Gulf Cooperation Council Countries' Electricity Sector Forecasting: Consumption Growth Issue and Renewable Energy Penetration Progress Challenges

Fahad Radhi Alharbi

This thesis is submitted for the degree of Doctor of Philosophy

Faculty of Science and Technology
School of Engineering

Graduate College July 2023

Declaration

The author declares that this project/thesis has never been submitted for a higher degree at this or any other university and that all of the contents are the author's original work, unless otherwise specifically cited. In addition, eight article papers from this thesis have been already published in leading international journals and proceeding IEEE conferences under the auspices of Lancaster University.

Signed:

Fahad Radhi Alharbi
Date: July 2023

Abstract

The Gulf Cooperation Council (GCC) countries depend on substantial fossil fuel consumption to generate electricity which has resulted in significant environmental harm. Fossil fuels also represent the principal source of economic income in the region. Climate change is closely associated with the use of fossil fuels and has thus become the main motivation to search for alternative solutions, including solar and wind energy technologies, to eliminate their reliance on fossil fuels and the associated impacts upon climate. This research provides a comprehensive investigation of the consumption growth issue, together with an exploration of the potential of solar and wind energy resources, a strict follow-up to shed light on the renewable energy projects, as currently implemented in the GCC region, and a critical discussion of their prospects. The projects foreshadow the GCC countries' ability to comply with future requirements and spearhead the renewable energy transition toward a more sustainable and equitable future. In addition, four forecasting models were developed to analyse the future performance of GCC power sectors, including solar and wind energy resources along with the ambient temperatures, based on 40 years of historical data. These were Monte Carlo Simulation (MCS), Brownian Motion (BM), and a seasonal autoregressive integrated moving average with exogenous factors (SARIMAX) model model-based time series, and bidirectional long short-term memory (BI-LSTM) and gated recurrent unit (GRU) model-based neural networks.

The MCS and BM prediction models apply a regression analysis (which describes the behaviour of an instrument) to a large set of random trials so as to construct a credible set of probable future outcomes. The MCS and BM prediction models have proven to be an exceptional investigative solution for long-term prediction for different types of historical data, including: (i) four types of fossil fuel data; (ii) three types of solar irradiance data, (iii) wind speed data; and, (iv) temperature data. In addition, the prediction model is able to cope with large volumes of historical data and different intervals, including yearly, quarterly, and daily. The simplicity of implementation is a strength of MCS and BM techniques.

The SARIMAX technique applies a time series approach with seasonal and exogenous influencing factors, an approach that helps to reduce the error values and improve the overall model accuracy, even in the case of close input and output dataset lengths. This

research proposes a forecasting framework that applies the SARIMAX model to forecast the long-term performance of the electricity sector (including electricity consumption, generation, peak load, and installed capacity). The SARIMAX model was used to forecast the aforementioned factors in the GCC region for a forecasted period of 30 years from 2021 to 2050. The experimental findings indicate that the SARIMAX model has potential performance in terms of categorisation and consideration, as it has significantly improved forecasting accuracy when compared with simpler, autoregressive, integrated, moving average-based techniques.

The BI-LSTM model has the advantage of manipulating information in two opposing directions and providing feedback to the same outputs via two different hidden layers. A BI-LSTM's output layer concurrently receives information from both the backward and forward layers. The BI-LSTM prediction model was designed to predict solar irradiance which includes global horizontal irradiance (GHI), direct normal irradiance (DNI), and diffuse horizontal irradiance (DHI) for the next 169 hours. The findings demonstrate that the BI-LSTM model has an encouraging performance in terms of evaluation, with considerable accuracy for all three types of solar irradiance data from the six GCC countries. The model can handle different sizes of sequential data and generates low error metrics.

The GRU prediction model automatically learned the features, used fewer training parameters, and required a shorter time to train as compared to other types of RNNs. The GRU model was designed to forecast 169 hours ahead in terms of forecasted wind speeds and temperature values based on 36 years of hourly interval historical data (1st January 1985 to 26th June 2021) collected from the GCC region. The findings notably indicate that the GRU model offers a promising performance, with significant prediction accuracies in terms of overfitting, reliability, resolution, efficiency, and generalisable processes. The GRU model is characterised by its superior performance and influential evaluation error metrics for wind speed and temperature fluctuations.

Finally, the models aim to help address the issue of a lack of future planning and accurate analyses of the energy sector's forecasted performance and intermittency, providing a reliable forecasting technique which is a prerequisite for modern energy systems.

Acknowledgements

"Everything begins with an idea."
"All you need is the plan, the road map,
and the courage to press on to your destination"
Quote by Earl Nightingale,
1921— 1989

The PhD study stage has been an enthralling and fulfilling experience in which I learned several analytical, research, and academic skills on a daily basis by combining an engaged academic community with scientific contributions. I would like to express my heartfelt gratitude to everyone who assisted me throughout my PhD journey.

First and foremost, my thankfulness goes to our *God, may He be praised and exalted!* Then, I would specifically like to express my deepest gratitude to my first supervisor, Dr. Denes Csala, for his tireless efforts, guidance, and advice, which have made a critical part in the success of this work since my first day as a PhD student at Lancaster University. I would also like to thank my second previous supervisor, Prof. Alastair Martin who retired in 2022. I wish him a prosperous retirement. I would also want to thank my second and third PhD supervisors, Dr. Ziwei Wang and Dr. M.S. Campobasso, for their comments and support during my PhD studies.

In addition, I would like to thank and highly appreciate the efforts of my PGR appraisal monitor Dr. Ahmed Badawy and the PGR coordinator Mrs. Laura Gracie. I am grateful to Dr. Richard Dawson and Prof. Sarah Green, my previous general mentors. I am also grateful to Dr. Xiaonan Hou, my current general mentor. Furthermore, my appreciation goes to all the Lancaster University engineering academic staff and my colleagues for their encouragement.

I would like to acknowledge the financial support from my main sponsor which is the government of the Kingdom of Saudi Arabia and the Saudi Arabian Cultural Bureau in London for their continuous assistance during my PhD studies.

I am also thankful to the International Renewable Energy Agency (IRENA) and the King Abdullah Petroleum Studies and Research Center (KAPSARC) for their support.

I dedicate this work to my dear mother and *'my father whom I lost during my PhD studies in 2019. May God have mercy on him.*' I would express my great thanks to them and to my siblings for their support throughout my life.

Finally, I would like to thank my young family, who are the shining light in the darkness of this life. I am indebted to my wife, my little girl and little son for their endless support, their continuous patience, and their participation on this long journey.

List of Journal Publications

- F. R. Alharbi and D. Csala, “A Seasonal Autoregressive Integrated Moving Average with Exogenous Factors (SARIMAX) Forecasting Model-Based Time Series Approach,” Inventions, vol. 7, no. 4, p. 94, Oct. 2022, doi: 10.3390/inventions7040094.

- F. R. Alharbi and D. Csala, “Wind Speed and Solar Irradiance Prediction Using a Bidirectional Long Short-Term Memory Model Based on Neural Networks,” Energies, vol. 14, no. 20, p. 6501, Oct. 2021, doi.org/10.3390/en14206501.

- F. R. Alharbi and D. Csala, “Gulf Cooperation Council Countries’ Climate Change Mitigation Challenges and Exploration of Solar and Wind Energy Resource Potential,” Applied Sciences, vol. 11, no. 6, p. 2648, Mar. 2021.Alharbi, F., Csala, D. 16/03/2021 In: Applied Sciences. 11, 6, 24 p. doi.org/10.3390/app11062648.

- F. R. Alharbi and D. Csala, "GCC Countries’ Renewable Energy Penetration and the Progress of Their Energy Sector Projects," in IEEE Access, vol. 8, pp. 211986-212002, 2020, doi: 10.1109/ACCESS.2020.3039936.

- F. Alharbi and D. Csala, “Saudi Arabia’s Solar and Wind Energy Penetration: Future Performance and Requirements,” Energies, vol. 13, no. 3, p. 588, Jan. 2020, doi.org/10.3390/en13030588.

List of Proceeding Conference Publications

- F. R. Alharbi and D. Csala, "Short-Term Wind Speed and Temperature Forecasting Model Based on Gated Recurrent Unit Neural Networks," 2021 3rd Global Power, Energy and Communication Conference (GPECOM), 2021, pp. 142-147, doi: 10.1109/GPECOM52585.2021.9587479.

- F. R. Alharbi and D. Csala, "Short-Term Solar Irradiance Forecasting Model Based on Bidirectional Long Short-Term Memory Deep Learning," 2021 International Conference on Electrical, Communication, and Computer Engineering (ICECCE), 2021, pp. 1-6, doi: 10.1109/ICECCE52056.2021.9514233.

- F. Al Harbi and D. Csala, "Saudi Arabia's Electricity: Energy Supply and Demand Future Challenges," 2019 1st Global Power, Energy and Communication Conference (GPECOM), 2019, pp. 467-472, doi: 10.1109/GPECOM.2019.8778554.

Contribution to Knowledge

Although several recent studies have discussed and analysed electrical power performance and consumption issues across the GCC region, this thesis provides a more comprehensive discussion of fossil fuel issues affecting the region.

GCC countries are fully dependent on fossil fuels to generate their electricity. Further, there is a dearth of (solar and wind) renewable energy research and feasibility studies in this region. These are essential in supporting renewable energy implementation and diversification of the energy mix system. This thesis fills this gap by assessing a long-term contribution to the sustainable energy strategy that protects the power supply from fluctuations and volatility, mitigates climate change implications, and ameliorates issues arising from carbon dioxide (CO_2) emissions across the region. This work is the first to provide such a synthesis between the past and present evolution of electricity generation capacity and energy consumption, and offers forecasts based on resources and preceding studies over the period spanning 1980 to 2020.

Four unique prediction models were developed and tested to forecast the future performance of the GCC's power sectors and evaluate the performance of solar irradiance, wind, and air temperature, respectively, based on historical data collated across a 36-year period (1985-2020). The models developed are MCS and BM model, SARIMAX model, BI-LSTM model and GRU based neural networks model. These prediction models have had a significant impact on the forecasting field.

As a result of this thesis's research output, eight article papers have already been published in Scopus international journals and at leading IEEE conferences under the auspices of Lancaster University with more than 125 citations in international organisations such as World Bank Study, ISI journals articles, including books, international conferences papers, and theses. Based on this research output, the findings presented in this thesis will open new avenues for future research and contribute to long-term research.

Table of Contents

List of Figures

List of Tables

Nomenclature

a_t	Zero average and the time series error term for SARIMAX model
$a_l(t)$	The input value of the layer for BI-LSTM model
b	The base vector for GRU and BI-LSTM models
e_t	The regression error for SARIMAX model
D	Drift for MCS and BM model
f	The ultimate valve for BI-LSTM model
f_t	Forget gate for BI-LSTM model
G	Backshift operator coefficient for SARIMAX model
g_t	Input node for BI-LSTM model
$1 - G$	Non-seasonal time series for SARIMAX model
$1 - G^s$	Seasonal time series for SARIMAX model
H	The general hidden layers for BI-LSTM model
H_1	Time series that does not have a unit root for SARIMAX model
H_0	Time series that has a unit root for SARIMAX model
$\overrightarrow{h}$	Forward hidden layers for BI-LSTM model
$\overleftarrow{h}$	Backward hidden layers for BI-LSTM model
$h\,t$	The hidden variable for BI-LSTM model
$h(t-1)$	The output vector of the past state or previous layer for GRU model
$h(t)$	The output vector current state layer for GRU model
$h_l^{(t)}$	Sharing status of the layer for BI-LSTM model
h^n	The hidden vector series for BI-LSTM model
i_t	Input gate for BI-LSTM model
l	The recurrent neural network (RNN) neuron layer
l_i	Lag degree for SARIMAX model
n	Sample numbers employed in the observation
N	Stack layers
o_t	Output gate for BI-LSTM model
r	Long-share value for MCS and BM model
R^2	Squared correlation coefficient
$r(t)$	Reset gate for GRU model
S	Standard deviation
s	The shape of the power-law profile
S_t	The value for the day for MCS and BM model
S_{t-1}	The value observed on the previous day for MCS and BM model
SS_{res}	The sum of squared residuals
SS_{Tot}	The absolute square number
U	The wind speed at a required height
u	Percentage drift for MCS and BM model
$Uref$	Reference wind speed
V	Variance
W	Weight of dust fallout

wQ (G^s)	Seasonal moving average for SARIMAX model
X	The exogenous factors for SARIMAX model
$x(t)$	The input vector at time t for GRU model
$x(t)$	The input vector for SARIMAX model
y	A commensurate sequential output
y_j	Actual value of the sample
$\hat{y}_j$	The forecasted observations
y_t	Autoregressive Integrated Moving Average with eXogenous output
$y(t)$	Corresponding prediction for BI-LSTM model
Z	The number of standard deviations for MCS and BM model
Zo	Surface roughness length
Zref	Anemometer height
$z(t)$	The update gate for GRU model

Mathematical Notation

$\boldsymbol{\beta}$	Time trend parameter
$\boldsymbol{\gamma}$	Null hypothesis
$\boldsymbol{\delta}$	Augmented Dickey-Fuller test coefficients
$\Delta\,\mathbf{y_t}$	The first difference operator
$\boldsymbol{\sigma_g}$	A sigmoidal element
$\boldsymbol{\sigma_h}$	The hyperbolic tangent
σ	Logistic sigmoid
$\odot$	Factor-wise multiplication
$\boldsymbol{\varphi_p}(\mathbf{G^s})$	Seasonal autoregressive
$\gamma(G)$	Moving average parameters

List of Acronyms

A	Amount of Dust Fallout
ACF	Autocorrelation function
ADF	Augmented Dickey-Fuller
AE	Autoencoder
AI	Artificial intelligence
ANN	Artificial neural network
AOD	Aerosol Optical Depth
ARIMA	Autoregressive Integrated Moving Average
APICORP	Arab Petroleum Investments Corporation
BM	Brownian Motion
BI-LSTM	Bidirectional long short-term memory
CAT	Climate Action Tracker
CAGR	Compound yearly growth rate
CCC	Committee on Climate Change
COVID-19	Coronavirus-2019
CNNs	Convolutional neural networks
CO_2	Carbon dioxide
CSP	Concentrating solar power
DBNs	Deep belief networks
DBMs	Deep Boltzmann machines
DNI	Direct Normal Irradiance
DHI	Direct Horizontal Irradiance
DL	Deep learning
DSM	Demand-side management
EnAppSys	Energy Applications Systems
FOA	Fruit fly optimisation algorithm
GCCIA	Gulf Cooperation Council Interconnection Authority
GCC	Gulf Cooperation Council
GC	Grey catastrophe
GDP	Gross Domestic Product
GHI	Global Horizontal Irradiance
GHG	Greenhouse Gas
GMDH	Group Method of Data Handling
GRU	Gated Recurrent Unit
Gt	Gigatonne
GW	Gigawatts
HELM	Hysteretic Extreme Learning Machine
IEMD	Integrated empirical mode decomposition (IEMD)
IEO	Independent Evaluation Office
IPCC	International Panel on Climate Change
IRENA	International Renewable Energy Agency

KAPSARC	King Abdullah Petroleum Studies and Research Center
KSA	Kingdom of Saudi Arabia
LSTM	Long short-term memory
MAE	Mean absolute error
MAPE	Mean absolute percentage error
MCS	Monte Carlo Simulation
MLPs	Multilayer perceptrons
MSE	Mean square error
Mt	Million Tonnes
MW	Megawatts
NPP	Nuclear power plants
NTP	National Transformation Programme
OECD	Organisation for Economic Cooperation and Development
OIES	Oxford Institute for Energy Studies
PACF	Partial Autocorrelation Function
PETA	Power Exchange Trading Agreement
PFI	Project Finance International
PV	Photovoltaic
QEWC	Qatar Electricity & Water Company
RBM	Restricted Boltzmann machine
RES	Renewable energy sources
RF	Random Forest
RNNs	Recurrent neural networks
SARIMA	Seasonal autoregressive integrated moving average
SARIMAX	Seasonal autoregressive integrated moving average with exogenous
SEM-VARIMAX	Structural equation modelling vector autoregressive with exogeneous
SVM	Support Vector Machine
SVR	Support vector regression
TWh	Terawatt-hour
UAE	United Arab Emirates
UNEP	United Nations Environment Programme
UNFCCC	United Nations Framework Convention on Climate Change
WEC	World Energy Council
WNN	Wavelet neural network

1 Introduction

As clean energy sources, renewable energy technologies (solar and wind) have grown considerably due to climate change, global warming, and carbon dioxide (CO^2) emissions. In particular, with the rapid growth of global industrial activities, climate change and global warming present the most serious global environmental issues. Currently, there is a sharp increase in CO_2 levels, which aggravates environmental issues [1-5]. The Met Office has reported that the global rate of climate warming and atmospheric CO_2 reached a near-record increase in 2019 [6]. The growth in CO_2 levels is driven by the continuous burning of fossil fuels [7], the expansion of heavy industries [8], and the destruction of forests due to rapid urbanisation [9]. This is further exacerbated by the exceptional population growth in developing countries [10]. Furthermore, climate variation leads to warm and dry conditions in the tropics, indicating that the growth of plants that absorb CO_2 from the air is limited while the average ambient temperature is increasing alongside decreasing precipitation. Human activities are continuously changing the climate as a result of natural life processes. A previous study has reported that more than 88% of human activities cause climate change, including persistent energy generation and consumption [11]. The threats of climate change and global warming have compelled policymakers and researchers to assess the effects of the world's warming on the global economy and to discuss ways of eliminating greenhouse gases and CO_2 emissions to mitigate global warming [3]. The countries of the Organisation for Economic Cooperation and Development (OECD) are striving to reduce greenhouse gas emissions, due to their stationary nature, and to comply with the international norms on environmental risks [12]. Thirty-four democratic countries of the OECD are working to address the environmental challenges of globalisation, corporate governance and economic development in addition to such social challenges as an ageing population.

According to the recommendation by the Committee on Climate Change (CCC), the power sectors must be entirely decarbonised by 2050. The decarbonisation of the power sector implies a reduction in its carbon intensity (i.e., emissions per unit of power generated measured as CO_2 per kWh). The CCC has reported that the UK must lead the global fight against climate change by reducing greenhouse gases to nearly zero by 2050. If all countries followed the example of the UK, there would be a 50% chance of staying below the recommended temperature rise by 2100 [13]. In 2015, Energy Applications

Systems and Information (EnAppSys) reported that, in the UK, the generation of renewable energy had grown to the same level as that of nuclear power plants (NPPs) while coal use had continued to decrease (claim made by Paul Verrill, Director of EnAppSys [14]). On the other hand, an independent adviser to the government on climate change in the UK reported that it may not be able to reach "net zero emissions, and it still remains an extremely significant goal" [13].

According to the CCC, the considerable drop in the cost of renewable energy, as promoted by government policies to nurture wind and solar power, will be the primary solution in addressing climate change and global warming issues [13]. Governments around the world are frequently called upon to contribute a major share of emission reductions, which entails the substitution of electricity generation based on fossil fuels with low-carbon technologies, such as RES and NPPs. In addition, these endeavours will minimise global dependence on imported fossil fuels and eliminate future exposure to long-term high electricity market prices. Nevertheless, it is difficult to achieve future low-carbon scenarios via RES alone as the support of NPPs is required. On the other hand, RES remain a variable source, introducing volatility that can affect the operational stability and reliability of the National Electricity Transmission System due to their specific physical characteristics. The challenges associated with such future mixed energy generation scenarios should be carefully considered and must be controlled as far as possible, as an imbalance in the electricity system is necessary to maintain the extremely high safety quality of the system. However, there are global regions where the pressure to shift away from fossil fuel-based energy sources is higher than ever. The GCC countries are among the top 25 in terms of CO_2 emissions per capita in the world, and are thus considered to be actors obstructing global climate change negotiations due to their larger oil and natural gas reserves [15]. In addition to energy reliance, the GCC countries exhibit a significant economic reliance on oil and natural gas as well, with fossil fuels being their primary source of income, representing some 31.6% to 55.7% of GDP and 60.8 to 93.8% of government revenues (Table 1-1) [16].

Recently, the GCC region has raised concerns about global climate change and associated environmental issues which require an integrated strategy to have a more proactive approach toward ecological modernisation and renewable energy policies. Regional authorities have identified requirements for the development of a strategic partnership, one that focuses on the sustainability of the GCC region and its well-being [11]. The GCC

countries are concerned with their large per capita energy consumption [17] as well as their depletion of water and other fossil fuel resources. Further, these are associated with the generation of waste, air pollution, and greenhouse gas emissions which are well above the global average. The region generates 99% of its electricity from fossil fuels, such as natural gas, crude oil, residual oil, and diesel owing to its large reserves of oil and natural gas, and the amount of electricity generated from fossil fuels is continuously being developed. Power consumption, as a result of activities from industries [18] such as the steel, iron, cement, and aluminium sectors, as well as construction, accounts for 34% of the total energy-related pollution in the region [11]. The CO_2 emissions of the GCC countries correspond to the burning of a considerable quantity of fossil fuels for energy generation and the emissions resulting from oil and natural gas exploration activities.

Table 1-1. Demographic data of GCC countries during 2022[16], [19].

Item	KSA	Oman	UAE	Kuwait	Qatar	Bahrain
Area (km^2)	2,149,690	309,500	71,002	17,818	93.8	778.3
Population (millions)	32.175	5.075	9.50	4.25	2.68	1.46
Population density (per km^2)	16	13	116	223	210	1696
GDP (billion dollars)	646	69.8	370.3	114	164.64	31.13
Per capita GDP (thousands of dollars)	20.8	16.8	48.33	28.7	59.331	22.71
Oil reserves (billions of barrels)	266	5.2	98.0	102	25.2	0.12
Natural gas reserves (in billion cubic feet)	8588	931	6,091	1784	24299	92
Oil & natural gas share of GDP (%)	47.8	47.7	31.6	51.5	55.7	44.2
Oil & natural gas as a % of Government revenues	90.4	81.7	75.9	93.8	60.8	80.1

Between 2000 and 2010, CO_2 emission levels increased by up to 80% across the region, averaging 8% per year and dominating 79% of other emissions [11], [19], [20]. Climate change and global warming are game changers, enormously affecting all sectors in the GCC region [11]. The dilemma is to define climate change and global warming via a precise understanding of its effects and to determine how one can heal those impacts and treat them in order to eliminate the associated risks. On the other hand, relatively few studies have discussed climate change and global warming across the GCC region, and those that have been published have typically ignored the crucial stages of the observed phenomena that require long-term effective solutions. The lack of GCC climate change studies and the clarification of the effects of this issue have led to uncertainties regarding future projections and risks [21]. Climate studies have reported that temperatures surged in the GCC region between 1960 and 2010, rising by up to 0.41°C per decade [11], [22]. Further, from 1960 to 2003, the number of winter cold days decreased and the number of hot days increased during the summer across the region [23]. In addition, the GCC region suffers from extremely arid conditions, and the climate is expected to become more severe with marginal quarterly rains attributed to the desalination of seawater [11], [24]. Climate studies have revealed a strong correlation between temperature rises and increases in energy consumption across the region.

1.1 Background

1.1.1 Gulf Cooperation Council Overview

In May 1981, the GCC was formed as a union of six countries in the Arabian Peninsula [25]. The six members of the council include the KSA, the Sultanate of Oman, the United Arab Emirates (UAE), the State of Kuwait, the State of Qatar, and the Kingdom of Bahrain. Table 1-1 presents additional relevant details of the GCC countries, such as their area in square kilometres; their respective populations in millions; and their gross domestic products (GDP) together with estimates of oil and natural gas reserves. The six GCC countries harbour approximately 30% of known global oil and a quarter of established natural gas reserves (Table 1-1) [26]. The GCC region's oil revenues exceeded 156 US$ billion in 1981 [27] and, until very recently, the GCC region's crude

oil deposits were the primary source of energy in the OECD [27]. The extremely rapid modern development of the GCC region and its sustained economic growth were defined by the ‘era of oil’ which defines the economics and politics of the region to a greater extent than it does anywhere else in the world. Further, massive development has been observed across the region in all sectors, including the energy sector, infrastructure, heavy petrochemical industry, educational systems, and other economic sectors [27]. On the other hand, the exports and savings of the GCC region far exceed its domestic investment requirements [27]. Rapid improvements have been achieved at the cost of substantial capital consumption, implying that the oil and natural gas reserves of the region have started to become depleted at rates that are considerably more rapid than the physical capital required created to replace oil and natural gas. On the other hand, the economic absorptive capacity of the GCC fell far short of the potential oil and natural gas revenues in the region due to a lack of long-term planning, scaled-up limitation issues, a lack of diversity of energy sources, and oversights in the monitoring and control of the economy [27]. In addition, oil and natural gas constitute non-renewable energy resources with limited lifetimes, leading to a skewed and unprotected economy. In fact, the GCC countries have not yet reached their required sustainable economic growth levels, which are independent of the oil and natural gas revenues, while the gestation period for the economic development of the GCC may be longer than the expected remaining lifespan of its remaining hydrocarbon resources [27]. These transformations have proven to be expensive, and the GCC region needs to diversify its economy, including replacing extant energy sources with viable alternatives, a matter that is both pressing and difficult.

1.1.2 Energy Consumption Overview of GCC Countries

The populations of the GCC countries are relatively small, while the oil and natural gas consumption levels of these countries are considerably greater than those of Japan or Indonesia and indeed greater than the primary energy consumption of the entire African continent [28]. Over the past 10 years, the energy demand in the region has increased by 6-8% per annum [28], [29]. The energy demand growth is associated with population development, mirroring GDP growth in the region. Currently, however, the main concern of the region is about delinking GDP growth from growth in energy demand for development. The shared challenges of the region include energy diversification, energy efficiency, domestic energy security, and long-term environmental sustainability. To

harness their climatic advantages, these energy challenges and visions were not given appropriate consideration within the GCC energy policies of the 1970s and 1980s. However, globally, several successful and ambitious plans for the reduction of energy consumption were implemented in China and India by incentivising efficiency and scaling up of RES [29]. Renewable energy is already a mature option as an alternative solution for the region in driving a fall in energy consumption and eliminating CO_2 emissions [30], [31]. Solar energy is abundant within onshore locations, while wind energy is abundant in offshore locations [30].

1.1.2.1 Electricity Overview of GCC Countries

In 2016, the GCC region recorded a generation capacity of 138 GW [32]. Figure 1-1 provides an overview of electricity generation capacity (dark blue) and peak demand (light blue) across the region in 2016 alongside projected demand in 2030 (green). However, according to the Arab Petroleum Investments Corporation (APICORP), the generation capacity increased to 151 GW in 2018 with the KSA being the largest producer with a generation capacity of 82 GW [33].

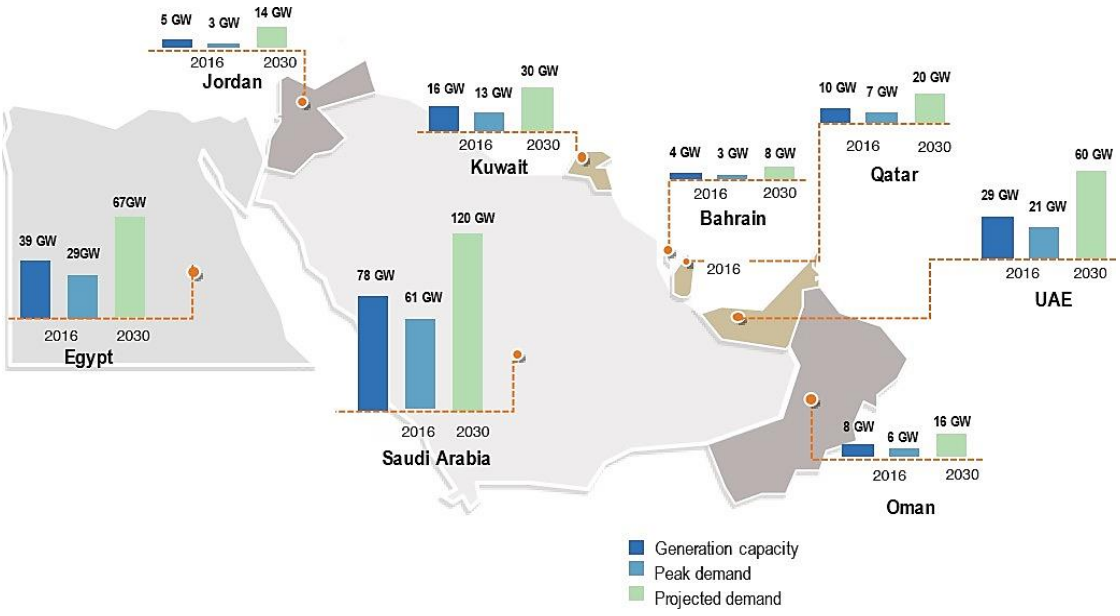

Figure 1-1. Electricity generation and peak demand across the GCC region and Egypt and Jordan in 2016 together with projected demand in 2030 [33].

The KSA generates more than half of all of the electricity produced in the GCC region, while Bahrain generates the least. The rising demand in KSA has led to the addition of more than 4 GW of power generation, annually [34]. APICORP has reported that the

GCC countries will need to add a further generative capacity of 43 GW within the next five years (by 2024) to meet the high levels of demand across the region [33]. The generation side faces challenges in terms of economic growth and demographic requirements. On the other hand, the main consumers in the region are broken down into residential, commercial, and industrial sectors. In 2017, the total annual electricity generated in the region increased to 680 TWh, rising to 691.5 TWh by 2018, corresponding to an increase greater than 11 GWh within a year (Figure 1-2) [35], [36]. In 2020, the electricity generated was reduced to 670 TWh due to COVID-19 restrictions enforced across the region.

In 2017, total annual consumption was recorded as 559.3 TWh, increasing to 573.11 TWh in 2018, corresponding to an increase of 13.8 TWh within a year (Figure 1-3). The consumption rate increased continuously, while the actions taken by the GCC governments failed to reduce consumption, an area which still requires improvement. However, total annual consumption was recorded as 613 TWh in 2020 and 614 TWh in 2019.

Over the past decade, peak load has surged across the region, contributing to the region's historic challenges in terms of electricity supply, challenges that necessitate increasing generative capacity. The arid desert conditions and extremely high summer temperatures require increased air conditioning capacity. This led to the highest peak load in the history of the region in 2015 in the KSA at 62.25 GW (Figure 1-4) [37]. Maximal peak loads are usually recorded during the months of July and August due to the very high temperatures.

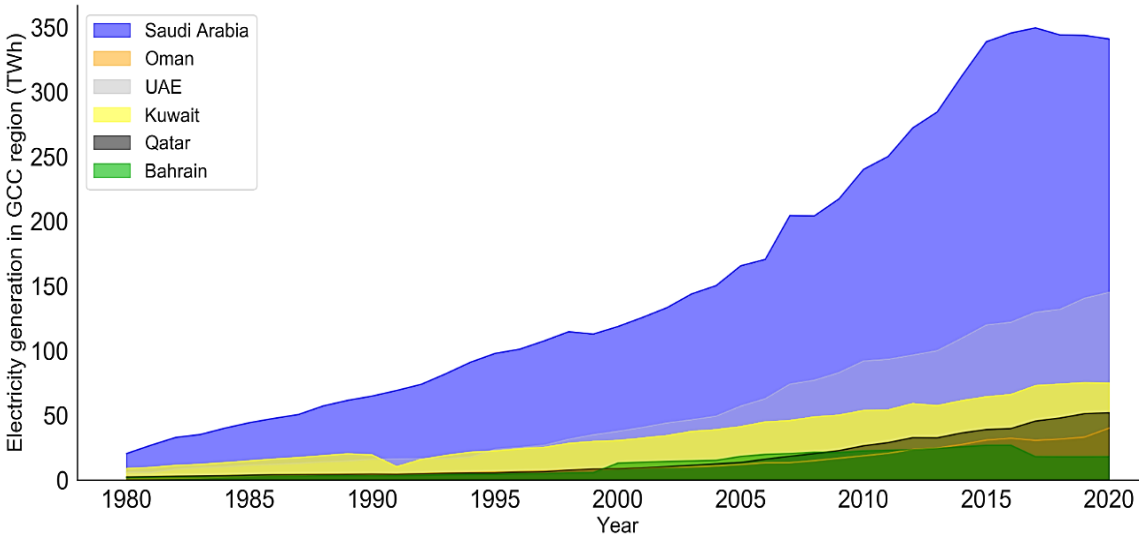

Figure 1-2. Electricity generation across the GCC region.

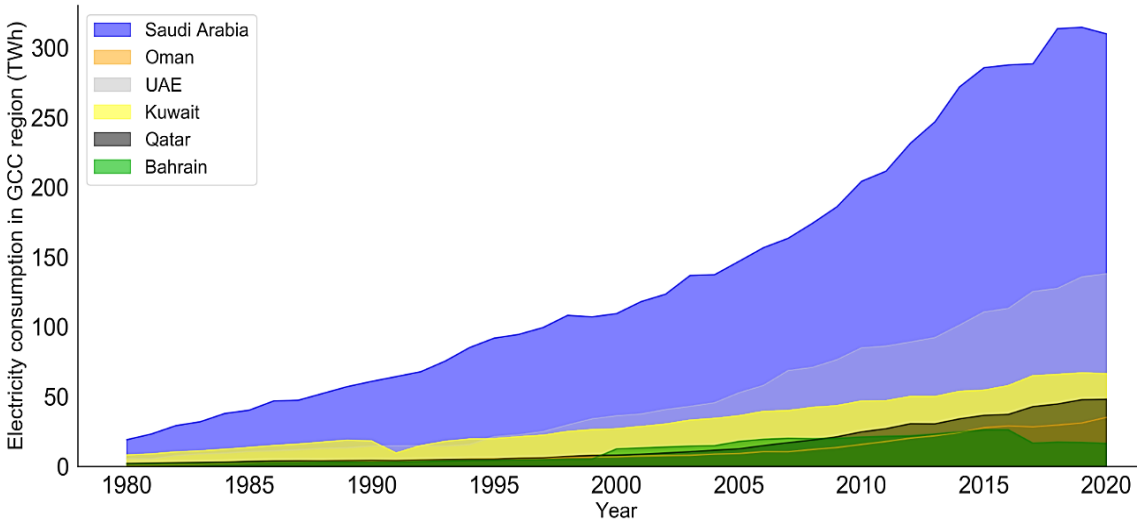

Figure 1-3. Electricity consumption in the GCC region.

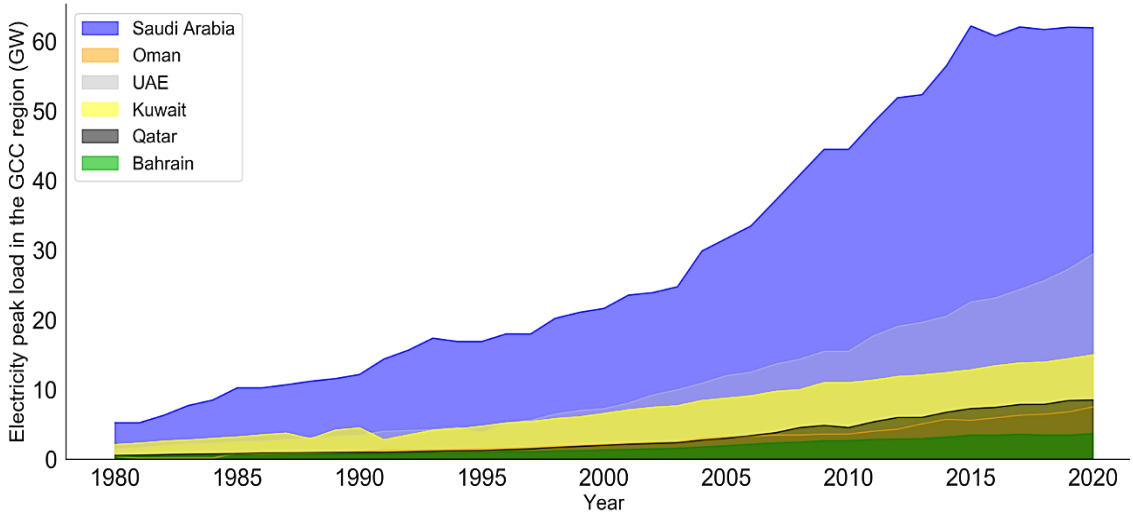

Figure 1-4. Electricity peak load across the GCC region.

On the other hand, the GCC countries can no longer continue to support the provision of electricity at heavily subsidised prices due to rising budget deficits and declining oil revenues. Improvements in income levels, as well as urbanisation, which has relatively low energy costs compared to international costs, have led to an increase in electricity demand. The electricity installed capacity performance in the GCC region is presented in Figure 1-5. To control power consumption, some of the GCC governments increased electricity prices twice between 2015 and 2018.

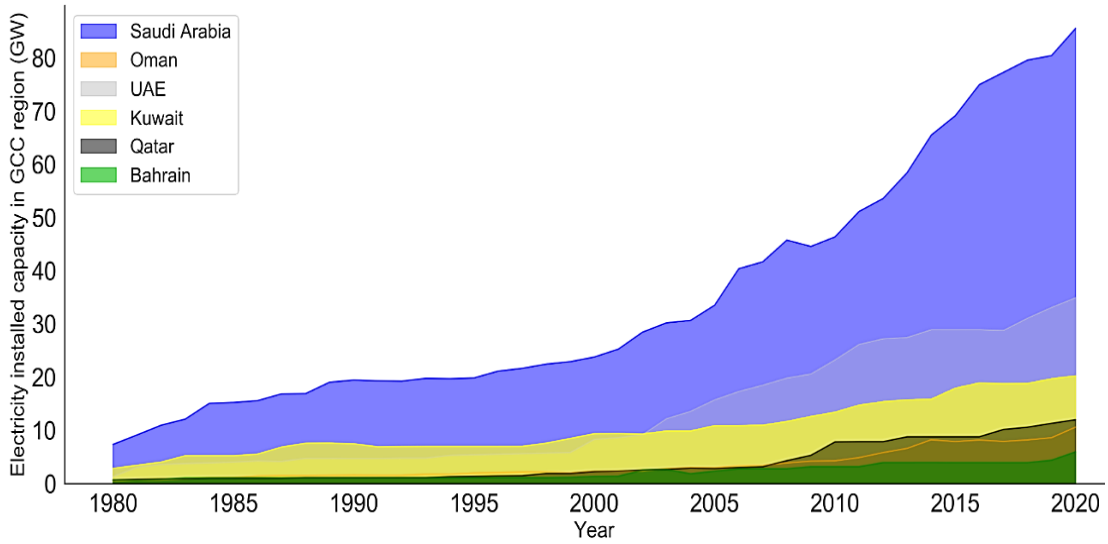

Figure 1-5. Electricity installed capacity in the GCC region.

Figure 1-6 shows the reduction in government subsidies from 2015 to 2019 [33]. The GCC governments implemented subsidy reform plans, causing domestic electricity tariffs to increase significantly by as much as 250% in KSA. The GCC governments have other reform plans for the power sector, such as kick-starting renewable energy initiatives across the region. However, the slowdown of this initiative, coupled with delayed electricity reforms, has adversely influenced the growth of domestic consumption across most of the GCC region.

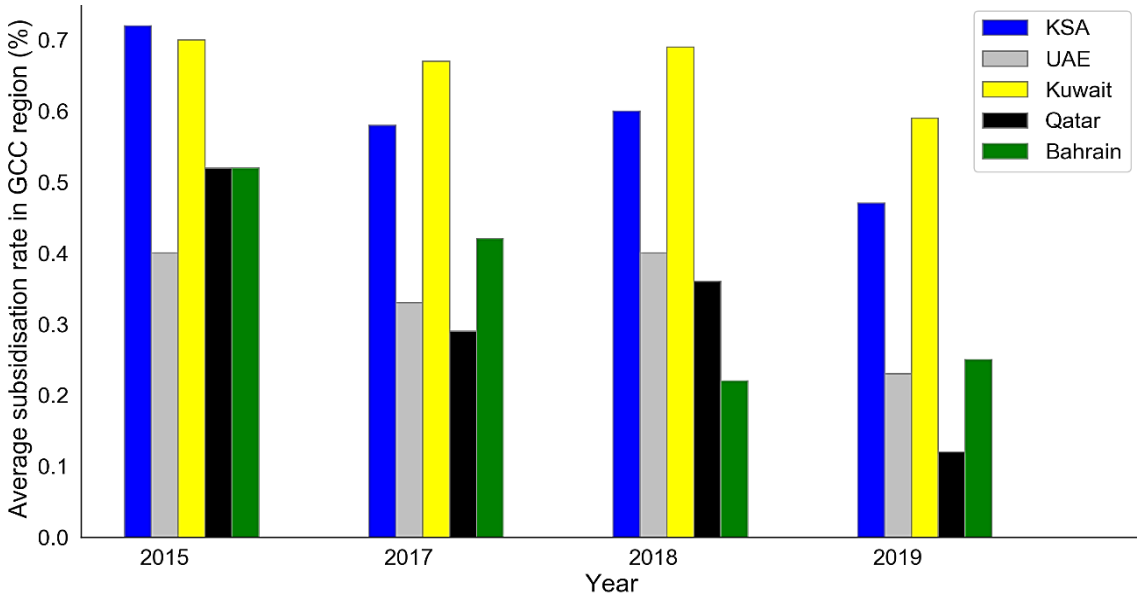

Figure 1-6. Reduction in government energy subsidies across the GCC region.

1.2 Problem Statement and Motivation

During the previous decade, energy consumption rates have raised rapidly across the GCC and are expected to continue increasing in the future, despite their full reliance on conventional energy supply technologies. The region has large reserves of oil and natural gas resources which is the key energy signature of these countries [38]. The countries of the GCC signed and ratified the United Nations Framework Convention on Climate Change (UNFCCC) as well as the Kyoto Protocol [39, 40]. The GCC considered climate change issues to be the world's primary environmental threat. As such, the GCC countries are required to support a global collaboration of energy technologies that addresses energy efficiency and the deployment of low-carbon technologies. The GCC's energy sector currently faces three major problems, as follows:

- Issues of the environment, namely the fact that the GCC's electricity sector must not be entirely dependent on evanescent oil resources or increasing natural gas prices.

- GCC countries started to suffer from an end to state energy subsidies, notably in the KSA which saw energy prices double over the past five years in an effort to reduce consumption.

- Increasing electricity demand and rising price constraints have prompted GCC governments to investigate more cooperative approaches in delivering reliable and affordable energy resources such as RES.

The development of integrated energy technologies will help to achieve the objectives of creating efficient and sustainable energy resources. Further, the economies of the GCC face a common problem through their economic dependence on oil and natural gas as a primary source of income. The GCC countries must diversify their revenues by introducing new industries such as the renewable energy sector. After highlighting the motivating problems of this research, the following questions were asked:

1. What is the level of awareness of GCC nations in terms of renewable energy resources and their potential to provide the energy security for the region?

2. Do the GCC countries have sufficient capabilities and resources to transition toward a clean energy system?

3. What are the possible future scenarios for the electricity sector in the GCC?

1.3 Research Aims

This research aims to meet the renewable energy engineering goals of Lancaster University to create a strategic real-world impact on a much-needed resolution for the world's energy problems, including the growth in energy consumption and greenhouse gas emissions.

In addition, this research presents an appropriate lens through which to examine and analyse future scenarios of renewable energy penetration and power performance in the GCC countries over the longer term. This will be essential to meet the growth in energy demand across the region and reduce dependence on conventional energy sources. The main aims of this research can be summarised as follows:

1. Assessing the ability of GCC countries to transition to renewable energy sources (RES) and comply with the energy share system by ensuring the penetration of RES into the GCC generation system.

2. Examine the future of the electricity sector in GCC countries, especially regarding the long-term growth capacity of RES and an investigation of potential future scenarios of development across the GCC region.

3. Analysing the transition towards decarbonisation technologies by evaluating potential solar and wind resources across the GCC to foster environmental sustainability and achieve climate change mitigation in the region.

4. Evaluating the future performance of the GCC power sectors by predicting future scenarios for power generation, electrical installation capacities, electricity consumption, peak load, wind speed, solar irradiance, and temperatures during several periods spanning 2025 to 2040. This will seek to target a minimisation of the use of fossil fuels in the region to comply with global consumption targets.

1.4 Objectives

The objectives of this research are delineated below:

1. To evaluate current and future GCC energy system requirements based on historic data and performance.

2. To investigate the flexibility of GCC countries in implementing a plan of renewable energy share via wind and solar technologies and their potential influence on the energy regimes of the future.

3. To investigate the sensitivity of RES in terms of installed capacity and generation for long-term energy sustainability across the GCC region.

4. To explore the influence of factors such as fluctuations in wind speed, temperatures and solar irradiance on RES and energy outputs over the longer term.

1.5 Research contributions and Significance

This research is distinguished by many points that make it unique in the field of electrical energy in the GCC region. The region's rapidly growing power consumption and the reasons that have led to its exacerbation over the past four decades are discussed and analysed, as is the energy future for the GCC region over the next thirty years, based on historical data and other studies conducted during the research period of interest (1980–2020). The use of energy sources in the GCC region over the past four decades, such as solar energy, wind speed, ambient temperatures, the dust effect and rainfall totals, are also addressed.

In addition to the above, four forecasting models have been developed to analyse the future performance of the power sector in the GCC region. These include solar and wind energy resources and data concerning ambient temperatures based on the past forty years. These models are the Monte Carlo Simulation (MCS) and Brownian Motion (BM) model, a seasonal autoregressive integrated moving average with exogenous factors; the SARIMAX model, which is based on time series data; the bidirectional long short-term

memory (BI-LSTM) model; and gated recurrent unit (GRU) model-based neural networks.

This study aims to help fill that gap by assessing a long-term contribution to sustainable energy strategies that protects power supplies from fluctuations and volatility, mitigates the implications of climate change and reduces carbon dioxide (CO2) issues in the region. This study is the first to include a synthesis between the past and present states of the GCC's power sectors and fills the research gap identified above in the following ways:

- This research contributes to reducing GCC countries' dependence on the fossil fuel industry by highlighting the ways in which the industry harms the environment and its explicit contributions to climate change, health problems and environmental harms not typically counted accounted for within the 'cost' of fossil fuels.

- Achieving equal opportunities regarding the diversification of electrical energy sources in the GCC region and identifying the main reasons and factors that have led to the growth of power consumption over the long term.

- Increasing investments in renewable energy and achieving a balance in energy prices, thus leading to stability in global energy markets.

- Reducing greenhouse gas and CO2 emissions to the levels closest possible to zero.

- Increasing the awareness of the need to rationalise the consumption of conventional energy sources, to provide opportunities for future generations to benefit from them.

- Increasing research on electrical energy over the long term in the GCC region, which has historically suffered from a severe shortage in this field, especially related to renewable energy.

- Promoting the research and development of renewable energy by highlighting the extent of the environmental risks facing humanity in the long term, should renewable energy not become the norm.

- Identifying effective transitional approaches and methods for renewable energy economies and promoting investment in this field

1.6 Structure of the Thesis

The structure of the thesis comprises of ten chapters, as follows:

Chapter 1 – Introduction. This chapter provides a contextual background and overview of the GCC region's energy sectors, including energy consumption growth issues. It focuses on the debate over the development of electricity systems in the region. In addition, this chapter provides a problem statement and motivation for the research together with aims and objectives (*this chapter was reviewed by external reviewers and published in a peer-review IEEE Journal*).

Chapter 2 – The GCC's Consumption Growth Issue and Review of Renewable Energy Deployment. This chapter presents the first phase of the literature review of the consumption growth issue and renewable energy deployment and analyses its requirements. In addition, this chapter discusses the GCC regional energy interconnectivity and provides a critical discussion of the progress of renewable energy projects across the region (*this chapter was reviewed by external reviewers and published in a peer-review IEEE Journal*).

Chapter 3 – Review of the Feasibility of Analysing Solar and Wind Energy Resources across the GGC. This chapter presents the second phase of the literature review which discusses the GCC's RES potential in terms of solar and wind energy, with a consideration of such atmospheric effects as dust and clouds. Moreover, this chapter discusses the GCC region's geographical factors (*this chapter was reviewed by external reviewers and published in a peer-review MDPI Applied Sciences Journal*).

Chapter 4 – Research methodology. This chapter outlines the research methodology, including the main research framework and a description of the collection, evaluation, and analysis of the historical data. This chapter provides an extended explanation of the "four models" development plan.

Chapter 5 – Monte Carlo Simulation and Brownian Motion Prediction Model Development. This chapter presents the first developed prediction model which is the

MCS and BM model including a consideration of its structure and method of operation along with its underlying mathematical concepts and simulation. In addition, this chapter presents the prediction model results together with a comprehensive discussion of the findings (*this chapter was reviewed by external reviewers and published in a peer-review MDPI Energies Journal, with the exception of section 5.3*).

Chapter 6 – Long-Term Seasonal Autoregressive Integrated Moving Average with Exogenous Prediction Model. This chapter comprises the second developed prediction model, namely the seasonal autoregressive integrated moving average with exogenous (SARIMAX) prediction model. This chapter presents the SARIMAX model's mathematical concepts together with a simulation and a comprehensive analysis of its predictions (*this chapter was reviewed by external reviewers and published in a peer-review MDPI Inventions Journal, except for section 6.3*).

Chapter 7 – Bidirectional Long Short-Term Prediction Model-Based Neural Networks. This chapter introduces the third developed prediction model which is the BI-LSTM. This chapter presents the BI-LSTM prediction model's structure, method of operation, underlying mathematical concepts and simulations together with an analysis of its results (*this chapter was reviewed by external reviewers and published in a peer-review MDPI Energies Journal, except for section 7.3).*

Chapter 8 – Short-Term Prediction Model Based on Gated Recurrent Unit Neural Networks. This chapter presents the fourth developed prediction model which is based on gated recurrent unit-based neural networks (GRU) including the model's structure, method of operation, underlying mathematical concepts and simulation, together with a discussion of its predicted results (*this chapter was reviewed by external reviewers and published at a peer-review IEEE Conference, with the exception of section 8.3).*

Chapter 9 – Synthesis and Interpretation of Findings. This chapter provides a comprehensive discussion of the GCC countries' characterisations and analysis, including an interpretation of the findings for the four predictive models' results as well as the main findings of the research.

Chapter 10 – Conclusions. This chapter presents the conclusions and highlights the main findings of the research. In addition, the strengths and limitations of the research are discussed, before offering recommendations for the GCC countries' renewable energy development as well as the scope for future research and forecasting techniques.

2 A Review of the GCC's Consumption Growth Issue and its Deployment of Renewable Energy Resources

This chapter consists of an overview of the published literature relating to historical energy consumption growth issues and renewable energy deployment across the GCC region. Here we discuss its prerequisites, including the interconnectivity of the GCC regional grid. In addition, this chapter provides a discussion of the progress of renewable energy projects across the region.

2.1 Progress of the Penetration of Renewable Energy Sources across the GCC

The GCC countries are facing rapid development in terms of infrastructure and energy investments which has resulted in electricity consumption increasing by 12.4% from 2005 to 2009, equivalent to an annual growth of 3.15% [41]. The largest rate of an increase in electricity consumption was recorded in Oman (22.6%), while the lowest rate of increase in consumption was in the KSA (6.3%). According to Alnaser and Alnaser [41], the increasing rate of electricity consumption across the GCC region (3.15% per annum) is greater than the world average (2.2%) over the same period. The average per capita power consumption across the GCC region reached 1,149 W per capita in 2005, as compared to 700 W per capita in the European Union [41], [42]. Based on Alnaser and Alnaser [41] figures, the electricity generation capacities of the region hovered at approximately 75 GW in 2011, although there was a need to add a further 60 GW to increase their electrical capacities to meet the projected growth in demand by 2015. The World Energy Council (WEC), on the other hand, estimates that the region will need a further 100 GW to meet its ever-growing demand over the next 10 years [41]. The governments of the GCC countries have recognised that their dependence on natural gas will not present a sustainable long-term solution due to their lack of alternative resources and extant environmental externalities. The GCC's share of total CO_2 emissions stands at approximately 2.2%. In 2011, KSA recorded its lowest CO_2 per capita values at 18 tonnes per capita, while the UAE recorded the highest at nearly 60 tonnes per capita [41]. Alnaser and Alnaser [41] estimated that up to 13 GW of renewable energy may have been generated across the GCC region in 2015. The GCC countries planned to invest a further

$200 billion in 14 to 20 renewable energy projects by 2020, reducing CO_2 by some 1,000,000 tonnes [41], [42].

Based on Weber [39], the oil and natural gas resources of the GCC region are ultimately finite and the region may face imminent declines in oil production. Thus, the increase in the domestic demand for natural gas and oil is contributing to the reduction in the national income of GCC exports [39], [43]. Since 2008, the domestic consumption of natural gas in the UAE and Kuwait has exceeded its actual production. Water desalination, residential demand, commerce, oil production and other industries are the major sinks for energy consumption across the GCC region. Another study reported that the low prices of oil and natural gas caused by government subsidies encouraged the overconsumption of water and energy in the region [39]. Taxes and tariffs can be implemented to reduce this consumption and ameliorate the increasing demand for power generation although these present risky policy decisions [39], [44]. The citizens of the GCC region are accustomed to low water and energy prices, which they view as citizens' rights and thus view their governments as the distributors of oil revenues and the creators of employment opportunities [39]. This places further pressure on GCC governments to substitute existing energy generation solutions with more climate-compliant alternatives in preference to fostering a reduction in demand. The recent interest in RES has been driven entirely by the high growth in demand for desalinated water, electricity generation, reuse schemes, and the competitively low cost of solar and wind energy [39]. As the GCC countries seek opportunities to diversify their economies, renewable energy provides an effective option to recycle their huge financial surpluses from oil production and opens the prospects for energy export to Europe's grid [39], [45].

According to a study conducted by Bhutto et al. [46] in 2014, the transfer to renewable energy technologies would reduce fossil fuel consumption in the GCC countries and mitigate their environmental challenges [47]. The population growth and brisk economic expansion in the region, which is linked to the growth of energy-intensive industries such as the petrochemical, aluminium and steel industries, has led to an increased electricity consumption [46]. As a result, regional governments needed to take advantage of inexpensive energy and review their taxation policies [46], [48]. While Howarth et al. [48] reported that the GCC countries have a common strategic target to transition towards economies which are less reliant on oil and natural gas resources. However, economic growth and energy consumption are strongly correlated across all sectors in the GCC.

This relationship has profound geopolitical implications and necessitates important policy development decisions driven by considerations of economic growth, future energy demand and climate change. Further, increasing consumption in the GCC countries far outpaces their GDP growth. This is in stark contrast to OECD economies which have been declining and have exhibited relatively slower energy consumption growth over recent years. According to Howarth et al. [48], to shape future domestic energy demand, the GCC countries need the following broad, strategic diversification models to be available to them:

- Improving path dependence of access to low-cost energy to support industrialisation in energy-intensive sectors such as cement, petrochemicals, aluminium and steel. This model would lead to rising domestic energy consumption and reduce the need for oil exports.

- Improving path dependence to include essential diversification into non-energy sectors, such as financial services, medical services, tourism and education. This model would moderate domestic energy consumption and ensure reliable energy exports which can be channelled into investments in high-value-added sectors.

According to Bhutto et al. [46] there is a strong correlation between a country's electricity consumption and its level of economic growth. This assertion is also supported by the findings of Howarth et al. [48]. It also found that the region is likely to experience one of the fastest growth rates in terms of economic and energy demand in the world over the next 20 years. The region requires widespread investments to meet rising energy demand over the next 20 years [46]. The real opportunity for the GCC countries thus lies in the development and adoption of new technologies and in building a strong management system for an alternative energy mix associated with increased energy efficiency and carbon sequestration. Renewable energy investments would support their long-term energy security by facilitating the diversification of the energy mix and reducing reliance on finite fossil fuel resources in addition to creating opportunities for capital investment in the region. The investments in renewable energy could also potentially create high-value jobs within the GCC energy sector and may thus contribute to a full energy value chain, including local and international deployment, manufacturing research and development.

Griffiths [49] wrote that each member country of the GCC had stated targets and ambitions for renewable energy, yet their deployment to date has essentially been minimal. The majority of the GCC countries have simply announced renewable energy targets rather than applying concrete policies to spur their adoption [49]. Therefore, the GCC countries need to address the gap between political ambition and the requirements of the power sector by reforming and enforcing appropriate policies and implementing clear strategies to guide regional energy development. The GCC's plans must be explicated into real actions via defined regulations and policies to achieve success to reflect the regional context [49]. Renewable energy auctions, which stimulate renewable energy deployment, are one suitable method. However, in keeping with international trends, GCC governments may no longer be focused on bridging the price gap between RES and fossil fuel-based energy generation [49]. Rather, the major trend in renewable energy is to support its sustainable integration into the energy mix. This trend is most pertinent to the GCC energy sector, where RES, including solar and wind, present attractive and economically viable options due to the region's abundant wind and solar resources [49]. GCC policymakers have begun to consider these types of renewable energy which have since been widely deployed as significant contributors to the global energy system as they have become increasingly cost-competitive. IRENA expects that, by 2025, utility-scale installations of solar and wind costs may have fallen even further, reducing solar costs by up to 57%, onshore wind costs by up to 12%, and offshore wind costs by up to 15% relative to 2015 [49]. However, progress is slow, possibly due to the region's lack of experience in implementing such renewable energy projects. The region has unique circumstances that must be considered, such as its high temperatures, occasionally low wind speeds, and its dependence on the oil industry as its primary source of income. The differences between energy policies and objectives are thus driven by differences in those economic, social and political contexts which shape policy formation. Additionally, the most important considerations in these types of new projects are those public financing, fiscal incentives and regulatory frameworks which support their demonstration, research and deployment lifecycle to achieve technology push and market pull. Regulations can create fiscal incentives for improving market support regarding the quality, quantity, costs and access to renewable energy. Although these classifications are adequate, there are many variations and overlaps in terms of the performance of each policy instrument. These have made discussions regarding the optimal policies for various GCC contexts a topic of significant debate.

Ahmad and Babar [50] discussed the impact of the globalisation energy markets over the power sector of GCC countries. The globalisation of the energy market has changed the energy philosophy of the GCC region and has pushed it to pay more attention to controlling the supply and consumption of power [50]. Nevertheless, the globalisation of the energy market in the GCC region not only reinforces free-flowing global trade but also invites foreign investment, industrialisation and market-driven domestic economies. According to Ahmad and Babar [50] the rapid and uneven growth in the world's population and its consumption of energy have created some seismic challenges for policymakers and security planners. According to the Independent Evaluation Office (IEO), the world's net renewable energy generation will increase by 80% driven by consumption requirements [51]. The globalisation of the energy market is not a new phenomenon for the GCC region, as it has been trading energy internationally for decades [50], [52]. The GCC countries plan to unbundle political barriers towards the privatisation of appreciating investments in the region by emboldening the private sector to invest in the power sectors [50]. Prior to 1990, all the GCC's power utilities were government-owned, although the deterioration of the GCC's economies as oil prices plunged in the 1980s and stayed low until the late 1990s had an impact on the global consumption of petroleum [50], [53]. The recent surge in fossil fuel prices, which power plants use to operate oil refineries, has raised additional concerns in the region.

These studies provide an expanded review of fossil fuel energy developments in the region together with adequate estimations of renewable energy as a new technology to meet anticipated growth in energy demand, a dimension which the GCC governments started to consider in the 1990s. In 2014, the GCC governments began executing their ambitious plans for renewable energy implementation after they realised that higher oil demand had driven up global CO_2 emissions [54]. Unfortunately, renewable energy technology has still not been widely featured in the GCC region, as renewable energy planning started late and its implementation has not been fast enough to meet increasing energy demand, even though the GCC countries have been the primary investors in renewable energy in the Middle East since 2014. However, the GCC governments have adopted a more proactive approach towards renewable energy technology, one that will likely lead the GCC region towards greater environmental sustainability. The extension in renewable energy projects is supported by a simultaneous fall in the cost of renewable energy technology and the rising prices of fossil fuels, such as natural gas, forcing the

GCC governments to increase the volume of exported fossil fuels and decrease their domestic consumption. Aside from the financial benefits of reducing subsidies for the domestic consumption of oil and increasing export capacities, the region could make transformational ecological gains that may prepare it for an inevitable "post-oil age" or, if oil and natural gas prices stay low for sustained periods (as they did the during the 1980s or from the end of 2018 until the outbreak of the Russo-Ukrainian War).

Another – and perhaps more important – factor supporting the use of renewable energy technology is the increasing environmental pressure from international organisations on the GCC countries to review their energy strategies and improve their green credentials. These investments will not only fulfil the regional requirements for renewable energy but may also make the region a world leader in renewable energy markets.

2.1.1 GCC Regional Energy Interconnectivity

One important aspect that must be considered when analysing the future of renewable energy development in the region is the existence of the high-capacity interconnections between the various countries of the region. The GCC's regional energy interconnection was proposed at an early stage of the Council's formation to connect the six member countries electrically through overhead lines and submarine cables [55]. According to Zhang et al. [55], the project was executed in three phases from 2009 to 2011 by the Gulf Cooperation Council Interconnection Authority (GCCIA; see Figure 2-1 and Table 2-1). The Power Exchange Trading Agreement (PETA) and associated General Agreement were signed in 2009 by the respective governments of the GCC countries and the GCCIA to start the operating services [55]. The General Agreement set out the terms among the member states, while the PETA determined the overarching laws and established a legal framework for the trading parties to exchange energy between countries through the GCC power grid [55], [56]. In 2011, a study was conducted by El-Katiri [56] of the Oxford Institute for Energy Studies (OIES) and also by a research group that mentioned that the GCC interconnection was constructed as an emergency mechanism for energy security in the region rather than for the purposes of trade. Later, it was improved for energy trading to create a common market for electricity. El-Katiri's [56] view is that, at present, the GCC energy interconnection may not be accruing economic benefits due to the high cost of maintaining its excess capacity. Rather, it merely serves as an emergency supplier with enormous future economic potential. According to Wogan et al. [57], in 2018 the GCC

interconnection trade market will augment the region's annual economic gains by circa. $1.1 billion. The GCC interconnection has successfully provided reliable services across the region, even if it has not yet realised its full operational potential. Based on the findings of Wogan et al. [57], this economic barrier was created by domestic energy subsidies, which reduce the benefits of electricity exchange between member states. This means that, with the broadly supported subsidies across the region, the other GCC countries are purchasing the generated electricity at below-market prices. The associated legal framework defines the obligations and rights of all the parties concerned, whether it is for the purposes of power generation or energy procurement within the GCC countries themselves [55]. Additional committees were founded to fully regulate the environment and to support a cooperative for energy exchange. Energy experts and specialists have demonstrated that the GCC interconnection is not only technically feasible and applicable to renewable energy, but also capable of developing at an optimistic pace to secure and accommodate the GCC's future anticipated power requirements [55], [57].

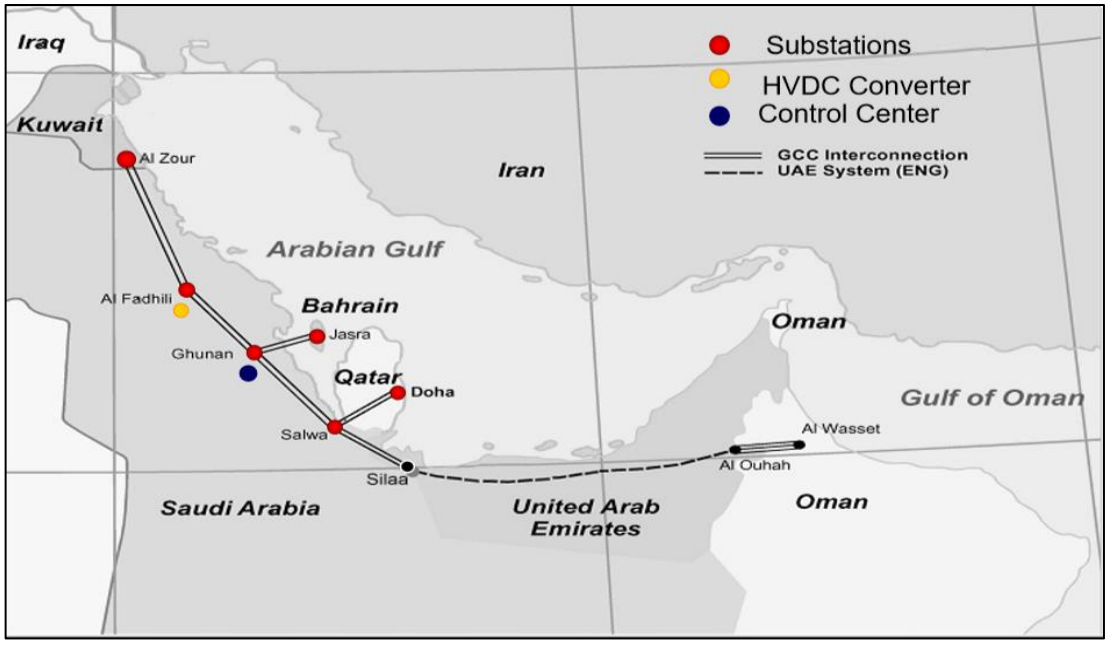

Figure 2-1. GCC regional energy interconnectivity [58].

The GCC ministries and regulators are working on unbundling the electricity utilities and initiating electricity sector reforms to integrate them more tightly within the GCC interconnecting network, given that it offers more than just energy security and economic benefits – it is arguably the region's most strategic project, one which reflects the strong bonds between GCC member states.

The GCCIA facilitates a bilateral energy trading system, one which renders the energy capacities of all member countries transparent, enabling them to place bids through yearly, monthly, or daily options. Two main methods exist for trading on the GCC energy interconnection (i.e., scheduled and unscheduled energy exchanges) [55],[59]. The scheduled energy exchanges are prearranged bilateral trades between member countries and are freely negotiated [55]. Unscheduled energy exchanges are those that may be required when unexpected events arise [55]. The GCCIA is the first cross-border electrical interconnector in the GCC region and the Middle East, serving the region and beyond by developing greater reliability and efficiency within the power market via the integration of its power systems. The main target of energy interconnection is to achieve complete interlinking between the GCC countries, especially as regards emergencies, communication, transportation and information exchange [55]. In addition, it aims to share common energy reserves, achieve a higher level of stability, and improve the reliability of supply to increase investments in power generation capacity across the region – a property that is deemed highly valuable in the context of increasing intermittent renewable energy generation. The GCCIA is supporting GCC countries by providing numerous benefits such as reducing the costs of installed capacity expansions and serving as an operations reserve with the most modern utilisation of available fuel resources [55],[60]. Additionally, the GCCIA continuously conducts interactive forums, workshops and seminars to create common ground among the GCC power authorities and it regularly launches various programmes for promoting energy trading within the Middle East. The GCCIA is a joint-stock commercial entity and is considered to be independent of any other organisation [55],[61]. The GCC countries possess nearly 50% of the estimated installation power generation capacity of the Middle East [55]. According to Zhang et al. [55], the GCC countries have the expected technical potential for achieving a renewable energy output of 65 GW of grid-connected wind energy and 34 GW of off-grid wind energy. In addition, the estimated technical potential for solar energy stands at 505 GW of grid-connected energy and 283 GW of off-grid energy [55]. In 2016, the energy trading volume between GCC countries had already reached 1.32 TWh, with member countries concluding more than 15 contracts (Table 2-1) [55].

Table 2-1. Sharing of the costs of interconnection [62], electricity export, and import by GCC Countries in 2016 [63, 64].

GCC countries	Phase I (%)	Phase I & II (%)	System size (MW)	Electricity export (GWh)	Electricity import (GWh)
KSA	40.0	31.6	1200	622	560
Oman	–	5.6	400	–	–
UAE	–	15.4	900	203	180
Kuwait	33.8	26.7	1200	238	236
Qatar	14.8	11.7	750	116	117
Bahrain	11.4	9.0	600	105	110

Nevertheless, the extent of energy exchange in the GCC region is much lower than that of other regional energy interconnections. Although the transfer capacity of the GCC countries is comparatively high, the scheduled energy exchanges are limited due to the prevailing emphasis on reserve collaboration and the lack of experience in trading under the new agreements. The most significant problem is the lack of power grid connections with other countries outside the region. Thus, the GCC countries have recently started to coordinate energy interconnections with other countries in the region, including Iraq, Egypt, and Jordan. Developing a wider regional energy interconnective system will lead to flexible renewable energy trading and will, ultimately, enable more countries beyond the GCC to balance demand and supply. The GCC regional energy interconnection also encourages energy exchange during periods of peak demand allowing for seasonal and regional climactic variations. This will be facilitated by other locations across the GCC which have a relatively low level of demand at that particular time. Further, in the longer term, the GCC countries might seek to export their surplus electricity during the winter season, when domestic demand is low, to places where demand is high, such as Eastern Europe. In any case, the improvements in the GCC regional energy interconnection system will provide alternative solutions to importing and exporting energy through the regional market. This will serve to support the GCC's broader economy and promote the private sector's participation in regional energy projects.

2.1.2 The GCC's Renewable Energy Projects

Recently, the use of renewable energy as a clean alternative has become the primary focus in reducing CO_2 emissions and slowing climate change [65]. Energy security and renewable energy development are now common future challenges for bottom-line value creation (both environmental and economic) across the GCC. According to Ramady [66], one of the sustainability project's primary issues is that private investors, such as banks, are particularly reluctant to support projects situated in arid areas. In 2018, the First Abu Dhabi Bank [67] agreed that renewable energy will be the primary means of change for the GCC markets in the longer term, despite its limited extant impact on oil demand on account of the vast infrastructural network that it requires. In addition, several environmental, economic and social considerations need to be carefully considered to identify the optimal energy mix. Without a doubt, however, the environmental advantages afforded by wind and solar renewable energy make them the cleanest sources of electricity generation available to the GCC. According to Patlitzianas and Flamos [68], investments in the unexploited renewable energy potential in the GCC countries (which are synchronous with the growth in cash liquidity within the new climate regimes), will lead the way to the application of renewable energy technologies. According to El-Katiri and Husain [69], the relatively strong economic position of the GCC countries allows them to move forward with investments in such renewable energy projects. In the longer term, the GCC countries can even gain from the deployment of alternative energy technologies [69]. Ferroukhi et al. [70] reported that the commercial side of renewable energy is actually the main concern of energy investors in the region, as they favour revenue over environmental sustainability. The key factor determining the deployment of renewable energy, in other words, is its cost [70].

Muench et al. [71] concluded that the use of renewable energy on a large-scale would trigger the following two major developments: raising the amount of volatile energy supply and raising the total number of renewable energy suppliers on the national grids. This concern is shared by Alnaser and Alnaser [42] in that the extension of large solar and wind energy projects and their accelerated execution in the GCC region might lead to disturbances of existing interconnections between the grids. The conventional electricity system has a baseline for its generation and depends on the rotation mass of its generators to maintain a steady frequency of (50–60 Hz) and provide systemic inertia [42]. However, renewable energy via wind and solar sources has no generation baseline,

does not provide synchronous frequency support to the system, and further provides no inertia [42],[72]. This becomes a primary concern at high penetrations. Such an unstable renewable energy generation system would likely lead to grid instability and systemic desynchronisation [42], [72]. This leads to a careful discussion of the most important aspects of renewable energy technologies such as operation planning, the quality and security of the supply, and the safety requirements resulting from matching the demand and supply side. The nature of the generation, operation and transmission of renewable energy is different from that of conventional energy. Understanding this specific nature and its interaction with each element of the national grids and their distribution systems is the basis for the integration of renewable energy with existing grids, especially when seeking to increase renewable energy capacity which will result in significant changes pertaining to uncertainty and variability. Although, as previously mentioned, the renewable energy (wind and solar) market in the GCC countries is still in its nascent stages, it has become a subject of great interest to the government's development plans. Future energy systems will need different models to control new demand and supply characteristics.

The KSA started to concentrate on RES such as solar energy to minimise the risk of rising electricity prices when energy subsidies were eventually reduced [73]. In October 2018, the government of the KSA issued installation approval for small-scale solar systems to encourage the implementation of solar energy, expecting to invest some $500 billion in renewable energy by 2030 [73],[74]. In 2018, the KSA began constructing a 300 MW solar energy project (the Sakaka project) and announced a 400 MW wind energy project (the Dumat Al Jandal project) – both ongoing – in the northwest based on the plans to construct the new city of Neom in this locale. Neom is projected to be an urban area based on a line of some 26,500 km^2 and will be fully powered by renewable energy [73],[74]. In the early part of 2020, the Dumat Al Jandal project, which is the first wind farm project in KSA and the largest development of its kind in the Middle East and Africa, won "Renewable Deal of the Year" at the annual Project Finance International (PFI) Awards. Such PFI awards are one of the financial industry's most prestigious global events, attracting hundreds of the world's most senior project finance professionals. The KSA renewable energy generation target is set at 54 GW, wherein the first phase of the National Transformation Programme (NTP) has a target of 3.4 GW by 2020, while a second phase

seeks to achieve a further 9.5 GW of capacity by 2023, with 2030 set as the target date for achieving the remaining renewable energy generation targets [75].

Pursuant to these goals, the Saudi Vision 2030 blueprint involves increasing the share of renewables within the energy mix from 0 to 4% by 2030 [75]. Qatar has also announced similar plans to generate 20% of its electricity from renewable energy by 2030 [70]. The UAE began focusing on renewable energy in 2006 when it built Abu Dhabi's Masdar City, a 6 km^2 sustainability project under the auspices of the Mubadala Investment Company. The country plans to go even further, with an 800 MW solar energy project scheduled for 2020 and the concentrated solar power (CSP) Mohammed bin Rashid Al-Maktoum Solar Park in Dubai, which plans to generate 5 GW of photovoltaic (PV) and CSP by 2030, covering some 48 km^2 of land [66]. In 2017, Nebras Power and the Qatar Electricity & Water Company (QEWC) signed a cooperation agreement with Masdar to develop renewable energy projects in Qatar and the UAE [73],[76]. That same year, Oman planned to integrate renewable energy into its energy mix through the 50 MW Harweel wind farm and 200 MW of associated solar energy [73]. In addition, the 100 kW Hiji solar project; 292 kW Al-Mazyonah solar project; 4,200 kW Saih Al-Khairat wind project; and a wind project on Masirah Island that will produce approximately 500 kW are also planned [77]. In 2016, Bahrain endorsed a planned energy mix that seeks to improve electrical energy efficiency by 6% by 2025 and by a further 10% by 2035 [73]. Kuwait has its own plans to transform its power system into an alternative power-dependent country by producing circa. 15% of its total electricity consumption from renewable energy by 2035, necessitating over 4.5 GW of capacity [73],[78].

The GCC countries have increasingly recognised the challenges of growing demand which are forcing them to seek alternative energy options. Table 2-2 and

Table 2-3 present all the GCC countries' future targets for renewable energy projects, many of which are moving forward rapidly, depending on the individual ambitions of each country. Achieving such targets also depends on market size and readiness. Table 2-4 shows the updated GCC renewable energy project statuses at the end of 2020.

Table 2-2. The Primary GCC Renewable Energy Project Targets and Plans [18], [73], [79-81].

Project name	Capacity	Project type	Country	Start date	End date	Client	(US$ Mn)
Renewable Energy.	9.5 GW	Complex	KSA	-	2023	Renewable Energy Project Development Office. (REPDO)	-
Dumat Al Jandal.	400 MW	Wind	KSA	Q3 2018	Q3 2021	REPDO	1000
Wadi Ad Dawasir - Layla.	200 MW	Solar	KSA	2020	-	REPDO	-
Ar Rass - Saad.	1000 MW	Solar	KSA	2020	-	REPDO	-
Jeddah	300MW	Solar	KSA	2021	-	REPDO	-
Sudair	1500 MW	Solar	KSA	2021	2023	ACWA and Aramco	906
Sakaka.	300 MW	Solar	KSA	Q2 2018	-	REPDO	500
Energy plants.	-	Waste	KSA	Q4 2018	Q4 2021	Constructions Industrielles de la Mediterranee, France.	300
Al Aflaj.	-	Solar	KSA	Q3 2017	-	Taqnia, King Abdul Aziz University & Saudi Electricity Company.	100
Yanbu	850 MW	Wind	KSA	2022	-	REPDO	-
Al-Ghat	600 MW	Wind	KSA	2022	-	REPDO	-
Waad Al-Shamal	500 MW	Wind	KSA	2022	-	REPDO	-
Henakiyah	1100 MW	Solar	KSA	2022	-	REPDO	-
Tubarjal	400MW	Solar	KSA	2022	-	REPDO	-
Power Plant in Misfah.	500 MW	Solar	Oman	Q4 2018	Q2 2021	Oman Power & Water Company (OPWC).	800
Dhofar, Phase II,	150 MW	Wind	Oman	-	-	OPWC	-
Manah.	1000 MW	Solar	Oman	-	2025	OPWC	-
Ibri, Al Dhahirah.	500-600 MW	Solar	Oman	-	2022	OPWC	-
Duqm.	200 MW	Wind	Oman	-	2024	OPWC.	-
Duqm.	1200 MW	CSP	Oman	-	-	OPWC.	-
OPWP - Dhofar	100MW	Wind	Oman	2021	2026	OPWC.	-
Manah 1	500 MW	Solar	Oman	2021	2024	OPWC.	-
Manah 2	500 MW	Solar	Oman	2021	2025	OPWC.	-
Jaalan Bani Bu Al.	100 MW	Wind	Oman	-	2023	OPWC.	-
ukhaizma Field.	2 GW	Solar	Oman	-	-	Occidental of Oman, Inc.	-

Table 2-3. The Primary GCC Renewable Energy Project Targets and Plans [18], [74], [80-82].

Project name	Capacity	Project type	Country	Start date	End date	Client	(US$ Mn)
Dhafra	2GW	Solar	UAE	2020	2023	Abu Dhabi National Energy Company and Masdar	-
Adwea Sweihan plant	1.2 GW	Solar	UAE	Q3 2017	-	Abu Dhabi Department of Energy	868
Mohammed Bin Rashid Al-Maktoum Park	5 GW	PV & CSP	UAE	Q2 2013	Q4 2030	Dubai Electricity & Water Authority	3200
Power Plant	-	Solar	UAE	Q1 2018	-	Expo 2020 Bureau	25
Hatta in Dubai	250 MW	Wind	UAE	-	-	Dubai Water & Electricity Authority	-
Jebel Ali Free Zone and Mina Rashid Port.	55 MW	Solar	UAE	-	-	DP World PLC.	-
Ras Al Khaimah.	200 MW	Solar	UAE	-	2025	Federal Electricity & Water Authority	-
Floating solar Jebel Ali.	60 MW	Solar	UAE	-	-	Dubai Electricity & Water Authority	-
Solar Energy.	1 GW	Solar	Kuwait	Q2 2018	Q2 2020	Kuwait National Petroleum Company	1200
Southwest of Kuwait.	30 GWh	Solar	Kuwait	-	2030	Ministry of Electricity and Water	-
Al Dibdibah/Shagaya.	1500 MW	Complex	Kuwait	Q2 2015	Q4 2033	Ministry of electricity & Water – Kuwait Institute for Scientific Research	5610
Ratqa field	100 MW	Solar	Kuwait	-	-	Kuwait Oil Company K.S.C.	-
Shakaaya	10 MW	Wind	Kuwait	-	-	Institute for Scientific Research	-
Power Plant.	640 MW	Solar	Qatar	-	2020	Qatar government	-
Al Kharsaah, Doha	800 MW	Solar	Qatar	Q1 2020	Q1 2022	Ministry of Energy and Industry	-
Al Kharsaah, Al Jumaliyah	700 MW	Solar	Qatar	-	-	Siraj Energy Q.P.S.C.	-
Askar Industrial Area	100 MW	Solar	Bahrain	-	2025	Electricity & Water Authority	-
Awali, Central	5 MW	Solar	Bahrain	-	-	Bahrain Petroleum Company	-
Askar landfill site	100 MW	hybrid	Bahrain	-	-	Electricity & Water Authority	-
Multi-site Sakhir	72 MW	Solar	Bahrain	2022	-	Electricity and Water Affairs	-
landfill site	100MW	solar	Bahrain	2022	-	Electricity and Water Affairs	-
Solar Park	100MW	solar	Bahrain	2021	2023	Electricity and Water Affairs	-

Table 2-4. Status of GCC Renewable Energy Projects in 2020 (Source: IRENA) [79-83].

Country	Project name	Capacity	Project type	Project status in 2023
KSA	Waad Al-Shamal	50 MW	Solar Thermal	Completed
	Sakaka	300 M	Solar PV	Completed
	Dumat Al Jandal	400 MW	Wind	Completed
	Wadi Ad Dawasir – Layla	200 MW	Solar	Under construction
	Ar Rass – Saad	1000 MW	Solar	Under construction
Oman	Dhofar, Phase I	50 MW	Wind	Completed
	Dhofar, Phase II	150 MW	Wind	Completed
	PEO Amin PV Plant	100 MW	Solar PV	Completed
	Miraah Solar EOR	1000 MW	Solar PV-thermal	Completed
	Duqm, Al Wusta	200 MW	Wind	Completed
	Ibri PV Plant	500 MW	Solar PV	Completed
	Duqm, Al Wusta	1200 MW	Solar - CSP	Completed
UAE	Shams 1	100 MW	Solar Thermal	Completed
	Sweihan	350 MW	Solar PV	Completed
	Mohammed bin Rashid Al-Maktoum, Phase I	13 MW	Solar PV	Completed
	Mohammed bin Rashid Al-Maktoum, Phase II	200 MW	Solar PV	Completed
	Mohammed bin Rashid Al-Maktoum, Phase III	800 MW	Solar PV	Completed
	Mohammed bin Rashid Al-Maktoum, Phase IVa	700 MW	CSP	Completed
	Mohammed bin Rashid Al-Maktoum, Phase IVb	250 MW	Solar PV	Completed
	Mohammed bin Rashid Al-Maktoum, Phase V	900 MW	Solar PV	Completed
	Noor Abu Dhabi	1177 MW	Solar PV	Completed
	Hatta in Dubai	250 MW	Wind	Under construction
	Jebel Ali Floating	60 MW	Solar PV	Completed
	Jebel Ali Free Zone and Mina Rashid Port	15-20 MW	Solar PV	Completed
	Ras Al Khaimah	200 MW	Solar	On hold
Kuwait	Shagaya, Phase I	50 MW	Solar Thermal	Completed
	Shagaya, Phase I	10 MW	Solar PV	Completed
	Shagaya	10 MW	Wind	Completed
	Al Dibdibah/Shagaya Phase II	1200 MW	Solar PV	Cancelled
	Southwest of Kuwait City	30 GW/h	Solar PV	Under construction
	Ratqa field	100 MW	Solar	Under construction
Qatar	Al Kharsaah, Al Jumaliyah	700 MW	Solar PV	Under construction
	Al Kharsaah, Doha	800 MW	Solar PV	Under construction
	Kahramaa	220 MW	Solar PV	Completed
	Mesaieed W2E	38 MW	Waste to Energy	Completed
Bahrain	Tatweer Petroleum	3 MW	Solar PV	Completed
	Al Dur Hybrid	5 MW	Wind & Solar PV	Completed
	Awali Township, Manama	5 MW	Wind & Solar PV	Completed
	Askar Industrial Area	100 MW	Solar	Under construction
	Askar landfill site	100 MW	Solar	Under construction

While Figure 2-2 summarises the renewable energy targets of the GCC countries, including the development of generation efficiency, the reduction of electricity consumption, and the reduction of peak demand. By the end of 2018, the GCC countries had a total of 146 GW of installed energy generation capacity, of which renewable energy accounted for less than 1% at 867 MW [82]. The UAE accounted for 68% of renewable energy as a share of planned installation, followed by the KSA at 16% and Kuwait at 9%, as shown in Figure 2-3a and Table 2-4.

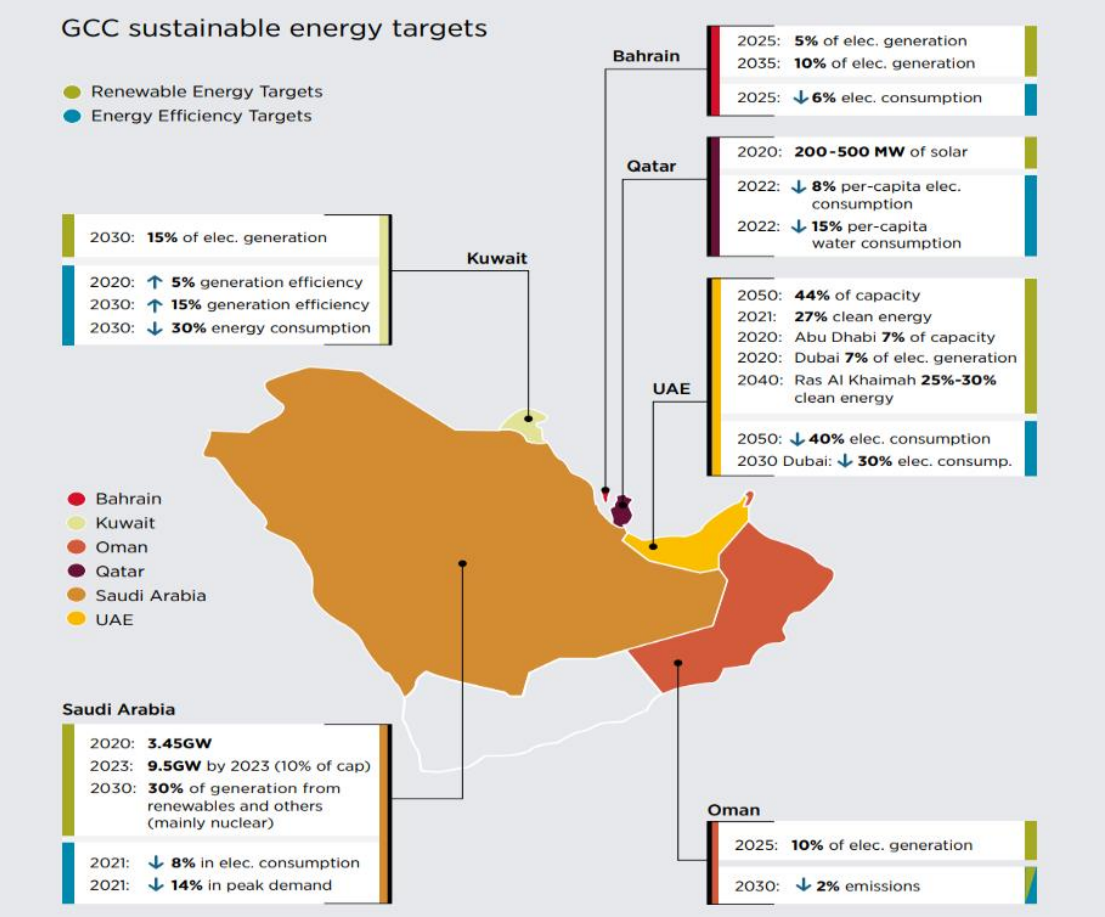

Figure 2-2. The estimated sustainable energy targets of the GCC countries (source: IRENA) [82].

The development of the renewable energy sector is not only the responsibility of governments, but also the private sector. Such collaborations can be facilitated by liberalising government policies to expedite renewable energy projects. Most of the energy stakeholders in the GCC region anticipate that, by 2030, there will be both a substantial growth in renewable energy generation to 78 GW and a total global investment of $13.5 trillion in low-carbon technologies [84]. According to the KAPSARC [84], in

addition to being competitive, renewable energy is an economically suitable option for diversifying the GCC's energy mix.

The KAPSARC reported that, based on the renewable energy tenders in 2017, it can successfully complete these targets under specific conditions if the GCC energy reform embraces three main factors [84]. First, it needs a credible economic plan with a realistic schedule to improve the regulations required to achieve the stated objectives [84]. Second, it requires the reform of large energy subsidies for long-term viability and to adapt to changing global energy markets [84]. Third, renewable energy must be integrated into the generation portfolio with natural gas serving as an effective reserve [84]. In 2020, AlKhars et al. [85] conducted a comprehensive systematic review based on 59 articles to analyse the relationship between energy consumption and economic growth in the GCC countries over a period of 13 years (2006–2019). AlKhars et al. [85] reported that there is an urgent requirement for the expansion of renewable energy technologies within the energy supply mix of the GCC countries to meet sustainable development targets, achieve economic growth, and mitigate environmental challenges in the region. Another study from 2020 by Haque [86] studied the relationship of energy consumption with specific key indicators including crude oil prices, GDP per capita, population growth, trade, and CO_2 emissions in the GCC region over a span of 29 years (1985–2014). Based on Haque's [86] analysis, there is a need to upscale the adoption of renewable energy technologies in the GCC region. Recent research by Abul et al. [87] discussed the energy consumption performance and economic growth in GCC countries during the period from 1980 to 2014. Abul et al. [87] highly recommended the implementation of energy technologies in the GCC region as a suitable alternative to deal with potential environmental issues. Many long-term studies have since called for investment in clean energy technologies in the GCC region as well as for the exploitation of those abundant natural resources to serve as effective long-term solutions. According to Abdmouleh et al. [18], short-term investments in renewable energy projects in the GCC region may not create adequate financial returns. Further, the GCC countries face common challenges to renewable energy deployment, such as a misunderstanding of its true cost, the "dust effect," high temperatures, and the paucity of research on regional weather patterns. However, the extreme growth rate in terms of regional energy demand will certainly drive the GCC governments to seize the initiative as regards emerging opportunities to kick-start more renewable energy projects.

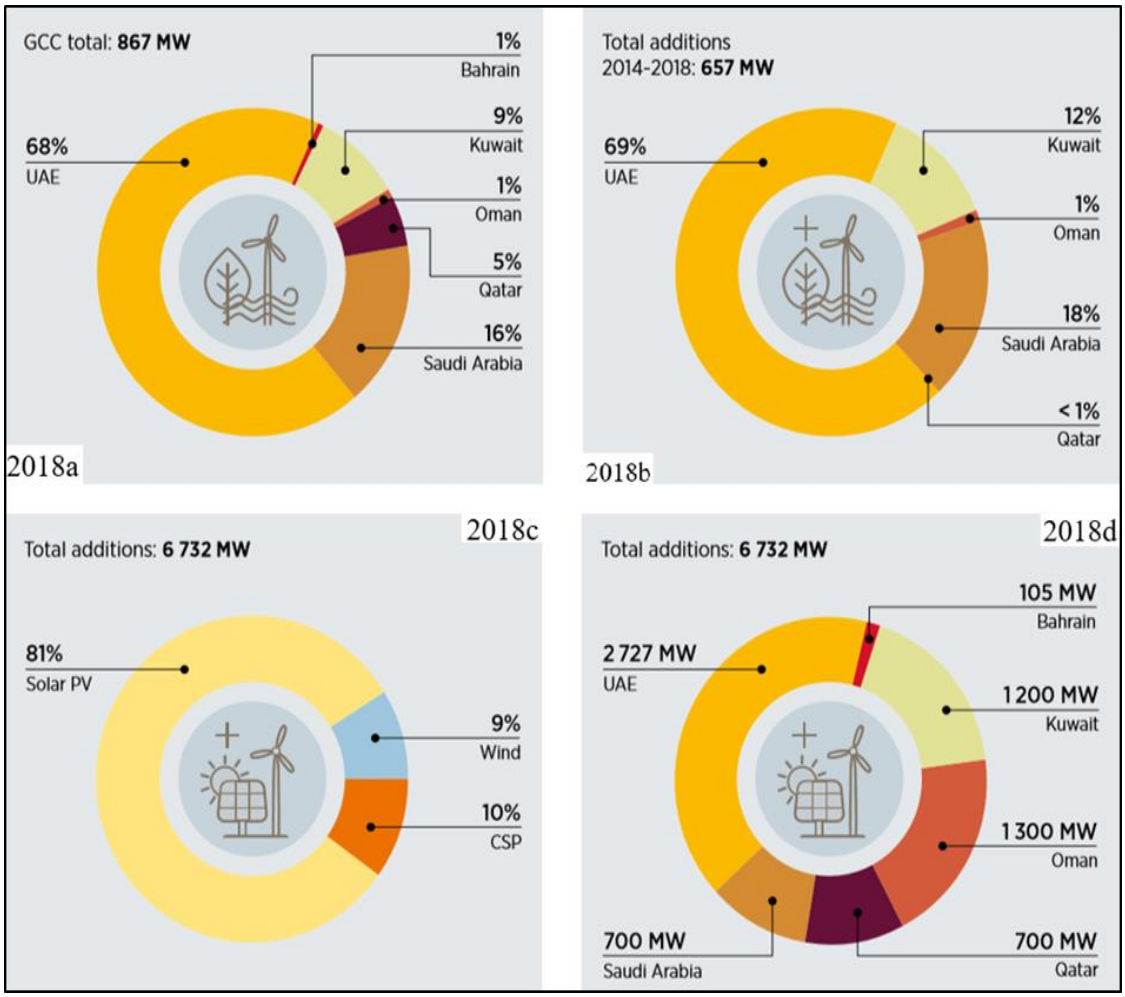

Figure 2-3. Installed renewable energy capacity share in 2018a; the growth of capacity from 2014–2018 in 2018b; planned installation of technology in 2018c, and installation planned by country in 2018d (source: IRENA) [82].

Table 2-5. Installed energy generation capacities for RES. Capacity presented in MW from 2014–2018 (Source: IRENA) [88].

GCC Country	2014	2015	2016	2017 - 2018					
	Total RES	Total RES	Total RES	PV	CSP	Wind	Biomass & waste	Total RES	Share of RES in the total electricity capacity (%)
KSA	24	74	74	89	50	3	0	142	0.2
Oman	1	2	2	8	0	0	0	8	0.1
UAE	137	137	144	487	100	1	1	589	2.0
Kuwait	0	1	20	19	50	10	0	79	0.4
Qatar	42	42	43	5	0	0	38	43	0.4
Bahrain	6	6	6	5	0	1	0	6	0.1
Total	210	262	289	613	200	14	39	867	0.6

In the past, the GCC countries have faced sharp criticism for their complete dependence on conventional energy and for ignoring the implementation of renewable energy. Even after the activation of renewable energy projects in the region, the region still faces criticism for its slow progress and limited performance. In 2014, OIES [89] reported that there was a lack of a long-term energy strategy in the GCC, one that provided visible plans with a timeline to promote alternative supply and demand-side energy policies. The policies addressing such alternative new energy options, such as renewable energy, suffer from the absence of any sense of urgency in the region [89]. The lack of expertise in terms of renewable energy technologies such as CSP, wind and solar-driven desalination, coupled with the immaturity of renewable energy technologies, reduces investment from ready-made solutions to mere experiments [89],[90]. Private sector investors have little status or incentive to invest in renewable energy projects, while consumers do not have clear means to control their levels of consumption [89]. The OIES reported that this attitude of 'business-as-usual' in the GCC region can no longer be sustained, and the region must devise concrete, modern policies and strategies to meet both medium- and long-term challenges of energy demand and the energy mix [89]. In 2014, Munawwar and Ghedira [91] reported that the realistic accomplishments of low-carbon projects and renewable energy deployment in the GCC region are limited and only represent a future vision with no real demonstration of success or explicit progress updates. Many GCC countries have undertaken projects, sector-wide efforts and policies that still only exist on paper. In 2018, Malik et al. [88] pointed out that the lack of an adequate policy framework in the region is obvious, especially for wide-scale renewable energy utilisation, as this requires well-articulated policies to advance renewable energy deployment in each GCC country. Al-Maamary et al. [30] mentioned that the renewable energy projects in the GCC region continue to fall shy of ambitions, as thousands of renewable energy projects across the region were suspended due to a drop in oil prices which caused a temporary constraint on funding.

To successfully deploy renewable energy in the region, the GCC governments need to commit to a regulatory framework that involves financial incentives [91]. The OIES mentioned that the strong fiscal position of the GCC countries, however, may enable them to deploy alternative energy systems with savings derived from domestic energy price reforms [89]. In 2017, Al-Saidi and Elagib [92] indicated that, although barriers exist to the implementation of renewable energy mega-projects across the GCC region,

modernisation policies are still emerging. Further, Al Shidi et al. [21] stated that the GCC countries do indeed have a strategic plan, since the slow transition from fossil fuel economies to low-carbon economies is necessary to improve their global image. They contend that they will undoubtedly deploy renewable energy, albeit at their own pace. Apostoleris et al. [93] reported that the unexpected leaders of large-scale and low-price solar energy projects in the Middle East are the UAE and KSA due to the falling cost of solar energy technologies. According to IRENA, since 2010, the average cost of electricity generated from PV technologies and wind energy has fallen by 73% and 22%, respectively [94]. In countries as dissimilar as India and KSA, Chile and the United States, electricity is being generated in optimal locations for approximately 30 USD per MWh [94]. Furthermore, both low tax regimes and the low prices of hardware and labour should lead to large rapid renewable energy contributions within the region.

Governmental policies, of course, remain an important factor in removing obstacles, the most aggressive of which are claims in terms of costs, returns and risks. The cost of clean energy technologies is expected to continue to decline in the future, creating great opportunity in facilitating renewable energy deployment and increasing both participation and diversification across these sectors. In addition, given the decline in the cost of renewable energy technologies and the region's fiscal challenges, there is no room for delay, indecision, or incoherence. Further, this advantage must attract significant interest from developers and investors alike, with governments supporting access to very low-cost project financing. It is worth noting that the focus should not however be on the cost of energy alone, but must also include energy efficiency, and these two elements are intertwined.

2.2 A Discussion of the GCC's Consumption Growth Issue and Renewable Energy Deployment

Based on this analysis of recent evolutions in energy generation and consumption patterns, extant energy-related investments, plus several key efficiencies and trade-oriented energy policies, it is apparent that the GCC countries have realised the importance of renewable energy and the urgent need to diversify their sources of energy. Such diversification can increase the sources of their economic income which have traditionally depended on oil and natural gas production and export. In addition, the energy sector has always been the cornerstone of the region's economic development and

social growth and thus, the future of each member country has been closely aligned with the future of its energy sector. Meanwhile, the GCC countries have also recognised the great responsibility they must bear in regard to addressing climate change and global warming issues and are obligated to reduce their collective carbon footprint.

Indeed, remarkable developments in renewable energy projects—even considering such slow progress—have been achieved in the GCC region during the past five years (*see Section 2.1.2 GCC Renewable Energy Projects* and

Table 2-3). Given the context of energy policy, which has been described in some detail, these steps can be considered a strong step in the desired direction and thus deserve commendation, given that they have set the GCC countries on a path towards a transition to sustainable energy. However, these advances are relatively small as compared to those achieved by other countries, such as India, China, Russia, the USA, and members of the European Union. Undoubtedly, in terms of the relatively cautious and sedate progress in terms of renewable energy deployment achieved in the GCC region so far, a gap exists between what has actually been achieved to date and the huge potential financial windfall which, when coupled with the great renewable energy resource potentials of the region, could be better exploited. This gap may be explained by the different energy management techniques that renewable energy production requires due to the intermittent nature of these resources and their efficiency and reliability as continuous sources of power. These factors continue to be the major concerns for GCC countries. However, the UAE and KSA are exerting major efforts in the field of renewable energy projects, as are Oman and Kuwait, which have also shown strong progress with their projects. Meanwhile, Bahrain and Qatar are languishing behind their peers and have shown unclear progress in their endeavours. Greater transparency in terms of announcing the developments of their sustainable and renewable energy projects would help clarify their progress towards targets. So far, both countries have only announced initial plans and set their primary targets for future renewable energy generation, given that they have yet to announce any real progress rates for any actual project (Table 2-2 and

Table 2-3). Improved transparency is required for all the countries in the region to achieve long-term sustainability in their policy support mechanisms and accelerate the sustainable deployment of renewable energy across the entire region.

Moreover, several factors in combination support the primary goal of spreading the implementation of renewable energy across the GCC region, including:

- The GCC region is one of the most attractive regions in the world in regard to the development of large-scale renewable energy projects due to its abundant solar energy as well as the winds that impact Oman, Kuwait, KSA, and the coastal areas of the Arab Gulf and the Red Sea. Such exploitation can be coupled with historical prominence within the global energy trade.

- The six GCC countries are already connected electrically by a large, modern regional energy interconnection grid (currently with significant overcapacity) through overhead lines and submarine cables. This grid can support the implementation of significant amounts of renewable energy in the region as well as balance regional disparities in energy supply and demand.

- The availability of capital and the liquidity of competitive financing resources are supported by strong prevailing socioeconomic conditions in the GCC countries, qualifying them to move forward and achieve success with their renewable energy projects.

- The sharp reduction in the prices of PV energy systems, hardware and modules, the very low taxes imposed, and the relatively low cost of labour can facilitate the faster completion of renewable solar energy projects.

- The surge of growth in energy demand and the increased social and political pressure to build a diversified energy mix in the region would ensure the region's energy security over the longer term.

The GCC countries' decisive move towards renewable energy projects is a signal to global investors and the energy community that the region is experiencing the start of an energy transition. These projects also provide further evidence of a change in global energy dynamics. The GCC countries have an opportunity to double the gains they can expect from expanding their sustainable projects and accelerating their completion to reach the stage of self-sufficiency and the abandonment of fossil fuels while still maintaining a globally significant position within the energy trade.

This chapter provided a deep dissection and critical analysis of all previous technical studies directly relevant to this research, such as [82,65,69]. It should be noted that most previous works have not only dealt with countries independently, they also need updating and should be considered relative to a variety of scenarios and other occurrences. This research is differentiated by its modern and thorough approach, which connects all previous studies and analyses them properly.

3 Feasibility Analysis for Solar and Wind Energy Resources in the GCC – A Review

This chapter presents an overview of the published literature that addresses (i) The importance of the GCC region's geographical factors; (ii) the GCC's solar and wind energy resource potential as well as the effects of dust and clouds; (iii) solar and wind power generation in the region; and, (iv) GCC climate justice. Finally, section (v) discusses the feasibility of deploying solar and wind energy resources across the region.

3.1 Global CO_2 Performance and the Temperature Reduction Plan

In the 21st century, the shift in global energy networks to low-carbon technologies is considered a significant challenge [95]. Climate change issues have forced nations around the world to explore low-carbon and other sustainable energy options. The average global temperature could increase by up to 6 °C by the end of this century if the world continues to emit greenhouse gases (GHGs) at today's levels [96]. However, the average global temperature increase must not exceed 2°C if we are to avoid the most severe impacts of climate change [96]. In addition, the Paris Agreement on climate change (December 2015) and the International Panel on Climate Change (IPCC, 2018) have striven to restrict the increase in global temperature to below 2°C or, ideally, to less than 1.5°C [97]. This means that global emissions must be reduced to at least 50% below their recorded levels in 1990, to reach 'zero emissions' by 2050. Several international organisations support this goal, including the United Nations Environment Programme (UNEP, 2018). Figure 3-1 provides more details regarding the CO_2 emissions performance and the temperature reduction plan, including the effects of COVID-19 during the international lockdown. The United States (USA), European Union (EU), China, and Russia are the largest sources of CO_2 emissions, while the KSA, USA, Canada, and South Korea are the largest producers of CO_2 per capita. In terms of actual figures, CO_2 per capita in the KSA is 18 tonnes versus 16.6 tonnes for the USA [98], with Canada and South Korea at 15.3 and 12.4 tonnes per capita, respectively. Coal provides approximately 60% of the energy in China despite the increased provision of renewable energy [98]. Based on the Global Carbon Project [98], China was the largest source of CO_2 emissions in 2018 at 27% and, while its emissions are growing, China is firmly on target to reach its peak reduction emissions by 2030 in accordance with its Paris Agreement commitments. The USA's

global share of CO_2 emissions surged in 2018 to 15%, although CO2 has fallen over the last decade due to the decline in coal consumption in favour of renewable energy and natural gas. However, President Donald Trump scaled back measures to curtail GHG emissions and withdrew the nation from the Paris Agreement. On his very first day in office, President Biden recommitted to the Paris Agreement. In 2018, the EU recorded a 9% global share of CO_2 emissions, representing a fall of 20% since 1990. This means that the EU is on track to reach its Paris Agreement goals. India's share of global CO_2 emissions was recorded at 7%, indicating that it has contributed to climate change to a far lesser extent relative to other large countries. Despite the fact that its energy and coal consumption is rising rapidly, India is emerging as a competitor in sustainable energy technologies. Russia recorded a 5% global share of CO_2 emissions in 2018, and the climate action tracker (CAT) reported that Russia has made significant renewable energy investments. Since the collapse of its industry after the break-up of the Soviet Union, its CO_2 emissions are continuing to plunge. The Global Carbon Project [98] reported a 2% global share of CO_2 emissions for Iran, South Korea, KSA, and Canada, whereas Japan stood at 3%. Values of 2-3% of the global share of CO_2 emissions are relatively low in the UK, Italy, France, Poland, Australia, Turkey, Brazil, South Africa, and Mexico, which each produces around 1% of global CO_2 emissions [99], despite their high populations. However, no country has been able to reach zero emissions. The rest of the world accounted for around 21% of global CO_2 emissions [99].

To support the transition towards decarbonisation technologies, governments around the world (industrialised and non-industrialised countries) must issue the world's first-ever legally binding agreement to reduce CO_2 emissions by as much as 80% before 2050. A strong and effective global framework is required to achieve this decarbonisation transition and to prevent any exacerbation of climate change issues. This review chapter analyses the transition towards decarbonisation technologies by evaluating the potential for solar and wind resources in the GCC countries to foster environmental sustainability and climate change mitigation across the region.

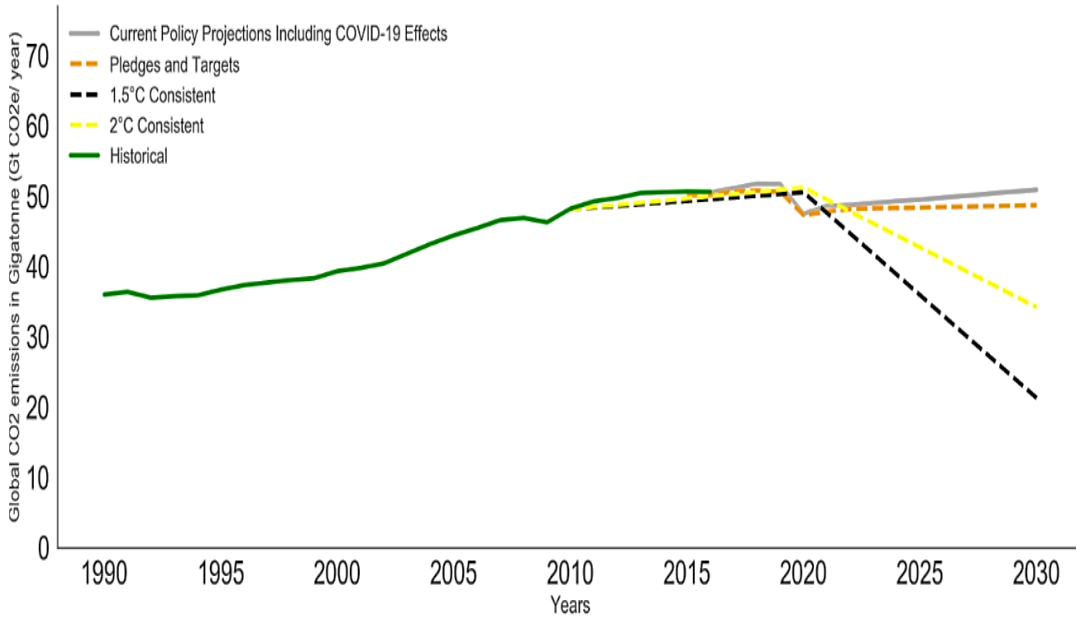

Figure 3-1. Global CO_2 performance and the temperature reduction plan (data obtained from climate action tracker, 2020). The 2030 Emissions Gap. Updated September 2020. Copyright © 2020 Climate Analytics and New Climate Institute. All rights reserved [100]).

3.2 Geographical Factors of the GCC Region

The GCC countries' geographical location serves as the point that links the West to the East [101]. The advantages of the GCC region stem from its strategic geographical location (Appl. Sci. 2021, 11, 2648 5 of 23) at one of the world's most important crossroads. The GCC region is located in the Arabian Peninsula, southwest of Asia between latitudes 13° and 32° north of the equator and longitudes 35° and 60° east of Greenwich [102]. The GCC region covers a large area of desert, one that occupies most of the wilderness of the Arabian Peninsula. The regional grouping known as the GCC constitutes approximately 2.5 million km^2 of land area, representing some 82% of the Arabian Peninsula's total area [103]. The region's land mass represents a rectangular shape tracking some 2,000 km along the Tropic of Cancer, with a north-south axis some 2,300 km in length [103]. In addition, the GCC region is bounded by three important waterways, namely the western Red Sea, the eastern Arabian Gulf, and the southern Arabian Sea. The region occupies the western coast of the Arabian Gulf from Oman to Kuwait. The Arabian Gulf is comprised of the Straits of Hormuz in the inner Arabian Gulf and the Oman Gulf, or outer Gulf. According to Riad [103], since the 1950s, the Straits of Hormuz in the Arabian Gulf have been of exceptional global importance, unsurpassed by any other seaway as the main route of the world's fleet of oil tankers. The vital importance of the Arabian Gulf to the GCC and the entire globe is obvious. All of

the eastern coastlines of the Red Sea overlook the KSA (except the short Yemeni coast), from Gizan in the south of KSA to the tip of the Aqaba Gulf, and these represent the critical border zones of the KSA with Jordan, Egypt, and the occupied Palestinian territories [103]. The northern boundaries of Kuwait and KSA are generally viewed as marking the borders of the GCC region. In addition, the Red Sea brings the GCC region into contact with the Suez Canal in Egypt, a key waterway that links the Red Sea with the Mediterranean. The facts of geography and the strategic location of the region are all points in the GCC countries' favour, as are their abundance of natural resources. All of the countries have a large open area and extensive beaches, which means that they all have coastlines on the Arabian Gulf, thereby explaining why the peninsula is often called "the Island of the Arabs". However, major difficulties arise with the ambitious development of renewable energy projects. Moreover, RES differ across geographical locations and so not all renewable energy technologies are optimal for every area. For instance, the GCC countries have extensive deserts and subtropical desert regions. The diversity of geographical locations may present advantages for the GCC region, in that various renewable energy techniques can be applied across different parts of the region. In addition, most of the areas of the GCC are incompatible with settled agriculture due to a lack of water and are therefore not of enormous significance. This means that the construction of new renewable energy projects will not affect its agricultural sectors. Further, there are no forests in the region subject to deforestation. The absence of any such geographical barriers or obstructions, the available infrastructure, and the favourable tax laws in the GCC region all contribute to a positive environment for new project development.

3.2.1 Solar and Wind Energy Resource Potential of the GCC

Across the GCC region, the development of solar and wind energy projects has been relatively slow despite their significant geographical potential, as RES could provide effective solutions to meet expected growth in electricity consumption, unprecedented increases in energy costs, and climate change issues. According to Patlitzianas et al. [104], while the GCC countries have not considered renewable energy as a clean alternative solution to these issues for many years, something seems to have changed recently due to their accession to the Kyoto Protocol and the UNFCCC, agreements which place climate change issues at the top of their list of priorities. As a result, the GCC countries are raising

their level of ambition in accelerating the deployment of RES. The imperatives for enhancing sustainable progress to tackle climate change are further strengthening the momentum of a renewable energy transition in this region. The GCC countries must capitalise on their promising resources for renewable energy generation, along with associated applications in terms of transport, buildings, cooling, and direct heat. RES have made striking gains in the GCC region over the past five years and are expected to become competitive with conventional energy technologies in the next five years. The ambition of each country differs, as does market size and readiness, while the overall picture is similar across the region.

3.2.1.1 Solar Energy

The importance of implementing large-scale photovoltaic (PV), CSP, and other solar energy applications and their economic benefits across several territories around the world has been analysed in many previous studies [105-114]. The success of various governments in developing solar energy technology primarily relies on an in-depth awareness of solar intensity levels and the distribution of global solar radiation, which is a challenging task because, to date, the available data is limited at a global scale. Singh et al. [115] and Meltzer et al. [116] mention that, based on the geographic situation of the GCC and its high levels of annual insolation (aggregated hours of sun, adjusted for solar intensity), places the region highly in terms of the development of solar power. The annual average global solar radiation in the GCC region is estimated at 6 kWh/m^2 per day, while the DNI is around 4.5 kW/m^2 per day [116]. The abundance of solar energy resources depends on the sun's irradiance parameters and associated spectral distribution. Prăvălie et al. [117] note that, if the countries of the Arabian Peninsula collaborate strongly to this end, then the entire GCC region would become a primary solar energy hotspot. Among the alternative RES available to the GCC region, solar energy stands out. Doukas et al. [38] mention that the GCC countries have a remarkable opportunity for the use of alternative energy sources, particularly solar energy and, therefore, should take a more proactive role in terms of investment in such emerging technologies. According to Al-Badi et al. [118] and Alnaser and Alnaser [42], the highest annual solar radiation range, 2,200 to 2,500 kWh/m^2, was recorded in Oman. The UAE has the second highest annual solar radiation at 2,285 kWh/m^2, which is supported by average sunshine of 10 h per day [119, 120] due to its location. The KSA and Kuwait have equivalent levels of

annual solar radiation of 2,200 kWh/m^2 [44, 121, 122]. Kuwait is also characterised by a high average daily sunshine of around 12 h per day. A mean of nearly 2,180 kWh/m^2 was recorded in Bahrain for annual solar radiation [41], while the lowest value of annual average solar radiation was measured in Qatar at 2,113 kWh/m^2/year together with average daily sunshine of 9.5 h [123]. Nowadays, the GCC countries pay particular and increasing attention to the adoption of solar energy to reduce the energy costs associated with their growth in demand. Dasari et al. [124] stated that the total annual mean of GHI across the entire Arabian Peninsula, including the GCC region, stands at between 6 and 8.5 kW/m^2 with an associated DNI of between 3 and 6.5 kW/m^2. The values of diffuse direct horizontal irradiance are high among the majority of locations across the region and are curtailed along the Red Sea and surrounding coastal shorelines at 1.2 and 4 kW/m^2, respectively [124]. This study provided a comprehensive evaluation of solar energy resources using high-resolution spatial data across the GCC region, gathered from 46 in situ radiometer stations over the region and supported by assimilative weather research, based on historical data spanning 37 years from 1980 to 2017. Figure 3-2 summarises the performance in terms of GHI, DNI, and DHI in W/m^2, including the diffuse fraction (DHI/GHI) of the GCC region. The diffuse fraction (DHI to GHI ratio) indicates enhanced cloud cover and/or a higher aerosol load above the average duration [125] and is particularly high over northern locations and lower over the southern regions of the central GCC region during the winter months, whereas it is high across the southern and central regions and lower over the northern territories during the summer [124]. The main elements that drive DHI variability are the cloud cover over the northern part of the GCC region in the winter and the loading of aerosols over the southern and central portions of the GCC during the summer due to atmospheric desert dust. According to Dasari et al. [124], the evaluation of such diverse parameters including solar radiation and aerosol characteristics suggests that the region possesses considerable solar energy potential, with the southeast and northwest identified as the most appropriate locations for exploiting solar energy given their minimal cloud coverage across the GCC countries.

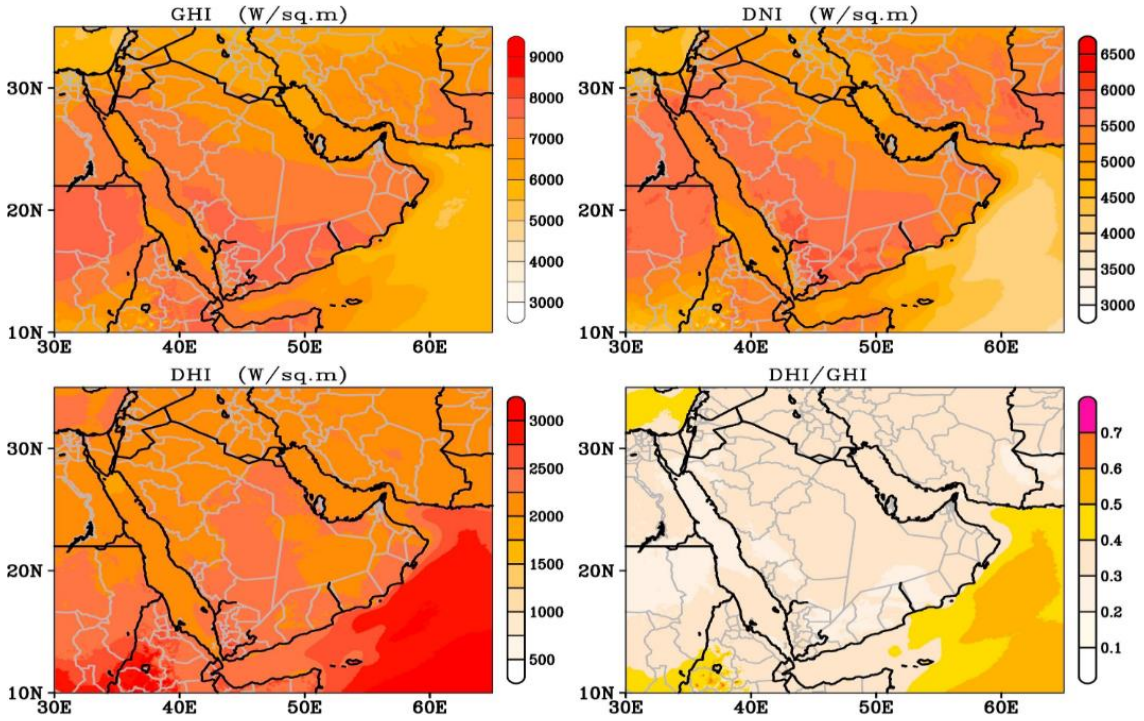

Figure 3-2. The annual mean of global horizontal irradiance (GHI), DNI, and DHI in W/m^2 and the performance of the diffuse fraction (DHI/GHI) over a 37 year period (1980–2017) across the GCC region [124].

There are considerable variations in the values of DNI and GHI between the winter and summer months, indicative of a high seasonal variance in the solar energy potential across the GCC region due to the sensitivity of the regional climate. Figure 3-3 and Figure 3-4 provide more details on the monthly variance in DNI and GHI. Moreover, the monthly values of DNI, GHI, and DHI exhibited a gradual development from January to April, with higher values occurring from May to September [55]. Between February and November, the position of the highest mean values of DHI shifted to the south, while from January to September, the position of maximum mean values of GHI and DNI migrated from the south to the north. The maxima of DHI from April to September arise due to the effect of dust across the southern and central regions during the summer and the impacts of winter cloud cover on the northern region. The transitional seasons, spring and fall, show intermediate DNI and GHI values, although their distributions are similar to those of the winter months. GHI and DNI have higher percentage values in terms of variation coefficient over the northern region during winter and can reach around 17% south of 15°N during the summer owing to the monsoon-related clouds and the distribution of dust. The northwestern and southeastern parts of the region are more desirable for harvesting solar energy despite the atmospheric dust pollution. The evaluation of various solar irradiance parameters provides an overview of the solar energy

resource potential of the GCC region, thereby promoting significant sustainable opportunities in the development of solar energy applications across the GCC region. Nonetheless, insufficient awareness, a paucity of experience, and technological deficiencies have hampered any comprehensive evaluation of solar energy characterisation across the region. An analysis of long-term solar energy resource conditions over the GCC region can be used to develop viable renewable energy project capabilities and fill any territorial gaps in terms of solar resources. Further, the Arabian Peninsula, and in particular the GCC countries with their 2030 goals, are among the fastest-growing solar energy markets. This research provides significant granular detail for policymakers and researchers to establish effective strategies for the harvesting of such renewable energy.

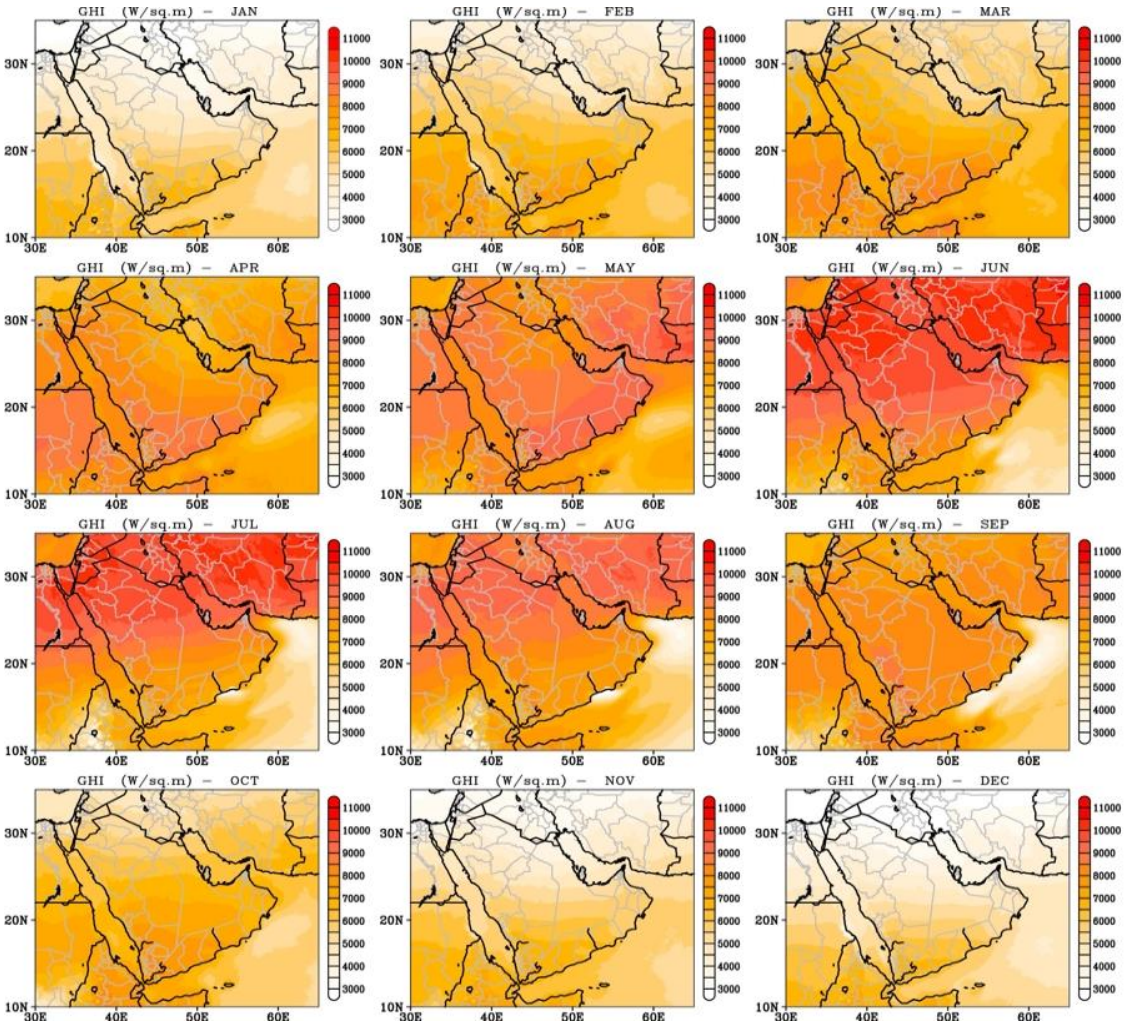

Figure 3-3. Monthly performance in terms of GHI (W/m^2) over a 37-year period (1980–2017) in the GCC region [124].

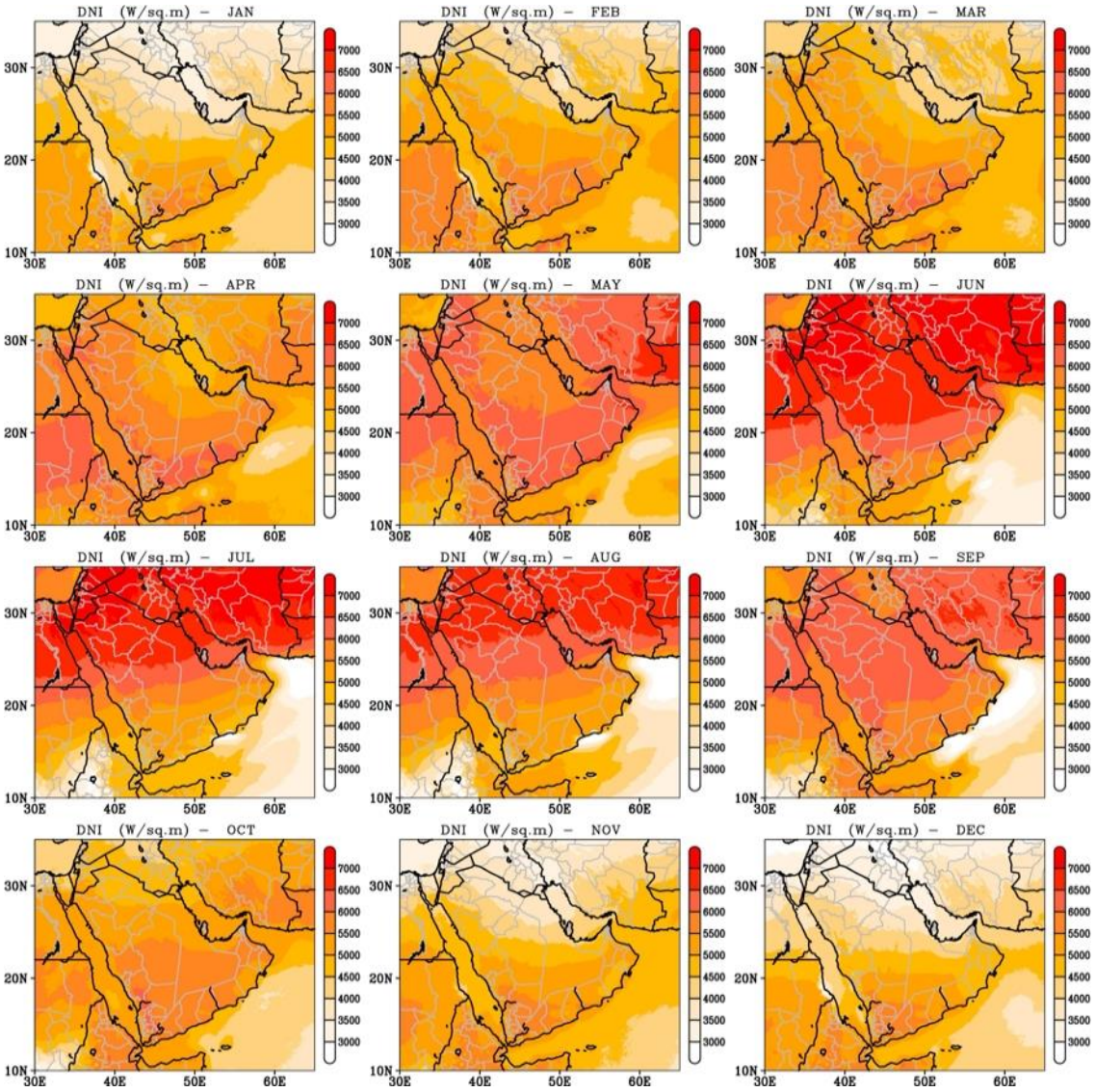

Figure 3-4. Monthly performance in terms of DNI (W/m²) over a 37-year period (1980–2017) in the GCC region [124].

3.1.1.2 Effects of Dust and Clouds

The impact of clouds and dust is identified with respect to geographical location and local conditions, and these are extremely clear in terms of diurnal variations in solar irradiance [126]. Moreover, clouds, dust particles, and high levels of atmospheric humidity all act to reduce solar intensity [127]. The observed intermittencies in solar radiation are also related to issues of dust and sand deposition on PV panels. Moreover, if dust particles are mixed with severe fog such atmospheric conditions may be exacerbated during the winter months, thereby affecting the performance of PV panels. However, clouds and dust are the main factors that determine the installation feasibility of solar energy projects [128-131]. The real challenge, as reported by Middleton [132] and Prospero et al. [133], is the

dusty environment of the Arabian Peninsula (including the circumambient deserts). Such dust emissions are triggered by other external factors, such as regional storms caused by large-scale instabilities of the atmosphere and high-speed winds, in some cases [134-136].

Awad and Mashat [137] mention that, as an influence on the strong pressure system gradient between the Arabian Peninsula's thermal low pressure and the Azores' high pressure, a huge amount of dust is carried toward Asia from the Northeastern African desert. Notaro et al. [138] identified three main sources of dust that can impact the region during the year, specifically the Rub Al Khali Desert, which is a large regional source of dust; the deserts of Iraq, which are major dust sources for northern and eastern KSA; and the Saharan Desert, which is the main remote source of dust for western KSA. Moreover, Mashat and Awad [139] categorise various Arabian Peninsula locations into permanent and temporary dust locations, while the eastern region is identified as a permanent source of dust. Table 3-1 provides more data on individual GCC countries and their effective average annual dust.

The presence of clouds and dust over the GCC region is attributable to storms. These have a major influence on a substantial portion of the region. Figure 3-5 shows the cloud coverage and aerosol optical depth (AOD) performance, indicating those areas with a high sky index clearness over the GCC region. Mainly, the high values of the AOD across the southern region of the GCC arise during the summer months [123] and are caused by the loads of aerosol and clouds that are correlated with the Indian summer monsoon [140,141]. A clear sky, supported by lower AOD values, prevails over the northern region of the GCC except during some summer months when the dust is carried by the winds of the Shamal, which act as an opaque filter of solar irradiance [142]. The increasingly diffuse fraction values are caused by those clouds which occur as a consequence of the mid-latitude weather systems during the winter over the northern region (see Figure 3-2). Further, seasonal variations in the diurnal patterns of the clearness index that affects the convective cycles' performance are evident in all parts of the region. The northwestern region is characterised by the symmetrical uniform clearness index during the entire year with a low difference, excluding the winter period (November to February), while high uncertainty is observable during the daytime. The clearness indicator shows major diurnal variation during the summer (June to September) in southwestern KSA and high diurnal variation in the eastern region between October and March [123]. During low-dust periods, the southern surface wind is dominant, while the prevailing wind during heavy-

dust activities across the eastern part of the Peninsula is a northern surface wind. The eastern region exhibits high diurnal variabilities during the year associated with high cloud coverage and greater AOD values, in some cases. In addition, the southwestern region is influenced by greater cloud coverage and a higher AOD, while the northwestern Red Sea is impacted by a mid-latitude cloud system in the winter. The clouds and dust over the southern region and the dust over the northern region play a significant role in modulating high diffuse fractions.

Table 3-1. Average annual dust in GCC countries and effective locations.

No	Location	Region/City	Annual dust (tonnes km^{-2})	Reference
1	**KSA**	Central Riyadh Northeastern Riyadh Najran*[1] Sharurah* Wadi Al-Dawasir* Al-Baha* Hail* Jeddah* Yenbo* Tabuk* Turaif* Al Ahsa* Hafar Al Batin* Arar*	392 454 420 416 382 298 298 267 198 164 271 355 397 279	[143] [144] This study This study This study This study This study This study This study This study This study This study This study This study
2	**Oman**	Fahal coastal area	89	[145]
3	**UAE**	Coastal areas of UAE*	256	This study
4	**Kuwait**	Central (Kuwait City)	216—339	[146]
5	**Qatar**	Doha	50—113	[147, 148]
6	**Bahrain**	Bahrain	60—144	[149]
7	**Arabian Gulf**	Northern parts of Arabian Gulf	373	[150]
8	**Sahara Desert**	western and southern Sahara Desert	913—10,446	[151, 152]
9	**Red Sea**	Red Sea	43.3	[153]
10	**Iraq**	Baghdad Um Qasr	220 193	[154] [155]

[1] The dust values were calculated in this study (*see section 3.4*).

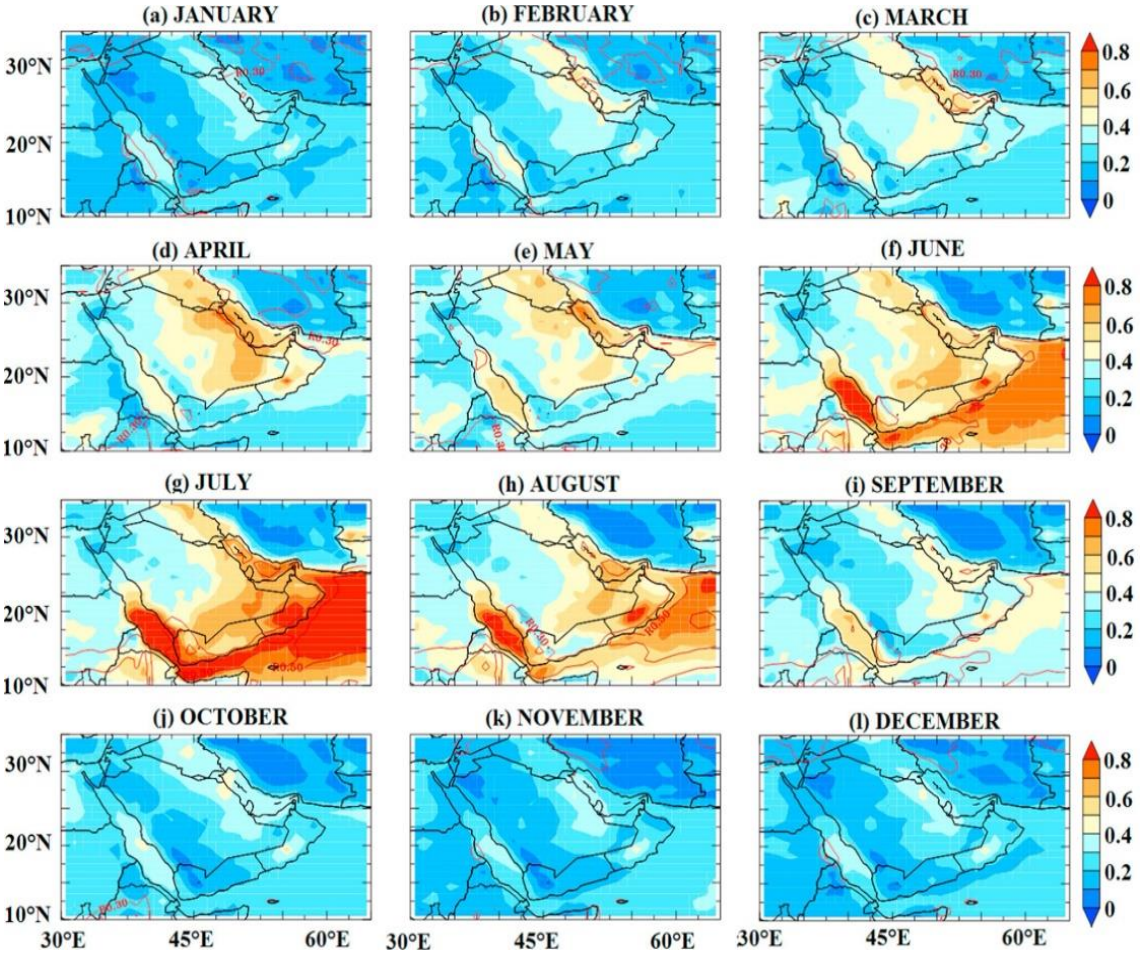

Figure 3-5. Monthly means of AOD and clearness of the sky over the GCC region computed for the period from 2003-2017 [119].

3.2.1.2 Wind Energy

Power generation from wind energy in the GCC countries is estimated to grow dramatically in the future and it is further expected that this will introduce significant challenges, such as intermittency, as well as hitherto unknown locations of high wind abundance. These challenges are rarely identified in the assessment of wind resources in the Middle East, including the GCC region, due to sparse meteorological observations and varying record lengths [156]. However, powering the GCC countries requires developing wind farms through a careful utilisation of available wind energy resources. To promote wind energy implementation in the GCC region, the Masdar Institute and other researchers have conducted several studies on the feasibility and potential of wind energy and other low-carbon technologies [157-164]. However, the majority of these studies are focused on the coastal locations of the GCC region. Al-Nassar et al. [165] note that there are trends toward commercial investments in offshore wind farms in most GCC

countries due to the reasonably promising offshore wind potential. In addition, Al-Salem et al. [166] examined the Arabian Gulf's wind energy map based on an analysis of historical data from 1979 to 2015 and found that the central locations of the Arabian Gulf have a high annual average wind speed (8-9 $m.s^{-1}$), with the highest wind speeds recorded at a 50 m elevation. This study has provided valuable information on wind energy resources in the Arabian Gulf. In addition, the wind energy potential in the coastal areas of the KSA was studied by Rehman and Ahmad [162]. They pinpointed Yanbo and Dhahran as the best locations for wind resources. Another 20 sites across KSA were studied by Rehman et al. [167] to assess wind power costs. The 20 locations selected cover three regions of the KSA, specifically the eastern, central, and western zones. Langodan et al. [168], Jiang et al. [169], Dasari et al. [170], Langodan et al. [171], Menezes et al. [172], and Zhai and Bowe [173] investigated potential RES, including wind energy, in the Red Sea and adjoining regions. These comprehensive studies have discussed the advantages and significance of the Red Sea for the GCC region. Research was performed by Rehman et al. [163] to evaluate wind resources at 60 m for Rafha, KSA. They found that the wind speeds in Rafha vary between 2.5 and 4.9 $m.s^{-1}$. Yip et al. [156] conducted a comprehensive study to assess wind resource characterisation in the Arabian Peninsula, including the GCC region. Furthermore, Nematollahi et al. [174] and Munawwar and Ghedira [91] mention that Oman is among the top countries for wind energy and that Kuwait also has abundant wind energy resources. Northwestern KSA and the Red Sea coast also have an abundance of wind. Ouarda et al. [175] and Gastli et al. [176] reported that the UAE and northeastern Oman present only low to average wind energy resources. Figure 3-6 presents the highlighted wind speed ranges in Oman (3-6.3 $m.s^{-1}$), Kuwait (4.5–5.5 $m.s^{-1}$), and northwestern KSA (3–6 $m.s^{-1}$) at a height of 50 m. Those sites that are characterised by greater height displayed higher wind speeds. Thus, the measurement scale and the height of wind turbines are important. Moreover, Shawon et al. [177] conducted a study of the wind technology deployment potential of all of the GCC countries and noted that these countries are good candidates for wind energy applications. Additionally, they observed that the wind speeds ranged between 2.35 and 5.1 $m.s^{-1}$ at a height of 10 m. These studies highlight wind resource locations and opportunities for accelerating and supporting further wind energy applications across the region. Figure 3-6 and Figure 3-7 show more details of average wind speeds of the GCC region at heights of 50 to 100 m. This indicates that wind energy distribution in the region is heterogeneous and clustered in specific locations. Furthermore, wind energy resources

in the GCC region are described in detail when assessing suitable technologies for the region. In particular, the western mountains of the GCC region offer an abundance of wind energy resources. High wind energy is detected along the coastal areas of the Arabian Gulf. In general, wind energy resources in the Arabian Gulf coast area are variable when compared to wind energy along the Red Sea shoreline at the same latitude. It is worth noting that the GCC countries all overlook the Arabian Gulf, which is characterised by high wind speeds. The GCC region is characterised by different wind speed performances due to various aspects, such as resolution, climatic scales, metrics of temporal variations in the wind, annual variability, and intermittency.

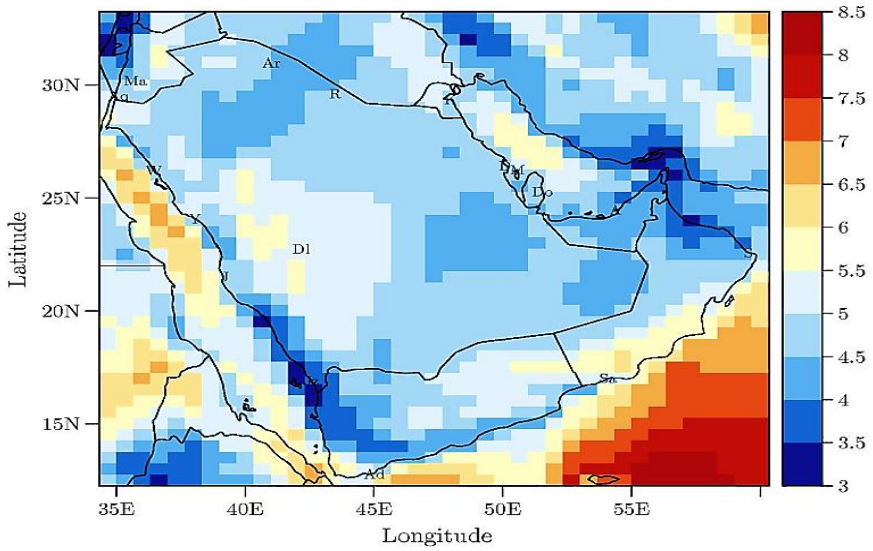

Figure 3-6. Average wind speed (m.s⁻¹) of the GCC region computed at an altitude of 50 m [156].

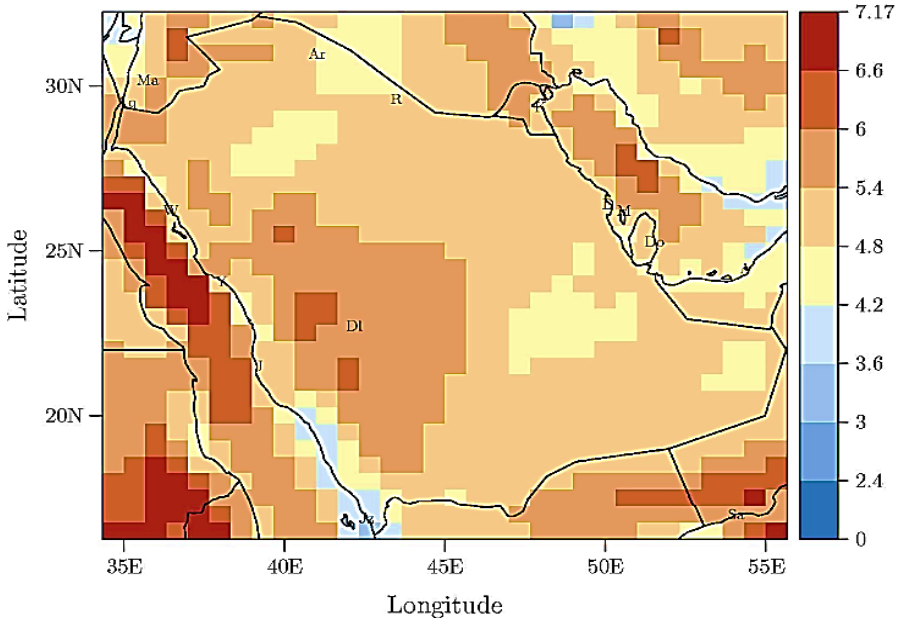

Figure 3-7. Average wind speed (m.s⁻¹) of the GCC region computed at an altitude of 100 m [156].

Further, each region has distinctive diurnal wind energy variations that vary with the seasons. Figure 3-8 presents the average monthly wind speed over the Red Sea in the GCC region at an altitude of 50–120m, based on an analysis of historical data spanning an 18 year period. An assessment of the spatial distribution of wind energy in the Red Sea shows that energy concentrations usually occur in three main locations over the 18 years of observations in which the density of wind energy is stronger as compared to other locations of the Red Sea (Figure 3-8). Moreover, it was observed that there is a stronger southeast wind over the southern Red Sea and a weaker northwest wind along the northern Red Sea throughout the El Niño periods, and a weaker southeast wind along the southern Red Sea with stronger northwest wind speeds along the northern Red Sea throughout La Niña periods. The mountain chains overlooking the Red Sea affect the prevailing local wind speed patterns and transform the Red Sea into a practical and realistic wind channel in which where the prevailing wind speeds are on the main axis. However, the monthly wind speed performance over the Red Sea affords great opportunity for harvesting wind energy from the Red Sea due to its many significant high wind speed locations. The most suitable sites for wind energy applications are however located in the KSA, the only GCC country adjacent to the Red Sea.

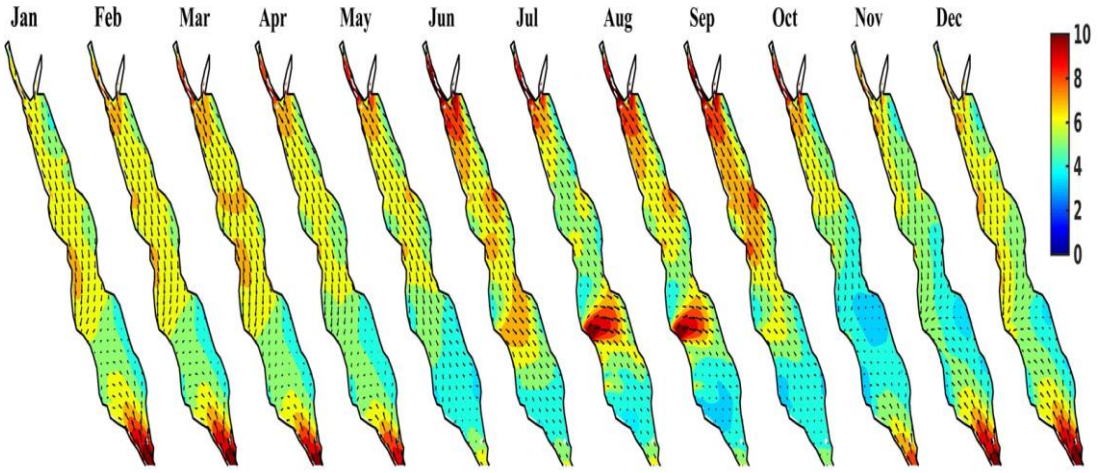

Figure 3-8. Average monthly wind speed ($m.s^{-1}$) over the Red Sea in the GCC region at an altitude of 50–120 m based on historical data spanning a period of 18 years [168].

3.3 Solar and Wind Power Generation

Despite the substantial potential solar and wind energy resources available across the GCC region, current use of these resources is extremely low. Based on the data from a 2020 IRENA report, the total electrical power generated from renewable energy (solar and wind energy) presently represents only 0.6% of the total energy generated in the GCC [82,178], while power consumption in the GCC has grown at an average annual rate of 8%, higher than any region of the world [179]. To meet this rising demand, the GCC countries will need to add some 100 GW of installed power generation capacity [179]. Elrahmani et al. [178] reported that the GCC region has a potential wind power generation capacity of 5.2 GW, assuming power generation under conditions of low to average wind speed. Potential power generation from solar power stands at 15.6 GW, some 96.7% of the total renewable energy generation in the GCC.

However, these may be underestimated, based on the abundant wind and solar resources available to the region. Recently, the GCC countries have recognised the significance of RES in their power generation systems. Critical factors contributing to the need for renewable alternatives include the need for economic diversity, continued urban expansion, the increasing growth in the rate of power consumption, the continued decline in solar and wind energy costs, and the need to reduce the region's carbon footprint. Recently, the GCC countries announced plans for solar and wind energy development through 2030. The plans call for an installed solar-generating capacity of 65 GW and an associated 5.2 GW of wind-generated energy. The plan's objectives are summarised in Table 3-2 [82,180,181]. Further, all the GCC countries have specifically focused on solar energy as a comprehensive solution to all their energy issues due to significantly high annual rates of solar radiation in the region [42]. Figure 3-9 and Figure 3-10 reveal the state of energy generation from solar and wind energy in the GCC region over the period from 2010 to 2020. In addition, Figure 3-11and Figure 3-12 show the development of the installed capacity for solar and wind energy in the GCC region for the period from 2010 to 2020 [182]. Based on Figure 3-9, 3-10, 3-11 and 3-12, the region had a combined total of 146 GW of total installed power capacity in 2017, with solar and wind energies representing only 1% of the total installed capacity at 867 MW. In 2018, the UAE increased the proportion it derives from solar and wind energy to 68% of its total installed capacity. In the KSA it accounted for 16% and in Kuwait 9%, respectively. While this

growth is not substantial in terms of installed solar and wind energy capacity, it does reflect a nearly four-fold increase from 2014 and this is expected to increase further after 2021 due to ambitious future targets for the GCC as presented in Table 3-2.

Table 3-2. Projected installed capacity in 2030 from solar and wind energy in the GCC region [82, 180, 181].

Country	Solar (MW)			Wind (MW)	Total
	CSP	Utility PV	Building Integrated PV		
KSA	9,500	10,500	750	3,500	24,250
Oman	770	2,420	990	1,210	5,390
UAE	6,000	18,900	4,200	300	29,400
Kuwait	1,000	5,800	1,000	200	8,000
Qatar	600	2250	150	—	3,000
Bahrain	70	520	70	20	680
GCC Total	17,940	4,0390	7,160	5,230	70,720

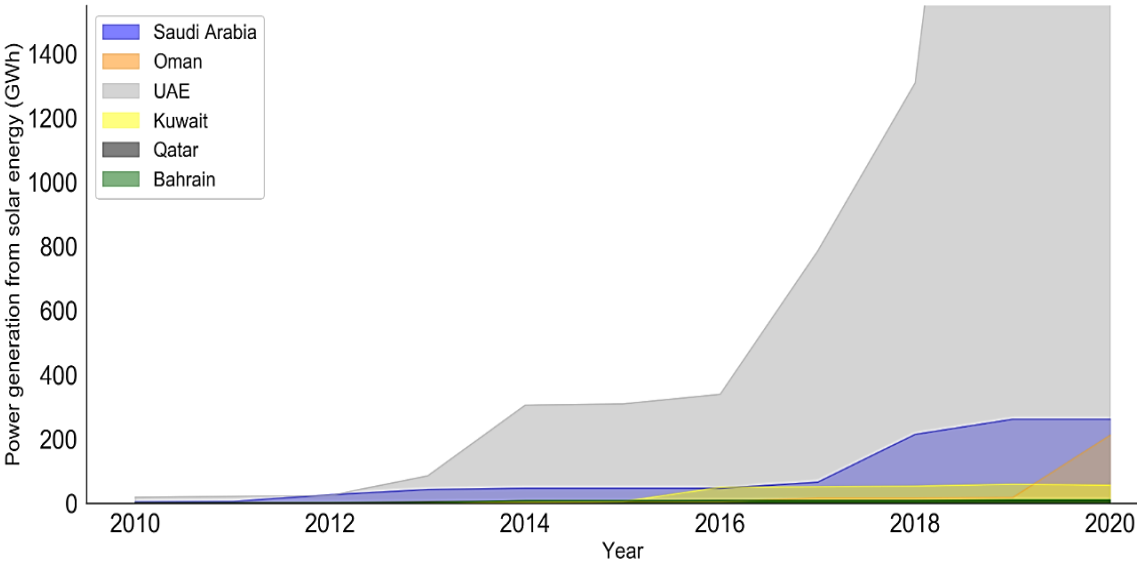

Figure 3-9. Energy generation from solar energy in the GCC region for the period from 2010 to 2020.

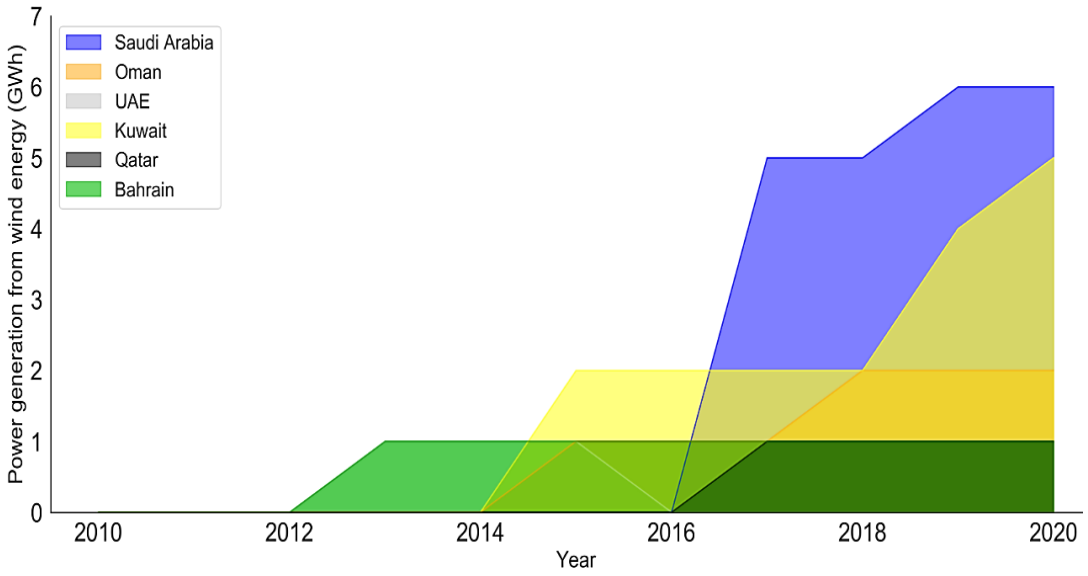

Figure 3-10. Energy generation from wind energy in the GCC region for the period from 2010 to 2020.

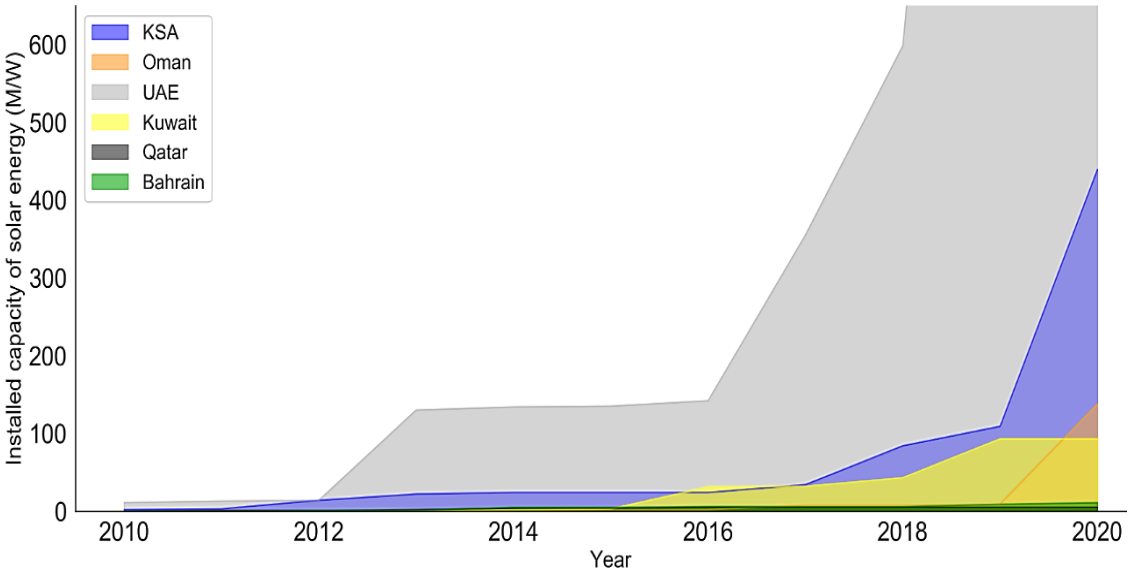

Figure 3-11. Power installed capacity from solar energy in the GCC region for the period from 2010 to 2020.

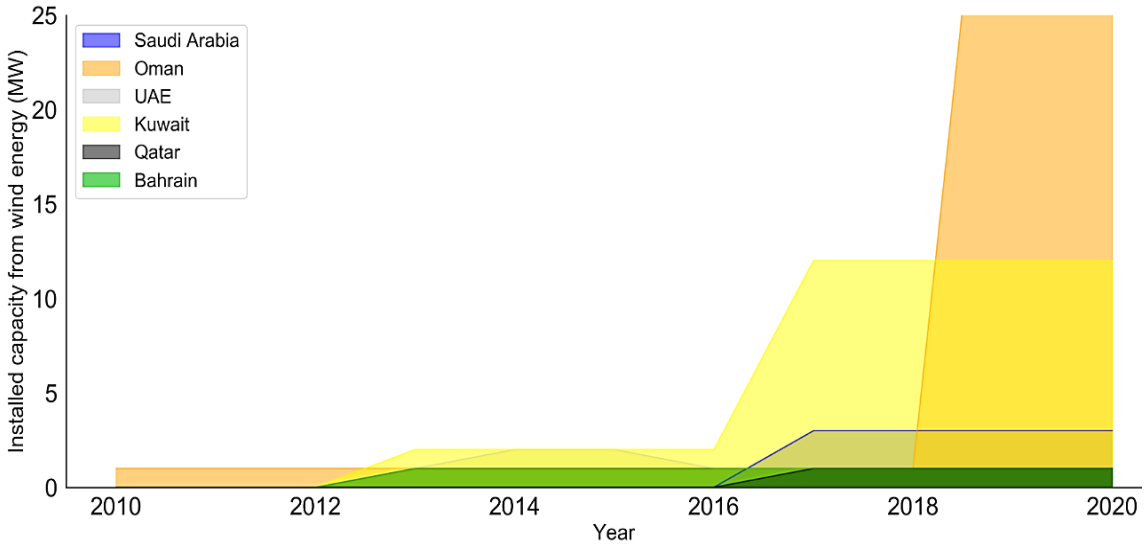

Figure 3-12. Power installed capacity from wind energy in the GCC region for the period from 2010 to 2020.

3.4 Climate Justice

The pursuit of climate justice forces us to ask serious questions about how we properly measure and address environmental inequalities. Climate justice politics are rife with controversy about the existence and geographic scope of both the issue and its potential remedies. Adger [183] mentioned that the UNFCCC is the main body organising international cooperation in response to the dangers of global climate change. Adaptation is used as a justification for international transfers in the convention framework, both to compensate for and brace for any potential future impacts. The argument that improving sustainability will improve adaptive capability and that planning activities are a vital part of overall adaptation can be used to justify this strategy [183]. Schlosberg [184] reported that environmental justice campaigns are not solely concerned with individual consumer approaches to climate change issues given that they do not just imply the use of solar panels on rooftops. Schlosberg [184] believes that the emphasis must be on developing innovative sustainable strategies and structures, practices and institutions that reflect not only environmental justice values, but also demand a broader definition of sustainability. In addition, effort must be put into eliminating harmful activities, such as coal mining and burning, the mishaps and misdeeds of mining corporations, and controlling for the growth of consumption. As the main producers and exporters of oil and gas, the GCC countries will be constantly criticised by the international community and environmental lobbying

groups. The region needs new environmental regulations, as well as increased governmental support, including an acceleration of the pace at which renewable energy projects are realised. In the GCC region, more sustainability legislation and cooperation with the international community are required to address climate change issues and close the gaps in the current environmental laws.

3.5 Discussion of Geographical Factors Unique to the GCC Region

Chapter 3 presents the second phase of the comprehensive review of the feasibility and evaluation of solar and wind energy resources in the GCC region. The first phase in Chapter 2 highlighted issues with energy consumption growth and addressed the rapid growth of solar and wind energy infrastructure projects and their development in the region. Chapter 3 includes a review of several previous works that assess the potential of solar and wind energy in the GCC region. Topics covered include dust fallout, solar energy and wind energy performance, with data collated from a 37-year period across the GCC. The chapter highlights the potential for solar and wind energy to serve as alternative solutions for reducing CO2 emissions and the slowing growth of fossil fuel consumption. The studies reviewed are divided into two groups: (1) those covering the entire GCC and based on high quality tools and maps, such as those featured in [124, 140, 156], and (2) those covering specific cities or locations in the GCC region. The present study is distinguished by its comprehensive approach to all aspects of energy use in the GCC region.

Both types of studies provide comprehensive details for the GCC region and highlight the issue of dust fallout over time. Moreover, the review's findings demonstrate that compliance with the Paris Agreement under the auspices of the UNFCCC would be feasible in the GCC region, given its significant potential for solar and wind energy development. Based on this review, the area from the southeast to the northwest part of the GCC region appears the most suitable for solar energy production, despite the potential for dust fallout.

Oman receives the most substantial annual solar radiation of up to 2,500 kWh/m^2, followed by the UAE with 2,285 kWh/m^2. The KSA and Kuwait have equivalent levels of up to 2,200 kWh/m^2, while Bahrain has a mean annual solar radiation of 2,180 kWh/m^2, and Qatar receives some 2,113 kWh/m^2/year. In addition, encouraging solar energy

radiation rates were recorded in western locations and the Red Sea's southwestern shores. These findings indicate that there are significant untapped solar energy resources that could support the energy needs of the entire region.

Dust fallout is a concern in the region during the summer months. However, it should be noted that the periodic waves of dust and clouds do not envelop the entire GCC region at the same time due to relative differences in geographic features and terrain and the large distances between them. However, the northwestern GCC region is characterised by clearer skies, and substantial diurnal variability was recorded in southwestern and eastern locations throughout the year.

The highest annual dust fall recorded was 454 tonnes km^{-2} in northeast Riyadh. Kuwait receives the second highest annual amount dust fall in the region at 216-339 tonnes km^{-2}, followed by the UAE at 256 tonnes km^{-2}. The lowest amount of dust was recorded is in Qatar at 50-113 tonnes km^{-2}, and Bahrain at 60-144 tonnes km^{-2}. Table 3-1 shows the annual dust falls for several locations based on data obtained from previous studies. We calculated the annual dust fallout at some locations in Table 3-1 using the equation $A = w \times 31.85$, based on the procedure presented in [145]. Here, A is the amount of dust fallout in tonnes/km^{-2}, and w is the weight. The weight (w) values were obtained from [138]. The data for the UAE were obtained from [185] to calculate the dust values.

The impacts of dust are to increase construction and maintenance costs of solar energy systems. However, a combination of bifacial panels, solar monitoring panels, and robotic cleaning technology will serve to improve system performance and reduce the effects of dust.

Our review showed that the western mountains of the GCC region are characterised by abundant onshore winds. Oman has the highest recorded average wind speeds of 3-6.3 $m.s^{-1}$, followed by Kuwait with 4.5-5.5 $m.s^{-1}$. Northwestern KSA has relatively abundant onshore winds with speeds of 3-6 $m.s^{-1}$. The UAE has the lowest average wind speeds at 3-4.8 $m.s^{-1}$. At this speed, wind energy development is not economically viable.

In contrast, offshore winds are substantial along the coastal areas of the Arabian Gulf, an expanse of water that links all of the GCC countries. Persistent and abundant offshore winds were recorded at various locations on the Red Sea coast, with average wind speeds of 4.5-7 $m.s^{-1}$. Three primary areas for favourable offshore winds on the Red Sea are characterised by high performance as compared to the other coastal locations in the region

(see Figure 3-6 and Figure 3-8). In particular, the findings of a long-term analysis of offshore wind speeds over the Red Sea indicate a great opportunity for KSA to harvest energy there.

To achieve the ambitious CO_2 reduction targets and achieve climate change mitigation, it is first essential to reduce fossil fuel use and phase out coal consumption. Although the GCC countries are among the largest carbon-producing countries, they do not rely on coal for all of their industrial activities and energy generation, as does much of the rest of the developed world. Coal produces significant CO_2 emissions relative to other types of fossil fuels. Based on Figure 3-8, 3-9, 3-10, and 3-11, the GCC countries have yet to fully harness their potential RES and should pay more attention to wind and solar energy to increase their use of clean energy. One mitigation strategy is to levy a substantial local carbon tax on those organisations and companies that produce high rates of CO_2 emissions and increase the current international carbon tax on all countries until the required decrease in CO_2 emissions is achieved.

Reducing energy consumption is essential, especially in the GCC which is experiencing growing energy demand. The deployment of solar and wind energy and accelerated decarbonisation technologies are critical solutions to climate change. Furthermore, decarbonisation processes must be sufficiently developed to have an impact at a scale sufficient to reduce CO_2 emissions. Based on IRENA's 2019 report and the findings of this review, implementing renewable energy in the GCC region power sector can reduce oil consumption by 23% (354 million barrels) by 2030. Low-carbon technologies will further lower CO_2 emissions by 22%, equivalent to 136 million tonnes ($MtCO_2$) in the region. In addition, the water used for power generation and oil extraction can be reduced by 17%, equivalent to 11.5 trillion litres. These deployments would have a positive impact on the GCC region and the world in terms of supporting climate change mitigation and global sustainability and some 220,500 jobs in the energy sector to support both local and global economies.

Adopting stricter regulations, including a reduction in energy subsidies, is one approach. Raising awareness and educating the public about the risks of climate change and its consequences would further reduce CO_2 emissions. In addition, granting countries and organisations committed to reducing CO_2 emissions some advantages and powers of encouragement could play a significant role. The desired outcomes are contingent upon

the carbon emissions goals set for developing countries, such as those in the GCC, as they are distinct from those assigned to developed countries. The GCC is considered a promising region because of its tremendous wealth and significant potential for alternative energy development. This potential must be harnessed to serve its nations, contribute to climate change mitigation, and build a prosperous future. However, the overall impacts are hard to predict, as oil and natural gas extraction may have unexpected consequences.

Progress in the contribution of solar and wind energy to climate change mitigation is expected to be essential for the GCC region due to their governments' plans regarding low-carbon technology deployments. Increasing the proportion of solar and wind energy in the generation of energy would decrease fossil fuel consumption in the region, tackle the issue of single-resource reliance, and have a positive effect on the environment and economic growth. This review provides background information and opportunities for researchers and policymakers to develop an effective strategy for solar and wind energy to support the deployment of low-carbon technologies and improve the traditional energy system in the GCC region.

4 Research Methodology

This chapter outlines the main research framework processes including historical data collection and description. Moreover, four predictive models were designed based on the methodology framework to meet the research aims and will be discussed in chapters 5, 6, 7 and 8 alongside their methodologies with underlying concepts and theories. The four predictive models comprised the (i) MCS and BM prediction model; (ii) the long-term seasonal autoregressive integrated moving average with exogenous model; (iii) the solar irradiance prediction model based bidirectional long short-term model; and (iv) the short-term wind speed and temperature prediction model based on GRU neural networks.

4.1 Research Framework

In order to build a sufficient and effective framework for the research methodology, the research requirements are required to be defined so as to determine the tasks and the target of this methodology. The framework is a technique that is applied to organise and ensure that the whole process of the methodology will go smoothly by addressing the basic stages, rules, procedures, and tasks of the research methodology, including data collection, data analysis, selection of the required tools and building the models which will be employed in this research. The framework is introduced to carry out the activities and tasks in a clear application form together with their objectives to achieve the research aims and deliver high quality results and accurate outputs. Organising a framework provides an overview of how the research process can be implemented and performed under clear guidelines. Nevertheless, the methodology design process must have an efficient management system and must be sufficiently flexible to meet both current requirements and changing situations as may be needed, given that the research is rarely implemented exactly according to the plan set out in the initial methodology, while monitoring the progress of the methodology and procedure is the main system's management responsibility. The main task of the monitoring is to ensure that research inputs (historical data) and outputs are in line with the original plan and that the process enacted complies with the rules of eligibility criteria. For these reasons, planned monitoring is important to maintain continuous activity during the ongoing process and not simply an activity left for the end of the work. The framework's emphasis is thus on

the monitoring methodology processes and as such is one of the main tasks of this research. The main reasons for the monitoring process are as follows:

- It provides vital information and significant achievements on the overall performance process in terms of how key targets and objectives have been met.
- Provides a clear picture of the status of the implementation of the methodology tasks.
- To keep track of whether tasks are being implemented based on the plan and thus monitor the progress of all the major elements including time, scope, and quality.
- It identifies or verifies the problems and issues in order to solve them.

4.1.1 Defining the Research Target

Definition and analysis of the target and the overarching requirements of the research will lead to a determination of the required data type, size, and models' associated specifications. This is especially the case where the problems being solved are ambiguously defined and the research target is sufficiently complex that they collectively cannot be easily grasped and instead are set in a changing context where the final solution can influence the nature of this research [186]. In addition, understanding the research target involves mapping and situating the insights of solution requirements, integrating any necessary changes and helping to reduce the duration and iterations of a project. In proposing renewable energy as a viable energy source in the region, this research aims to design future scenarios for the GCC electricity power sectors to evaluate their future performance, including generative capacity and consumption growth, leading to a proposal of renewable energy as an available and viable energy source in the region. Moreover, determining future temperatures, wind speed and solar irradiances, including GHI, DNI, and DHI are integral to this analysis.

4.2 Data Collection Challenges

To comprehend and provide more detailed insights into the big data requirements and data analytics, several challenges regarding these approaches must be addressed. The

main challenge is how to select the type, size, and lifecycle of the data. The reliability of data sources, their classification, overall quality, being able to identify any inaccuracies, understanding the characteristics of the data and executing suitable analyses are other significant challenges. Table 4-1 presents the data classification challenge. In addition, data process challenges include a series of techniques such as devising efficient methods of capturing, transforming and integrating data as well as selecting suitable tools for its evaluation.

Table 4-1. Classification challenges of data.

No	Challenge	Definition	Example
1	Data challenges	The group of challenges related to the characteristics of the data itself.	Volume, velocity, variety, variability, veracity, visualisation, and value.
2	Process challenges	All the challenges encountered while processing the data.	Data mining & cleansing, data interpretation, analysis & modelling, data aggregation & integration.
3	Management challenges	Includes the privacy, security, governance, and lack of skills related to understanding and analysing data.	Privacy, security, data governance, data & information sharing, cost, and data ownership.

4.2.1 Data Analytics

Data Analysis is a process of cleansing, inspecting, transforming, and preparing to receive raw data to discover useful and important information. In addition, finding patterns and connections and, further, identifying any relationships arising between the elements of data is part of the data analytics. Data analytics has key components that are required for any initiative and by combining these components, a successful data analytics initiative will provide a clear picture of the data's advantages and limitations. In addition, regression analysis is an excellent tool when working on predictions and future forecasts, as this can effectively measure the relationship between a dependent variable and an independent variable.

4.2.2 Data Description

In this research, GCC countries were identified as a study area. The historical energy data were collected from the KAPSARC [32], the Saudi Water and Electricity Regulatory Authority [187], and U.S. Energy Information Administration [35]. The historical energy data for KSA and other GCC countries consisted of electricity generation, consumption, peak load, and installed capacity data, as presented in Figure 1-2 to Figure 1-5. The actual historical data pertained to quarterly intervals over a 39-year period from 1981 to 2020 and were used to evaluate and predict the behaviour of the power sector in GCC countries across a 30-year span (2021–2050).

The historical weather data were collected from the Meteoblue weather service's portal [188] for GCC countries. The data comprised GHI, DNI, DHI, wind speeds ($m.s^{-1}$) at 80 m altitude, and ambient temperature (°C) at 2 m above ground. These are presented in Figure 4-1 to Figure 4-16 for the KSA and also in *A.5 Appendix 5*. For the other GCC countries, these are represented in Figure A.5–1 to Figure A.5–80. The actual historical data spans 36 years in the form of daily and hourly intervals for the period from the 1st of January 1985 to the 26th of June 2021 and were used to evaluate and predict the future behaviours of GHI, DNI, DHI, wind speed, and ambient temperature. The meteorological conditions have changed and varied over the previous 36 years. This large quantity of historical data can provide details that the four prediction models can accurately reflect. The data were analysed, verified, and cleaned to ensure that no values were missing or duplicated. Moreover, Dickey-Fuller theory confirmed that all the data were stationary (p-values < 0.05). As the p-values were less than 0.05, the p-value hypothesis was tested and validated. Further, the quality of the historical data was a key element, allowing the four prediction models to extract the essential components and produce accurate results.

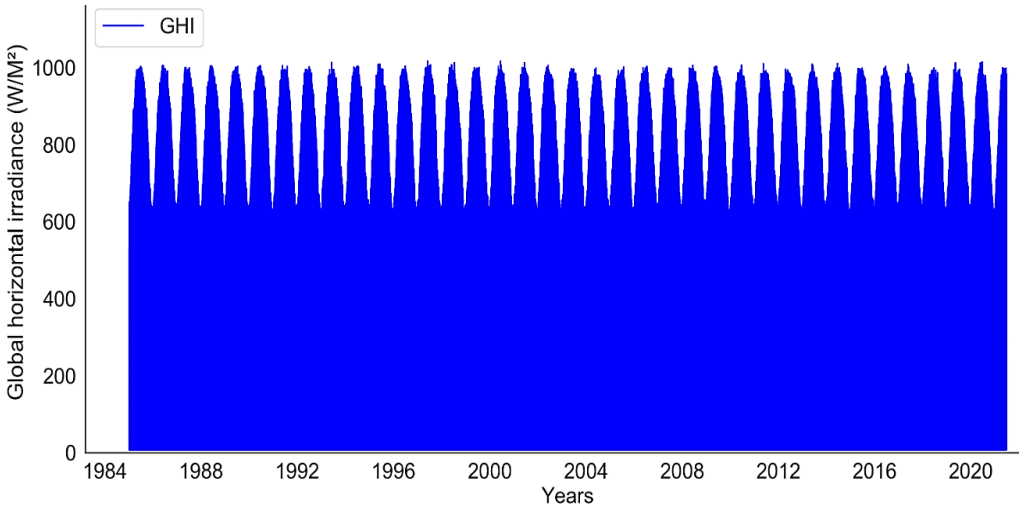

Figure 4-1. KSA hourly intervals - historical performance of the GHI over 36 years.

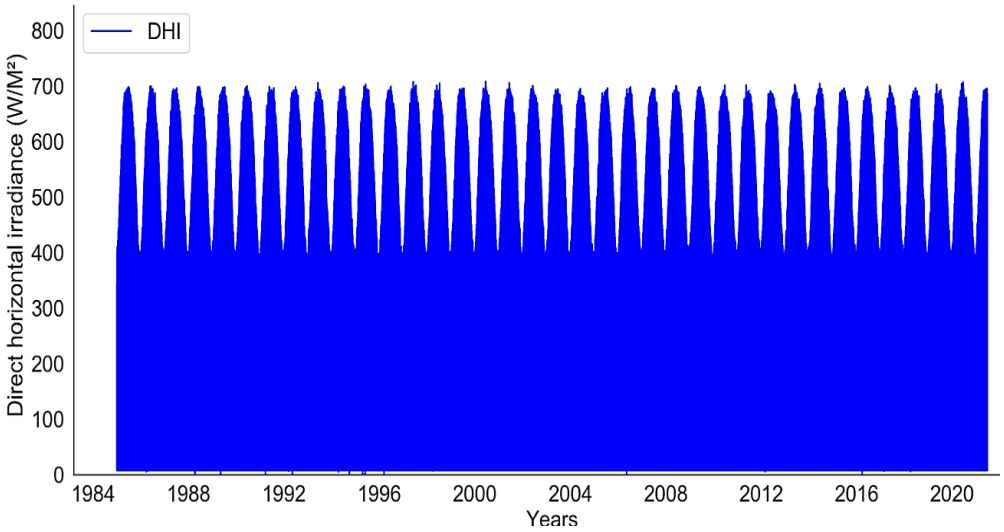

Figure 4-2. KSA hourly intervals - historical performance of the DNI over 36 years.

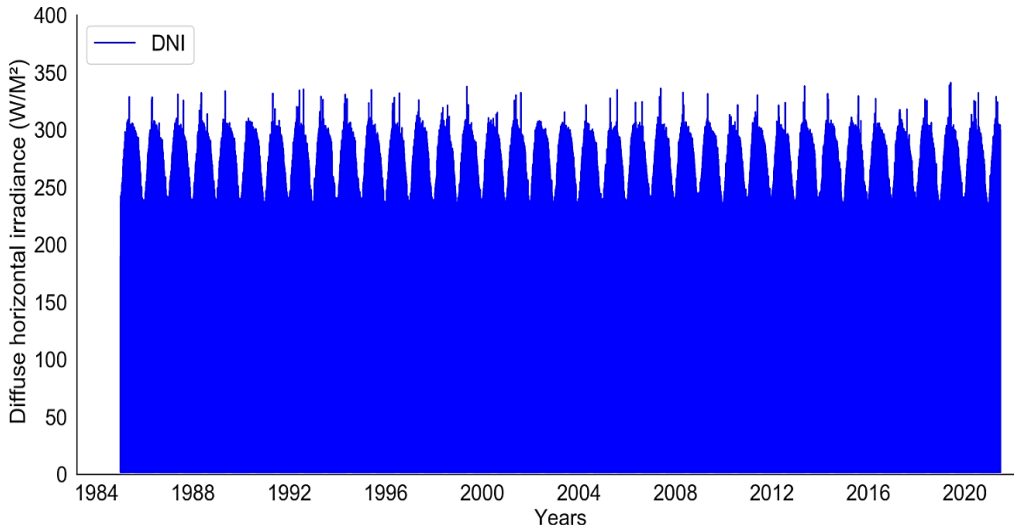

Figure 4-3. KSA hourly intervals - historical performance of the DHI over 36 years.

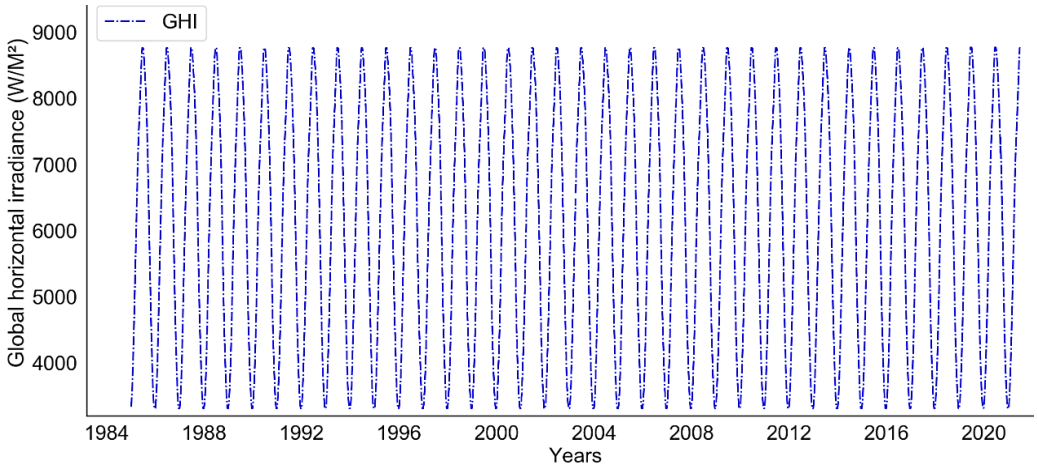

Figure 4-4. KSA daily intervals historical performance of the GHI over 36 years.

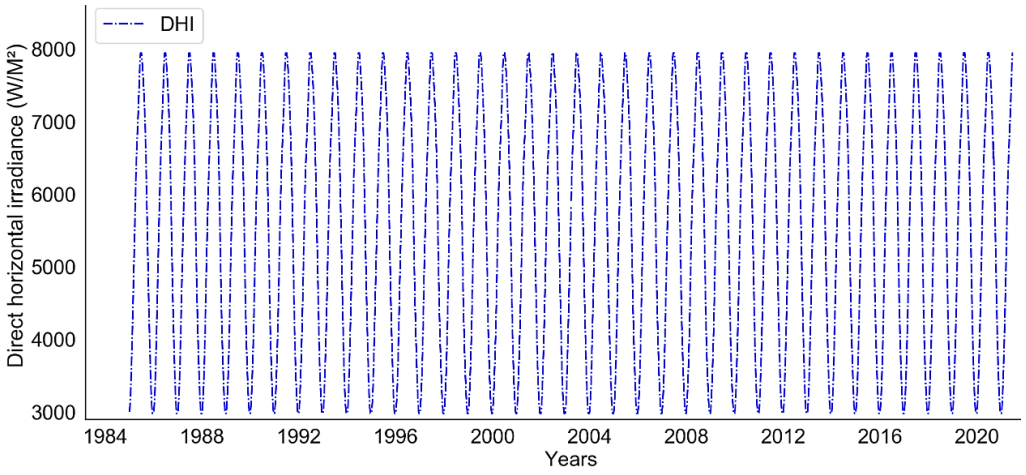

Figure 4-5. KSA daily intervals historical performance of the DNI over 36 years.

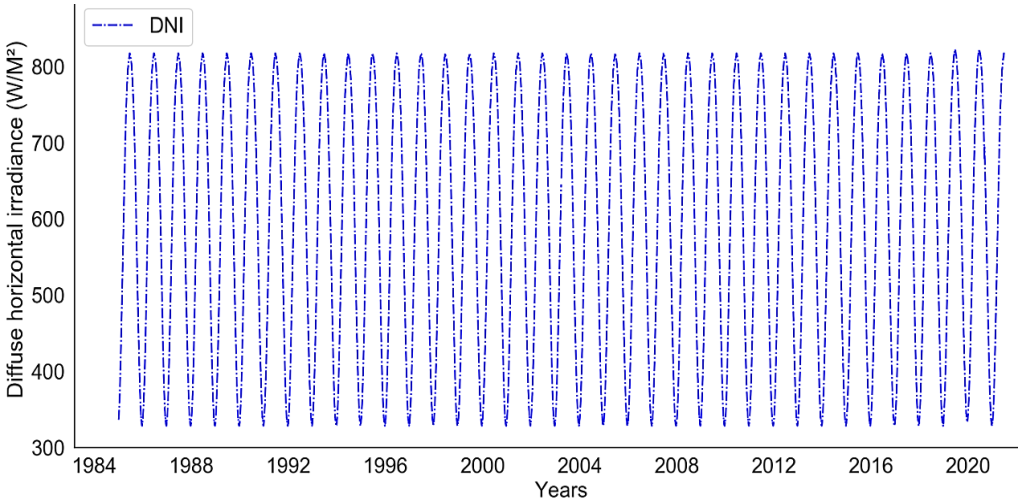

Figure 4-6. KSA daily intervals historical performance of the DHI over 36 years.

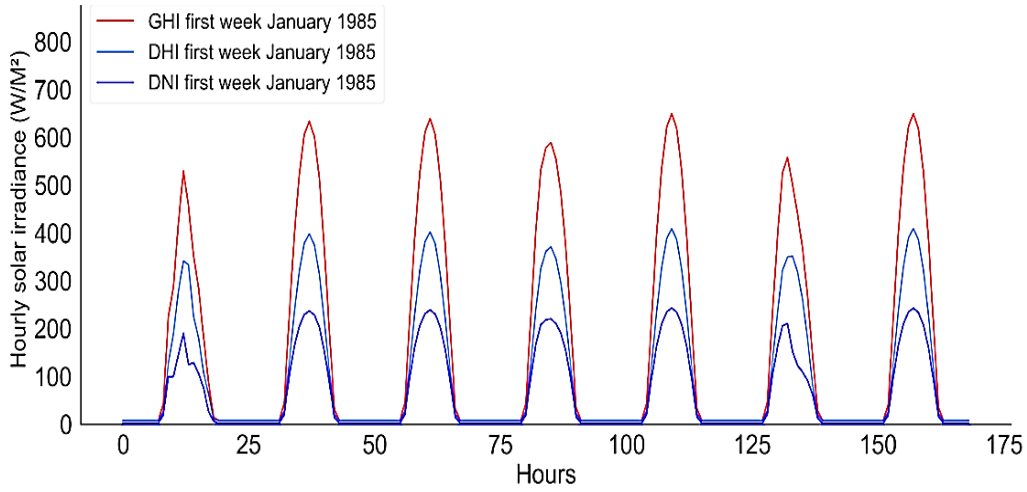

Figure 4-7. KSA hourly intervals historical performances of the GHI, DHI, and DNI.

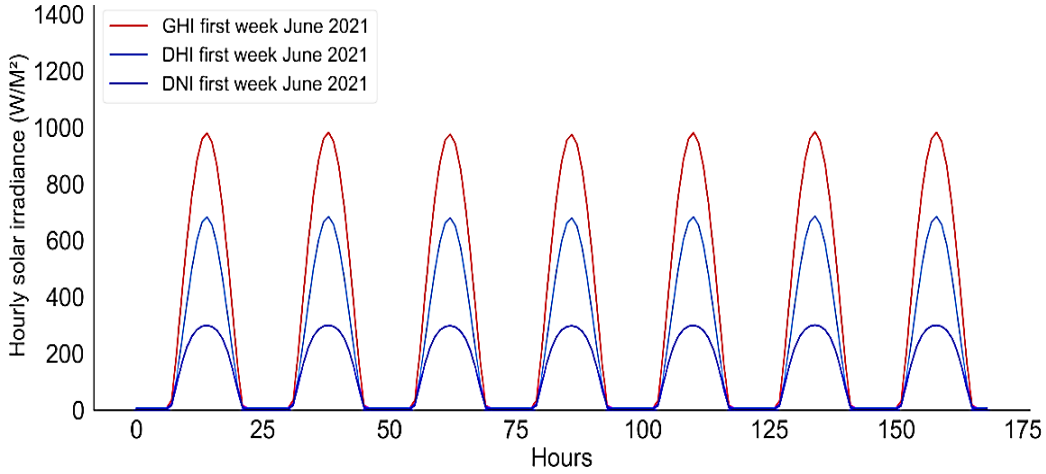

Figure 4-8. KSA hourly intervals historical performances of the GHI, DHI, and DNI.

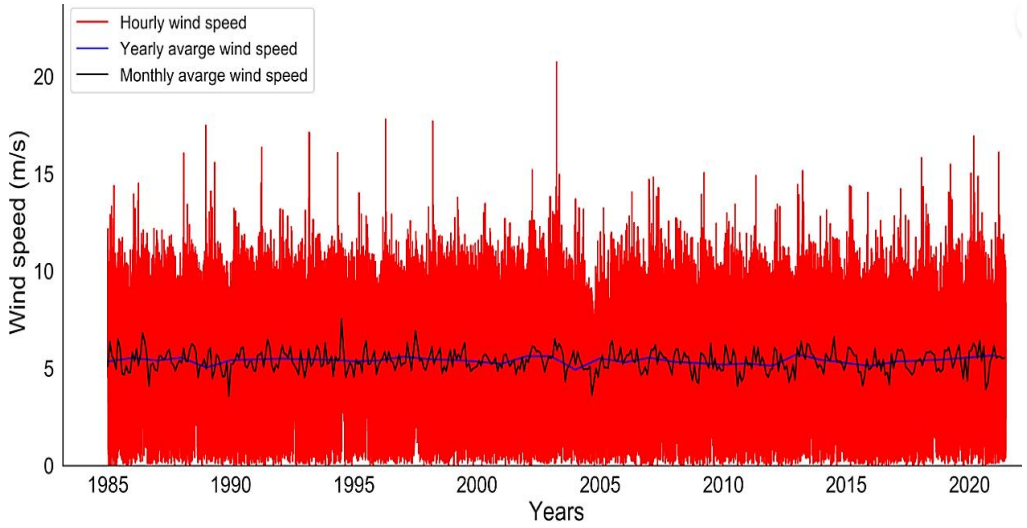

Figure 4-9. KSA hourly, monthly and yearly intervals historical wind speed performance over 36 years.

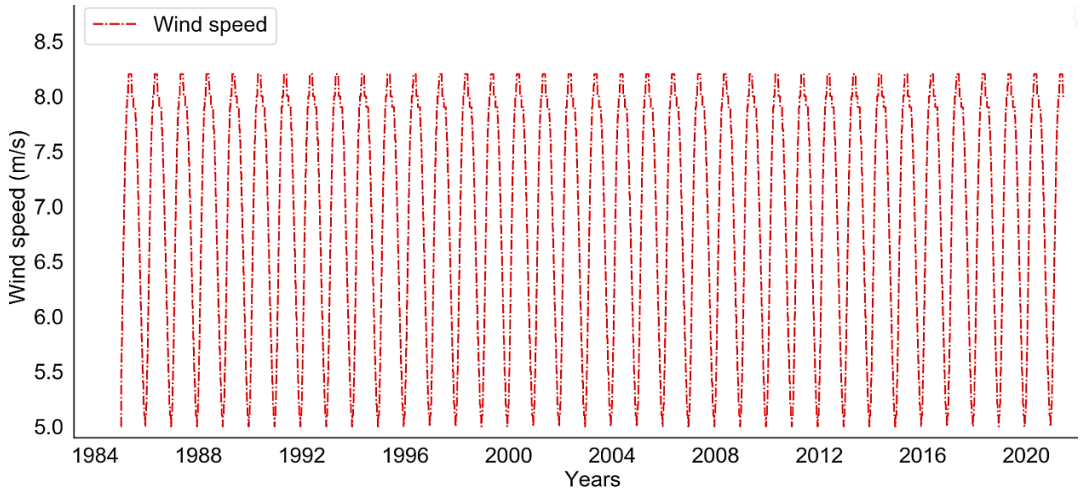

Figure 4-10. KSA daily intervals historical wind speed performance over 36 years.

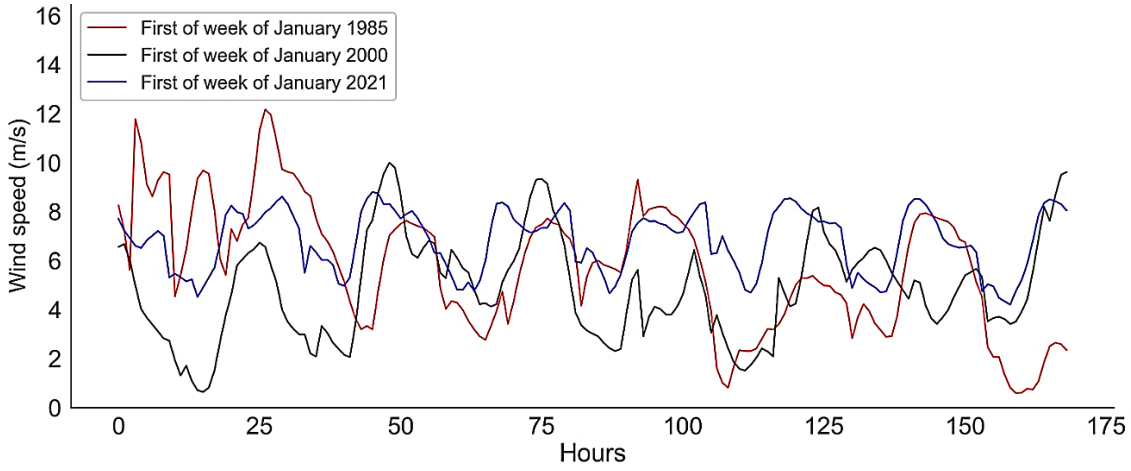

Figure 4-11. The first three historical weeks of wind speed performance for KSA.

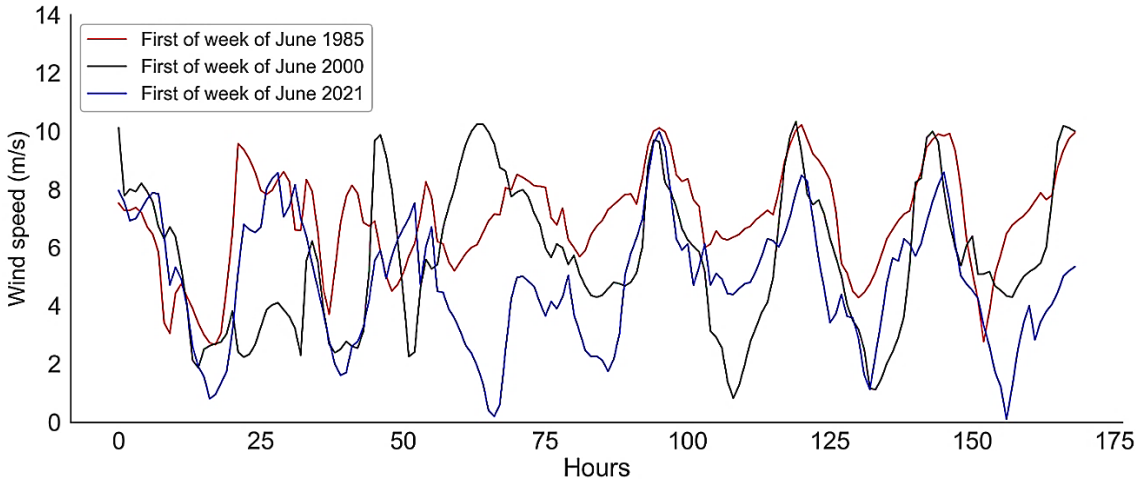

Figure 4-12. The first three historical weeks of wind speed performance for KSA.

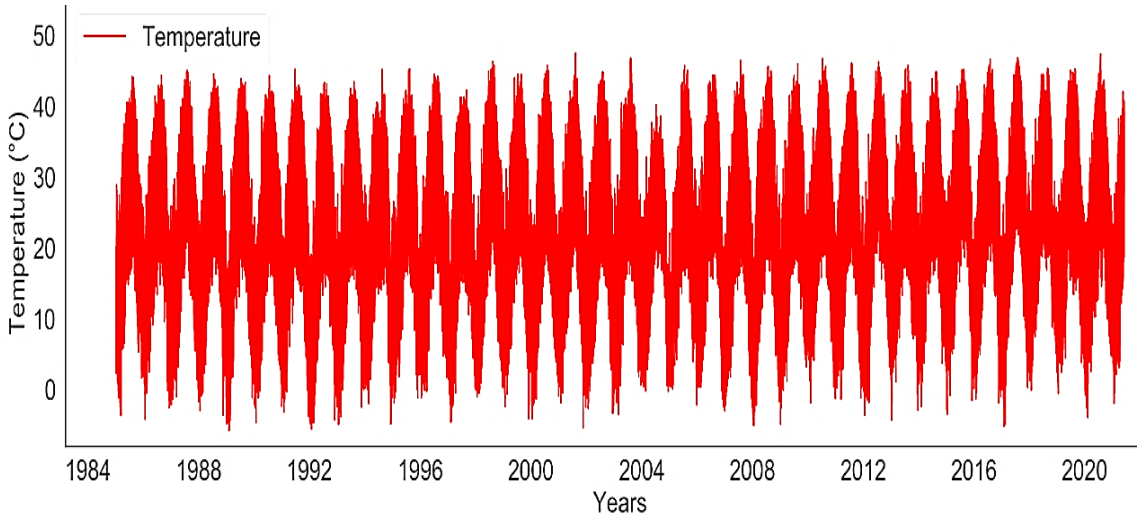

Figure 4-13. The historical temperature performance over 36 years at hourly intervals for KSA.

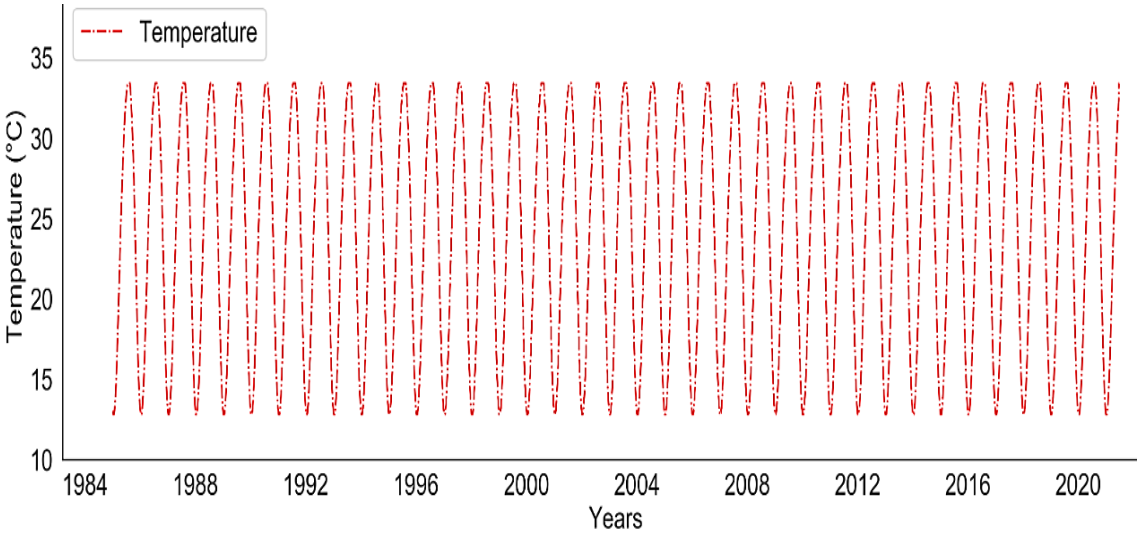

Figure 4-14. The historical temperature performance over 36 years at daily intervals for KSA.

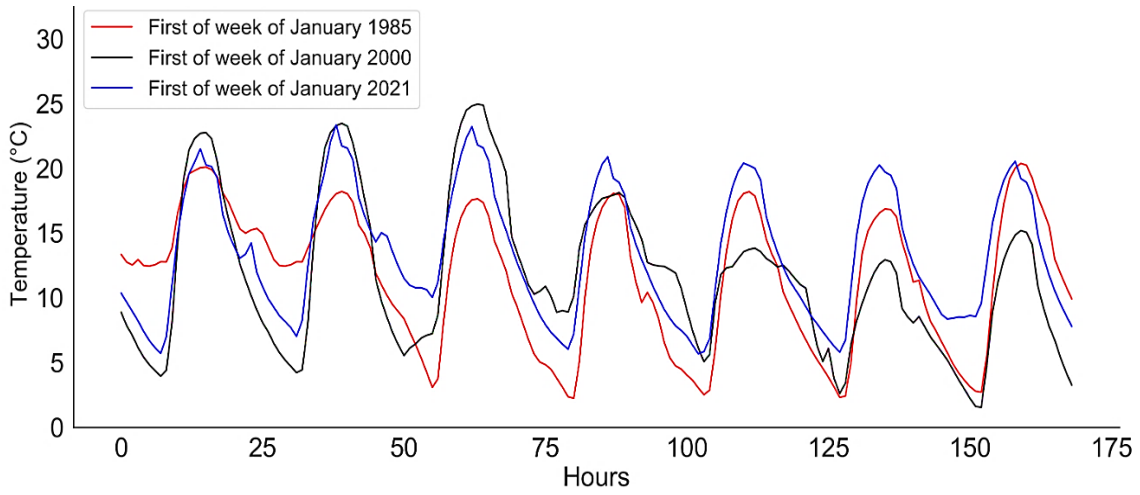

Figure 4-15. The first three historical weeks of temperature performance for KSA.

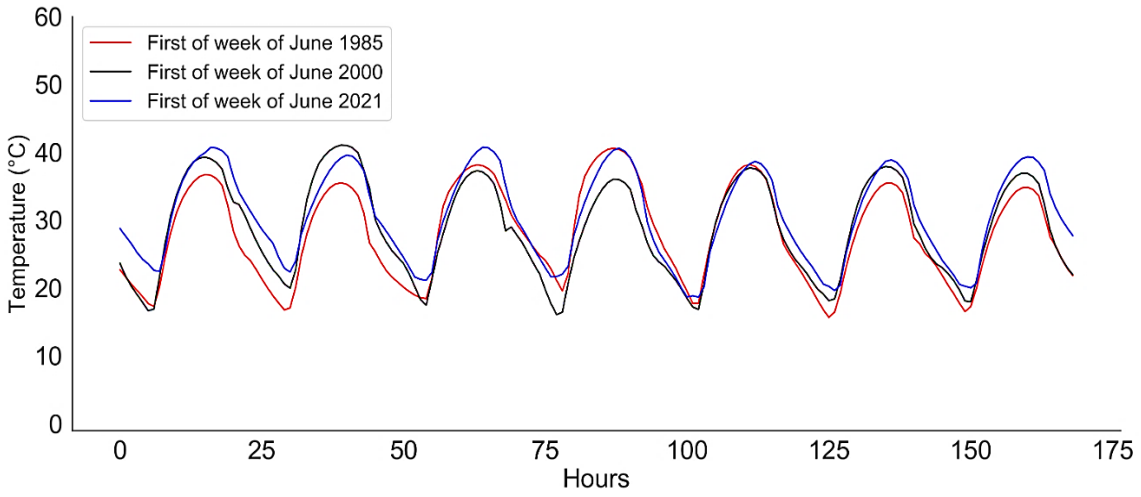

Figure 4-16. The first three historical weeks of temperature performance for KSA.

4.3 Development of Four Predictive Models

Predictive modelling encompasses a range of tools and techniques that are built based on computational mathematical methods in order to predict a future outcome based on a given model's inputs, including historical data. Mathematical approaches employ equations based on a specific model's requirements which describe the phenomena under consideration. The models can be developed accordingly to meet the specific aims of the research methodology, while the type and size of the data play important roles in selecting the preferred model type. However, while the model's performance must be accurate to reflect the data quality, its creation is only delimited by the imagination of the developer or the researcher's aims and goals [189]. In general, securing confidence in the believability of the actionable outcomes results from the support provided by the analysis of multiple sources of historical data, its interpretations, and ensuing predictions based on relevant theoretical considerations [189]. Energy forecasting for the short and long-term is a complex process and one which requires high quality models. The general plan of this methodology was to design and develop four predictive models for use in different approaches sharing a common aim albeit from different points of view. From this, we will provide an easy method of comparing the results of the four models and the extent to which they support each other (e.g, to perform all the tasks that may not be covered by one of them). Moreover, the contexts, characteristics, advantages, practical applications, and limitations were considered in the design of these models. The models can be meaningfully grouped based on the characteristics of the research-targeted situation and the overall purpose of each model [190]. Since there is no specific technique that works

consistently better in all conditions, several statistical techniques need to be evaluated to select the best predictive models with more options for the data [191]. Hold-out analysis and cross-validation should be performed to compare the predictive power of various models. These processes will help to avoid choosing models that limit fitting to the data and do not demonstrate strong predictive power for the test data. Figure 4-17 summarises the selection and testing process for the predictive models.

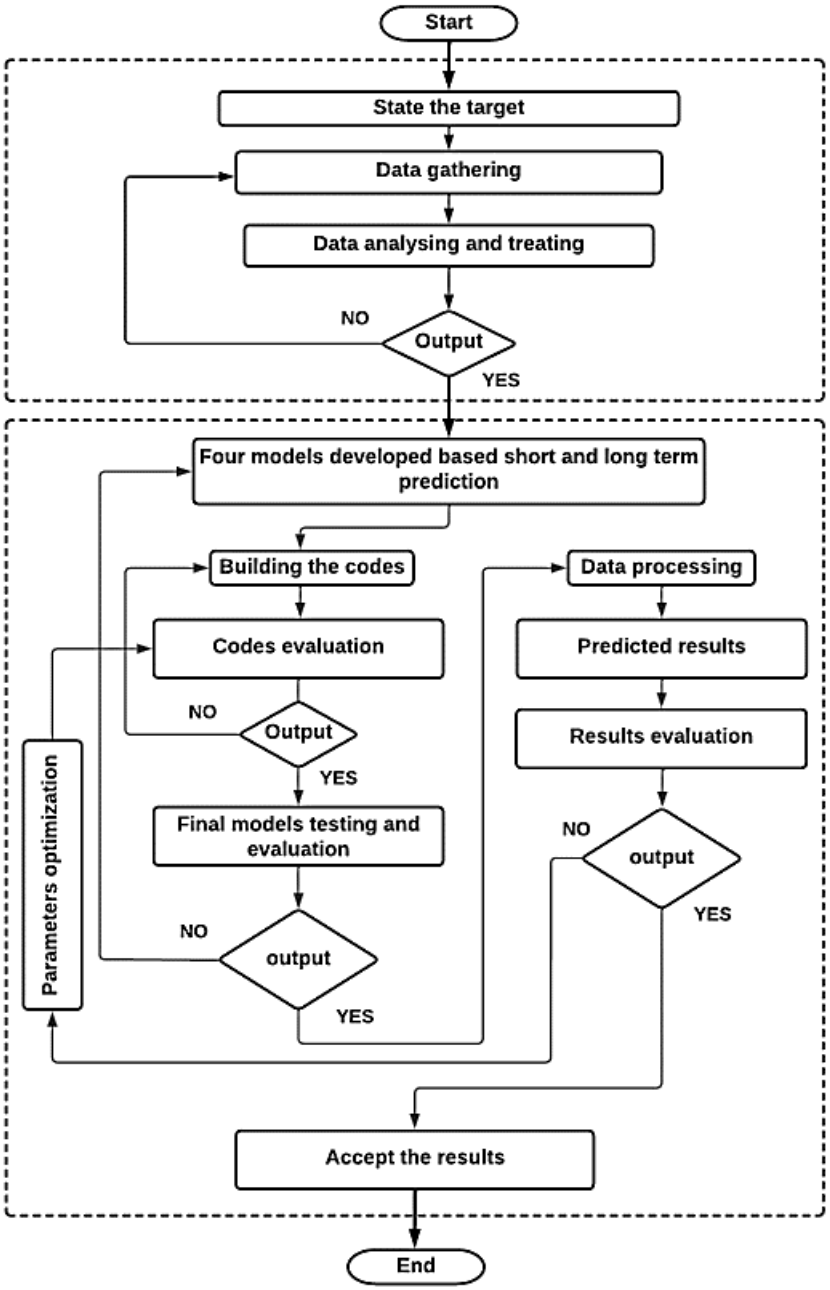

Figure 4-17. Selection and testing process for the predictive models.

5 Monte Carlo Simulation and Brownian Motion Prediction Model Development

In this chapter, the MCS and BM prediction model was developed to predict the long-term performance of the power sectors in the GCC region. The MCS and BM prediction model applies regression analysis (which characterises the behaviour of an analytical technique) to a large sample of random trials to provide a plausible set of probable future outcomes. In addition, the power sectors of the GCC countries will be predicted to analyse and compare with historical data. The predicted power sector values include electricity generation, consumption, peak load, and installation capacities for the next 30 years spanning from 2021 to 2050. The power sector historical dataset was gathered from the GCC countries at quarterly intervals from 1980 to 2020. Moreover, the wind speeds and solar irradiance measurements, including GHI, DNI and DHI, will be predicted and analysed, including temperature performance based on the historical weather data. The historical weather data was collated for the period from 1985 to 2021 as daily intervals for all the GCC countries (*see section 4.2.2 and A.5 Appendix 5*). The results of the MCS and BM prediction model were analysed and discussed in this *chapter* for the KSA, while the Figures for the other GCC countries are presented in *A.1 Appendix 1*.

5.1 Model Background

CO_2 and GHG emissions can be reduced by applying renewable energy technologies, thereby reducing the consumption of fossil fuels such as oil and coal. Since the late 19th Century, the global average temperature of the Earth's surface has increased by 0.6°C (±0.2°C) due to climate change and global warming [192]. Regionally, during the dry seasons, the temperature has risen by 0.72 °C per decade [192]. As the climate becomes warmer, evaporation increases, leading to an increase in average worldwide precipitation [193]. The combined impacts of fossil fuels on global warming have made implementing solar and wind energy in the 21st century a top priority [106]. The absence of harmful emissions, the rapid development of these technologies, and the decreasing cost of renewable energy have made solar and wind energy the most promising alternatives to fossil fuels in recent years [194,195]. However, the dependence on weather and nature fluctuations, which are difficult to predict, is a common drawback of solar and wind energy resources [194,196]. These issues could be partially confronted by applying the

strengths of one source to overcome the weaknesses of another, but this integration makes hybrid solar and wind generation systems more difficult to analyse in some cases [194, 196]. The variability and uncertainty of solar and wind energy resources have created new challenges that can cause quick increases or decreases in power generation [197]. Solar and wind energy inputs vary over time due to the influence of meteorological fluctuations. These normal variations occur across periods of seconds, minutes, hours, days, weeks, months, seasons, and even years. Solar and wind energy resources at prospective geographical locations must therefore be investigated for their potential economic utilisation [198]. The key to optimal utilisation and the integration of solar and wind power is understanding these variations and their predictability. Forecasting modelling tools are widely used to assist utilities to manage grid operations by advising estimated renewable generation in advance [199]. Various research has been conducted across the world to discuss forecasting models to assess future electricity generation from solar and wind sources.

A great predictive solution was proposed by Shafiullah [199] in the form of a hybrid integration system that can predict solar and wind generation in advance, supported by a model that can analyse the techno-economic and environmental prospects of renewable energy; as well as a load management system to manage customer load demand efficiently. The comprehensive proposed system was developed to be applied in the subtropical climate of Central Queensland. Moreover, these types of effective models can support the implementation of solar and wind energy across many locations due to the high quality of efficiency and cost reductions. To maximise the resultant benefits and maintain reliability at the required level, advanced tools for handling solar and wind energy, such as future forecasting and management algorithms, can be employed. Solar and wind energy forecast tools that predict the next few hours, days, or weeks can play a crucial role in the processes of management operator systems. Al-Alawi and Al-Hinai [200], Lopez et al. [201], and Mohandes et al. [202] developed predictive models to forecast solar irradiation based on an Artificial Neural Network (ANN) through machine learning. Most of these models achieved a high forecasting accuracy. The field of power system forecasting has developed quickly due to the increasing proportion of total energy share provided by renewables in many countries. Ji et al. [203] discussed a forecasting model which was used to predict mean hourly wind speed using a Support Vector Machine (SVM) technique. The proposed model is a novel algorithm for wind speed

prediction, wherein forecasting error is improved by a support vector classifier which outperforms transitional support vector regression algorithms. More and Deo [204] applied a technique to predict daily, weekly, and monthly wind speeds at two coastal sites in India using an ANN. Satisfactory prediction values with low deviations and high levels of correlation were observed. This type of forecasting technique was applied and trained with past data in an autoregressive manner by backpropagation and cascade correlation algorithms. However, prediction accuracy was reduced as the interval of prediction decreased from a month to a day. The majority of predictive models discussed in previous studies were built to cover short or medium-term projections, although there remains a requirement to build a long-term predictive model due to cost-effectiveness, energy saving, and climate requirements. The analysis of large sets of historical solar and wind speed data from meteorological measurements and system operators at typical site locations allows the determination of likely future variations in net generated power over the long run. Further, to assess the economic feasibility of solar and wind power generation projects, several optimisation approaches can be employed to analyse the performance of solar and wind resources over the long-term [4]. Optimisation modelling and statistical analyses can be employed to provide an effective solution in selecting suitable sites for the deployment of solar plants and wind farms to generate large-scale power from RES, significantly reducing the cost of power generation and CO_2 emissions [205]. There is a need to develop predictive solutions due to sustainability requirements and climate change issues. Probabilistic forecasting is one of the flexible management tools that enable a shift from deterministic to stochastic methods to find robust solutions. The probabilistic approach can be implemented in this research to evaluate future power system performance and the behaviour of solar and wind resources based on MCS and BM models using a large volume of historical data to provide a wide range of options for future predicted values.

Therefore, this chapter aims to analyse and predict the future performance of the power systems, solar energy, and wind speed resources of the GCC region to support the integration of solar and wind energy generation projects. The predictive results of the GCC countries are presented in *A.1 Appendix 1*. Further, this chapter synthesises the positive criteria of solar and wind energy's benefits and attempts to compensate for its deficiencies. In addition, this chapter simulates the future performance of power system, solar and wind energy penetration scenarios in those GCC countries which represent

divergent climate profiles. This study examines the distributions of changes in solar irradiance, wind speed, and temperature that may occur at different times over a long period. Although this chapter studies the future performance of the power system and solar/wind resources in GCC countries, it can be applied to other countries once a large amount of historical data is available.

5.2 Development of the Monte Carlo Simulation and Brownian Motion Model

MCS and BM were employed to estimate the future performance of power sectors, including solar and wind energy, based on temperature fluctuations across the GCC region. MCS is a computerised mathematical technique that is employed to produce random values based on a known distribution of historical data. MCS was applied to model the probabilities of several outcomes that cannot be easily predicted, due to the intervention of random variables, to understand distribution and uncertainty in a prediction model. This approach is a form of quantitative analysis that is employed to randomly calculate the Sharpe ratio for thousands of selected allocations. MCS and BM were employed to refer to a universe of different simulation approaches, including future energy prediction scenarios, helping researchers to make informed decisions. BM is technically a Markov process, which means the values follow a random walk and are consistent with the weak form in which past value information is already incorporated. Thus, the next estimated value's movement is "conditionally independent" on the movements of past values. Standard BM is a stochastic process in that $B = [B(t): t \geq 0]$ as continuous sample paths [206]. The ultimate aim of describing the details of MCS and BM processes is to use these concepts for real option theory applications. The newly generated dataset is larger than the historical initial dataset, which would provide immense opportunities to understand and analyse the produced scenarios. It would be a big challenge to generate an accurate long-term prediction, which depends on the size of the historical data and suitably selected approaches. These are common issues with all approaches that are used to build future scenarios, although MCS and BM approaches have the great advantage of using a small amount of historical data, including generating unlimited future values, which can avoid this issue to generate long-term scenarios.

5.2.1 Monte Carlo Simulation and Brownian Motion Structure

Python software simulates and predicts the development of values from 1,000 to 10,000 times which would generate maximum and minimum expected average values. Python's package library is very extensive, offering a wide range of facilities and providing access to system functionality with large memory. Such a large memory is essential in statistical processes given the huge historical data sets and large future predicated data sets involved. The holistic method process of preparing such historical data and building the predictive model is shown in Figure 5-1. In addition, equations (5–1 to 5–3) [206] were employed to yield future values of power, wind speed, solar irradiance, and temperature, where D is the drift, V is the variance, S is the standard deviation, u is the average log value (or percentage drift), and r is the long-share value and the natural logarithm of BM. S_t is the value for day (t), while S_{t-1} is the value observed on the previous day (t − 1) when S = 1, the mean = 0, while Z is the number of standard deviations, and δ is the step size of the latent variables. Furthermore, equations (5–1 to 5–3) were implemented and integrated into the codes in order to build a sufficiently accurate long-term predictive model. All the algorithms and variables of the MCS and BM approaches were defined based on Python libraries, including NumPy, Pandas, and SciPy functions. The codes and predictive model were evaluated at multiple stages based on comparing different algorithms, oftentimes in terms of computational and predictive performance, and selecting the best model efficiency from a specific hypothesis space, as shown in Figure 5-1.

$$D = u - \frac{1}{2} * V \tag{5-1}$$

$$r = D + S * e^{r} \tag{5-2}$$

$$S_t = S_{t-1} * e^{\left(r - \frac{1}{2} * S^2\right) \delta_t + S\,[\sqrt{\delta}_t . Z_t]} \tag{5-3}$$

Equations 5–4 and 5–5 represent the velocity profile rendered by a power function and the logarithmic function, respectively, which are used to measure the wind speed at different altitudes [207]. U is the wind speed at a required height; Uref is the reference wind speed; Zref is the anemometer height; Z is the required height; s is the shape of the power-law profile; and Zo is the surface roughness length. Compound yearly growth rate

(CAGR) formula can be used to compute the annual growth rate (5-6). In addition, f represents the ultimate valve, s represents the initial value, and y represents the total number of years.

$$\frac{U}{U\,ref} = \left(\frac{z}{z\,ref}\right)^{S} \tag{5-4}$$

$$\frac{U}{U\,ref} = \left(\frac{Ln(z/zo)}{Ln(z\,ref/zo\,)}\right) \tag{5-5}$$

$$CAGR\ = \left(\frac{f}{s}\right)^{1/y} - 1 \tag{5-6}$$

5.2.1.1 Data preparation

Historical data was collected for GCC countries to predict the long-term performance of their respective power sectors and the three types of solar irradiance across the region. In addition, the MCS and BM model is used to predict future wind speeds and temperatures. The power sector data encompasses electricity generation, consumption, peak load, and installation capacities, as presented in Figure 1-2 to Figure 1-5, given at quarterly intervals. Furthermore, the historical data for the three types of solar irradiance for KSA, specifically GHI, DNI, and DHI, are presented in Figure 4-4 to Figure 4-8 as daily intervals. The historical data for other GCC countries, including the three types of solar irradiance, wind speed and temperature values are presented in *A.5 Appendix 5*. Historical wind speeds and temperature data for the KSA are presented in Figure 4-9 to Figure 4-16 in daily intervals. To achieve better future prediction values, the quality and quantity of the datasets are important. The data were reviewed, checked, and analysed to control for any missed or duplicated values. All the datasets were maintained as stationary with p-values of less than 0.05 (p-values < 0.05).

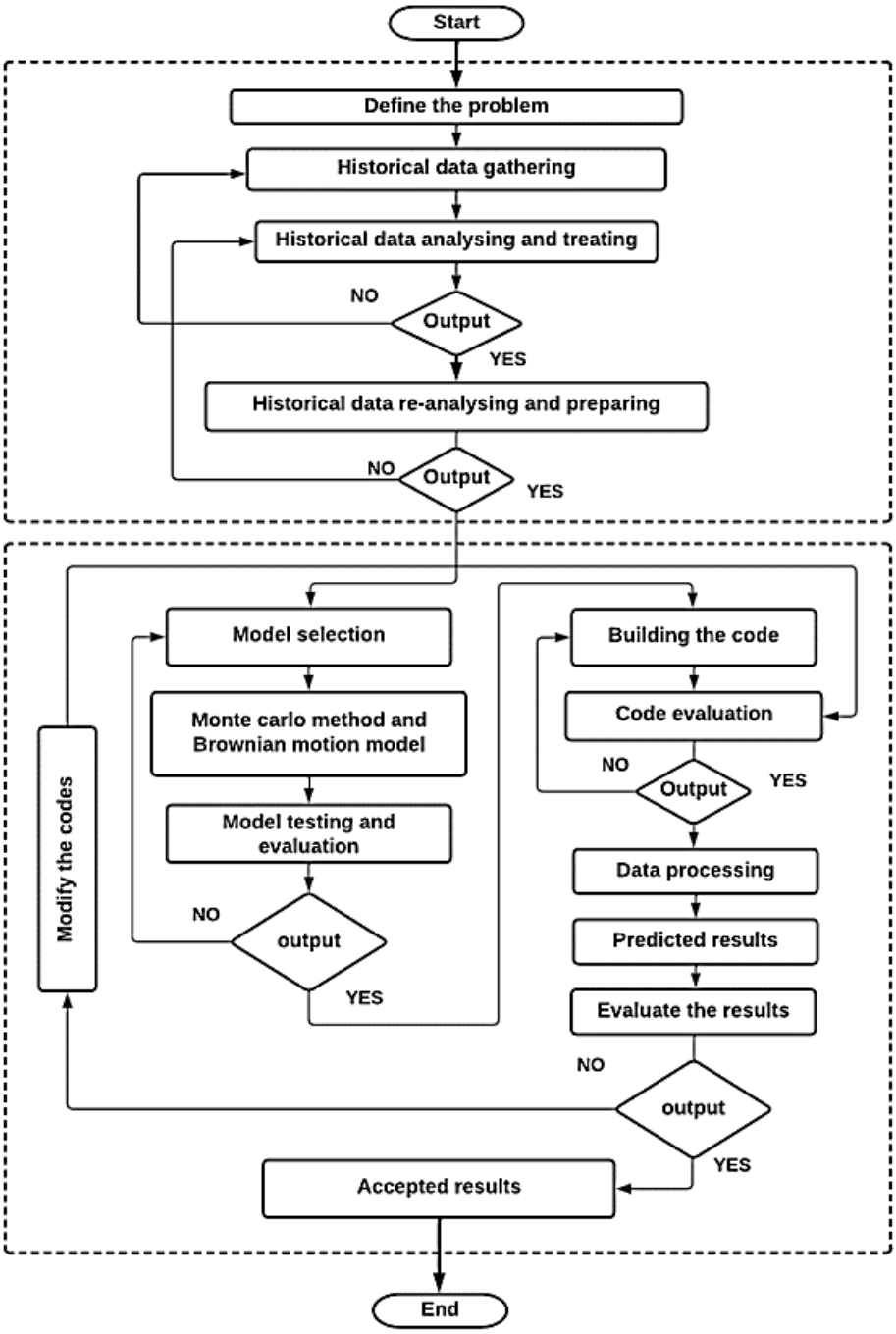

Figure 5-1. The processes of developing the MCS and BM predictive model.

5.3 Analysis and Discussion of Results

The MCS and BM predictive model was developed to predict the values for the GCC electricity power sector until 2050 at yearly intervals. Moreover, the MCS and BM predictive model was employed to predict the weather values for the GCC region for 1,000 days in the future until the 26th of March 2024, again as daily interval values. The electricity power sector data set includes electricity generation, consumption, peak load and installed capacity, while the weather values are comprised of irradiance, wind speed and temperature. All the estimated values will be analysed and discussed in this section. The results for the KSA will be presented in this section, while the results for the other GCC countries will be presented in *A.1 Appendix 1*.

5.3.1 Predictions for Electrical Power

Based on the future estimated results of the MCS and BM predictive model and the 40 year generative history of the GCC power sector, energy generation in KSA, the largest member state, is forecasted to be 398 TWh in 2030, rising to 478 TWh in 2040, and 600 TWh in 2050, as illustrated in Figure 5-2a. In addition, Figure 5-2b shows the range of distribution values for KSA electricity generation in TWh for the next three decades until 2050, while the grey range shows the highest concentration of forecasted values. It is however possible that the next dispersed value intervals can fall inside the grey range. Moreover, Oman's power generation is forecasted to be 52 TWh in 2030 and 61.7 TWh in 2040, rising to 82.30 TWh in 2050, as shown in Figure A.1–1. The UAE's power generation is expected to be 192 TWh in 2030, 223 TWh in 2040, and 239 TWh in 2050, as presented in Figure A.1–10. Kuwait's future power requirements are calculated to be 92 TWh in 2030, 106 TWh in 2040, and 118 TWh in 2050, as illustrated in Figure A.1–19. Further, as indicated in Figure A.1–28, Qatar's future power generation is predicted to reach 65 TWh in 2030, then climbing to 77 TWh in 2040 and 106 TWh in 2050. According to Figure A.1–37, Bahrain's electricity generation is forecast to be 21.30 TWh in 2030, falling to 19.88 TWh in 2040, and then increasing to 22.5 TWh by 2050.

The electricity generated normally seeks to approximate to demand, although generation usually seeks to exceed consumption due to a requirement for balance between supply and demand. Figure 5-3a reveals that the electricity consumption in KSA will be 377

TWh in 2030, rising to around 460 TWh in 2040; while the predicted electricity consumption in KSA is estimated at 540 TWh in 2050. Figure 5-3b shows the long-term distribution values for forecasted KSA electricity consumption. In contrast, Oman is expected to consume 43.82 TWh in 2030, 59.65 TWh in 2040, and 69.12 TWh in 2050, as presented in Figure A.1–2. Predicted electricity consumption values for the UAE are 165 TWh in 2030,184.50 TWh in 2040, and 245.50 TWh in 2050 (Figure A.1–11). The corresponding figures for Kuwait are 85.70, 107, and 123.40 TWh, respectively (Figure A.1–20). On the other side of the GCC region, Qatar is anticipated to consume 57.40 TWh in 2030, 73.22 TWh in 2040, and 83.32 TWh in 2050 (see Figure A.1–29). As shown in Figure A.1–37, Bahrain's power consumption is expected to reach 21.45 TWh in 2030, then decreasing to 20.33 TWh in 2040, and eventually rising to 23.50 TWh in 2050.

In addition, the MCS and BM prediction model reveals an important aspect of the development for the maximum and minimum electrical load values in GCC countries over the next 30 years, as evidenced by the evolution in values. The electrical load values for the KSA are forecasted to be 72.5 GW in 2030 and 82 GW in 2040, continuing to rise to reach 96 GW in 2050 (see Figure 5-4). Oman’s peak load is predicted to reach 8.76 GW in 2030, 9.43 GW in 2040, and 14.89 GW in 2050, as shown in Figure A.1–3. During the summer, temperatures rise across all GCC countries, which has an obvious influence on the change in the expected peak load values, yet the most significant aspect is the long-term consequences of climate change in the GCC region. According to Figure A.1–12, the predicted electricity peak load values for the UAE are calculated as 37.3 GW in 2030, 42.20 in 2040, and 54.97 GW in 2050. Kuwait’s predicted electricity peak load values are 16.64 GW in 2030, 16.90 GW in 2040, and 18.79 GW in 2050, as illustrated in A.1–21. Geographically speaking, Kuwait is situated in the northeastern corner of the GCC region and is considered a small country in terms of population and area. The dry, sandy Arabian desert dominates most of Kuwait’s landscape and hence, the country's energy consumption is minimal and easily controlled. The predicted electricity peak load values for Qatar are expected to reach 10.35 GW in 2030, 12.42 GW in 2040, and 16.20 GW in 2050, as shown in Figure A.1-30. As Bahrain is the smallest country in the GCC region, its estimates are lower at 21.30 GW in 2030, 19.99 GW in 2040, and 23.17 GW in 2050, as presented in Figure A.1-37.

To meet the forecasted growth and development in the GCC power sector, electrical installation capacities must be considered. The electricity installation capacity for the

KSA was expected to be 106 GW in 2030, increasing to 117.5 GW in 2040, until finally reaching 128 GW in 2050, as illustrated in Figure 5-5. The electrical installation capacity values for Oman are predicted to be developed to 13.98 GW in 2030, 18.87 GW in 2040, and 21.88 GW in 2050, as shown in Figure A.1–4. Based on Figure A.1–13, the predicted installed electrical capacities for the UAE are estimated to be 44.88 GW in 2030, 48.50 in 2040, and 60.98 GW in 2050. In addition, Kuwait's predicted installed electrical capacity values are 24.50 GW, 28 GW in 2030, and 35.79 GW in 2050 (see Figure A.1–22). Qatar's predicted installed electrical capacity values are forecasted to be 16.99 GW in 2030, 21.98 in 2040, and 25.78 GW in 2050 (see Figure A.1–22); while Bahrain's predicted installed electrical capacity values are 9.98 GW in 2030, 13.98 GW in 2040 and 17.99 GW in 2050 (see Figure A.1–40).

The estimated results of the MCS/ BM prediction model revealed that predicted electricity generation, consumption, peak load and installed capacities in the GCC region will continue to increase due to an increasing population and higher summer temperatures. Further, the rapid desertification of the region is one of the greatest environmental issues of our time. Those water-scarce regions of the GCC area are deteriorating due to the combined effects of climate change, land mismanagement, and unsustainable freshwater usage. The lack of drinking water in the region necessitates an increase in the construction of desalination plants. The great urban and economic renaissance of the GCC region has contributed to an increase in energy consumption in recent decades. Nevertheless, the region is still on the verge of very large future development projects and these obligate more energy consumption. Therefore, the best solution is to harness the region's RES, including wind and solar energy, as well as regulating energy consumption more effectively in the region.

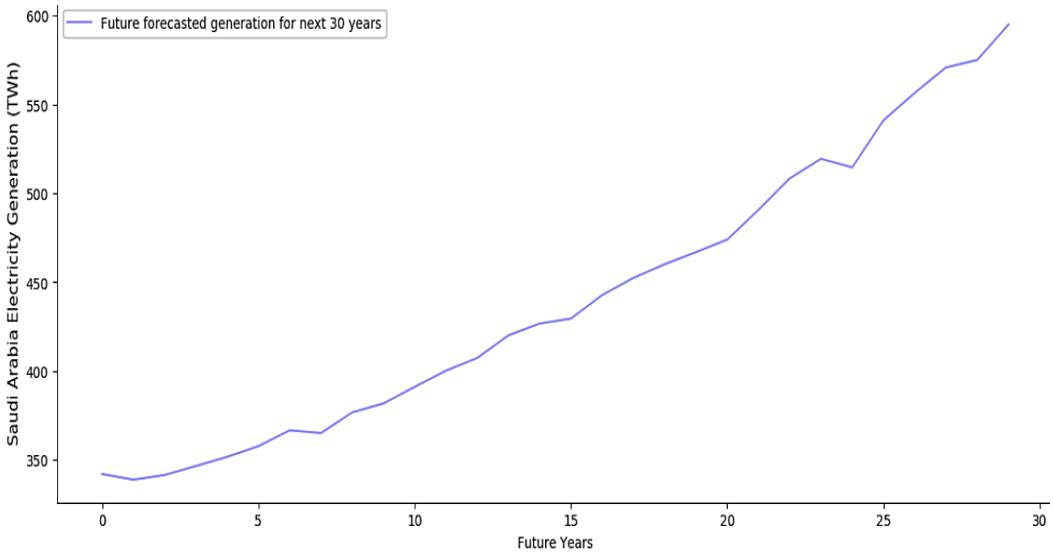

(a)

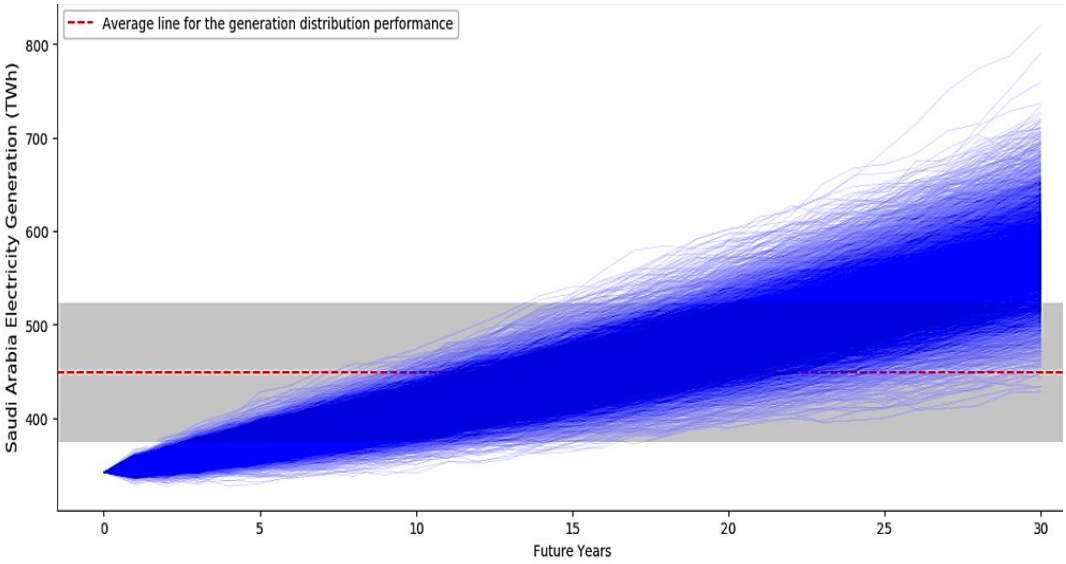

(b)

Figure 5-2. (a) Randomly selected sample predicted electricity generation values for a 30-year period from 2021 to 2050 for the KSA and (b) the predicted electrical generation distribution performance by MCS and BM.

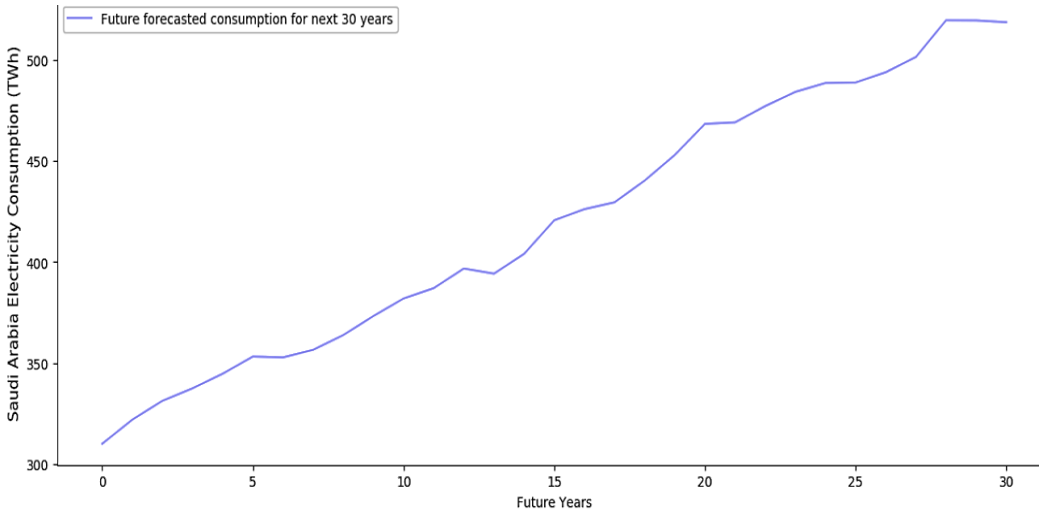

(a)

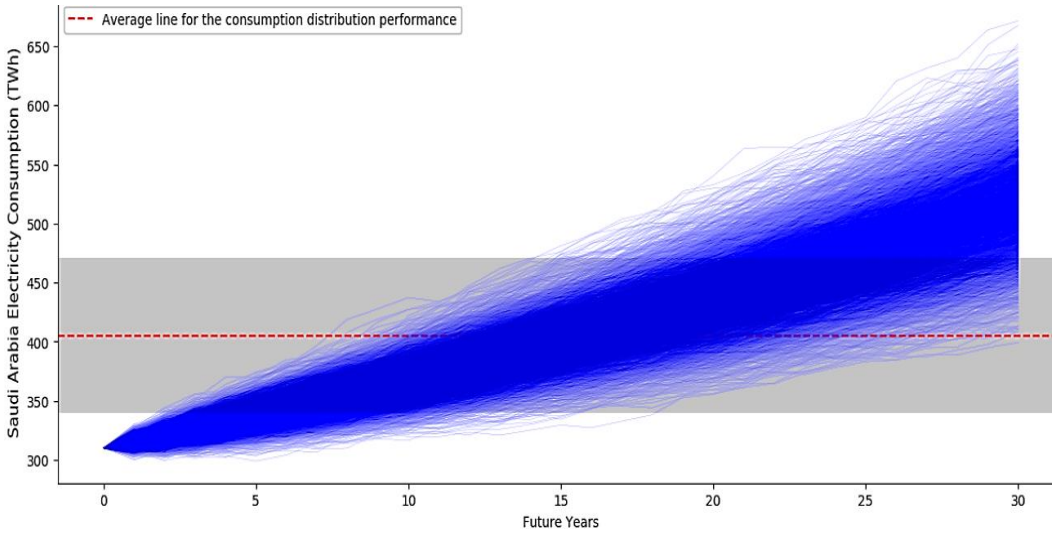

(b)

Figure 5-3. (a) Randomly selected sample predicted electricity consumption values for the 30-year period from 2021 to 2050 for the KSA and (b) predicted electricity consumption distribution performance by MCS and BM.

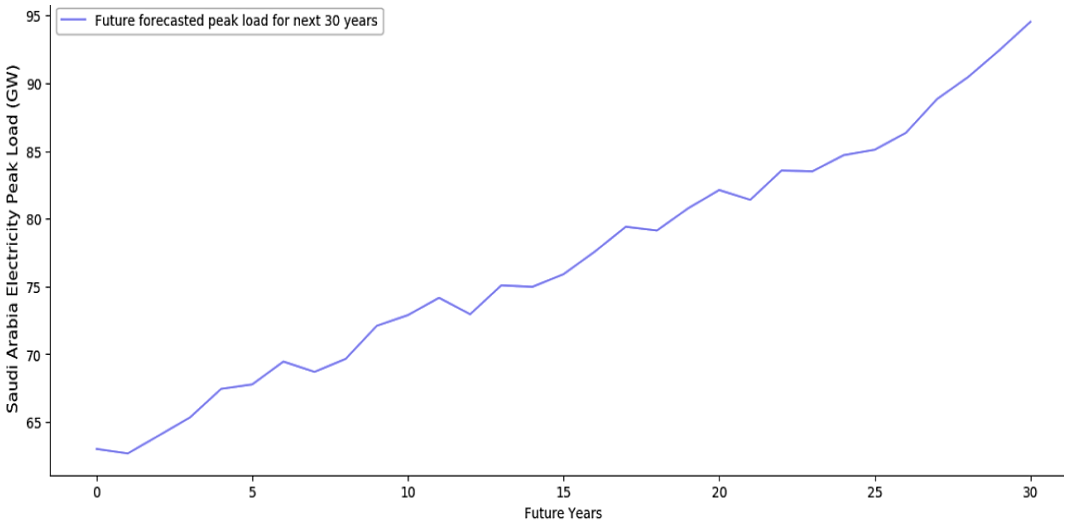

(a)

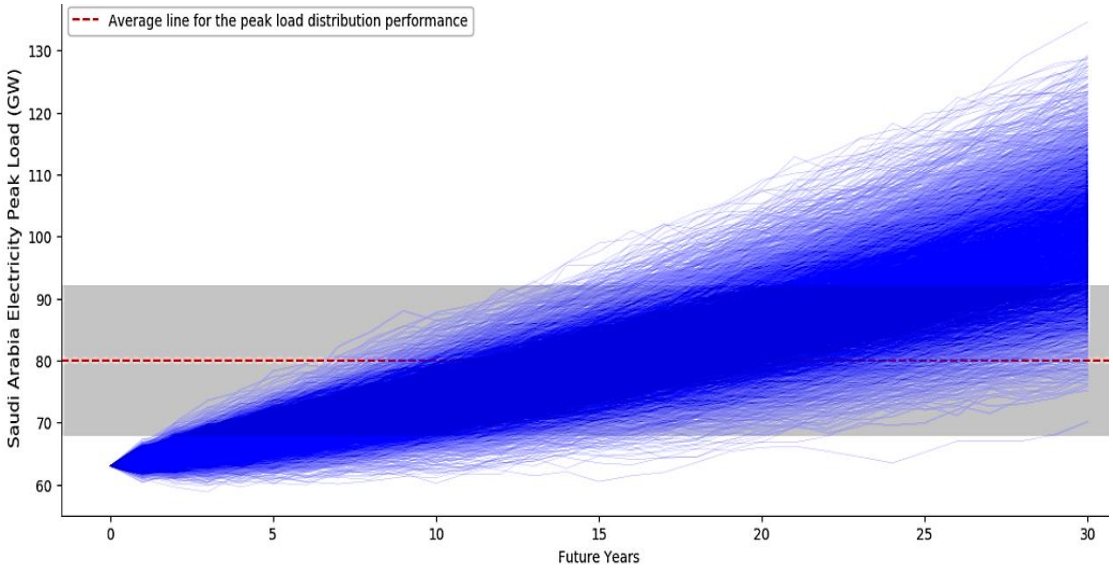

(b)

Figure 5-4. (a) Randomly selected sample predicted electricity peak load values for the 30-year period spanning 2021 to 2050 for the KSA and (b) predicted electricity peak load distribution performance by MCS and BM.

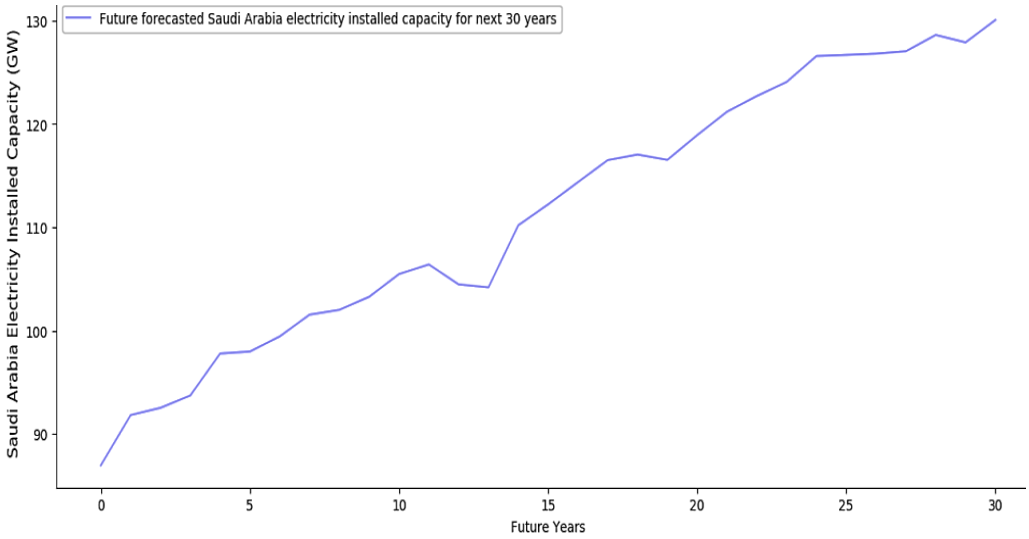

(a)

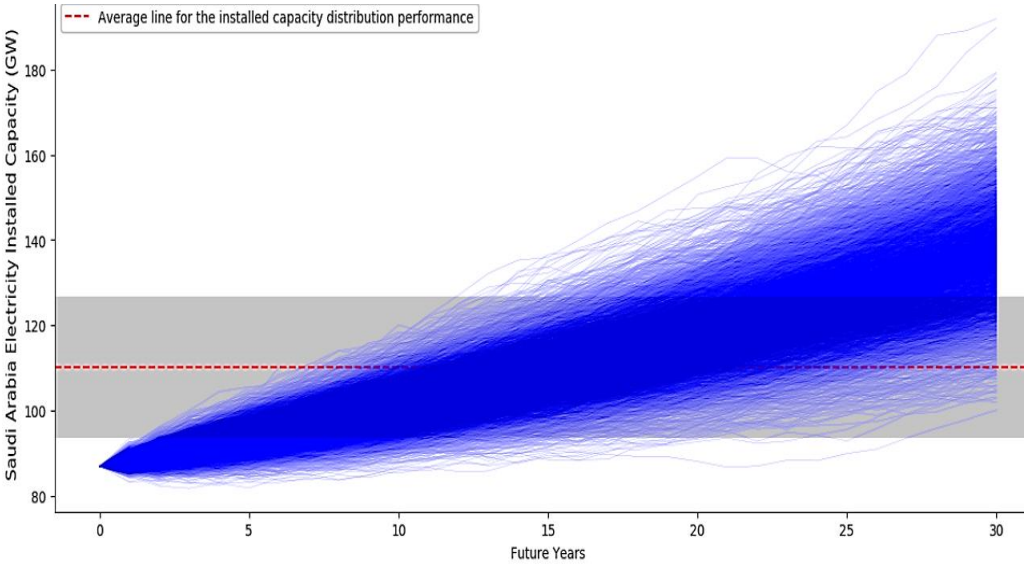

(b)

Figure 5-5. (a) Randomly selected sample predicted electrical installed capacity values for the 30-year period from 2021 to 2050 for the KSA and (b) predicted electricity installed capacity distribution performance by MCS and BM.

5.3.2 Prediction Results for Irradiance, Wind Speed and Temperature

To encourage the implementation of solar and wind energy across the GCC region, long-term predictive models of solar irradiance, wind speeds, and temperatures must be designed and exhaustively tested. Thus the KSA, Oman, UAE, Kuwait, Qatar, and Bahrain were selected for weather analysis and evaluation to cover a range of different climatological conditions across the GCC region. The daily total values for GHI, DNI, and DHI were estimated to enable an analysis of their future behaviours for the next thousand days from 26th June 2021. Weather patterns are somewhat random and therefore extremely difficult to predict without historical data. The inherent variability of future values of solar irradiance, wind speed, and temperature means that historical records are extremely useful for programming analytical and predictive tools across a wide range of applications.

According to the MCS and BM future analyses, the forecasted daily total values of GHI in the KSA were predicted to reach 9,620 watts per square metre (W/M^2) as the maxima and 6,835 W/M^2 as the minima, as shown in Figure 5-6a. In addition, the distribution performance describes the future daily behaviours of solar GHI in the KSA, as illustrated in Figure 5-6b. As shown in Figure A.1–6a, the greatest daily solar GHI value in Oman was 10,465 W/M^2, while the lowest was 8,188 W/M^2. In addition, the predicted solar GHI distribution performance in Oman for the following 1,000 days is presented in Figure A.1–6b. The solar GHI for the UAE was forecast to be 10,111 W/M^{2}as a maxima and 7,460 W/M^2 as a minima over the next 1,000 days (Figure A.1–14). Kuwait's estimated solar GHI maxima and minima are 9,560 W/M^2 and 8,100 W/M^2, respectively, as shown in Figure A.1–23. According to Figure A.1–32, Qatar's solar GHI maxima and minima are predicted to be 9,230 W/M^2 and 6,145 W/M^2, respectively; whereas Bahrain's solar GHI is anticipated to reach a maxima of 9,000 W/M^{2}and a minima of 6,115 W/M^2 (see Figure A.1–41).

Further, the estimated maximum daily total value for DNI was 4,998 W/M^{2}with a minima of 3,500 W/M^2 in the KSA, as shown in Figure 5-7. Based on Figure A.1-6, the highest and lowest anticipated solar DNI values for Oman are 8,090 and 7,400 W/M^2, respectively; while the forecast solar DNI values for the UAE are 8,288 W/M^2 as a maxima and 6,700 W/M^2 as a minima (see Figure A.1–15). As shown in Figure A.1–24a, the maxima for Kuwait's estimated solar DNI is 8,374 W/M^2 while the minima is 7,161

W/M^2. Figure A.1–24b shows the predicted solar DNI distribution performance for Kuwait. The highest forecasted value of Qatar's estimated solar DNI is 4,337 W/M^2, while the lowest is 2,911 W/M^2 as shown in Figure A.1–33a. Meanwhile, the expected solar DNI distribution performance for Qatar is given in Fig A.1–33b. The future predictions of the MCS and BM model anticipate that Bahrain's daily total DNI values will vary from 8,474 W/M^2 to 5,750 W/M^2, as shown in Figure A.1–42.

Moreover, the daily total of DHI in the KSA was expected to range from 862 W/M^2 to 681 W/M^2, as shown in Figure 5-8a. As indicated in Figure A.1–7, the daily total DHI in Oman was anticipated to range between 990 W/M^2 and 763 W/M^2 (as shown in Figure A.1–16); whereas the corresponding figures for the UAE's solar DHI are expected to be 838 W/M^2 and 665 W/M^2, respectively. As illustrated in Figure A.1-25, the maxima for Kuwait's predicted solar DHI is 920 W/M^2, with a minima of 934 W/M^2. The highest forecasted value for Qatar's solar DHI is 450 W/M^2 and the lowest 286 W/M^2, as shown in Figure A.1–34. The solar DHI in Bahrain is expected to reach 829 W/M^2 as a maxima and 711 W/M^2 as a minima (see Figure A.1–43).

Based on the results of this research, the GCC region exhibited extremely promising daily solar irradiance. This makes the GCC countries suitable for solar power plant projects, especially Oman, the KSA, Kuwait and the UAE. In addition to the fact that the KSA's northern region is supported by vast open tracts of land with relatively low temperature values, its southern region is characterised by mountainous areas with relatively cloudy weather in some parts and lower temperatures. These results can be ascribed to the GCC central region generally, which has a history of long dust storm spells plus typhoons, terrain issues and arid conditions, especially during the summer. Meanwhile, the GCC's northwestern region is characterised by a distinguished location with clear skies which are free from dust, have relatively low temperatures, and a moderate climate throughout the year, thereby explaining the divergence in the results. The GCC's southern region is characterised by lower temperatures, dusty, cloudy weather and foggy days. The fact is that, on a clear day, direct solar irradiance represents between 85% and 90% of the total amount of solar irradiance reaching the surface of the earth. On a foggy or cloudy day when we "cannot see the sun", the direct component of solar irradiance is essentially very low. The variation of all of these factors, including geographical locations and climate change issues, attenuate the direct component and change solar irradiance values. In general, a considerable amount of effort has been spent cataloguing, measuring, and

developing predictive analytical models to forecast these effects. However, the future evaluation of solar energy resources has shown that the GCC region possesses abundant potential solar energy resources with more than ample opportunities to diversify the GCC's energy mix. Theoretically speaking, the findings of this research offer great incentives to push ahead with investments in solar energy.

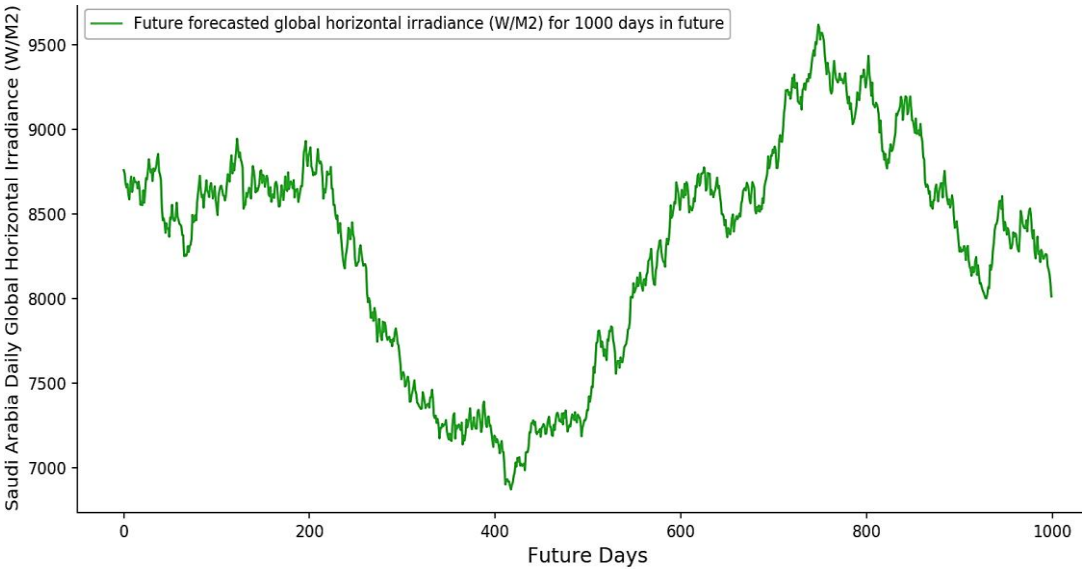

(a)

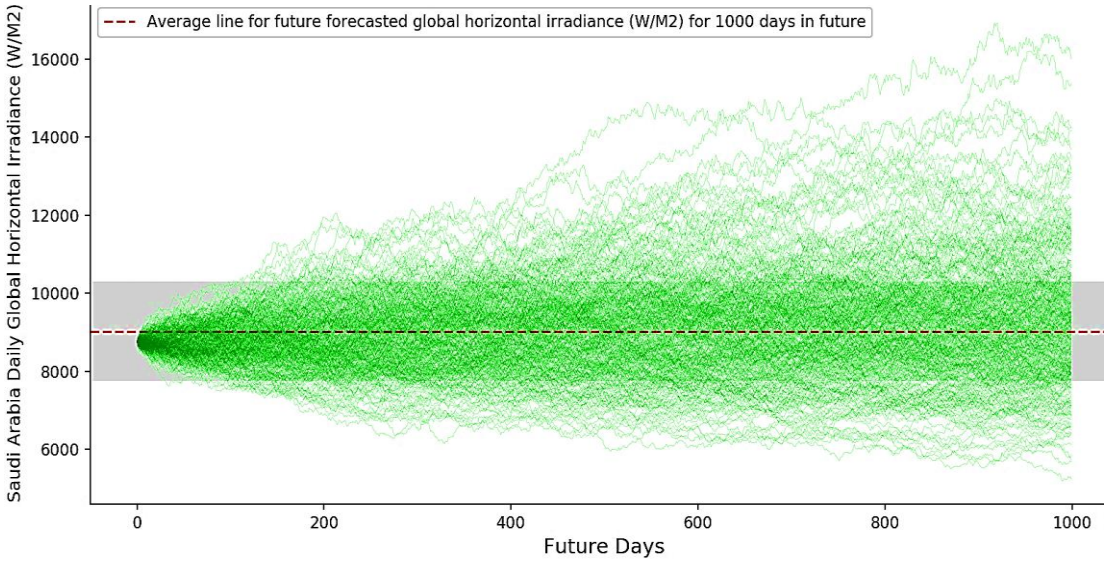

(b)

Figure 5-6. (a) Randomly selected sample predicted solar GHI values for a future 1,000 days for the KSA and (b) predicted solar GHI distribution performance by MCS and BM.

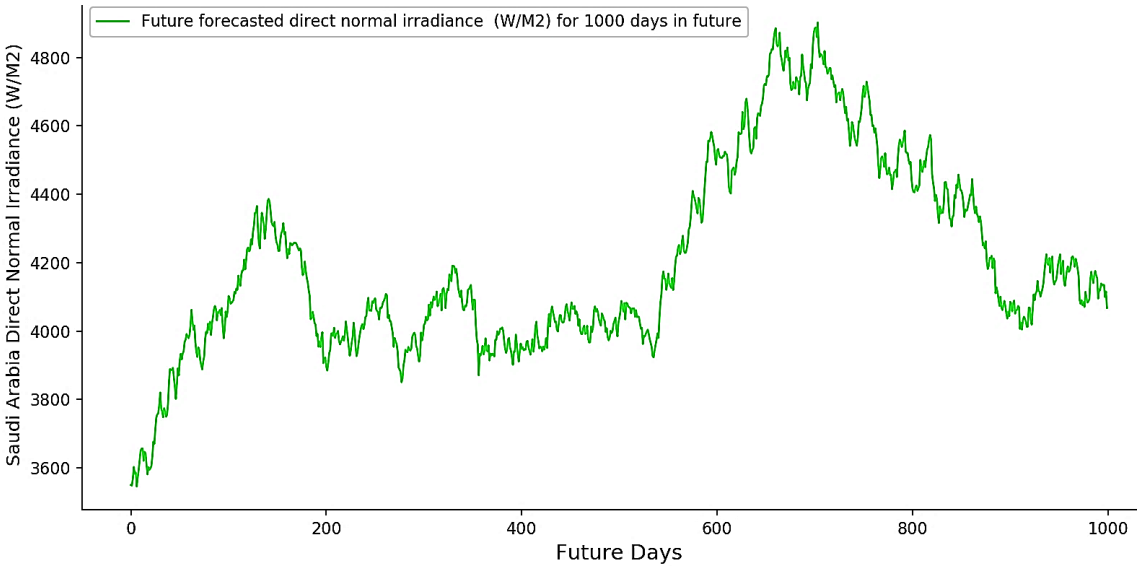

(a)

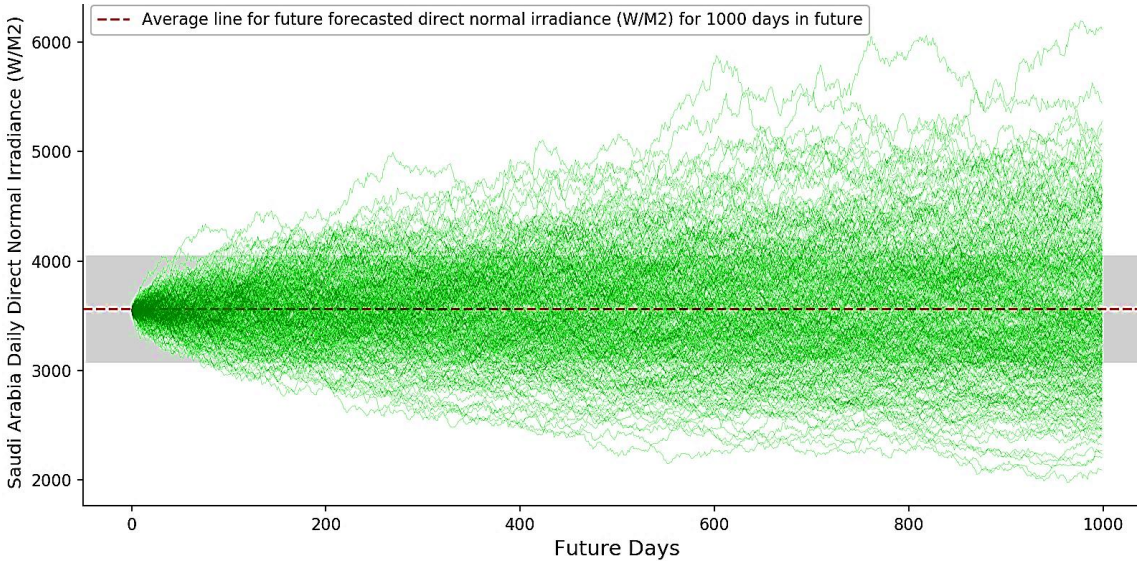

(b)

Figure 5-7. (a) Randomly selected sample predicted solar direct irradiance (DNI) values for 1,000 future days for the KSA and (b) predicted solar DNI distribution performance by MCS and BM.

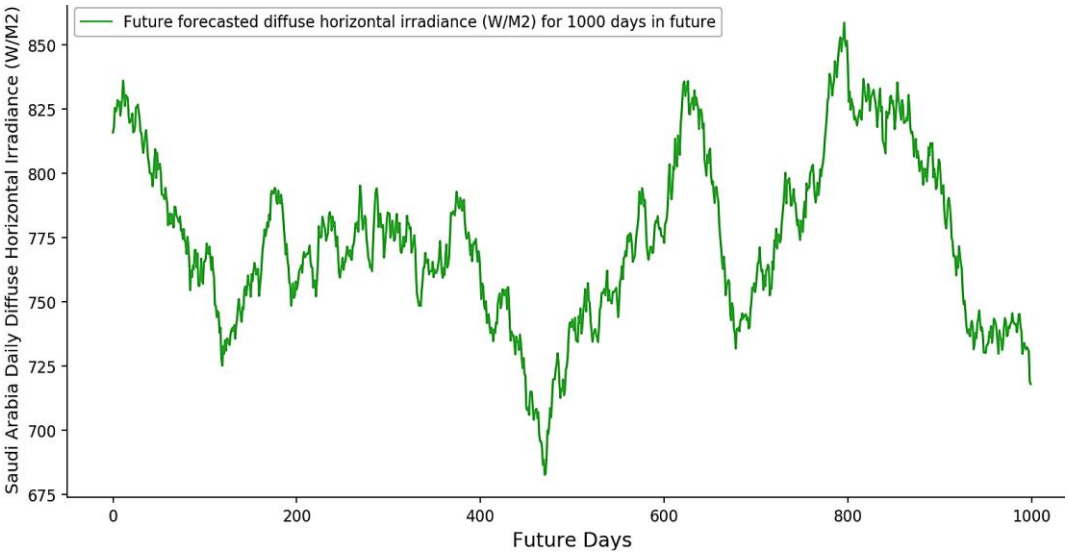

(a)

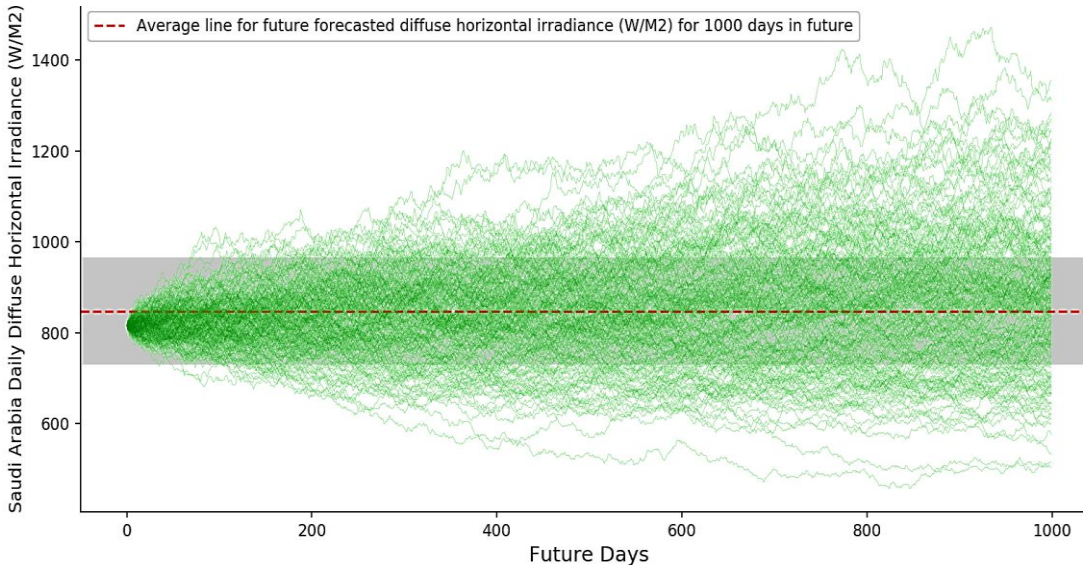

(b)

Figure 5-8. (a) Randomly selected sample predicted solar DHI values for 1,000 future days for the KSA and (b) predicted solar DHI distribution performance by MCS and BM.

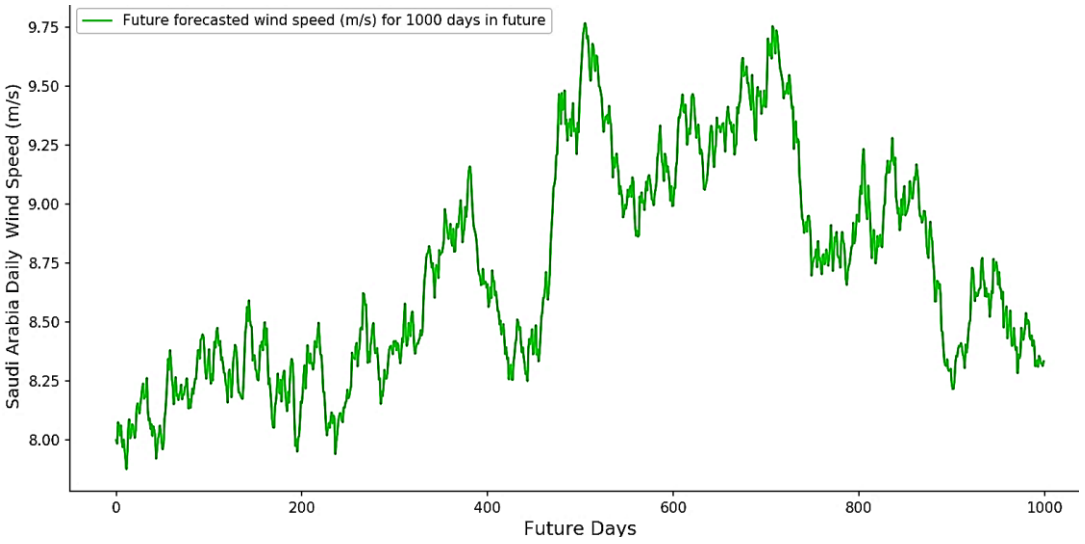

(a)

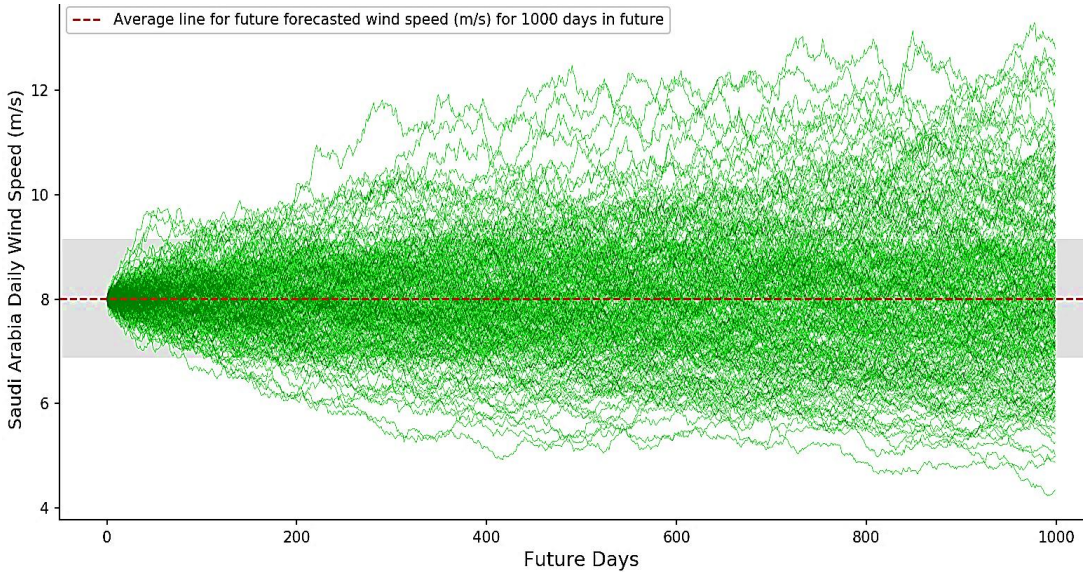

(b)

Figure 5-9. (a) Randomly selected sample predicted wind speed values for 1,000 future days in the KSA and (b) predicted wind speed distribution performance by MCS and BM.

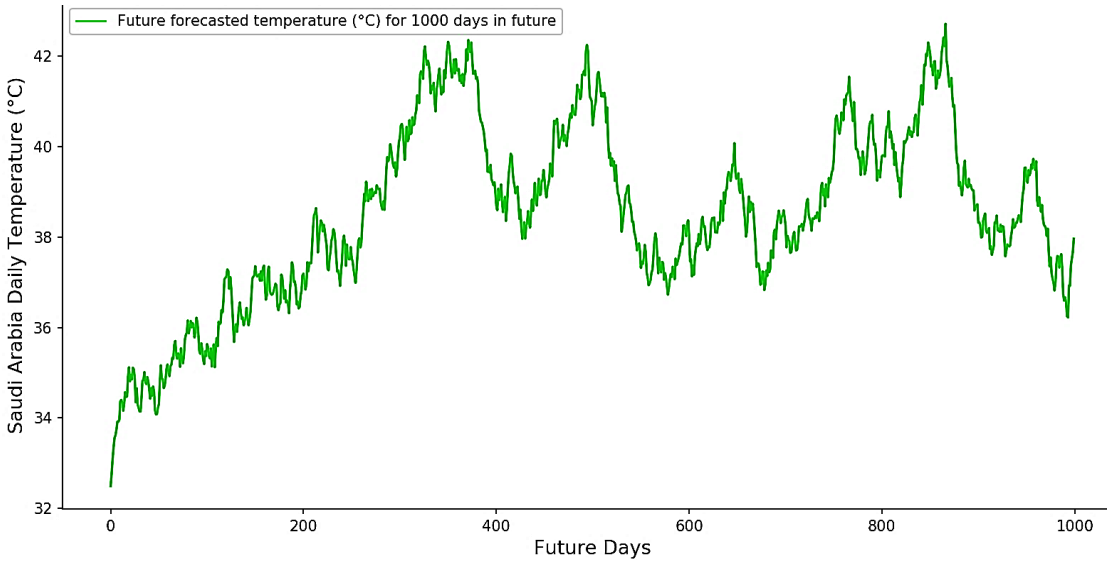

(a)

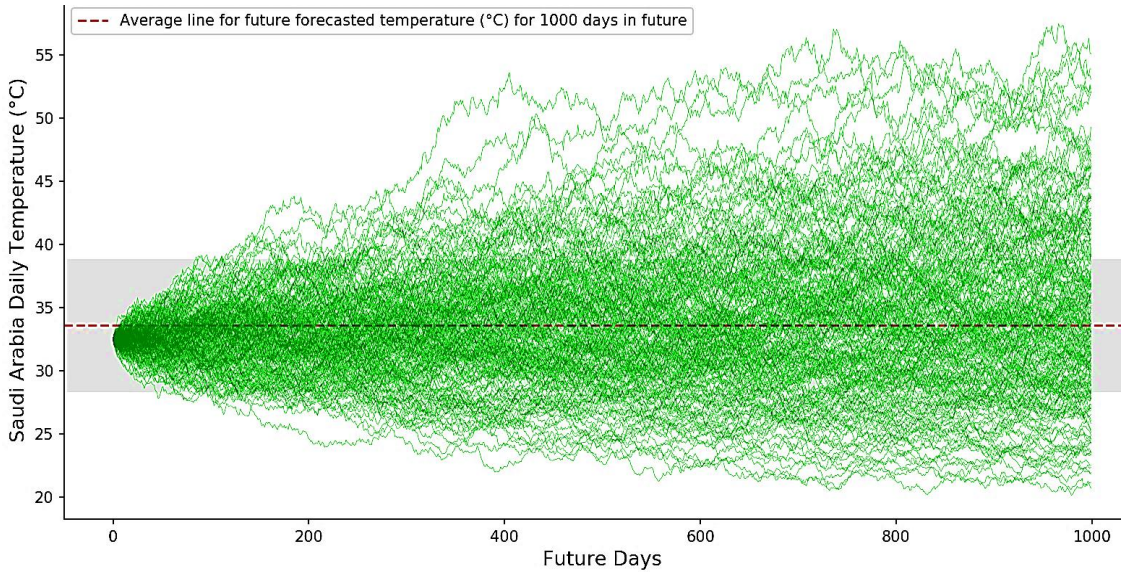

(b)

Figure 5-10. (a) Randomly selected sample predicted temperature values for 1,000 future days for the KSA and (b) future temperature distribution performance as predicted by MCS and BM.

The wind speed distribution levels were plotted to gain further insight into the GCC region to permit extrapolation between the various sites and the predicted results. The daily wind speed, as measured in the KSA, was predicted and it was expected that the maxima and minima would be 9.77 and 7.76 $m.s^{-1}$, respectively, as shown in Figure 5-9a together with good wind speed distributions (Figure 5-9b). The maxima and minima of the daily wind speeds in Oman were forecast to be 12.85 and 9.24 $m.s^{-1}$, respectively, as illustrated in Figure A.1–8. For the UAE, the daily wind speed was anticipated to be between 5.35 and 1.33 $m.s^{-1}$ (see Figure A.1–17). Based on Figure A.1–26, it is observed

that the daily wind speed in Kuwait varies between 11.95 and 8.40 $m.s^{-1}$ and, for Qatar, 8.95 and 5.30 $m.s^{-1}$ (see Figure A.1–35). With respect to Bahrain, the daily wind speed was found to vary between 8.3 and 5.75 $m.s^{-1}$, as shown in Figure A.1–44.

The wind speed changes from one site to another due to various factors, including different geographical locations and meteorological conditions in relation to differences in atmospheric pressure. In general, the GCC region is characterised by a wide desert area with some mountainous areas in the south, valleys in the central region, and small hills in the northwest. In addition, Oman, and the southern and western regions of the KSA are characterised by high plateaus and mountains containing agricultural areas. The effect of terrain features that may cause local variations in wind speed was reflected in the predicted values for wind speeds. Based on the historical data derived from the GCC region over the past 36 years (1st January 1985 to 26th June 2021), in terms of daily performance and MCS and BM future analyses, Oman recorded the highest wind speed range in the region (12.85 to 9.24 $m.s^{-1}$), followed by Kuwait (11.95 to 8.40 $m.s^{-1}$). In addition, the northwestern and southern regions of the KSA have acceptable wind energy resources for the longer term (9.77 to 7.76 $m.s^{-1}$) and these two regions are suitable for wind farm projects, as are Qatar (8.95 to 5.30 $m.s^{-1}$) and Bahrain (8.3 to 5.75 $m.s^{-1}$), respectively. However, the UAE recorded very low wind speed values (5.30 to 1.33 $m.s^{-1}$) according to the MCS and BM forecasting model. Modern wind turbines are variable-speed machines and have different wind speeds that depend on the characteristics of the selected and installed wind turbines, such as their size. In this regard, the cut-in and cut-out wind speeds of such wind turbines are 3.5 and 25 $m.s^{-1}$, respectively. Thus wind speeds are required to achieve at least 6 to 8 $m.s^{-1}$ to be economically viable.

According to the MCS and BM model's future predictions, the maximum and minimum daily temperatures of the KSA were 43°C during the winter and 32.6°C during the summer months, respectively. Figure 5-10a shows the performance, in terms of the daily temperature, for the following 1,000 days from the 26th June 2021. Figure 5-10b presents a high concentration of temperature intensity in the KSA, which varies between 20°C in the winter and 57°C in the summer during the course of the next 1,000 days. Based on Figure A.1–9, the estimated daily temperature for Oman is 35.3℃ in the summer (maxima) and 23.75 ℃ in the winter (minima). The highest daily temperature for the UAE is expected to be 41.2°C and the lowest 33.2°C (see Figure A.1–18). For Kuwait, the maximum estimated daily summer temperature is 48°C while the lowest winter

daytime temperature is 25.2°C, as illustrated in Figure A.1–27. For Qatar, the figures are 44.6°C and 33.0°C, respectively (see Figure A.1–36). Figure A.1–45 indicates that the greatest estimated daily temperature for Bahrain is 43°C in the winter and the lowest is 31°C in the summer.

Based on the historical data set for the GCC countries and MCS and BM future analyses, Oman recorded a very low daily temperature value range as compared to the other GCC countries (35.3 to 23.75°C, respectively) due to its geographical location, high mountains, and agricultural lands, while the UAE recorded the second lowest daily temperature value range (41.2 to 33.2°C). In addition, the KSA and Bahrain recorded very close lowest daily temperature values, ranging between 43°C and 32.6°C and 43°C and 31°C, respectively. The northwestern and southern regions of the KSA recorded lower daily temperature values due to low dusty weather during the summer, in some instances, and cloudy weather during the winter. However, these regions can support the implementation of solar power plants due to the large distances involved and the different types of geographical locations. While Kuwait observed the greatest daily temperature variations, the range in the GCC region as a whole was between 48.0°C and 25.2°C due to its proximity to the Iraqi desert. Meanwhile, Oman and the northwestern region of the KSA are characterised by clear skies throughout the year and less dustfall, which makes them more suitable for solar system power plants due to the low cost of cleaning the solar panels. The other GCC countries such as the UAE, Kuwait, Qatar, and Bahrain, recorded high values of solar irradiance with acceptable temperatures during the summer. The temperature values play an important role in solar power generation. As the temperature values increase, the current values rise very slightly while voltages tend to decrease more rapidly. Higher temperatures generally attenuate the power output of solar plants.

Based on the historical data and MCS and BM validation exercises, GCC countries are highly recommended for the deployment of solar and wind energy applications due to the abundance of solar and wind energy resources. Except for the UAE, which had extremely low wind speed values, the GCC countries were classified based on their 36 years of historical data for daily solar irradiance, wind speed, and daily temperature, the values for which were estimated for a thousand future days. Further, one interesting aspect of this research is that this study can be considered a roadmap to meet climate and sustainability goals by providing long-term projections for solar, wind, and average temperature performances for the GCC region as a whole. The findings of this research

can be used by a decision-maker to inform renewable energy development in the GCC region.

5.3.3 MCS and BM Model Evaluation

The MCS and BM prediction model applies a regression analysis (which describes the behaviour of an instrument) to a large set of random trials in order to construct a credible set of probable future outcomes. This is accomplished by applying the model to the data generated by the trials. The MCS and BM are alternative methods for generating potential asset changes or variance-covariance factors. The MCS and BM both presume that random shocks accompany a continuous drift. In addition, the periodic outputs obtained using the prediction model tend to follow a normal distribution. However, the subsequent multi-period data range follows a lognormal distribution instead. The MCS and BM prediction model has proven to be an exceptional investigative solution for long-term predictions for different types of historical data, including (i) four types of fossil fuel data; (ii) three types of solar irradiance data; (iii) wind speed data; and (iv) temperature data.

In addition, the MCS and BM prediction model was implemented here because it is an attempt to predict the future many times over. By the end of a simulation using this model, thousands or millions of ‘random trials’ are produced, allowing for the distribution of their outcomes to be analysed. The research motivation for applying the MCS and BM prediction method is aimed at improving decision-making capabilities, despite uncertain conditions, with a faster time resolution. The prediction model is able to cope with large volumes of historical data and different temporal intervals. The simplicity of implementation is a strength of MCS and BM techniques. Concerning the problem of time-scale separation, BM demonstrates improvements over data movement dynamics. Both MCS and BM approaches, with their relative sophistication, appear to serve as particularly effective modelling techniques for applications with demanding complexity, not only for high-level particle concentration determinations (in physical and chemical engineering) and financial applications, but also for data analysis and future forecasting relationships. Using controlled replicates, MCS and BM approaches have proven their capability to convey a random quantitative estimate. Therefore, to imitate randomness, a mechanism for generating random integers is essential. Through each MCS and BM generation, the accuracy of the findings needs to generate "excellent" pseudorandom

numbers. These approaches will doubtless have a potentially fruitful impact on the development of more accurate forecasting models.

6 Seasonal Autoregressive Integrated Moving Average with eXogenous Factors Prediction Model

In this chapter, the seasonal autoregressive integrated moving average with exogenous (SARIMAX) prediction model based on time series approach was designed to predict the long-term performance of the power sector in the GCC region based on historical data. The SARIMAX model incorporates time series data to improve its generalisation by considering the effects of the parameters selected on the expected historical data values for the next step. The historical dataset was collated from the GCC region at quarterly intervals for the period from 1980 to 2020 (*see section 6.2.7.1*). The predicted values include electrical generation, consumption, electricity peak load and installation capacities for the next 30 years (2021 to 2050). The results of the SARIMAX prediction model were analysed and discussed in this chapter, while the Figures for the other GCC countries are presented in *A.1 Appendix 1*.

6.1 Model Background

In this section, several previous studies of relevance to the SARIMAX prediction model are reviewed. Stylianos et al. [208] conducted an objective assessment of four unique forecasting models, specifically an ANN, SARIMAX, seasonal autoregressive integrated moving average (SARIMA), and the modified SARIMA model for short-term PV generation. The ANN, SARIMAX, and modified SARIMA models outperformed the SARIMA model in terms of next-day forecasting, and their analysis also revealed discrepancies in precision among these models. Sheng and Jia [209] developed a SARIMAX-LSTM-based load time series forecasting model that could enhance the accuracy of short-term load forecasting. In this hybrid model, the SARIMAX model showed a good fit, obtained the fitting residual, and then predicted the results. LSTM was used to predict the forecasting error of the SARIMAX model and modified the model's final forecasting results. The experiments demonstrated that the model is well suited for short-term load forecasting. According to Alasali et al. [210], the forecasting accuracy and precision of the rolled stochastic ARIMAX model for electricity demand and load forecasting exceeded those of the benchmark models (e.g., ANN). The developed forecasting model enhanced the forecasting performance by providing probabilistic demand scenarios to capture non-smooth demand.

Sutthichaimethee and Ariyasajjakorn [211] proposed an ARIMAX long-term energy consumption forecasting model for generating three scenarios in Thailand over the next 10, 20, and 30 years. The results of the model indicated that it offers good performance, although the model could be improved to generate scenarios in one step. In addition, the outcomes of Sutthichaimethee and Ariyasajjakorn's long-term forecasting study must be considered in terms of decision-making to reach the maximum benefit of sustainable development. Sutthichaimethee and Naluang [212] developed a long-term forecasting model based on the structural equation modelling vector autoregressive with exogeneous variables (SEM-VARIMAX) model for predicting energy consumption over a 17-year period (2020–2036). This approach is efficient for analysing causal relationships and optimising predictions. Moreover, the SEM-VARIMAX model is more appropriate for long-term forecasting than the autoregressive integrated moving average (ARIMA), MLR, backpropagation neural network, ANN, or grey models. Elamin and Fukushige [213] used a short-term SARIMAX forecasting model to forecast load demand. This model significantly outperformed MLR models with interactions, although the model needs to reduce its error metrics values. Lee and Cho [214] conducted a study to forecast Korea's electricity peak load using several forecasting models including SARIMAX, ANN, SVR, LSTM, SARIMAX-ANN, SARIMAX-SVR, and SARIMAX-LSTM. The findings outperformed the hybrid SARIMAX models and the single LSTM model. However, this study did not demonstrate that these models are more accurate in countries in terms of meteorological variations. Tarsitano and Amerise [215] developed a forecasting system based on the SARIMAX model to predict the electricity load in six Italian macro-regions. This model uses a backward stepwise regression to estimate the regression coefficients in order to generate the residual sequence. In addition, the model's performance in terms of 1 and 9-day forecasting demonstrated a good integration of the linear regression-based time series into a unique method that was able to make reliable forecasts of electricity demands. Bennett et al. [216] proposed an ARIMAX-neural network hybrid model for forecasting next-day energy consumption and peak demand, one which could be used to schedule battery system charging and discharging. The two models making up the hybrid model had specific advantages in that the ARIMAX model was better at accounting for large demand spikes, while the neural network (NN) model was better at dealing with small variations. The results of these two models were somewhat reasonable. In addition, Liu et al. [217] compared the ANN and ARIMAX models in terms of next-week temperature-driven electricity load forecasting. The results

showed that, despite the ANN model's better fitting to the temperature data, the SARIMAX model forecasts had greater accuracy. The ANN model performed better than the SARIMAX model in the estimation stage, yet underperformed the SARIMAX model in the forecasting stage. Furthermore, the pre-whitening approach was used to assess the delayed effect of temperature on electrical energy consumption.

Soares and Medeiros [218] compared the SARIMA and ANN models for electrical load forecasting in southeastern Brazil as these types of models can be used for estimating power demand in tropical regions. However, they observed that, while the ANN model could deal with non-linearities in the dataset, the results did not significantly improve. Moreover, Mohamed et al. [219] developed double SARIMA models to improve short-term load estimates in Malaysia. These models consistently outperformed the single SARIMA forecasting model. In addition, using more complicated non-linear models did not improve prediction accuracy. Kim [220] developed a seasonal autoregressive moving average model for forecasting electricity demand in Korea based on a multiplicative mechanism process to identify double seasonal cycles, intraday effects, and intra-week effects. The double SARMA mechanism can detect the intraday and intra-week autocorrelations of daily and weekly fluctuations in power demand. These experimental findings showed that the proposed model outperformed comparable models. Fan et al. [221] proposed a novel short-term load forecasting model, one which combined support vector regression (SVR), grey catastrophe (GC), and random forest (RF) approaches. The proposed approach achieved very successful outcomes in terms of short-term forecasting although, nevertheless, this model needs further development to perform long-term forecasting adequately. Moreover, Yu and Xu [222] improved an enhanced backpropagation NN to predict short-term gas consumption. Applying this approach had the potential to boost both the effectiveness of the learning speed and the functionality of the forecasting model.

Alharbi and Csala [187] conducted a study to forecast the long-term power performance for the KSA using a Group Method of Data Handling (GMDH)-based NN. Although these methods are widely used, these models lack high accuracy or evaluation methods. Chen et al. [223] and Zhang et al. [224] suggested short-term electrical load forecasting hybrid models that integrated SVR, enhanced empirical mode decomposition (IEMD), a seasonal ARIMA, and a wavelet neural network (WNN) which was optimised using the fruit fly optimisation algorithm (FOA). The drawbacks of these forecasting models, such as the

complicated optimisation procedure and the sluggish convergence rate, were overcome by the hybridisation models. Such hybrid methods have the potential to successfully increase forecasting accuracy and complement each other and the shortcomings of preceding models.

6.2 Time Series Analysis Approach

6.2.1 Autoregressive Integrated Moving Average and Seasonal ARIMA

The ARIMA model is a statistical tool, one that provides complementary approaches to time series and predicts future values in series for gaining meaningful insights with random errors. Although exponential smoothing approaches are constructed based on capture of trend and seasonality in the data, the ARIMA model describes an ARMA linear model type in terms of statistical prediction [225, 226]. Furthermore, one significant stumbling block in the adoption of ARIMA prediction models is the fact that the order selection procedure is often considered subjective and difficult to implement [227]. The seasonal series data performance renders the standard ARIMA model ineffective for utilisation [228]. ARIMA has the disadvantage of not being able to handle seasonal data, which is frustrating. Therefore, the ARIMA model was upgraded to the seasonal ARIMA (or SARIMA) model [229] to maintain the time series when it comprises both seasonal and non-seasonal data to process the univariate time series [228]. The main components of the ARIMA model are autoregression (AR), integration (I), and moving average (MA) and defines the data in terms of stationary, non-stationary, and seasonal processes of order (p, d, q). While p refers to autoregressive lag observations included in the model, d is the difference order (or the number of times that the raw observations are differenced), while q is the MA lag or the size of the MA window [230]. Considering the seasonal ARIMA

(p, d, q) * $(P, D, Q)^S$ as non-negative integers designed to handle seasonality, X_t is the observed value at time (t); while s represents the number of periods per season. Equation (6-1) represents the general form of the SARIMA prediction model [231]:

$$\varphi_p(G)\varphi_p(G^s)\,(1-G)^d\;(1-G^s)^D\,X_t = \gamma_q(G)\,w_Q(G^s)\;e_t \tag{6-1}$$

The coefficients $\varphi_p(G)$ and $\gamma_q(G)$ refer to the order of the non-seasonal autoregressive (AR) and non-seasonal MA components' characteristic polynomials; while the polynomials $\varphi_p(G^s)$ and $w_Q(G^s)$ denote the seasonal autoregressive (SAR) and seasonal moving average (SMA) polynomials, respectively [231]. The non-seasonal and seasonal time series are termed $(1 - \mathrm{G})$ and $(1 - G^s)$ and represent the differencing components. In addition, d and D denote the non-seasonal ARIMA's ordinary and seasonal differenced terms; while e_t refers to the prediction error, s indicates the duration of the seasonal pattern (e.g., s = 12 monthly series), and G denotes backshift operator coefficient. Equations (6-2 to 6-5) represent the SARIMA prediction model, as follows:

$$RA: \varphi_p(G) = 1 - \varphi_1 G - \varphi_2 G^2 - \varphi_3 G^3 - \cdots - \varphi_p G^p \quad (6\text{-}2)$$

$$MA: \gamma_q(G) = 1 - \gamma_1 G - \gamma_2 G^2 - \gamma_3 G^3 - \cdots - \gamma_q G^q \quad (6\text{-}3)$$

$$SRA: \varphi_p(G^s) = 1 - \varphi_1 G^s - \varphi_2 G^{2s} - \varphi_3 G^{3s} - \cdots - \varphi_p G^{ps} \quad (6\text{-}4)$$

$$SMA: w_Q(G^s) = 1 - w_1 G^s - w_2 G^{2s} - w_3 G^{3s} - \cdots - w_Q G^{Qs} \quad (6\text{-}5)$$

6.2.2 ARIMA with eXogenous Factors

The ARIMAX prediction model is another variant of the ARIMA model which can utilise a univariate time series in historical data to analyse and predict its own trend and future values. While the ARIMAX model with extra independent factors or explanatory variables was introduced and subsequently compared to the ARIMA model to solve the issue of the univariate time series, it is also a multiple regression model that consists of one or more (AR) terms and one or more (MA) terms. In addition, the ARIMAX prediction model is suitable for any type of data pattern, such as stationary or non-stationary data, and univariate data with trends. Mathematically, the ARIMAX model can be presented in equation form (6-7) [232], where $\varphi(G)$ refers to the AR parameters and $\gamma(G)$ to the MA parameters. In addition, the regression error e_t and a_t donate a zero average and the time series error term, while l_i refers to the lag degree and y_t is the output.

$$e_t = \frac{\gamma(G)}{\varphi(G)} \; a_t \quad (6\text{-}6)$$

$$y_t = \alpha + \sum_{i=1}^{m} \frac{\gamma_i(G)}{\varphi_i(G)} \; Gl_i X_t + e_t \tag{6-7}$$

6.2.3 Seasonal ARIMA with eXogenous Factors

The seasonal ARIMA with exogenous factors (SARIMAX) is an improved version of the SARIMA as it incorporates exogenous factors (X) as external feature parameters to enhance the model's performance, thereby reducing prediction errors, overcoming autocorrelation issues and improving prediction performance [231]. The SARIMAX comprises both seasonal effects and eXogenous factors (X) that can be used as SARIMAX (p, d, q) $*$ (P, D, Q), while the exogenous factors (X) are optional parameters. Exogenous factors (X) can be in the form of external parallel time series data such as wind speed or temperature values that have the same correlation with the original data that requires prediction. Exogenous factors (X) are used to support the prediction model and provide more details. The SARIMAX model is presented in equation (6-8) [231]. $y_{k,t}$ refers to the number of external exogenous factors at time t, while α_k is the correlation coefficient value of the external exogenous (X) input factors.

$$\varphi_p(G)\varphi_p(G^s)\,(1-G)^d\;(1-G^s)^D\,X_t = \alpha_k y_{k,t} + \gamma_q(G)\,w_Q(G^s)\;e_t \tag{6-8}$$

6.2.4 Autocorrelation (ACF) and Partial Autocorrelation (PACF)

The autocorrelation function (ACF) and partial autocorrelation function (PACF) concepts are fundamental tools for analysing linear time series and are utilised in selecting the p and q values for the ARIMA model. Graphically, a correlogram shows how linearly related two pairs of observations are with different time lags and this gives us an idea of how they are interrelated. In addition, the ACF and PACF functions can be used to identify the models, fit autoregressive models, find periodicities, outliers, categorise time series, and forecast future values [233]. When the ACF has values close to (-1), the outliers will have the most influence. For large positive values of the ACF, a few successive outliers can enhance the prediction by offsetting and overcoming the small sample bias. However, some transformations can eliminate the impact of outliers on the ACF, although their bias persists asymptotically [233]. The PACF provides an attractive

vantage point from which to observe the structure of time series and provides adequate criteria for a sequence of real numbers to describe the weak stationary time series [234].

6.2.5 Augmented Dickey-Fuller (ADF) Test and Null Hypothesis

The ADF test can be employed to determine whether a set of data is stationary or non-stationary [230, 235]. In the case of non-stationary data, high-order differencing can be applied to make the data stationary [206]. ADF results perform evaluations based on two types of values, namely the statistic and the $p - value$. The large negative statistic value leads to a strong rejection of the unit root hypothesis while the time series has no unit root, indicating that it is stationary. If the ADF test statistic result is positive, the null hypothesis of a unit root is not rejected and the time series has a unit root, indicating it is non-stationary. In addition, the general concept of the ADF test involves the implementation of the null hypothesis to evaluate data as being either stationary or non-stationary by denoting H_1 or H_0 [230]; where H_1 refers to the time series that does not have a unit root. In this case, the null hypothesis is rejected, and the data is deemed to be stationary [230]. In addition, H_0 refers to a time series that has a unit root and, in this case, the null hypothesis is not rejected and the data is deemed to be non-stationary. On the other hand, $p - values$ used to control between H_1 and H_0 are as follows:

- If the ($p - value \leq 0.05$), the mean time series does not contain a unit root, the null hypothesis is rejected, and the data is stationary [230, 235].

- If the ($p - value > 0.05$), the mean time series contains a unit root, the null hypothesis is not rejected, and the data is non-stationary [230, 235].

Mathematically, the ADF test can be presented in equation (6-9); where α is a constant and β is a time trend parameter, and γ and δ are coefficients. The autoregressive process's lag order is p; γ is the null hypothesis, y_t is the dependent variable, and $\Delta\, y_t$ the first difference operator.

$$\Delta\, y_t = \alpha + \beta_t + \gamma\, y_{t-1} + \delta_1 \Delta\, y_{t-1} + \cdots + \delta_{p-1} \Delta\, y_{t-p+1} + e_t \qquad (6\text{-}9)$$

6.2.6 Error Indices

Various indices were identified as common error indicators to comprehensively evaluate the proposed SARIMAX forecasting model's efficiency. Moreover, modelling error indicators (i.e., mean square error [MSE], root mean square error [RMSE], mean absolute percentage error [MAPE], and mean absolute error [MAE]) were used to assess the model's reliability and correctness, as shown mathematically in Equations (6-10)–(6-13). The variable y_j is the actual value, whereas $\hat{y}_j$ refers to the forecasted observations, and (n) refers to the sample numbers employed in the observation. Further, the standard deviation of the regressions (forecast error) is indicated by the term "RMSE," which is the square root of the mean square errors and is recognised as an effective general-purpose error indicator for numerical predictions due to its low sensitivity to noise. In addition, R-squared (the squared correlation coefficient, or R^2), indicates how much of a dependent variable's fluctuation can be described by exogenous factors. In Equation (6–14), SS_{res} is the sum of squared residuals and SS_{Tot} is the absolute square number.

$$MSE = \frac{1}{n}\sum_{j=1}^{n}(y_j - \hat{y}_j)^2 \tag{6-10}$$

$$RMSE = \sqrt{\frac{1}{n}\sum_{j=1}^{n}\frac{(y_j - \hat{y}_j)^2}{n}} \tag{6-11}$$

$$MAPE = \frac{1}{n}\sum_{j=1}^{n}\left|\frac{y_j - \hat{y}_j}{y_j}\right| * 100 \tag{6-12}$$

$$MAE = \frac{1}{n}\sum_{j=1}^{n}|\, y_j - \hat{y}_j \,| \tag{6-13}$$

$$R^2 = 1 - \frac{SS_{res}}{SS_{Tot}} \tag{6-14}$$

6.2.7 Model Setup and Configuration

Using Python programming, we developed a SARIMAX forecasting model based on the time series concepts, principles, and computational approaches presented in Equations (1)–(9). Python programming offers a vast amount of memory, is capable of handling massive amounts of data, and has a wide range of pre-built libraries. The datasets were

prepared and cleaned in preparation for processing. Due to the size and nature of the datasets, various parameter settings were necessary for each type of data to improve the model fit. To this end, we developed a method that automatically splits the training and testing data to match the model's specifications. The total dataset length was 164 steps and the data were divided into training and testing data, accounting for 30% and 70% of all the data, respectively. Further, we developed a robust and effective code which monitors the performance of the model, generates an automatic report to identify any weak points in the code, defines the parameters (p, d, q) and (P, D, Q), and then automatically sets the values for the variables (p, d, q) to (1, 0, 6) as well as their orders (P, D, Q) to (3, 1, 1). In addition, the exogenous factors were set as 0. Many developers split the training and testing data manually and define the parameters of the variables randomly, a process that might result in incorrect values and negatively impact the model's performance. Any unknown variables that might produce data fluctuations will make it impossible to predict them unless there is a known variable that explains such variations.

The flowchart of the proposed SARIMAX forecasting model is presented in Figure 6-1 which summarises the research process. This started with defining the problem, followed by data collection, data testing, and analysis. The process also included selecting the approach, developing the forecasting model, evaluating the forecasting model, and testing the final forecasting results.

6.2.7.1 Data preparation

The historical power sector data for the GCC region comprises electricity generation, consumption, peak load, and installed capacity data, as presented in Figure 1-2 to Figure 1-5. The actual historical data pertained to quarterly intervals taken over a 40-year period (1981–2020) and were used to evaluate and predict the behaviour of the power sector over a 30-year period (2021–2050). Furthermore, the quality of the historical data could provide details that could increase the SARIMAX model's forecasting accuracy. The historical data were evaluated, validated, and cleaned to ensure that there were no missing or duplicate values. The Dickey-Fuller test revealed that the data were stationary, with a $p < 0.05$.

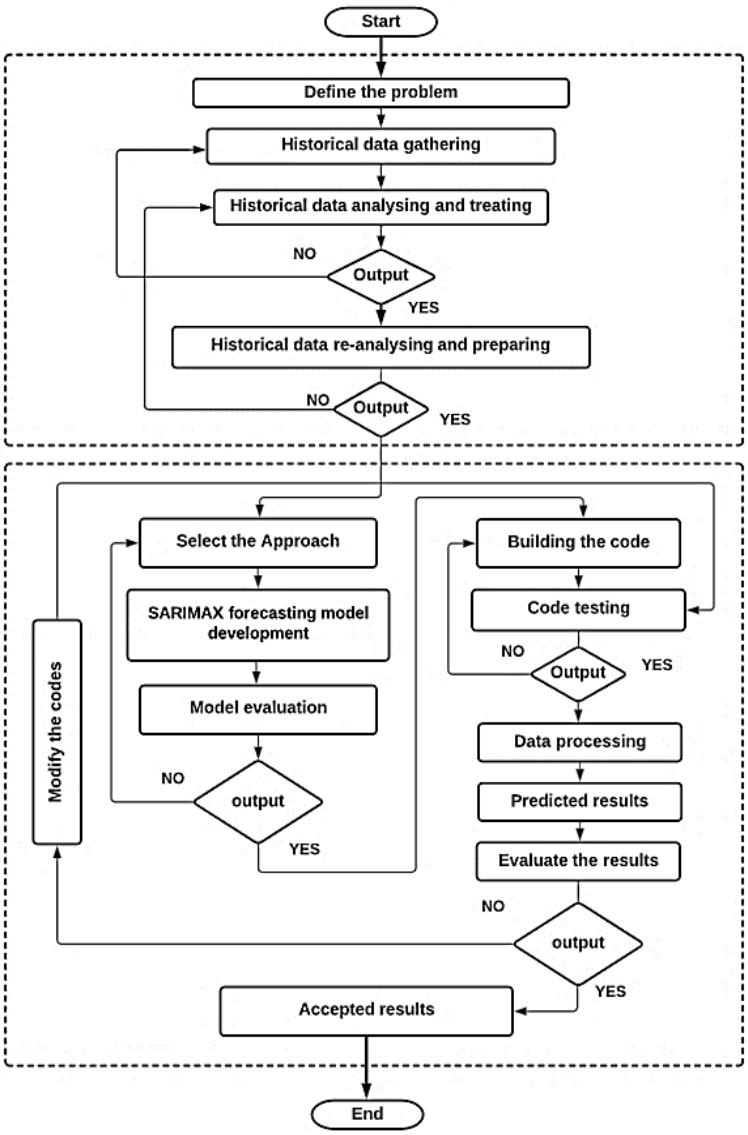

Figure 6-1. Flowchart of the proposed SARIMAX forecasting model.

6.3 Results Analysis and Discussion

The SARIMAX model was developed to forecast future electricity generation, consumption, peak load, and installed capacity values of the GCC region for a 30-year period (2021–2050) based on historical data collected over the previous 40 years. In addition, as energy demand rises, new dynamic energy markets emerge. This leads to an imbalance in energy prices and has a direct influence on the world's energy security. These forecasting technologies present new opportunities for the energy market, including developments, performance, price controls, cost savings, and optimisation that can solve obstacles for those businesses operating in this industry. Further, determining which energy markets provide the most opportunities for the power generation profile of

the organisation thereby minimises the likelihood of grid congestion while simultaneously improving electricity flow. Moreover, forecasting technologies are critical in ensuring the stability of the energy system, since the efficiency of the energy markets is dependent on the availability of a dependable supply, flexible bidding, system assistance, predictive maintenance, and enhanced power quality. Forecasting is a challenging task owing to several confounding factors which must all be considered, such as the links between regressors that have major effects on the power sector, as well as the intermittency and fluctuations, which cause apparent effects resulting from multiple errors. The developed model was used to forecast the future performance of the power sector in the GCC region, as presented in Figure 6-2 to Figure 6-5 for the KSA and in *A.2 Appendix 2* for the other GCC countries. The estimates and findings showed that the SARIMAX model was able to effectively handle the four types of electricity data as a multimodal dataset from the six countries.

The main and cross effects were evaluated by repeatedly plotting, analysing, and testing the data for the KSA. Electricity generation (Figure 6-2a), electricity consumption (Figure 6-3a), electricity peak load (Figure 6-4a), and installed power capacity (Figure 6-5a) data did not exhibit any significant overfitting between the experimental and forecasted values, indicating that the SARIMAX model offers a promising performance based on the KSA historical data. Moreover, the model produced remarkable error metrics for the KSA in terms of accuracy indicators, as shown in Table 6-1. The error metrics of electricity generation for KSA were as follows: RMSE = 1.2 TWh, MAE = 0.6 TWh, MSE = 1.5 TWh, and MAPE = 0.3%. Furthermore, electricity generation had an R2 of 99%. A reduction in the KSA's consumption RMSE to 1 TWh was achieved, but the MAE recorded the same value as the generation MAE (0.6 TWh) due to the similarity between historical electricity consumption and generation data. The KSA's consumption MSE and MAPE were recorded as 1 TWh and 0.3%, respectively, with an R2 = 99%. The MAPE values were influenced by the small values in the historical data. The KSA's peak load error indicators dropped, with RMSE = 0.3 GW, MAE = 0.1 GW, MSE = 0.1 GW, MAPE = 0.4%, and R2 = 99%. The error metric values for KSA's installed capacity were significantly smaller than the error values for electricity generation, consumption, and peak load. The error metrics for KSA's installed capacity showed significant improvements, with RMSE = 0.2 GW, MAE = 0.1 GW, MAPE = 0.3%, and R2 = 99%, as presented in Table 6-1. In addition, the MSE decreased to 0.07 GW.

Based on Figure A.2–1, Oman's electrical generation error metrics values are reduced but the MAPE value is raised as per the following: RMSE = 0.2 TWh, MAE = 0.1 TWh, MSE = 0 TWh, and MAPE = 0.5%, as shown in Table A.2–1. In addition, Oman's R^2 for electricity generation is 99 % and the associated p-value is 0%. A decrease in Oman's consumption error metrics values were recorded as a RMSE to 1 TWh, MAE recorded 0 TWh, MAE attained 0 TWh, and MAPE was lowered to 0.4 % (see Figure A.2–2). R2 is 99% and the p-value is 0% for Oman's electricity consumption. Oman's peak load error indications were reduced to 0 GW for RMSE, MAE, and MSE, as displayed in Figure A.2–3. While Oman's peak load MAPE, p-value and R^2 remained the same at 0.4%, 0% and 99%, respectively. According to Figure A.2–4, the MAPE value for Oman's installed capacity rose to 0.9%, while the corresponding values for RMSE = 0.1 GW, MAE = 0 GW, MSE = 0 GW, R2 = 99%, and p-value = 0%. The quality of the finding in terms of error metrics revealed extraordinary values in Oman, and this is related to the peculiarity of its historical data as compared to that of the KSA.

Figure A.2–5 and Table A.2-2 show a reduction in UAE's electrical generation error metrics values wherein the RMSE is 0.4 TWh, MAE is 0.2 TWh, MSE is 0.2 TWh, and MAPE = 0.3%. The UAE's power generation R^2 is 99% and the p-value is 1×10^{-12} %. Moreover, the RMSE recorded 0.4 TWh, MAE reached 0.3 TWh, MSE is 0.2 TWh, and MAPE = 0.4 % for the UAE's electricity consumption (see Figure A.2–6). The UAE's electricity consumption R^2 is 99% and the p-value = 4×10^{-12} %. Figure A.2–7 shows that RMSE is reduced to 0.1 GW, MAE to 0, and MSE to 0. The UAE's peak load MAPE, p-value, and R^2 retained are 0.6%, 2×10^{-11} %, and 99%, respectively. Figure A.2–8 shows that the UAE's installed capacity MAPE climbed to 0.5%, RMSE = 0.1 GW, MAE = 0, MSE = 0, R^2 = 99%, and the p-value = 3×10^{-10} %.

Kuwait's electrical generating error metrics include RMSE as 0.2 TWh, MAE as 0.1 TWh, MSE as 0 TWh, and MAPE as 0.3%, as shown in Figure A.2–9 and Table A.2-3. R^2 is 99% and the p-value is 6×10^{-8}. Kuwait's power consumption had the same error metrics as for electrical generation, except the p-value = 1.6×10^{-8} (see Figure A.2–10). Figure A.2–11 indicates that the RMSE, MAE, and MSE are 0 TWh. Kuwait's peak load MAPE, p-value, and R^2 are 0.2%, 2 × 10−11, and 99%, respectively; while the RMSE, MAE, and MSE are 0 TWh for Kuwait's installed capacity and the R^2 is 99%, MAPE is 0.3%, and p-value is 0% as shown in Figure A.2–12.

Qatar's electrical generation error parameters consist of an RMSE of 0.1 and TWh and MAE and MSE values of 0. Figure A.2–13 and Table A.2-4 show that the MAPE = 0.3%, R^2 = 99%, and the p-value = 0%. According to Figure A.2–14, Qatar's power consumption and electrical generation had the same error metrics values. Figure A.2–15 reveals that the RMSE, MAE, and MSE are all 0 TWh. The MAPE, p-value, and R^2 for Qatar's peak load are 0.3%, 8.6×10^{-8}, and 99%, respectively. The RMSE, MAE, and MSE for Qatar's installed capacity are all 0 TWh. Figure A.2–16 demonstrates that the R^2 = 99.0%, the MAPE = 0.7%, and the p-value = 4.3×10^{-9}%.

Bahrain's electrical generation error indicator values include a MAPE of 0.7%, an RMSE of 0.3 TWh, a MAE of 0.1 TWh, and a MSE of 0 TWh, as presented in Figure A.2–17 and Table A.2–5. Bahrain's electrical generation R^2 = 99% with a p-value = 1.2×10^{-9}%. According to Figure A.2–18, Bahrain's power consumption recorded 0.1 TWh for MAPE, MAE, and MSE, while its power consumption RMSE = 0.3 and R^2 = 99% with a p-value = 3.6×10^{-9} %. Bahrain's peak load error parameters are 0.3 TWh for RMSE, 0.5 for MAPE, and 0 TWh for MAE and MSE, respectively, while the R^2 = 99% and the p-value = 0%. Bahrain's installed capacity error parameters recorded an RMSE = 0.1 TWh, 0 TWh for both MAE and MSE, with a MAPE = 1.8% (Figure A.2–20). In addition, R^2 = 99% and the p-value = 5.3×10^{-8}%. This is a clear demonstration of the remarkable performance of the SARIMAX model, as it demonstrates that the outcomes of predictions for all the different types of historical data for the six countries of the GCC region exhibited extremely low error values for these long-term predictions. The model developed has been able to deal with the nature of historical data, which is characterised by variations in geography, climate, and weather conditions. These differences were properly considered in the development of the model. Although the MAPE is the most important measurement for predicting accuracy within the electrical forecasting literature, the MAE, MSE, and RMSE are also presented in this work. Applying a range of forecasting accuracy indicators is important in the evaluation of the SARIMAX model. However, it is essential to carry out investigations as to whether the values of the four-error metrics are consistent with each other.

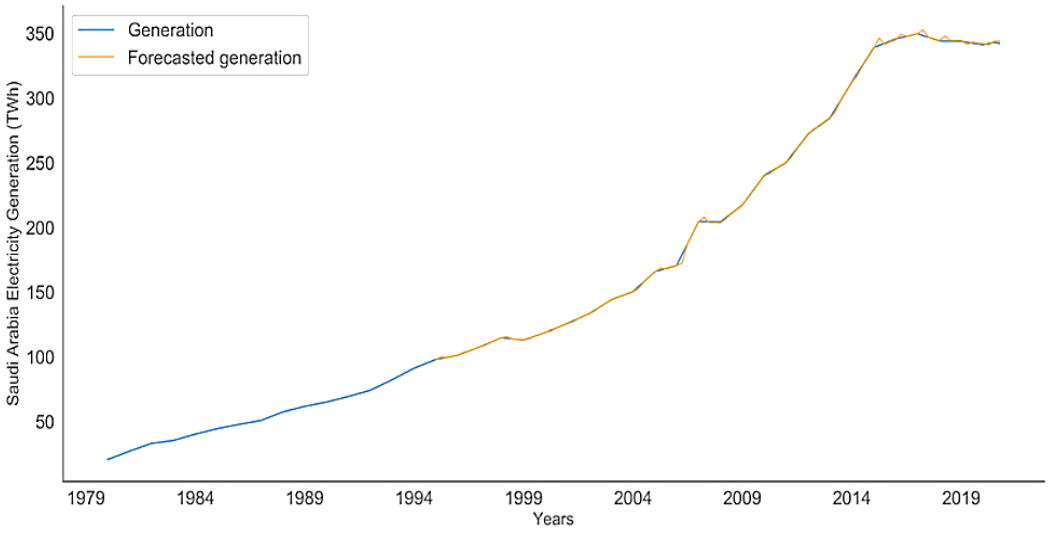

(a)

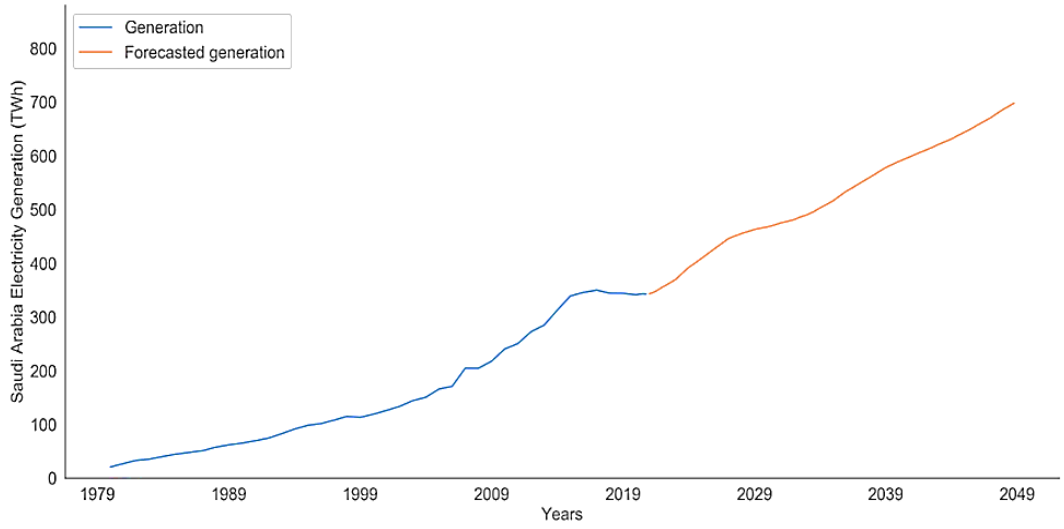

(b)

Figure 6-2. (a) Real and forecast values of electricity generation which show the good fit and performance of the SARIMAX model. (b) Forecast electricity generation values for a 30-year period from 2021 to 2050.

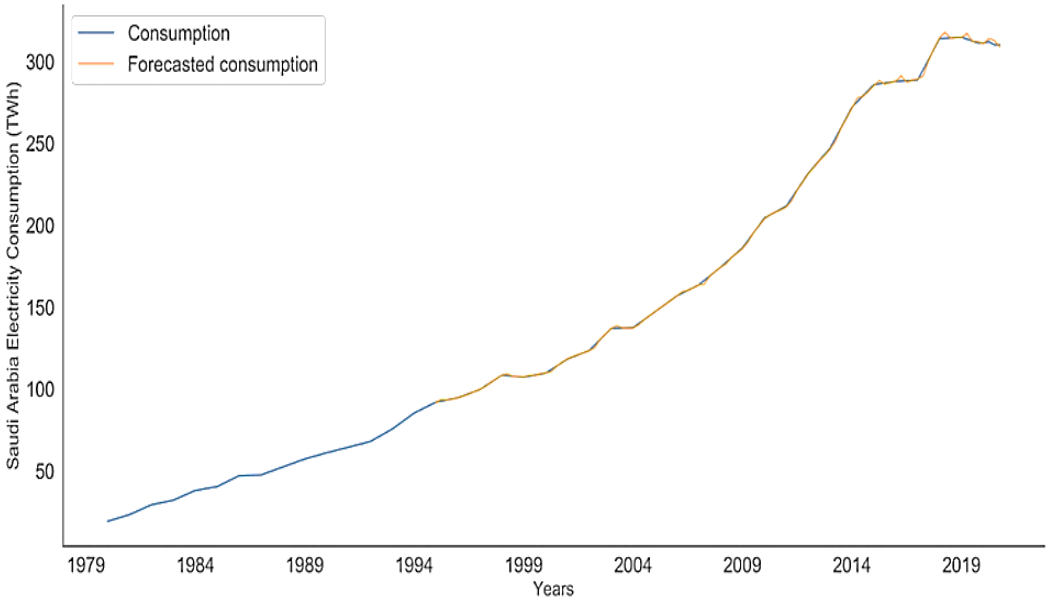

(a)

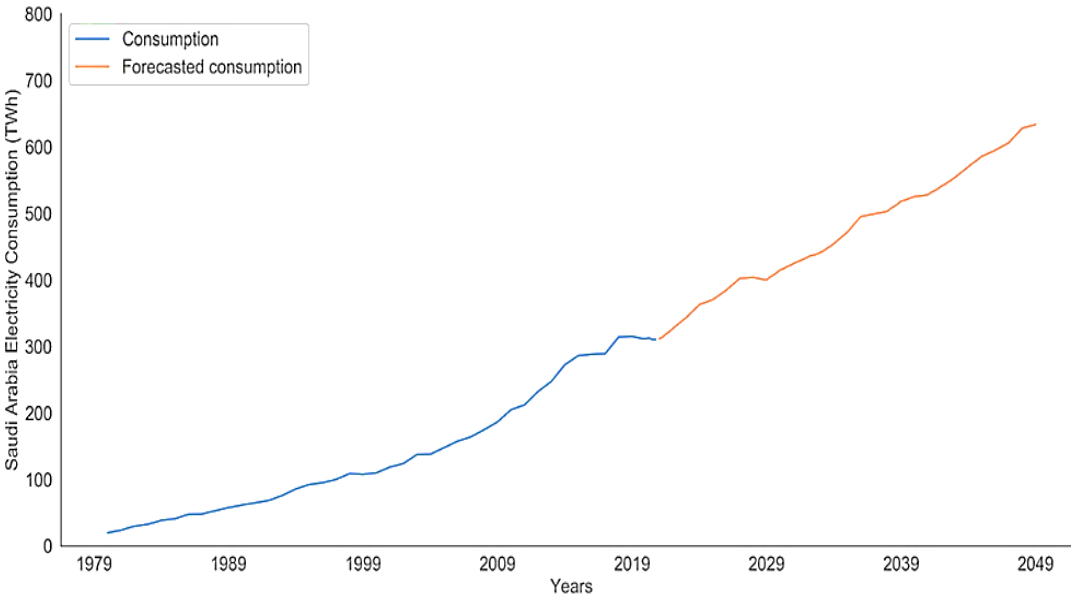

(b)

Figure 6-3. (a) Real and forecast values of electricity consumption which show the good fit and performance of the SARIMAX model. (b) Forecast electricity consumption values for a 30-year period from 2021 to 2050.

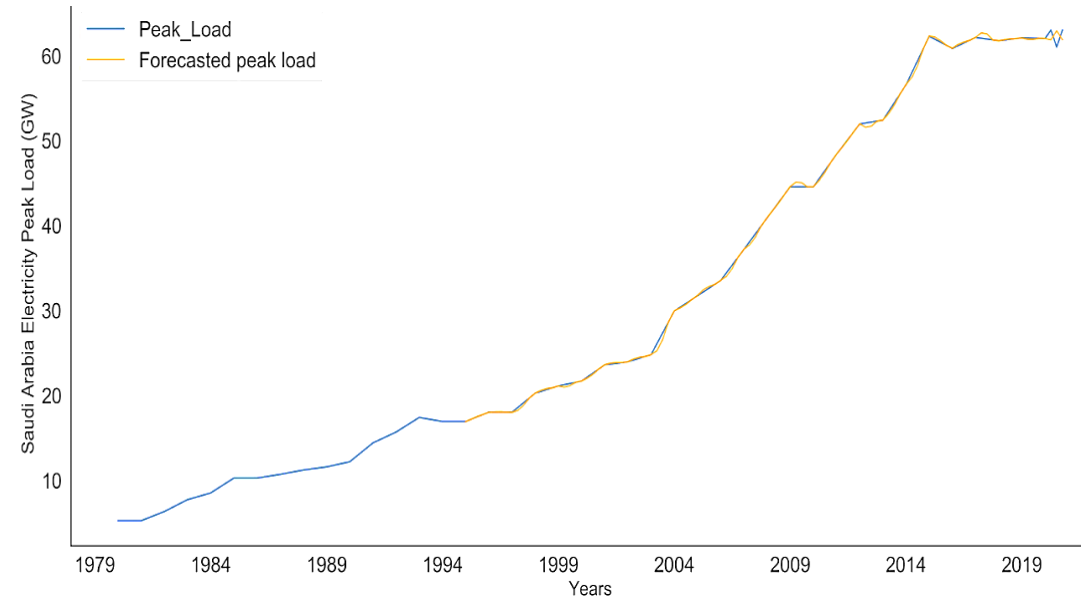

(a)

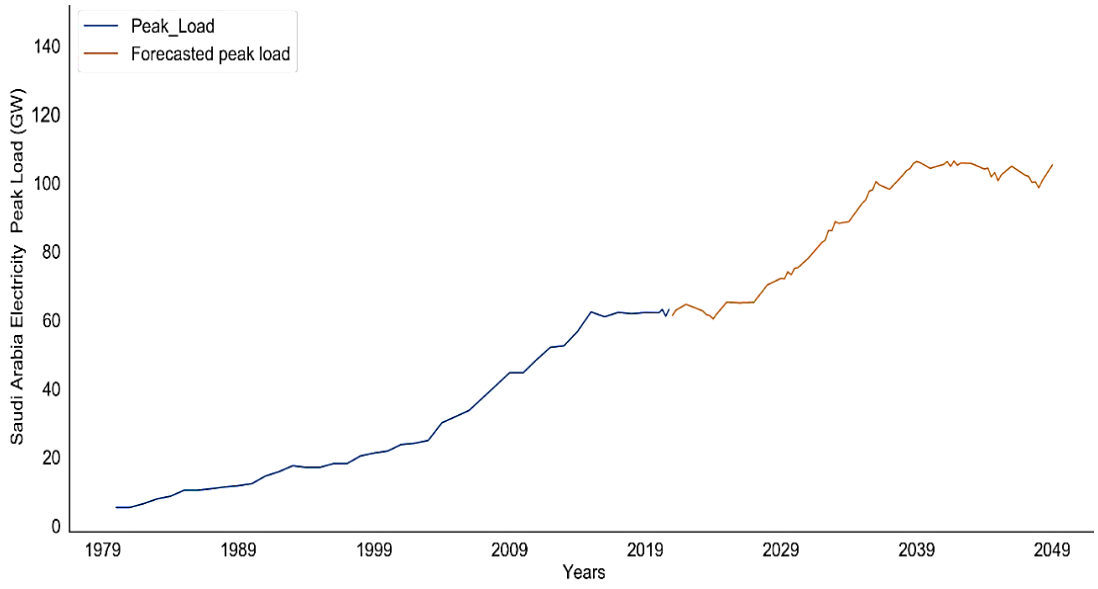

(b)

Figure 6-4. (a) Real and forecast values of the electricity peak load which show the good fit and performance of the SARIMAX model. (b) Forecast peak electricity load values for a 30-year period from 2021 to 2050.

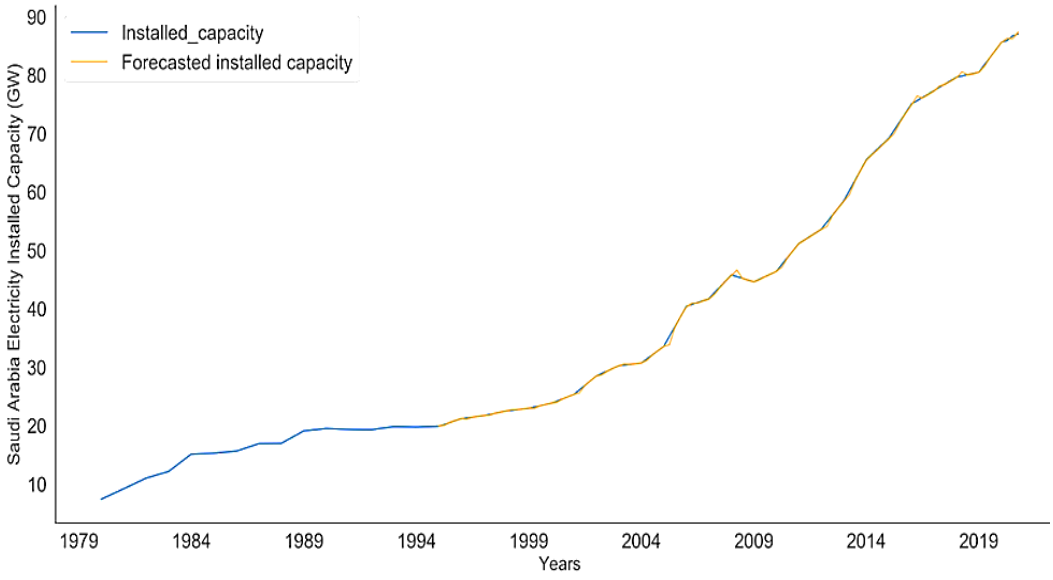

(a)

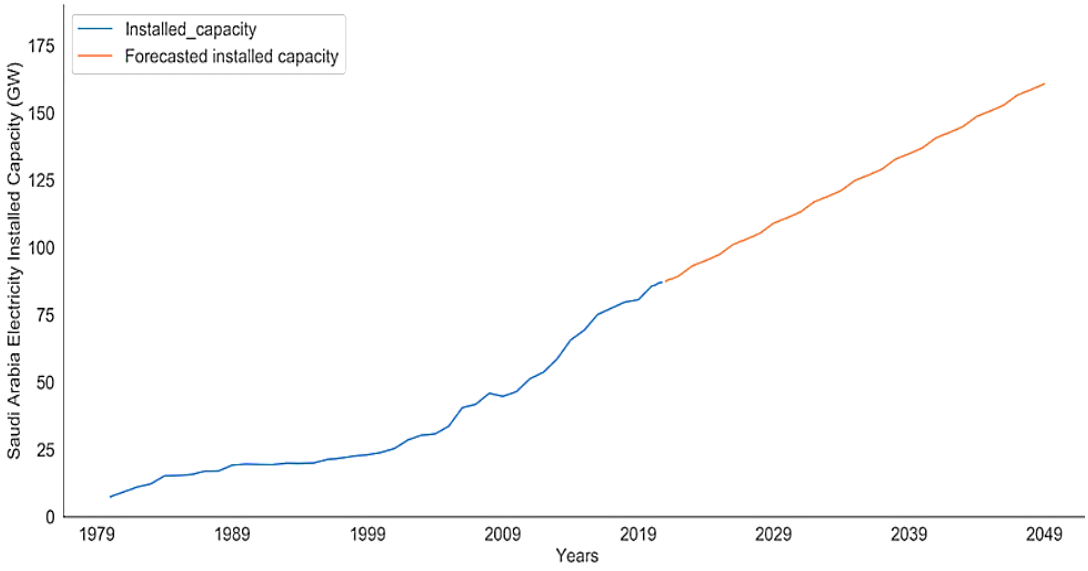

(b)

Figure 6-5. (a) Real and forecast values of the installed electricity capacity which show a good fit and performance of the SARIMAX model. (b) Forecast electricity installed capacity values for a 30-year period from 2021 to 2050.

Table 6-1. Forecast accuracy indicators for the proposed SARIMAX model.

No.	Metric	Generation (TWh)	Consumption (TWh)	Electric Peak Load (GW)	Installed Capacity (GW)
1	RMSE	1.2	1	0.3	0.2
2	MAE	0.6	0.6	0.1	0.1
3	MSE	1.5	1	0.1	0.07
4	MAPE (%)	0.3	0.3	0.4	0.3
5	*p*-value (%)	3×10^{-7}	2×10^{-8}	0	0
6	R^2 (%)	99	99	99	99

6.3.1 Future Performance Analysis for the Electricity Sector of the GCC Region

In addition, Figures (A.2-1b to A.2-20b), Figure 6-2b, Figure 6-3b, Figure 6-4b and Figure 6-5b illustrate the forecast values for electricity generation, consumption, peak load, and installed capacity of the GCC region for the 30 years spanning 2021 to 2050. It is evident, among all the types of historical data, that the historical peak load and installed capacity data values showed unique erroneous indicator values that decreased commensurately (except for the MAPE value). This was caused by the unique nature of the historical electricity peak load and installed capacity data. Significant and acceptable correlations between the variables' fluctuations for the four categories of historical power data were shown by the R^2 values, indicating that the correlations were both considerable and suitable. A statistical analysis of the historical power data and the SARIMAX forecasts showed that electricity consumption is likely to continue growing swiftly until 2050, although the estimated electricity generation values were higher than the estimated electricity consumption values, despite their proximity. The predicted installed capacity values showed an increasing trend over the three decades from 2021 to 2050, a reasonable forecast for meeting the anticipated growth in electrical consumption. The electrical peak load did not show continuous growth as it depends on different factors, including weather and seasonality. In general, the main factors that cause surges in electricity consumption and major variations in the electricity peak load are GHG emissions, changes in GDP, and population growth. This demonstrates how crucial it is to include cross effects in both short-term and long-term forecasting models. In addition, evaluating the other external factors and their interconnections might further enhance the investigation and the accuracy of forecasts.

According to Figure 6-2b, forecasted electricity generation in the KSA will be 369 TWh in 2023, a figure which is estimated to continue to increase to 409 TWh in 2025. Moreover, electricity generation is forecast to reach 470 TWh in 2030 and 516 TWh in 2035. In 2040, electricity generation is forecast to be 589 TWh, reaching 643 TWh in 2045 and 700 TWh in 2050. In comparison, Oman will generate some 39 TWh of energy in 2023 and 43 TWh in 2025. In 2030 and 2035, Oman's generated electricity output will reach 49 and 56 TWh, respectively. Electricity generation will climb to 66 TWh in 2040, 73 TWh in 2045, and 80 TWh in 2050, as presented in Figure A.2–1b. The UAE will generate 152 TWh in 2023 and 157 TWh in 2025, outputs that are forecasted to rise to

169 and 178 TWh in 2030 and 2035, respectively. Figure A.2–5b indicates that the UAE will generate some 186 TWh in 2040, 190 TWh in 2045, and 195 TWh by 2050. In addition, Kuwait will generate 77 TWh of electricity in 2023 and 80 TWh in 2025, rising to 91 and 99 TWh in 2030 and 2035, respectively. According to Figure A.2–9b, Kuwait's power generation will reach 107 TWh in 2040, 116 TWh in 2045, and 126 TWh in 2050.

Qatar will generate 54 TWh of power in 2023, increasing to 56 TWh in 2025. In 2030 and 2035, Qatar will likely generate 66 and 75 TWh of electricity, respectively. Figure A.2–13b indicates that power generation will reach 83 TWh in 2040, 93 TWh in 2045, and 102 TWh in 2050. Bahrain's power generation fell from 17 TWh in 2020 to 17 TWh in 2023, although it will likely increase to 21 TWh in 2030. For 2035, 2045, and 2050 Bahrain will generate an estimated 22, 26 and 28 TWh of electricity, respectively (see Figure A.2–17b). It is worth mentioning that Bahrain demonstrated a decline in power generation in 2016, with generation falling from 26 TWh in 2016 to 17 TWh in 2020.

The electrical generative output of the GCC nations faces demographic and economic challenges as the growth in demand continues to outpace economic growth. Oil and gas have until now been the main sources of energy used to generate power, and the GCC regions continue to burn a considerable amount of oil to generate a substantial proportion of their electricity.

Figure 6-3b indicates that the KSA's electricity consumption will reach 342 TWh in 2023 and will continue to rise to 373 TWh in 2025. In addition, the consumption of electricity will reach 421 TWh in 2030 and 483 TWh by 2035. In 2040, a forecasted 524 TWh of electricity will be consumed, followed by 590 TWh in 2045, and 644 TWh in 2050. In the case of Oman, the nation is estimated to be consuming 38 TWh by 2023 and 42 TWh by 2025. In 2030 and 2035, Oman will be forecasted to consume 47 and 54 TWh of electricity, respectively. As shown in Figure A.2–2b, the consumption of electricity will reach 58 TWh in 2040, rising to 62 TWh in 2045, and reaching 64 TWh in 2050. The UAE will utilise 147 TWh in 2023 and 152 TWh by 2025. In 2030 and 2035, the UAE will need 164 and 174 TWh, respectively, rising still further to 185 TWh by 2040, 190 TWh by 2045, and in 2050 the nation is expected to demand 195 TWh, as depicted in Figure A.2–6b. In 2023 and 2025, Kuwait will consume 72 and 76 TWh of energy, respectively, rising to 84 and 99 TWh by 2030 and 2035, respectively.

Figure A.2–10b indicates that Kuwait's energy consumption will reach 107 TWh in 2040, 116 TWh by 2045, and 126 TWh in 2050. In 2023, Qatar will use a forecasted 49 TWh of power, increasing to 51 TWh in 2025. Qatar's consumption will increase to 61 and 67 TWh of power in 2030 and 2035, respectively; 75 TWh in 2040, 84 TWh in 2045, and 93 TWh by 2050, as illustrated in Figure A.2–14b.

Bahrain's power consumption in contrast decreased from 16 TWh in 2020 to 15 TWh in 2023, and is anticipated to increase to 20 TWh in 2030, continuing to fluctuate between 19 and 20 TWh between 2035 and 2050 (see Figure A.2–17b). Bahrain's power consumption actually fell from 26 TWh in 2016 to 17 TWh in 2020. Bahrain has compensated for the decrease in electricity generation from GCC regional electricity interconnections as it relies heavily upon it to provide it with electricity, explaining the significant decrease in domestic energy production. The increase in electricity consumption in the GCC countries has always been linked to three main factors, namely increases in temperature that require the use of air conditioners, especially during the summer, and the scarcity of water sources which requires the use of seawater desalination plants. In addition, large increases in population, economic and urban growth all further affect electricity consumption.

The results of analysing future and historical data of peak electricity loads in the KSA anticipates maxima of 62 GW in 2023 and 66 GW in 2025 (Figure 6-4b), rising to 74 GW in 2030 and 94 GW in 2035. By 2040 the KSA's electricity peak load will be 103 GW, increasing still further to 104 GW in 2045 and 105 GW in 2050. The main reason for the fluctuations in load values across the GCC region is the increase in electrical loads at peak times, especially during the summer, official working hours, and Ramadan. Figure A.2–3b reveals that Oman's peak load will reach 9 GW in 2023 and 10 GW in 2025, increasing to 11.73 GW in 2030, 13 GW by 2035, 14.84 GW by 2040, 16 GW in 2045, and 17 GW in 2050. In addition, Figure A.2–7b shows that the UAE's peak load will exceed 33 GW in 2023 and 35 GW by 2025. The UAE's peak load is forecast to reach 40 GW in 2030 and 48 GW in 2035, showing no signs of abating in 2040 at 53 GW, 59 GW in 2045, and 66 GW in 2050. Our results indicated that the rise in peak load rate in the UAE is within the range of natural variation over the next thirty years.

Figure A.2–11b demonstrates that Kuwait's peak demand will reach 13 GW in 2023 and subsequently decline to 12 GW by 2025 remaining at around 12 GW and 13 GW for 2030

and 2035, respectively. The peak demand in Kuwait will however be slightly elevated toward 14.50 GW in 2040, 15.60 GW in 2045, and 16.82 GW by 2050. The peak load in Qatar is expected to reach 9 GW in 2023 and increase to 10 GW in 2025, as shown in Figure A.2–13b. Expected peak demand in Qatar is 12 GW for 2030 and 14 GW for 2035, rising still further to 16 GW in 2040, 17.60 GW in 2045, and 19 GW by 2050. Figure A.2–13b illustrates that Bahrain's peak load will rise to 3.80 GW in 2023 and 4 GW in 2025. There are forecasted to be steady increases in Bahrain's peak electrical demand to 4.39 GW in 2030 and 4.80 GW in 2035, rising still further in 2040, 2045, and 2050 to 5.30 GW, 6 GW, and 6.20 GW, respectively. Bahrain however demonstrates negligible growth in its electricity load owing to its limited size and population. In addition, it is imperative that the countries of the GCC set up efficient pricing and demand-side management (DSM) systems to reduce consumption, not only at peak periods, but also during all other hours of the day. Such systems would improve not only the power consumption in GCC countries as a whole, but also in each individual country.

The KSA’s installed electricity capacity is continuing to rise to meet consumption. According to Figure 6-4b, the installed electrical capacity in KSA will be 93 GW in 2023, and it is expected to continue increasing to 97 GW in 2025 and beyond to 110 GW in 2030, 124 GW in 2035, 136 GW in 2040, 150 GW in 2045, and 160 GW in 2050. Figure A.2–4b shows that Oman will have an estimated 12.70 GW of installed electrical capacity in 2023 and 14 GW by 2025, rising to 16.50 GW in 2030, 19.50 GW in 2035, 22 GW in 2040, 25 GW in 2045, and 28 GW in 2050.

Figure A.2–7b indicates that the UAE's installed capacity will be 38 GW in 2023, with an expected growth to 40 GW by 2025. Furthermore, the UAE's installed capacity will continue to rise from 45 GW in 2030 to 51 GW in 2035, rising still further to 56 GW in 2040, 61 GW in 2045, and 66 GW by 2050. Figure A.2–12b illustrates that Kuwait's installed capacity will reach 20 GW in 2023 and 22 GW in 2025. In addition, Kuwait's installed capacity will increase from 24 GW in 2030 to 26 GW in 2035, 28 GW in 2040, 31 GW in 2045, and 33 GW by 2050. Between 2021 and 2050, Kuwait's installed capacity will grow approximately 2 GW. According to Figure A.2-16b, by 2023 Qatar will have an installed capacity of 13 GW and, by 2025, it will have an installed capacity of 14 GW. The country's installed capacity is however expected to increase from 16 GW in 2030 to 18 GW in 2035, 21 GW in 2040, 23 GW in 2045, and 25 GW by 2050. Figure A.2–20b shows the calculations projecting that Bahrain's installed capacity will reach 7.60 GW in

2023 and 8.49 GW in 2025, before further increments to 11 GW in 2030, 14 GW in 2035, 16 GW in 2040, 19 GW in 2045, and 22 GW in 2050. Note that Bahrain's electricity consumption is predicted to decline over the next 30 years which is reasonable given the country's small size and the presence of an efficient strategy to cut consumption. However, there will be a growth in installed capacity, possibly due to efforts to export electricity to the international energy markets.

There are many potential contributing factors to the issue of rising energy consumption in the GCC region, including cheap energy costs, the hot environment, the abundance of oil and natural gas resources in the GCC countries, technological development, and inadequate public awareness. All of these factors contribute to higher levels of energy consumption. Special air conditioning and cooling systems are needed from April to October due to the hot, arid climate, which doubles energy consumption relative to the winter months. In the GCC region, the primary consumers of energy are the desalination industry, followed by the industrial sector, the cooling industry, and, finally, household consumers. The GCC countries rely on desalinated seawater for their drinking water needs which requires a lengthy and energy-intensive treatment procedure. They possess a huge number of such desalination plants, and the number of these plants is expected to grow over the next thirty years to fulfil their drinking water demands as the number of housing units and public facilities increases. Such rapid population expansion is accompanied by a rise in demand for energy and other amenities in the region. In contrast to the pattern seen in the vast majority of countries, the GCC region's energy consumption has been rising faster than its GDP. As the GCC's electricity costs are still much lower than the average prices in the region and around the world, this exacerbates consumption.

6.3.2 SARIMAX Model Evaluation

Eleven external models that predict long-term power consumption were selected to compare their performance with that of the proposed SARIMAX model based on the MAPE, RMSE, MAE, and MSE error metrics and R^2. However, the authors of the study, from which forecasting models 5–11 originated, used only two error metrics to evaluate their models (MAPE and RMSE) and did not provide R^2 values. The evaluation metrics of our proposed model were superior to those of the other external power consumption models (see Table 6-2). Moreover, the R^2 of our SARIMAX model was 99% for all four

types of historical data, which is higher than the R^2 values of the external models. Based on the comparison in Table 6-2, machine learning (ML) and deep learning (DL) forecasting models perform worse than univariate time series forecasting. The comparison of the proposed SARIMAX model with the external models adds value to this paper, since it allows us to evaluate our work both independently and in relation to other works. Therefore, it is important that future studies use different tools and procedures to evaluate their work and compare it with published papers. This could be useful for researchers who make predictions under similar conditions.

Table 6-2. Comparison of the performance of the proposed SARIMAX model and external models.

No.	Forecasting Model	MAPE (%)	RMSE (GW)	MAE (GW)	MSE (GW)	R^2 (%)
1	SARIMAX [214]	5.42	4298.65	3614.03	18,478.39	79.60
2	LSTM [214]	2.98	3106.64	2027.57	9651.24	86.10
3	ANN [214]	4.97	4109.63	3562.24	16,889.12	81.80
4	SVR [214]	4.16	3615.72	3004.19	13,073.43	82.20
5	MLR model [212]	20.06	22.91	-	-	-
6	BP model [212]	13.50	16.87	-	-	-
7	Grey model [212]	12.11	14.48	-	-	-
8	ANN model [212]	8.65	10.15	-	-	-
9	ANFIS model [212]	6.42	6.89	-	-	-
10	ARIMA model [212]	6.29	3.41	-	-	-
11	SEM-VARIMAX model [212]	1.06	1.19	-	-	-
12	SARIMAX proposed model	0.30	1	0.60	1	99

In addition, the forecasting performance of the SARIMAX model was checked at quarterly dataset intervals with different volumes and types of historical data to test its forecasting accuracy under different conditions. Overall, all of the SARIMAX model's error values for the four types of historical data were minimal compared with those of the other forecasting models, proving the model's capacity to adapt to new historical data observations. Further, the proposed model easily coped with different types of historical data and generated promising forecasting results with very low error metrics in terms of accuracy and interpretability. The model's performance is particularly impressive in terms of installed power capacity. The error values also decreased while the training time increased. Further, the integration of a substantial quantity of historical data with a sizeable amount of training data extended the duration of the simulation. However, because of the interdependence of the succeeding phases, the SARIMAX prediction

model must be treated sequentially. The most difficult tasks are strengthening the generalisation capabilities of the model while simultaneously attaining better outcomes. Generalisation is described as the fluctuation in the recognition rate of the model's performance when matching the training data to previously observed datasets, such as the testing data. The model lacked generalisation results because of the significant overfitting of the training and testing data, but it did not exhibit significant overfitting (see Figure 6-2a, Figure 6-3a, Figure 6-4a and Figure 6-5a). The SARIMAX model incorporates time series to improve its generalisation by considering the effects of the selected parameters on the expected historical data values for the next step. When a significant number of sufficient historical data are selected, the SARIMAX model's efficiency becomes evident, its long-term forecasting quality improves, and its accuracy increases. In this research, several error metrics were used to evaluate the proposed model and to provide other model developers with more options for comparing their work using these error metrics. This research also aimed to provide future researchers with guidelines and a roadmap based on our experimental findings. This research could provide solid alternative procedures for future research by emphasising the importance of the time series approach and how to choose the most appropriate forecasting technique for long-term forecasts, such as for the next 30 years.

7 Bidirectional Long Short-Term Prediction Model Based Neural Networks

In this chapter, a BI-LSTM prediction model was designed to predict short-term performance in terms of solar irradiance of the GCC region. BI-LSTM confers the advantages of manipulating information in two opposing directions and providing feedback to the same outputs via two different hidden layers. A BI-LSTM's output layer concurrently receives information from both the backward and forward layers. Predicted solar irradiance values include GHI, DNI and DHI based on historical weather data collated for the period from the 1st January 1985 to the 26th June 2021 at hourly intervals for all the GCC countries (*see section 4.2.2 and A.5 Appendix 5*). The results of the BI-LSTM prediction model were analysed and discussed in this chapter for the KSA while the Figures for the other GCC countries are presented in *A.3 Appendix 3*.

7.1 Model Background

In recent years, AI technologies, including DL, have become incredibly influential as a promising branch of ML [236]. They are supported by several advantages, including high generalisation capabilities and big data processing when compared to shallow models and, as such, offer both supervised and unsupervised feature learning algorithms [237]. Supervised learning algorithms are applied to the pre-labelled original dataset. The original dataset has input and output variables, while the supervised learning process employs algorithms for learning the mapping functions [238]. The supervised learning algorithms enable the model to relate the signal dataset to an activity class [238], while the unsupervised learning algorithms can extract the learning features from the original dataset [239] and can reconstruct their patterns. These technologies are characterised by multiple linear processing layers and large-scale hierarchical data representation [240]. The large numbers of layers and increased computational complexity refer to a more complex DL architecture which can utilise and analyse major issues inherent in big data, including the extraction of complex patterns from large volumes, semantic indexing, data tagging, the fast retrieval of information, and the simplification of discriminatory tasks. DL has several approaches, including autoencoder (AE) coding [241], deep belief networks (DBNs) [242], deep Boltzmann machines (DBMs) [243], convolutional neural networks (CNNs) [244], and RNNs [245]. DL provides a comprehensive solution for

various engineering applications including energy prediction and the monitoring of power systems. In terms of optimal power system operation and planning, wind speed and solar energy interval prediction are gaining vital importance. However, forecasting efficiency is an arduous process due to the obvious issues of fluctuations in wind speed and solar irradiance. Therefore, numerous advanced DL-based approaches have been developed in previous studies to enhance prediction accuracy and foster potential innovations in the field. Wang et al. [246] predicted PV power output via wavelet transformation and a deep CNN. This technique decomposes the input signal into multiple frequency sequences. In addition, Piazza et al. [247] used a non-linear autoregressive function with exogenous input based on a NN to predict hourly intervals of solar irradiation and wind speed. This approach required the use of external data, including temperature or wind direction values, to provide the model with more detail. Another important study was conducted by Wang et al. [248] to predict short-term solar irradiance based on an ANN model. In addition, Sözen et al. [249] employed the ANN model to predict potential solar energy in Turkey. However, these forms of models can be improved by increasing the number of hidden layers. Altan et al. [250] developed a LSTM neural network with a decomposition technique and grey wolf estimator to predict short-term wind speeds. Moreover, combining multiple techniques to develop a hybrid prediction model can serve to improve the model's performance and prediction accuracy.

Hu et al. [251] created a non-linear hybrid model based on LSTM, a differential evolution algorithm, a non-linear hybrid mechanism, and a hysteretic extreme learning machine to enhance the accuracy of wind speed prediction. The differential evolution algorithm is utilised to upgrade the model, although it is difficult to balance. Alli et al. [252] used the time series model-based LSTM NN to predict solar radiation, wind speed, precipitation, relative humidity, and temperature values. Moreover, this model is able to cope with different types of weather data. Liu and Lin [253] conducted a study to predict the daily load performance in the UK during the COVID-19 pandemic restrictions using a multivariate time series forecasting-based BI-LSTM NN. The prediction model considered both solar and wind power, including wind speed, biomass, and temperature values. Further, the model recorded high values of the RMSE with obvious overfitting. K.U. and Kovoor [254] proposed a wind speed prediction model-based ensemble empirical mode decomposition and BI-LSTM NN. The model enhanced the accuracy valuesdue to its data denoising and disintegrating characteristics. Zhen et al. [255]

developed a short-term prediction model using the BI-LSTM and genetic algorithm to estimate PV power output. This model is capable of comprehending the connection between several PV output as a series. In addition to the aforementioned studies, numerous studies have been presented that offer many promising ideas in the field of energy prediction.

In this chapter, a prediction model was designed based on the BI-LSTM. This model can estimate the future performance of solar irradiance, including GHI, DNI, and DHI, with associated wind speeds and ambient temperature values based on a time series. In addition, the model predicts future values for one week (169 h) at hourly intervals. Moreover, the chapter aims to contribute to the issues of wind and solar energy fluctuation and intermittence that can be used to investigate their implications on the stability of conventional power systems as they are influenced by such factors alongside ambient temperatures. Analysing the performance of significant quantities of historical data for a specific region can assist in our understanding of the variability of wind and solar energy in this region.

7.1.1 Overview of DL Approaches

ANNs are designed from hundreds of single units as a variety of interconnected processing elements, called neurons (connected to coefficients weighted as adjustable parameters) which represent the neural structures and are organised in layers [256]. ANNs are designed to simulate specific biological neural processes and process information similarly to the human brain to solve more complex problems [257]. The basic principle of an ANN is to infer and extract knowledge by detecting patterns, analysing the relationships arising between the data and then learning them based on experience and not pre-programming [256-258] by using a series of processes that are dependent on evaluating the available inputs. Each neuron receives input signals as aggregated data from other neurons or external stimuli from outside the network which are then analysed and processed locally through transfer functions to generate an output signal that is converted to other neurons or classified as external output [257]. Moreover, each processing element contains a transfer function (i.e., an output) and a weighted sum of the inputs which is termed the neuron activation function [256]. The processing element is an equation that is used to balance the inputs and outputs. The single output of the

neuron is produced by multiplying the input signals by the connection weights to combine them and then transferring the activation signal via a transfer function (see Figure 7-1). The transfer function can be calculated by incorporating the time-lagged observations and predictor variables into an ANN model [257]. The transfer function can specify the relationship arising between a node and a NN's inputs and outputs. This introduces the nonlinearity that is necessary for most ANN applications [257]. The transfer functions of the neurons are those basic elements that influence the behaviour of the NN which, in turn, depends on its learning rules and architecture [256]. In addition, the neurons are the basic components of an ANN and are considered the NN power that simulates the function of biological human neurons (as shown in Figure 7-1 [256]). The effective predictive approaches of ANNs are summarised in the following subsections.

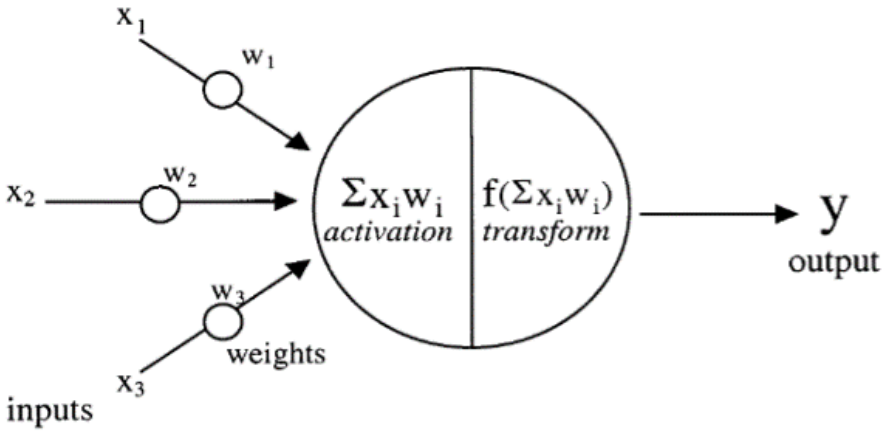

Figure 7-1. Basic components of ANN neuron model [256].

7.1.2 Autoencoder (AE)

The AE is an unsupervised learning [258] feeding forward NN approach that is trained to replicate its inputs to its outputs via the hidden layers [259, 260]. An AE can comprise of stackable units to create a deep and complex structure that forms a multilayer NN. The stacked autoencoder produces fewer reconstruction errors as compared to shallow models [261]. The AE consists of four major components, namely the encoder, decoder, reconstruction loss, and bottleneck [258]. There are two advantages of the AE in that (i) it applies the latent representations of features to improve model efficiency, and (ii) the reduction in dimensionality decreases training time [262].

7.1.3 The Restricted Boltzmann Machine (RBM)

The RBM is a commonly used deep probabilistic model and represents undirected probabilistic approaches employing two basic layers called the Boolean visible neuron layer and the binary-valued hidden layer [237,260]. The first layer comprises visible inputs (v), while the second layer consists of hidden variables (h). Figure 7-2 represents the configuration of an RBM, where W stands for weight, and a and b are both biases. The layers of the RBM are stacked one on top of the other to make it deeper [260]. The RBM is used for learning the distribution of probability through its data input space to demonstrate desirable potential in its configuration [263]. The distribution is learned by reducing this model that was developed as a feature of thermodynamic-based network parameters [237]. The assumption procedure includes defining reconstructed data driving probabilities through both the visible layers and the hidden layer.

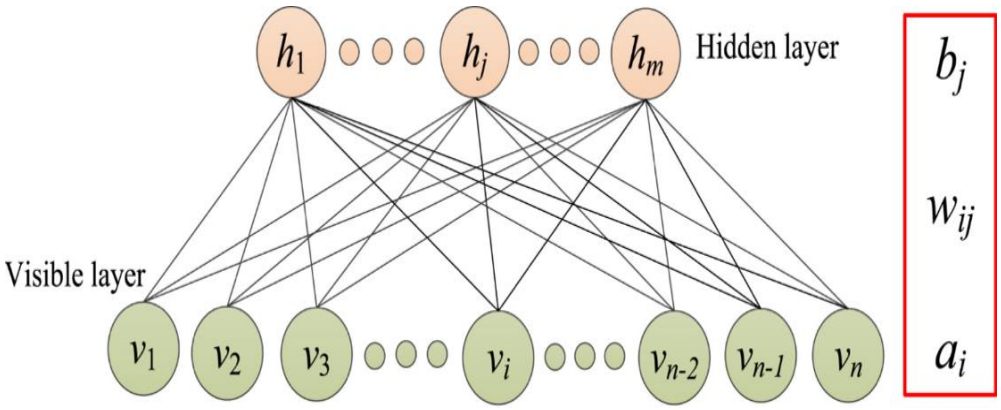

Figure 7-2. Two-layer configuration of the RBM [264].

7.1.4 Deep Belief Network (DBN)

The DBN is considered a form of NN that comprises multiple hidden layer units [265]. The DBN acts as a stacked RBM made up of several hidden layers and employs the backpropagation algorithm for training [260, 266]. Each DBN layer contains an RBM. However, the RBM can be used with only one hidden layer. In the DBN architecture, there is no interconnection to link the units of each layer [242]. The connections link each unit in a layer to the next layer's units [260]. Figure 7-3 illustrates the configuration of a 4-layer DBN with three hidden and one visible layer. While the top three layers remain undirected, all of the intermediate layers' connections are oriented toward the data layer.

As such, the DBN can be trained with unsupervised learning to extract discriminant features [242] by contrastive ramification and the DBN algorithm can decrease the dimensionality of the input dataset [267]. Two steps must be carried out to perform DBN training for regression. First, the DBN is trained by learning through divergence in an unsupervised method which leads to a reduced set of features from the data [267, 268]. Then, appending the ANN as a single layer for fully linked neurons to the pretrained architecture is the second training step [267, 268]. For forecasting, the new attached layers must be trained for the desired target [267].

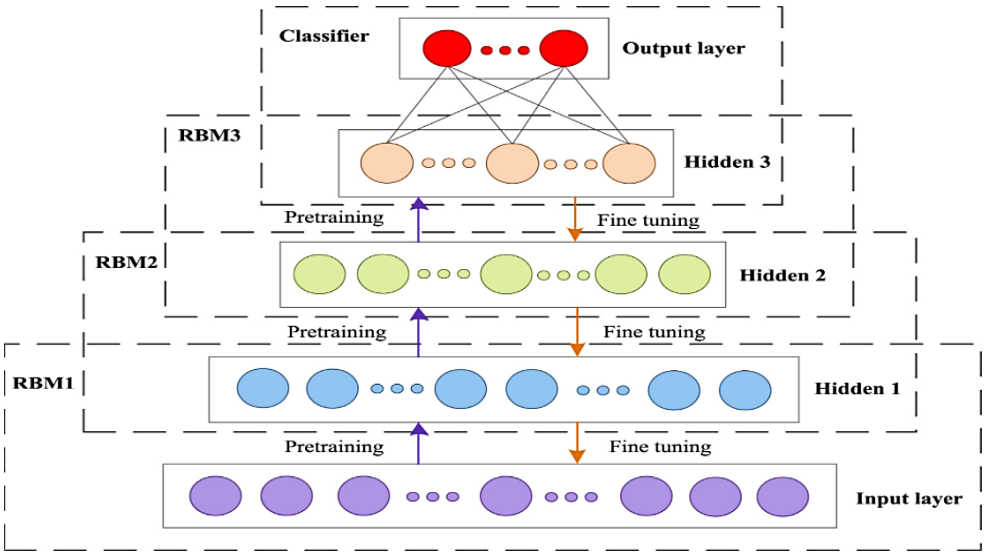

Figure 7-3. The configuration of the DBN consists of three main stacked RBMs with an output layer [264].

7.1.5 Deep Boltzmann Machine (DBM)

The DBM is a type of deep structure NN approach with a similar design to the RBM. The DBM has more hidden layers with many more variables as compared to the RMB [260], and the DBM's hidden units are organised into a layer hierarchy rather than a single layer [243]. The connectivity restriction of the RMB enables complete connectivity between subsequent layers, while there are no connections between the layers or between non-neighbouring layers [243]. A DBM consists of undirected connections connecting all layers between the variables, including the visible and multiple hidden layers. Higher-order correlations can be captured by each layer arising between the hidden features in the lower layer (see Figure 7-4 [243]). Along with a bottom-up pass, the approximate inference method can integrate top-down feedback which allows the DBM to spread ambiguity and interact with uncertain information more robustly. The DBM can learn

more complicated internal representations – a promising approach to overcoming problems [243]. The DBM is trained as a joint model and represents a graphical model that is absolutely undirected, while the DBN can be a directed and undirected model and trained appropriately in layers [243]. In terms of computing, DBM training is costlier than DBN training.

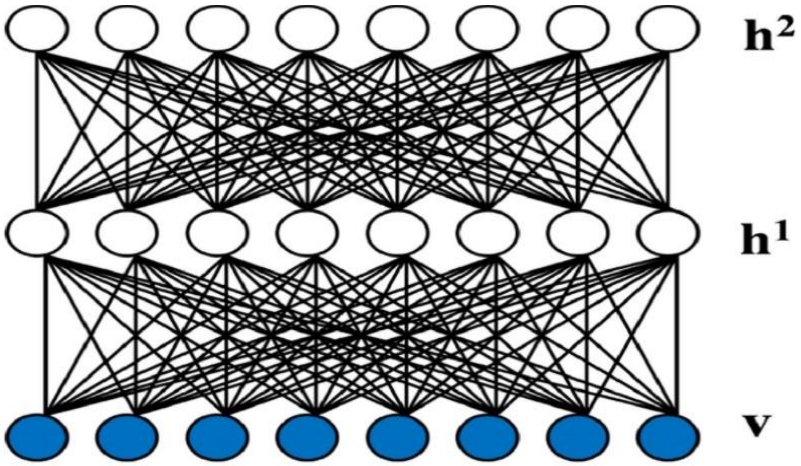

Figure 7-4. The configuration of the DBM [269].

7.1.6 Convolutional Neural Network (CNN)

The CNN is considered a neuronal feed-forward NN and has a completely connected network with fewer parameters to learn [258, 260]. In addition, the CNN model consists of three main layer types, namely completely connected layers, pooling layers, and convolutional layers (see Figure 7-5). Usually, the data input applied to the CNN is 2D [240]. The convolutional layers contain feature maps and multiple filters in the form of parallel layers which are the neuronal layers with weighted inputs to generate output values [270, 271]. The pooling layer is used to minimise overfitting, generalise the feature representations, and sample the feature map of the previous layer [271]. The completely connected layer is applied for prediction applications at the end of the network as the detector stages with modified linear activations. CNN models are commonly used in several applications, such as imaging and audio processing, video recognition, speech recognition, and natural language processing (NLP).

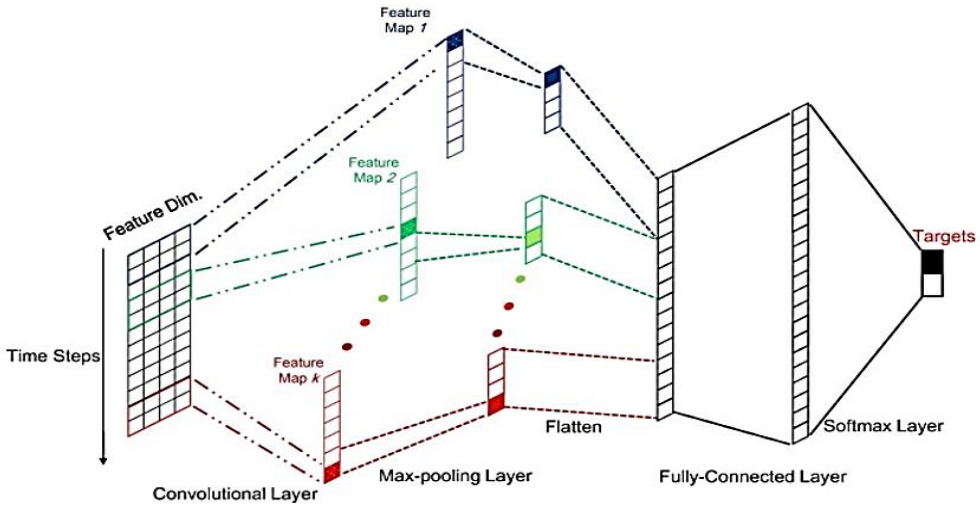

Figure 7-5. The three main layers of a CNN including softmax layer [240].

7.2 Model Configurations Based Neural Networks

This section discusses the main approaches that we used to develop the prediction model based on an RNN, LSTM, and a BI-LSTM to predict the future performance of solar irradiance, including GHI, DNI, and DHI values. Further, the prediction model configurations and error metrics are discussed in this section.

7.2.1 Recurrent Neural Network (RNN)

An RNN is a NN designed to perform sequence data processing and utilise each sequence variable iteratively [272]. RNNs consist of an internal memory, which is used for updating neuronal status in the network system based on the preceding input(s), and to employ backpropagation for training over time [260,273]. RNNs essentially provide one-way information transfer from the inputs to the hidden units with unidirectional information transfer synthesis from the previous temporal unit [274]. Moreover, the RNN identifies a directional loop that can learn and utilise previous data as an important difference from standard feed-forward NNs to the current output. RNNs have unique advantages due to the increased number of stacking layers in their architecture [273]. Such a vanishing gradient descent can be a disadvantage of RNNs in some cases [275]. In addition, several intermediate steps are needed by RNN-based approaches, which do not support training and configuration in an end-to-end manner [276]. However, the algorithm is able to learn uncertainties replicated in previous time measurements due to the sharing advantages of RNN. Further, the RNN obtains much deeper learning over time. RNNs seek to map the

input in the computational algorithms to graph the sequential (N) of x value in a commensurate sequential output (y), as shown in Equations (7-1)–(7-3), while the learning process is carried out for each time step from ($t = 1$ to $t = \tau$) [277]. The RNN neuronal parameters at the layer l can update their sharing states at each time step (t). The $x(t)$ indicates the data input, $h_l^{(t)}$ is sharing status of layer (l), and $y(t)$ refers to the corresponding prediction. In addition, $a_l(t)$ is the input value of the layer, and b indicates the base.

$$a_1(t) = b_1 + W_1 * h_1^{(t-1)} + U_1 * x^{(t)} \quad (7\text{-}1)$$

$$a_l(t) = b_l + w_l * h_l^{(t-1)} + U_l * h_l^{(t)} \quad (7\text{-}2)$$

$$y(t) = b_N + W_N * h_N^{(t-1)} + U_N * h_N^{(t)} \quad (7\text{-}3)$$

7.2.2 Long Short-Term Memory (LSTM)

LSTM is a complex computing unit that can produce strong results across a range of sequence modelling tasks due to its exceptional capacity to retain sequence information over time. In the training process of RNNs, LSTM can address the exploding and vanishing gradient phenomenon [278]. The remarkable findings from the implementation of LSTM in numerous fields indicate that it is capable of capturing the data variance pattern and defining the data associated with the time series dependency and relationship. This type of NN has been created to overcome the limitations of RNNs in learning long-term incompatibilities [279]. The memory cells incorporated into the LSTM architecture which store data are the strongest approach for identifying and manipulating the long-range context [280,281]. Each LSTM block is comprised of three main gates: an input gate, a forget gate, and an output gate equipped with a memory cell [282]. These gates and the sigmoid activation feature regulate changes in cell status. Figure 7-6 shows the LSTM cell configuration with the key components of the LSTM, such as the adding element level and the multiplication symbol, which correspond to the multiplication of the element levels. Additionally, the con represents the vector merging.

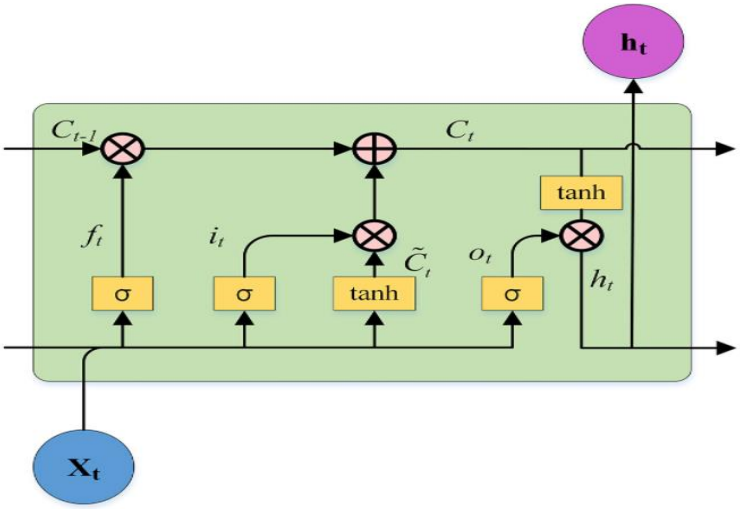

Figure 7-6. The long short-term memory cell unit [283].

The input gate (i_t) specifies the magnitude of the values flowing into the cell and stored in the memory of the processor. The forget gate (f_t) specifies the degree of the values that remain in the cell and removes those data which are not required from the memory. The output gate (o_t) triggers the LSTM's output activation and defines which information is used as the output. In addition, the input node (g_t) is a vector of cell activation. Equations (7-4)–(7-8) represent the mathematical performance of the LSTM, where h_t represents the hidden variable and the logistic sigmoid is denoted by σ.

$$f_{(t)} = \sigma\left(W_{xf}\ x_t + W_{hf}\ h_{t-1}\ + W_{cf}\ c_{t-1}\ + b_f \right) \tag{7-4}$$

$$i_{(t)} = \sigma\left(W_{xi}\ x_t + W_{hi}\ h_{t-1}\ + W_{ci}\ c_{t-1}\ + b_i \right) \tag{7-5}$$

$$g_{(t)} = f_t\ g_{t-1}\ + i_t \tanh\left(W_{xg}\ x_t + W_{hg}\ h_{t-1}\ + b_g \right) \tag{7-6}$$

$$o_{(t)} = \sigma\left(W_{xo}\ x_t + W_{ho}\ h_{t-1}\ + W_{co}\ c_t\ + b_o \right) \tag{7-7}$$

$$h_{(t)} = o_t\ \tanh(g_t) \tag{7-8}$$

7.2.3 Bidirectional Long Short-Term Memory (BI-LSTM)

BI-LSTM is developed using the approach of LSTM [284] to increase classification process performance. BI-LSTM is created by combining RNNs with LSTM approaches (see Figure 7-7) which can access a long-range context [285]. BI-LSTM networks outperform unidirectional networks such as LSTM, and they are significantly faster and more accurate than both conventional RNNs or time-windowed multilayer perceptrons (MLPs). Moreover, BI-LSTM has comprehensive detail for the sequential information for all the stages before and after each step in the given sequence [285]. In addition, BI-LSTM employs the LSTM algorithm to compute the hidden layers. Unlike LSTM, one characteristic of BI-LSTM is that it is capable of processing data in two different directions by utilising two hidden layers and forwarding the results to the same output layer [286,287].

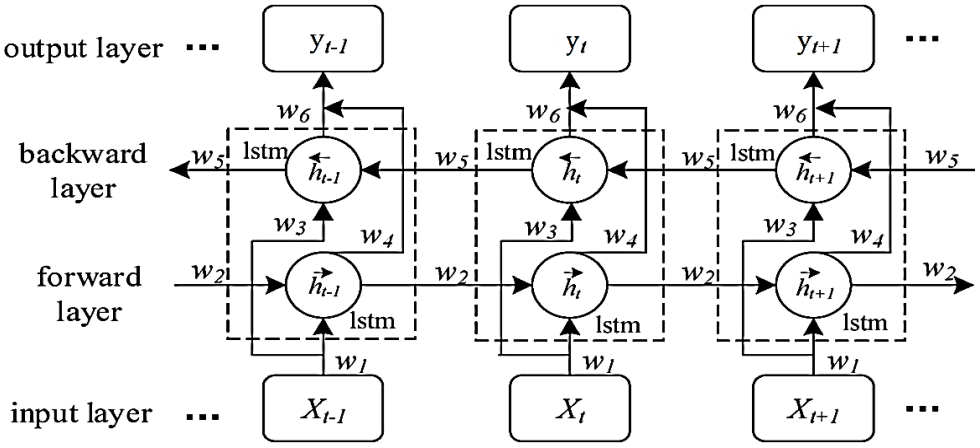

Figure 7-7. The structure of the bidirectional long short-term memory unit [288].

The forward hidden $\overrightarrow{h}$ and the backward hidden $\overleftarrow{h}$ layers are the main parameters of the BI-LSTM as presented in Equations (7-9) and (7-10), respectively. Equation (7-11) represents a combination of the forward hidden $\overrightarrow{h}$ and the backward hidden $\overleftarrow{h}$ layers. Backpropagation over time is employed to learn the necessary parameters from the training data, using the output sequence $y_{(t)}$ to iterate the backward layers based on the error function. The hidden layers (Ḥ) are used for N stack layers, while the hidden vector series h^n is computed sequentially via n (n = 1) to N (t = 1,…, T), as indicated in Equation (7-12). In addition, $h^0 = x$. y_t denotes the network's ultimate output, as illustrated in Equation (7-13).

$$\vec{h}_{(t)} = \mathrm{H}\left(W_{x\vec{h}}\ x_t + W_{\vec{h}\vec{h}}\ \vec{h}_{t-1} + b_{\vec{h}} \right) \quad (7\text{-}9)$$

$$\overleftarrow{h}_{(t)} = \mathrm{H}\left(W_{x\overleftarrow{h}}\ x_t + W_{\overleftarrow{h}\overleftarrow{h}}\ \overleftarrow{h}_{t+1} + b_{\overleftarrow{h}} \right) \quad (7\text{-}10)$$

$$\mathrm{y}_{(t)} = \left(W_{y\vec{h}}\ \vec{h}_t + W_{y\overleftarrow{h}}\ \overleftarrow{h}_t + b_y \right) \quad (7\text{-}11)$$

$$h^n{}_{(t)} = \mathrm{H}\left(W_{h^{n-1}h^n}\ h^{n-1}{}_t + W_{h^n h^n}\ h^n{}_{t-1} + h^n{}_h \right) \quad (7\text{-}12)$$

$$y_{(t)} = \left(W_{h^N \mathrm{y}}\ h^N{}_t + b_y \right) \quad (7\text{-}13)$$

7.2.4 The Bidirectional Long Short-Term Memory Model Structure

The prediction model was built using Python programming which has a large memory and can handle datasets of vast volumes. It also incorporates a wide range of pre-built libraries. The datasets were prepared and cleaned in preparation for processing. A suitable BI-LSTM model was developed based on computational approaches (*section 3*) using various layer numbers and model parameters. The number of layers, the setting of the neurons, and the training, test, and validation split size are presented in Table 7-1. Moreover, each type of data required different parameter settings to optimise the BI-LSTM fit owing to variations in the dataset's size and nature. Further, in the factorisation of the learning machine network, the two most essential BI-LSTM model parameters are the number of inputs and the number of neurons within the hidden layer. The error metrics remain nearly constant, with only very minor fluctuations when the number of neurons exceeds 150 and is less than 300, which is a result of the extreme learning machine networks' randomisation of input weight(s). The BI-LSTM model architecture can be used for a variety of prediction tasks based on several parameters, including its ability to enable additional training by iterating the input data twice, and the common requirement of fewer neurons than are needed for standard LSTMs. In addition, increasing the number of timesteps or lagging features to predict the label will work up to a point. It must use a basic LSTM each time, which increases the timesteps to set a baseline. However, the nature of the historical data, its size, its intervals, inputs, outputs and the type of predication—whether it is short-term or long-term—and the error metrics' values all

determine the number of layers, hidden neurons and the parameter settings.Figure 7-8 shows the flowchart of the proposed BI-LSTM model.

Table 7-1. Number of layers and the parameters hyperparameters settings of the BI-LSTM model.

No.	Element	Number of Layers	Size of Layer Neuron	Epoch Size	Batch Size	Validation Split (%)	Training Size (%)	Test Size (%)
1	GHI	4	12	30	64	0.03	79	20.97
			24					
			12					
			6					
2	DNI	5	12	50	84	0.02	79	20.98
			24					
			12					
			12					
			6					
3	DHI	2	100	40	74	20	79	20
			50					

7.2.4.1 Data preparation

Historical solar data was collated from the Meteoblue weather service's portal [188] for the GCC countries, including GHI, DNI, and DHI values, as presented in Figure 4-1 to Figure 4-3 for the KSA and *A.5 Appendix 5* for the other GCC countries. The actual historical data covers a period of over 36 years at hourly intervals for the period from the 1st January 1985 to the 26th June 2021. This data was used to evaluate and predict future GHI, DNI, and DHI values for the next 169 h across the GCC region. The geological conditions have changed and varied widely over the previous 36 years. This large quantity of historical data can be accurately forecasted by the BI-LSTM NN prediction model. The data were analysed, verified, and cleaned to ensure that no values were missing or duplicated. Moreover, Dickey-Fuller theory confirmed that all the data were stationary with p-values of less than 0.05. Further, historical data quality was key to enabling the BI-LSTM model to extract essential components and produce accurate results.

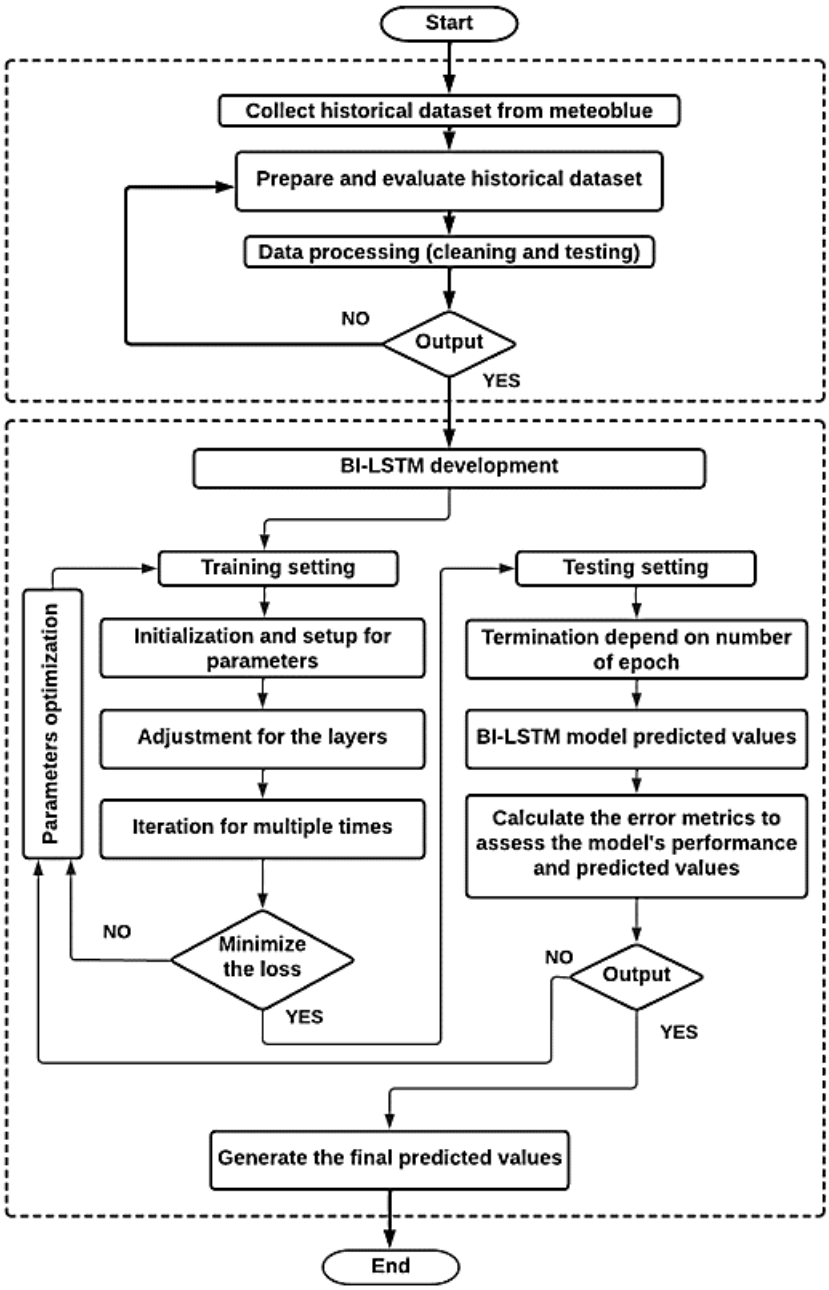

Figure 7-8. The flowchart of the proposed BI-LSTM model.

7.3 Results Analysis and Discussion

The developed BI-LSTM model was implemented to predict the future values of the three types of solar irradiance (GHI, DNI and DHI) 169 h in advance from 23:00 h 27th June 2021 to 23:00 h 3rd July 2021, based on an historical dataset covering over 36 years for different locations across the GCC region. Based on the predicted results for solar irradiances, shown in Figure 7-9 to Figure 7-14 for the KSA and Figures A.3–1 to A.3–30 in *Appendix 3* for the other GCC countries, the BI-LSTM model effectively handled the three different types of irradiance as a multimodal dataset. The values for GHI (Figure 7-9), DNI (Figure 7-11), and DHI (Figure 7-12) for the KSA and Figures A.3–1 to A.3–30 in *Appendix 3* for the other GCC countries did not exhibit any major overfitting between experimental and predicted results, which means the BI-LSTM model offers a promising performance with this type of dataset.

Further, in terms of forecasting accuracy indicators, the BI-LSTM model achieved notable error metrics for all GCC countries, as presented in Tables 7–2, A.3–1, A.3–2, A.3–3, A.3–4 and A.3–5. The forecasting error metrics for GHI for the KSA were as follows: RMSE = 7.8 W/M^2; MAE = 5 W/M^2; MSE was 61 W/M^{2}and the MAPE = 2.5%. In addition, the p-value was 4.01×10^{-21} with an R^2 recorded of 99% for the three types of solar irradiance in the KSA (see Table 7-2).

The GHI error metrics of Oman are RMSE = 17.9 W/M^2, MAE = 6.3 W/M^2 and MSE = 312 W/M^2, which is the highest value recorded for Oman's GHI. While the MAPE = 2.6% (all Oman's p-values are 0% with R^2 values of 99% as presented in Table A.3–1), the UAE's GHI forecasting accuracy indicator rates for the three types of solar irradiance were lower than those for Oman. The corresponding error metrics for the UAE for GHI are an RMSE = 16.2 W/M^2, MAE = 9.85 W/M^2, MSE = 262.5 W/M^2, and a MAPE = 2.8%. A p-value of 2.47×10^{-27} % and R^2 values are 99 % for the three types of solar irradiance in the UAE (Table A.3–2).

Kuwait's GHI forecasting accuracy indices were superior to those of Oman and the UAE. Kuwait's GHI error metrics are RMSE = 8.5 W/M^2, MAE 5.4 W/M^2, MSE = 72.7 W/M^2, and MAPE = 1.5% (with a p-value of 2.47×10^{-27} % and an R^2 of 99% for the three kinds of solar irradiance) as shown in Table A.3–2. Qatar outperformed Kuwait, Oman, and the UAE in terms of GHI forecasting accuracy, wherein RMSE = 8.1 W/M^2, MAE = 4.9 W/M^2, MSE = 65.6 W/M^2, and MAPE = 4.4%. Qatar's p-value = 2.47×10^{-27} % with an

R^2 of 99% for all three solar irradiance categories (see Table A.3–2). The proposed BI-LSTM forecasting model continues to record the best values for Bahrain's GHI error indicators, as illustrated in Table A.3–5. Bahrain's GHI error metrics are RMSE = 7.2 W/M^2, MAE = 4.3 W/M^2, MSE = 52.1 W/M^2, and MAPE = 2.4%. Bahrain's p-value = 2.97×10^{-28}%, with an R^2 = 99% for all three solar irradiance categories.

The RMSE of the KSA's DNI is reduced to 7.7 W/M^2, while the MAE increased to 6.3 W/M^2 due to two main factors: (i) the type of dataset; and (ii) the different parameter settings in Table 7-1. In addition, the MSE of the KSA's DNI is reduced to 59 W/M^2, while the MAPE value grew rapidly to 45%. Oman's DNI error metrics include an RMSE = 8.5 W/M^2, MAE = 6.1 W/M^2, MSE = 73.2 W/M^2, and MAPE = 36.6%. Oman has remarkably different DNI error values than those observed for GHI, except for its MAPE value. The UAE's DNI error metrics are RMSE = 8.1 W/M^2, MAE = 6.2 W/M^2, MSE = 8.1 W/M^2, and MAPE = 27% with a p-value of 8.66×10^{-30}%. The UAE's DNI errors are significantly lower than those of Oman. Kuwait's DNI error indicators are as follows: RMSE = 9.1 W/M^2, MAE = 7.7 W/M^2, MSE = 82.6 W/M^2, and MAPE = 30.1% with a p-value = 2.13×10^{-29}%. Except for MAPE, Kuwait has higher error percentages than Oman or the UAE. Qatar's DNI error measurements are RMSE = 8.9 W/M^2, MAE = 7.5 W/M^2, MSE = 79.5 W/M^2, and MAPE = 44.4% with a p-value = 2.60×10^{-29}%. Qatar has lower DNI error levels than Kuwait, excepting the MAPE value. The DNI error measured values for Bahrain are RMSE = 9.7 W/M^2, MAE = 7.8 W/M^2, MSE = 94.8 W/M^2, and MAPE = 40.9% with a p-value = 8.56×10^{-30}%. Bahrain's DNI error rates are significantly higher than those for GHI.

The MAPE values were affected by the nocturnal zero values of solar irradiance in the historical data. The MAPE values contrast with the other data, particularly as regards the value of MSE when considering all three types of solar irradiance data from the six different countries. When there is a rise in the value of MAPE, MSE values fall, and vice versa. Moreover, the error metrics of KSA's DHI recorded a sharp decrease, with an RMSE value of 2.4 W/M^2, while the MAE = 1.7 W/M^2, the MSE = 6 W/M^2, and the MAPE value was reduced to 14.3% with p-value = 1.19×10^{-22}%. Oman's HDI error measures show a significant improvement as compared to Oman's GHI and DNI, except for MAPE. The error metrics of Oman's DHI are RMSE = 3.8 W/M^2, MAE = 2.7 W/M^2, MSE = 14.2 W/M^2, and MAPE = 44.9% (see Table A.3–1). The UAE's DHI error measurements indicate an RMSE = 4.6 W/M^2, MAE = 2.8 W/M^2, MSE = 21.6 W/M^2,

and a MAPE = 30.6 %, with a p-value = 2.27×10^{-28} % as illustrated in Table A.3–2. Kuwait's DHI error measurements indicate an RMSE = 1.7 W/M^2, MAE = 1.2 W/M^2, MSE = 2.8 W/M^2, a MAPE = 28.5 %, and a p-value = 1.92 × 10−25%. The error rates for the DHI in Kuwait were lower than those of the KSA, Oman, and the UAE. The RMSE, MAE, MSE, MAPE, and p-value for the DHI in Qatar were 2.6 W/M^2, 2 W/M^2, 6.7 W/M^2, 36.7%, and 9.49×10^{-27} %, respectively. For the DHI in Bahrain, the RMSE was reported as 2.6 W/M^2, the MAE = 1.9 W/M^2, the MSE = 6.7 W/M^2, and the MAPE = 24.9%, with a p-value = 8.15×10^{-28}.

The BI-LSTM model revealed remarkable outcomes and performance with the short-term predictive values for solar irradiance. Despite the massive quantity of training data, the BI-LSTM model did not demonstrate any overfitting. Tables 7–2, A.3–1, A.3–2, A.3–3, A.3–4 and A.3–5 illustrate the future predicted values for the GHI, DHI, and DNI for 169 h ahead. Overall, the BI-LSTM forecasting model was notable for GHI, DNI and DHI error values. The DHI recorded low values for the error metrics of all six countries. However, all the error values of the BI-LSTM model, using these different types of historical datasets, were considered to be relatively small when compared to other prediction models, demonstrating their flexibility in terms of new historical data observations. The performance comparison between the proposed BI-LSTM model and the other external solar irradiance models (Table 7-3) also revealed that the proposed model's evaluation metrics were superior to those of the other external solar irradiance models tested.

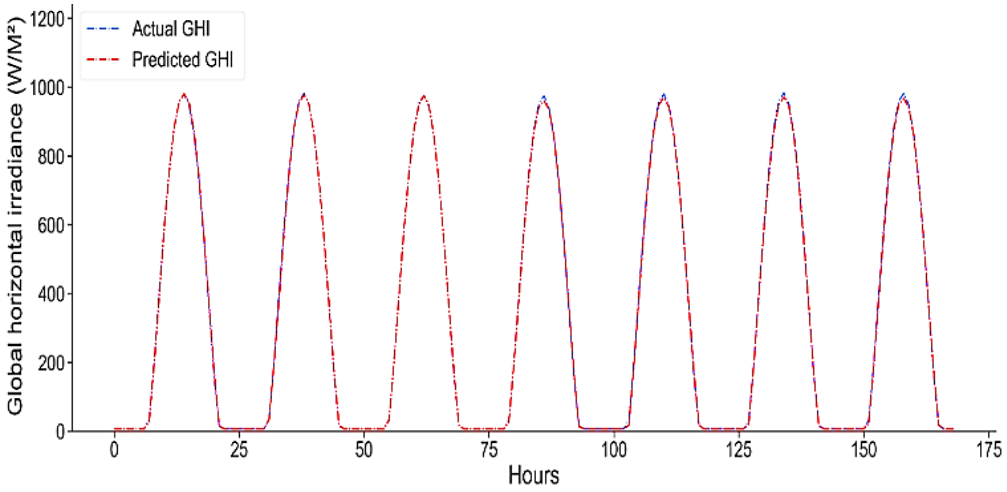

Figure 7-9. Real and predicted values of GHI for the KSA showing the fit and performance of BI-LSTM model.

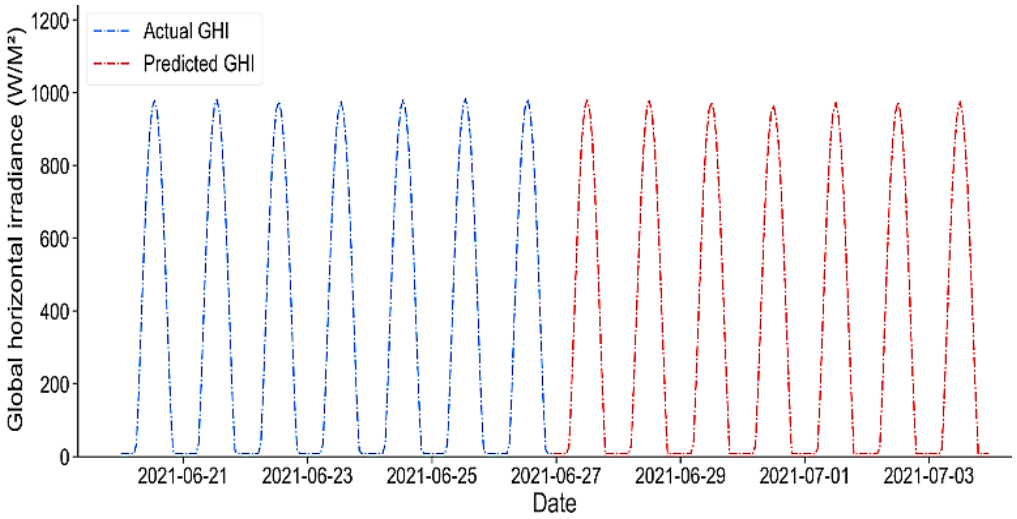

Figure 7-10. The GHI's predicted future values for the next 169 hours for the KSA.

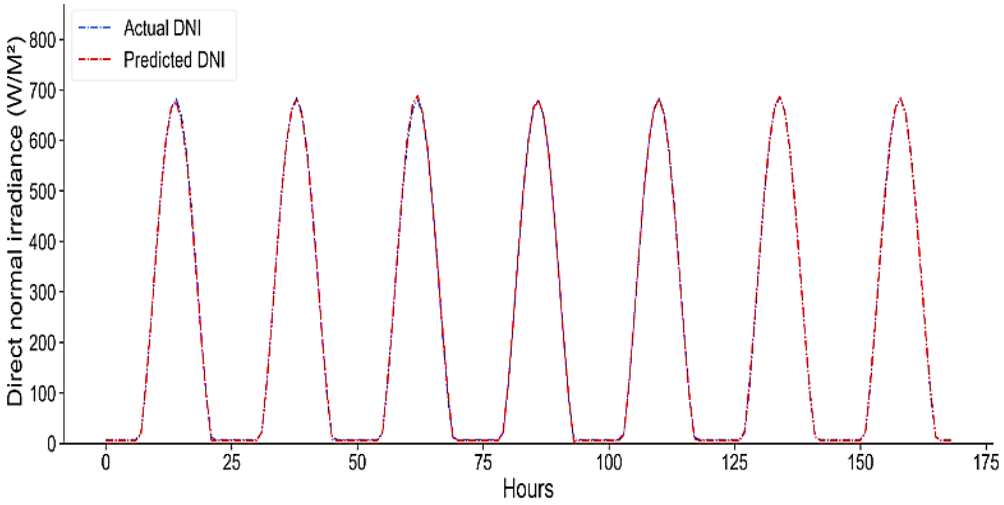

Figure 7-11. KSA's real and predicted values for DNI showing the fit and performance of BI-LSTM model.

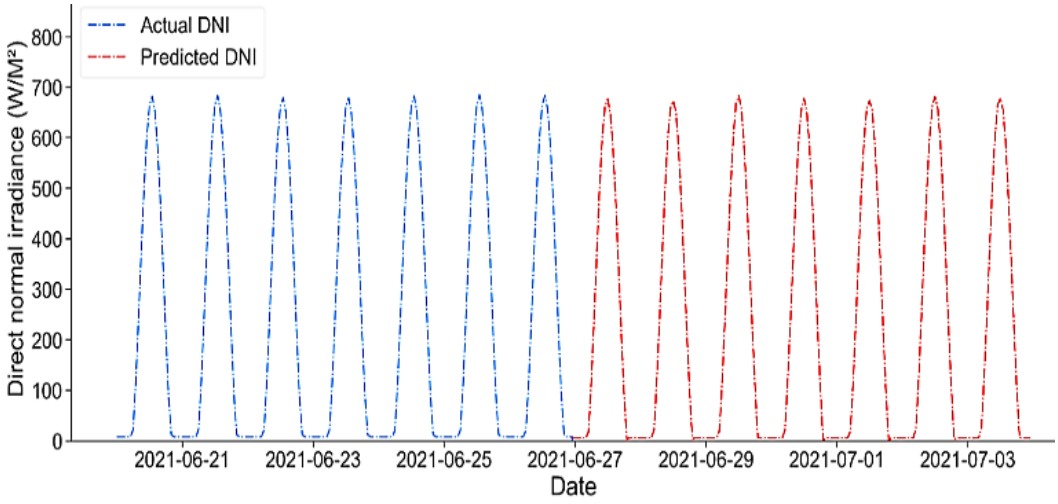

Figure 7-12. The DNI's predicted future values for the next 169 hours for the KSA.

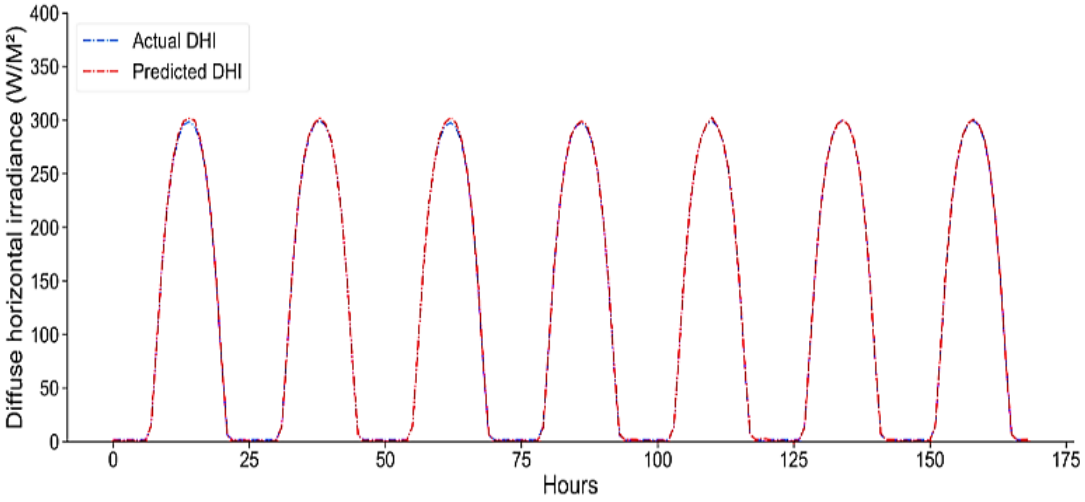

Figure 7-13. Real and predicted values of DHI for KSA showing the fit and performance of BI-LSTM model.

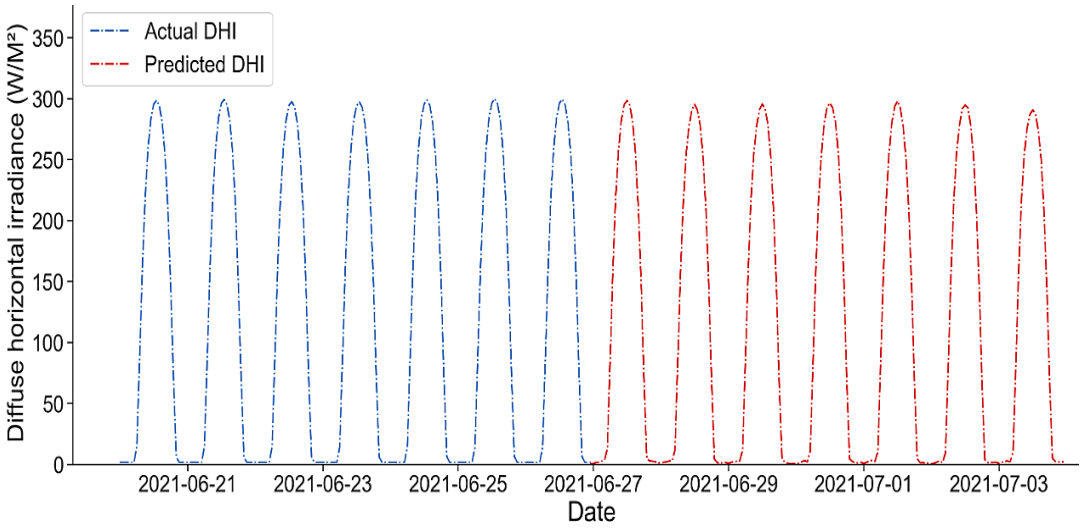

Figure 7-14. The DHI's predicted future values for the next 169 hours for the KSA.

Table 7-2. Forecasting accuracy indicators for the KSA using the BI-LSTM model.

No.	Metric	GHI (W/M²)	DNI (W/M²)	DHI (W/M²)
1	RMSE	7.82	7.68	2.44
2	MAE	5	6.28	1.73
3	MSE	61.21	59.01	5.98
4	MAPE (%)	2.45	42	14.29
5	*p*-value (%)	4.01×10^{-21}	2.78×10^{-23}	1.19×10^{-22}
6	R^2 (%)	99	99	99

7.3.1 BI-LSTM Model Evaluation

The BI-LSTM prediction model was evaluated by implementing the three main types of historical datasets for all six GCC countries (covering the three types of solar irradiance), based on the parameter settings detailed in Table 7-1. In addition, the proposed BI-LSTM model was compared with several external ANN prediction models to evaluate its performance, as presented in Table 7-3.

Table 7-3. Comparison of proposed BI-LSTM model performance with external solar irradiance models.

No.	Model	RMSE (W/m^2)	MSE (W/m^2)	MAE (W/m^2)	MAPE (%)	R^2 (%)
1	BI-LSTM [289]	20.71	-	7.60	17.40	98
2	PCA-BI-LSTM [290]	-	6063.90	42	-	94
3	SCA-BI-LSTM [291]	119.71	69.50	79.62	-	89
4	CEN-BI-LSTM [291]	85.60	56	66.40	-	95
5	CEN-SCA-BI-LSTM [291]	81.30	52	61.80	-	95
6	BI-LSTM [291]	124	70.30	82.22	-	88
7	CEN-ANN [291]	93.42	61	71.51	-	94
8	**BI-LSTM proposed model**	**5.98**	**42.06**	**4.33**	**19.58**	**99**

In comparison to the observational results and ANN models presented in Table 7-3, the BI-LSTM offered significant advantages over other models in terms of its accuracy and interpretability. The BI-LSTM prediction model showed strong performance with all three principal types of historical dataset, especially DHI values. The epoch numbers and error indicators had a significant connection, implying that, as the epoch numbers rise, so error values decrease, although the training time also increases. Moreover, by combining a large amount of historical data with a significant amount of training data, the duration of the simulation periods is extended even further. The subsequent steps are reliant on the preceding stages and so the BI-LSTM prediction model must be handled sequentially. Nevertheless, one of the most challenging problems was enhancing this model's generalisation capabilities and achieving improved outcomes. Generalisability is defined as the variation in the recognition rate of the BI-LSTM model as compared to earlier observational datasets (training data) with a dataset that the model has not previously seen (testing data). Further, the lack of generalisability of the model leads to excessive overfitting of training and testing datasets. The BI-LSTM model processes the dataset in two directions, with two hidden layers feeding the data forward to the same output layer.

In addition, the BI-LSTM model employs a time series to enhance generalisability by taking into consideration the impacts of the features of the predicted historical dataset values of the upcoming instant. The BI-LSTM model can be configured to predict the next 1 h in the future, 24 h ahead, or up to 4 weeks in the future, although increasing the future predicted interval values would raise the error metric indicators. Whenever a sufficient number of historical datasets are chosen, the effectiveness of the BI-LSTM model becomes apparent and its short-term predictive performance and accuracy are improved.

8 Gated Recurrent Unit Prediction Model Based NNs

In this chapter, the GRU NN prediction model was developed to predict the short-term wind speed and temperature values of the GCC region one week in advance. The GRU prediction model automatically learned the features, used fewer training parameters, and required a shorter time to train as compared to other types of RNN. The wind speed and temperature historical dataset was gathered from GCC countries at hourly intervals for the period from the 1st January 1985 to 26th June 2021 (*see section 4.2.2 and Appendix 5*). The results of the GRU prediction model were analysed and discussed in this chapter for the KSA while the Figures for the other GCC countries are presented *in Appendix 4*.

8.1 Model Background

Wind power generation has grown exponentially in recent years due to growing awareness of the global climate change crisis. This has required a transition from fossil fuel sources to renewable energy technologies. Although it has shown rapid growth in its deployment, wind energy's performance is restricted due to fluctuations in power generation as compared to other types of energy generation. The increase in wind power generation creates significant implications for operating systems, including variations in wind speed and intermittent/non-dispatchable power generation. These factors have an impact on the power generation system's quality, operation protection, distribution effectiveness, and cost [292]. In addition, the unstable nature of wind energy reduces the reliability of national grids when connected to large-scale wind farms. Wind energy variations can be counterbalanced using battery storage technologies. On the other hand, battery systems will play a significant role in raising the cost of wind energy generation and using diesel generators to support the national grid is not a decarbonisation solution. Forecasting approaches such as NN-DL can be employed to predict the future performance of wind speed based on the analysis of historical data or previous observations. Further, forecasting can reduce energy consumption, balance demand and supply, and optimise grid performance [293]. DL forecasting technology has sparked a great deal of interest in investigating comparable challenges with common uncertain effects [294]. Moreover, RNNs are a type of DL framework that are effective in interacting with time series. The operation of wind farms can be properly controlled and maintained ahead of time sequences using prediction technology and statistic models.

NNs are an active research topic in the AI field for generating predictive capabilities with fault-tolerant capacities [292]. In addition, prediction accuracy was enhanced by NN-DL approaches and statistical time sequence models. Nonetheless, the main issue with RNNs is the vanishing gradient problem, one which restricts RNN learning of long data sequences [292]. The gradient contains information that is used to update the RNN parameters and, when the gradient declines, the updating of the parameters becomes minimal, indicating that no meaningful learning occurs. The LSTM neural network, with its complex principles and architecture, was introduced to solve the vanishing gradient issue [281], which was proven to have effective performance and outperformed traditional prediction approaches for short-term predictions [267,295,296]. On the other hand, the challenges are that prediction models must be fast, efficient, and accurate. In 2014, the first basic model of a GRU NN was proposed by Cho et al. [297]. The GRU has a simple principle and architecture enabling it to be faster, more efficient, and more accurate, as it has fewer parameters than an LSTM. GRUs have been shown to perform on smaller and less frequent datasets relative to an LSTM block [293]. In this chapter, a prediction model based on a GRU approach is developed for predicting and analysing the future performance of wind speed and temperature values across short-term hourly intervals for a period of one week in advance (169 h). In addition, this chapter aims to contribute to the issue of the high volatility of wind energy which, alongside temperature considerations, can be used to investigate its impacts on the performance of power generation systems.

8.2 Gated Recurrent Unit Neural Networks

Gated Recurrent Unit Neural Network (GRU) theory is a gating mechanism approach that was developed based on ANNs. The GRUs inherit the LSTM's characteristics of the lack of an output gate, automated learning of features, the use of fewer training parameters, and a shorter time required to train in comparison to other RNN models, including the LSTM [298,299]. In contrast to the LSTM, the GRU can process different sizes of dataset frequencies and time series, including a smaller data range. The GRU block consists of two main gates, specifically the update gate $z_{(t)}$ and the forgetting, or reset gate $r_{(t)}$ with associated input gate, as illustrated in Figure 8-1 [300,301]. GRUs modulate the data via the gate unit. However, memory access is not provided by a separate memory unit. The update gate is used to regulate the prior information state which is required for the current state. In addition, the update gate facilitates the prediction model in estimating and

evaluating the size of previous data that must be transferred to the future [298]. The higher the value of the update gate, the greater the amount of state information gathered from the previous instant [302]. However, the reset gate is used to govern the flow of state information from the previous instant which is required to be disregarded. The reset gate primarily controls the amount of activation information that reaches the input as well as how the new input is combined with the previous memory [298]. The lower the value of the reset gate, the greater the amount of information that is ignored.

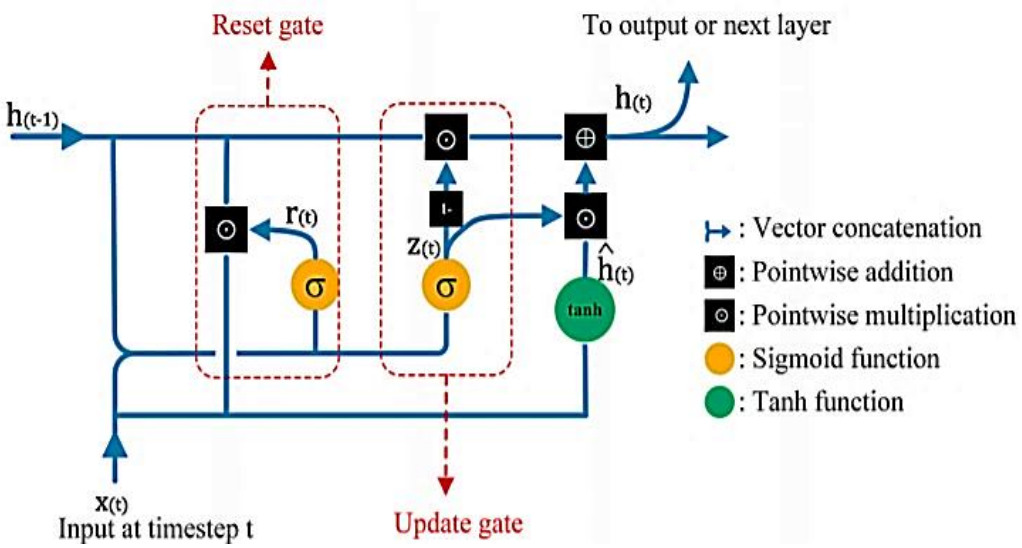

Figure 8-1. Architecture of a GRU network.

Mathematically speaking, the GRU network can be delineated by equations (8-1 to 8-4), where $z(t)$ is the update gate, $r(t)$ is the reset gate, and $x(t)$ is the input vector at time t [301]. In addition, W and U are the weight parameter matrices that are required to be learned for training. The terms $h(t-1)$ and $h(t)$ represent the output vector of the past state or previous layer and the current state, respectively. Moreover, b is the base vector, (σ_g) is a sigmoidal element, (σ_h) is the hyperbolic tangent, $(\odot)$ is a factor-wise multiplication, and the tan$h$ is the activation function that is used to control the flowing values via the network. The extracted features of the (σ_g) and tan$h$ functions are set to be (0, 1) and (1, 1), respectively [300]. The gradient descent technique is used to train the GRU and the elements are updated continuously until convergence [302].

$$r_{(t)} = \sigma_g(\, W_r \;\; x_t + \; U_r \;\; h_{t-1} \;\; + b_r \,) \tag{8-1}$$

$$z_{(t)} = \sigma_g(\, W_r \;\; x_t + \; U_z \;\; h_{t-1} \;\; + b_z \,) \tag{8-2}$$

$$h_{(t)} = 1 - z_t \odot h_{t-1} \; + \; z_t \odot \hat{h}_{(t)} \tag{8-3}$$

$$\hat{h}_{(t)} = \sigma_h(W_h \; x_t + \; U_h \; (r_t \; \odot h_{t-1} \;) + b_h \;) \tag{8-4}$$

8.2.1 Gated Recurrent Unit Model Structure

Python software was used to build and process the codes of the GRU model. The GRU prediction model was developed as a set of coding functions based on mathematical algorithms, including the definition of the model parameters (Figure 8-2). The training and testing sets accounted for 70% and 28% of the historical data, respectively, with the remaining data being used to validate the proposed method's predictive capabilities. The number of neurons in the first and second layers was adjusted to 64. The predicted errors were drastically reduced as the number of hidden neurons increased. When the number of neurons was 64, the RMSE caused by the randomisation of the input weights for the extreme learning network remained practically constant with only minor fluctuations. The number of epochs was set to 10, the batch size to 64, and the validation split to 0.02, which improved the model's fit. Further, in factorisation learning networks, the numbers of inputs and neurons of the hidden layer is the most important parameter in a GRU model.

8.2.1.1 Data preparation

The GCC region was selected as a case study for this research. A historical dataset was gathered in order to analyse and predict the behaviour of wind speed ($m.s^{-1}$) at an altitude of 80 m and temperature (°C) at a height of 2m for the following week at hourly intervals (169 h). All the real historical data utilised in this research cover the 36-year period from the 1st January 1985 to the 26th June 2021 at hourly intervals. This data is presented in *Section 4.2.2 and A.5 Appendix 5*. This research used an anemometer to collect the data from the Meteoblue weather service portal [189] which provided the historical wind speeds and temperature data. During the last 36 years, meteorological conditions have differed and varied over time, and so this large amount of historical data can provide more granular detail that can be considered by the GRU NN prediction model. Moreover, the quantity and quality of datasets are a basic factor for GRU models to extract the required features and obtain accurate prediction outcomes. To guarantee that no values were

missed or duplicated, all the data were reviewed, validated, and evaluated. The Dickey-Fuller test was applied to ensure that all the data were stationary, as was confirmed by p-values < 0.05.

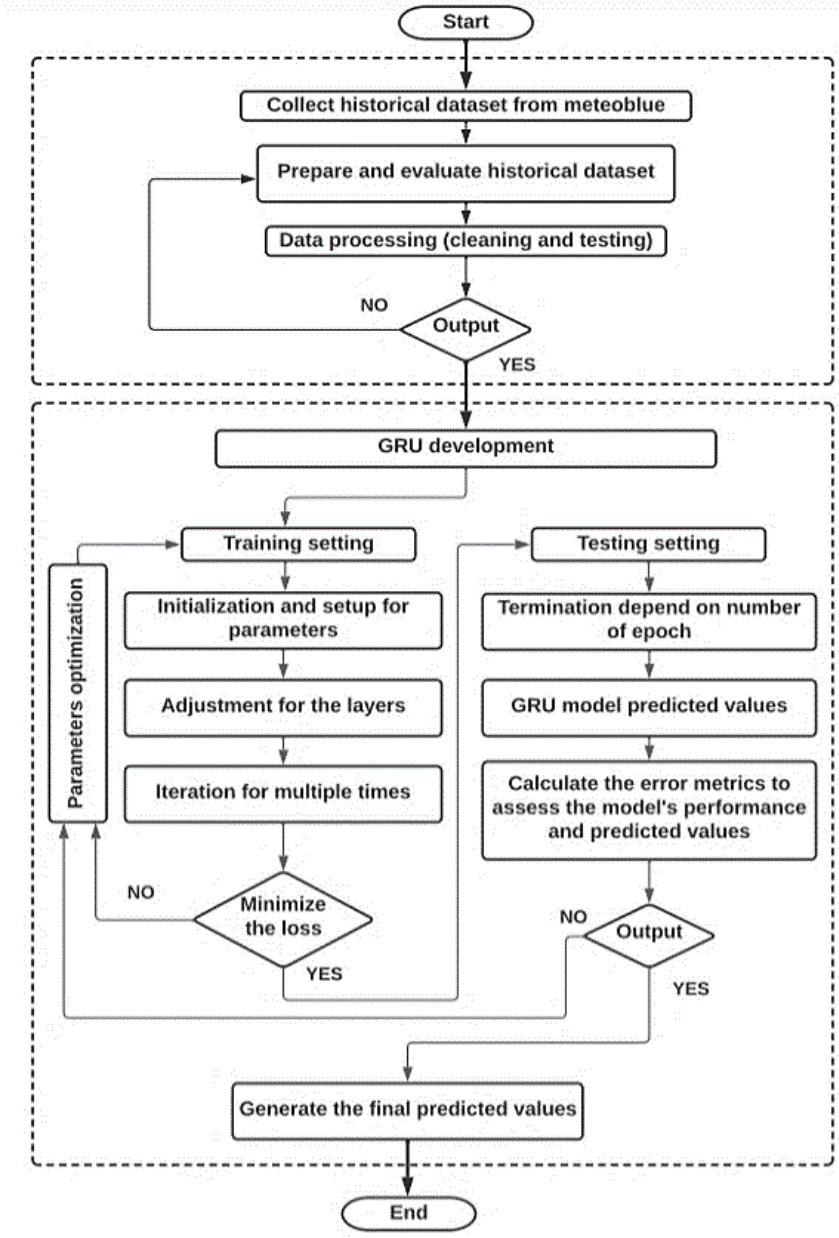

Figure 8-2. Flowchart of the GRU prediction model.

8.3 Results Analysis and Discussion

The short-term future performance of wind speed and temperature across the GCC countries was predicted based on a historical dataset spanning a period of 36 years using the GRU NN prediction model. The results revealed a strong performance and notable model fitting as presented in Figure 8-3 to Figure 8-8 for the KSA and in *Appendix 4* for the other GCC countries. Despite the enormous quantity of training data, the GRU model did not exhibit overfitting for wind speed forecasting results, as shown in Figure 8–3, Figure 8–4, Figure A.4–2, Figure A.4–7, Figure A.4–13, Figure A.4–19 and Figure A.4–25. In addition, the forecast wind speed values for the subsequent 169 hours from 23:00 h on the 26th of June 2021 to 23:00 h on the 3rd of July 2021 were obtained along with significant error metrics, as shown in Figure 8–6, Figure A.4–3, Figure A.4–8, Figure A.4–14, Figure A.4–20 and Figure A.4–26.

For the KSA, the RMSE = 0.66 m.s^{-1}, the MAE = 0.47 m.s^{-1}, and the MSE = 0.43 m.s^{-1}. Moreover, the KSA's p-value = 0% and its MAPE = 14.98%, highlighting the quality of the GRU model (see Table 8-1). The R^2 = 93%, which indicates that the variables exhibit reasonable correlation and variance. The error indicators have improved with Oman's historical data, and the decline of these values becomes obvious, even when the R^2 value improved. The RMSE for Oman = 0.41 m.s^{-1}, the MAE = 0.29 m.s^{-1}, and the MSE = 0.14 m.s^{-1}. In addition to this, the p-value for Oman = 0%, the MAPE = 5.04%, and the R^2 value = 95%, as shown in Table A.4–1. The error metrics continued to improve and decrease with the UAE's historical data. The UAE has an RMSE = 0.36 m.s^{-1}, an MAE = 0.22 m.s^{-1}, and an MSE = 0.13 m.s^{-1}. Further, the p-value for UAE = 0.01%, the MAPE = 4.39, and the R^2 = 97%, as illustrated in Table A.4–2. The error metrics for Kuwait increased with its historical data. The RMSE, MAE, and MSE values for Kuwait are 0.66 m.s^{-1}, 0.44 m.s^{-1}, and 0.43 m.s^{-1}, respectively, as shown in Table A.4–3. The p-value for Kuwait = 0%, the MAPE = 5.40% and the R^2 = 94%. For Qatar, the RMSE = 0.52 m.s^{-1}, the MAE = 0.32 m.s^{-1}, and the MSE = 0.27 m.s^{-1}. In addition, as shown in Table A.4–4, Qatar has a p-value = 0%, a MAPE = 9.77%, and an R^2 = 96%. The MAPE values increased for Qatar and Bahrain, with RMSE, MAE, and MSE values for the latter of 0.54 m.s^{-1}, 0.34 m.s^{-1}, and 0.29 m.s^{-1}, respectively. For further clarification, Table A.4–5 shows that the p-value, MAPE, and R^2 for Bahrain are 0.01%, 9.77%, and 94%,

respectively. The number of variables had a significant impact on the accuracy of the forecasted models.

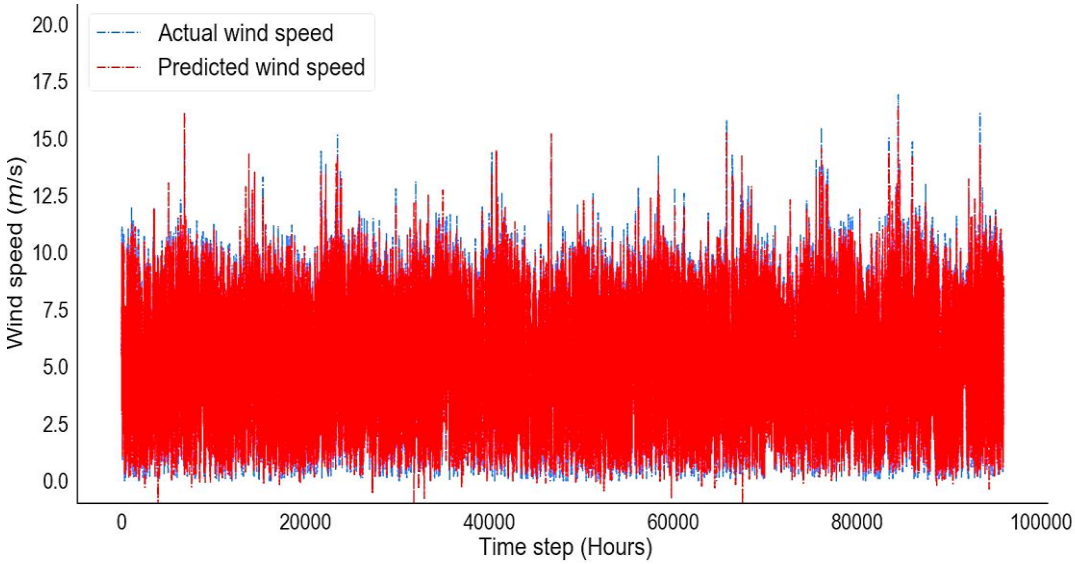

Figure 8-3. The actual and predicted wind speed performance for the KSA.

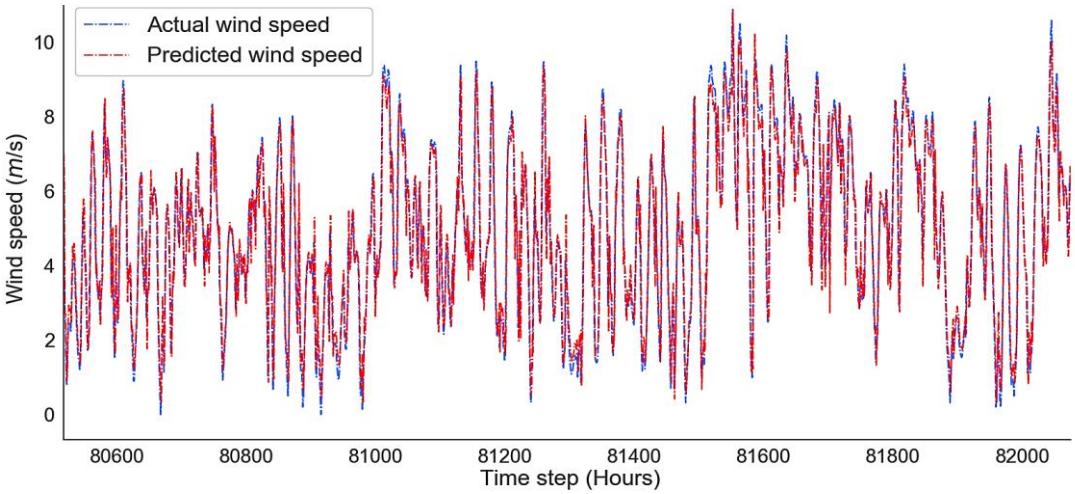

Figure 8-4. Real and predicted values of wind speed for KSA showing the fit and performance of the GRU model.

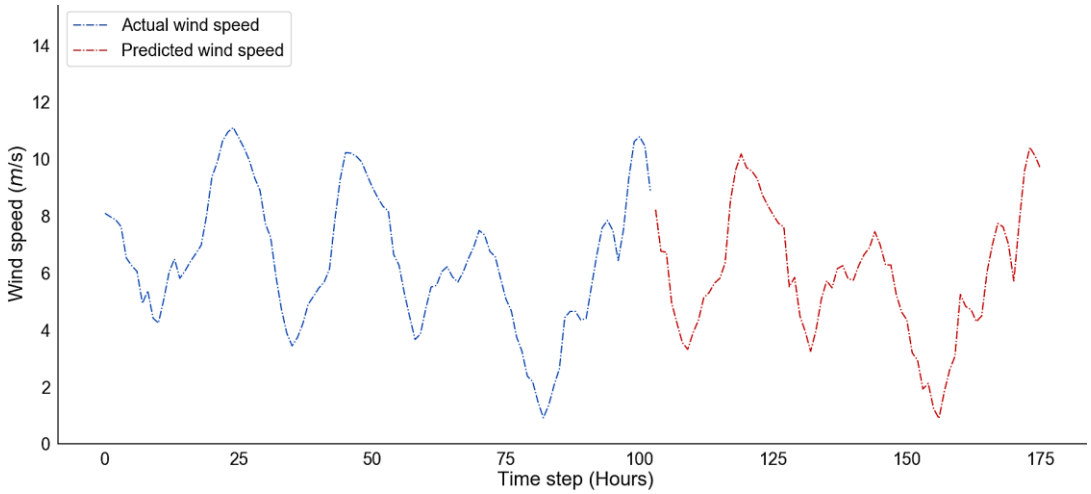

Figure 8-5. The wind speed's predicted future values for the next 169 hours in the KSA.

The future performance of the temperature values for the forthcoming week (169 h) from 23:00 h on the 7th of June 2021 to 23:00 h on the 14th of June 2021 were predicted, as presented in Figure 8–5, Figure A.4–6, Figure A.4–11, Figure A.4–17, Figure A.4–23 and Figure A.4–29. In addition, the GRU model did not demonstrate any indications of overfitting and exhibits a fine fit for the results of the temperature prediction, as seen in Figure 8–7, Figure A.4–5, Figure A.4–10, Figure A.4–16, Figure A.4–22 and Figure A.4–25.

The RMSE, MAE and MSE error metrics for temperature in the KSA are 0.87°C, 0.65°C and 0.76°C, respectively. In addition, the MAPE, p-value and R^2 were all improved at 2.19%, 0%, and 99%, respectively. Moreover, the RMSE, MAE, and MSE error metrics for Oman's temperature readings are 0.91°C, 0.68°C, and 0.83°C, as presented in Table A.4–1. Oman's MAPE has increased to 2.5 %. The p-value and R^2 for Oman are 5.43×10^{-23}% and 97%, respectively. The UAE's RMSE, MAE, and MSE temperature error measurements are 0.78°C, 0.53°C, and 0.60°C, respectively. Additionally, the UAE's MAPE, p-value, and R^2 are increased to 1.77%, 5.58×10^{-15}%, and 98%, correspondingly (see Table A.4–2). The error metrics for Kuwait's temperature readings have significantly risen. According to Table A.4–3, the RMSE, MAE, and MSE values for Kuwait are 1.17°C, 1.04°C, and 1.61°C, respectively. The p-value for Kuwait = 1.39×10^{-12} %, the MAPE is 2.69%, and the R^2 is 98%. Qatar's temperature RMSE = 0.91°C, MAE = 0.63°C, and MSE = 0.83°C. In addition, as shown in Table A.4–4, Qatar has a p-value = $.87 \times 10^{-15}$%, a MAPE of 1.84%, and an R^2 of 98%. The RMSE, MAE, and MSE values for Bahrain's temperature values are 0.81°C, 0.66°C, and 0.67°C, respectively. For further

clarification, Table A.4–5 shows that the p-value, MAPE, and R^2 for Bahrain are all 1.86 × 10^{-12} %, 2.04%, and 97%, respectively.

The MSE, RMSE, and MAE of the predicted temperature results increased compared to the predicted wind speed error values, although these error metric values of the GRU model are considered relatively small values when compared to other prediction models (see Table 8-2 and Table 8-3), demonstrating their flexibility in new dataset observations. Further, improving this model's generalisation capabilities and producing highly accurate results was one of the most difficult challenges. The variation in model performance, when assessing previously observed data (i.e., training data), over data that the model has never seen before (i.e., testing data), is referred to as generalisability. Moreover, the model's insufficient generalisability will tend to lead to overfitting of the training data.

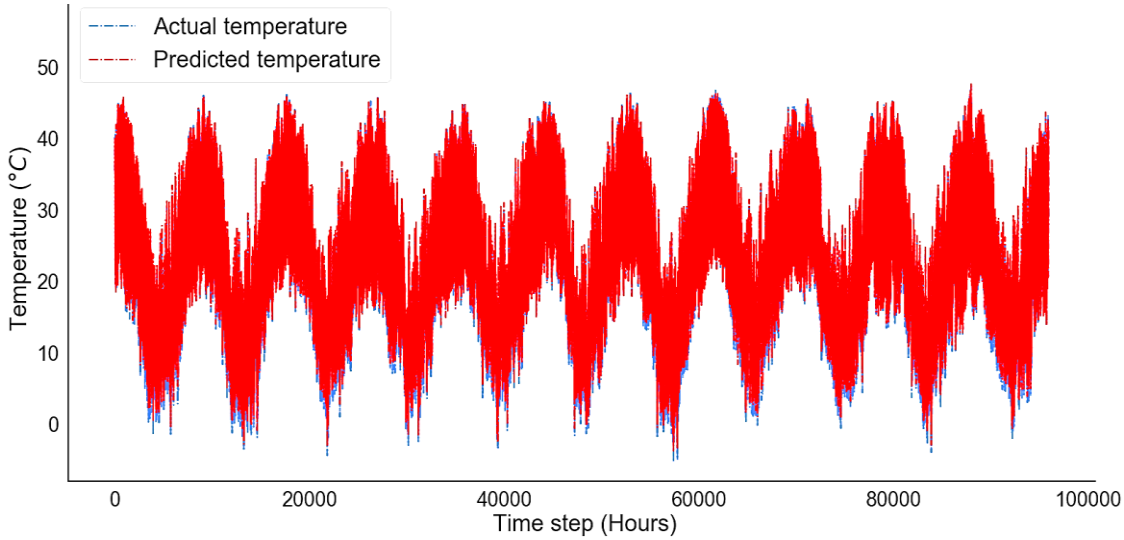

Figure 8-6. Actual and predicted temperature performance for the KSA.

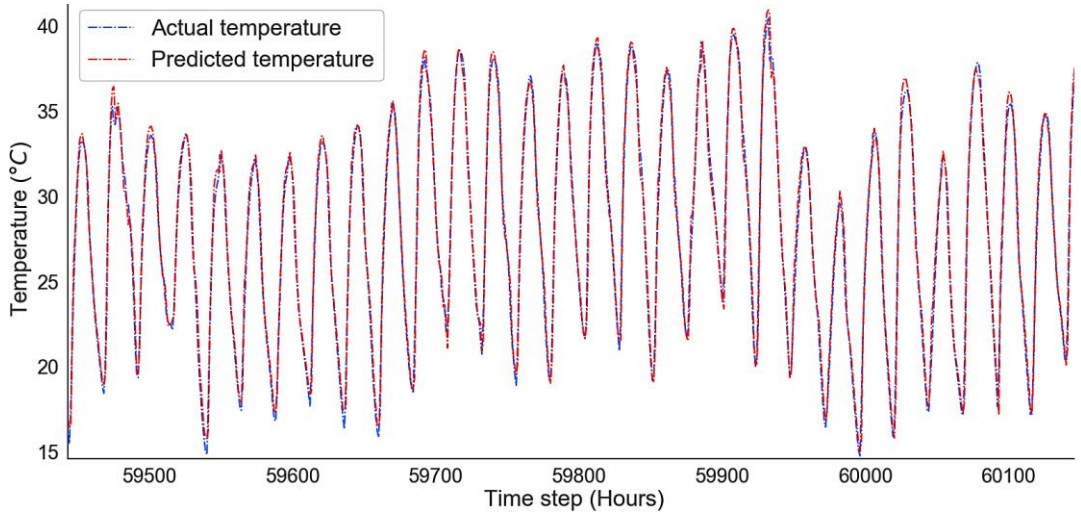

Figure 8-7. Actual and predicted temperature performance for KSA showing the model fitting.

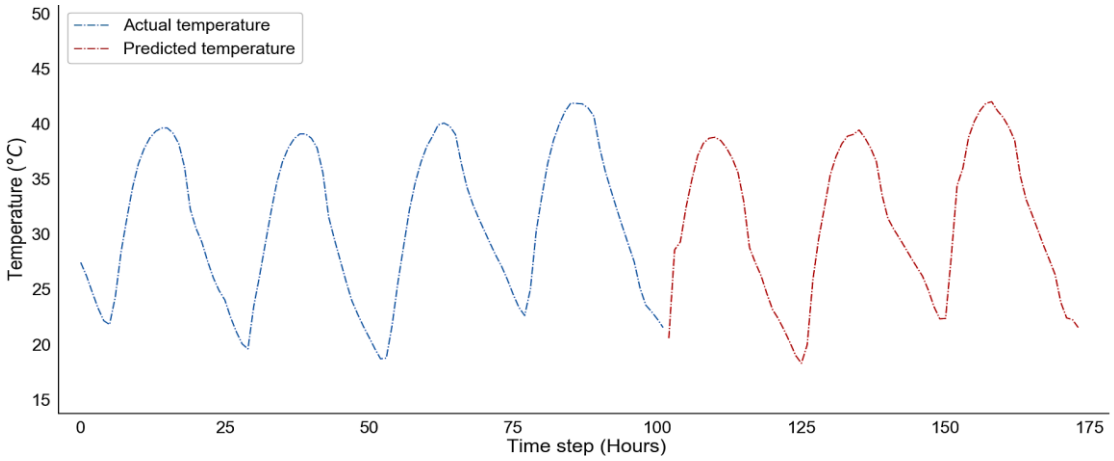

Figure 8-8. Future predicted values of the temperature for the next 169 hours in the KSA.

Table 8-1. Forecasting accuracy indicators for the KSA using the GRU model.

No.	Metric	Wind speed (m s^{-1})	Temperature (°C)
1	RMSE	0.66	0.87
2	MAE	0.47	0.65
3	MSE	0.43	0.76
4	MAPE (%)	14.98	2.19
5	*p*-value (%)	0.00	0.00
6	R^2 (%)	93	99

8.3.1 GRU Model Evaluation

Based on the parameter settings shown in *section 8.2.1*, the GRU prediction model was assessed by applying two different types of historic dataset for the six GCC countries, specifically wind speed and temperature. In addition, the performance of the proposed GRU model was evaluated by comparing it to numerous external ANN prediction models, as shown in Table 8-2 and Table 8-3. In terms of accuracy and interpretability, the GRU model showed substantial successes relative to other models, especially when compared to the results of the observational ANN models.

Table 8-2. Comparison of GRU proposed model performance with other wind speed models [251].

No.	Model	RMSE (m s^{-1})	MSE (m s^{-1})	MAE (m s^{-1})	MAPE (%)	R^2 (%)
1	HELM1	1.65703	-	1.25618	21.00415	92
2	HELM2	1.64881	-	1.25159	20.90677	92
3	HELM3	1.67172	-	1.24861	20.98445	93
4	LSTM1	1.62832	-	1.24653	20.76933	93
5	LSTM2	1.62999	-	1.21817	20.71264	93
6	LSTM3	1.63093	-	1.23705	20.77809	93
7	LSTMDE-HELM	1.59568	-	1.20192	20.56069	93
8	**GRU proposed model**	**0.66**	**0.43**	**0.47**	**14.98**	**93**

Table 8-3. Comparison of GRU proposed model performance with other temperature models [303].

No.	Model	RMSE (°C)	MSE (°C)	MAE (°C)	MAPE (%)	R^2 (%)
1	LSTM	4.48	-	3.49	-	89
2	BLSTM	4.42	-	3.40	-	91
3	CNN-BLSTM	3.98	-	3.09	-	92
4	CNN	4.77	-	3.78	-	89
5	UM(RDAPS)	3.74	-	2.81	-	96
6	**GRU proposed model**	**0.87**	**0.76**	**0.65**	**2.19**	**99**

The GRU prediction model demonstrated a commendable performance when coping with historical datasets such as wind speed and ambient temperature. Generally speaking, the GRU model uses historical time series data to increase prediction accuracy by considering the effects of characteristics on anticipated wind speed and temperature values of the next instant, in comparison to other networks such as LSTM, BI-LSTM, CNN and CNN-LSTM. The GRU prediction model does not require the use of memory to monitor the transferred information; instead, it uses all extracted features immediately and without any supervision. When a suitable number of historical time series data are selected, the efficiency of the GRU model becomes increasingly clear, and short-term prediction accuracy develops. The size and the error values of the epochs show a significant correlation, indicating that, if the number of epochs increases, then the errors will obviously decrease, although the attendant training time increases. Furthermore, utilising a large amount of historical data with a huge volume of training data resulted in long simulation periods and significant error readings. The GRU prediction model must be processed sequentially, as the succeeding steps are dependent on the previous stages. The GRU model achieved an acceptable improvement in the wind speed and temperature discrimination tasks when combining large historical data. Additionally, by integrating a substantial amount of historical data with a sizeable quantity of training data, GRUs will be able to lengthen the duration of the simulation periods still further.

9 Synthesis and Interpretation of the Findings

This chapter provides a comprehensive analysis and discussion of the GCC countries' power sectors perspective based on 40 years of significant previous studies and historical data integrated with 30 years of predicted future performance. An interpretation of the main findings for all four prediction models is related to the primary research findings.

9.1 Overview

This work assesses the long-term contribution to sustainable energy strategy that protects a given power supply from fluctuations and volatility, mitigates climate change implications and reduces CO_2 emissions in the GCC region. In addition, this research addresses the rapid growth issue of power consumption in the GCC region over the last 40 years (*see Chapter 2*) and how this impacts the climate change mitigation process. The development of renewable energy projects and their progress across the GCC region is debated with a view to solving the power consumption growth issue. Climate change mitigation challenges and an exploration of solar and wind energy resource potential in the GCC region was discussed in *Chapter 3*. Moreover, four prediction models were developed to study and analyse the future performance of the GCC's power sectors over the next 30 years and evaluate the region's solar and wind energy resource potential alongside ambient temperature based on 40 years of historical data. The four prediction models developed included; (i) the long-term MCS and BM prediction model which was used to predict the future performance of the power sectors in the GCC region alongside the potential performance of solar energy, wind, and ambient temperature over the next 1,000 days (*Chapter 5*); (ii) the SARIMAX long-term prediction model was employed to forecast the behaviour of the GCC's electricity sectors, including generation, consumption, electrical peak load and installation capacities over the next 30 years (*Chapter 6*); (iii) the BI-LSTM short-term prediction model based on neural networks was designed to analyse and examine the future performance of solar energy over the next 7 days ahead (*Chapter 7*); (iv) the GRU short-term prediction model based on NNs was developed to study and investigate the future performance of wind speed and ambient temperature over the next 7 days across the GCC region (*see Chapter 8*).

9.2 A Perspective on the Future Power Sectors of the GCC Countries

The GCC countries presently depend on fossil fuels such as oil and natural gas to generate their electricity. Fossil fuels have a finite lifespan and a history of fluctuating costs that are prone to shocks such as the COVID–19 pandemic and the Russian invasion of the Ukraine, events which have created multiple issues that affect the energy security of GCC region and the international world energy system over the long-term. Energy supplies have been impacted by the COVID–19 pandemic as a result of the disruption of supply chains, the curtailing of international transportation, and the long-term shutdown of the whole system. As a consequence, the globe was unable to completely recover from the pandemic before the current Russian-Ukrainian conflict generated a worldwide energy shock in which global energy markets were influenced by existing rates owing to Russian sanctions, compelling many countries to return to coal and fossil fuels. This prompted the President of the USA to put pressure on other oil-producing countries to increase their production, a demand that directly contradicts climate change policy and affects the plan to reduce carbon emissions in the world and the GCC region as a whole. The GCC countries have recognised the necessity of minimising their future fossil fuel consumption and have begun to consider renewable and sustainable energy resources, representing a significant step forward.

The findings of the long-term prediction MCS and BM model showed a rise in the consumption of electrical energy in all GCC countries (*see sections 5.3.1 and 6.3.1*). Based on this model, the KSA expected increments in its power consumption to 377 TWh in 2030, representing a 2% annualised growth from its 309 TWh figure in 2020, further developing capacity to 540 TWh in 2050. For Oman we estimated an increase in electricity consumption from 34 TWh in 2020 to 44TWh in 2030, a 2.6% annualised rise over the next 10 years, climbing to 69 TWh in 2050. In addition, the UAE predicts a 1.8% annualised growth in power consumption from 138 TWh in 2020 to 165 TWh in 2030, rising still further to 245TWh in 2050. Kuwait forecasted an increase in power consumption from 66.40 TWh in 2020 to 86 TWh in 2030, constituting 2.6% annualised growth, increasing still further to 123.40 TWh in 2050. For Qatar we predicted a 2% annualised growth in electricity consumption over the next decade from 48 TWh in 2020 to 57.40 TWh in 2030, reaching 83.32 TWh in 2050. For Bahrain we estimated a 2.6% annualised growth in electricity consumption during the next 10 years from 16.40 TWh

in 2020 to 21.45 TWh in 2030, rising to 24 TWh in 2050. Forecast growth in Oman, Kuwait and Bahrain lies within normal limits and is not exceptional.

The other long-term prediction model, SARIMAX, indicated a growth in electricity consumption across all GCC countries, except for the Kingdom of Bahrain, which observed a considerable fall in consumption. The KSA anticipated a 3% annualised increase in electricity demand over the next ten years, resulting in 421 TWh in 2030 and 644TWh in 2050. Oman forecasted an increase in power consumption of 3.2% per annum over the following decade from 47 TWh in 2030 to 64 TWh in 2050. UAE expects a 1.7% annual increase in electricity demand to 164 TWh in 2030, rising to 195 TWh in 2050. For Kuwait we estimated a 2.4% annualised rise in electricity demand to 84 TWh in 2030 and 126 TWh in 2050. Qatar might anticipate a 2.4% annual increase in energy demand over the next decade, reaching 61 TWh in 2030 and 93 TWh in 2050; whereas for Bahrain we predicted a 2% annual increase in power demand, reaching 20 TWh in 2030 and dropping to 19.5 TWh in 2050.

According to the findings of the SARIMAX model, the Kingdom of Bahrain is one of the smallest countries in the GCC region and the world. Consequently, its energy consumption is relatively low, which explains why its consumption is forecasted to remain stable between 2030 and 2050. However, applying two long-term prediction models with different approaches and principles contributes to our conceptual understanding from several resources. The consumption values for all countries show a clear convergence, especially in terms of annualised consumption. The rapid economic development in the area is a primary contributor to these increases. Considering the limited alternatives available in GCC countries and the significant increases in population growth, the lack of water resources, urbanisation, and other social and economic activities, it is anticipated that power consumption will continue to play an increasingly important role in the region's energy supply profile towards 2030. However, these challenges will persist until 2050. Furthermore, increasing fossil fuel energy consumption impacts GCC countries' economic growth and exacerbates environmental issues by increasing CO_2 emissions. The regional and international scientific communities consistently indicate that GHG emissions caused by human activity and the combustion of hydrocarbons (coal, oil, and gas), have already contributed to a one-degree rise in global temperatures beyond pre-industrial levels, forcing GCC countries to commit to mitigating the effects of these damages. Incorporating a share of renewable energy

technologies into GCC countries' total energy generation portfolio could be a suitable solution to all of their fossil fuel-related issues. Renewable energy technologies can maintain the GCC countries' energy consumption growth rates by supporting the region's power sectors in achieving consumption control targets and managing load balances during peak demand.

The long-term and short-term prediction models, including MCS and BM, BI-LSTM and GRU were used to study the future performance of solar energy, wind speed and ambient temperatures over the GCC region. The results of these predictions have proven that the GCC region possesses large potential solar and wind energy resources, placing it amongst the best regions in the world for RES. This makes the GCC region attractive for solar energy plant development. Oman has the greatest solar irradiation in the region, followed by the UAE and the KSA (*See Chapters 5,7 and 8*), followed by Kuwait, Qatar and Bahrain, respectively. Determining the optimal locations for solar energy, reliable wind speeds are among the challenges facing the large-scale implementation of solar and wind energy projects. Oman possesses the highest values of potential solar energy and wind speeds alongside the lowest temperature values in the region. Kuwait has the second highest wind speeds in the region, followed by the KSA (*see Chapters 5, 7 and 8*). Qatar is the fourth-ranked country in the region, followed by Bahrain. The highest temperature values were recorded in Kuwait, then Qatar, with the KSA and Bahrain having equivalent temperatures.

According to the evaluation of the progress of renewable energy projects and an examination of the potential solar and wind energy resources in the region, the GCC countries can spearhead the renewable energy transition toward a more sustainable and equitable future. The GCC region can become a hotspot for renewable energy investments that have the potential to make it a global leader in the field. The abundance of solar and wind energy resources and the strategic location of the GCC region can support a future mixed energy plan, one which would offer great opportunities to implement low-carbon technologies and build strong power sectors to comply with future requirements. Overall, there seems to be some evidence to indicate that acceleration of the deployment of renewable energy technologies in the GCC region will shift the trajectory of climate change, allowing for quick and substantial emission reductions whilst simultaneously advancing technologies towards near-zero carbon energy generation. However, there is a dearth of (solar and wind) renewable energy research and feasibility studies in the GCC

region, that could serve as pathways towards faster decarbonisation and support renewable energy implementation and diversification of the energy mix.

9.3 Evaluation of the Developed GCC Forecasting System

Forecasting technologies are the best solutions for the integration of power generation optimisation with real-time components of consumption to create a system that operates efficiently with multiple generation sources such as wind and solar energy. That can create an intelligent power system, managing change in the demand to maximise systemic efficiency, reduce CO_2 emissions, and enhance reliability. Asset integration is a major factor of decarbonisation in that the power sector makes the system more efficient by adjusting the power generation and the associated loads. In addition, the GCC's power sectors will need to optimise the deployment of assets based on the availability of resources which requires long-term and short-term forecasting tools to manage the real costs of operating each type of generation technology. This will be accomplished while taking into consideration the actual operational expenses of such energy generation. This is of importance as the region continues to increase its renewable energy. Four different types of highly accurate forecasting models have been developed for this research. The development of a comprehensive system comprising four models for long and short-term forecasting was an effective strategy for meeting the GCC region's energy system requirements. The most appropriate approaches for long- and short-term forecasting were identified based on a number of experiments performed in this study. Furthermore, several relevant published works were analysed and divided into two groups: (i) ones that specialise in long-term forecasting, and (ii) ones that specialise in short-term forecasting. Based on these divisions, it was possible to determine the appropriate approaches for long- and short-term forecasting.

The forecasting system was evaluated using multiple types of historical data (see Figure 9-1). The results of the tests showed the high performance of the four forecasting models as an integrated forecasting system.

The MCS and BM long-term prediction model was characterised by its extraordinary capacity to handle all types of historical data and provided unexpected results for all GCC countries. In fact, it is difficult to formulate and design a forecasting model that performs so many tasks simultaneously and deals with fossil fuel, solar energy, wind energy, and

temperature data. However, the MCS and BM prediction model has already accomplished this. One of the most significant characteristics of this model is that it provides an accurate and unambiguous representation of the performance of future forecasts, including evidence of the flow of future values and their distribution based on BM approaches. In business, BM is widely used to describe the assumed path that random variables such as stock prices will follow. In addition, stochastic differential applications of BM and MCS are typical assessment techniques used in risky and uncertain environments. BM can be characterised as a Markoff process, which indicates that the values at a particular time are completely reliant on their position at a previous point in time. Consequently, it has been discovered that, for a Markoff process such as BM, the system's behaviour is totally governed by conditional probabilities. However, one of the limitations of the MCS and BM prediction models is that they do not fit shorter periodicities of historical data, such as hourly intervals, and their performance is far higher for yearly, quartile, and daily intervals. The MCS and BM prediction model provides a comprehensive estimation, explaining the absence of conventional error indicators for this type of forecasting. On the other hand, the SARIMAX long-term prediction model demonstrated its superior capacity to forecast future GCC power sector performance across a range of circumstances, generating very low error metric values, as presented in Tables 6–1, A.2–1, A.2–2, A.2–3, A.2–4 and A.2–5. Further, the performance of the SARIMAX model outperformed published external models (see Table 6-2). The SARIMAX long-term prediction model is characterised by very effective performance and was able to cope with the very large size of historical data for fossil fuels, including electricity generation, consumption, electricity peak load and installation capacities for all the GCC countries. In addition, the SARIMAX model can accommodate environmental factors such as seasonality and data temporal sequences. The findings revealed that the SARIMAX model is effective across all criteria for seasonal forecasting with strong fitting. The SARIMAX model delivers a highly dependable in-sample fit and a bigger record of the most accurate forecasting of power system values, while maintaining acceptable error metrics. The SARIMAX model generated more accurate predictions by considering the most significant variables that influence the dynamics of the power system series. Nonetheless, the multivariate non-linear input data are extremely skewed, which greatly affects the performance of the SARIMAX model.

Further, the GCC region's short-term predictions were considered for their effectiveness in terms of evaluating solar energy and wind speed resources. As the penetration of various solar and wind energy sources increases, the system’s reliability and flexibility become more difficult and costs will be further increased. The short-term prediction for solar and wind energy can reduce the risks and costs associated with integrating RES. The short-term BI-LSTM prediction model was employed to predict the three types of solar irradiance, namely GHI, DNI, and DHI, for the GCC countries for the next 7 days. The model's performance was remarkable, yielding very low error metrics values as illustrated in Tables 7–2, A.3–1, A.3–2, A.3–3, A.3–4 and A.3–5. This type of prediction model is intended for forecasting periods as short as one hour, a day, or a solitary week, at most. The BI-LSTM is a sequence processing model comprising two LSTMs. One of the LSTMs processes the input(s) in a forward direction, while the other processes them in a backward direction. The BI-LSTM significantly raises the quantity of data that can be accessed by the network, hence enhancing the context that can be used by the algorithm. The model's maximum forecasting range is a week. Based on a comparison of the performance of the proposed BI-LSTM model with external solar irradiance models, it outperformed its competitors and achieved very low error metric values (see Table 7-3). In addition, one of the main challenges was in developing a model that is capable of predicting wind speeds as they can change in a fraction of a second. The short-term GRU prediction model was designed to predict wind speed and temperature values for the next 7 days as for the BI-LSTM model. It is intended that we will be able to predict future periods spanning no longer than a week. GRU promises to accomplish ML tasks involving memory and clustering by connecting nodes in a sequence. GRU's advantage is that its computational time is more efficient, while its complexity is lower due to having fewer parameters than LSTM with faster training times. The GRU forecast model offered a highly distinguished performance, especially in terms of wind speed values, and this performance was reflected in the very small error metrics values observed, as shown in Tables 8–1, A.4–1, A.4–2, A.4–3, A.4–4 and A.4–5. The proposed GRU model outperforms its competitors and generates extremely low error metric values based on a comparison of its performance with other external models, as presented in Table 8-2.

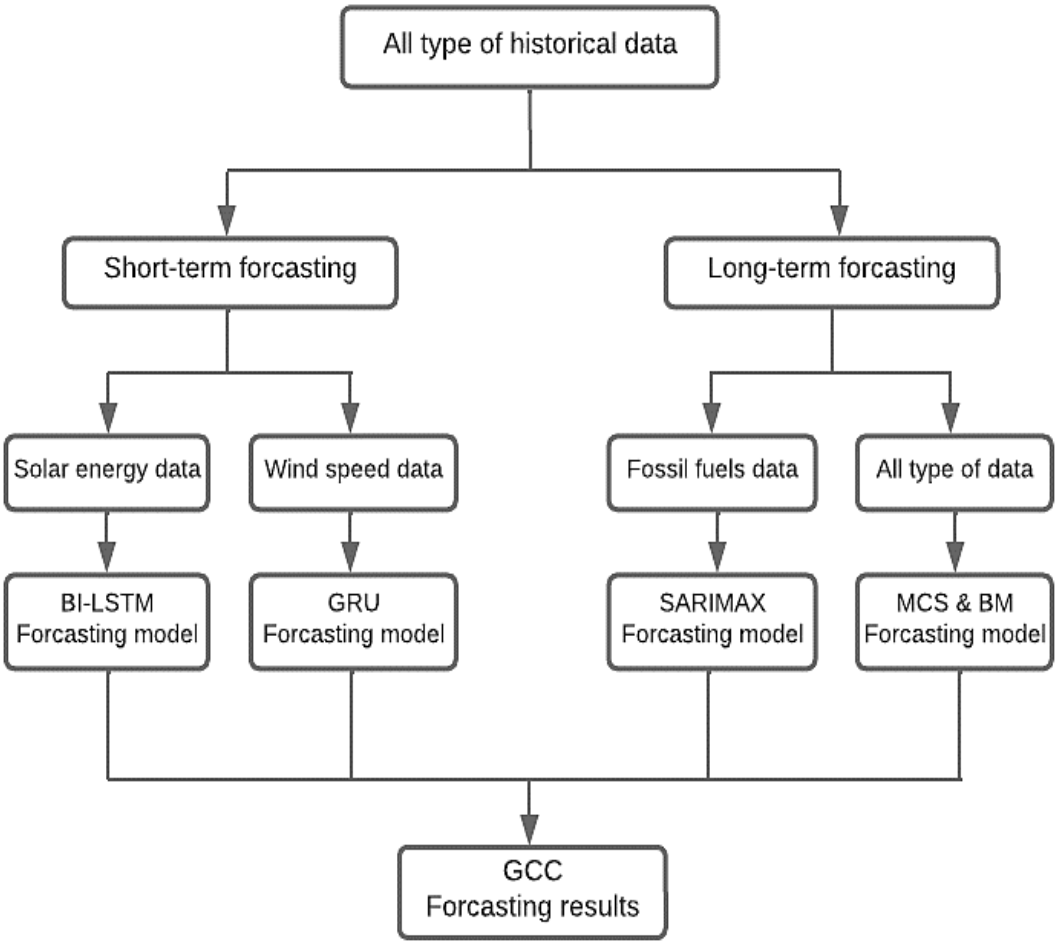

Figure 9-1. GCC forecasting system comprising four models.

9.4 Contribution to Society

One of the goals of this study is to raise community awareness, develop it and provide the best energy solutions in the GCC region for the long term, especially the next five years. This research also contributes to society's efforts to slow energy consumption. In addition, the work contributes to the progress of society in all aspects of life that depend on energy security by playing a major role in promoting the ongoing development of renewable energy.

10 Conclusions and Recommendations for Future Work

This chapter presents the overall findings of this thesis, which are intended to present a step towards clean, competitively priced energy by investigating the long-term impacts of an exclusive reliance on fossil fuels over the previous four decades. Predicting the future of energy over the next 30 years and elucidating the potential of solar and wind RES in the GCC region is pivotal to this end. In addition, this chapter addresses the strengths and limitations of this study along with recommendations for future work.

10.1 Conclusions

Even though coal consumption has declined considerably in recent years, the persistent increase in fossil fuel energy usage far outstrips any growth in low-carbon technologies and activities. This has exacerbated the escalation of climate change concerns in the GCC region. The accelerated increase in the consumption of conventional energy sources will swiftly deplete any remaining fossil fuel resources. Per capita emissions continue to grow in the wealthier oil-producing nations of the GCC region, including the KSA, Oman, the UAE, Kuwait, Qatar, and Bahrain. Although the GCC region has significant reserves of natural gas and non-associated gas sources; the majority of the GCC countries are now faced with a shortage of domestic natural gas supply due to high demand, with the exception of Qatar. In fact, the GCC countries play a significant role in the global energy sector and are extremely susceptible to several energy issues relating to their economies.

The low cost of energy, government subsidies, and the abundance of fossil fuel sources has supported the alarming growth of energy consumption across the region. The region is unusual in its strong dependence on thermal desalination and electricity generation from fossil fuel sources. Although each country in the GCC region has stated goals and objectives regarding the decarbonisation of energy technology, there have been few transitions to date. The GCC region has abundant fossil fuel sources and enormous solar and wind energy potential, and any delays in implementing renewable energy have been due to bureaucracy. Of course, the geographical location of the region has very favourable characteristics for solar and wind energy. The challenges raised by the consumption of fossil fuels are generally similar in each GCC country due to their respective geographical locations, weather conditions, and economic activities. There are many options for

mitigating climate change, both environmentally and economically, with solar and wind energy offering the best options for achieving forecasted emission reduction targets at the required rate. Moreover, the road map to the transition towards decarbonisation, in terms of solar and wind energy technologies, can be divided into two categories, specifically the status and nature of a geographical locale and its associated weather conditions, prompting a regional analysis. This long-term analysis provides an extended exploration of potential solar and wind energy resources in the GCC region. The research evaluated cloud coverage and dust fallout in the area based on 40 years of historical data. The main findings of this research indicate that the daily solar GHI in Oman reaches 10,465 W/M^2, the highest solar radiation in the region. The UAE has the second highest daily solar GHI with 10,111 W/M^2, followed by the KSA with 9,620 W/M^2 and Kuwait with 9,560 W/M^2. Qatar ranks fifth with 9,230 W/M^2, followed by Bahrain with 9,000 W/M^2. In addition, Oman has the highest recorded daily wind speeds, ranging from 12.85–9.24 $m.s^{-1}$. Kuwait has the second highest daily wind speed range in the region with 11.95–8.40 $m\ s^{-1}$, followed by Saudi Arabia with 9.77–7.76 $m.s^{-1}$, and Qatar with 8.95–5.30 $m.s^{-1}$. Bahrain ranks fifth with a wind speed range of 8.30–5.75 $m.s^{-1}$, while the UAE has the lowest average wind speeds from 3–4.8 $m.s^{-1}$, below the economically feasible threshold. The region's lowest recorded temperatures were in Oman, whereas Kuwait had the highest temperatures, followed by Qatar, the KSA and Bahrain, which experienced similar temperatures. The KSA recorded the highest annual dustfall at 454 tonnes km^{-2}, which would have major effects on solar energy collection systems. The lowest annual dust amount was observed in Qatar at 50–113 tonnes km^{-2}. In addition, the cloud coverage across the GCC countries is minimal over the course of the year. However, the potential value of solar and wind energy resources in the GCC region is considered high compared to the global average. This analysis proves that there are no real obstacles that prevent the development of decarbonisation technologies in the region given the vast amounts of solar and wind energy resources available. Accelerating the implementation of decarbonisation energy technology is the responsibility of all countries, especially major oil-exporting industrialised countries. Implementing renewable energy deployment will support the GDP of the GCC countries and it would have a positive impact on the region in the long term.

The MCS and BM long-term prediction model was employed in this research to evaluate the future requirements of the GCC power sector as well as the potential for solar and

wind energy (alongside temperature performance). The MCS and BM model provided wide details to analyse the future behaviour of the trans-GCC power sector. In particular, solar and wind energy fluctuations may be challenging in terms of the selection of both time and location for solar and wind energy projects, and this requires careful study of the visibility and availability of resources. Fortunately, variations in solar and wind energy technologies can complement each other. For instance, when solar plants are dormant at night, wind turbines are at work. Solar plants generate their maximum power outputs in the summer season and minimum power in the winter. The MCS and BM models presented many different potential outcomes in addition to the probabilities associated with each, based on a huge pool of random data samples. A deterministic prediction is easier to understand in comparison to the image that it provides. The fundamental premise behind the MCS and BM is ergodicity, which defines the statistical behaviour of a moving point in a closed system. In such a system, the moving point will ultimately examine all potential locations. The precision of the results is dependent on the number of simulations. In other words, 1,000 simulations yield more precise results than 100. The system recreates the intrinsic uncertainty of the input parameters using random number generators which are computer programmes that create an unexpected series of random numbers. The MCS and BM model utilises samples of input data and a specified computational formalism to forecast the probabilities of system outcomes. Moreover, the MCS and BM forecasting model has proven its long-term capabilities with impressive performance using all types of historical data.

In addition, this research helped fill knowledge gaps in terms of the long-term forecasts for the electricity generating sector by developing a SARIMAX long-term forecasting model, one which considers the implications of the GCC's regional electricity generation, consumption, peak load, and installed capacity. Not only does this address future performance and demand, but also planning implications to address fluctuation and uncertainty issues that can impact the future stability of the power system and associated energy markets. Further, enhancing the quality of the power system will have a major effect on the scheduling, operation, and integration of energy markets. Moreover, the forecasting model can be used to enhance their efficiency. Therefore, applying forecasting techniques and paradigms can improve the performance of the energy markets, which is especially useful where there is uncertainty. These forecasting models provide robust methodological approaches to crucial challenges pertaining to

unpredictability in electricity markets and to improving the microeconomics, energy policies, and evolution of global energy markets.

In this research, the SARIMAX forecasting model was developed and validated using a variety of selected features, including the time series algorithm and hypotheses regarding the most effective forecasting sequence and processes for the future performance of the power sector. The present research provides evidence that classical approaches are superior to the complex methods such as decision trees, MLPs, LSTM NN models and other DL methods, at least for those challenges investigated. The experimental findings conducted in this research strongly encourage the use of classical models like SARIMAX. This research emphasises the need, not only to carefully use model preparation strategies, but also actively test several combinations of models and data preparation schemes for particular situations to determine which method is the most effective. In addition, the most important issue and greatest difficulty is improving their accuracy and maximising their vast potential.

The model was evaluated and validated using four different types of historical electricity sector data, specifically electricity generation, consumption, peak load, and installed capacity. The historical data covered a span of 40 years (1980–2020) and had been gathered from GCC countries as quarterly interval data for forecasting the aforementioned values over a 30-year period from 2021 to 2050. The SARIMAX forecasting model demonstrated the ability to cope with a variety of historical data types. The model's effectiveness was tested using error indices, such as the RMSE, MAE, MSE, and MAPE values and the R^2 (*see section 6.3*). As shown in Table 6-2, the comparison of the proposed SARIMAX model with 11 external prediction models strengthened these research findings and validated the SARIMAX model's performance, making a significant contribution to the literature by allowing us to analyse this research work independently and in comparison to other benchmarks. The study findings also revealed that the SARIMAX model outperformed its competitors in terms of forecasting accuracy, overfitting, redundancy elimination, training time, and testing execution time, proving that it offers remarkable performance. However, the model can be further improved and its error indications can be further reduced by improving learning performance, optimising the parameters, using monthly historical interval datasets, and adjusting the duration of the iterations.

A proposed DL BI-LSTM short-term prediction model based on an RNN time series was trained and validated through a set of selected features, including the algorithms' neural connection strength, gated units, and layers, which are deemed the best prediction sequence processes for the future performance of solar irradiance in GCC region. The BI-LSTM prediction model was examined and evaluated by implementing five different types of historical datasets, including three types of solar irradiance comprising GHI, DNI, and DHI metrics. In addition, a historical dataset (1st January 1985 to 26th June 2021) was collated from the GCC region in hourly intervals to predict the next 169 h. The BI-LSTM prediction model proved its capacity to handle different types of historical data. The efficacy of the proposed model was evaluated in terms of the performance of the error indexes, including the RMSE, MAE, MSE, and MAPE values with R^2 (*see section 7.3*). In addition, the results indicate that the proposed BI-LSTM model had a substantial edge over its competitors in terms of the prediction accuracy, overfitting, minimisation of redundancies and training, and testing execution time, and it demonstrated significant performance. These results were supported by a comparison of the proposed BI-LSTM model with external ANN prediction models, as shown in Table 7-3. Nevertheless, the BI-LSTM model can be upgraded, and the error indicators minimised by upgrading the learning performance, optimising the hidden layers, and modifying the epoch size or learning iterations.

The GRU short-term prediction model was built based on RNNs using the algorithm's strength in terms of neural connections, gated units, and layers, which are the most accurate prediction sequence procedures for wind speed and temperature. The GRU model was validated to predict the ensuing 169 h. The hourly historical dataset from the 1st January 1985 to the 26th June 2021 was utilised to test the GRU prediction model's ability to cope with this type of data. The GRU model's underlying architecture provided an efficient cell structure, one which required fewer training parameters, especially for short-term prediction. The experimental results show that the significant advantages of the GRU model over its competitors (see Table 8-2 and Table 8-3) include a good degree of prediction accuracy, overfitting, redundancy reduction, and training and testing execution time, all of which showed good performance. The GRU prediction model generated notable error metric values such as MSE, RMSE, MAE, and MAPE for the GCC region wind speed and temperature values (*see section 8.3*). Further, the representation of the results demonstrated a remarkable level of the model's learning

features, computing efficiency, fast convergences, and the capability of the GRU approach. However, the model can be improved and the error metrics reduced by enhancing learning performance, improving the hidden layers, and setting the epoch number or learning iterations.

The prediction models contribute to extant knowledge gaps in the power sectors, including wind and solar energy forecasting, by considering the impacts of solar irradiance, wind speed fluctuation, uncertainty, and intermittence issues, along with ambient temperatures, all of which affect power system stability. The scheduling and operation of wind and solar energy integration power systems would be greatly influenced by improving the quality of wind and solar energy predictions.

10.2 Strengths and Limitations

This research is distinguished by its comprehensiveness and capability to investigate the issues concerning the development of electricity consumption across a region that has historically been one of the top exporters of oil and natural gas and whose primary source of income is petroleum. Consequently, energy is a very sensitive topic for the GCC countries. This research relied on authentic sources and historical data that explored the last four decades of the GCC countries and shed light on the region's latent energy capacities, including solar and wind, which are among the most significant RES. This research has presented its vision and findings for the future of energy in the GCC region for the next 30 years using various tools and forecast models based on AI (*see the contribution to knowledge section*). The region has always needed this kind of research, an investigation that bridges the past with the present and deduces the likely future of the power sector.

As for other researchers in this field, we faced some obstacles and challenges, which were represented in collating historical data which simultaneously covered a 40-year period across six countries. We suffered tremendously from indifference and a lack of communication with the agents and representatives of the energy ministries in the GCC region. With the exception of Kuwait, the GCC countries publish their energy data every two years, unlike the European countries, which publish theirs every three months. In addition, the spread of COVID-19 affected my work at the university and forced me to work from home for much of 2020. This suffering increased during the comprehensive

lockdown due to the pandemic and the GCC countries stopped publishing their 2019 data. Finally, all contact with their representatives was lost until the end of 2021. Then during 2022, the data from 2020 was gathered, which was extremely important to reflect the impact of COVID-19 on the GCC power sector. Obtaining this historical data was one of the most difficult tasks of this study due to its large volume.

10.3 Recommendations for Future Work

The GCC region requires further analyses and investigation into the future performance of energy in the region, particularly in light of the region's rising energy consumption. In addition, all the GCC counties overlook the Arabian Gulf, particularly Oman, which borders both the Arabian Gulf and the Arabian Sea, and the KSA, which accesses both the Arabian Gulf and the Red Sea. This paves the way for research into the possibility of generating tidal power from sea waves. This effort may be broadened to cover the possibilities of using hydrogen and developing new techniques for reducing CO_2 emissions in the region. As there has been so little formal investigation of the GCC power sectors, this work can be expanded in innumerable directions.

As we look to the future, we placed most emphasis on energy forecasting and its modelling, while also considering data aspects and other requirements of the industry. Future forecasting solutions will be required to incorporate statistical data, although this should be provided in a manner that is suited to the end user and their specific decision-making issues. These forecasting models can be upgraded by decreasing the error metric values, maintaining flexibility, and shortening simulation times. In the meantime, the increased size of the database has created additional difficulties in terms of data pre-treatment and error post-processing. The evolution of contemporary computers and storage techniques enables the management of bigger databases. The computational times required for the proposed models are 15 minutes for the SARIMAX model and 20 minutes for the MSC and BM model. The BI-LSTM model required 1 hour for resolution to perform the forecasting, while the GRU took 30 minutes. In the case of long-term forecasting models, it is preferable to use longer epochs of historical data for annual, semi-annual or quarterly resolution. By contrast, for short-term forecasting models, it is preferable to use very small periods, such as 5-minute, 15-minute or 1-hour resolutions, as this reduces error rates and provides extremely accurate information. Several variables

can impact the accuracy of such a predictive model, including the sizes and sample rates of training, testing, validation datasets, the algorithms used, and model modifications.

Improved energy forecasting requires the development of more sophisticated and economic prediction technologies. In addition, a management system for organising and managing the operations of these forecasting models can be developed. Moreover, these models can be adapted for use across diverse locations and regions across the world. Specifically, it is recommended that we use new hybrid approaches, such as numerical simulations and NNs, as well as more sophisticated combinations, including ensemble learning methods. Expanding the scope of this work will serve to increase trust in the outcomes of comparisons across forecasting models and provide more reliable information for assessing the performance of other research studies in the forecasting field.

References

[1] R. M. Ramirez, R. K. Kopparapu, V. Lindner, and J. F. Kasting, "Can increased atmospheric CO2 levels trigger a runaway greenhouse?," *Astrobiology,* vol. 14, no. 8, pp. 714-731, 2014.

[2] J. Hansen, M. Sato, G. Russell, and P. Kharecha, "Climate sensitivity, sea level and atmospheric carbon dioxide," *Philosophical Transactions of the Royal Society A: Mathematical, Physical and Engineering Sciences,* vol. 371, no. 2001, p. 20120294, 2013.

[3] B. Ozcan, "The nexus between carbon emissions, energy consumption and economic growth in Middle East countries: a panel data analysis," *Energy Policy,* vol. 62, pp. 1138-1147, 2013.

[4] Z. Kothavala, "The duration and severity of drought over eastern Australia simulated by a coupled ocean–atmosphere GCM with a transient increase in CO2," *Environmental modelling & software,* vol. 14, no. 4, pp. 243-252, 1999.

[5] G. A. Meehl and W. M. Washington, "El Niño-like climate change in a model with increased atmospheric CO_2 concentrations," *Nature,* vol. 382, no. 6586, pp. 56-60, 1996.

[6] D. Carrington, "Worrying' rise in global CO2 forecast for 2019 " in *The Guardian News*, ed. UK: Guardian, 2019.

[7] D. S. Siqueira, J. de Almeida Meystre, M. Q. Hilário, D. H. D. Rocha, G. J. Menon, and R. J. da Silva, "Current perspectives on nuclear energy as a global climate change mitigation option," *Mitigation and Adaptation Strategies for Global Change,* vol. 24, no. 5, pp. 749-777, 2019.

[8] B. Zhu, W. Zhou, S. Hu, Q. Li, C. Griffy-Brown, and Y. Jin, "CO2 emissions and reduction potential in China's chemical industry," *Energy,* vol. 35, no. 12, pp. 4663-4670, 2010.

[9] T. Krackeler, L. Schipper, and O. Sezgen, "Carbon dioxide emissions in OECD service sectors: the critical role of electricity use," *Energy Policy,* vol. 26, no. 15, pp. 1137-1152, 1998.

[10] M. R. Qader, "Electricity consumption and GHG emissions in GCC countries," *Energies,* vol. 2, no. 4, pp. 1201-1213, 2009.

[11] H. M. S. Al-Maamary, H. A. Kazem, and M. T. Chaichan, "Climate change: the game changer in the Gulf Cooperation Council region," *Renewable and Sustainable Energy Reviews,* vol. 76, pp. 555-576, 2017.

[12] OECD and NEA., "Nuclear Energy and Renewables–System Effects in Low-carbon Electricity Systems," 9264188517, 2012. Accessed: 30/12/2019. [Online]. Available: www. oecd-bookshop. org, https://www.oecd-nea.org/ndd/pubs/2012/7056-system-effects.pdf

[13] R. Harrabin, "Climate change: UK 'can cut emissions to nearly zero' by 2050,"

[14] Renewable Energy Focus. "Renewable power generation in UK grows to same level as nuclear amid continued demise of coal." Renewable Energy Focus. http://www.renewableenergyfocus.com/view/43575/renewable-power-generation-in-uk-grows-to-same-level-as-nuclear-amid-continued-demise-of-coal/ (accessed 25/06/2019).

[15] D. Reiche, "Energy Policies of Gulf Cooperation Council (GCC) countries—possibilities and limitations of ecological modernization in rentier states," *Energy Policy,* vol. 38, no. 5, pp. 2395-2403, 2010.

[16] B. Fattouh and L. El-Katiri, *Energy and Arab economic development*. Citeseer, 2012.

[17] M. Asif, "Growth and sustainability trends in the buildings sector in the GCC region with particular reference to the KSA and UAE," *Renewable and Sustainable Energy Reviews,* vol. 55, pp. 1267-1273, 2016.

[18] Z. Abdmouleh, R. A. M. Alammari, and A. Gastli, "Recommendations on renewable energy policies for the GCC countries," *Renewable and Sustainable Energy Reviews,* vol. 50, pp. 1181-1191, 2015, doi: 10.1016/j.rser.2015.05.057.

[19] Secretariat General of the Gulf Cooperation Council. TheCooperation Council for the Arab States of the Gulf.Accessed: Jun 29, 2023. [Online]. Available: http://www.gcc-sg.org/enus/CooperationAndAchievements/Pages/Home.aspx

[20] M. Salahuddin and J. Gow, "Economic growth, energy consumption and CO2 emissions in Gulf Cooperation Council countries," *Energy,* vol. 73, pp. 44-58, 2014.

[21] H. Al Shidi, H. Sulaiman, and P. Amoatey, "Shifting to Renewable Energy to Mitigate Carbon Emissions: Initiatives by the States of Gulf Cooperation Council," *Low Carbon Economy,* vol. 7, no. 03, p. 123, 2016.

[22] D. Carrington, "Extreme Heatwaves Could Push Gulf Climate Beyond Human Endurance, Study Shows," in *The Guardian*, ed, 2015.

[23] F. M. Al Zawad and A. Aksakal, "Impacts of climate change on water resources in Saudi Arabia," in *Global Warming*: Springer, 2010, pp. 511-523.

[24] Z. Li, A. Siddiqi, L. D. Anadon, and V. Narayanamurti, "Towards sustainability in water-energy nexus: Ocean energy for seawater desalination," *Renewable and Sustainable Energy Reviews,* vol. 82, pp. 3833-3847, 2018.

[25] D. Wogan, S. Pradhan, and S. Albardi, "GCC Energy System Overview – 2017," The King Abdullah Petroleum Studies and Research Center (KAPSARC), Saudi Arabia, 2017. Accessed: 10/06/2019. [Online]. Available: https://www.kapsarc.org/research/publications/gcc-energy-system-overview-2017/

[26] H. M. S. Al-Maamary, H. A. Kazem, and M. T. Chaichan, "Renewable energy and GCC States energy challenges in the 21st century: A review," *International Journal of Computation and Applied Sciences IJOCAAS,* vol. 2, no. 1, pp. 11-18, 2017.

[27] A. A. Kubursi, "Oil, influence, and development: the Gulf states and the international economy," *International Journal,* vol. 41, no. 2, pp. 362-382, 1986.

[28] P. S. Glada Lahn and F. Preston, "Saving oil and gas in the gulf," *The Royal Institute of International. Chatham House Report Affairs,* 2013.

[29] H. M. S. Al-Maamary, H. A. Kazem, and M. T. Chaichan, "The impact of oil price fluctuations on common renewable energies in GCC countries," *Renewable and Sustainable Energy Reviews,* vol. 75, pp. 989-1007, 2017.

[30] H. Fath, A. Sadik, and T. Mezher, "Present and future trend in the production and energy consumption of desalinated water in GCC countries," *International Journal of Thermal & Environmental Engineering,* vol. 5, no. 2, pp. 155-165, 2013.

[31] D. Gielen, F. Boshell, D. Saygin, M. D. Bazilian, N. Wagner, and R. Gorini, "The role of renewable energy in the global energy transformation," *Energy Strategy Reviews,* vol. 24, pp. 38-50, 2019.

[32] King Abdullah Petroleum Studies and Research Center (KAPSARC), "Electricity Market Integration in the GCC and MENA: Imperatives and Challenges," King Abdullah Petroleum Studies and Research Center, Saudi Arabia, 2018 2018. Accessed: 29/06/2019. [Online]. Available: https://www.kapsarc.org/research/publications/electricity-market-integration-in-the-gcc-and-mena-imperatives-and-challenges/

[33] Arab Petroleum Investments Corporation, "MENA power investment: reforms slowing demand growth," Saudi Arabia, 2018, vol. 03 No. 07. Accessed: 08/07/2019. [Online]. Available: http://www.apicorp.org/Research/EnergyReseach/2018/APICORP_Energy_Research_V03_N07_2018.pdf

[34] Oxford Business Group. "Saudi Arabia Report: Saudi Arabia works to meet rising water and energy demand." Oxford Business Group. https://oxfordbusinessgroup.com/overview/path-privatisation-kingdom-works-meet-rising-demand-energy-and-water (accessed 07/07/2019).

[35] "Independent Statistics & Analysis - U.S. Energy Information Administration (EIA)." Eia.gov. https://www.eia.gov/international/data/world#/?pa=0000002&c=4100000002000060000000000000g000200000000000000001&tl_id=2-A&vs=INTL.2-2-AFRC-BKWH.A&vo=0&v=H&end=2016 (accessed 25/08/2020).

[36] "BP Statistical Review of World Energy 2018," London, UK, 2019. Accessed: 22/09/2019. [Online]. Available: https://www.bp.com/content/dam/bp/business-sites/en/global/corporate/pdfs/energy-economics/statistical-review/bp-stats-review-2018-full-report.pdf

[37] C. Cosgrove, "Energy consumption in GCC countries. Power on, power up," 2017: IEEE, pp. 1-6.

[38] H. Doukas, K. D. Patlitzianas, A. G. Kagiannas, and J. Psarras, "Renewable energy sources and rationale use of energy development in the countries of GCC: Myth or reality?," *Renewable Energy,* vol. 31, no. 6, pp. 755-770, 2006.

[39] A. S. Weber, "Review of sustainable and renewable energy activities in the state of Qatar," in *2013 International Renewable and Sustainable Energy Conference (IRSEC)*, 7-9 March 2013 2013, pp. 91-95, doi: 10.1109/IRSEC.2013.6529703.

[40] K. D. Patlitzianas, H. Doukas, and D. T. Askounis, "An assessment of the sustainable energy investments in the framework of the EU–GCC cooperation," *Renewable energy,* vol. 32, no. 10, pp. 1689-1704, 2007.

[41] W. E. Alnaser and N. W. Alnaser, "The status of renewable energy in the GCC countries," *Renewable and Sustainable Energy Reviews,* vol. 15, no. 6, pp. 3074-3098, 2011, doi: 10.1016/j.rser.2011.03.021.

[42] N. W. Alnaser and W. E. Alnaser, "The impact of the rise of using solar energy in GCC countries," *Renewable Energy and Environmental Sustainability,* vol. 4, p. 7, 2019.

[43] J. Krane, "Stability versus sustainability: energy policy in the Gulf monarchies," *The Energy Journal,* pp. 1-21, 2015.

[44] M. A. Salam and S. A. Khan, "Transition towards sustainable energy production–A review of the progress for solar energy in Saudi Arabia," *Energy Exploration & Exploitation,* vol. 36, no. 1, pp. 3-27, 2018.

[45] M. Davies, B. Hodge, G. Schellekens, and S. Ahmad, "Developing renewable energy projects: A guide to achieving success in the middle east," *Egypt: EverSheds, Shahid Law Firm, Pwc,* 2015.

[46] A. W. Bhutto, A. A. Bazmi, G. Zahedi, and J. J. Klemeš, "A review of progress in renewable energy implementation in the Gulf Cooperation Council countries," *Journal of Cleaner Production,* vol. 71, no. C, pp. 168-180, 2014, doi: 10.1016/j.jclepro.2013.12.073.

[47] A. Al-Badi and I. AlMubarak, "Growing energy demand in the GCC countries," *Arab Journal of Basic and Applied Sciences,* vol. 26, no. 1, pp. 488-496, 2019.

[48] N. Howarth, M. Galeotti, A. Lanza, and K. Dubey, "Economic development and energy consumption in the GCC: an international sectoral analysis," *Energy Transitions,* vol. 1, no. 2, p. 6, 2017.

[49] S. Griffiths, "Renewable energy policy trends and recommendations for GCC countries," *Energy Transitions,* vol. 1, no. 1, p. 3, 2017.

[50] A. Ahmad and M. Babar, "Effect of energy market globalization over power sector of GCC region: a short review," *Smart Grid and Renewable Energy,* vol. 4, no. 03, p. 265, 2013.

[51] J. M. Pedraza, "Electrical energy generation in Europe," in *The Current Situation and Perspectives in the Use of Renewable Energy Sources and Nuclear Power for Regional Electricity Generation*: Springer, 2015.

[52] B. Wang and Z. Yu, "The Gulf Regional Cooperation after the Cold War," *Journal of Middle Eastern and Islamic Studies (in Asia),* vol. 8, no. 1, pp. 100-120, 2014.

[53] K. Mohaddes and M. H. Pesaran, "Oil prices and the global economy: Is it different this time around?," *Energy Economics,* vol. 65, pp. 315-325, 2017.

[54] N. Ghaffour, J. Bundschuh, H. Mahmoudi, and M. F. A. Goosen, "Renewable energy-driven desalination technologies: A comprehensive review on challenges and potential applications of integrated systems," *Desalination,* vol. 356, pp. 94-114, 2015.

[55] X.-P. Zhang, O. U. Mingyu, S. Yanmin, and L. I. Xiaolu, "Review of Middle East energy interconnection development," *Journal of Modern Power Systems and Clean Energy,* vol. 5, no. 6, pp. 917-935, 2017.

[56] L. El-Katiri, *Interlinking the Arab Gulf: Opportunities and Challenges of GCC Electricity Market Cooperation*. Oxford Institute for Energy Studies, 2011.

[57] D. Wogan, F. Murphy, and A. Pierru, "The costs and gains of policy options for coordinating electricity generation in the Gulf Cooperation Council," *Energy policy,* vol. 127, pp. 452-463, 2019.

[58] H. Fraser and H. K. Al-Asaad, "Engaging in cross-border power exchange and trade via the Arab Gulf states power grid," *The Electricity Journal,* vol. 21, no. 10, pp. 19-29, 2008.

[59] H. Al-Asaad and A. A. Ebrahim, "The GCC Power Grid: Benefits & Beyond," *Oil, Gas & Energy Law Journal (OGEL),* vol. 6, no. 3, 2008.

[60] H. K. Al-Asaad, A. I. Al-Mohaisen, and S. Sud, "GCC power grid: Transforming the GCC power sector into a major energy trading market," 2006, pp. 27-29.

[61] A. Al-Mohaisen, L. Chaussé, and S. Sud, "Progress report on the GCC electricity grid system interconnection in the Middle East," 2007: IEEE, pp. 1-7.

[62] A. Al-Mohaisen and S. Sud, "Update on the Gulf Cooperation Council (GCC) electricity grid system interconnection," in *2006 IEEE Power Eng. Soc. General Meeting*, Montreal, Québec, Jun. 18–22 2006: IEEE, p. 6.

[63] X. P. Zhang, O. U. Mingyu, S. Yanmin, and L. I. Xiaolu, "Review of Middle East energy interconnection development," *J. Modern Power Syst. Clean Energy,* vol. 5, no. 6, pp. 917–935, Nov. 2017, doi: 10.1007/s40565-017-0335-7.

[64] A. M. H. A. Karim, N. H. A. Maskati, and S. Sud, "Status of Gulf cooperation council (GCC) electricity grid system interconnection," in *2004 IEEE Power Eng. Soc. General Meeting*, Denver, CO, Jun. 6–10 2004: IEEE, pp. 1385–1388.

[65] S. Bassi, A. Bowen, and S. Fankhauser, "The case for and against onshore wind energy in the UK," *Grantham Research Institute on Climate Change and Environment Policy Brief, London,* 2012.

[66] M. A. Ramady, *The GCC Economies [electronic resource] : Stepping Up To Future Challenges*. New York, NY: Springer New York, 2012.

[67] First Abu Dhabi Bank. "The GCC-Facts & Figures: FAB Market Insights & Strategy." First Abu Dhabi Bank. https://www.bankfab.com/en-ae/cib/market-insights/macro-strategy-and-economic-update (accessed 30/12/2018).

[68] K. D. Patlitzianas and A. Flamos, "Driving forces for renewable development in GCC countries," *Energy Sources, Part B: Economics, Planning, and Policy,* vol. 11, no. 3, pp. 244-250, 2016.

[69] L. El-Katiri and M. Husain, "Prospects for Renewable Energy in GCC States–Opportunities and the Need for Reform," 2014.

[70] R. Ferroukhi, N. Ghazal-Aswad, S. Androulaki, D. Hawila, and T. Mezher, "Renewable energy in the GCC: status and challenges," *International Journal of Energy Sector Management,* vol. 7, no. 1, pp. 84-112, 2013.

[71] S. Muench, S. Thuss, and E. Guenther, "What hampers energy system transformations? The case of smart grids," *Energy Policy,* vol. 73, pp. 80-92, 2014.

[72] S. C. Johnson, D. J. Papageorgiou, D. S. Mallapragada, T. A. Deetjen, J. D. Rhodes, and M. E. Webber, "Evaluating rotational inertia as a component of grid reliability with high penetrations of variable renewable energy," *Energy,* vol. 180, pp. 258-271, 2019.

[73] Ventures Onsite, "GCC POWER MARKET: PREPARED BY VENTURES ONSITE FOR MIDDLE EAST ELECTRICITY ENERGISING," UAE, 2017. Accessed: May 8,2019. [Online]. Available: https://www.venturesonsite.com/construction-report/189-gcc-power-market-%E2%80%93-october-2017

[74] A. A. Farag, "The story of Neom city: opportunities and challenges," in *New Cities and Community Extensions in Egypt and the Middle East*: Springer, 2019, pp. 35-49.

[75] National Renewable Energy Program (NREP). "About the National Renewable Energy Program." https://ksa-climate.com/making-a-difference/nrep/ (accessed May 9, 2019).

[76] K. E. Okedu and W. Z. A. L. Salmani, "Smart Grid Technologies in Gulf Cooperation Council Countries: Challenges and Opportunities," 2019.

[77] E. Coyle, "A Case Study of the Omani Electricity Network and Readiness for Solar Energy Integration," *SDAR* Journal of Sustainable Design & Applied Research,* vol. 5, no. 1, p. 4, 2017.

[78] O. Alsayegh, N. Saker, and A. Alqattan, "Integrating sustainable energy strategy with the second development plan of Kuwait," *Renewable and Sustainable Energy Reviews,* vol. 82, pp. 3430-3440, 2018.

[79] H. E. Murdock, D. Gibb, and T André, "Renewables 2019 Global Status Report," 2019.

[80] "Zawya."https://www.zawya.com/mena/en/projects/list/(accessed 28/08/2020).

[81] "The Renewable Energy Project Development Office (REPDO)." https://www.powersaudiarabia.com.sa/web/index.html (accessed 26/08/2020).

[82] IRENA(2019), "Renewable Energy Market Analysis: GCC 2019," IRENA, Abu Dhabi, 978-92-9260-096-9, 2019. Accessed: 20/03/2020. [Online]. Available: https://www.irena.org/publications/2019/Jan/Renewable-Energy-Market-Analysis-GCC-2019

[83] "Mohammed bin Rashid Al-Maktoum Solar Park - a leading project that promotes sustainability in the UAE." https://www.dewa.gov.ae/en/about-us/media-publications/latest-news/2019/03/mohammed-bin-rashid-al-maktoum-solar-park (accessed 28/8/2020).

[84] King Abdullah Petroleum Studies and Research Center (KAPSARC), "Future of the Electricity System in the GCC Countries," KAPSARC, Riyadh, Saudi Arabia, 2017. Accessed: 09/10/2018. [Online]. Available: https://datasource.kapsarc.org/explore/dataset/future-of-the-electricity-system-in-the-gcc-countries/information/

[85] M. AlKhars, F. Miah, H. Qudrat-Ullah, and A. Kayal, "A Systematic Review of the Relationship Between Energy Consumption and Economic Growth in GCC Countries," *Sustainability,* vol. 12, no. 9, p. 3845, 2020.

[86] M. I. Haque, "Oil price shocks and energy consumption in GCC countries: a system-GMM approach," *Environment, Development and Sustainability,* pp. 1-16, 2020.

[87] S. J. Abul, E. Satrovic, and A. Muslija, "The link between energy consumption and economic growth in gulf cooperation council countries," *International Journal of Energy Economics and Policy,* vol. 9, no. 5, p. 38, 2019.

[88] K. Malik, S. M. Rahman, A. N. Khondaker, I. R. Abubakar, Y. A. Aina, and M. A. Hasan, "Renewable energy utilization to promote sustainability in GCC countries: policies, drivers, and barriers," *Environmental Science and Pollution Research,* pp. 1-17, 2019.

[89] L. El-Katiri, "Future Energy Challenges for the GCC States," in *Oxford Institute for Energy Studies (OIES)*, ed. United Kingdom: OIES, 2014, p. 5.

[90] M. F. A. Goosen, H. Mahmoudi, and N. Ghaffour, "Today's and future challenges in applications of renewable energy technologies for desalination," *Critical Reviews in Environmental Science and Technology,* vol. 44, no. 9, pp. 929-999, 2014.

[91] S. Munawwar and H. Ghedira, "A review of renewable energy and solar industry growth in the GCC region," *Energy Procedia,* vol. 57, pp. 3191-3202, 2014.

[92] M. Al-Saidi and N. A. Elagib, "Ecological modernization and responses for a low-carbon future in the Gulf Cooperation Council countries," *Wiley Interdisciplinary Reviews: Climate Change,* vol. 9, no. 4, p. e528, 2018.

[93] H. Apostoleris, S. Sgouridis, M. Stefancich, and M. Chiesa, "Evaluating the factors that led to low-priced solar electricity projects in the Middle East," *Nature Energy,* vol. 3, no. 12, p. 1109, 2018.

[94] T. Van de Graaf, "A new world: the geopolitics of the energy transformation," ed, 2019.

[95] N. Bauer, L. Baumstark, and M. Leimbach, "The REMIND-R model: the role of renewables in the low-carbon transformation—first-best vs. second-best worlds," *Climatic Change,* vol. 114, no. 1, pp. 145-168, 2012.

[96] H. M. Government, "The UK low carbon transition plan: national strategy for climate and energy," ed: The Stationery Office London, 2009.

[97] U. Nyambuu and W. Semmler, "Climate change and the transition to a low carbon economy–Carbon targets and the carbon budget," *Economic Modelling,* vol. 84, pp. 367-376, 2020.

[98] J. Tollefson, "The hard truths of climate change---by the numbers," *Nature,* vol. 573, pp. 324-327, 2019.

[99] "Each Country's Share of CO_2 Emissions." Union of Concerned Scientists https://www.ucsusa.org/resources/each-countrys-share-co2-emissions (accessed 03-03-2021).

[100] "Climate Action Tracker: Global emissions time series." Climate Analytics and New Climate Institute. https://climateactiontracker.org/global/cat-emissions-gaps/ (accessed 01-03-2021, 2021).

[101] H. M. S. Al-Maamary, H. A. Kazem, and M. T. Chaichan, "Changing the energy profile of the GCC States: A review," vol. 11, no. 3, pp. 1980-1988, 2016.

[102] A. S. Alsharhan, Z. A. Rizk, A. E. M. Nairn, D. W. Bakhit, and S. A. Alhajari, *Hydrogeology of an arid region: the Arabian Gulf and adjoining areas*. Elsevier, 2001.

[103] M. Riad, "Geopolitics and politics in the Arab Gulf States (GCC)," *GeoJournal,* vol. 13, no. 3, pp. 201-210, 1986.

[104] K. D. Patlitzianas, H. Doukas, and J. Psarras, "Enhancing renewable energy in the Arab States of the Gulf: Constraints & efforts," *Energy policy,* vol. 34, no. 18, pp. 3719-3726, 2006.

[105] S. H. Madaeni, R. Sioshansi, and P. Denholm, "How thermal energy storage enhances the economic viability of concentrating solar power," *Proceedings of the IEEE,* vol. 100, no. 2, pp. 335-347, 2011.

[106] A. Hepbasli and Z. Alsuhaibani, "A key review on present status and future directions of solar energy studies and applications in Saudi Arabia," *Renewable and sustainable energy reviews,* vol. 15, no. 9, pp. 5021-5050, 2011.

[107] Y. Tian and C.-Y. Zhao, "A review of solar collectors and thermal energy storage in solar thermal applications," *Applied energy,* vol. 104, pp. 538-553, 2013.

[108] W. Li, P. Wei, and X. Zhou, "A cost-benefit analysis of power generation from commercial reinforced concrete solar chimney power plant," *Energy conversion and management,* vol. 79, pp. 104-113, 2014.

[109] X. Zhao, Y. Zeng, and D. Zhao, "Distributed solar photovoltaics in China: Policies and economic performance," *Energy,* vol. 88, pp. 572-583, 2015.

[110] E. Sermyagina, J. Saari, J. Kaikko, and E. Vakkilainen, "Integration of torrefaction and CHP plant: Operational and economic analysis," *Applied energy,* vol. 183, pp. 88-99, 2016.

[111] P. Guo, Y. Zhai, X. Xu, and J. Li, "Assessment of levelized cost of electricity for a 10-MW solar chimney power plant in Yinchuan China," *Energy Conversion and Management,* vol. 152, pp. 176-185, 2017.

[112] E. Du, N. Zhang, B.-M. Hodge, C. Kang, B. Kroposki, and Q. Xia, "Economic justification of concentrating solar power in high renewable energy penetrated power systems," *Applied Energy,* vol. 222, pp. 649-661, 2018.

[113] F. R. Pazheri, "Solar power potential in Saudi Arabia," *International Journal of Engineering Research and Applications,* vol. 4, no. 9, pp. 171-174, 2014.

[114] A. H. Almasoud and H. M. Gandayh, "Future of solar energy in Saudi Arabia," *Journal of King Saud University Engineering Sciences,* vol. 27, no. 2, pp. 153-157, 2015.

[115] T. Singh, M. A. A. Hussien, T. Al-Ansari, K. Saoud, and G. McKay, "Critical review of solar thermal resources in GCC and application of nanofluids for development of efficient and cost-effective CSP technologies," *Renewable and Sustainable Energy Reviews,* vol. 91, pp. 708-719, 2018.

[116] J. Meltzer, N. E. Hultman, and C. Langley, "Low-carbon energy transitions in Qatar and the Gulf cooperation council region," *Brookings Papers on Economic Activity,* 2014.

[117] R. Prăvălie, C. Patriche, and G. Bandoc, "Spatial assessment of solar energy potential at global scale. A geographical approach," *Journal of cleaner production,* vol. 209, pp. 692-721, 2019.

[118] A. H. Al-Badi, A. Malik, and A. Gastli, "Sustainable energy usage in Oman—Opportunities and barriers," *Renewable and Sustainable Energy Reviews,* vol. 15, no. 8, pp. 3780-3788, 2011.

[119] A. Mokri, M. A. Ali, and M. Emziane, "Solar energy in the United Arab Emirates: A review," *Renewable and Sustainable energy reviews,* vol. 28, pp. 340-375, 2013.

[120] A. Assi, M. Jama, and M. Al-Shamisi, "Prediction of global solar radiation in Abu Dhabi," *ISRN Renewable Energy,* vol. 2012, 2012.

[121] A. S. Alsharhan, *Hydrogeology of an arid region : the Arabian Gulf and adjoining areas*. Elsevier, 2001.

[122] S. AlYahya and M. A. Irfan, "Analysis from the new solar radiation Atlas for Saudi Arabia," *Solar Energy,* vol. 130, pp. 116-127, 2016.

[123] D. Bachour and D. Perez-Astudillo, "Ground-measurement GHI map for Qatar," *Energy Procedia,* vol. 49, pp. 2297-2302, 2014.

[124] H. P. Dasari, S. Desamsetti, S. Langodan, R. Attada, R. K. Kunchala, Y. Viswanadhapalli, O. Knio, and I. Hoteit, "High-resolution assessment of solar energy resources over the Arabian Peninsula," *Applied Energy,* vol. 248, pp. 354-371, 2019.

[125] F. Vignola, J. Michalsky, and T. Stoffel, *Solar and infrared radiation measurements*. CRC press, 2016.

[126] A. A. Mas'ud, A. V. Wirba, S. J. Alshammari, F. Muhammad-Sukki, M. M. Abdullahi, R. Albarracín, and M. Z. Hoq, "Solar energy potentials and benefits in the gulf cooperation council countries: A review of substantial issues," *Energies,* vol. 11, no. 2, p. 372, 2018.

[127] E. Zell, S. Gasim, S. Wilcox, S. Katamoura, T. Stoffel, H. Shibli, J. Engel-Cox, and M. Al Subie, "Assessment of solar radiation resources in Saudi Arabia," *Solar Energy,* vol. 119, pp. 422-438, 2015.

[128] P. A. Jimenez, J. P. Hacker, J. Dudhia, S. E. Haupt , J. A. Ruiz-Arias, C. A. Gueymard, G. Thompson, T. Eidhammer, and A. Deng, "WRF-Solar: Description and clear sky assessment of an augmented NWP model for solar power prediction," *Bulletin of the American Meteorological Society,* vol. 97, no. 7, pp. 1249-1264, 2016.

[129] S. E. Haupt, B. Kosović, T.Jensen, J. K. Lazo, J. A. Lee, P. A. Jiménez, J. Cowie, G. Wiener, T. C. McCandless, M.Rogers, S. Miller, M. Sengupta, Y. Xie, L. Hinkelman, P. Kalb, and J. Heiser,"Building the Sun4Cast system: Improvements in solar power forecasting," *Bulletin of the American Meteorological Society,* vol. 99, no. 1, pp. 121-136, 2018.

[130] A. A. Prasad, R. A. Taylor, and M. Kay, "Assessment of direct normal irradiance and cloud connections using satellite data over Australia," *Applied energy,* vol. 143, pp. 301-311, 2015.

[131] F. Crespi, A. Toscani, P. Zani, D. Sánchez, and G. Manzolini, "Effect of passing clouds on the dynamic performance of a CSP tower receiver with molten salt heat storage," *Applied Energy,* vol. 229, pp. 224-235, 2018.

[132] N. J. Middleton, "Dust storms in the Middle East," *Journal of Arid Environments,* vol. 10, no. 2, pp. 83-96, 1986.

[133] J. M. Prospero, P. Ginoux, O. Torres, S. E. Nicholson, and T. E. Gill, "Environmental characterization of global sources of atmospheric soil dust identified with the Nimbus 7 Total Ozone Mapping Spectrometer (TOMS) absorbing aerosol product," *Reviews of geophysics,* vol. 40, no. 1, pp. 2-1, 2002.

[134] N. W. Tindale and P. P. Pease, "Aerosols over the Arabian Sea: Atmospheric transport pathways and concentrations of dust and sea salt," *Deep Sea Research Part II: Topical Studies in Oceanography,* vol. 46, no. 8-9, pp. 1577-1595, 1999.

[135] W.-D. Chen, F. Cui, H. Zhou, H. Ding, and D.-X. Li, "Impacts of different radiation schemes on the prediction of solar radiation and photovoltaic power," *Atmospheric and Oceanic Science Letters,* vol. 10, no. 6, pp. 446-451, 2017.

[136] A. Awad and A.-W. Mashat, "The synoptic patterns associated with spring widespread dusty days in central and eastern Saudi Arabia," *Atmosphere,* vol. 5, no. 4, pp. 889-913, 2014.

[137] A. M. Awad and A.-W. S. Mashat, "Synoptic features associated with dust transition processes from North Africa to Asia," *Arabian Journal of Geosciences,* vol. 7, no. 6, pp. 2451-2467, 2014.

[138] M. Notaro, F. Alkolibi, E. Fadda, and F. Bakhrjy, "Trajectory analysis of Saudi Arabian dust storms," *Journal of Geophysical Research: Atmospheres,* vol. 118, no. 12, pp. 6028-6043, 2013.

[139] A. Mashat and A. M. Awad, "The classification of the dusty areas over the Middle East," *Bull Fac Sci Cairo Univ,* vol. 78, no. A, pp. 1-19, 2010.

[140] R. Attada, H. P. Dasari, A. Parekh, J. S. Chowdary, S. Langodan, O. Knio and I. Hoteit, "The role of the Indian Summer Monsoon variability on Arabian Peninsula summer climate," *Climate dynamics,* vol. 52, no. 5-6, pp. 3389-3404, 2019.

[141] R. Attada, R. K. Yadav, R. K. Kunchala, H. P. Dasari, O. Knio, and I. Hoteit, "Prominent mode of summer surface air temperature variability and associated circulation anomalies over the Arabian Peninsula," *Atmospheric Science Letters,* vol. 19, no. 11, p. e860, 2018.

[142] K. R. Kumar,R. Attada, H. P. Dasari, R. K. Vellore, S. Langodan, Y. O. Abualnaja, and I. Hoteit, "Aerosol Optical Depth variability over the Arabian Peninsula as inferred from satellite measurements," *Atmospheric Environment,* vol. 187, pp. 346-357, 2018.

[143] N. T. Al-Tayeb and B. M. Jarrar, "Dust fall in the city of Riyadh," 1993: Riyadh, pp. 66-74.

[144] A. Modaihsh, A. Ghoneim, F. Al-Barakah, M. Mahjoub, and M. Nadeem, "Characterizations of Deposited Dust Fallout in Riyadh City, Saudi Arabia," *Polish Journal of Environmental Studies,* vol. 26, no. 4, 2017.

[145] M. I. Badawy, M. D. Hernandez, and F. T. Al-Harthy, "Sources of pollution at Mina al Fahal coastal area," *Bulletin of Environmental Contamination and toxicology,* vol. 49, no. 6, pp. 813-820, 1992.

[146] A. Al-Dousari, W. Al-Nassar, A. Al-Hemoud, A. Alsaleh, A. Ramadan, N. Al-Dousari, and M. Ahmed, "Solar and wind energy: challenges and solutions in desert regions," *Energy,* vol. 176, pp. 184-194, 2019.

[147] H. Al-Thani, M. Koc, and R. J. Isaifan, "Investigations on deposited dust fallout in urban Doha: Characterization, source apportionment and mitigation," *Environ. Ecol. Res,* vol. 6, no. 5, pp. 493-506, 2018.

[148] W. Javed, Y. Wubulikasimu, B. Figgis, and B. Guo, "Characterization of dust accumulated on photovoltaic panels in Doha, Qatar," *Solar Energy,* vol. 142, pp. 123-135, 2017.

[149] N. W. Alnaser, A. A. Dakhel, M.J. Al Othman, I. Batarseh, J. K. Lee, S. Najmaii, and W. E. Alnaser, "Dust accumulation study on the Bapco 0.5 MWp PV project at University of Bahrain," *International Journal of Power and Renewable Energy Systems,* vol. 2, no. 1, p. 53, 2015.

[150] A. Al-Dousari, D. Doronzo, and M. Ahmed, "Types, indications and impact evaluation of sand and dust storms trajectories in the Arabian Gulf," *Sustainability,* vol. 9, no. 9, p. 1526, 2017.

[151] M. F. Yassin, S. K. Almutairi, and A. Al-Hemoud, "Dust storms backward Trajectories' and source identification over Kuwait," *Atmospheric research,* vol. 212, pp. 158-171, 2018.

[152] A. Al-Hemoud, A. Al-Dousari, H. Al-Dashti, P. Petrov, A. Al-Saleh, S. Al-Khafaji, W. Behbehani, J. Li, and P. Koutrakis,"Sand and dust storm trajectories from Iraq Mesopotamian flood plain to Kuwait," *Science of The Total Environment,* vol. 710, p. 136291, 2020.

[153] S. Kalenderski, G. Stenchikov, and C. Zhao, "Modeling a typical winter-time dust event over the Arabian Peninsula and the Red Sea," *Atmospheric Chemistry and Physics,* vol. 13, no. 4, pp. 1999-2014, 2013.

[154] M. A. Al-Dabbas, M. A. Abbas, and R. M. Al-Khafaji, "Dust storms loads analyses—Iraq," *Arabian Journal of Geosciences,* vol. 5, no. 1, pp. 121-131, 2012.

[155] I. Gharib, M. Al-Hashash, and M. Anwar, "Dust fallout in northern part of the ROPME sea area," *Kuwait Institute for Scientific Research, Report no. KISR2266. Kuwait,* 1987.

[156] C. M. A. Yip, U. B. Gunturu, and G. L. Stenchikov, "Wind resource characterization in the Arabian Peninsula," *Applied energy,* vol. 164, pp. 826-836, 2016.

[157] A. H. Marafia and H. A. Ashour, "Economics of offshore/onshore wind energy systems in Qatar," *Renewable Energy,* vol. 28, no. 12, pp. 1953-1963, 2003.

[158] B. L. Almutairi, "Investigating the feasibility and soil–structure integrity of onshore wind turbine systems in Kuwait," 2017.

[159] N. S. Al Bahrana and N. Al Mahdi, "Feasibility of wind energy applications in Bahrain," *Renewable energy,* vol. 1, no. 5-6, pp. 831-836, 1991.

[160] I. Janajreh, L. Su, and F. Alan, "Wind energy assessment: Masdar City case study," *Renewable energy,* vol. 52, pp. 8-15, 2013.

[161] S. Nader, "Paths to a low-carbon economy—The Masdar example," *Energy Procedia,* vol. 1, no. 1, pp. 3951-3958, 2009.

[162] S. Rehman and A. Ahmad, "Assessment of wind energy potential for coastal locations of the Kingdom of Saudi Arabia," *Energy,* vol. 29, no. 8, pp. 1105-1115, 2004.

[163] S. Rehman, I. M. El-Amin, F. Ahmad, S. M. Shaahid, A. M. Al-Shehri, and J. M. Bakhashwain, "Wind power resource assessment for Rafha, Saudi Arabia," *Renewable and Sustainable Energy Reviews,* vol. 11, no. 5, pp. 937-950, 2007.

[164] M. A. Baseer, J. P. Meyer, S. Rehman, and M. M. Alam, "Wind power characteristics of seven data collection sites in Jubail, Saudi Arabia using Weibull parameters," *Renewable Energy,* vol. 102, pp. 35-49, 2017.

[165] W. K. Al-Nassar, S. Neelamani, K. A. Al-Salem, and H. A. Al-Dashti, "Feasibility of offshore wind energy as an alternative source for the state of Kuwait," *Energy,* vol. 169, pp. 783-796, 2019.

[166] K. Al-Salem, S. Neelamani, and W. Al-Nassar, "Wind Energy Map of Arabian Gulf," *Natural Resources,* vol. 9, no. 5, pp. 212-228, 2018.

[167] S. Rehman, T. O. Halawani, and M. Mohandes, "Wind power cost assessment at twenty locations in the Kingdom of Saudi Arabia," *Renewable Energy,* vol. 28, no. 4, pp. 573-583, 2003.

[168] S. Langodan, Y. Viswanadhapalli, H. P. Dasari, O. Knio, and I. Hoteit, "A high-resolution assessment of wind and wave energy potentials in the Red Sea," *Applied energy,* vol. 181, pp. 244-255, 2016.

[169] H. Jiang, J. T. Farrar, R. C. Beardsley, R. Chen, and C. Chen, "Zonal surface wind jets across the Red Sea due to mountain gap forcing along both sides of the Red Sea," *Geophysical Research Letters,* vol. 36, no. 19, 2009.

[170] H. P. Dasari, S. Langodan, Y. Viswanadhapalli, B. R. Vadlamudi, V. P. Papadopoulos, and I. Hoteit, "ENSO influence on the interannual variability of the Red Sea convergence zone and associated rainfall," *International Journal of Climatology,* vol. 38, no. 2, pp. 761-775, 2018.

[171] S. Langodan, L. Cavaleri, Y. Viswanadhapalli, and I. Hoteit, "Wind-wave source functions in opposing seas," *Journal of Geophysical Research: Oceans,* vol. 120, no. 10, pp. 6751-6768, 2015.

[172] V. V. Menezes, J. T. Farrar, and A. S. Bower, "Westward mountain gap wind jets of the northern Red Sea as seen by QuikSCAT," *Remote Sensing of Environment,* vol. 209, pp. 677-699, 2018.

[173] P. Zhai and A. Bower, "The response of the Red Sea to a strong wind jet near the Tokar Gap in summer," *Journal of Geophysical Research: Oceans,* vol. 118, no. 1, pp. 421-434, 2013.

[174] O. Nematollahi, H. Hoghooghi, M. Rasti, and A. Sedaghat, "Energy demands and renewable energy resources in the Middle East," *Renewable and Sustainable Energy Reviews,* vol. 54, pp. 1172-1181, 2016.

[175] T. B. M. J. Ouarda, C. Charron, J. Y. Shin, P.R. Marpu, A. H. Al-Mandoos , M. H. Al-Tamimi , H. Ghedira , and T. N. Al Hosary,"Probability distributions of wind speed in the UAE," *Energy conversion and management,* vol. 93, pp. 414-434, 2015.

[176] A. Gastli, D. Y. Charabi, and M. S. Al-Yahyai, "Assessment of Wind Energy Potential Locations in Oman using Data from Existing Weather Stations," 2010.

[177] M. J. Shawon, L. El Chaar, and L. A. Lamont, "The GCC: wind technology deployment potential," 2011: IEEE, pp. 174-177.

[178] A. Elrahmani, J. Hannun, F. Eljack, and M.-K. Kazi, "Status of renewable energy in the GCC region and future opportunities," *Current Opinion in Chemical Engineering,* vol. 31, p. 100664, 2021.

[179] N. Sultan, "The challenge of shale to the post-oil dreams of the Arab Gulf," *Energy policy,* vol. 60, pp. 13-20, 2013.

[180] R. P. Praveen, V. Keloth, A. G. Abo-Khalil, A. S. Alghamdi, A. M. Eltamaly, and I. Tlili, "An insight to the energy policy of GCC countries to meet renewable energy targets of 2030," *Energy Policy,* vol. 147, p. 111864, 2020.

[181] F. Alharbi and D. Csala, "GCC Countries' Renewable Energy Penetration and the Progress of Their Energy Sector Projects," *IEEE Access,* pp. 1-1, 2020, doi: 10.1109/ACCESS.2020.3039936.

[182] IRENA (2020), "Renewable capacity statistics 2020," IRENA, Abu Dhabi, 978-92-9260-239-0, 2020. Accessed: 13/02/2021.

[183] W. N. Adger, "Scales of governance and environmental justice for adaptation and mitigation of climate change," *Journal of International development,* vol. 13, no. 7, pp. 921-931, 2001.

[184] D. Schlosberg, "Theorising environmental justice: the expanding sphere of a discourse," *Environmental politics,* vol. 22, no. 1, pp. 37-55, 2013.

[185] W. Hamza, M. R. Enan, H. Al-Hassini, J.-B. Stuut, and D. De-Beer, "Dust storms over the Arabian Gulf: a possible indicator of climate changes consequences," *Aquatic Ecosystem Health & Management,* vol. 14, no. 3, pp. 260-268, 2011.

[186] D. C. Wynn and C. M. Eckert, "Perspectives on iteration in design and development," *Research in Engineering Design,* vol. 28, no. 2, pp. 153-184, 2017.

[187] F. Al Harbi and D. Csala, "Saudi Arabia's Electricity: Energy Supply and Demand Future Challenges," 2019: IEEE, pp. 467-472.

[188] Meteoblue AG. Meteoblue AG,. https://www.meteoblue.com/en/historyplus (accessed Dec.02, 2020).

[189] W. N. Suter, "Qualitative data, analysis, and design," *Introduction to educational research: A critical thinking approach,* vol. 2, pp. 342-86, 2012.

[190] D. C. Wynn and P. J. Clarkson, "Process models in design and development," *Research in Engineering Design,* vol. 29, no. 2, pp. 161-202, 2018.

[191] E. Kabir, S. Guikema, and B. Kane, "Statistical modeling of tree failures during storms," *Reliability Engineering & System Safety,* vol. 177, pp. 68-79, 2018.

[192] S. A. Abdul-Wahab, Y. Charabi, R. Al-Maamari, G. A. Al-Rawas, A. Gastli, and K. Chan, "CO2 greenhouse emissions in Oman over the last forty-two years," *Renewable and Sustainable Energy Reviews,* vol. 52, pp. 1702-1712, 2015.

[193] S. S. Rashwan, A. M. Shaaban, and F. Al-Suliman, "A comparative study of a small-scale solar PV power plant in Saudi Arabia," *Renewable and Sustainable Energy Reviews,* vol. 80, pp. 313-318, 2017.

[194] H. H. Chen, H.-Y. Kang, and A. H. I. Lee, "Strategic selection of suitable projects for hybrid solar-wind power generation systems," *Renewable and Sustainable Energy Reviews,* vol. 14, no. 1, pp. 413-421, 2010.

[195] J. G. Slootweg and W. L. Kling, "The impact of large-scale wind power generation on power system oscillations," *Electric Power Systems Research,* vol. 67, no. 1, pp. 9-20, 2003.

[196] H. Yang, Z. Wei, and L. Chengzhi, "Optimal design and techno-economic analysis of a hybrid solar-wind power generation system," *Applied Energy,* vol. 86, no. 2, pp. 163-169, 2009.

[197] R. Bessa, C. Moreira, B. Silva, and M. Matos, "Handling renewable energy variability and uncertainty in power systems operation," *Wiley Interdisciplinary Reviews: Energy and Environment,* vol. 3, no. 2, pp. 156-178, 2014.

[198] N. M. Al-Abbadi, "Wind energy resource assessment for five locations in Saudi Arabia," *Renewable Energy,* vol. 30, no. 10, pp. 1489-1499, 2005.

[199] G. M. Shafiullah, "Hybrid renewable energy integration (HREI) system for subtropical climate in Central Queensland, Australia," *Renewable energy,* vol. 96, pp. 1034-1053, 2016.

[200] S. M. Al-Alawi and H. A. Al-Hinai, "An ANN-based approach for predicting global radiation in locations with no direct measurement instrumentation," *Renewable Energy,* vol. 14, no. 1-4, pp. 199-204, 1998.

[201] G. Lopez, M. A. Rubio, M. Martınez, and F. J. Batlles, "Estimation of hourly global photosynthetically active radiation using artificial neural network models," *Agricultural and forest Meteorology,* vol. 107, no. 4, pp. 279-291, 2001.

[202] M. Mohandes, S. Rehman, and T. O. Halawani, "Estimation of global solar radiation using artificial neural networks," *Renewable energy,* vol. 14, no. 1-4, pp. 179-184, 1998.

[203] G.-R. Ji, P. Han, and Y.-J. Zhai, "Wind speed forecasting based on support vector machine with forecasting error estimation," 2007, vol. 5: IEEE, pp. 2735-2739.

[204] A. More and M. C. Deo, "Forecasting wind with neural networks," *Marine structures,* vol. 16, no. 1, pp. 35-49, 2003.

[205] G. M. Shafiullah, M. T. O. Amanullah, A. B. M. S. Ali, D. Jarvis, and P. Wolfs, "Prospects of renewable energy–a feasibility study in the Australian context," *Renewable Energy,* vol. 39, no. 1, pp. 183-197, 2012.

[206] K. Naik, *Hands-On Python for Finance: A practical guide to implementing financial analysis strategies using Python*. Packt Publishing Ltd, 2019.

[207] V. Lam, "Development of wind resource assessment methods and application to the Waterloo region," 2013.

[208] S. I. Vagropoulos, G. I. Chouliaras, E. G. Kardakos, C. K. Simoglou, and A. G. Bakirtzis, "Comparison of SARIMAX, SARIMA, modified SARIMA and ANN-based models for short-term PV generation forecasting," 2016: IEEE, pp. 1-6.

[209] F. Sheng and L. Jia, "Short-term load forecasting based on SARIMAX-LSTM," 2020: IEEE, pp. 90-94.

[210] F. Alasali, K. Nusair, L. Alhmoud, and E. Zarour, "Impact of the covid-19 pandemic on electricity demand and load forecasting," *Sustainability,* vol. 13, no. 3, p. 1435, 2021.

[211] P. Sutthichaimethee and D. Ariyasajjakorn, "Forecasting energy consumption in short-term and long-term period by using arimax model in the construction and materials sector in thailand," *Journal of Ecological Engineering,* vol. 18, no. 4, 2017.

[212] P. Sutthichaimethee and S. Naluang, "The efficiency of the sustainable development policy for energy consumption under environmental law in Thailand: Adapting the SEM-VARIMAX model," *Energies,* vol. 12, no. 16, p. 3092, 2019.

[213] N. Elamin and M. Fukushige, "Modeling and forecasting hourly electricity demand by SARIMAX with interactions," *Energy,* vol. 165, pp. 257-268, 2018.

[214] J. Lee and Y. Cho, "National-scale electricity peak load forecasting: Traditional, machine learning, or hybrid model?," *Energy,* vol. 239, p. 122366, 2022.

[215] A. Tarsitano and I. L. Amerise, "Short-term load forecasting using a two-stage sarimax model," *Energy,* vol. 133, pp. 108-114, 2017.

[216] C. Bennett, R. A. Stewart, and J. Lu, "Autoregressive with exogenous variables and neural network short-term load forecast models for residential low voltage distribution networks," *Energies,* vol. 7, no. 5, pp. 2938-2960, 2014.

[217] N. Liu, V. Babushkin, and A. Afshari, "Short-term forecasting of temperature driven electricity load using time series and neural network model," *Journal of Clean Energy Technologies,* vol. 2, no. 4, pp. 327-331, 2014.

[218] L. J. Soares and M. C. Medeiros, "Modeling and forecasting short-term electricity load: A comparison of methods with an application to Brazilian data," *International Journal of Forecasting,* vol. 24, no. 4, pp. 630-644, 2008.

[219] N. Mohamed, M. H. Ahmad, and Z. Ismail, "Improving short term load forecasting using double seasonal arima model," 2011.

[220] M. S. Kim, "Modeling special-day effects for forecasting intraday electricity demand," *European Journal of Operational Research,* vol. 230, no. 1, pp. 170-180, 2013.

[221] G.-F. Fan, M. Yu, S.-Q. Dong, Y.-H. Yeh, and W.-C. Hong, "Forecasting short-term electricity load using hybrid support vector regression with grey catastrophe and random forest modeling," *Utilities Policy,* vol. 73, p. 101294, 2021.

[222] F. Yu and X. Xu, "A short-term load forecasting model of natural gas based on optimized genetic algorithm and improved BP neural network," *Applied Energy,* vol. 134, pp. 102-113, 2014.

[223] Y. Chen, P. Xu, Y. Chu, W. Li, Y. Wu, L. Ni, Y. Bao, and K. Wang, "Short-term electrical load forecasting using the Support Vector Regression (SVR) model to

calculate the demand response baseline for office buildings," *Applied Energy,* vol. 195, pp. 659-670, 2017.

[224] J. Zhang, Y.-M. Wei, D. Li, Z. Tan, and J. Zhou, "Short term electricity load forecasting using a hybrid model," *Energy,* vol. 158, pp. 774-781, 2018.

[225] A. Ampountolas, "Modeling and Forecasting Daily Hotel Demand: A Comparison Based on SARIMAX, Neural Networks, and GARCH Models," *Forecasting,* vol. 3, no. 3, pp. 580-595, 2021.

[226] D. Barrow and N. Kourentzes, "The impact of special days in call arrivals forecasting: A neural network approach to modelling special days," *European Journal of Operational Research,* vol. 264, no. 3, pp. 967-977, 2018.

[227] R. J. Hyndman and G. Athanasopoulos, *Forecasting: principles and practice*. OTexts, 2018.

[228] G. P. Papaioannou, C. Dikaiakos, A. Dramountanis, and P. G. Papaioannou, "Analysis and modeling for short-to medium-term load forecasting using a hybrid manifold learning principal component model and comparison with classical statistical models (SARIMAX, Exponential Smoothing) and artificial intelligence models (ANN, SVM): The case of Greek electricity market," *Energies,* vol. 9, no. 8, p. 635, 2016.

[229] S. Makridakis, S. C. Wheelwright, and R. J. Hyndman, *Forecasting methods and applications*. John wiley & sons, 2008.

[230] K. Naik, *Hands-On Python for Finance: A practical guide to implementing financial analysis strategies using Python*. UK: Packt Publishing Ltd, 2019, p. 378.

[231] P. Manigandan, M. S. Alam, M. Alharthi, U. Khan, K. Alagirisamy, D. Pachiyappan, and A. Rehman,"Forecasting Natural Gas Production and Consumption in United States-Evidence from SARIMA and SARIMAX Models," *Energies,* vol. 14, no. 19, p. 6021, 2021.

[232] H. J. Bierens, "ARMAX model specification testing, with an application to unemployment in the Netherlands," *Journal of Econometrics,* vol. 35, no. 1, pp. 161-190, 1987.

[233] A. Dürre, R. Fried, and T. Liboschik, "Robust estimation of (partial) autocorrelation," *Wiley Interdisciplinary Reviews: Computational Statistics,* vol. 7, no. 3, pp. 205-222, 2015.

[234] F. L. Ramsey, "Characterization of the partial autocorrelation function," *The Annals of Statistics,* pp. 1296-1301, 1974.

[235] E. Bengtsson and S. Påhlman, "The effect of rising interest rates on Swedish condominium prices," 2021.

[236] T. Ahmad and H. Chen, "Deep learning for multiscale smart energy forecasting," *Energy,* vol. 175, pp. 98-112, 2019.

[237] H. Wang, Z. Lei, X. Zhang, B. Zhou, and J. Peng, "A review of deep learning for renewable energy forecasting," *Energy Conversion and Management,* vol. 198, p. 111799, 2019.

[238] J. Brownlee, *Deep learning for time series forecasting: Predict the future with MLPs, CNNs and LSTMs in Python*. Machine Learning Mastery, 2018.

[239] Y. Netzer, T. Wang, A. Coates, A. Bissacco, B. Wu, and A. Y. Ng, "Reading digits in natural images with unsupervised feature learning," 2011.

[240] R. Zhao, R. Yan, Z. Chen, K. Mao, P. Wang, and R. X. Gao, "Deep learning and its applications to machine health monitoring," *Mechanical Systems and Signal Processing,* vol. 115, pp. 213-237, 2019.

[241] P. Vincent, H. Larochelle, Y. Bengio, and P.-A. Manzagol, "Extracting and composing robust features with denoising autoencoders," 2008, pp. 1096-1103.

[242] G. E. Hinton, S. Osindero, and Y.-W. Teh, "A fast learning algorithm for deep belief nets," *Neural computation,* vol. 18, no. 7, pp. 1527-1554, 2006.

[243] R. Salakhutdinov and G. Hinton, "Deep Boltzmann machines," 2009, pp. 448-455.

[244] P. Sermanet, S. Chintala, and Y. LeCun, "Convolutional neural networks applied to house numbers digit classification," 2012: IEEE, pp. 3288-3291.

[245] K.-i. Funahashi and Y. Nakamura, "Approximation of dynamical systems by continuous time recurrent neural networks," *Neural networks,* vol. 6, no. 6, pp. 801-806, 1993.

[246] H. Wang, H. Yi , J. Peng, G. Wang, Y. Liu, H. Jiang, and W. Liu, "Deterministic and probabilistic forecasting of photovoltaic power based on deep convolutional neural network," *Energy conversion and management,* vol. 153, pp. 409-422, 2017.

[247] A. Di Piazza, M. C. Di Piazza, and G. Vitale, "Solar and wind forecasting by NARX neural networks," *Renewable Energy and Environmental Sustainability,* vol. 1, p. 39, 2016.

[248] F. Wang, Z. Mi, S. Su, and H. Zhao, "Short-term solar irradiance forecasting model based on artificial neural network using statistical feature parameters," *Energies,* vol. 5, no. 5, pp. 1355-1370, 2012.

[249] A. Sözen, E. Arcaklioğlu, and M. Özalp, "Estimation of solar potential in Turkey by artificial neural networks using meteorological and geographical data," *Energy Conversion and Management,* vol. 45, no. 18-19, pp. 3033-3052, 2004.

[250] A. Altan, S. Karasu, and E. Zio, "A new hybrid model for wind speed forecasting combining long short-term memory neural network, decomposition methods and grey wolf optimizer," *Applied Soft Computing,* vol. 100, p. 106996, 2021.

[251] Y.-L. Hu and L. Chen, "A non-linear hybrid wind speed forecasting model using LSTM network, hysteretic ELM and Differential Evolution algorithm," *Energy conversion and management,* vol. 173, pp. 123-142, 2018.

[252] A. Abayomi-Alli, M. O. Odusami, O. Abayomi-Alli, S. Misra, and G. F. Ibeh, "Long short-term memory model for time series prediction and forecast of solar radiation and other weather parameters," 2019: IEEE, pp. 82-92.

[253] X. Liu and Z. Lin, "Impact of COVID-19 pandemic on electricity demand in the UK based on multivariate time series forecasting with bidirectional long short-term-memory," *Energy,* vol. 227, p. 120455, 2021.

[254] K. U. Jaseena and B. C. Kovoor, "EEMD-based Wind Speed Forecasting system using Bidirectional LSTM networks," 2021: IEEE, pp. 1-9.

[255] H. Zhen, D. Niu, K. Wang, Y. Shi, Z. Ji, and X. Xu, "Photovoltaic power forecasting based on GA improved Bi-LSTM in microgrid without meteorological information," *Energy,* vol. 231, p. 120908, 2021.

[256] S. Agatonovic-Kustrin and R. Beresford, "Basic concepts of artificial neural network (ANN) modeling and its application in pharmaceutical research," *Journal of pharmaceutical and biomedical analysis,* vol. 22, no. 5, pp. 717-727, 2000.

[257] G. Zhang, B. E. Patuwo, and M. Y. Hu, "Forecasting with artificial neural networks:: The state of the art," *International journal of forecasting,* vol. 14, no. 1, pp. 35-62, 1998.

[258] T. van Klompenburg, A. Kassahun, and C. Catal, "Crop yield prediction using machine learning: A systematic literature review," *Computers and Electronics in Agriculture,* vol. 177, p. 105709, 2020.

[259] I. Goodfellow, Y. Bengio, and A. Courville, *Deep learning*. MIT press Cambridge, 2016.

[260] A. Almalaq and G. Edwards, "A review of deep learning methods applied on load forecasting," 2017: IEEE, pp. 511-516.

[261] M. Saha, A. Santara, P. Mitra, A. Chakraborty, and R. S. Nanjundiah, "Prediction of the Indian summer monsoon using a stacked autoencoder and ensemble regression model," *International Journal of Forecasting,* 2020.

[262] A. Saeed, C. Li, M. Danish, S. Rubaiee, G. Tang, Z. Gan, and A. Ahmed, "Hybrid Bidirectional LSTM Model for Short-Term Wind Speed Interval Prediction," *IEEE Access,* vol. 8, pp. 182283-182294, 2020.

[263] H. Z. Wang, G. B. Wang, G. Q. Li, J. C. Peng, and Y. T. Liu, "Deep belief network based deterministic and probabilistic wind speed forecasting approach," *Applied Energy,* vol. 182, pp. 80-93, 2016.

[264] X. Yan, Y. Liu, and M. Jia, "Multiscale cascading deep belief network for fault identification of rotating machinery under various working conditions," *Knowledge-Based Systems,* vol. 193, p. 105484, 2020.

[265] X. Qiu, L. Zhang, Y. Ren, P. N. Suganthan, and G. Amaratunga, "Ensemble deep learning for regression and time series forecasting," 2014: IEEE, pp. 1-6.

[266] S. Ryu, J. Noh, and H. Kim, "Deep neural network based demand-side short term load forecasting," *Energies,* vol. 10, no. 1, p. 3, 2017.

[267] A. Gensler, J. Henze, B. Sick, and N. Raabe, "Deep Learning for solar power forecasting—An approach using AutoEncoder and LSTM Neural Networks," 2016: IEEE, pp. 002858-002865.

[268] G. E. Hinton, "A practical guide to training restricted Boltzmann machines," in *Neural networks: Tricks of the trade*: Springer, 2012, pp. 599-619.

[269] J. Wu, T. R. Mazur, S. Ruan, C. Lian, N. Daniel, H. Lashmett, L. Ochoa, I. Zoberi, M. A. Anastasio, H. M. Gach, S. Mutic, M. Thomas, and H. Li, "A deep Boltzmann machine-driven level set method for heart motion tracking using cine MRI images," *Medical image analysis,* vol. 47, pp. 68-80, 2018.

[270] J. Brownlee, *Deep learning with Python: develop deep learning models on Theano and TensorFlow using Keras*. Machine Learning Mastery, 2016.

[271] J. Brownlee, *Deep Learning for Computer Vision: Image Classification, Object Detection, and Face Recognition in Python*. Machine Learning Mastery, 2019.

[272] J.-T. Baillargeon, L. Lamontagne, and E. Marceau, "Mining Actuarial Risk Predictors in Accident Descriptions Using Recurrent Neural Networks," *Risks,* vol. 9, no. 1, p. 7, 2021.

[273] P.-F. Pai and W.-C. Hong, "Support vector machines with simulated annealing algorithms in electricity load forecasting," *Energy Conversion and Management,* vol. 46, no. 17, pp. 2669-2688, 2005.

[274] C. Yin, Y. Zhu, J. Fei, and X. He, "A deep learning approach for intrusion detection using recurrent neural networks," *IEEE Access,* vol. 5, pp. 21954-21961, 2017.

[275] D. L. Marino, K. Amarasinghe, and M. Manic, "Building energy load forecasting using deep neural networks," 2016: IEEE, pp. 7046-7051.

[276] L. Chen, G. Xu, S. Zhang, W. Yan, and Q. Wu, "Health indicator construction of machinery based on end-to-end trainable convolution recurrent neural networks," *Journal of Manufacturing Systems,* vol. 54, pp. 1-11, 2020.

[277] H. Shi, M. Xu, and R. Li, "Deep learning for household load forecasting—A novel pooling deep RNN," *IEEE Transactions on Smart Grid,* vol. 9, no. 5, pp. 5271-5280, 2017.

[278] Y. Liu, L. Guan, C. Hou, H. Han, Z. Liu, Y. Sun, and M. Zheng, "Wind power short-term prediction based on LSTM and discrete wavelet transform," *Applied Sciences,* vol. 9, no. 6, p. 1108, 2019.

[279] F. Kratzert, D. Klotz, C. Brenner, K. Schulz, and M. Herrnegger, "Rainfall–runoff modelling using long short-term memory (LSTM) networks," *Hydrology and Earth System Sciences,* vol. 22, no. 11, pp. 6005-6022, 2018.

[280] A. Graves, N. Jaitly, and A.-r. Mohamed, "Hybrid speech recognition with deep bidirectional LSTM," 2013: IEEE, pp. 273-278.

[281] S. Hochreiter and J. Schmidhuber, "Long short-term memory," *Neural computation,* vol. 9, no. 8, pp. 1735-1780, 1997.

[282] J. Zhao, F. Deng, Y. Cai, and J. Chen, "Long short-term memory-Fully connected (LSTM-FC) neural network for PM2. 5 concentration prediction," *Chemosphere,* vol. 220, pp. 486-492, 2019.

[283] X. Li, L. Peng, X. Yao, S. Cui, Y. Hu, C. You, and T. Chi, "Long short-term memory neural network for air pollutant concentration predictions: Method

development and evaluation," *Environmental pollution,* vol. 231, pp. 997-1004, 2017.

[284] L. He, D. Jiang, L. Yang, E. Pei, P. Wu, and H. Sahli, "Multimodal affective dimension prediction using deep bidirectional long short-term memory recurrent neural networks," 2015, pp. 73-80.

[285] A. Graves and J. Schmidhuber, "Framewise phoneme classification with bidirectional LSTM and other neural network architectures," *Neural networks,* vol. 18, no. 5-6, pp. 602-610, 2005.

[286] A. Graves, A.-r. Mohamed, and G. Hinton, "Speech recognition with deep recurrent neural networks," 2013: IEEE, pp. 6645-6649.

[287] M. Schuster and K. K. Paliwal, "Bidirectional recurrent neural networks," *IEEE transactions on Signal Processing,* vol. 45, no. 11, pp. 2673-2681, 1997.

[288] J. Yin, Z. Deng, A. V. M. Ines, J. Wu, and E. Rasu, "Forecast of short-term daily reference evapotranspiration under limited meteorological variables using a hybrid bidirectional long short-term memory model (Bi-LSTM)," *Agricultural Water Management,* vol. 242, p. 106386, 2020.

[289] F. R. Alharbi and D. Csala, "Short-Term Solar Irradiance Forecasting Model Based on Bidirectional Long Short-Term Memory Deep Learning," 2021: IEEE, pp. 1-6.

[290] D. Justin, R. S. Concepcion, H. A. Calinao, J. Alejandrino, E. P. Dadios, and E. Sybingco, "Using Stacked Long Short-Term-Memory with Principal Component Analysis for Short Term Prediction of Solar Irradiance based on Weather Patterns," 2020: IEEE, pp. 946-951.

[291] T. Peng, C. Zhang, J. Zhou, and M. S. Nazir, "An integrated framework of Bidirectional Long Short Term Memory (Bi-LSTM) based on sine cosine algorithm for hourly solar radiation forecasting," *Energy,* vol. 221, p. 119887, 2021.

[292] N. Sodsong, K. M. Yu, and W. Ouyang, "Short-Term Solar PV Forecasting Using Gated Recurrent Unit with a Cascade Model," 2019: IEEE, pp. 292-297.

[293] Y. Wang, M. Liu, Z. Bao, and S. Zhang, "Short-term load forecasting with multi-source data using gated recurrent unit neural networks," *Energies,* vol. 11, no. 5, p. 1138, 2018.

[294] Y. Zhang and L. Yang, "A novel dynamic predictive method of water inrush from coal floor based on gated recurrent unit model," *Natural Hazards,* vol. 105, no. 2, pp. 2027-2043, 2021.

[295] J. Zheng, C. Xu, Z. Zhang, and X. Li, "Electric load forecasting in smart grids using long short-term-memory based recurrent neural network," 2017: IEEE, pp. 1-6.

[296] W. Kong, Z. Y. Dong, Y. Jia, D. J. Hill, Y. Xu, and Y. Zhang, "Short-term residential load forecasting based on LSTM recurrent neural network," *IEEE Transactions on Smart Grid,* vol. 10, no. 1, pp. 841-851, 2017.

[297] K. Cho, B. v. Merrienboer, C. Gulcehre, D. Bahdanau, F. Bougares, H. Schwenk, and Y. Bengio,"Learning phrase representations using RNN encoder-decoder for statistical machine translation," *arXiv preprint arXiv:1406.1078,* 2014.

[298] Y.-D. Syu, J.-C. Wang, C.-Y. Chou, M.-J. Lin, W.-C. Liang, L.-C. Wu, and J.-A. Jiang, "Ultra-Short-Term Wind Speed Forecasting for Wind Power Based on Gated Recurrent Unit," 2020: IEEE, pp. 1-4.

[299] R. Zhao, D. Wang, R. Yan, K. Mao, F. Shen, and J. Wang, "Machine health monitoring using local feature-based gated recurrent unit networks," *IEEE Transactions on Industrial Electronics,* vol. 65, no. 2, pp. 1539-1548, 2017.

[300] Z. Zhang, X. Pan, T. Jiang, B. Sui, C. Liu, and W. Sun, "Monthly and quarterly sea surface temperature prediction based on gated recurrent unit neural network," *Journal of Marine Science and Engineering,* vol. 8, no. 4, p. 249, 2020.

[301] Y. Wang, W. Liao, and Y. Chang, "Gated recurrent unit network-based short-term photovoltaic forecasting," *Energies,* vol. 11, no. 8, p. 2163, 2018.

[302] X.-B. Jin, N.-X. Yang, X.-Y. Wang, Y.-T. Bai, T.-L. Su, and J.-L. Kong, "Hybrid deep learning predictor for smart agriculture sensing based on empirical mode decomposition and gated recurrent unit group model," *Sensors,* vol. 20, no. 5, p. 1334, 2020.

[303] S. Jeong, I. Park, H. S. Kim, C. H. Song, and H. K. Kim, "Temperature Prediction Based on Bidirectional Long Short-Term Memory and Convolutional Neural Network Combining Observed and Numerical Forecast Data," *Sensors,* vol. 21, no. 3, p. 941, 2021.

Appendices

A.1 Appendix 1 – GCC Countries Future Scenario Using MCS and BM Prediction Model

A.1.1 Fossil Fuel Prediction for Oman Using Monte Carlo Simulation and Brownian Motion Model

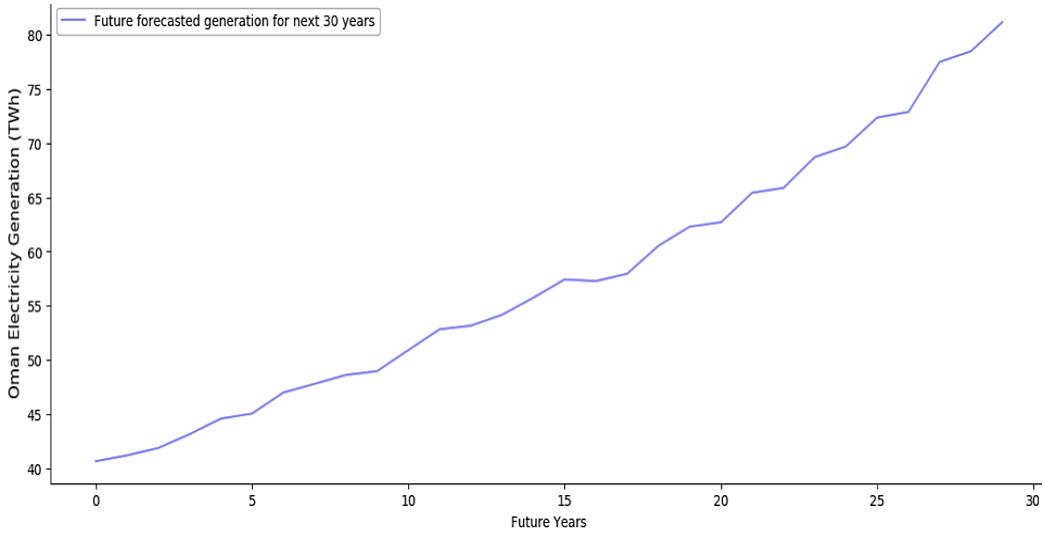

(a)

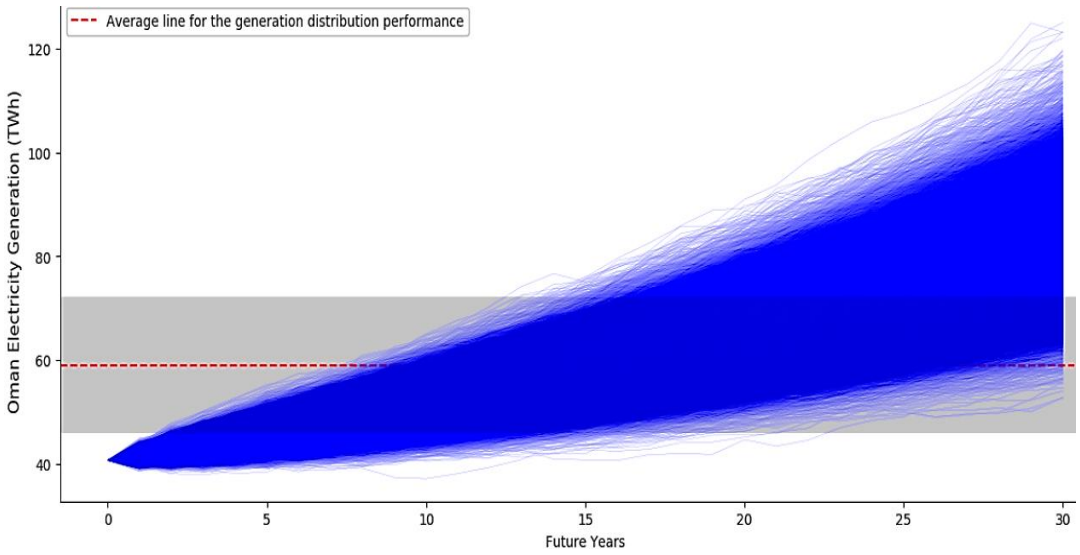

(b)

Figure A.1-1. (a) Randomly selected sample predicted electricity generation values for 30-year period from 2021 to 2050 for Oman and (b) Future electricity generation distribution performance, as predicted by MCS and BM.

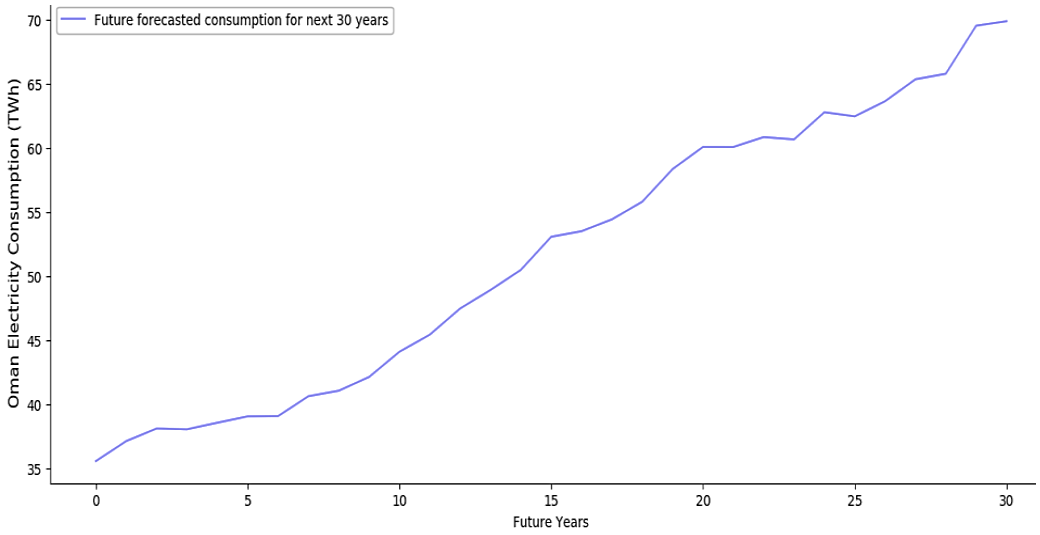

(a)

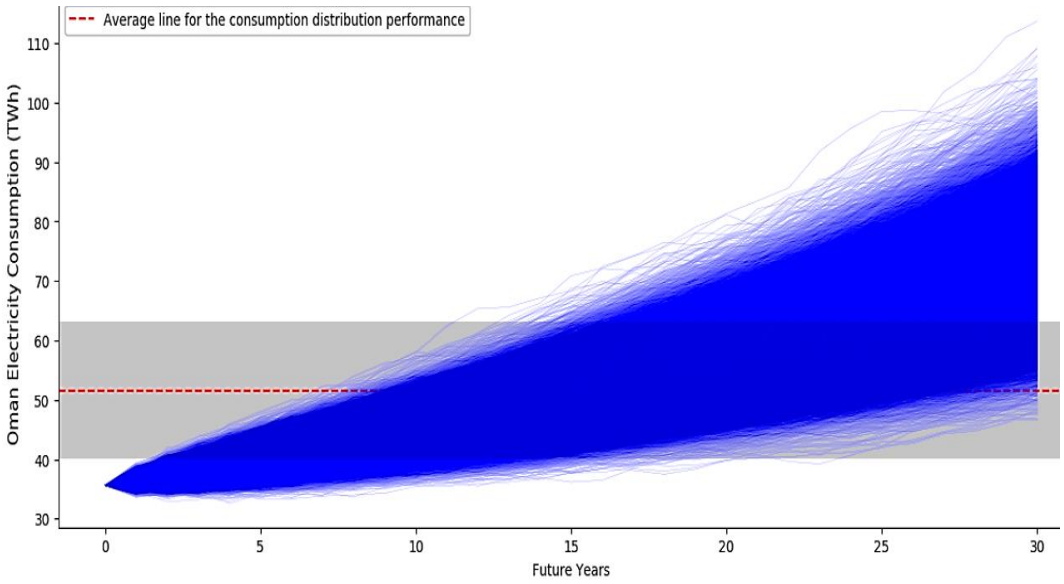

(b)

Figure A.1-2. (a) Randomly selected sample predicted electricity consumption values for 30-year period from 2021 to 2050 for Oman and (b) electricity consumption distribution performance, as predicted by MCS and BM.

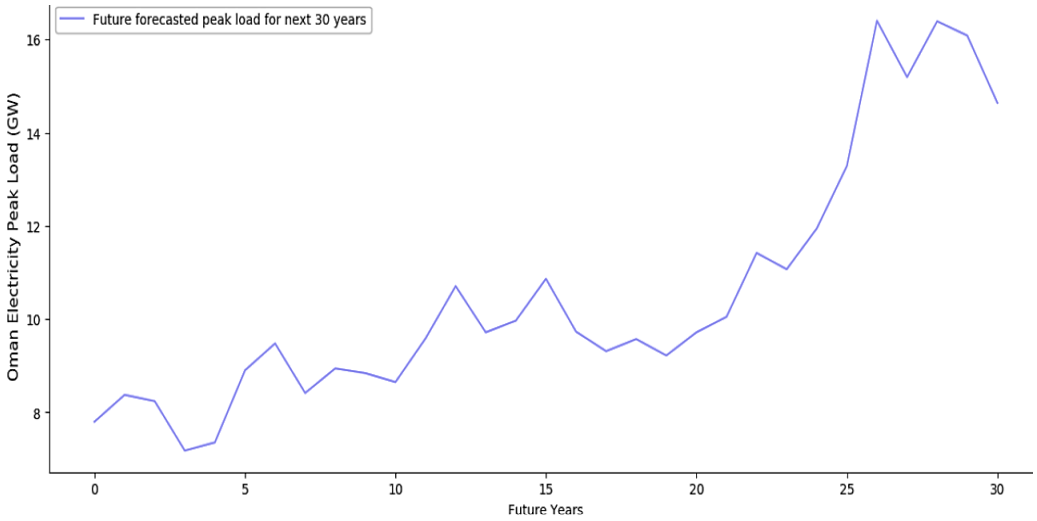

(a)

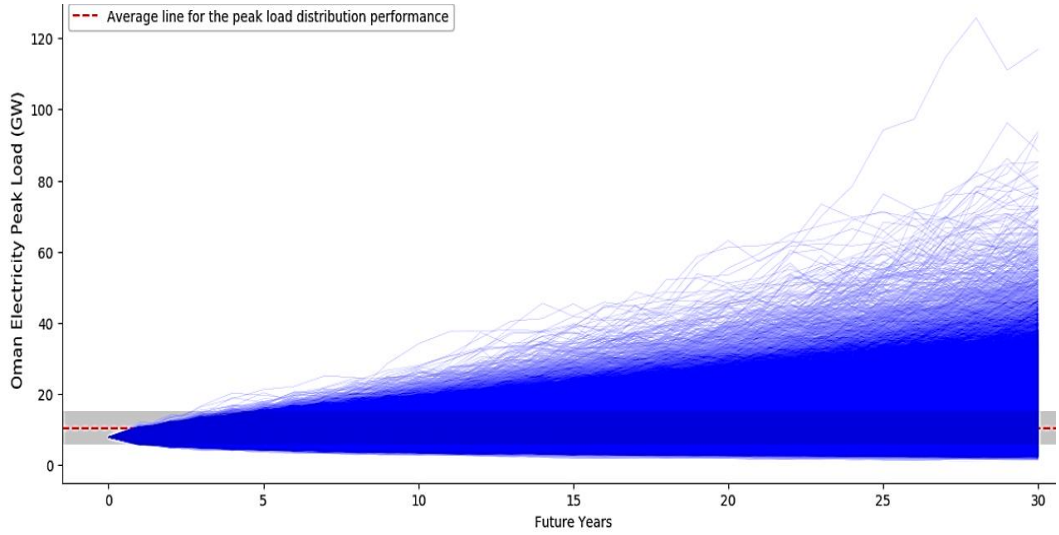

(b)

Figure A.1-3. (a) Randomly selected sample predicted electricity peak load values for 30-year period from 2021 to 2050 for Oman and (b) electricity peak load distribution performance, as predicted by MCS and BM.

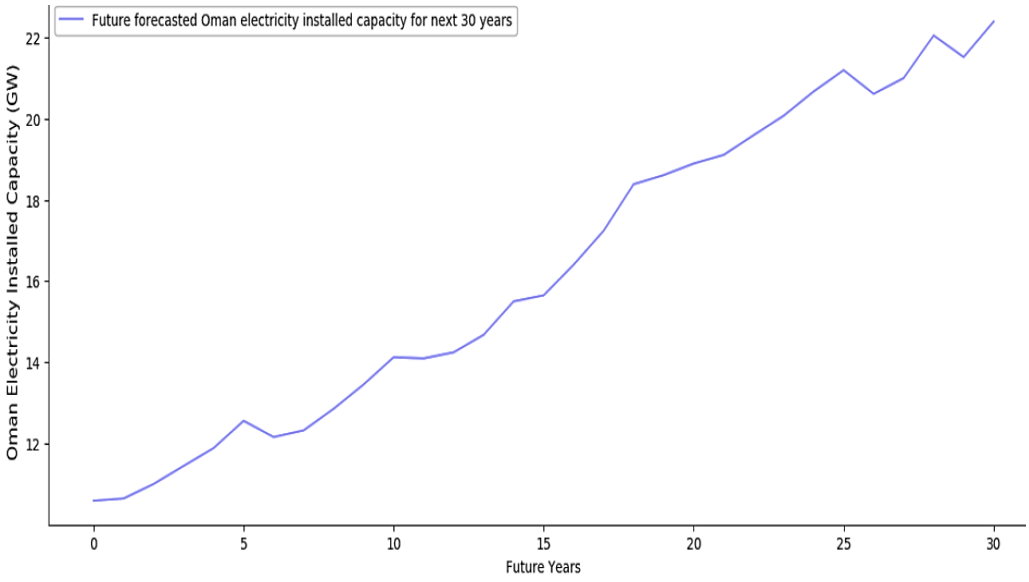

(a)

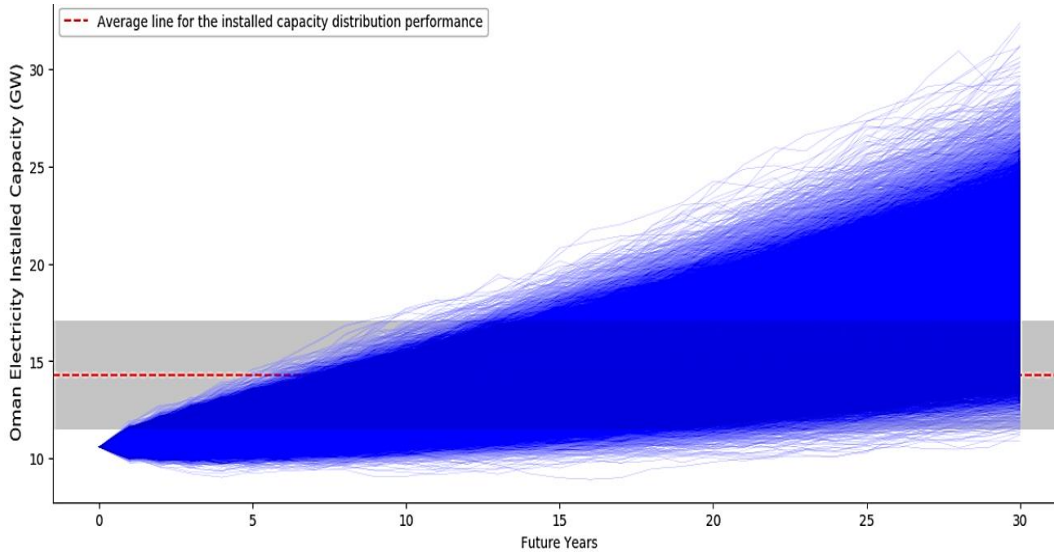

(b)

Figure A.1-4. (a) Randomly selected sample predicted electricity installed capacity values for 30-year period from 2021 to 2050 for Oman and (b) electricity installed capacity distribution performance, as predicted by MCS and BM.

A.1.1.1 Solar Irradiance, Wind speed and Temperature Prediction for Oman Using Monte Carlo Simulation and Brownian Motion Model

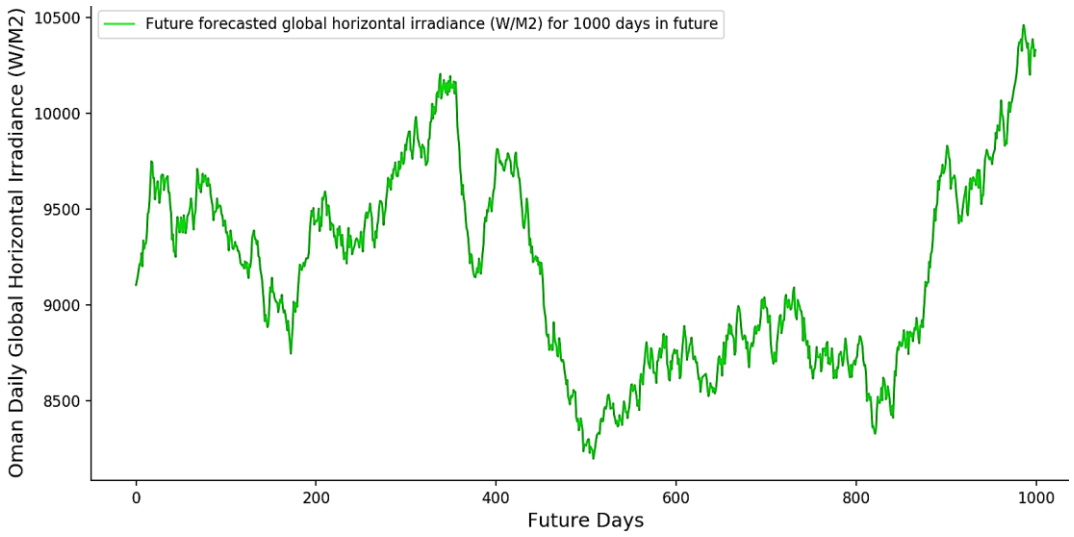

(a)

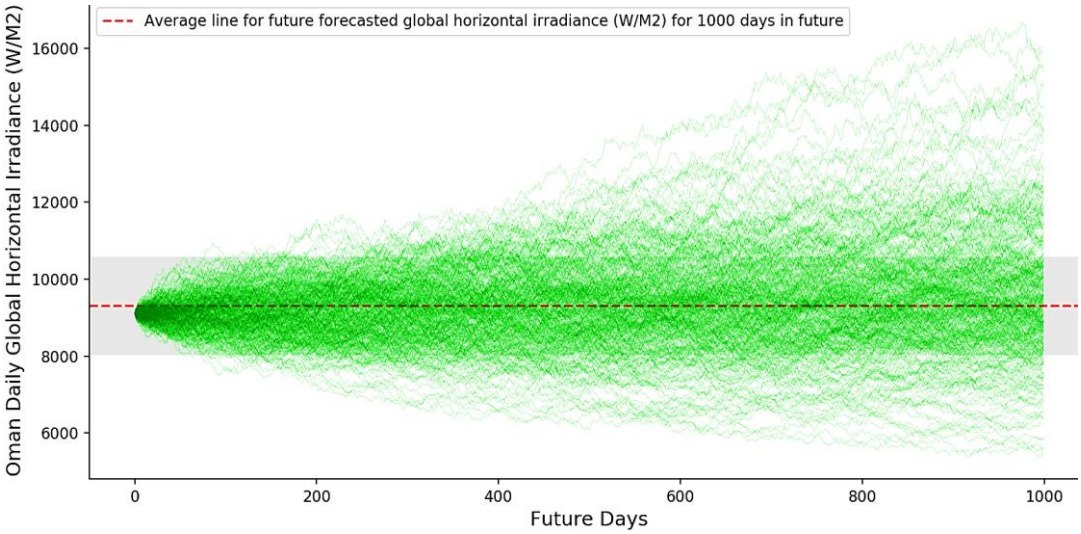

(b)

Figure A.1-5. (a) Randomly selected sample predicted solar GHI values for 1000-days in future for Oman and (b) forecast solar GHI distribution performance, as predicted by MCS and BM.

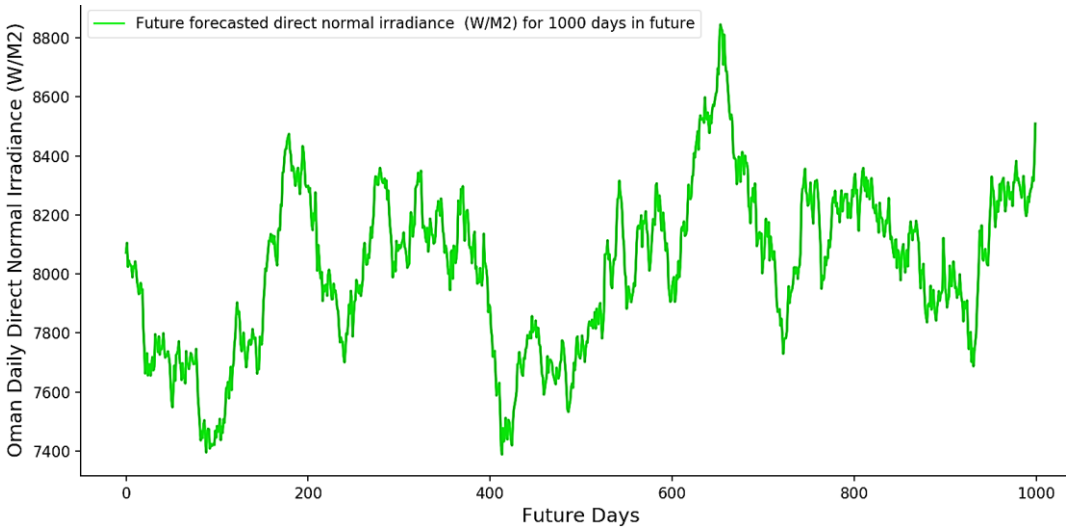

(a)

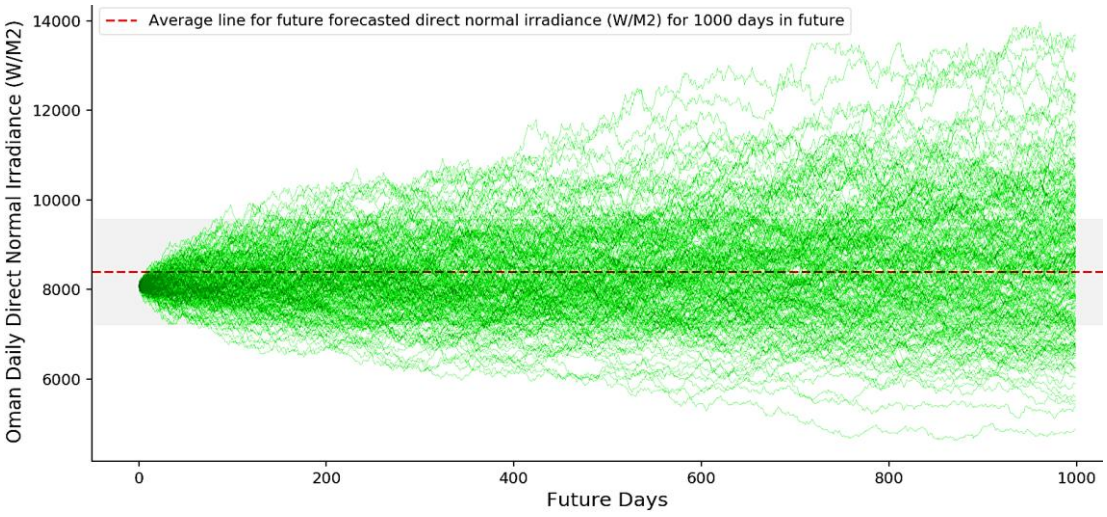

(b)

Figure A.1-6. (a) Randomly selected sample predicted solar direct irradiance (DNI) values for 1000-days in future for Oman and (b) The predicted solar DNI distribution performance, as predicted by MCS and Brownian (BM).

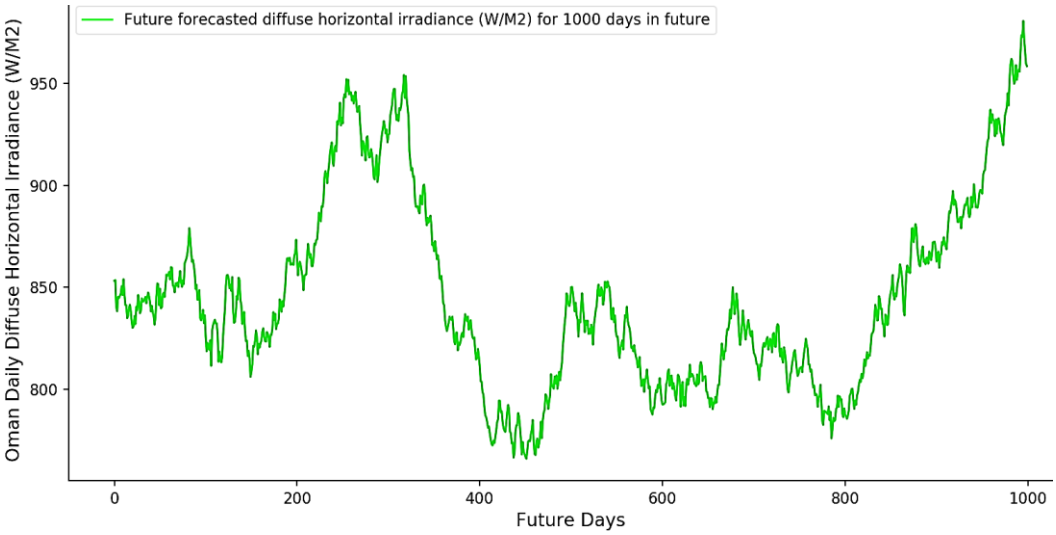

(a)

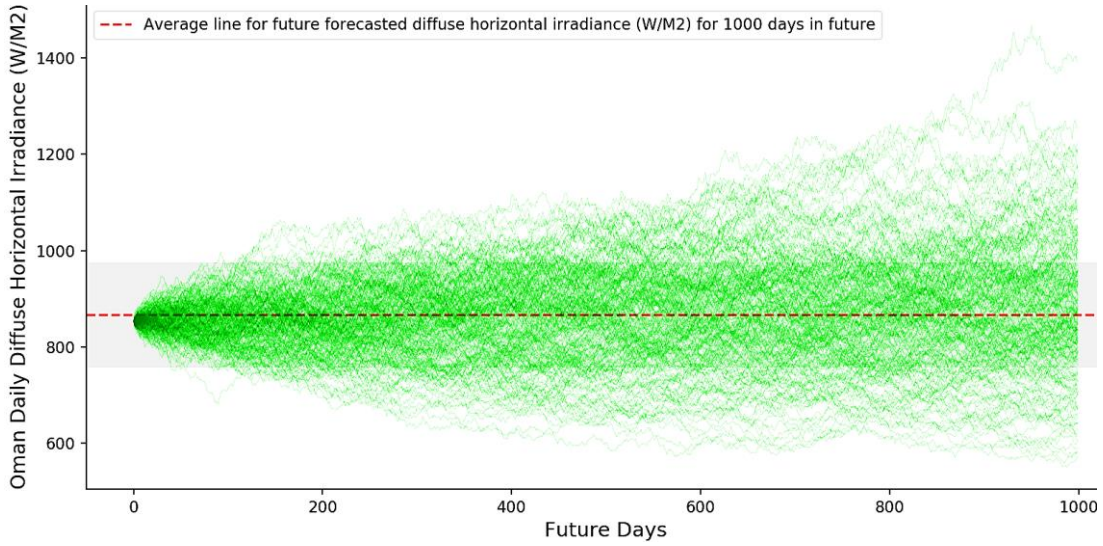

(b)

Figure A.1-7. (a) Randomly selected sample predicted solar DHI values for 1000-days in future for Oman and (b) The predicted solar DHI distribution performance, as predicted by MCS and Brownian (BM).

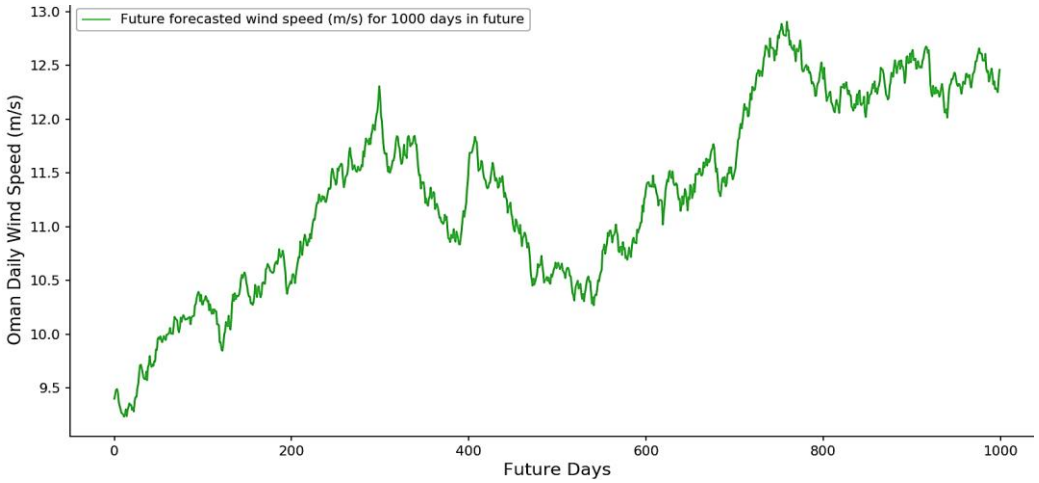

(a)

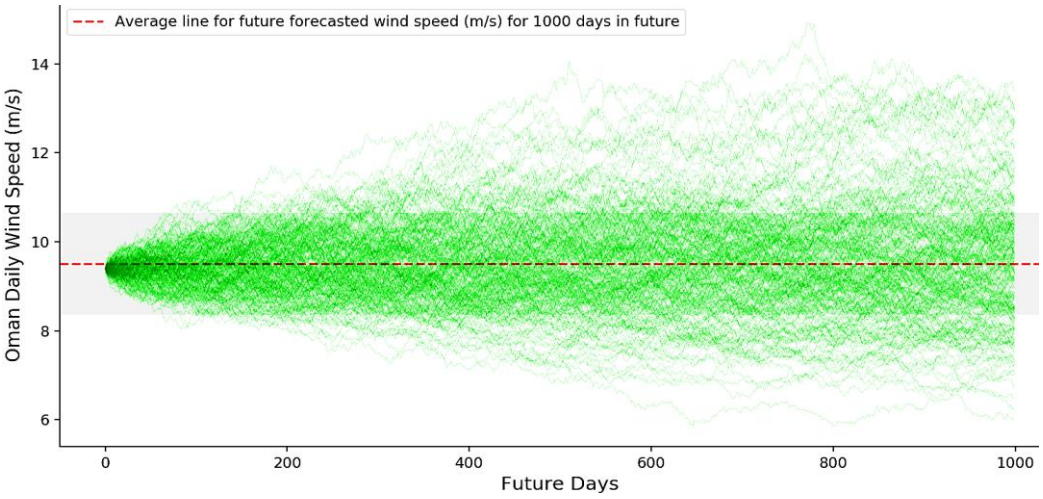

(b)

Figure A.1-8. (a) Randomly selected sample predicted wind speed values for 1000-days in future for Oman and (b) The predicted wind speed distribution performance, as predicted by MCS and Brownian (BM).

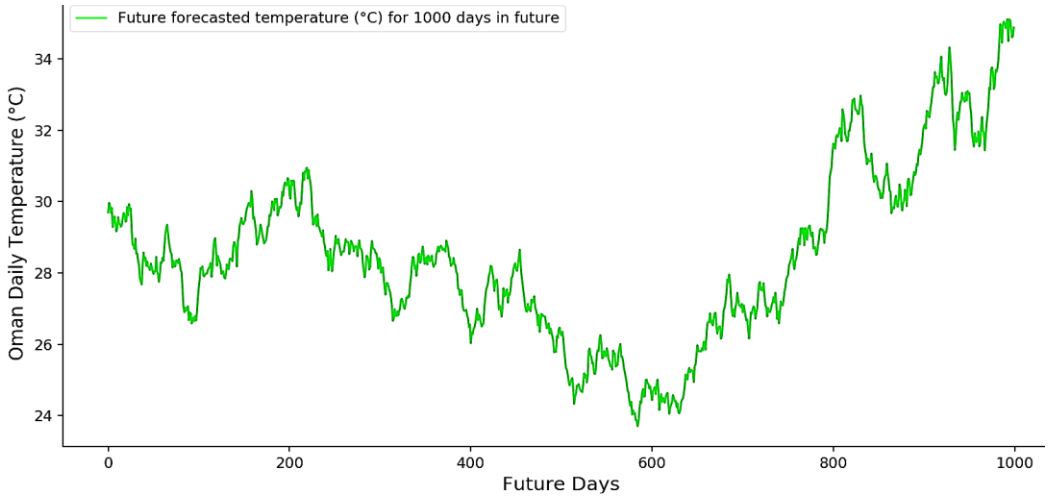

(a)

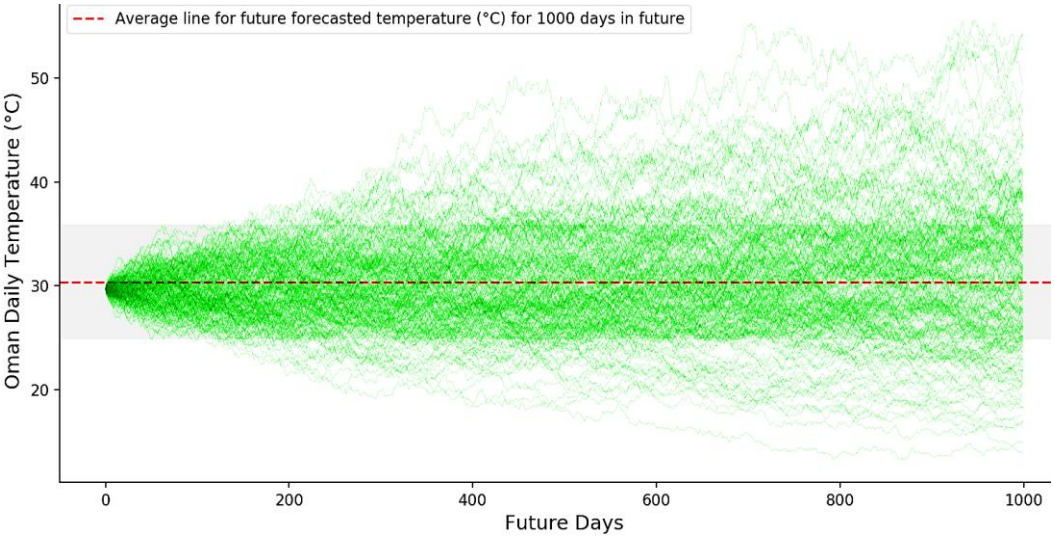

(b)

Figure A.1-9. (a) Randomly selected sample predicted temperature values for 1000-days in future for Oman and (b) The predicted temperature distribution performance, as predicted by MCS and Brownian (BM).

A.1.2 Fossil Fuel Prediction for UAE Using Monte Carlo Simulation and Brownian Motion Model

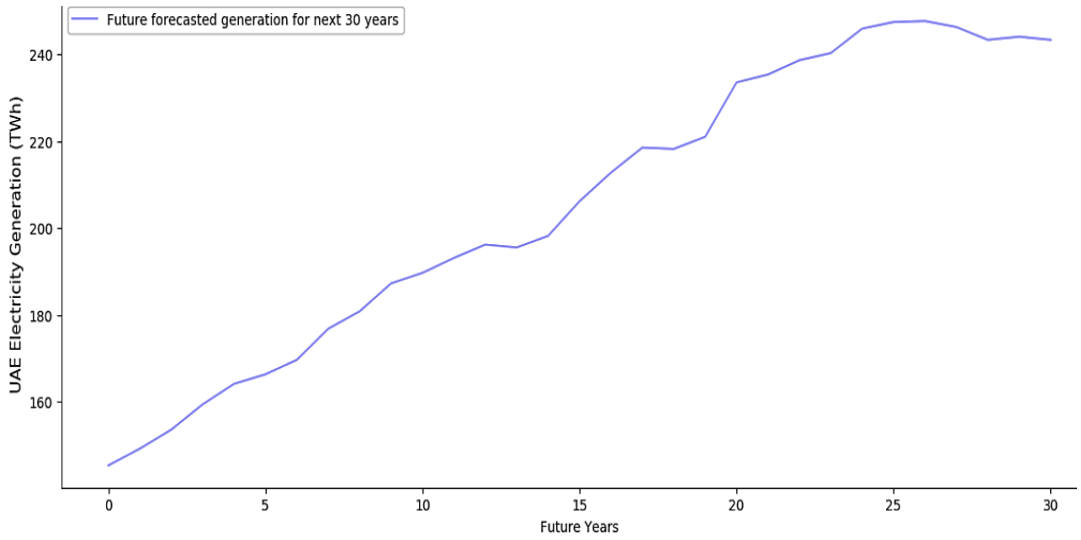

(a)

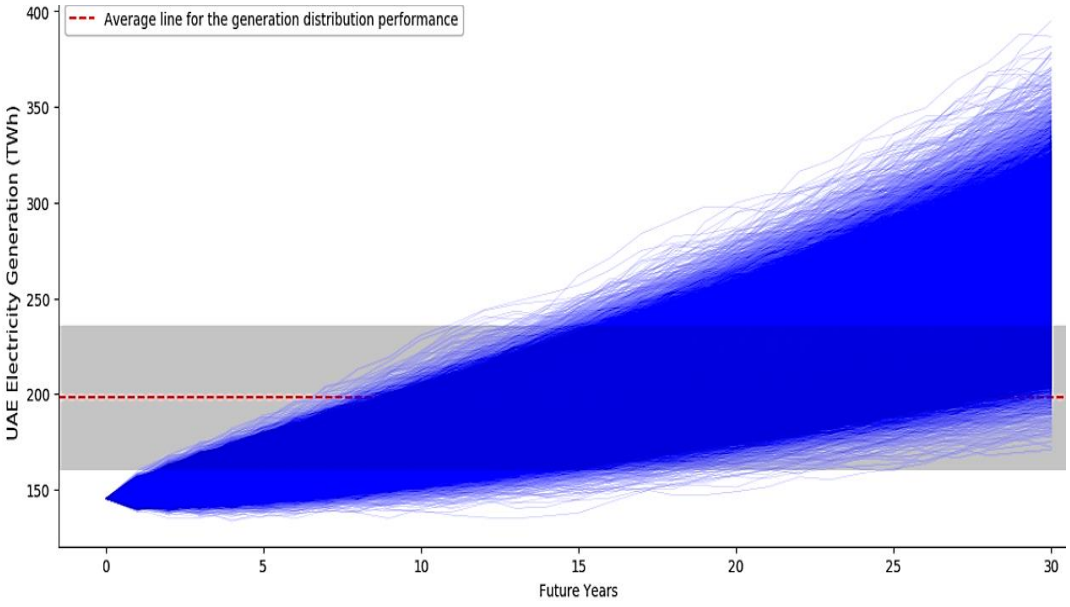

(b)

Figure A.1-10. (a) Randomly selected sample predicted electricity generation values for 30-year period from 2021 to 2050 for UAE and (b) The predicted electricity generation distributions performance, as predicted by MCS and BM.

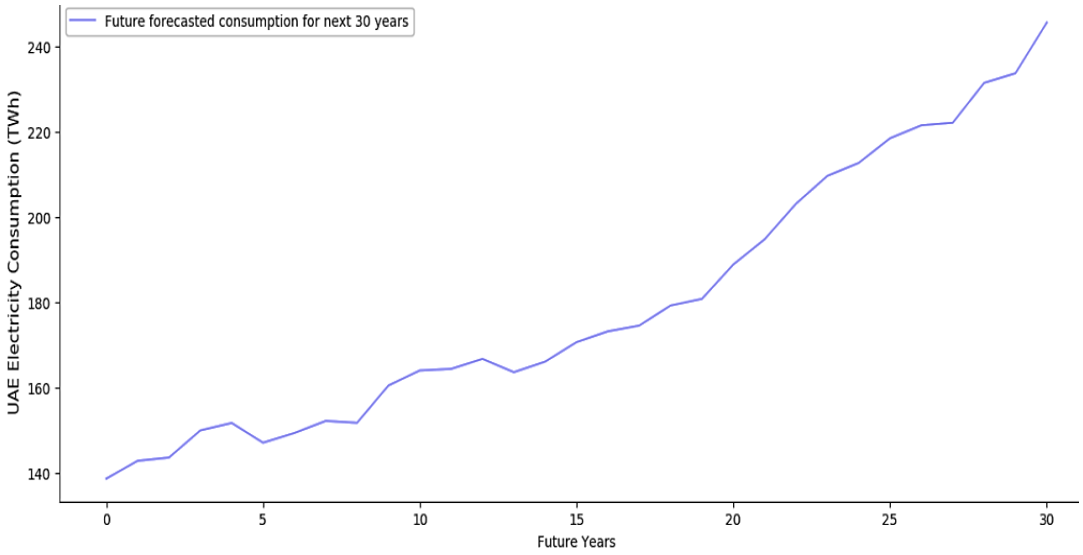

(a)

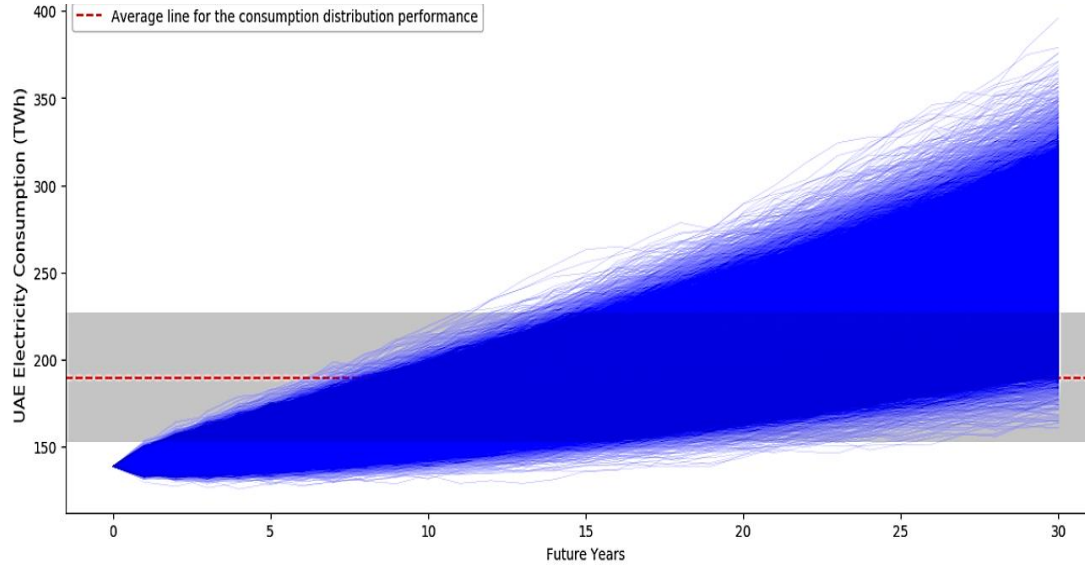

(b)

Figure A.1-11. (a) Randomly selected sample predicted electricity consumption values for 30-year period from 2021 to 2050 for UAE and (b) The predicted electricity consumption distributions performance, as predicted by MCS and BM.

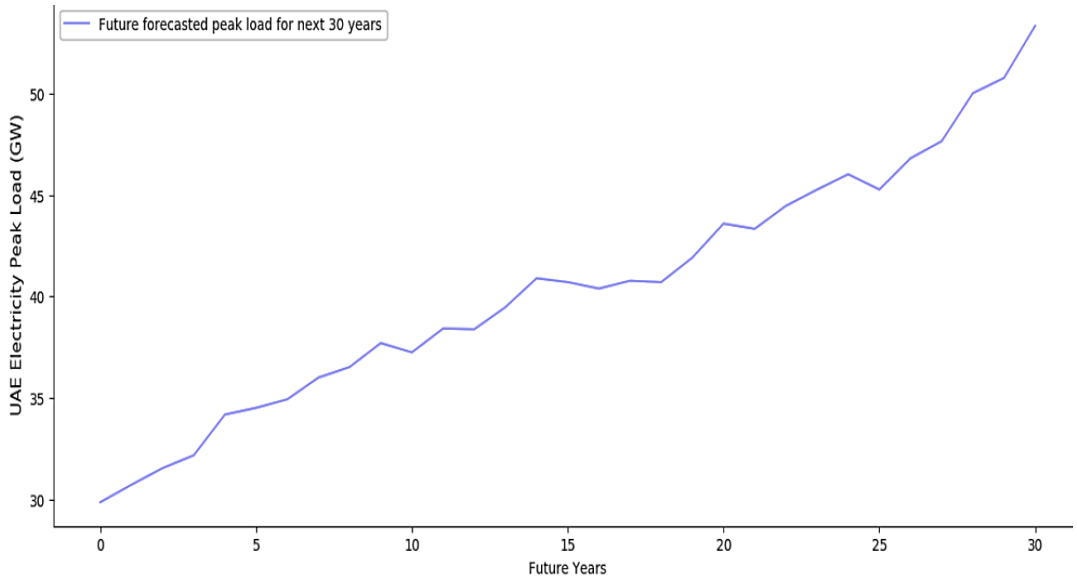

(a)

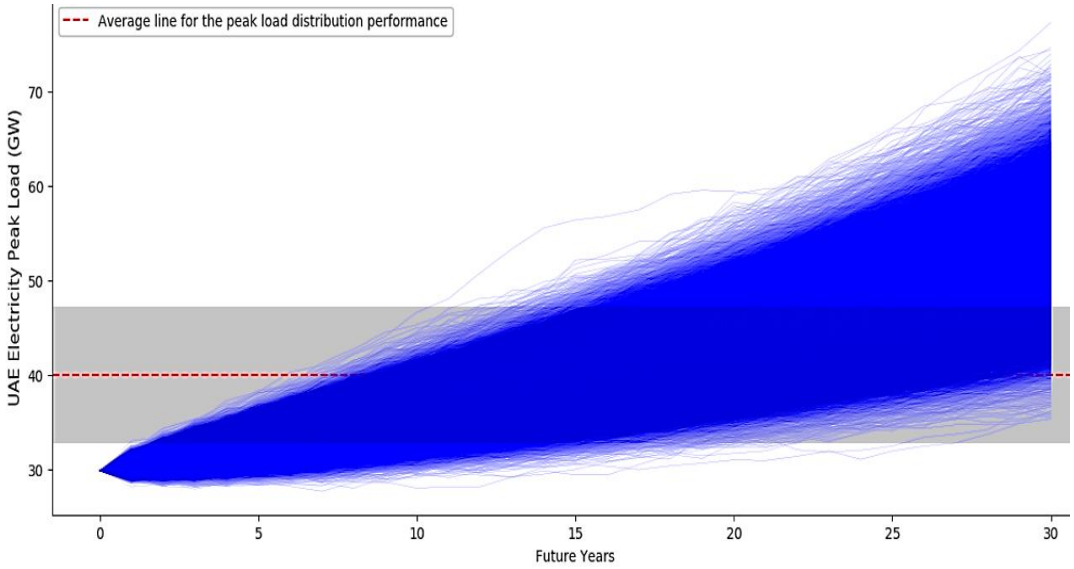

(b)

Figure A.1-12. (a) Randomly selected sample predicted electricity peak load values for 30-year period from 2021 to 2050 for UAE and (b) The predicted electricity peak load distributions performance, as predicted by MCS and BM.

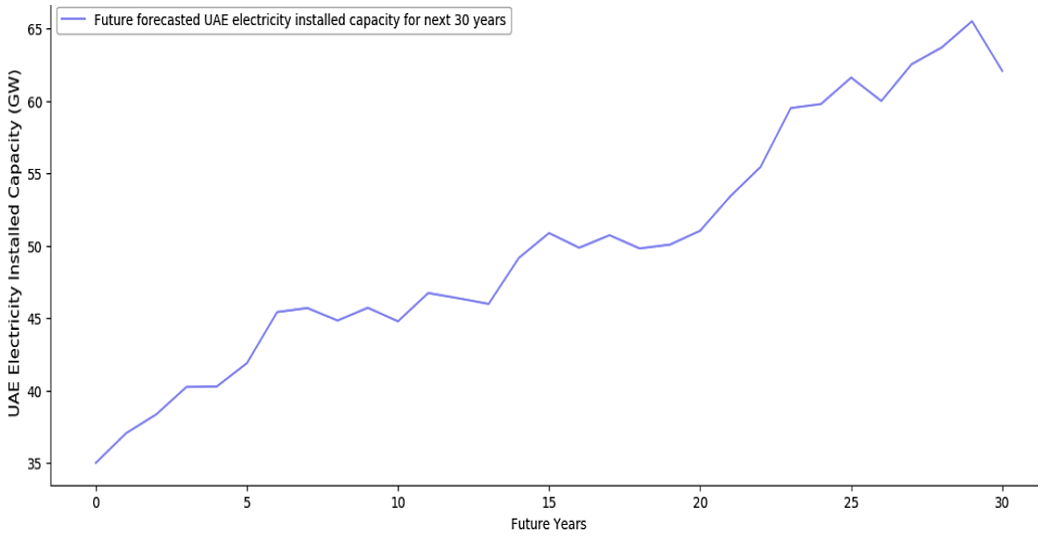

(a)

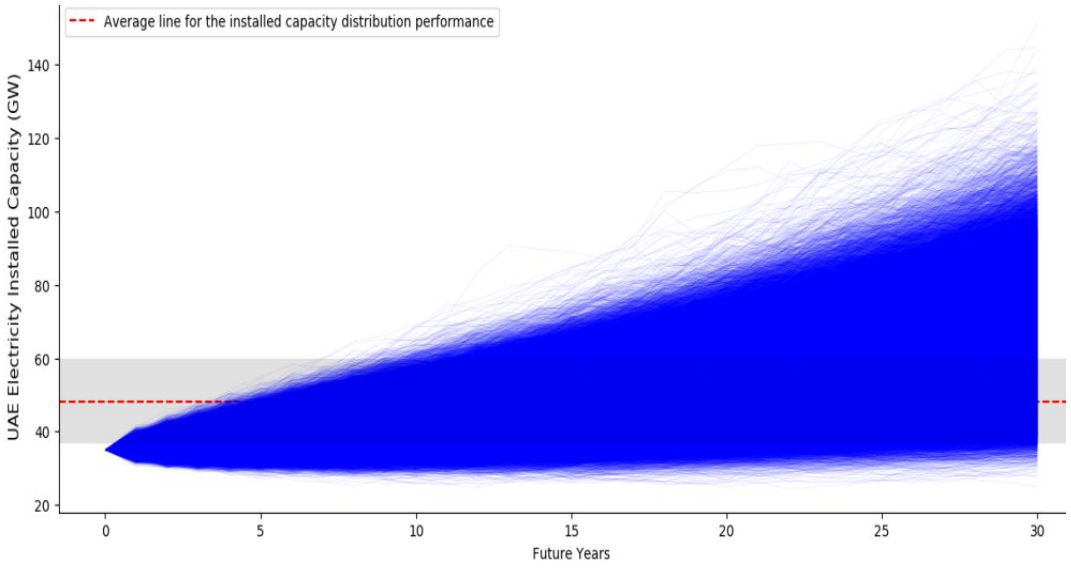

(b)

Figure A.1-13. (a) Randomly selected sample predicted electricity installed capacity values for 30-year period from 2021 to 2050 for UAE and (b) The predicted electricity installed capacity distributions performance, as predicted by MCS and BM.

A.1.2.1 Solar Irradiance, Wind speed and Temperature Prediction for UAE Using Monte Carlo Simulation and Brownian Motion Model

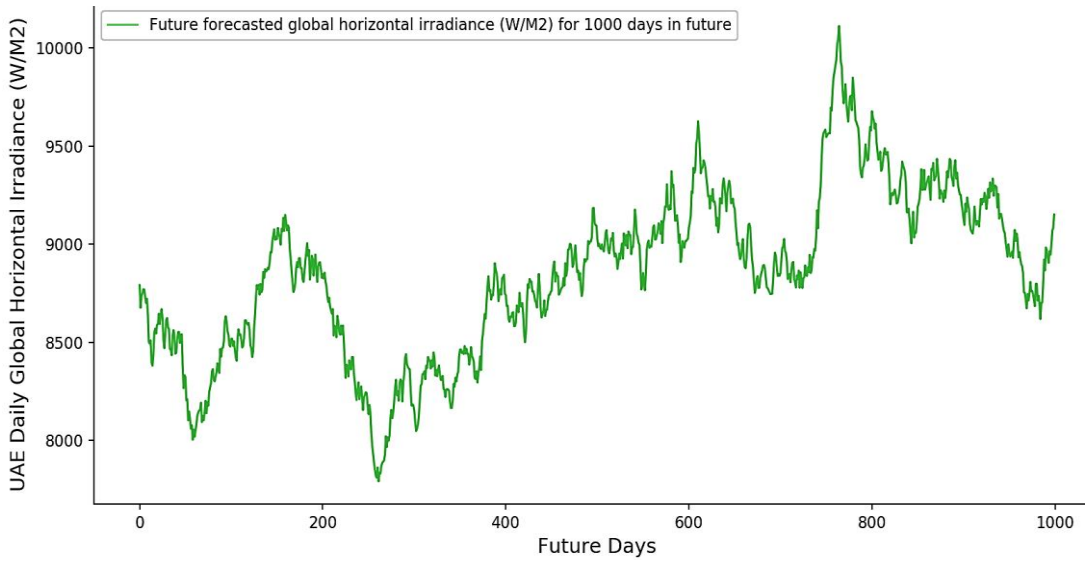

(a)

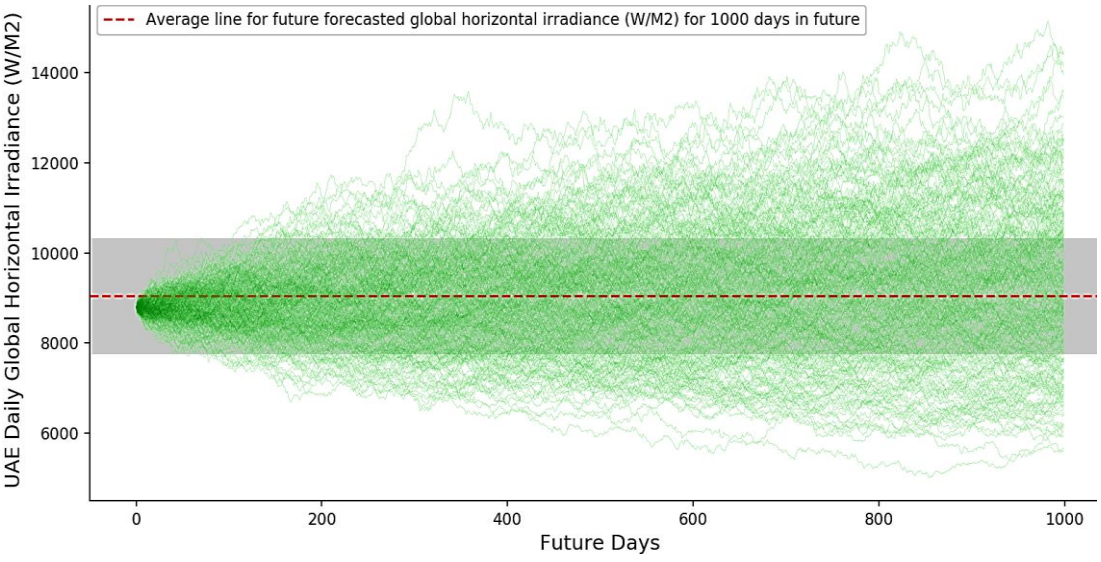

(b)

Figure A.1-14. (a) Randomly selected sample predicted solar GHI values for 1000-days in future for UAE and (b) The predicted solar GHI distribution performance, as predicted by MCS and Brownian (BM).

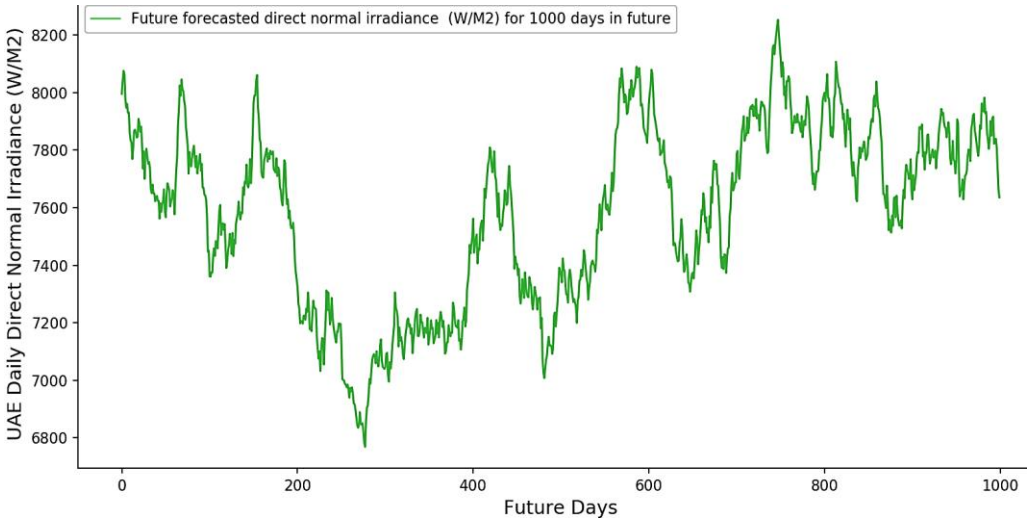

(a)

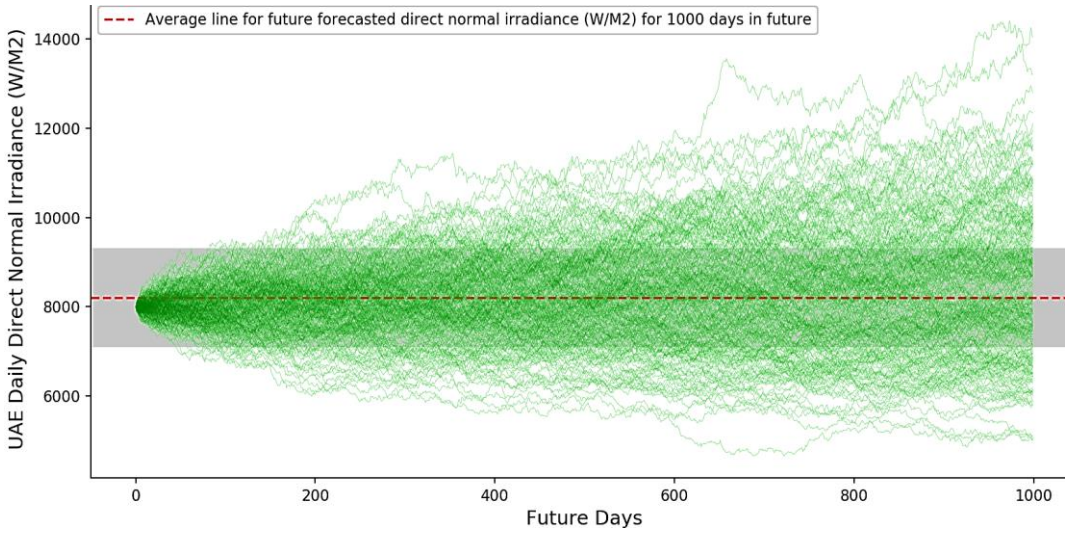

(b)

Figure A.1-15. (a) Randomly selected sample predicted solar direct irradiance (DNI) values for 1000-days in future for UAE and (b) The predicted solar DNI distribution performance, as predicted by MCS and Brownian (BM).

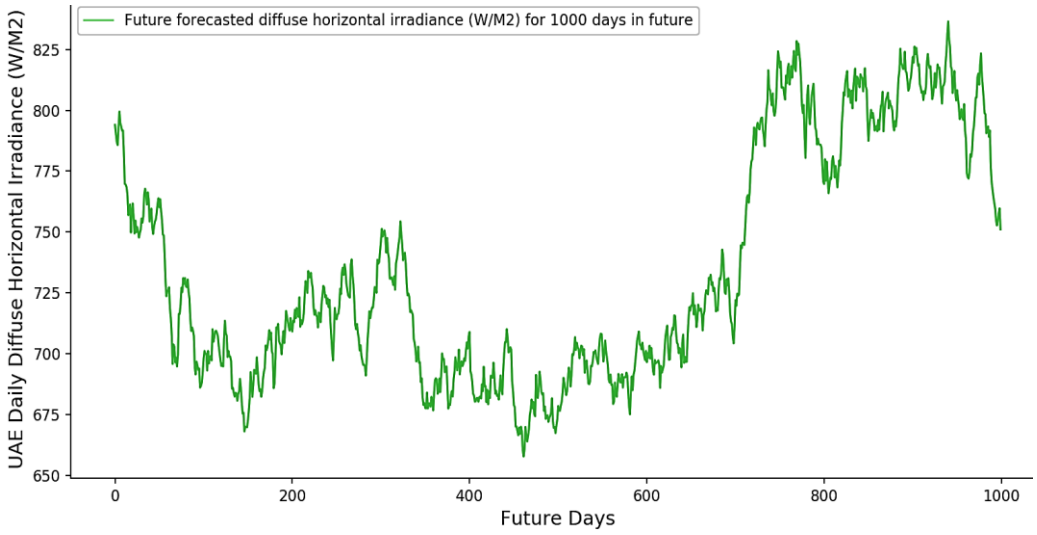

(a)

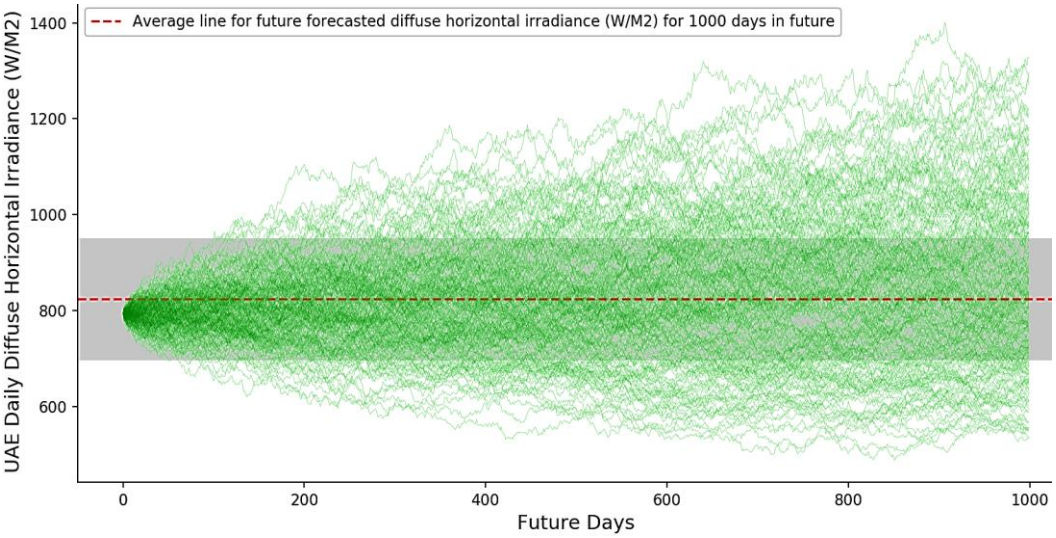

(b)

Figure A.1-16. (a) Randomly selected sample predicted solar DHI values for 1000-days in future for UAE and (b) The predicted solar DHI distribution performance, as predicted by MCS and Brownian (BM).

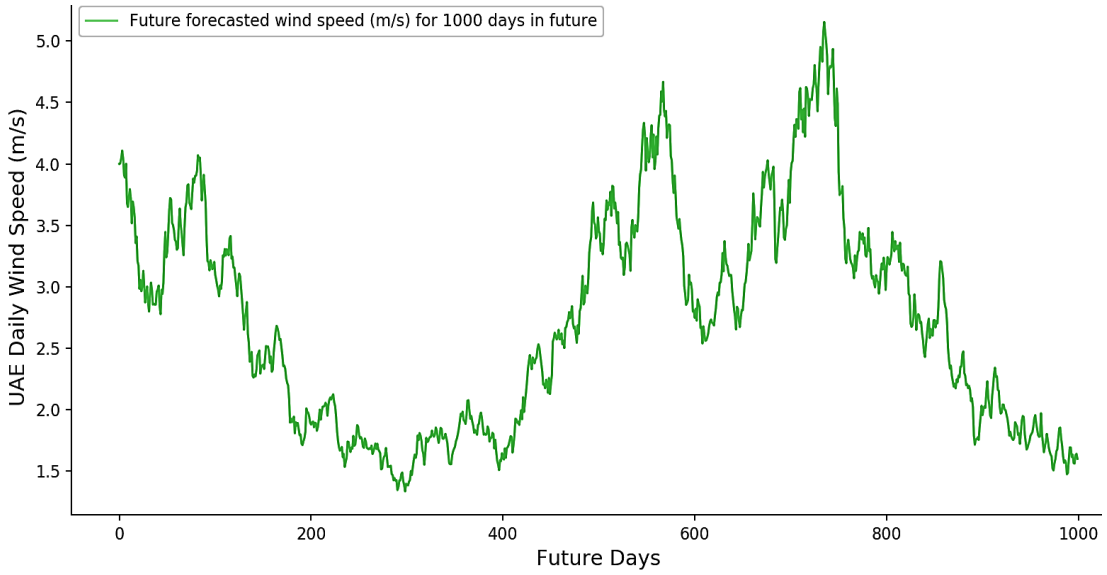

(a)

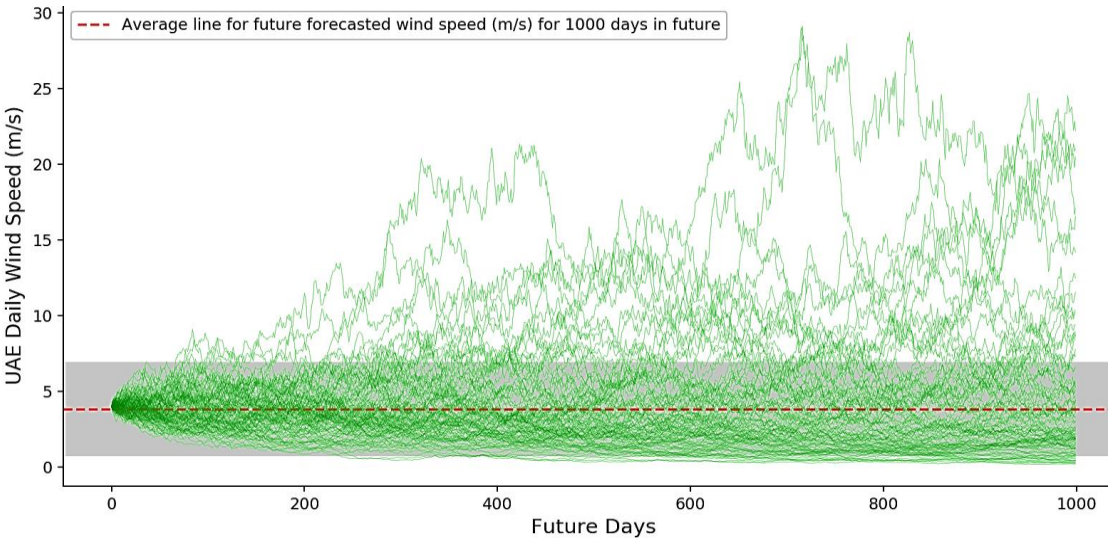

(b)

Figure A.1-17. (a) Randomly selected sample predicted wind speed values for 1000-days in future for Oman and (b) The predicted wind speed distribution performance, as predicted by MCS and Brownian (BM).

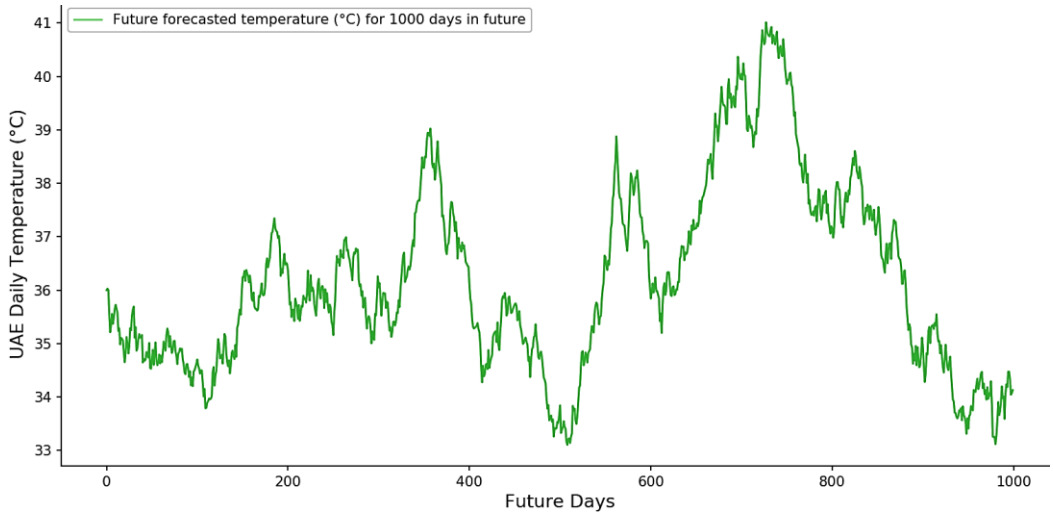

(a)

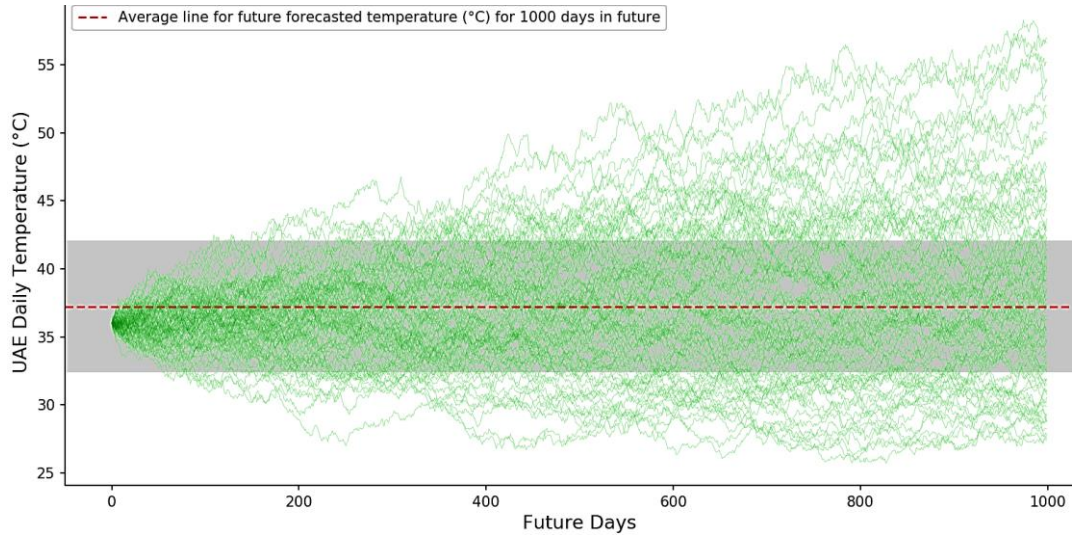

(b)

Figure A.1-18. (a) Randomly selected sample predicted temperature values for 1000-days in future for UAE and (b) The predicted temperature distribution performance, as predicted by MCS and Brownian (BM).

A.1.3 Fossil Fuel Prediction for Kuwait Using Monte Carlo Simulation and Brownian Motion Model

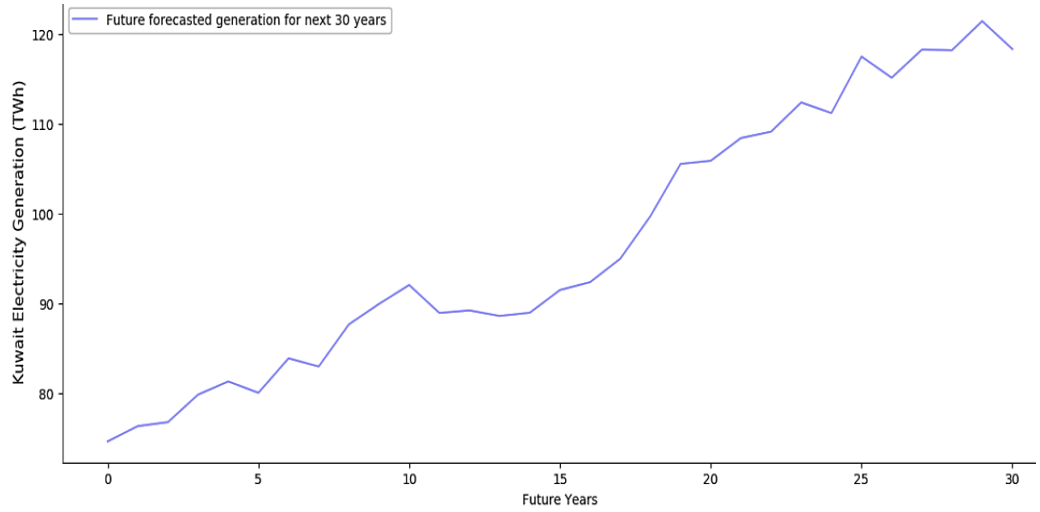

(a)

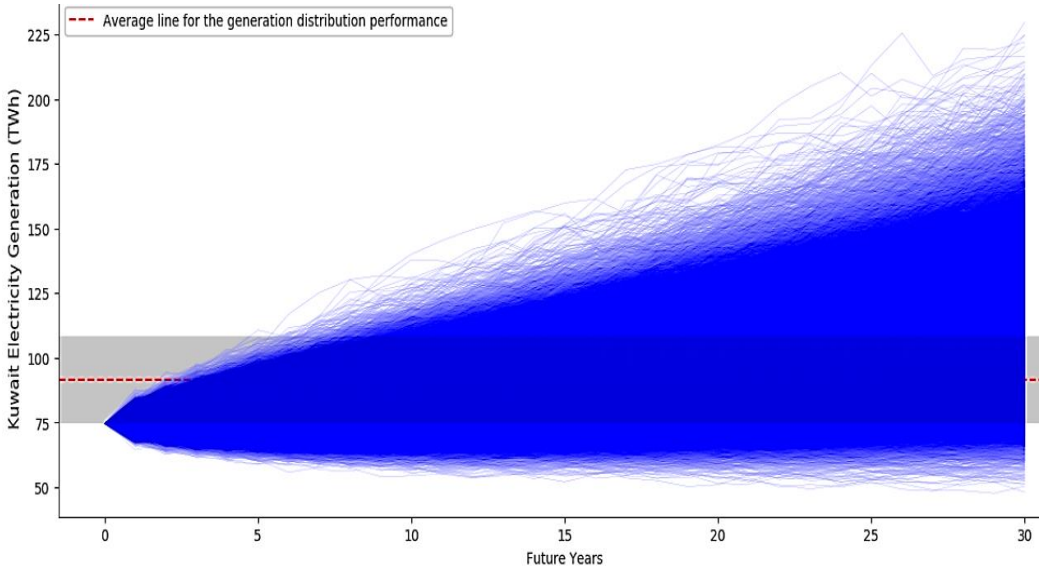

(b)

Figure A.1-19. (a) Randomly selected sample predicted electricity generation values for 30-year period from 2021 to 2050 for Kuwait and (b) The predicted electricity generation distributions performance, as predicted by MCS and BM.

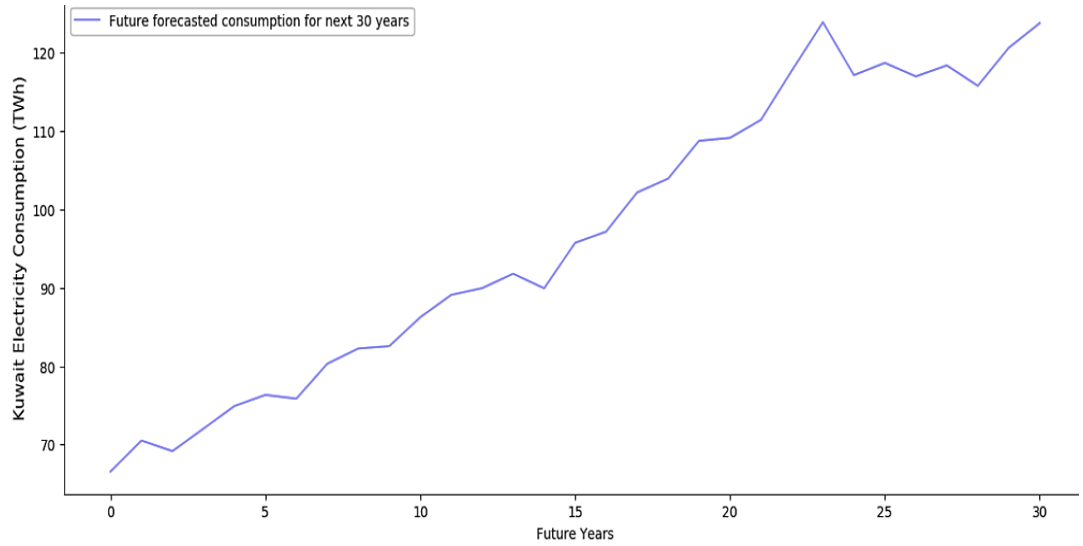

(a)

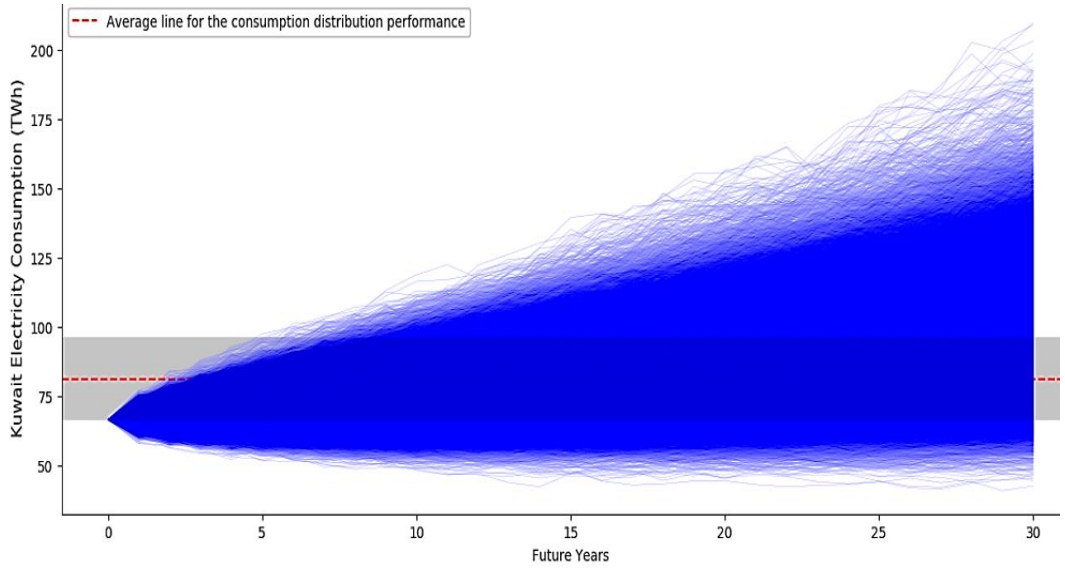

(b)

Figure A.1-20. (a) Randomly selected sample predicted electricity consumption values for 30-year period from 2021 to 2050 for Kuwait and (b) The predicted electricity consumption distributions performance, as predicted by MCS and BM.

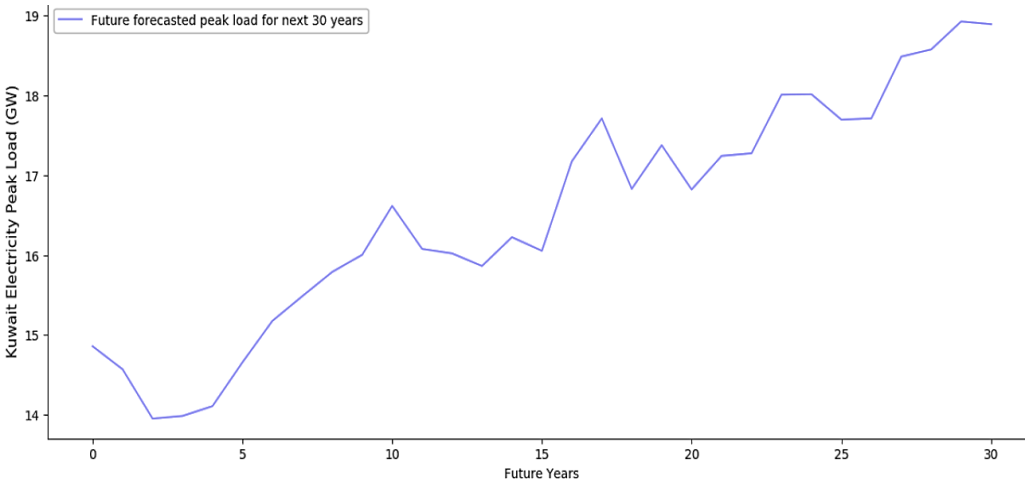

(a)

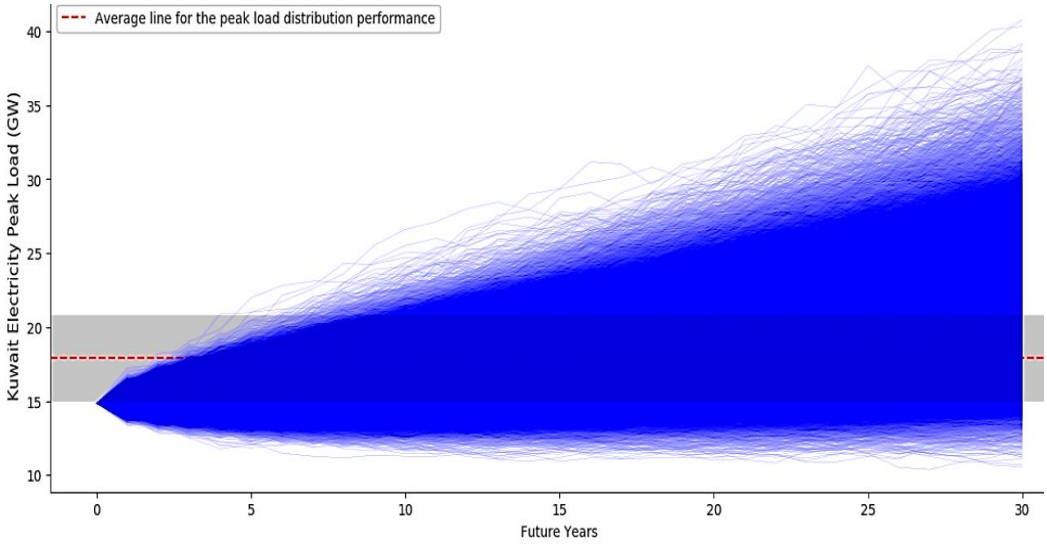

(b)

Figure A.1-21. (a) Randomly selected sample predicted electricity peak load values for 30-year period from 2021 to 2050 for Kuwait and (b) The predicted electricity peak load distributions performance, as predicted by MCS and BM.

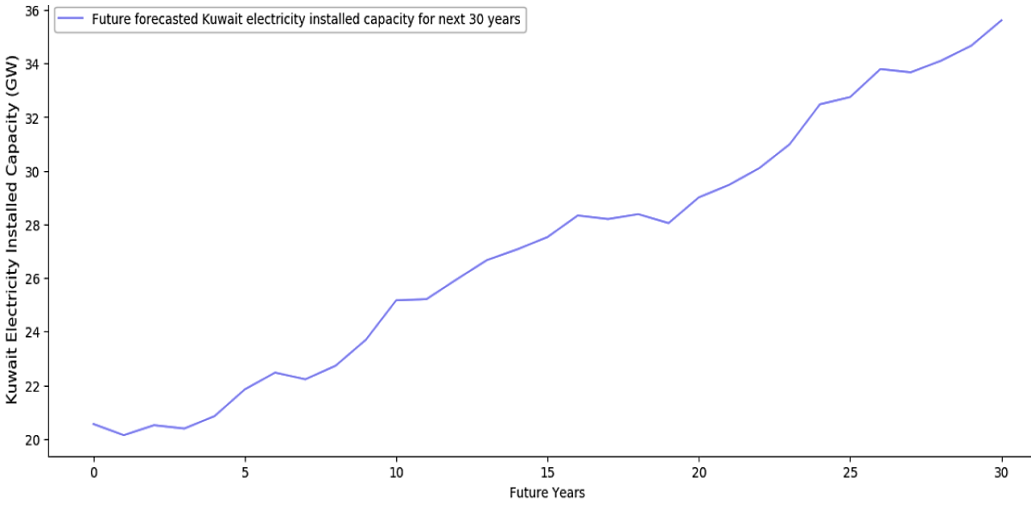

(a)

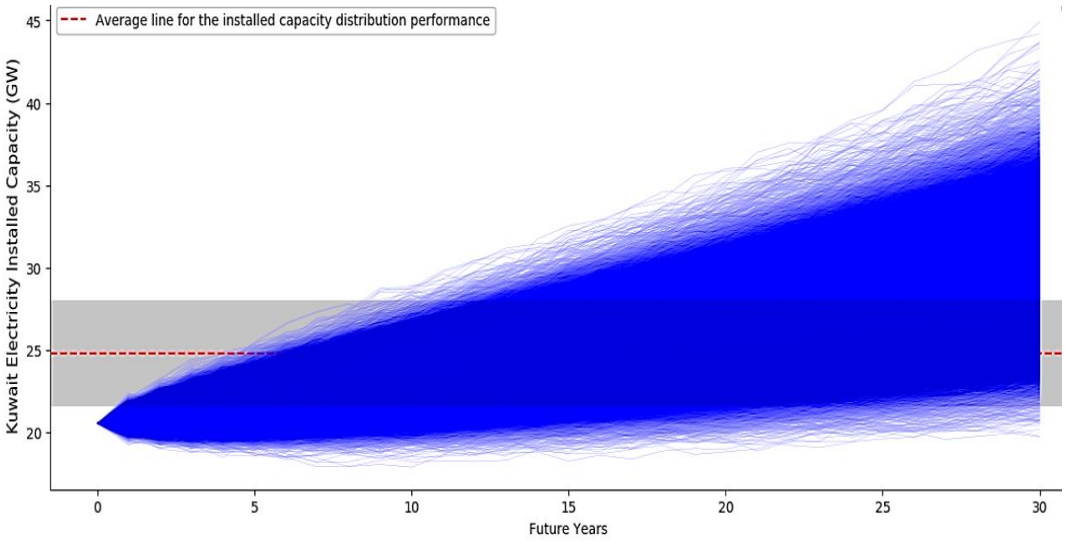

(b)

Figure A.1-22. (a) Randomly selected sample predicted electricity installed capacity values for 30-year period from 2021 to 2050 for Kuwait and (b) The predicted electricity installed capacity distributions performance, as predicted by MCS and BM.

A.1.3.1 Solar Irradiance, Wind speed and Temperature Prediction for Kuwait Using Monte Carlo Simulation and Brownian Motion Model

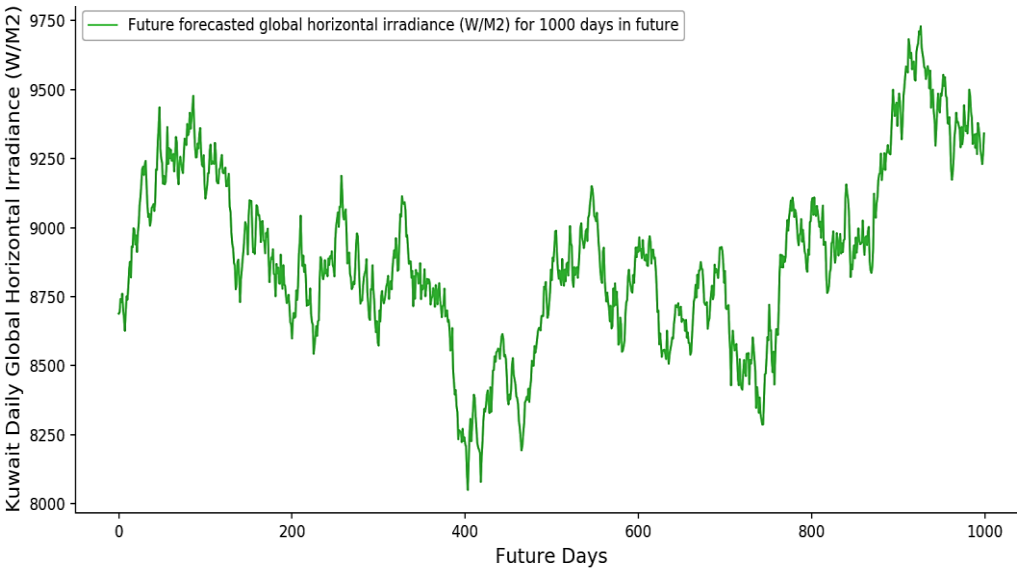

(a)

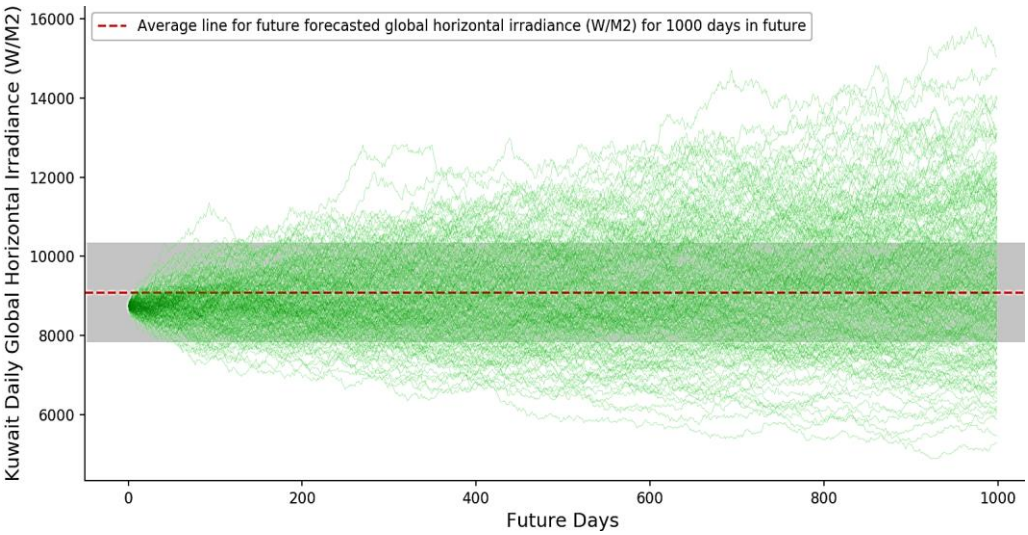

(b)

Figure A.1-23. (a) Randomly selected sample predicted solar GHI values for 1000-days in future for Kuwait and (b) The predicted solar GHI distribution performance, as predicted by MCS and Brownian (BM).

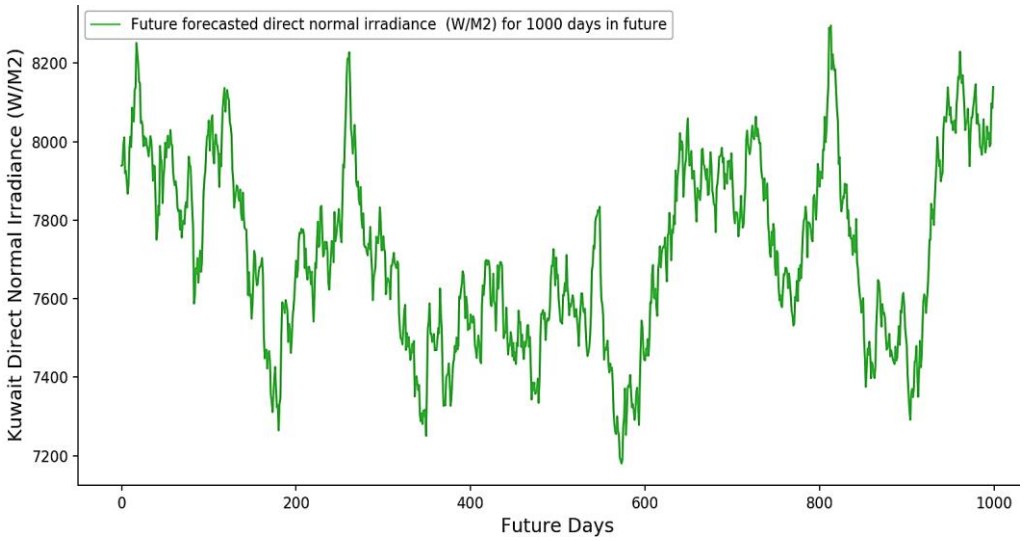

(a)

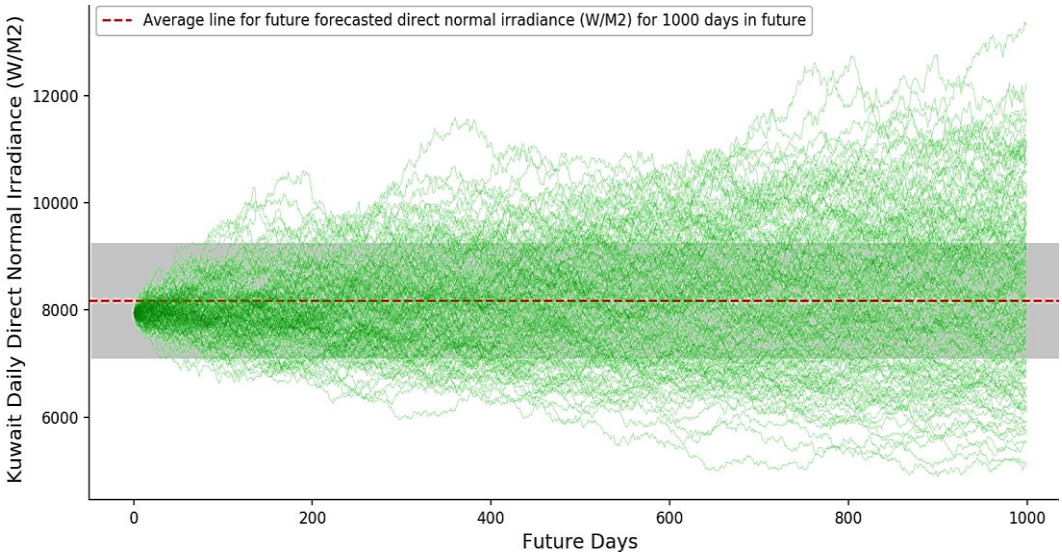

(b)

Figure A.1-24. (a) Randomly selected sample predicted solar direct irradiance (DNI) values for 1000-days in future for Kuwait and (b) The predicted solar DNI distribution performance, as predicted by MCS and Brownian (BM).

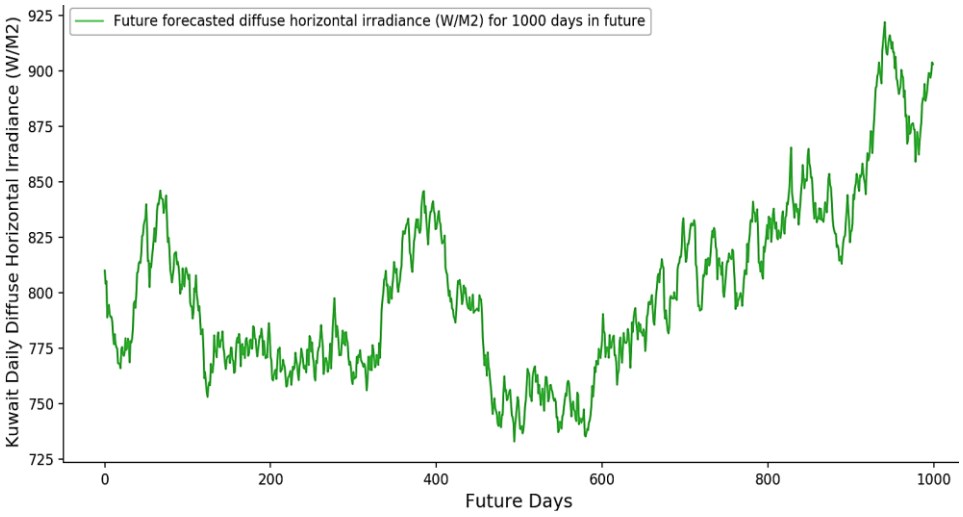

(a)

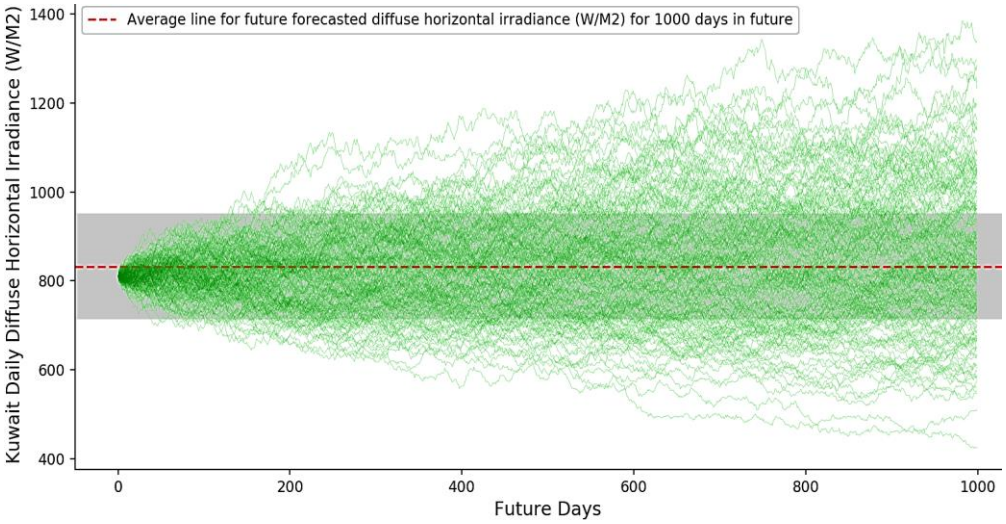

(b)

Figure A.1-25. (a) Randomly selected sample predicted solar DHI values for 1000-days in future for Kuwait and (b) The predicted solar DNI distribution performance, as predicted by MCS and Brownian (BM).

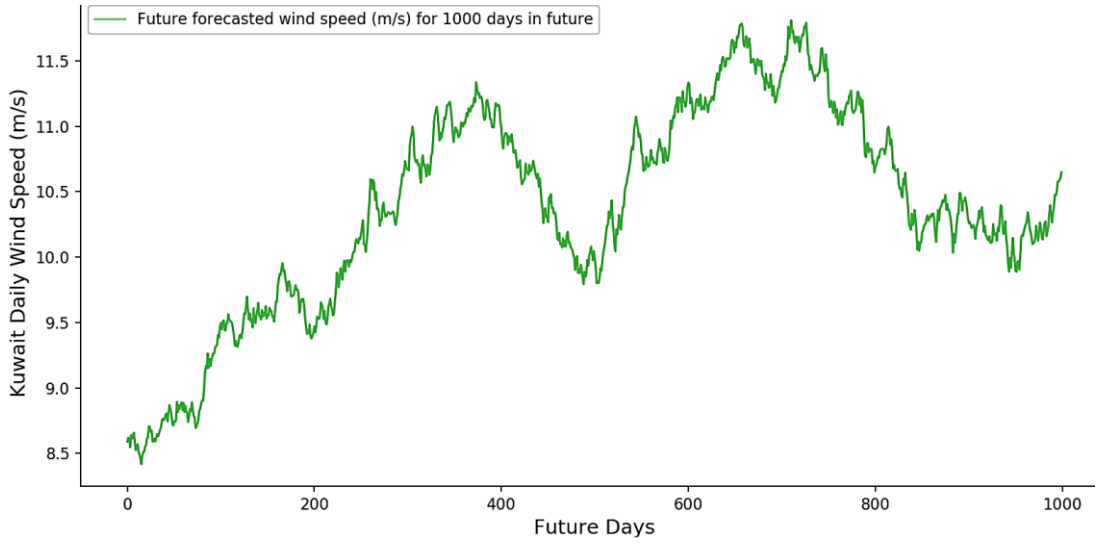

(a)

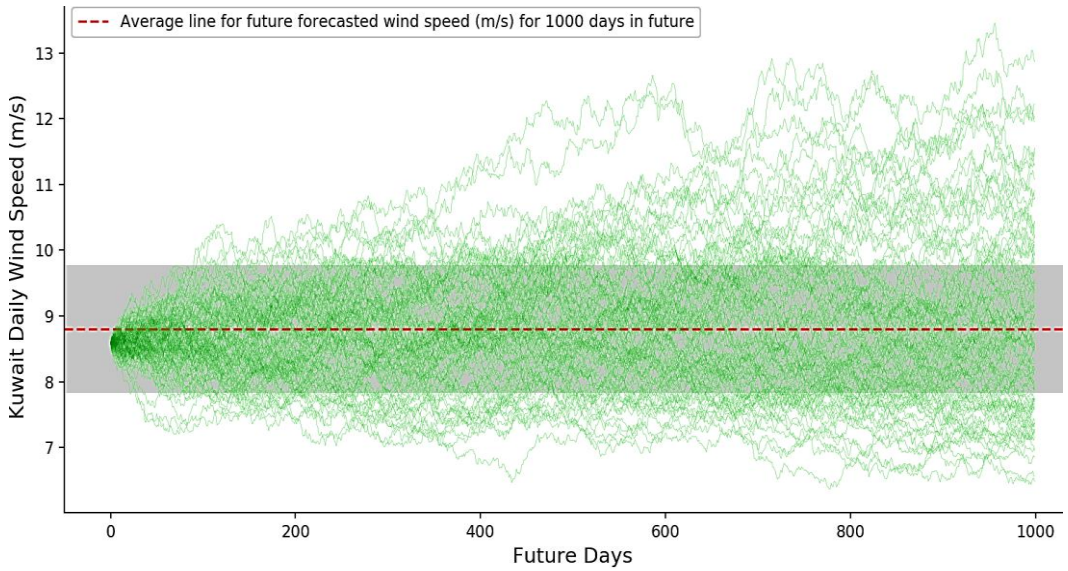

(b)

Figure A.1-26. (a) Randomly selected sample predicted wind speed values for 1000-days in future for Kuwait and (b) The predicted wind speed distribution performance, as predicted by MCS and Brownian (BM).

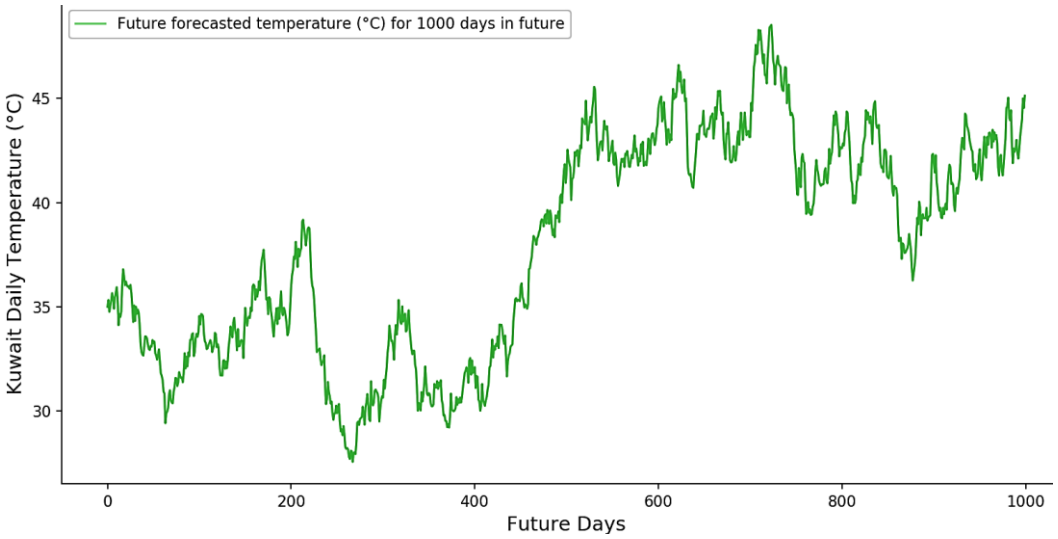

(a)

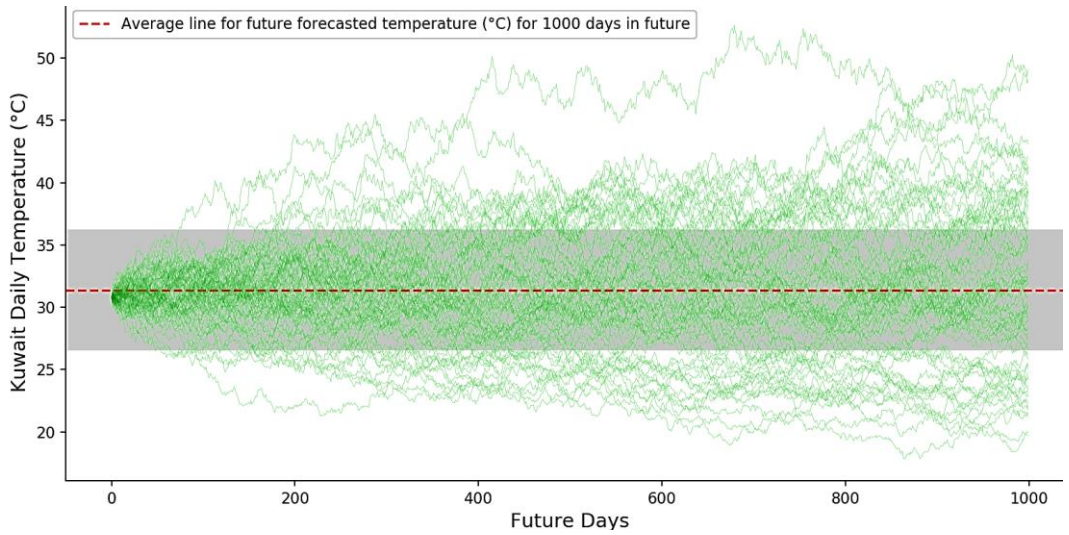

(b)

Figure A.1-27. (a) Randomly selected sample predicted temperature values for 1000-days in future for Kuwait and (b) The predicted temperature distribution performance, as predicted by MCS and Brownian (BM).

A.1.4 Fossil Fuel Prediction for Qatar Using Monte Carlo Simulation and Brownian Motion Model

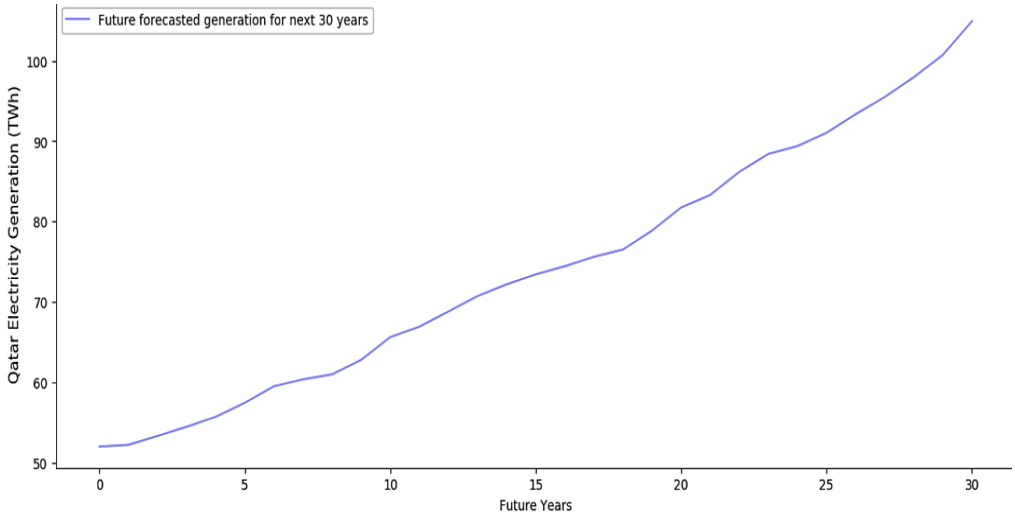

(a)

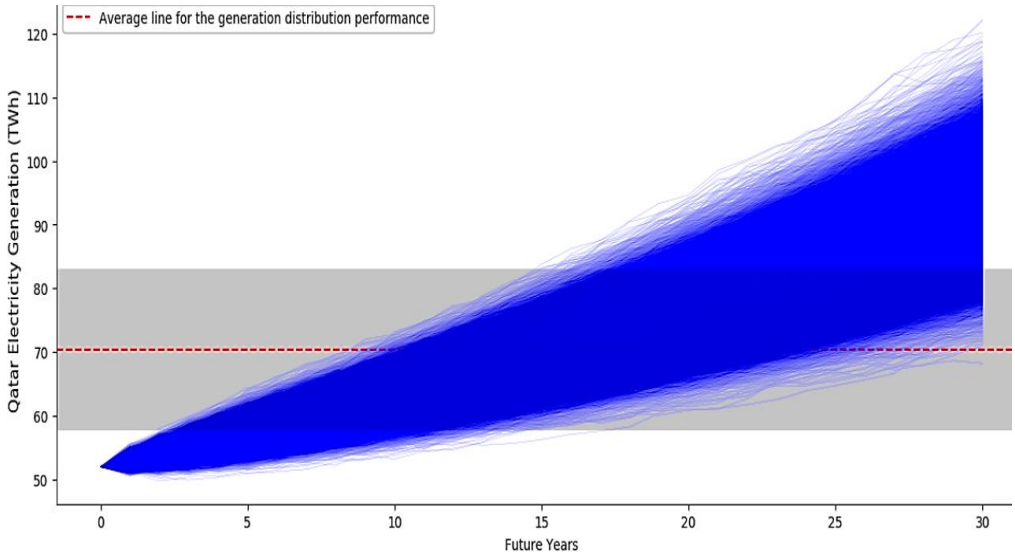

(b)

Figure A.1-28. (a) Randomly selected sample predicted electricity generation values for 30-year period from 2021 to 2050 for Qatar and (b) The predicted electricity generation distributions performance, as predicted by MCS and BM.

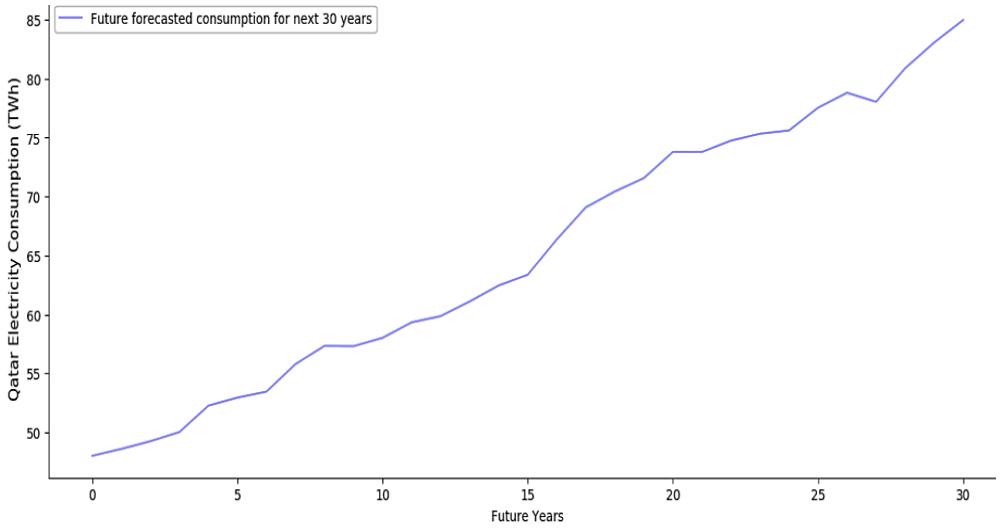

(a)

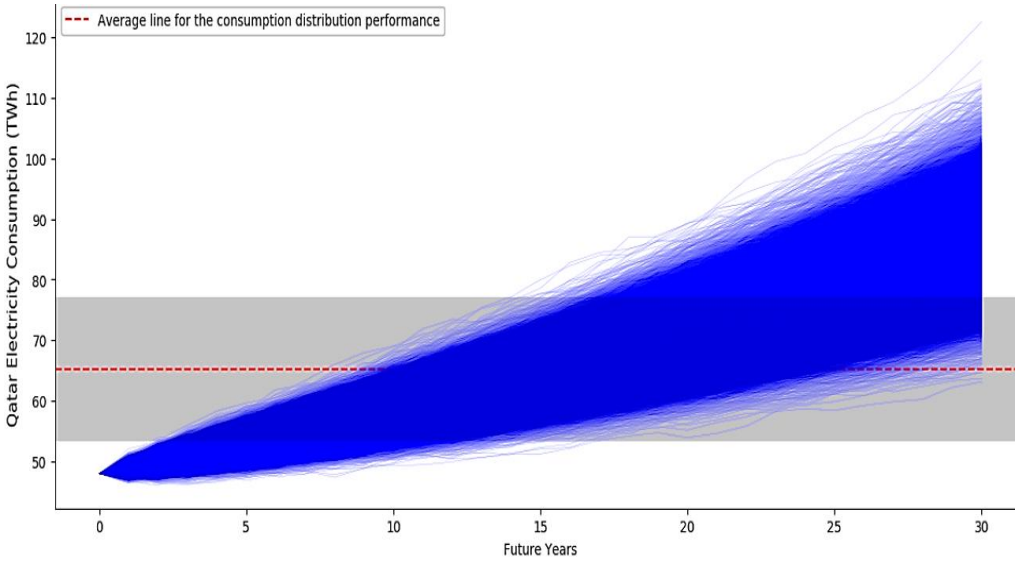

(b)

Figure A.1-29. (a) Randomly selected sample predicted electricity consumption values for 30-year period from 2021 to 2050 for Qatar and (b) The predicted electricity consumption distributions performance, as predicted by MCS and BM.

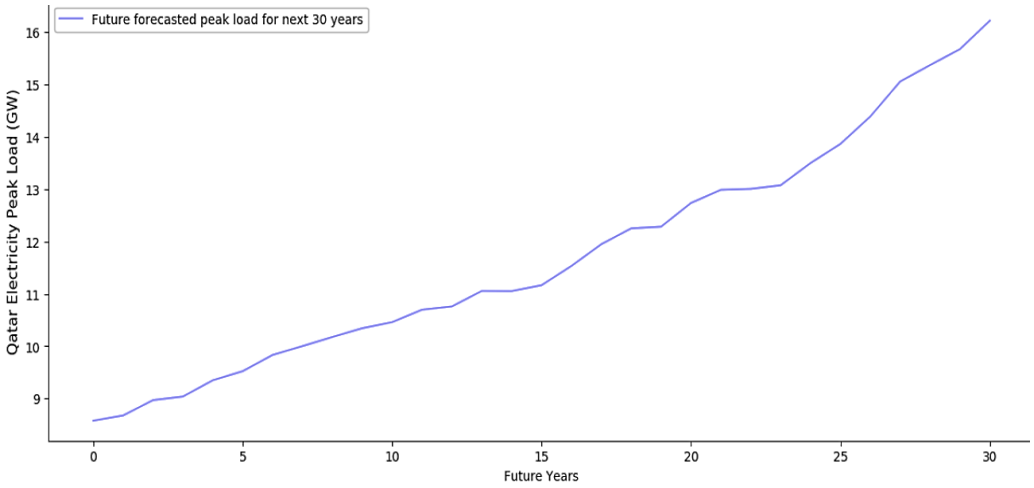

(a)

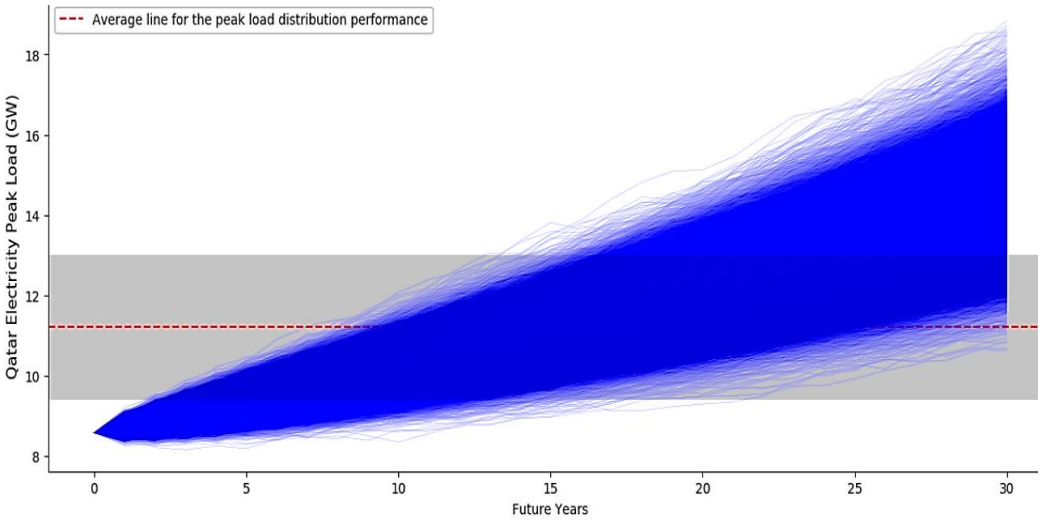

(b)

Figure A.1-30. (a) Randomly selected sample predicted electricity peak load values for 30-year period from 2021 to 2050 for Qatar and (b) The predicted electricity peak load distributions performance, as predicted by MCS and BM.

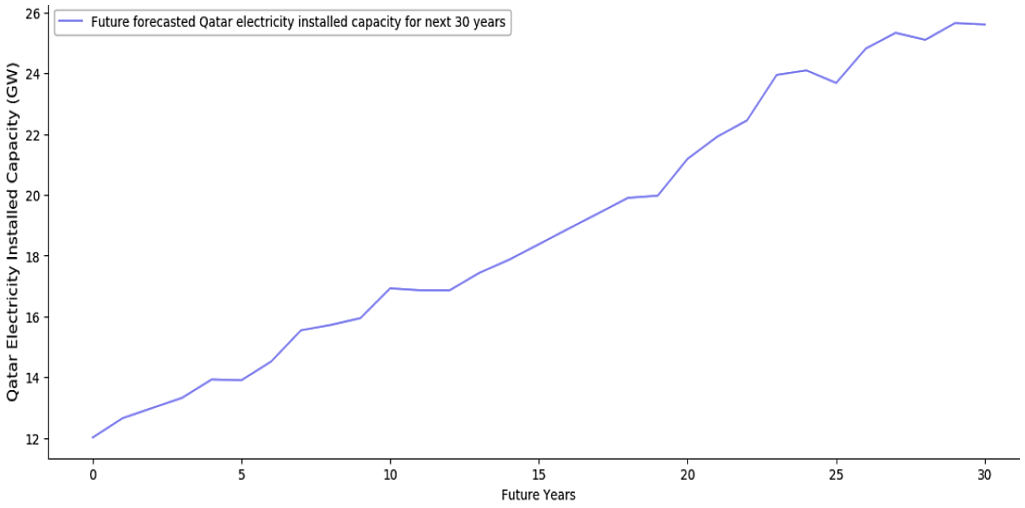

(a)

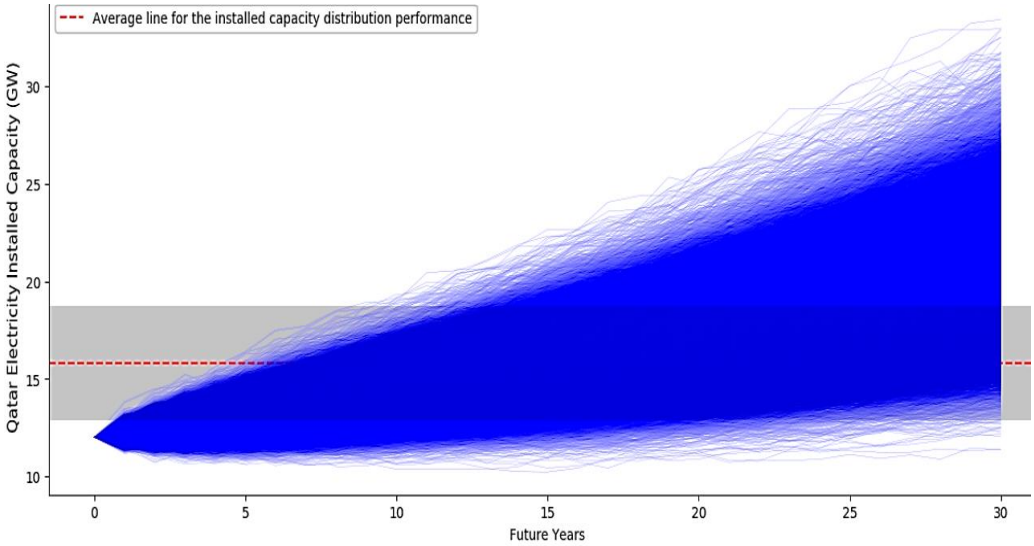

(b)

Figure A.1-31. (a) Randomly selected sample predicted electricity installed capacity values for 30-year period from 2021 to 2050 for Qatar and (b) The predicted electricity installed capacity distributions performance, as predicted by MCS and BM.

A.1.4.1 Solar Irradiance, Wind speed and Temperature Prediction for Qatar Using Monte Carlo Simulation and Brownian Motion Model

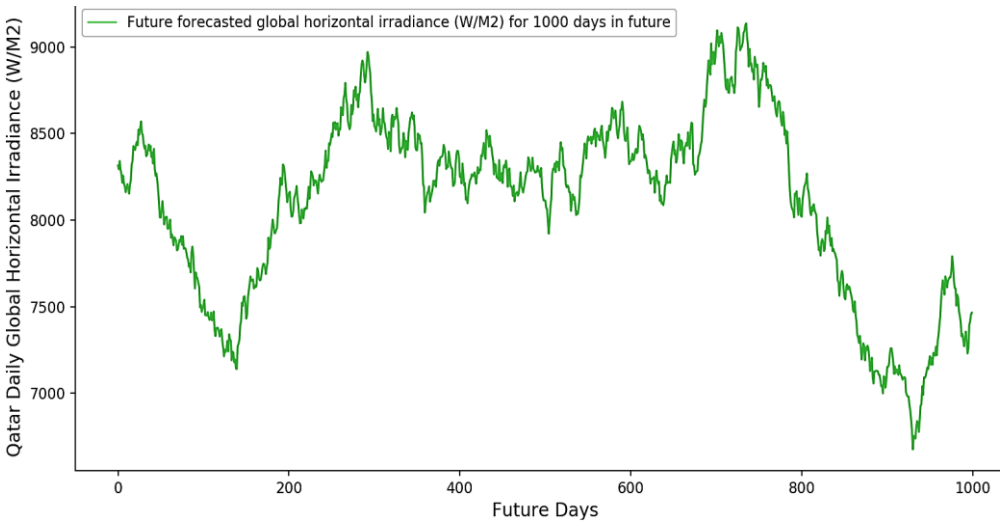

(a)

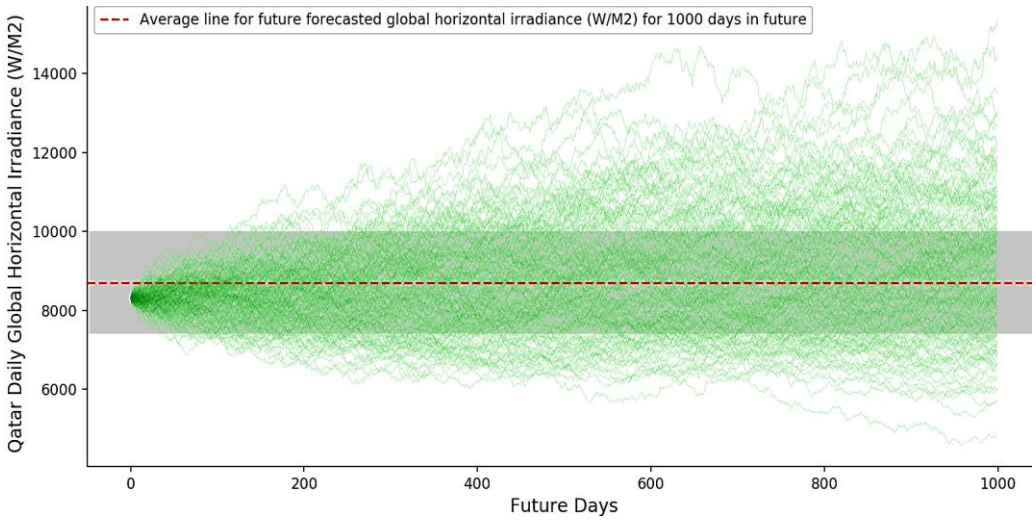

(b)

Figure A.1-32. (a) Randomly selected sample predicted solar GHI values for 1000-days in future for Qatar and (b) The predicted solar GHI distribution performance, as predicted by MCS and Brownian (BM).

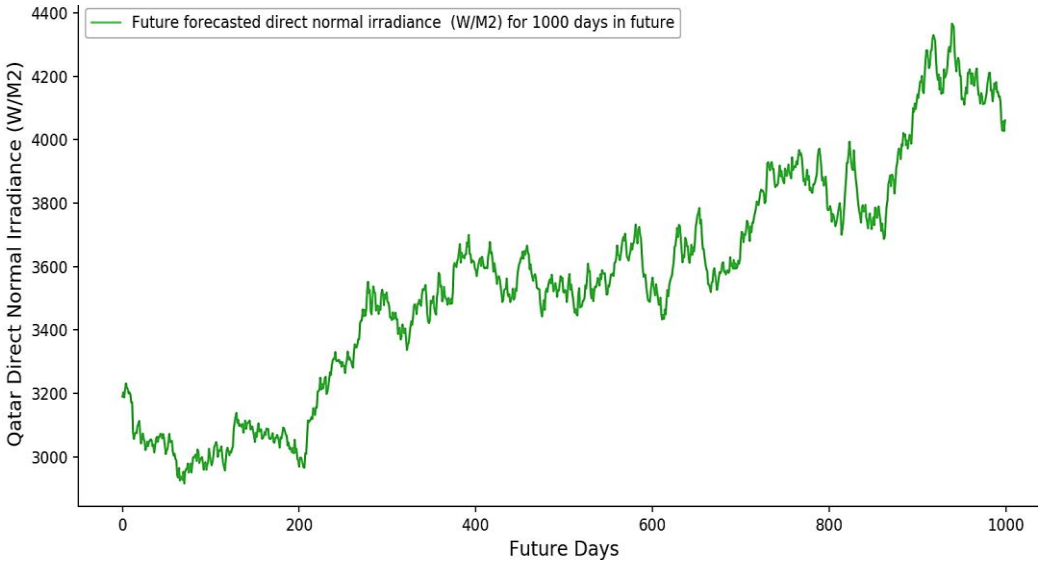

(a)

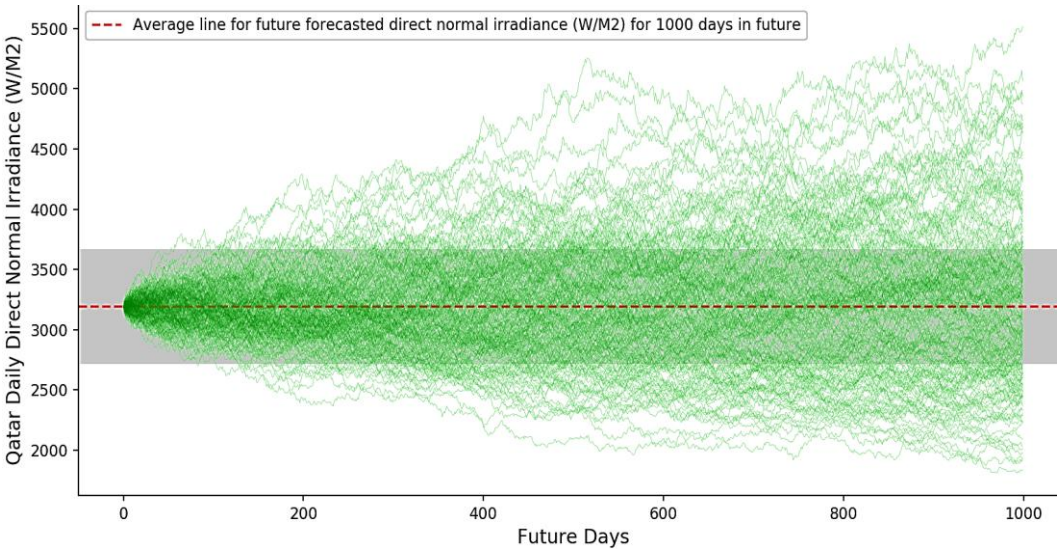

(b)

Figure A.1-33. (a) Randomly selected sample predicted solar direct irradiance (DNI) values for 1000-days in future for Qatar and (b) The predicted solar DNI distribution performance, as predicted by MCS and Brownian (BM).

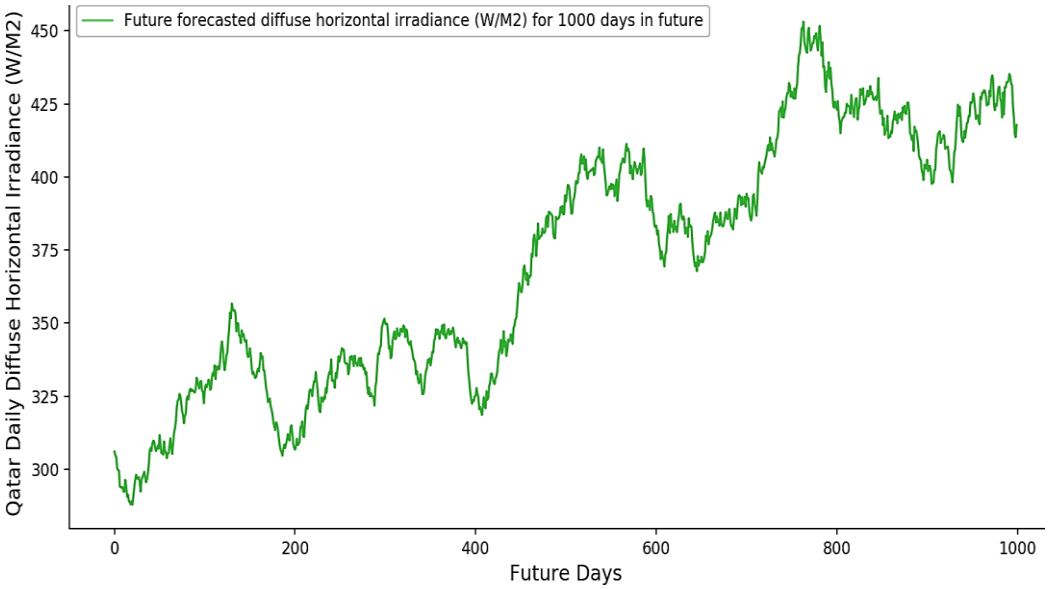

(a)

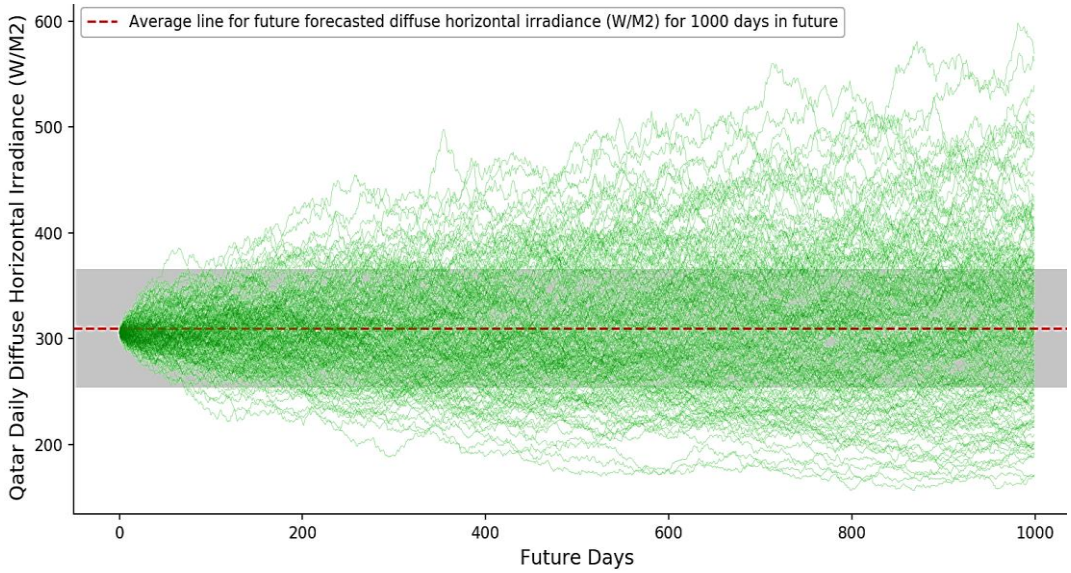

(b)

Figure A.1-34. (a) Randomly selected sample predicted solar DHI values for 1000-days in future for Qatar and (b) The predicted solar DNI distribution performance, as predicted by MCS and Brownian (BM).

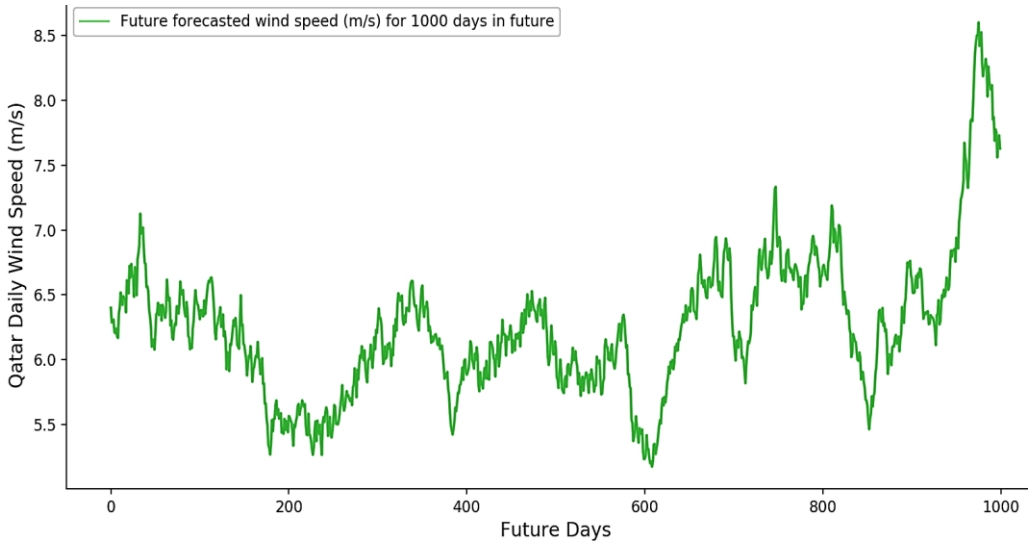

(a)

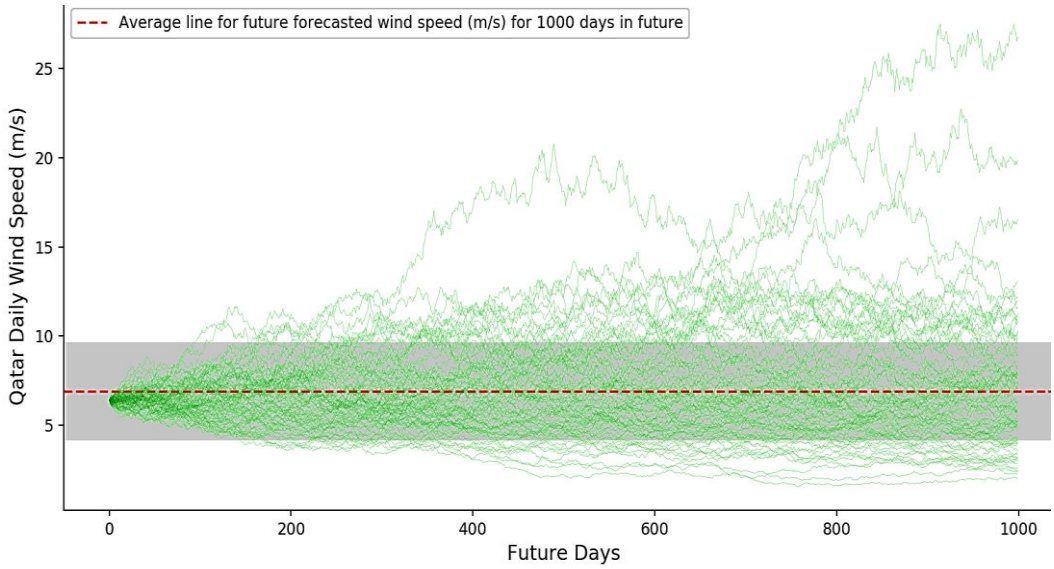

(b)

Figure A.1-35. (a) Randomly selected sample predicted wind speed values for 1000-days in future for Kuwait and (b) The predicted wind speed distribution performance, as predicted by MCS and Brownian (BM).

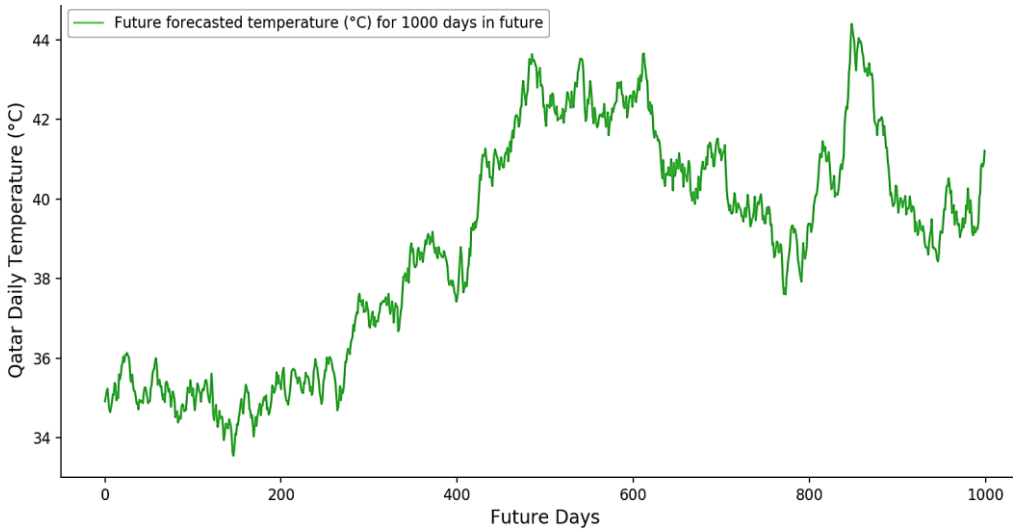

(a)

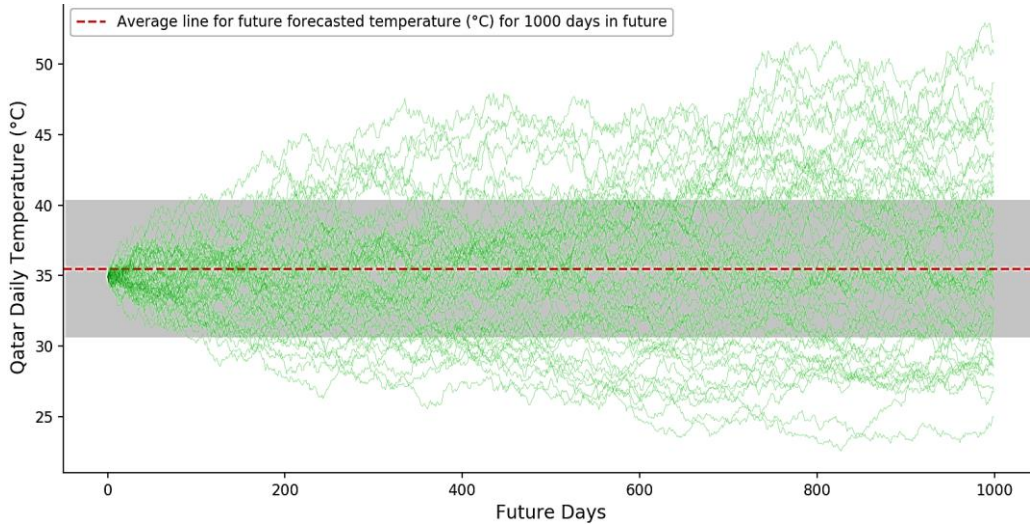

(b)

Figure A.1-36. (a) Randomly selected sample predicted temperature values for 1000-days in future for Qatar and (b) The predicted temperature distribution performance, as predicted by MCS and Brownian (BM).

A.1.5 Fossil Fuel Prediction for Bahrain Using Monte Carlo Simulation and Brownian Motion Model

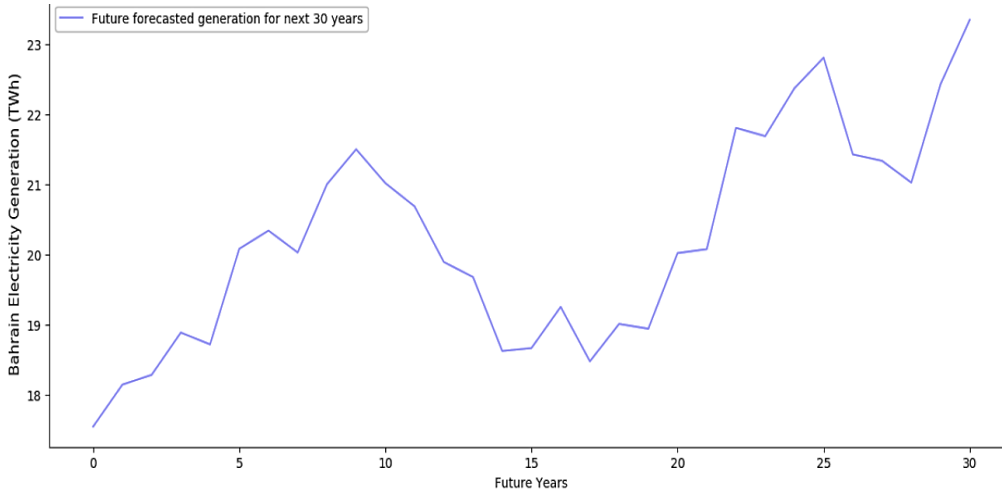

(a)

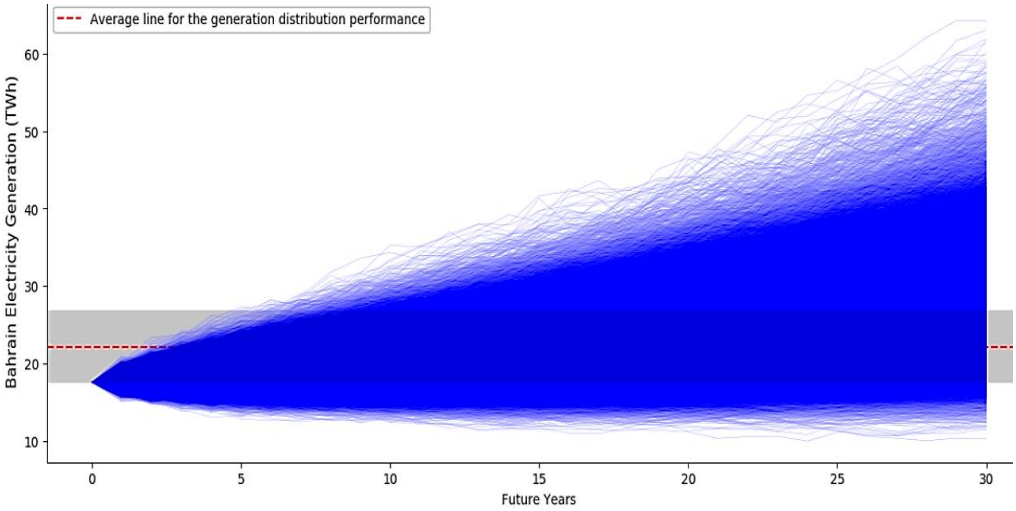

(b)

Figure A.1-37. (a) Randomly selected sample predicted electricity generation values for 30-year period from 2021 to 2050 for Bahrain and (b) The predicted electricity generation distributions performance, as predicted by MCS and BM.

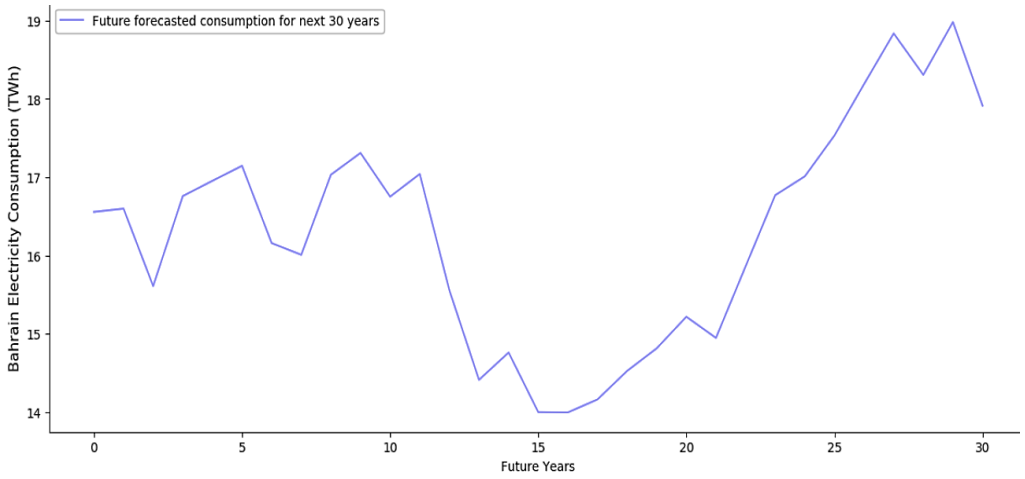

(a)

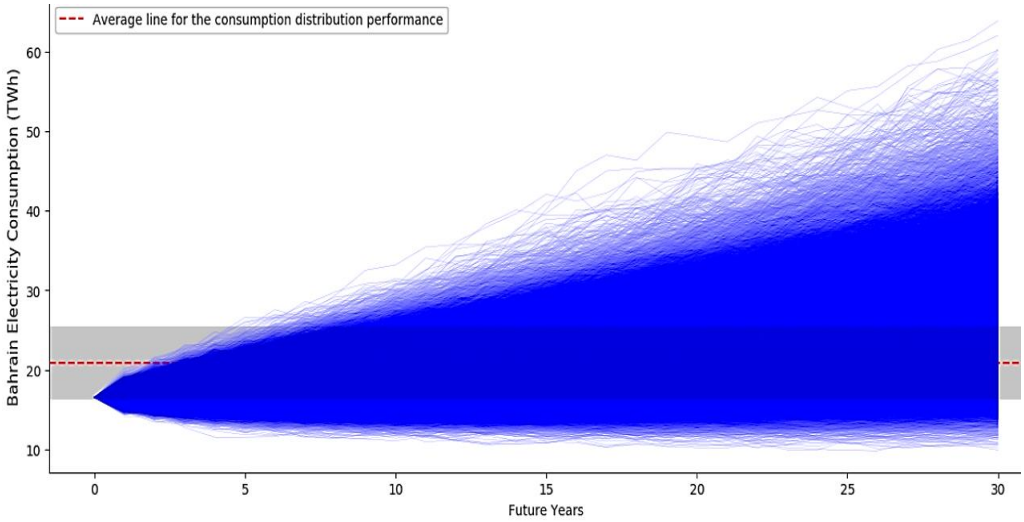

(b)

Figure A.1-38. (a) Randomly selected sample predicted electricity consumptionvalues for 30-year period from 2021 to 2050 for Bahrain and (b) The predicted electricity consumption distributions performance, as predicted by MCS and BM.

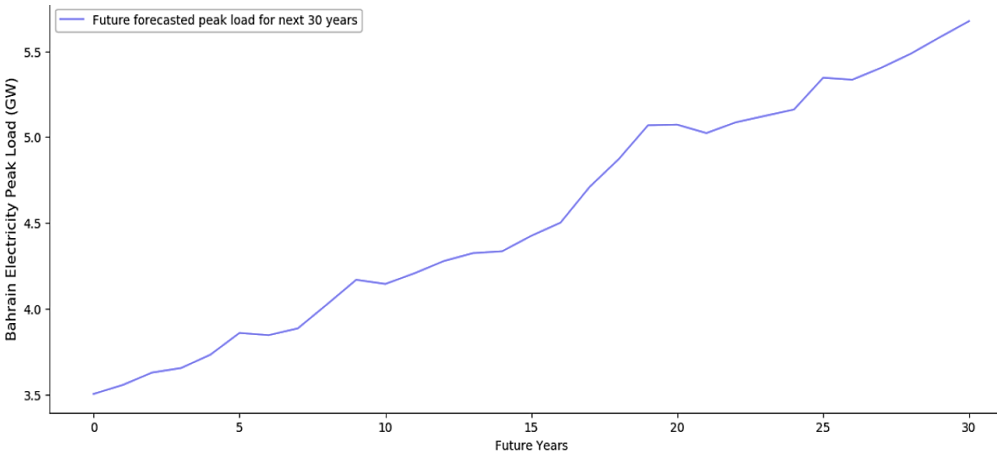

(a)

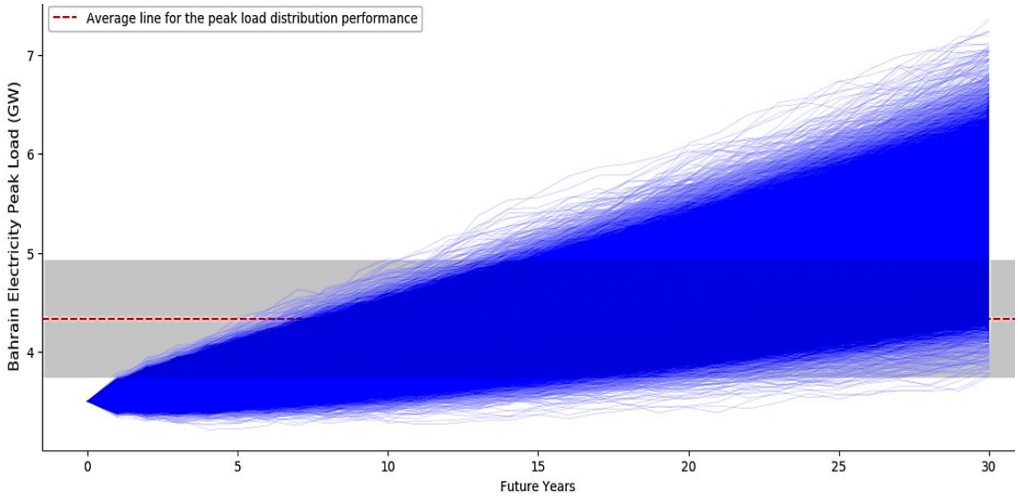

(b)

Figure A.1-39. (a) Randomly selected sample predicted electricity peak load values for 30-year period from 2021 to 2050 for Bahrain and (b) The predicted electricity peak load distributions performance, as predicted by MCS and BM.

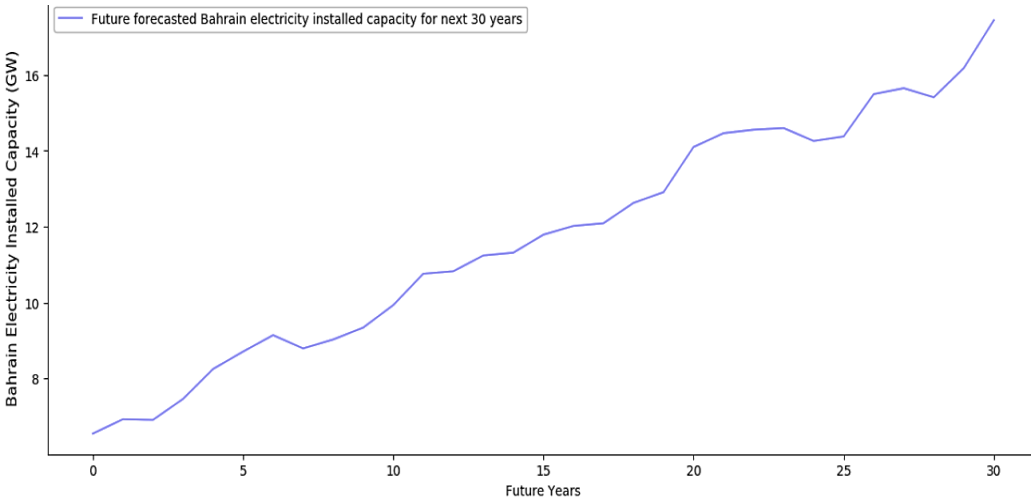

(a)

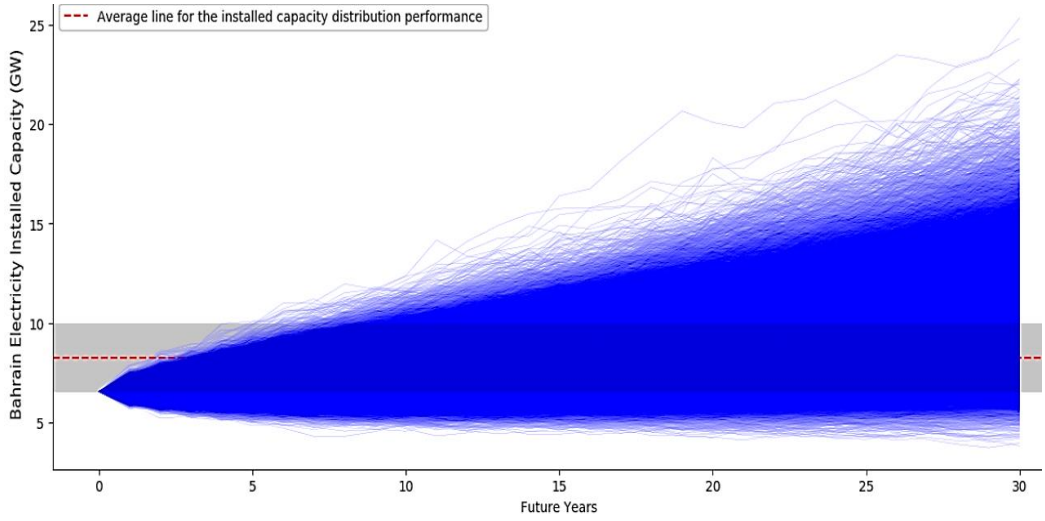

(b)

Figure A.1-40. (a) Randomly selected sample predicted electricity installed capacity values for 30-year period from 2021 to 2050 for Bahrain and (b) The predicted electricity installed capacity distributions performance, as predicted by MCS and BM.

A.1.5.2 Solar Irradiance, Wind speed and Temperature Prediction for Bahrain Using Monte Carlo Simulation and Brownian Motion Model

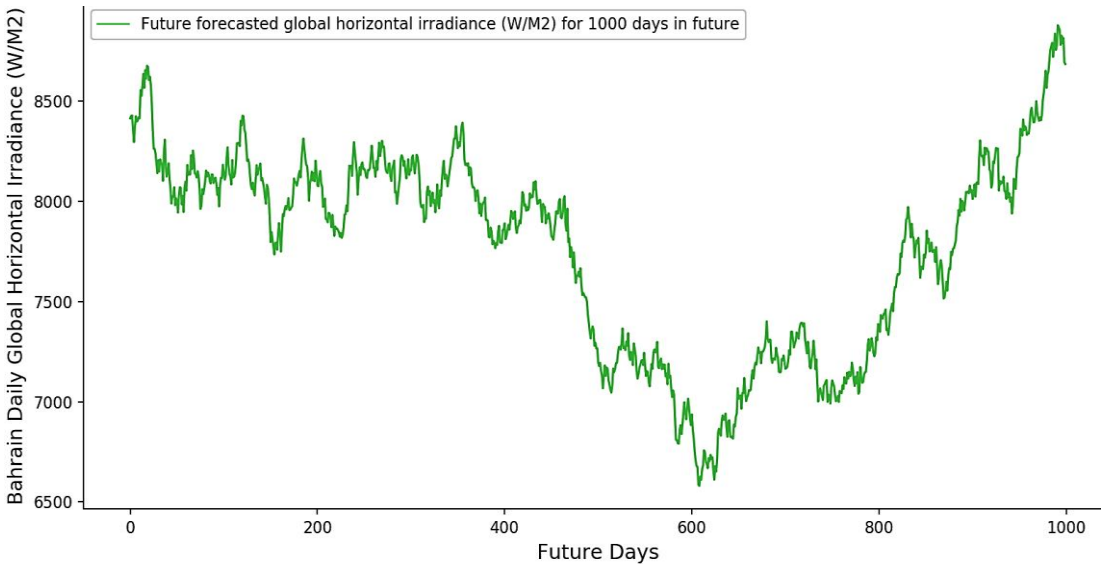

(a)

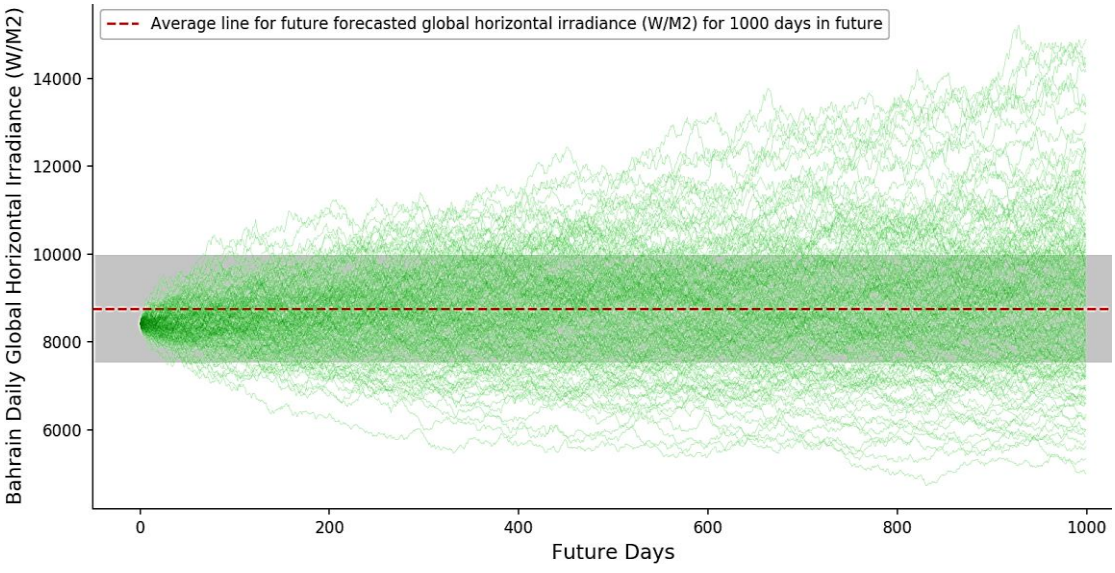

(b)

Figure A.1-41. (a) Randomly selected sample predicted solar GHI values for 1000-days in future for Bahrain and (b) The predicted solar GHI distribution performance, as predicted by MCS and Brownian (BM).

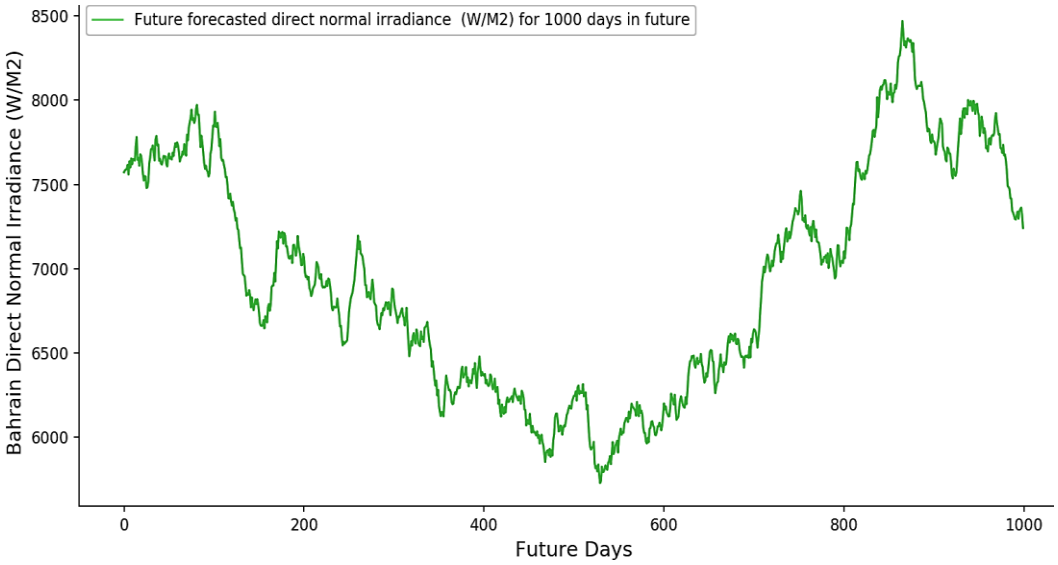

(a)

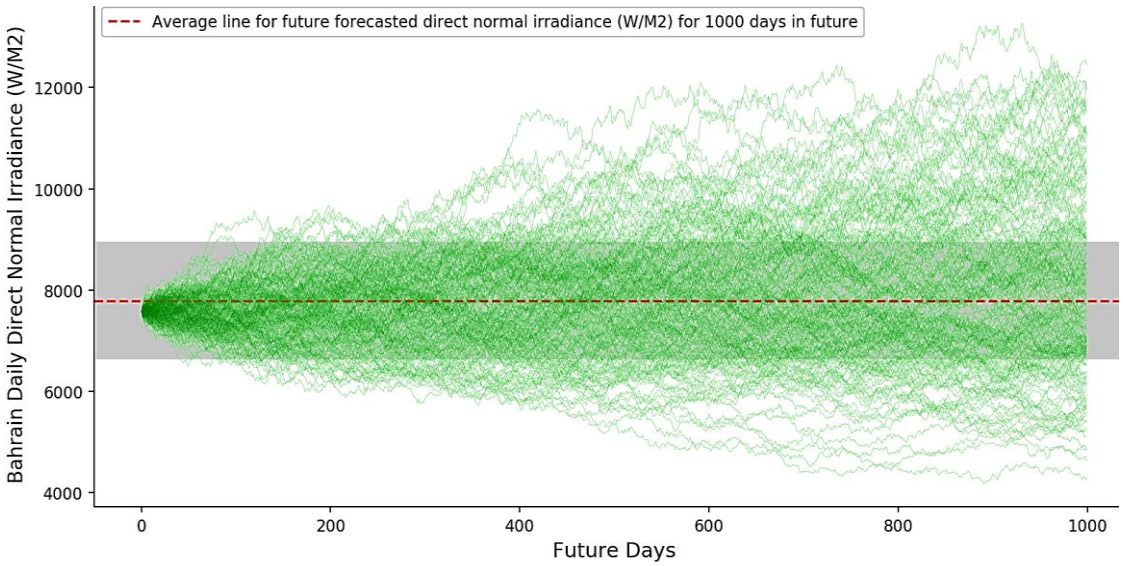

(b)

Figure A.1-42. (a) Randomly selected sample predicted solar direct irradiance (DNI) values for 1000-days in future for Bahrain and (b) The predicted solar DNI distribution performance, as predicted by MCS and Brownian (BM).

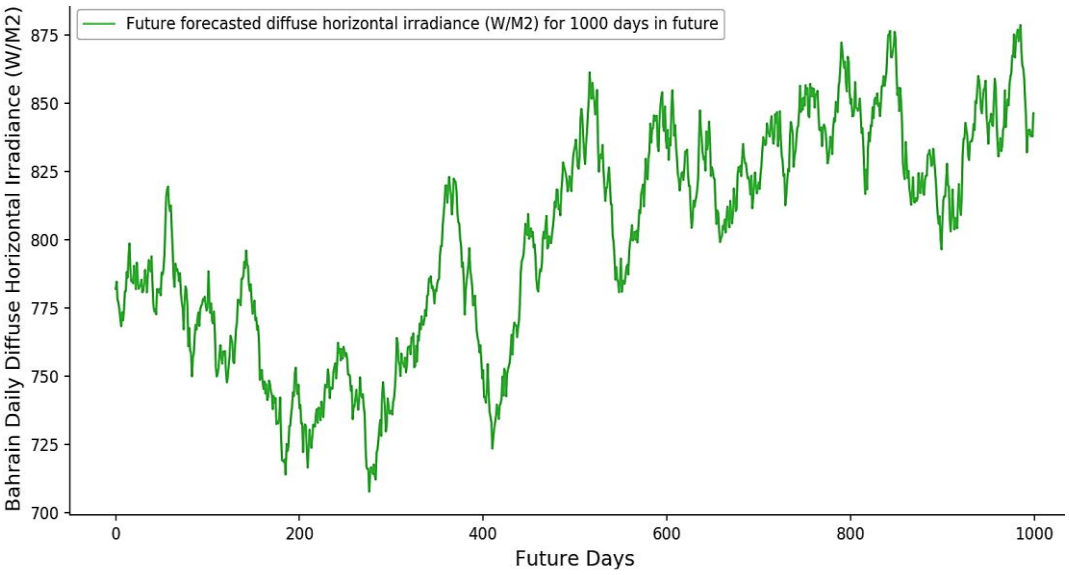

(a)

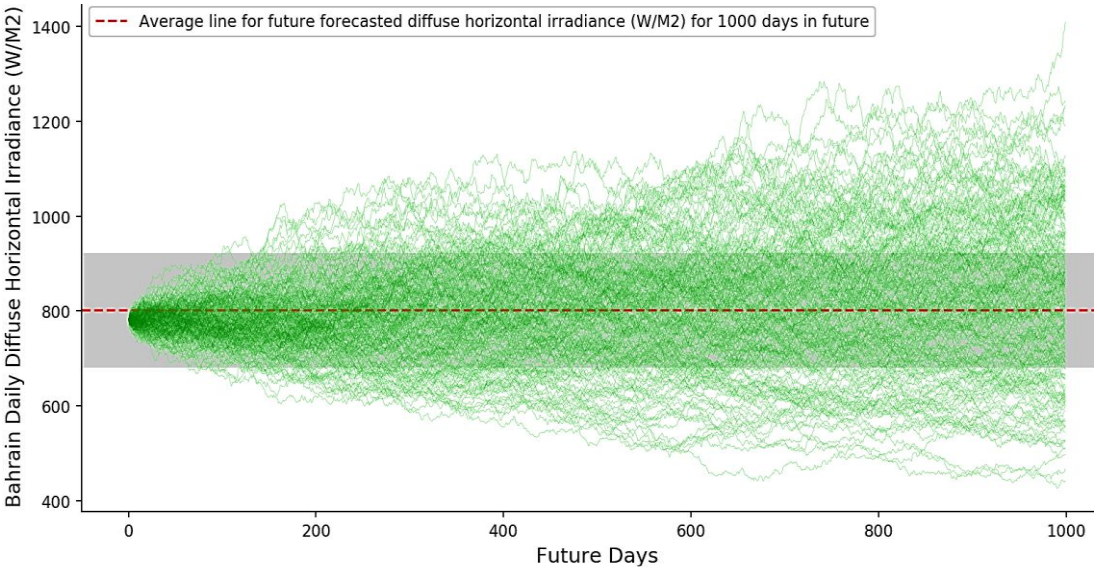

(b)

Figure A.1-43. (a) Randomly selected sample predicted solar DHI values for 1000-days in future for Bahrain and (b) The predicted solar DNI distribution performance, as predicted by MCS and Brownian (BM).

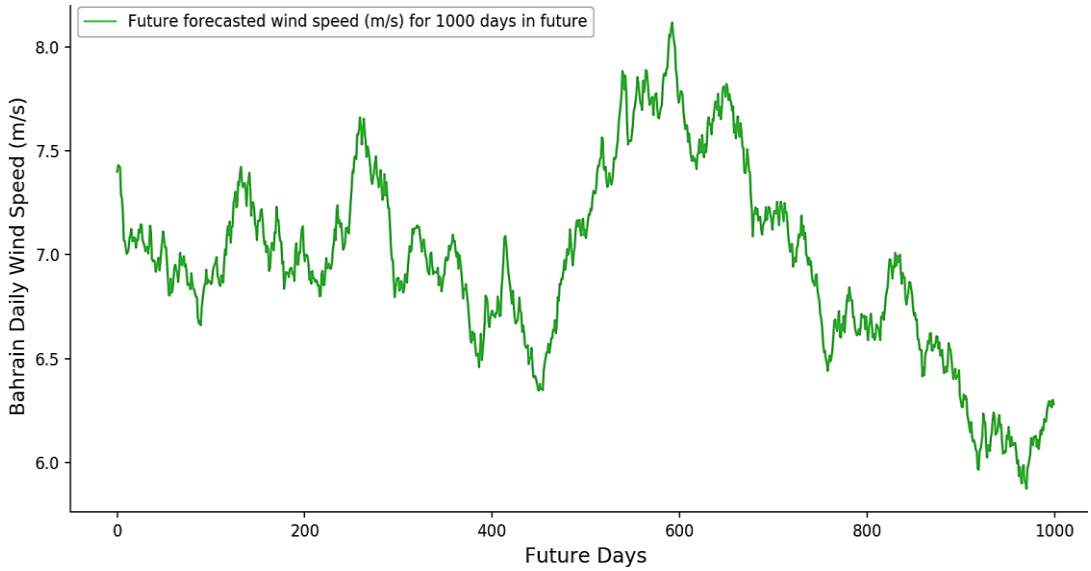

(a)

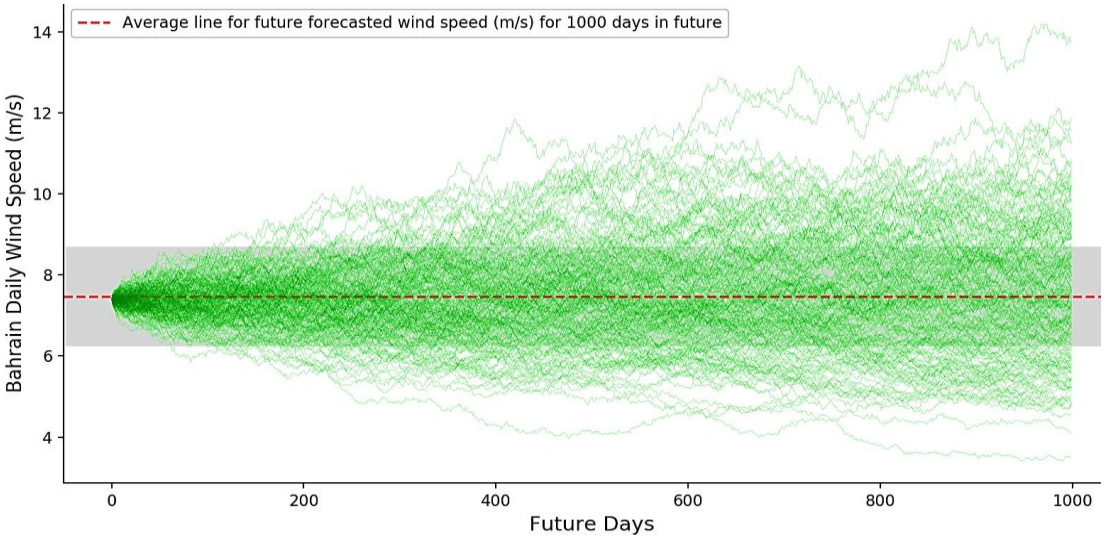

(b)

Figure A.1-44. (a) Randomly selected sample predicted wind speed values for 1000-days in future for Bahrain and (b) The predicted wind speed distribution performance, as predicted by MCS and Brownian (BM).

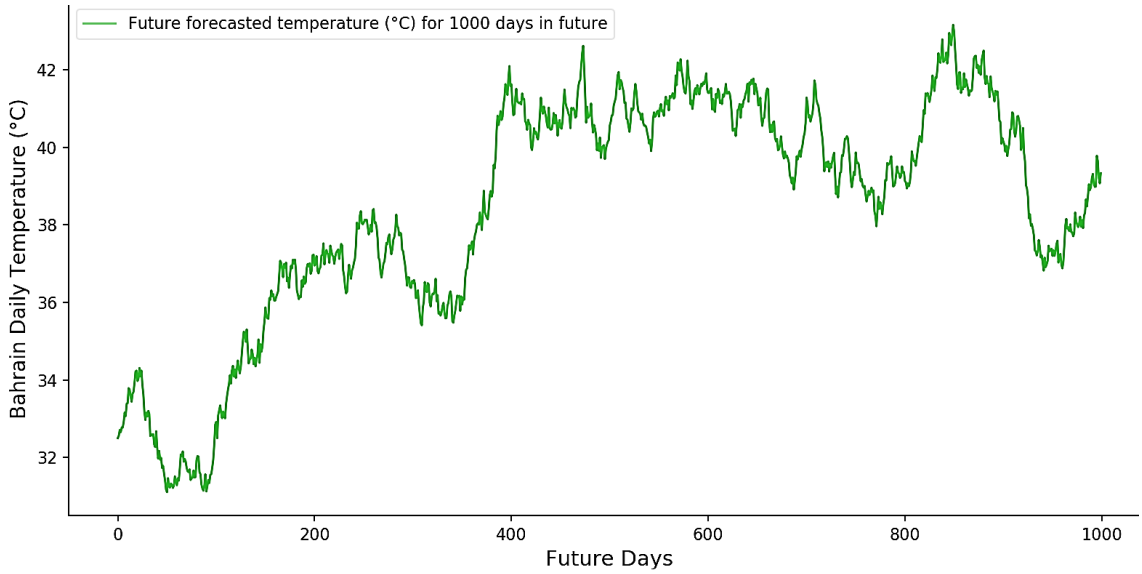

(a)

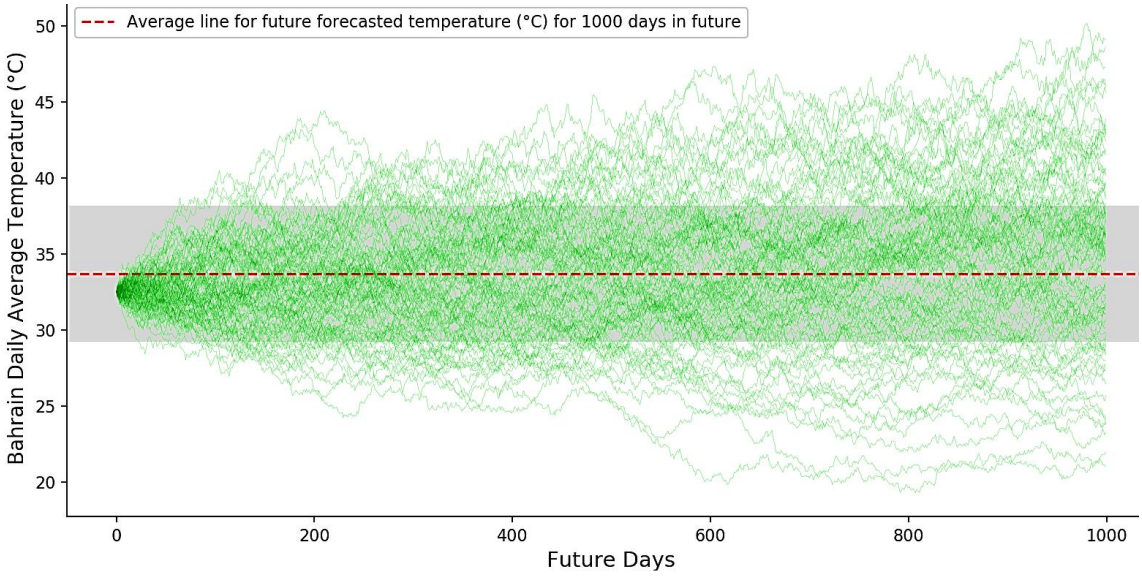

(b)

Figure A.1-45. (a) Randomly selected sample predicted temperature values for 1000-days in future for Bahrain and (b) The predicted temperature distribution performance, as predicted by MCS and BM.

A.2 Appendix 2 – GCC Countries Future Scenario Using SARIMAX Prediction Model

A.2.1 Fossil Fuel Prediction for Oman Using SARIMAX Model

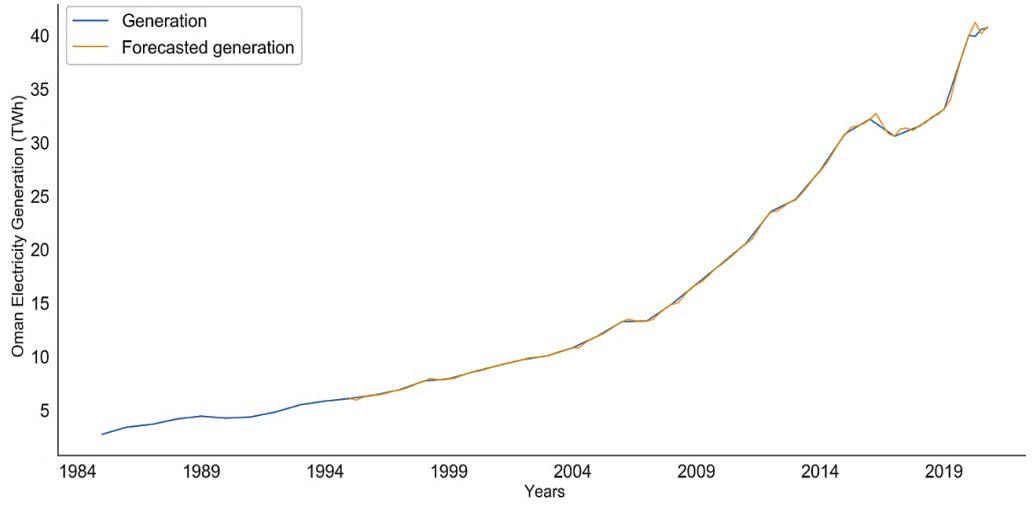

(a)

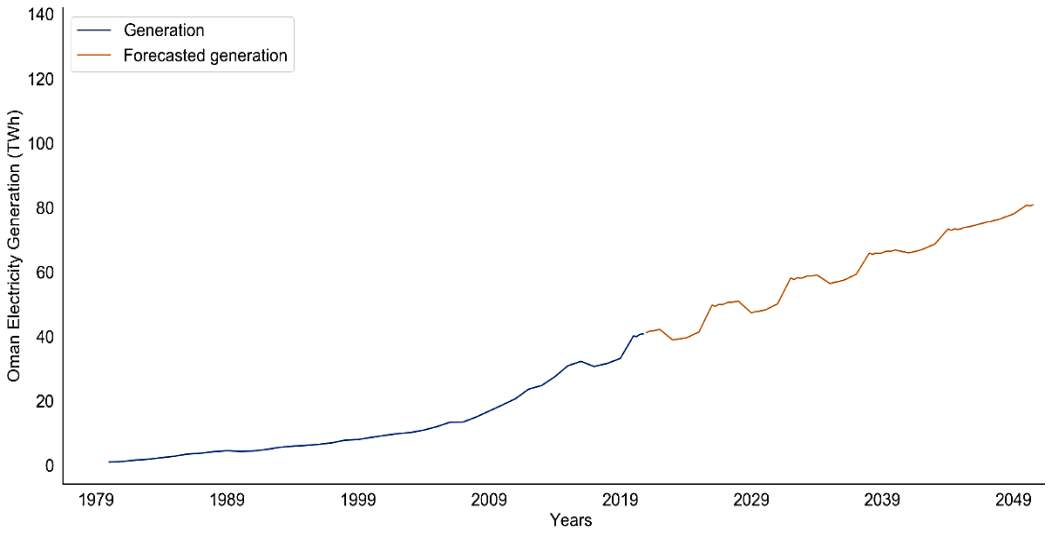

(b)

Figure A.2-1. (a) Real and forecasted values of electricity generation of Oman, which show the good fit and performance of the SARIMAX model. (b) Forecasted electricity generation values for 30-year period from 2021 to 2050.

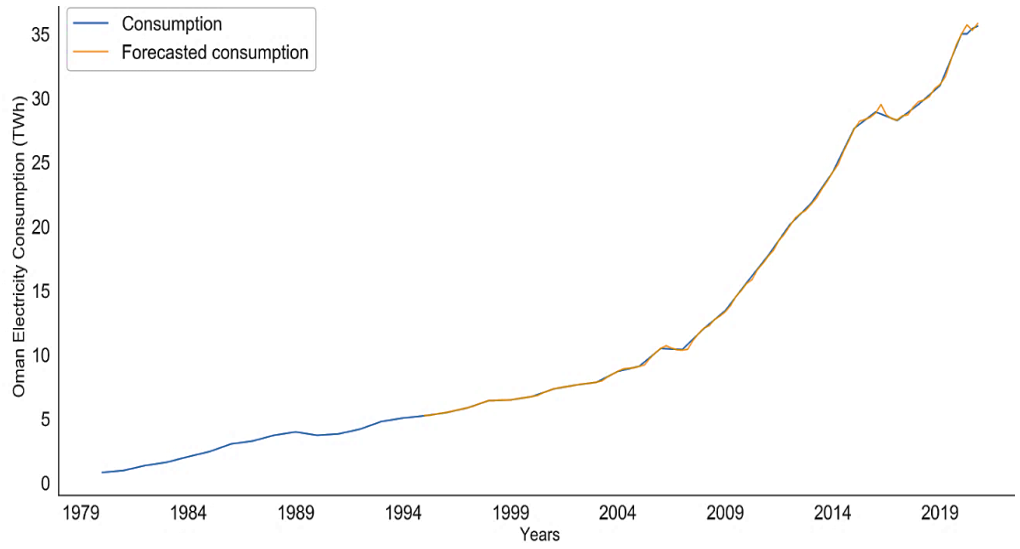

(a)

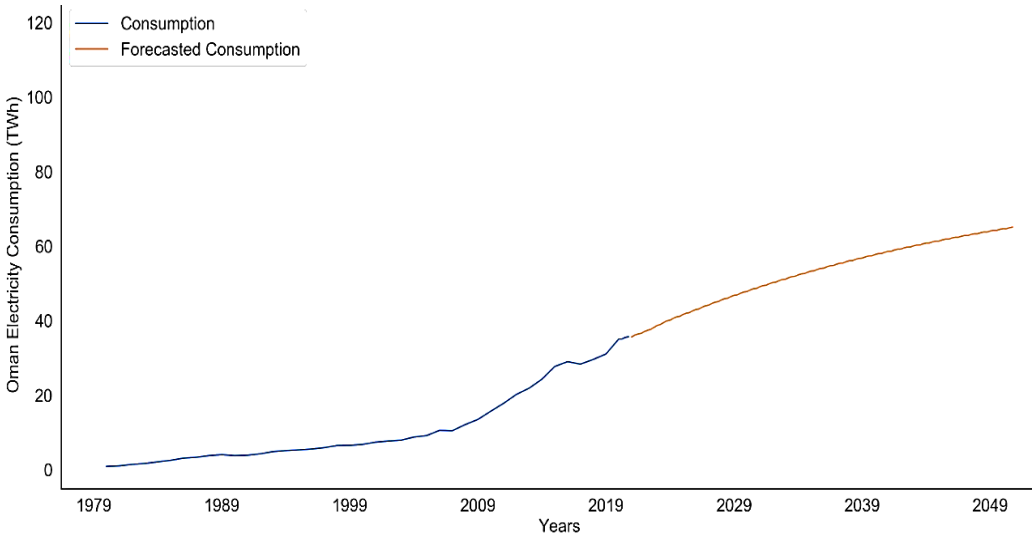

(b)

Figure A.2-2. (a) Real and forecasted values of electricity consumption of Oman, which show the good fit and performance of the SARIMAX model. (b) Forecasted electricity consumption values for 30-year period from 2021 to 2050.

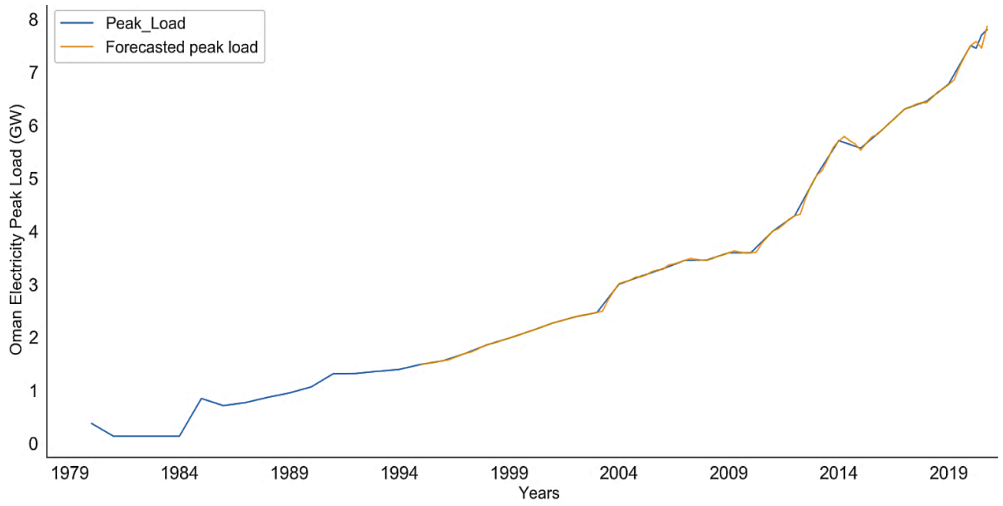

(a)

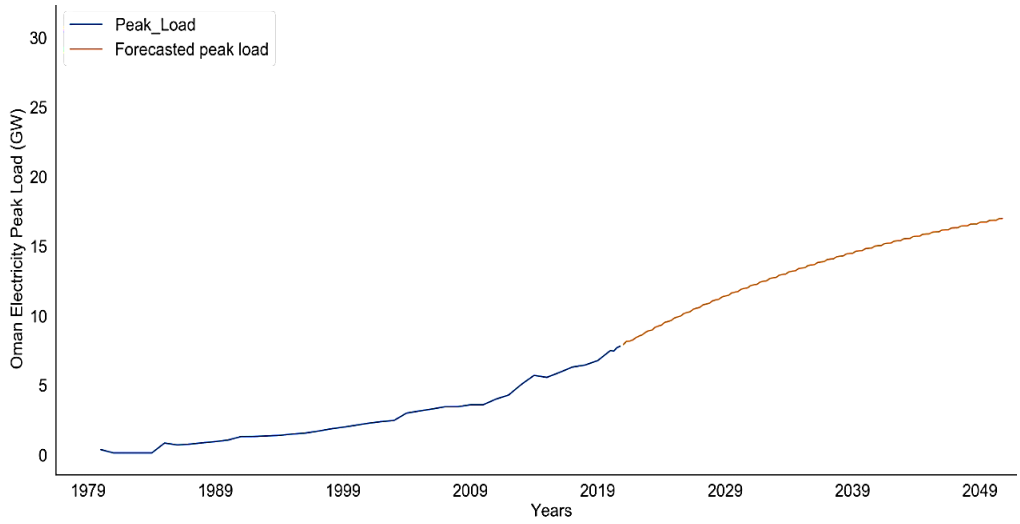

(b)

Figure A.2-3. (a) Real and forecasted values of electricity peak load of Oman, which show the good fit and performance of the SARIMAX model. (b) Forecasted electricity peak load values for 30-year period from 2021 to 2050.

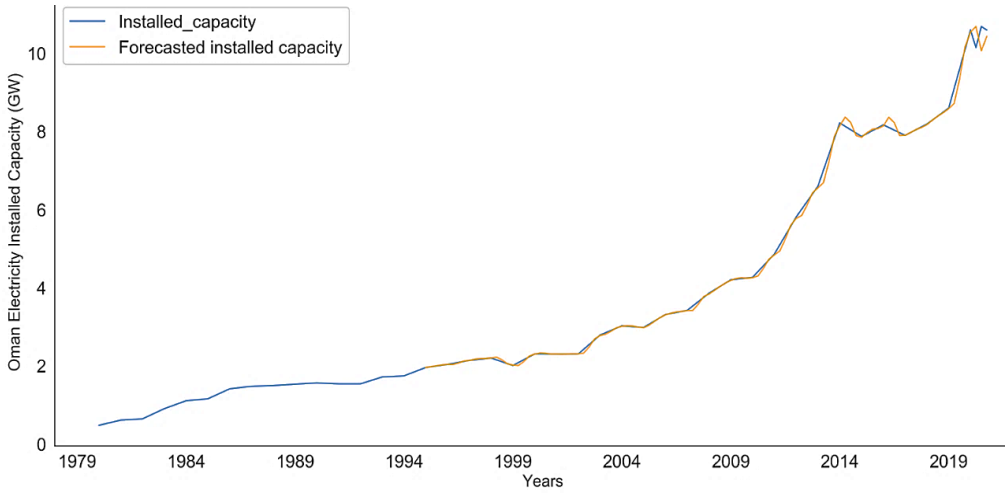

(a)

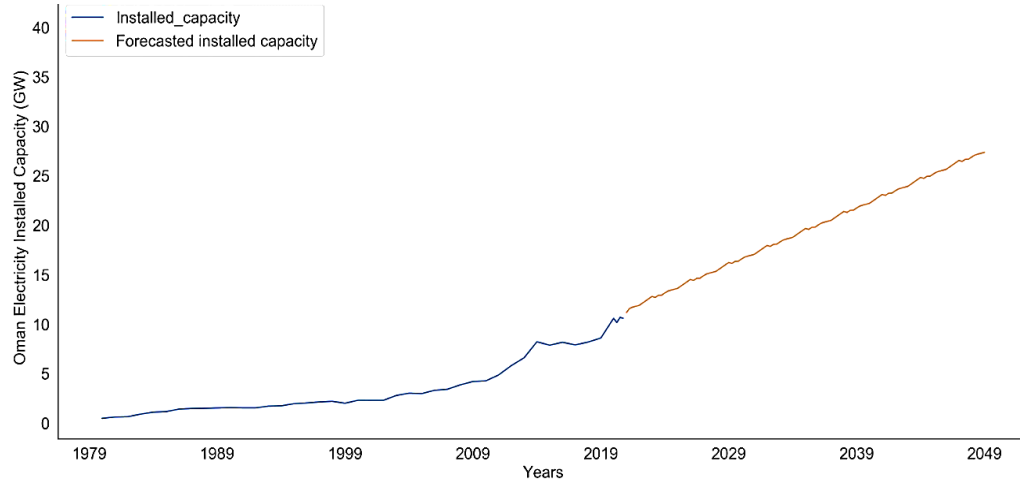

(b)

Figure A.2-4. (a) Real and forecasted values of electricity installation capacity of Oman, which show the good fit and performance of the SARIMAX model. (b) Forecasted electricity installation capacity values for 30-year period from 2021 to 2050.

Table A.2-1. Forecasting accuracy indicators for Oman prediction using the SARIMAX model.

No.	**Metric**	**Generation (TWh)**	**Consumption (TWh)**	**Electric peak load (GW)**	**Installed capacity (GW)**
1	RMSE	0.2	0.1	0.0	0.1
2	MAE	0.1	0.0	0.0	0.0
3	MSE	0.0	0.0	0.0	0.0
4	MAPE (%)	0.5	0.4	0.4	0.9
5	*p*-value (%)	0.0	0.0	0.0	0
6	R^2 (%)	99	99	99	99

A.2.2 Fossil Fuel Prediction for UAE Using SARIMAX Model

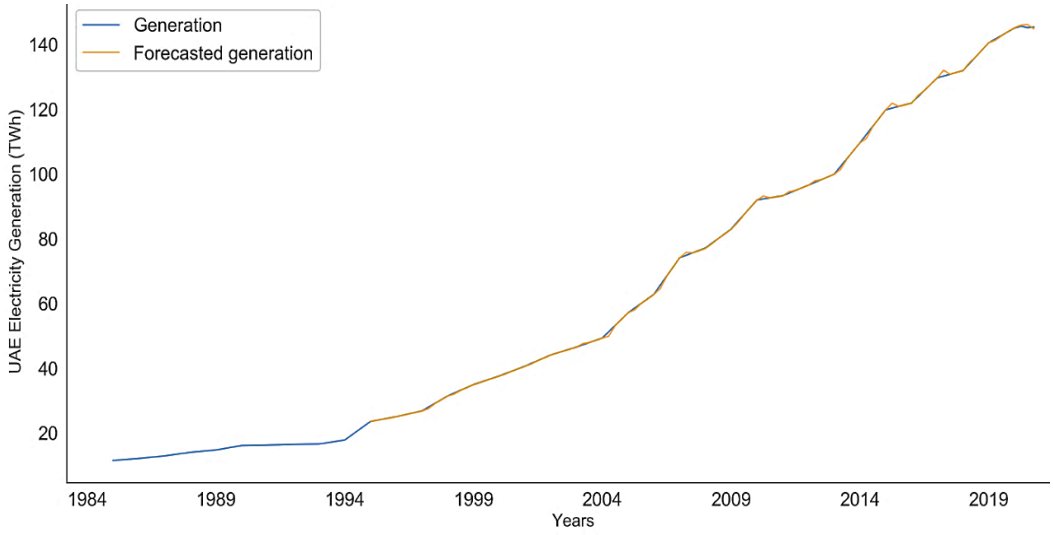

(a)

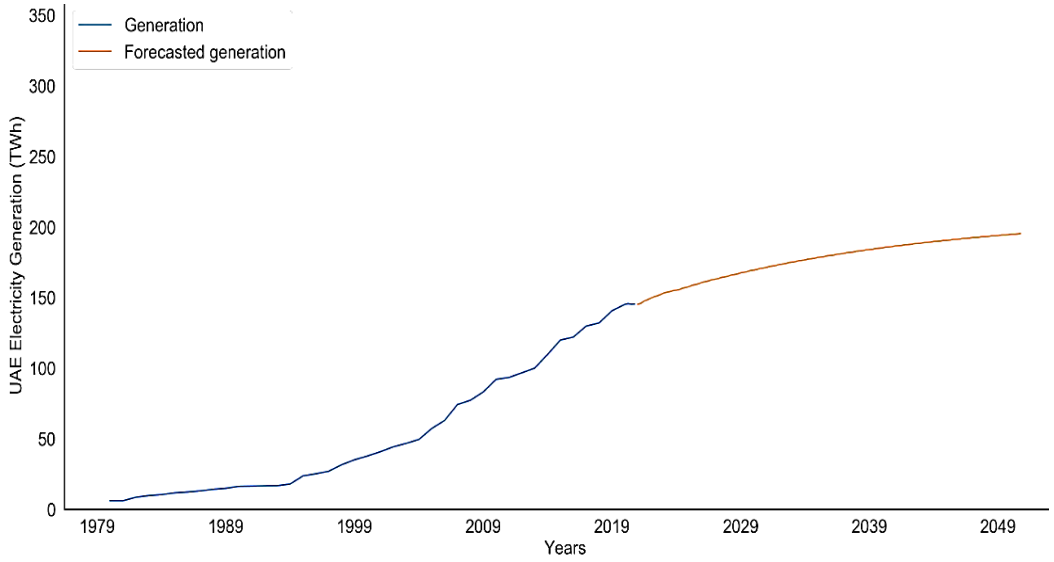

(b)

Figure A.2-5. (a) Real and forecasted values of electricity generation of UAE, which show the good fit and performance of the SARIMAX model. (b) Forecasted electricity generation values for 30-year period from 2021 to 2050.

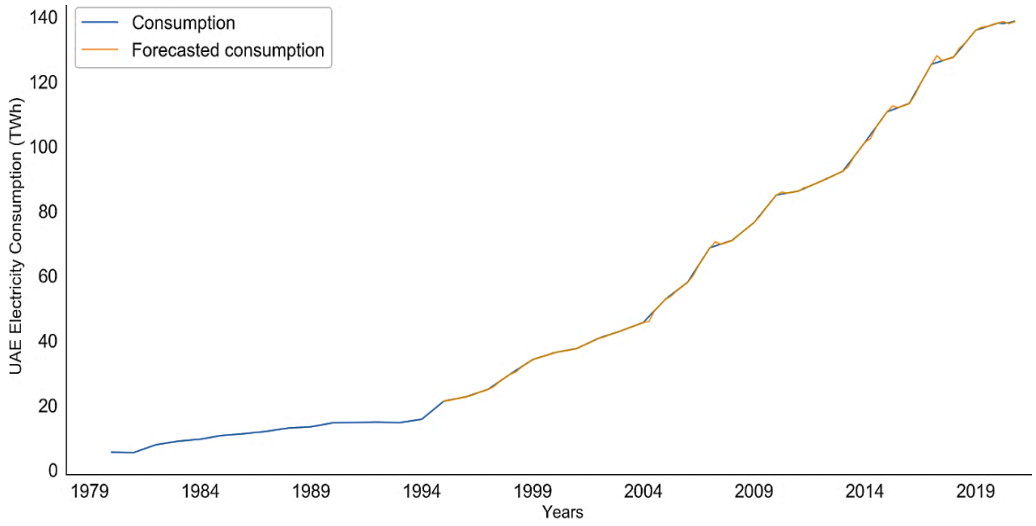

(a)

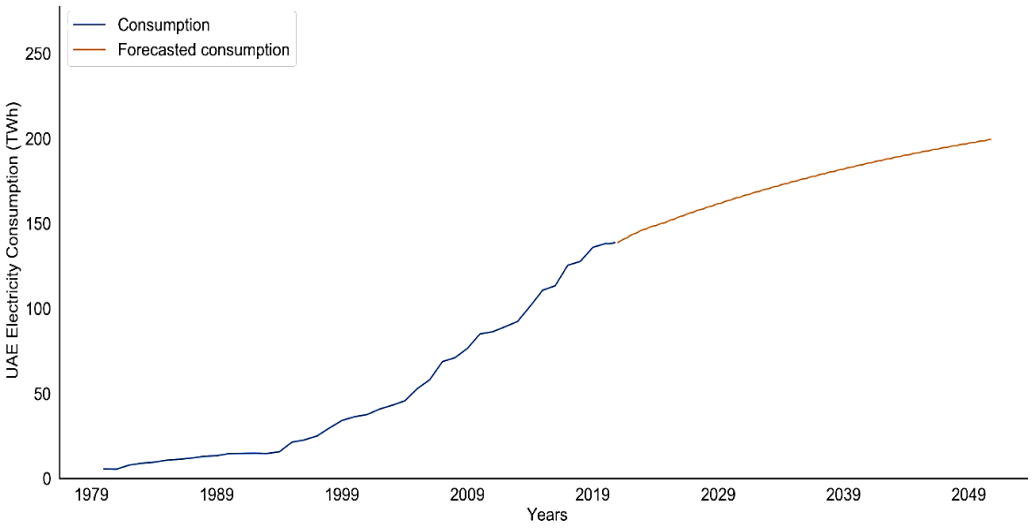

(b)

Figure A.2-6. (a) Real and forecasted values of electricity consumption of UEA, which show the good fit and performance of the SARIMAX model. (b) Forecasted electricity consumption values for 30-year period from 2021 to 2050.

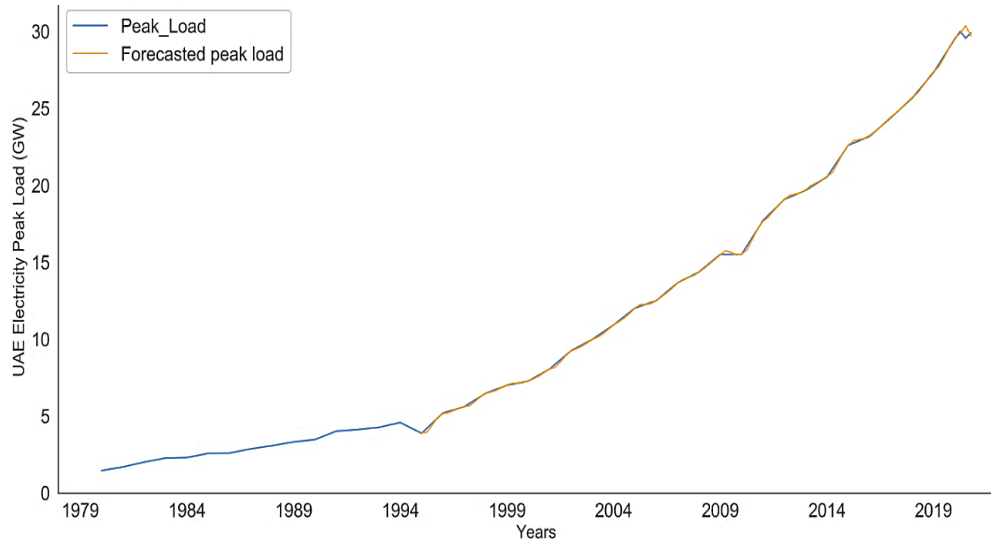

(a)

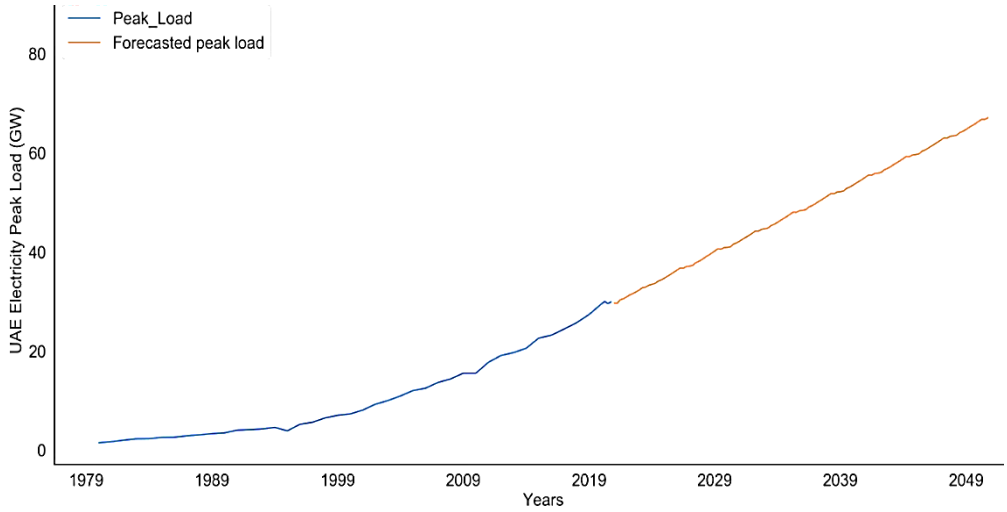

(b)

Figure A.2-7. (a) Real and forecasted values of electricity peak load of UEA, which show the good fit and performance of the SARIMAX model. (b) Forecasted electricity peak load values for 30-year period from 2021 to 2050.

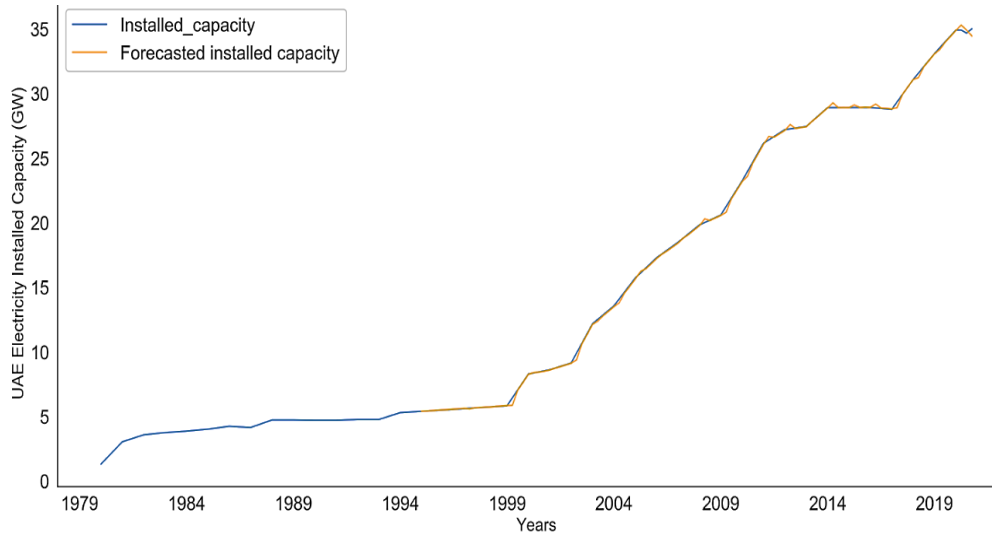

(a)

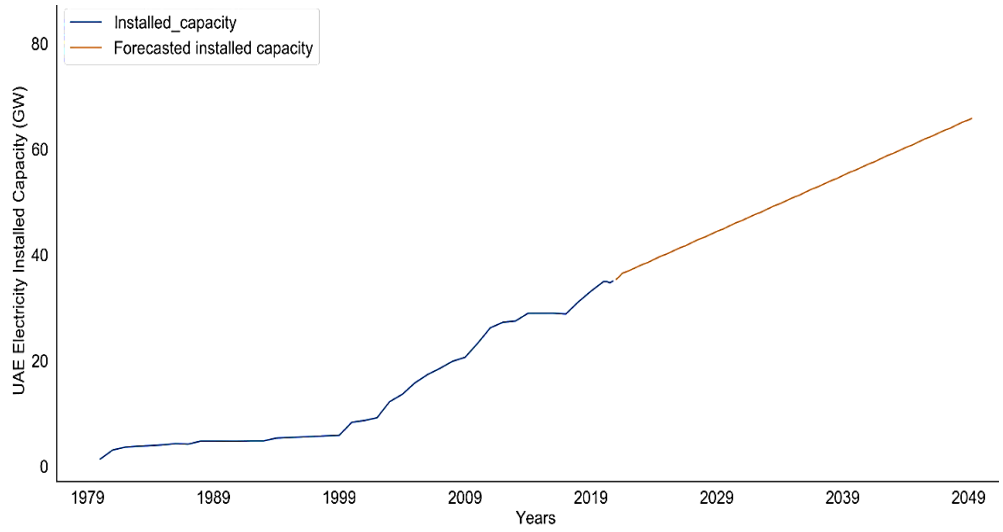

(b)

Figure A.2-8. (a) Real and forecasted values of electricity installed capacity of UEA, which show the good fit and performance of the SARIMAX model. (b) Forecasted electricity installed capacity values for 30-year period from 2021 to 2050.

Table A.2-2. Forecasting accuracy indicators for UAE prediction using the SARIMAX model.

No.	Metric	Generation (TWh)	Consumption (TWh)	Electric peak load (GW)	Installed capacity (GW)
1	RMSE	0.4	0.4	0.1	0.1
2	MAE	0.2	0.3	0.0	0.0
3	MSE	0.2	0.2	0.0	0.0
4	MAPE (%)	0.3	0.4	0.6	0.5
5	*p*-value (%)	1×10^{-12}	4×10^{-12}	2×10^{-11}	3×10^{-10}
6	R^2 (%)	99	99	99	99

A.2.3 Fossil Fuel Prediction for Kuwait Using SARIMAX Model

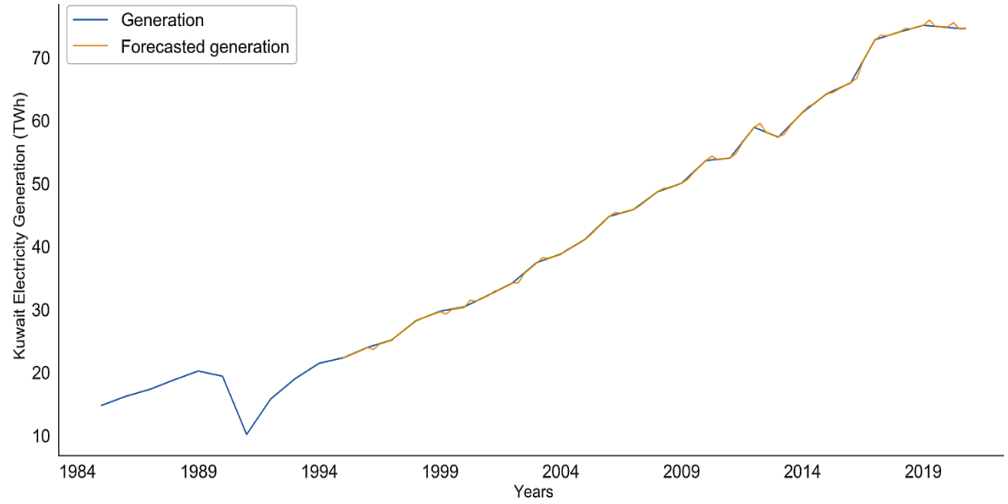

(a)

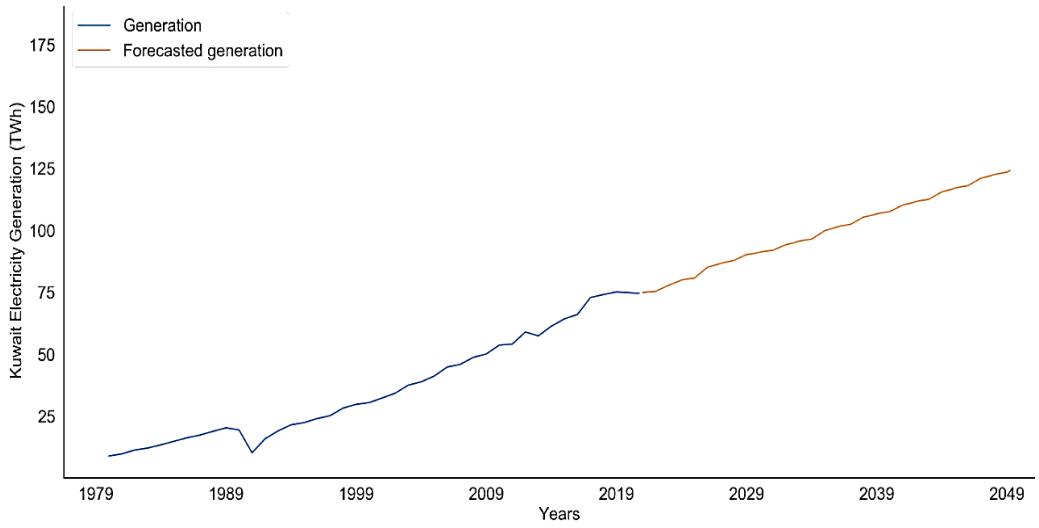

(b)

Figure A.2-9. (a) Real and forecasted values of electricity generation of Kuwait, which show the good fit and performance of the SARIMAX model. (b) Forecasted electricity generation values for 30-year period from 2021 to 2050.

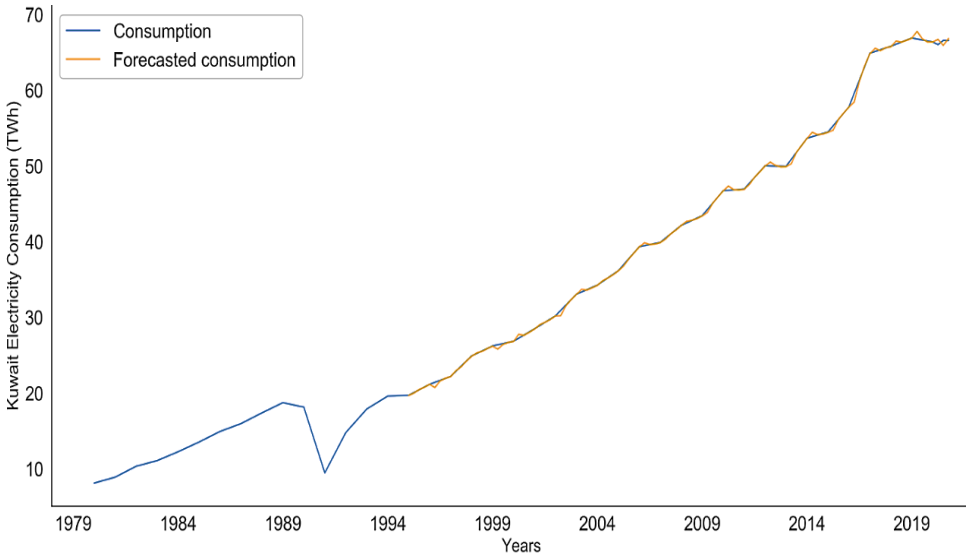

(a)

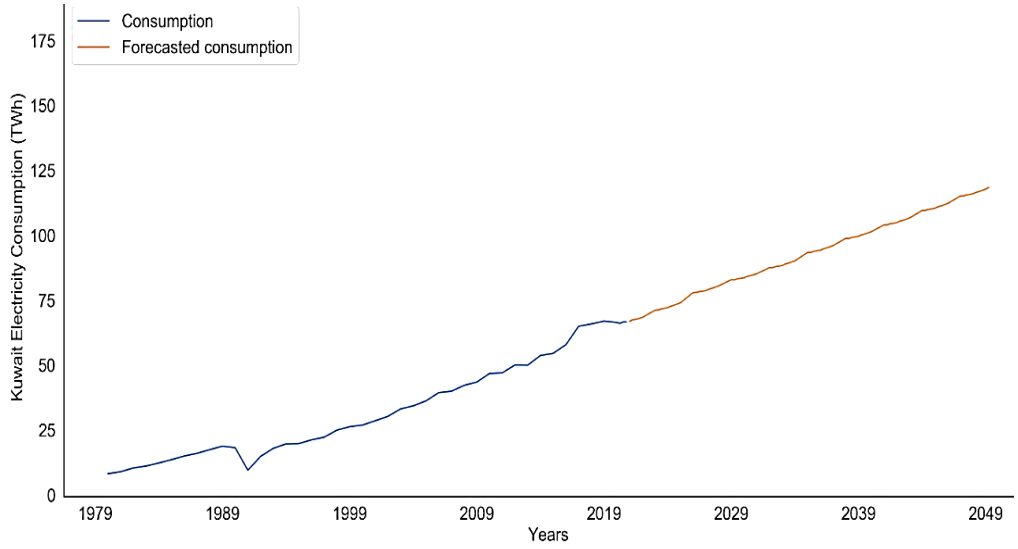

(b)

Figure A.2-10. (a) Real and forecasted values of electricity consumption of Kuwait, which show the good fit and performance of the SARIMAX model. (b) Forecasted electricity consumption values for 30-year period from 2021 to 2050.

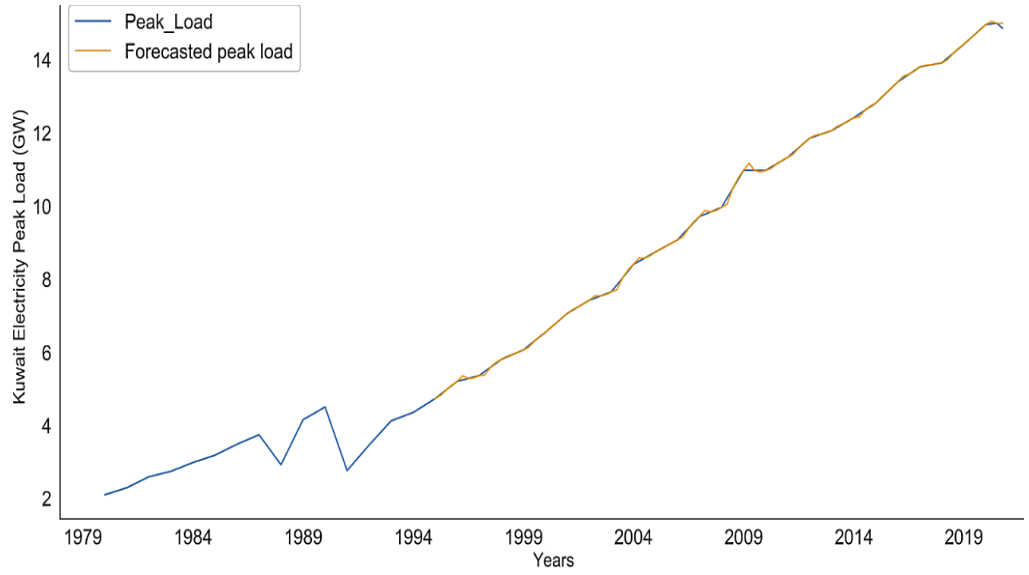

(a)

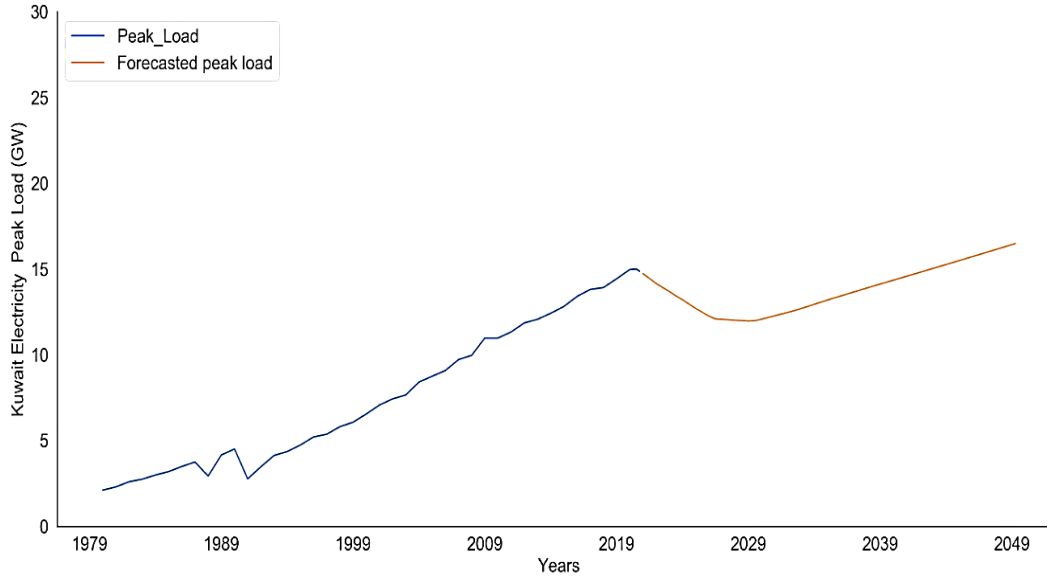

(b)

Figure A.2-11. (a) Real and forecasted values of electricity peak load of Kuwait, which show the good fit and performance of the SARIMAX model. (b) Forecasted electricity peak load values for 30-year period from 2021 to 2050.

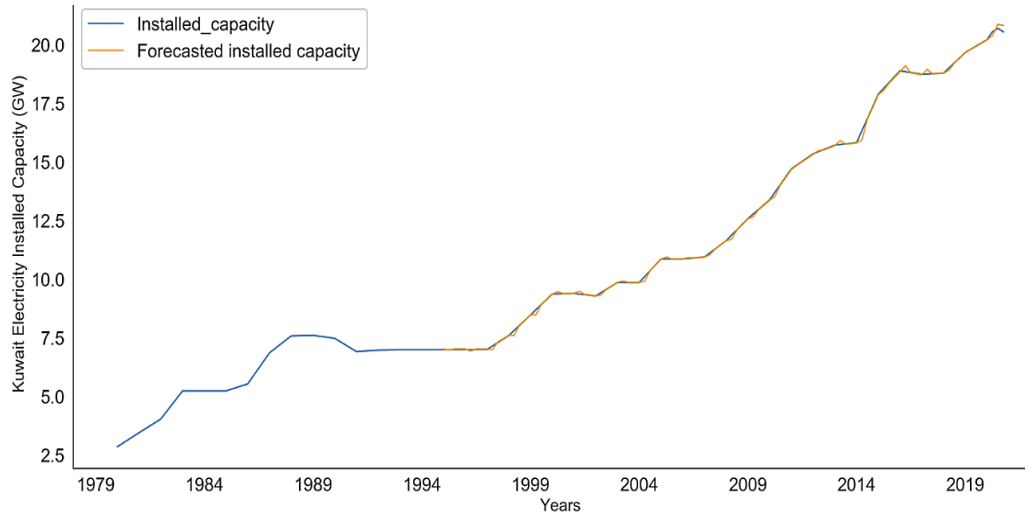

(a)

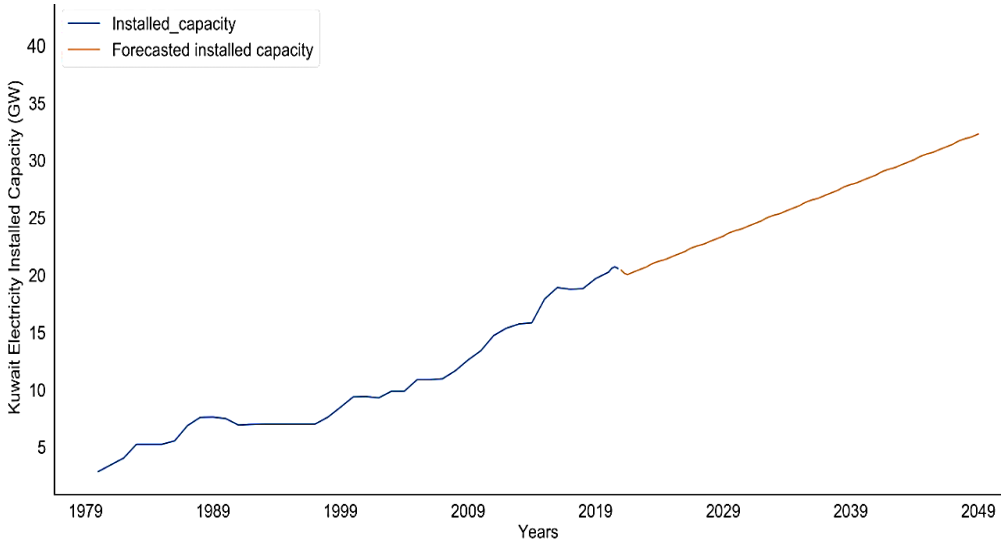

(b)

Figure A.2-12. (a) Real and forecasted values of electricity installed capacity of Kuwait, which show the good fit and performance of the SARIMAX model. (b) Forecasted electricity installed capacity values for 30-year period from 2021 to 2050.

Table A.2-3. Forecasting accuracy indicators for Kuwait prediction using the SARIMAX model.

No.	Metric	Generation (TWh)	Consumption (TWh)	Electric peak load (GW)	Installed capacity (GW)
1	RMSE	0.2	0.2	0.0	0.0
2	MAE	0.1	0.1	0.0	0.0
3	MSE	0.0	0.0	0.0	0.0
4	MAPE (%)	0.3	0.3	0.2	0.3
5	*p*-value (%)	6×10^{-8}	1.6×10^{-8}	3×10^{-11}	0.0
6	R^2 (%)	99	99	99	99

A.2.4 Fossil Fuel Prediction for Qatar Using SARIMAX Model

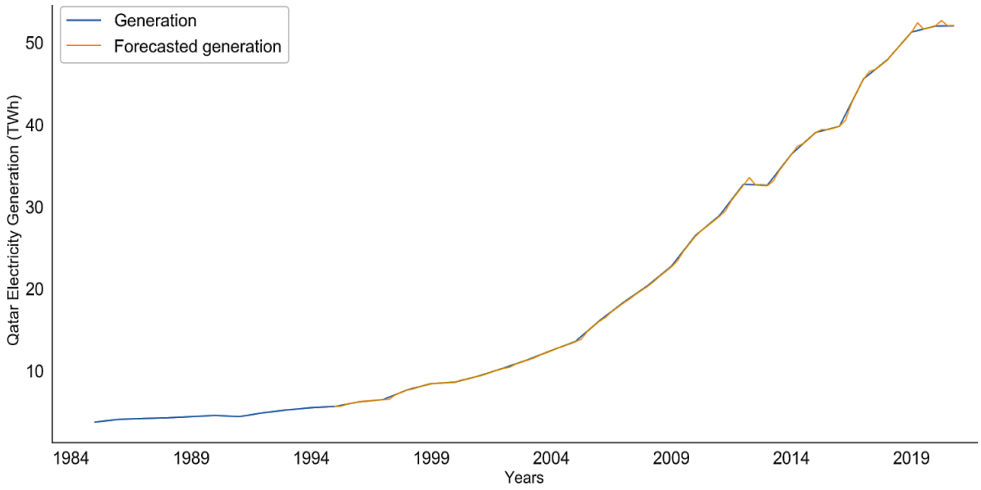

(a)

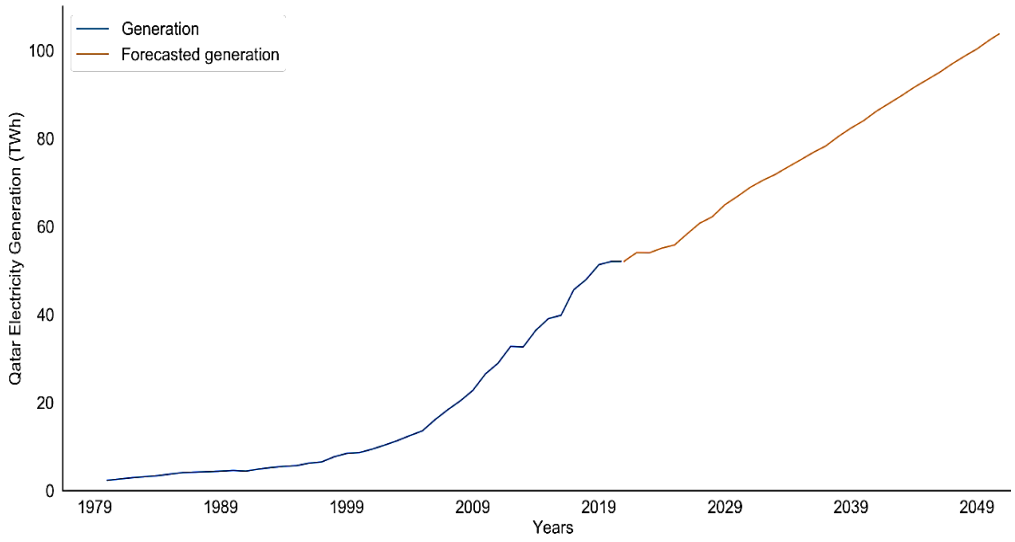

(b)

Figure A.2-13. (a) Real and forecasted values of electricity generation of Qatar, which show the good fit and performance of the SARIMAX model. (b) Forecasted electricity generation values for 30-year period from 2021 to 2050.

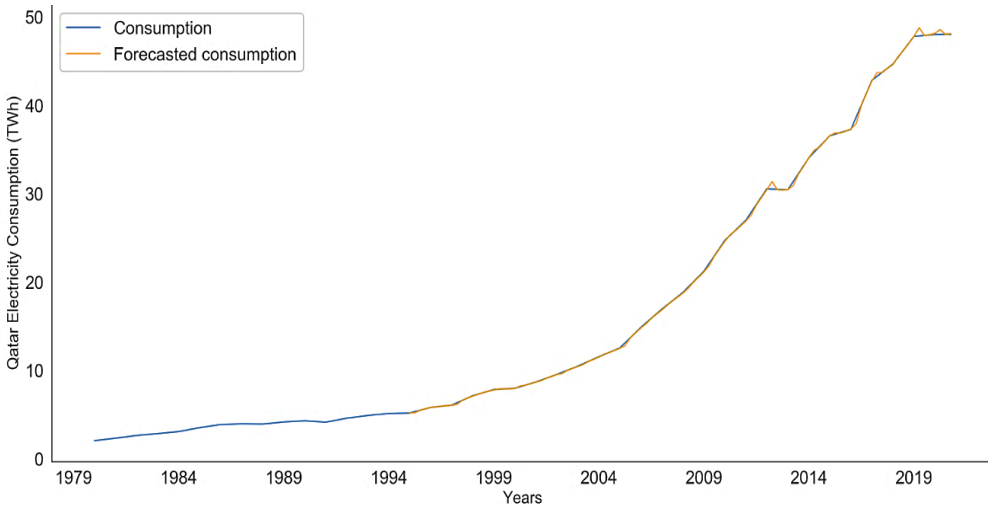

(a)

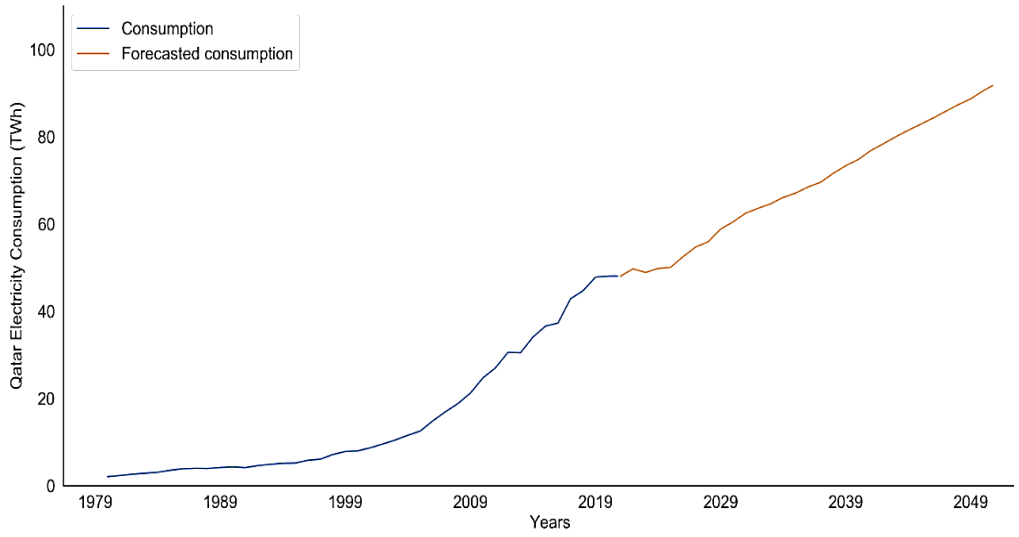

(b)

Figure A.2-14. (a) Real and forecasted values of electricity consumption of Qatar, which show the good fit and performance of the SARIMAX model. (b) Forecasted electricity consumption values for 30-year period from 2021 to 2050.

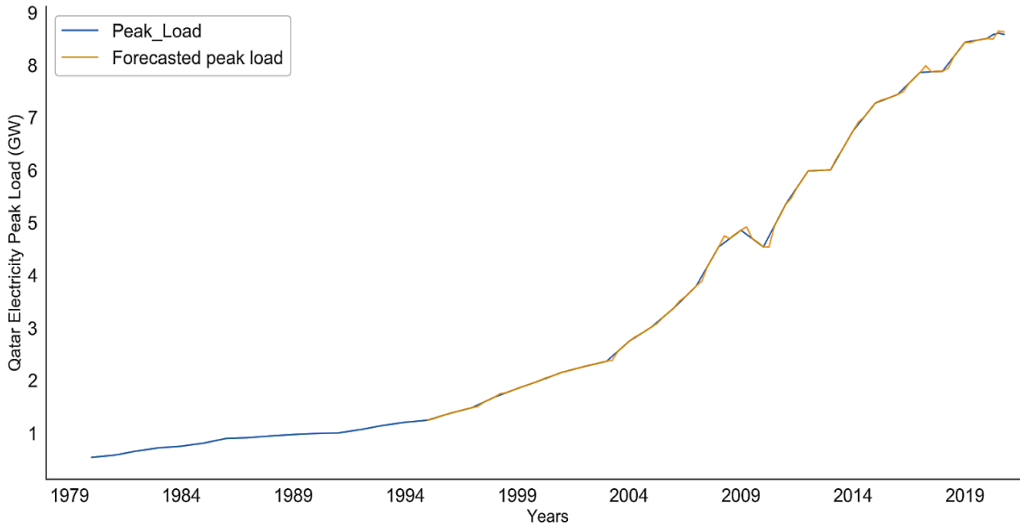

(a)

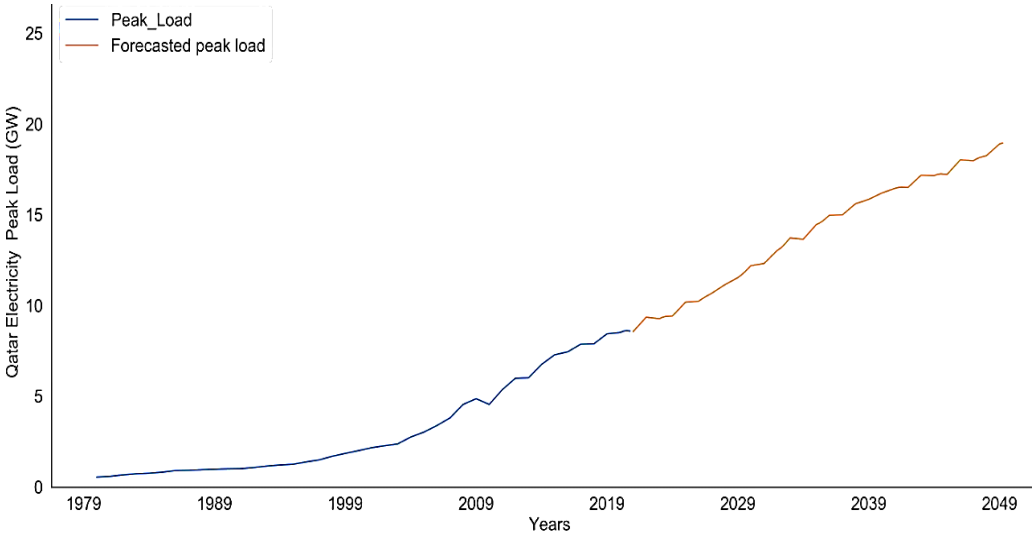

(b)

Figure A.2-15. (a) Real and forecasted values of electricity peak load of Qatar, which show the good fit and performance of the SARIMAX model. (b) Forecasted electricity peak load values for 30-year period from 2021 to 2050.

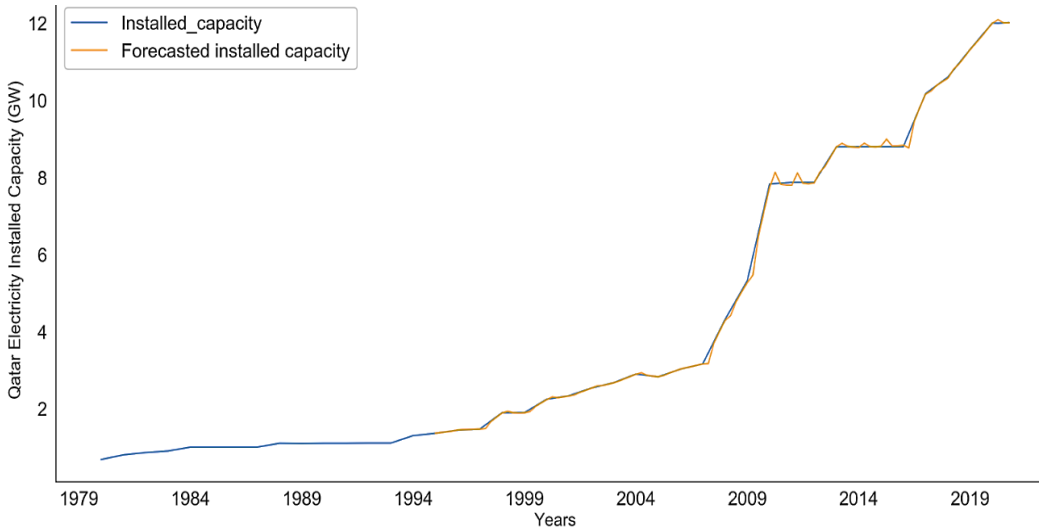

(a)

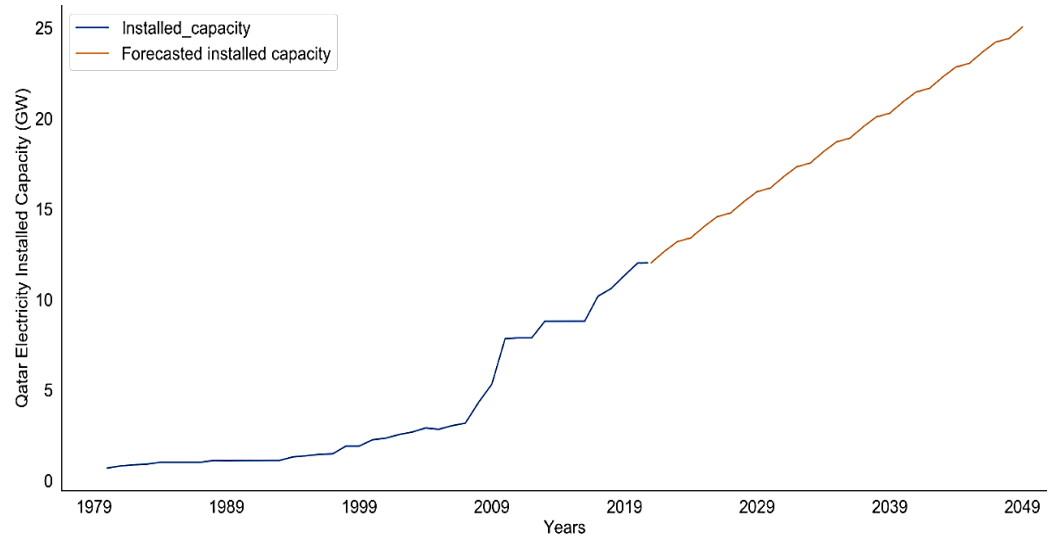

(b)

Figure A.2-16. (a) Real and forecasted values of electricity peak load of Qatar, which show the good fit and performance of the SARIMAX model. (b) Forecasted electricity peak load values for 30-year period from 2021 to 2050.

Table A.2-4. Forecasting accuracy indicators for Qatar prediction using the SARIMAX model.

No.	Metric	Generation (TWh)	Consumption (TWh)	Electric peak load (GW)	Installed capacity (GW)
1	RMSE	0.1	0.1	0.0	0.0
2	MAE	0.0	0.0	0.0	0.0
3	MSE	0.0	0.0	0.0	0.0
4	MAPE (%)	0.3	0.3	0.3	0.7
5	*p*-value (%)	0.0	0.0	8.6×10^{-8}	4.3×10^{-9}
6	R^2 (%)	99	99	99	99

A.2.5 Fossil Fuel Prediction for Bahrain Using SARIMAX Model

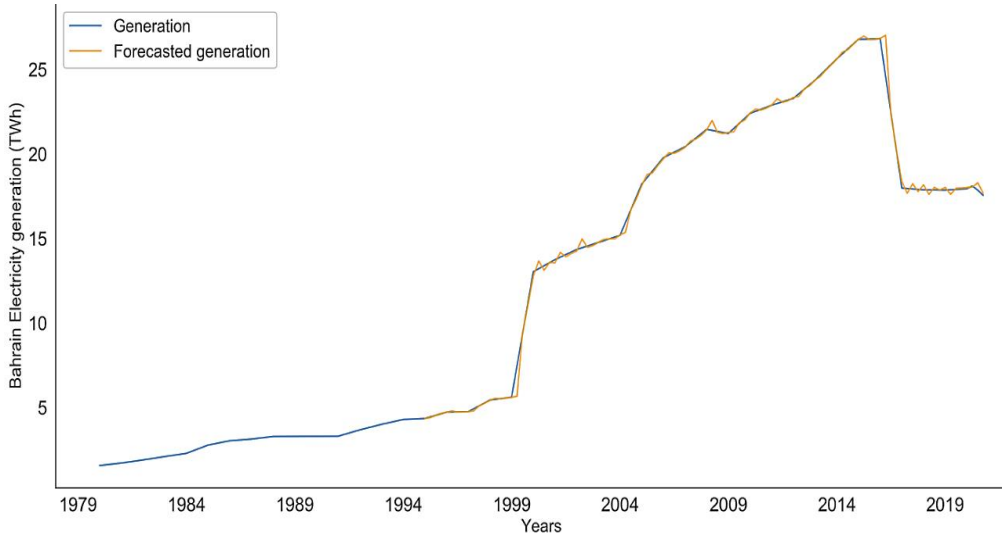

(a)

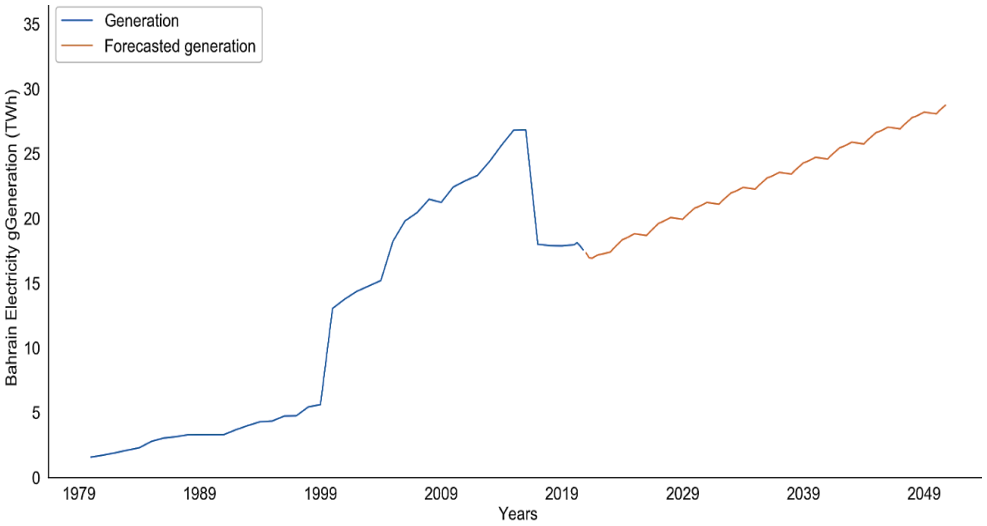

(b)

Figure A.2-17. (a) Real and forecasted values of electricity generation of Bahrain, which show the good fit and performance of the SARIMAX model. (b) Forecasted electricity generation values for 30-year period from 2021 to 2050.

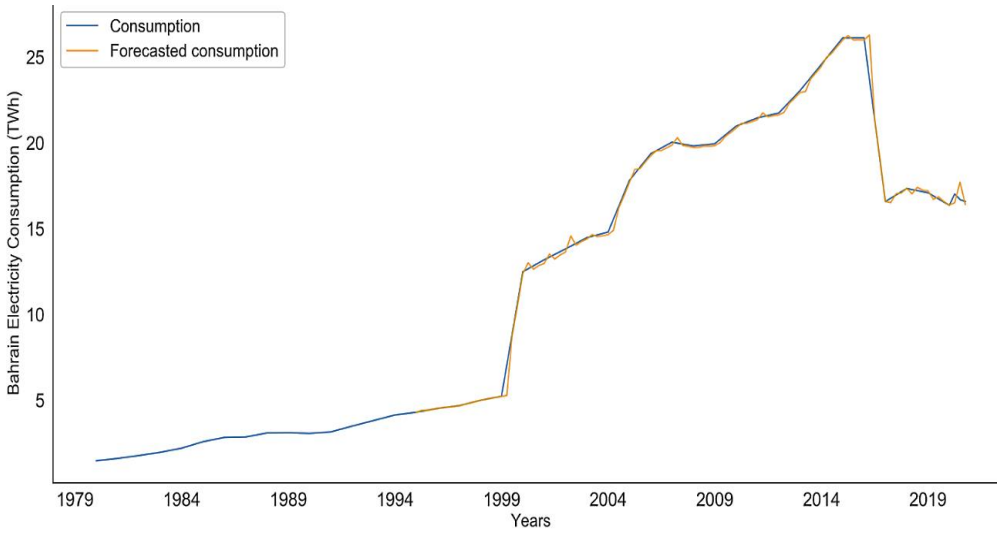

(a)

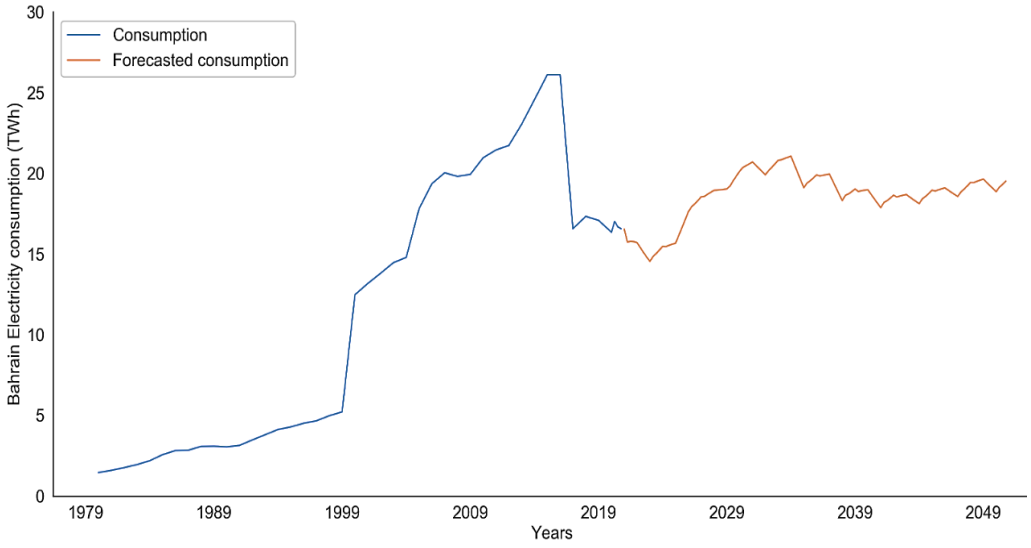

(b)

Figure A.2-18. (a) Real and forecasted values of electricity consumptionof Bahrain, which show the good fit and performance of the SARIMAX model. (b) Forecasted electricity consumption values for 30-year period from 2021 to 2050.

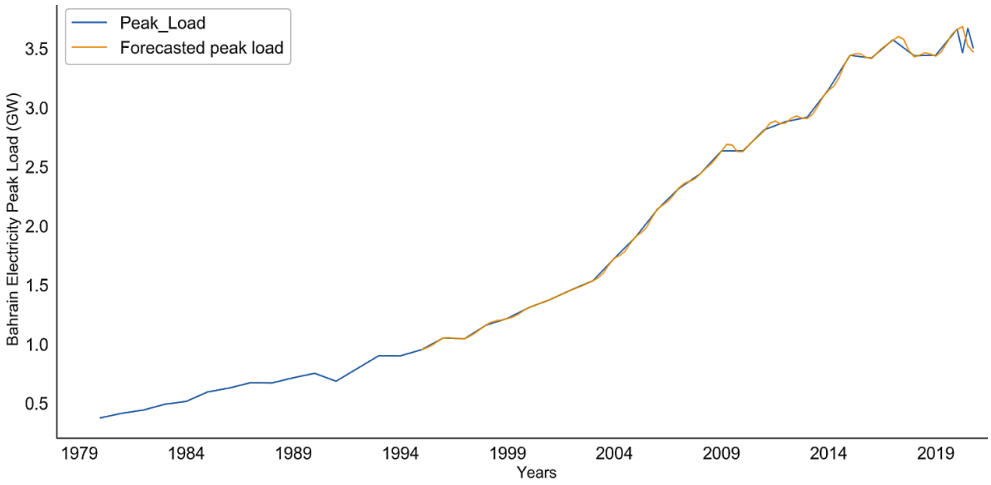

(a)

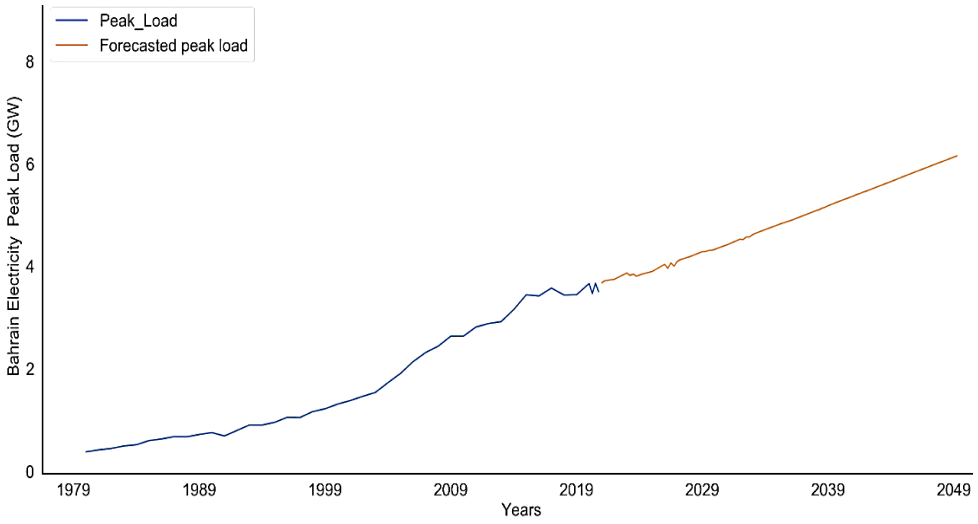

(b)

Figure A.2-19. (a) Real and forecasted values of electricity peak load for Bahrain, which show the good fit and performance of the SARIMAX model. (b) Forecasted electricity peak load values for 30-year period from 2021 to 2050.

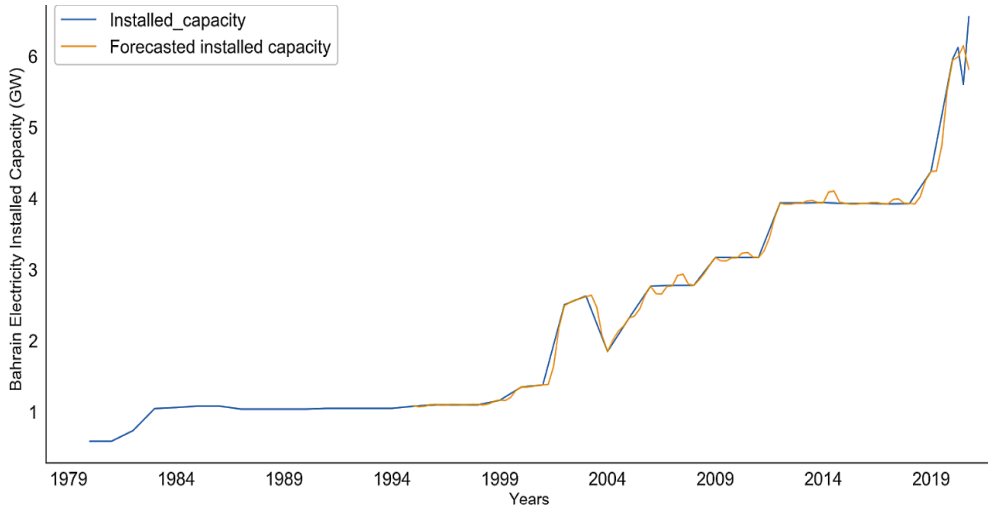

(a)

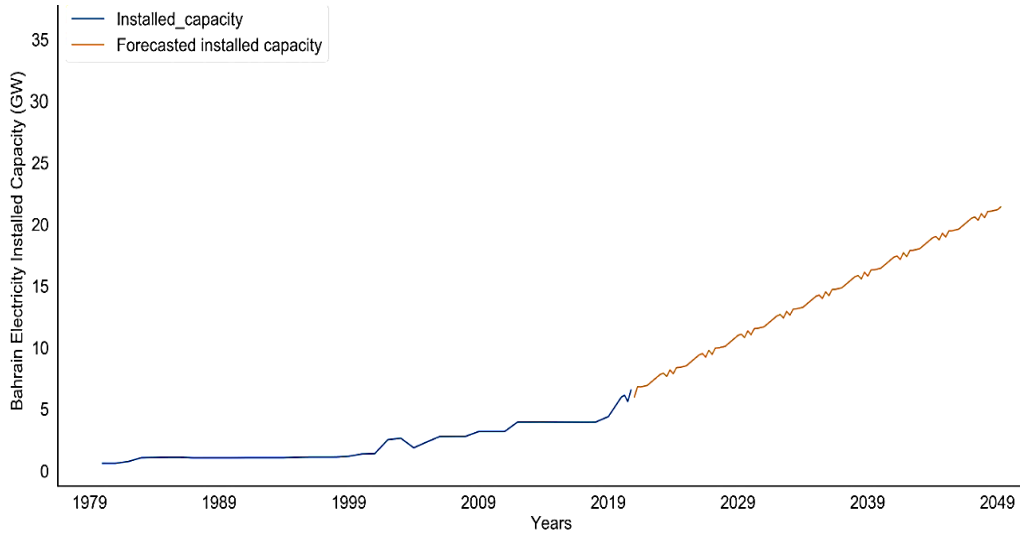

(b)

Figure A.2-20. (a) Real and forecasted values of electricity installed capacity for Bahrain, which show the good fit and performance of the SARIMAX model. (b) Forecasted electricity installed capacity values for 30-year period from 2021 to 2050.

Table A.2-5. Forecasting accuracy indicators for Bahrain prediction using the SARIMAX model.

No.	Metric	Generation (TWh)	Consumption (TWh)	Electric peak load (GW)	Installed capacity (GW)
1	RMSE	0.3	0.3	0.3	0.1
2	MAE	0.1	0.1	0.0	0.0
3	MSE	0.1	0.1	0.0	0.0
4	MAPE (%)	0.9	0.1	0.5	1.8
5	*p*-value (%)	1.2×10^{-9}	3.6×10^{-9}	0.0	5.3×10^{-8}
6	R^2 (%)	99	99	99	99

A.3 Appendix 3 – GCC Countries Future Scenario Using BI-LSTM Prediction Model

A.3.1 Solar Irradiance Prediction for Oman Using BI-LSTM Model

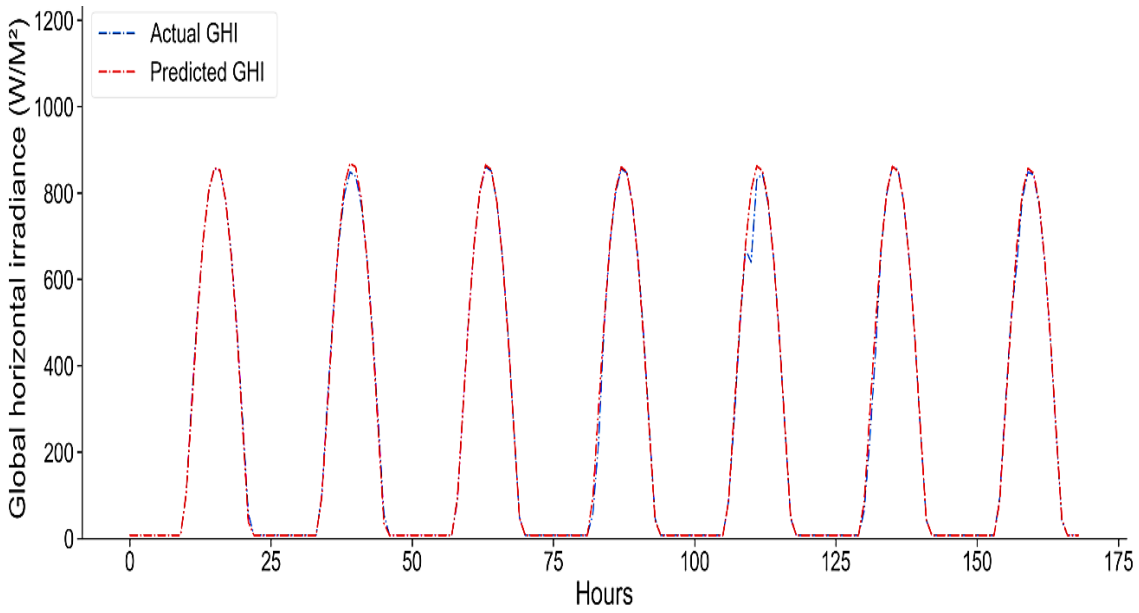

Figure A.3-1. Oman real and predicted values of GHI, which show the fit and performance of BI-LSTM model.

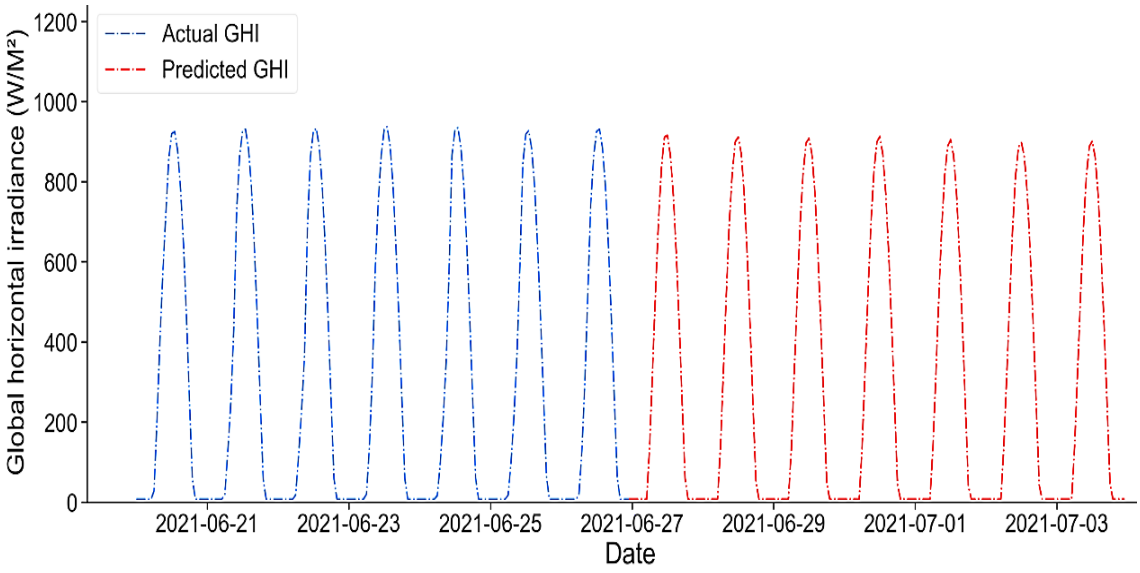

Figure A.3-2. The GHI's predicted future values for the next 169 hours for Oman.

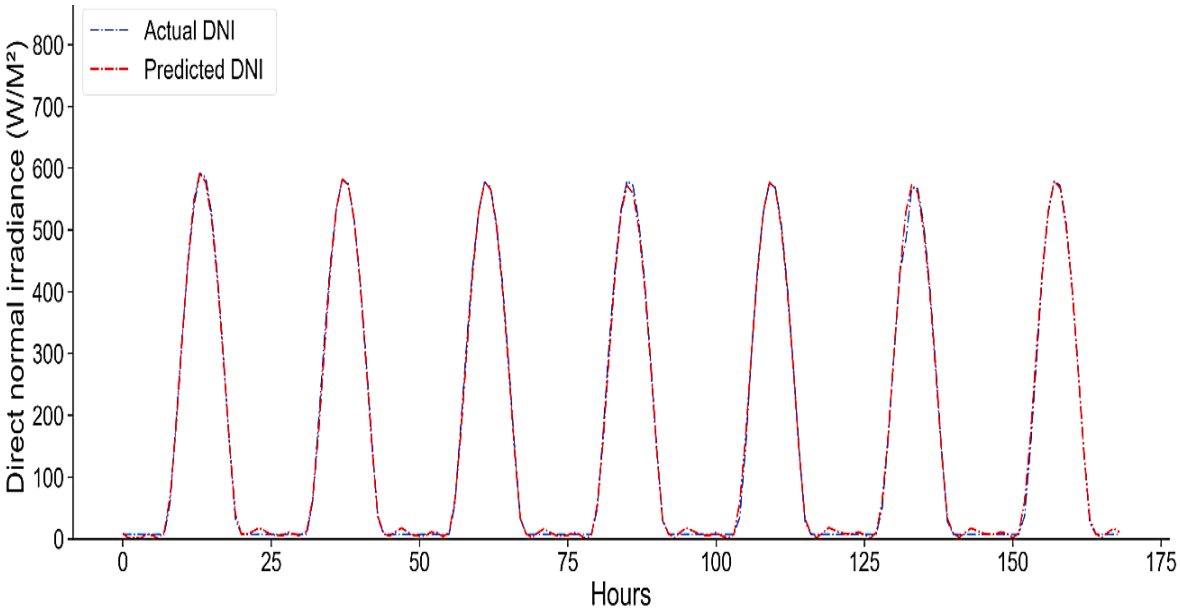

Figure A.3-3. Oman real and predicted values of DNI, which show the fit and performance of BI-LSTM model.

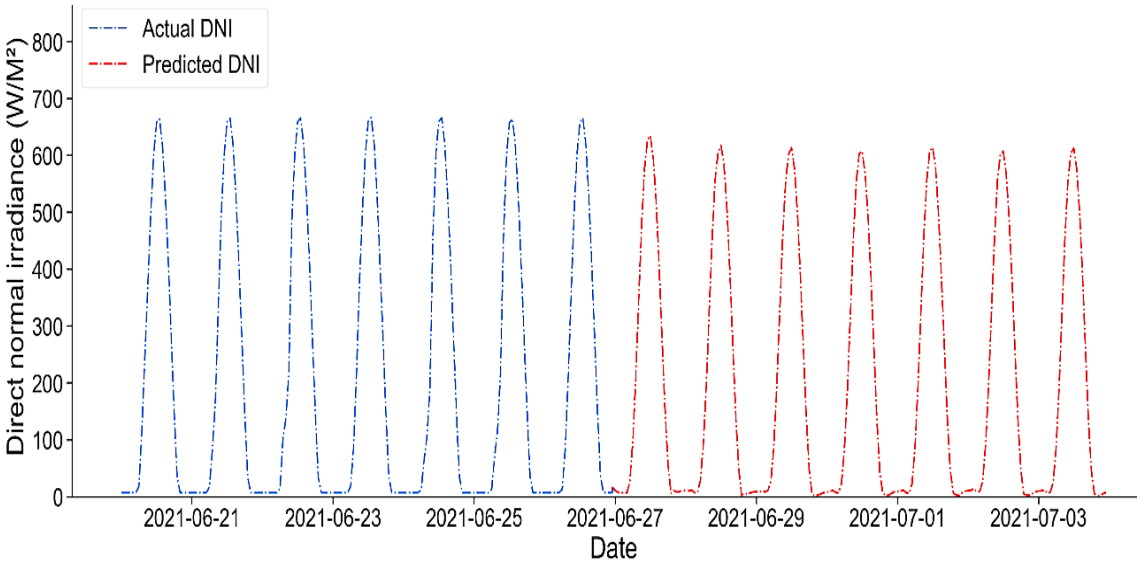

Figure A.3-4. The DNI's predicted future values for the next 169 hours for Oman.

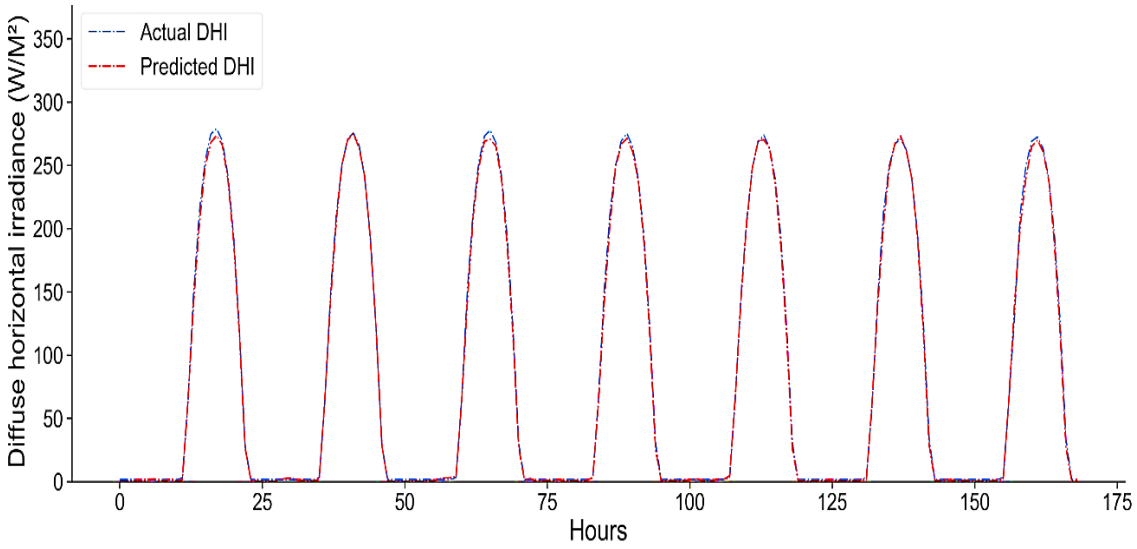

Figure A.3-5. Oman real and predicted values of DHI, which show the fit and performance of BI-LSTM model.

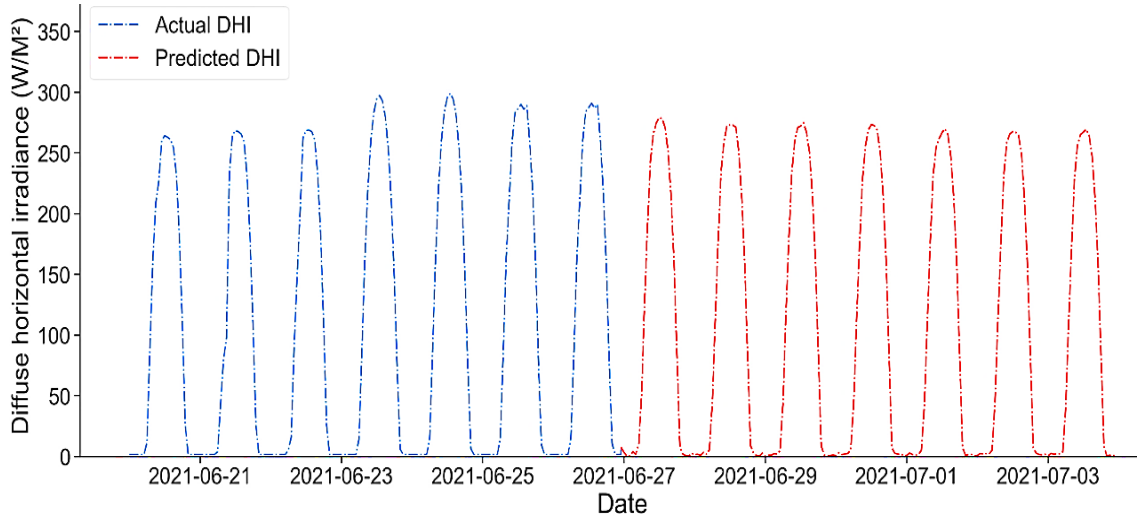

Figure A.3-6. The DHI's predicted future values for the next 169 hours for Oman.

Table A.3-1. Forecasting accuracy indicators for Oman prediction using the BI-LSTM model.

No.	Metric	GHI (W/M²)	DNI (W/M²)	DHI (W/M²)
1	RMSE	17.89	8.55	3.76
2	MAE	6.29	6.14	2.66
3	MSE	312.12	73.24	14.21
4	MAPE (%)	2.57	36.65	44.97
5	*p*-value (%)	0.00	0.00	0.00
6	R^2 (%)	99	98	99

A.3.2 Solar Irradiance Prediction for UAE Using BI-LSTM Model

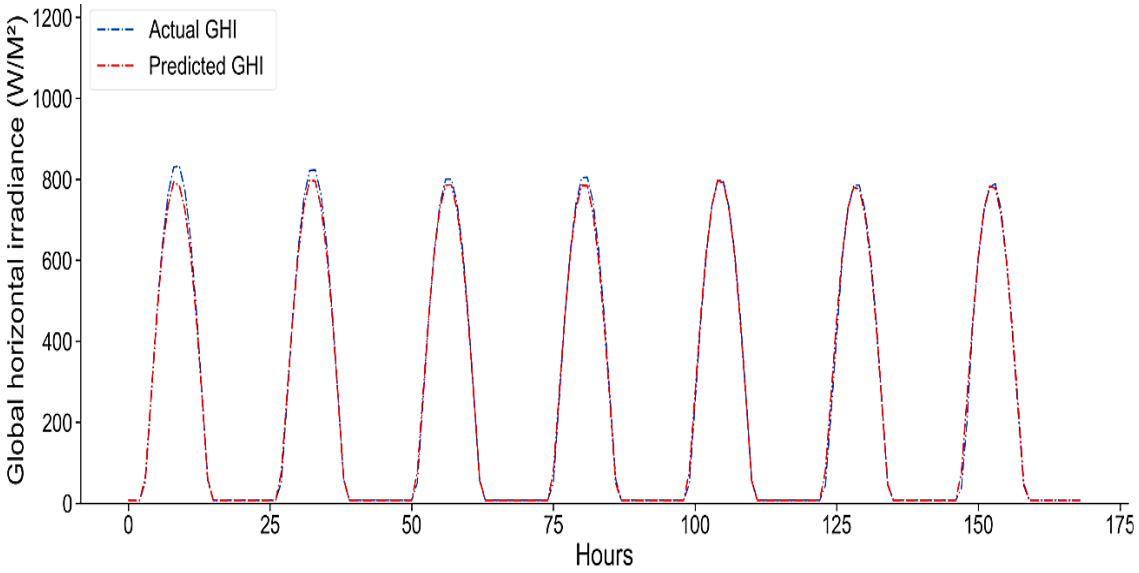

Figure A.3-7. UAE real and predicted values of GHI, which show the fit and performance of BI-LSTM model.

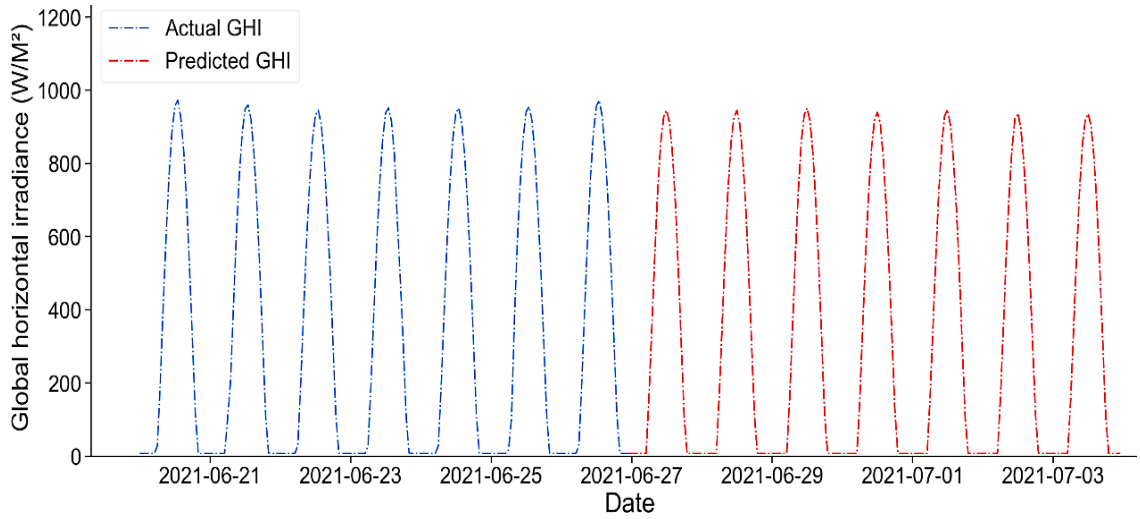

Figure A.3-8. The GHI's predicted future values for the next 169 hours for UAE.

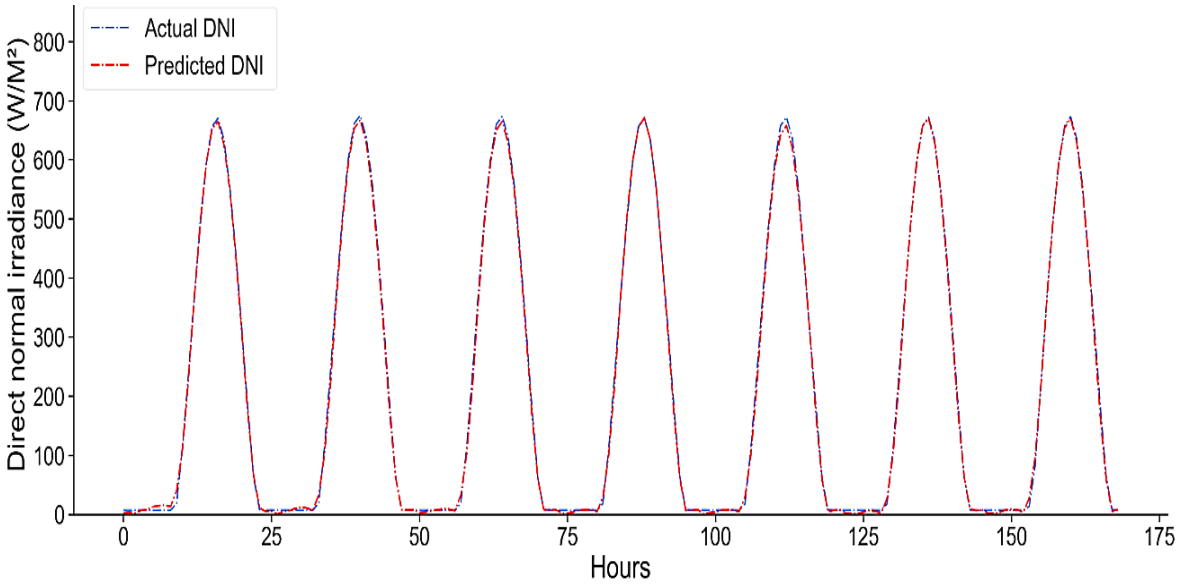

Figure A.3-9. UAE real and predicted values of DNI, which show the fit and performance of BI-LSTM model.

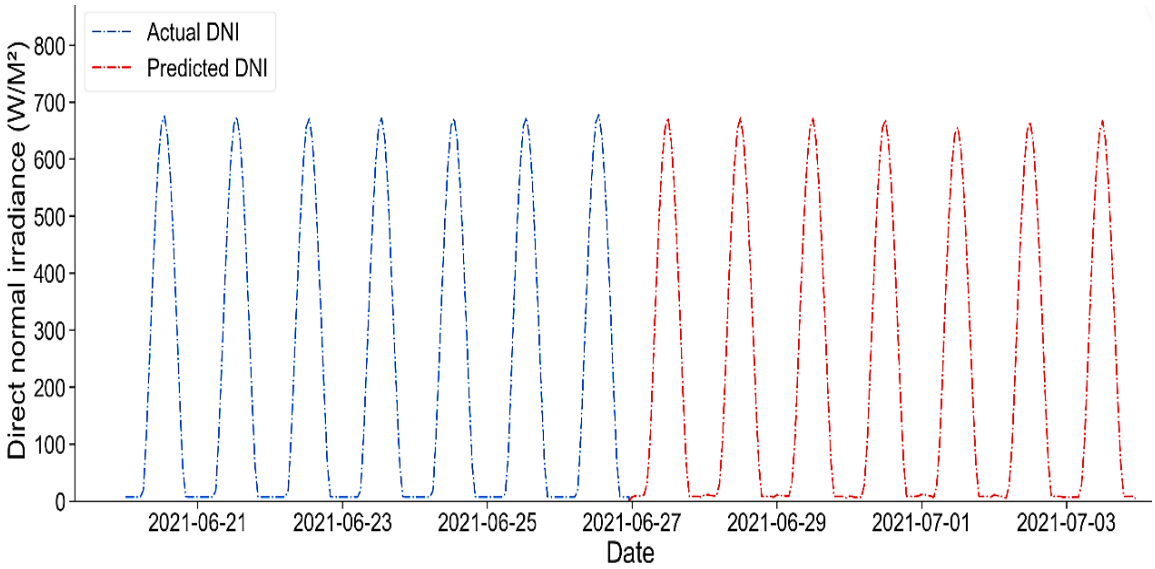

Figure A.3-10. The DNI's predicted future values for the next 169 hours for UAE.

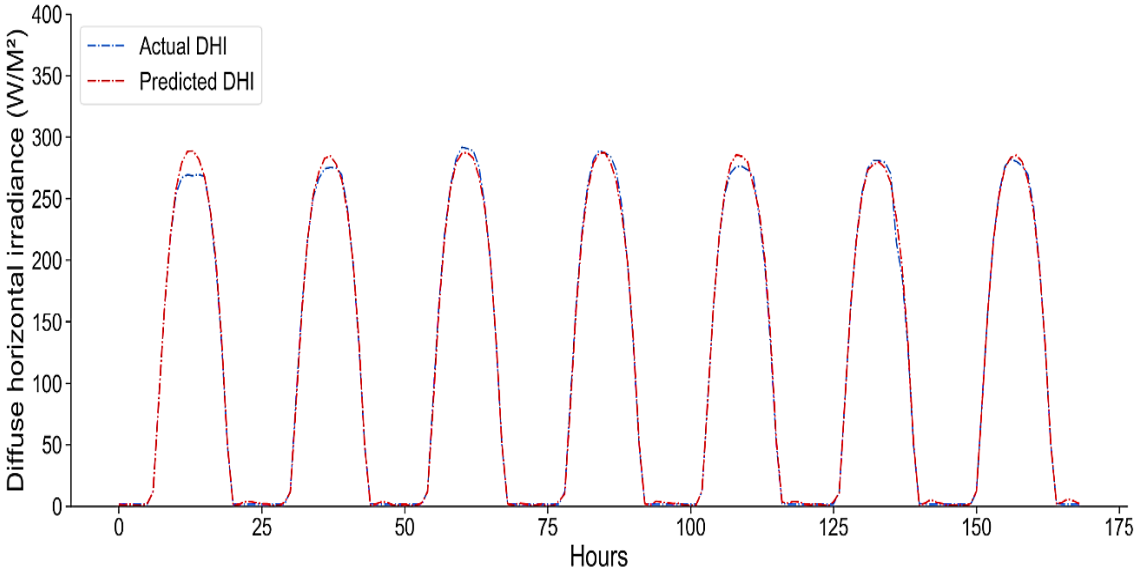

Figure A.3-11. UAE real and predicted values of DHI, which show the fit and performance of BI-LSTM model.

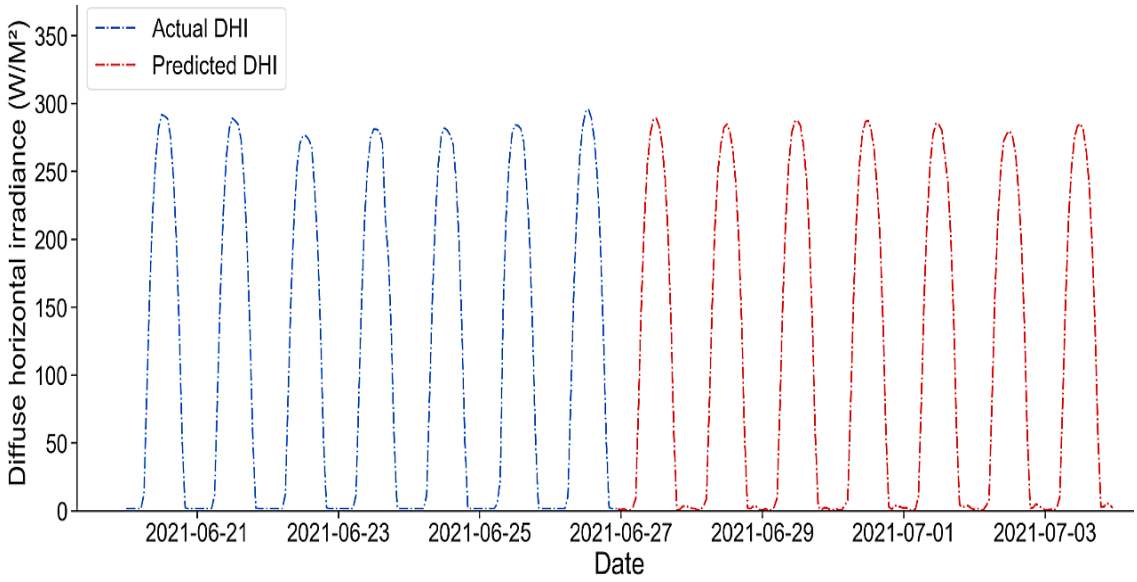

Figure A.3-12. The DHI's predicted future values for the next 169 hours for UAE.

Table A.3-2. Forecasting accuracy indicators for UAE prediction using the BI-LSTM model.

No.	Metric	GHI (W/M²)	DNI (W/M²)	DHI (W/M²)
1	RMSE	16.20	8.14	4.64
2	MAE	9.85	6.24	2.78
3	MSE	262.47	8.14	21.61
4	MAPE (%)	2.80	26.96	30.62
5	*p*-value (%)	2.72×10^{-28}	8.66×10^{-30}	2.27×10^{-28}
6	R^2 (%)	99	99	99

A.3.3 Solar Irradiance Prediction for Kuwait Using BI-LSTM Model

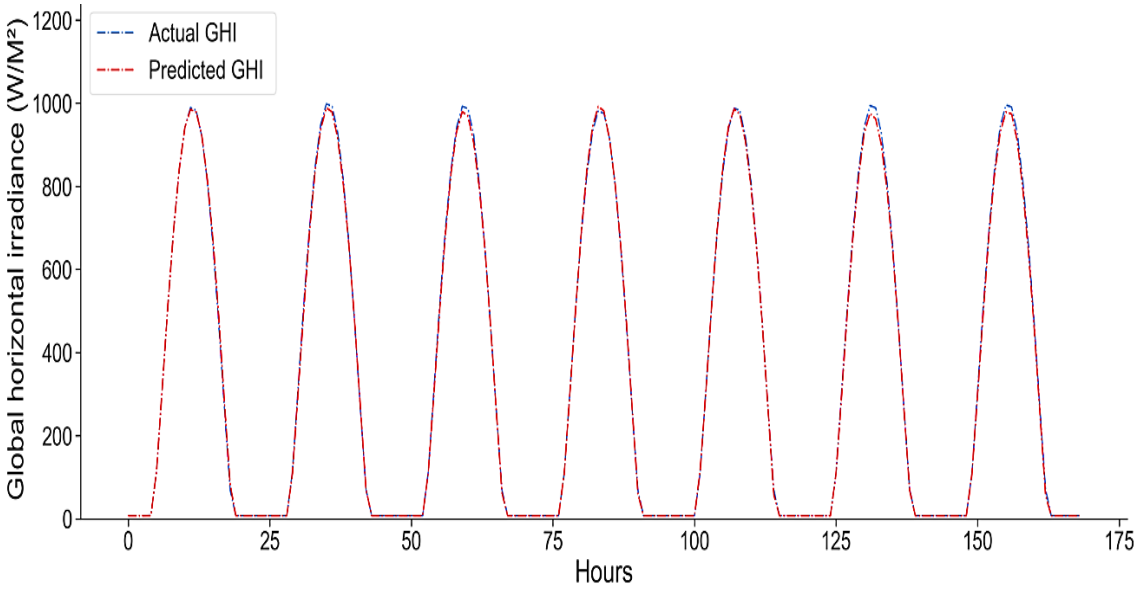

Figure A.3-13. Kuwait real and predicted values of GHI, which show the fit and performance of BI-LSTM model.

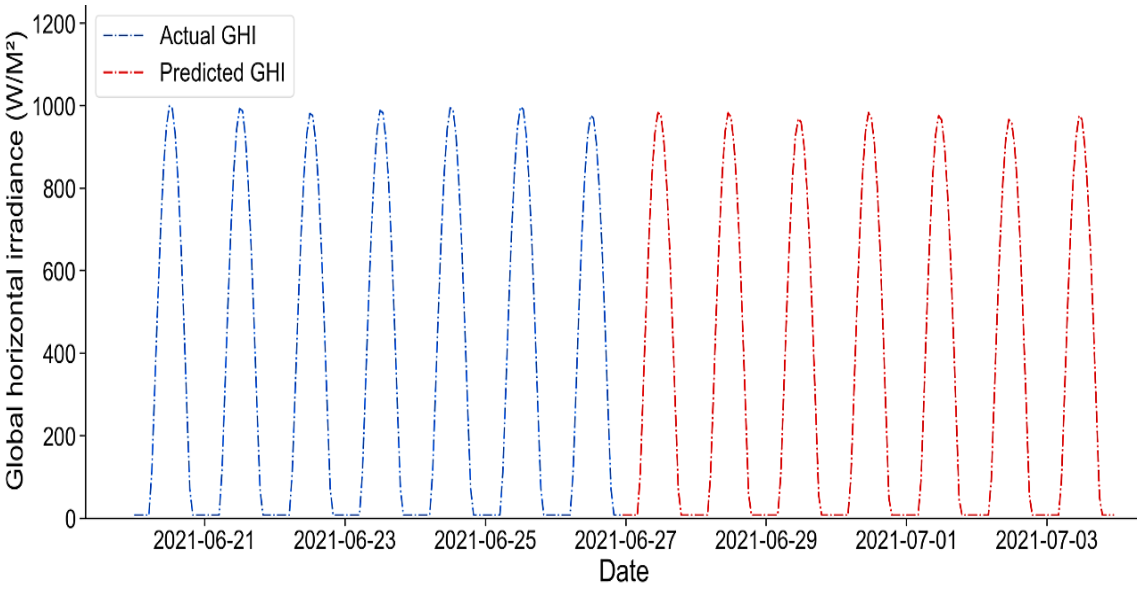

Figure A.3-14. The GHI's predicted future values for the next 169 hours for Kuwait.

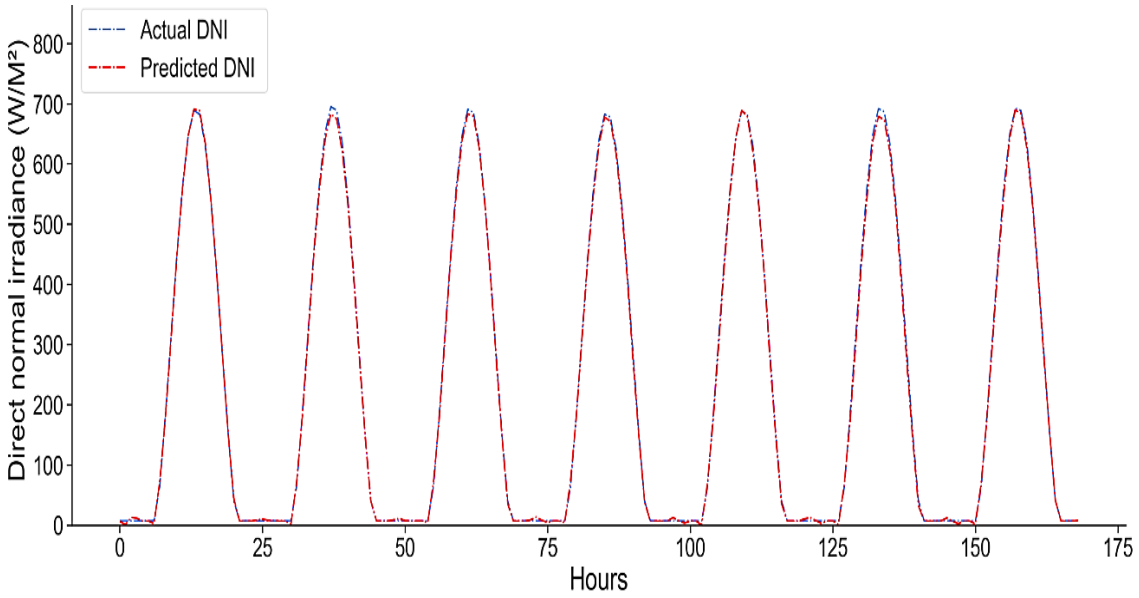

Figure A.3-15. Kuwait real and predicted values of DNI, which show the fit and performance of BI-LSTM model.

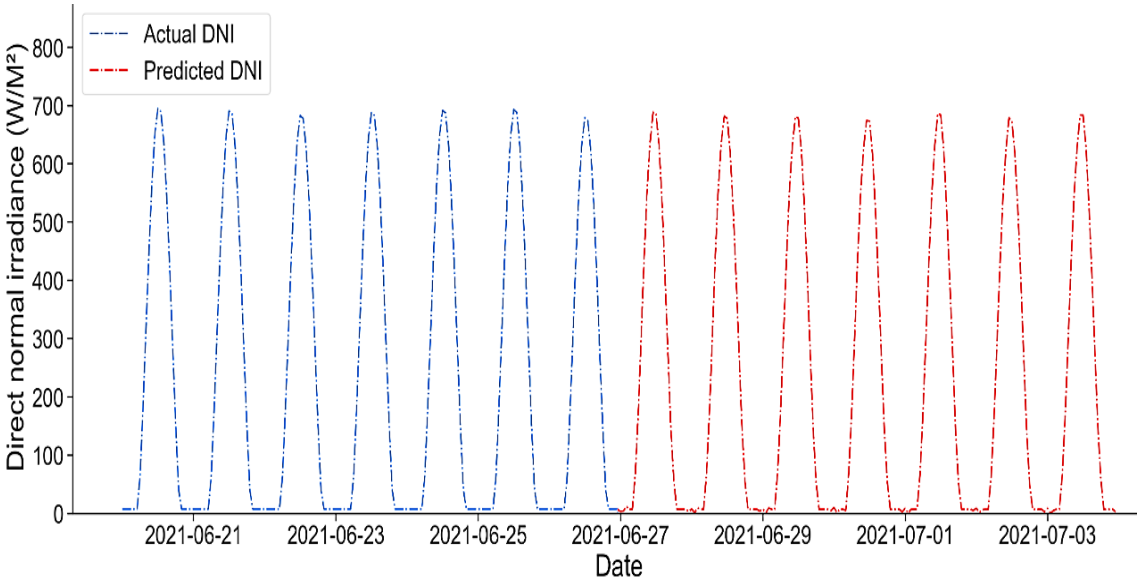

Figure A.3-16. The DHI's predicted future values for the next 169 hours for Kuwait.

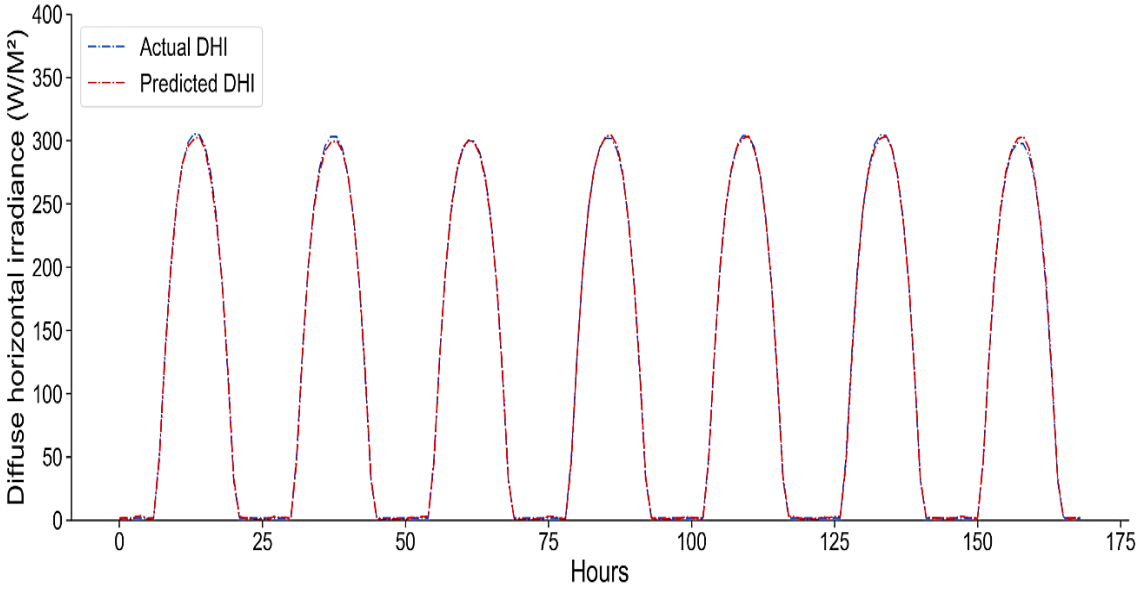

Figure A.3-17. Kuwait real and predicted values of DHI, which show the fit and performance of BI-LSTM model.

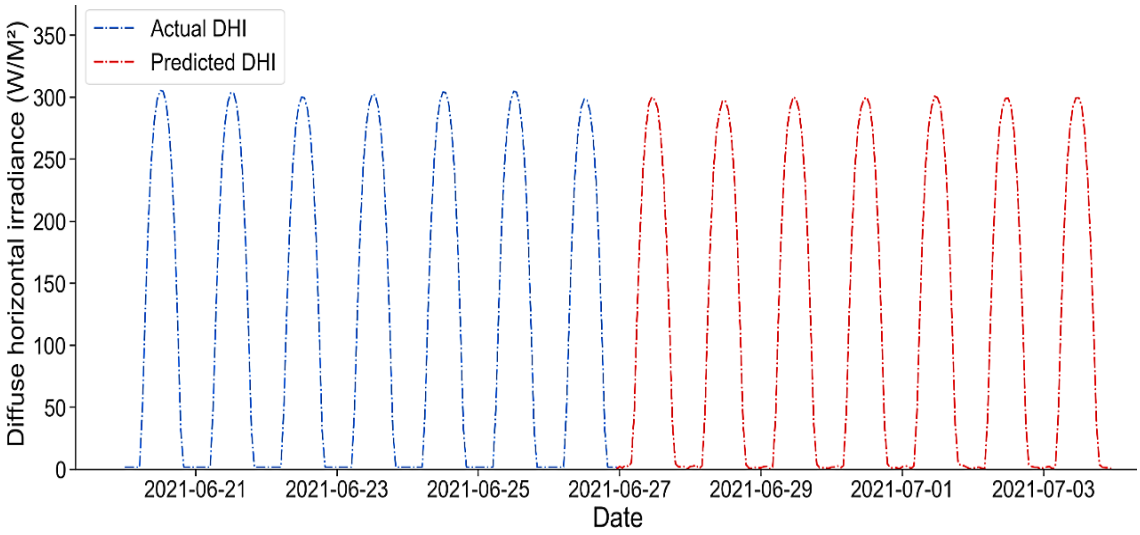

Figure A.3-18. The DHI's predicted future values for the next 169 hours for Kuwait.

Table A.3-3. Forecasting accuracy indicators for Kuwait prediction using the BI-LSTM model.

No.	Metric	GHI (W/M²)	DNI (W/M²)	DHI (W/M²)
1	RMSE	8.52	9.08	1.66
2	MAE	5.36	7.72	1.22
3	MSE	72.72	82.62	2.77
4	MAPE (%)	1.46	32.07	28.53
5	*p*-value (%)	2.47×10^{-27}	2.13×10^{-29}	1.92×10^{-25}
6	R^2 (%)	99	99	99

A.3.4 Solar Irradiance Prediction for Qatar Using BI-LSTM Model

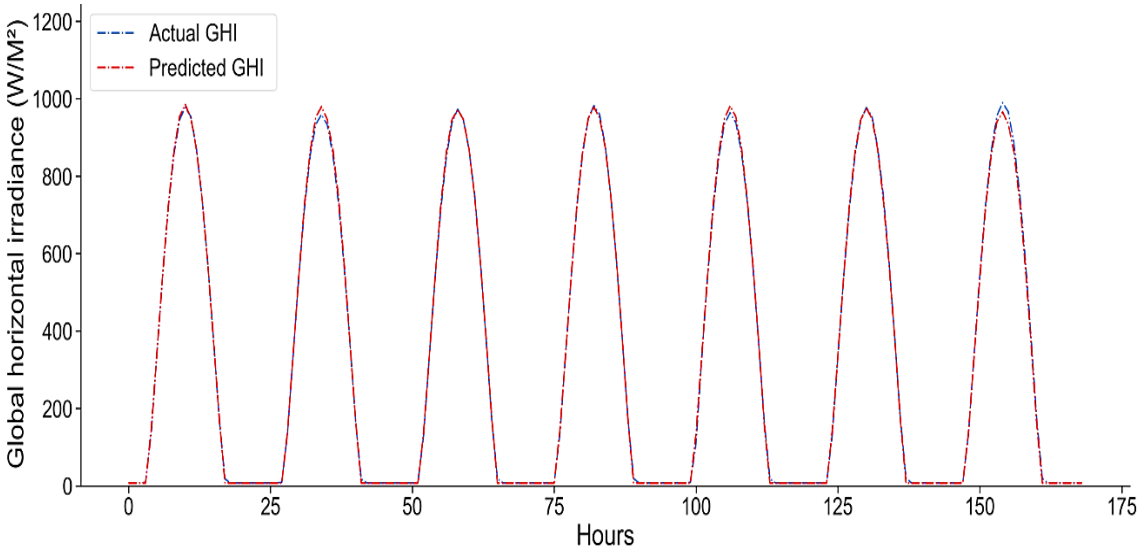

Figure A.3-19. Qatar real and predicted values of GHI, which show the fit and performance of BI-LSTM model.

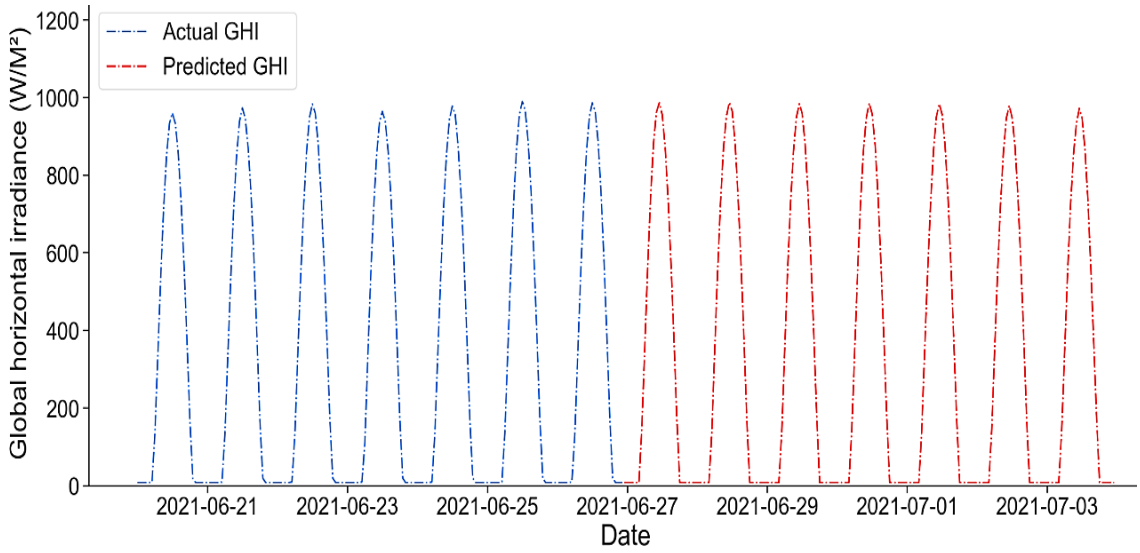

Figure A.3-20. The GHI's predicted future values for the next 169 hours for Qatar.

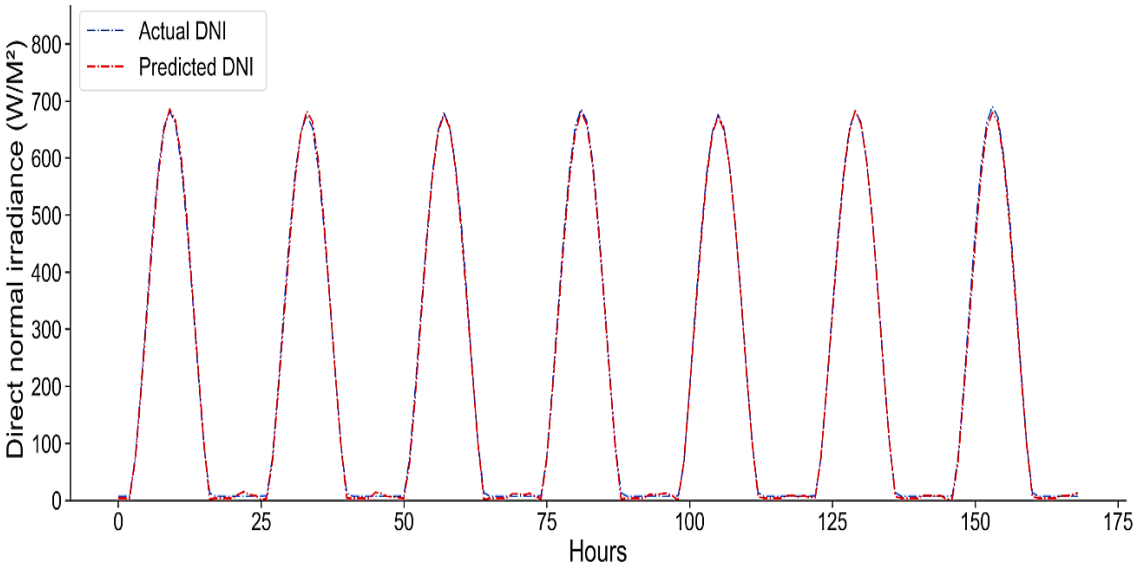

Figure A.3-21. Qatar real and predicted values of DNI, which show the fit and performance of BI-LSTM model.

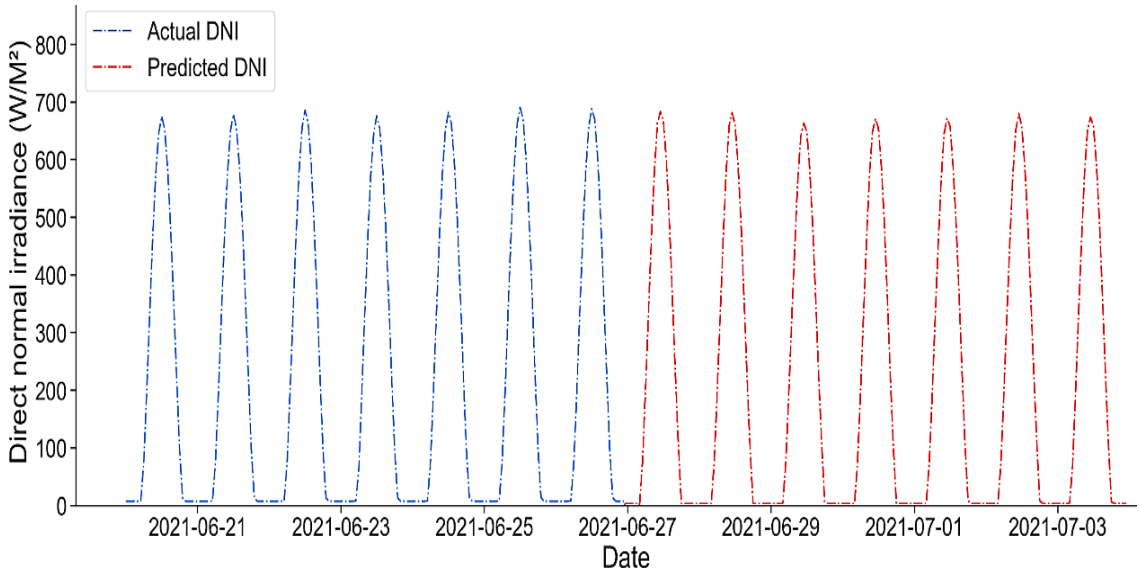

Figure A.3-22. The DHI's predicted future values for the next 169 hours for Qatar.

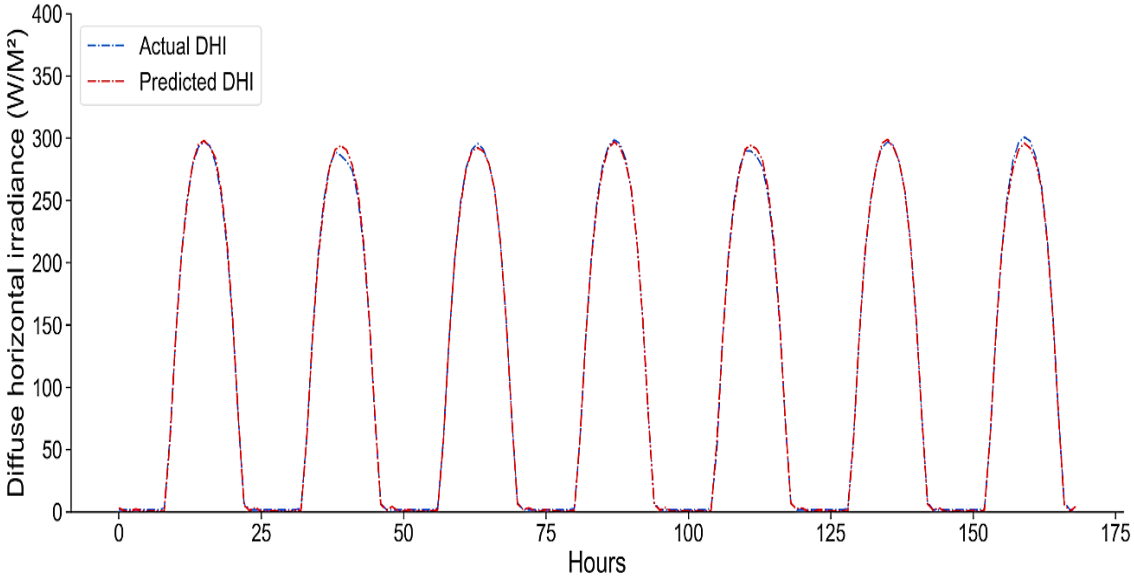

Figure A.3-23. Qatar real and predicted values of DHI, which show the fit and performance of BI-LSTM model.

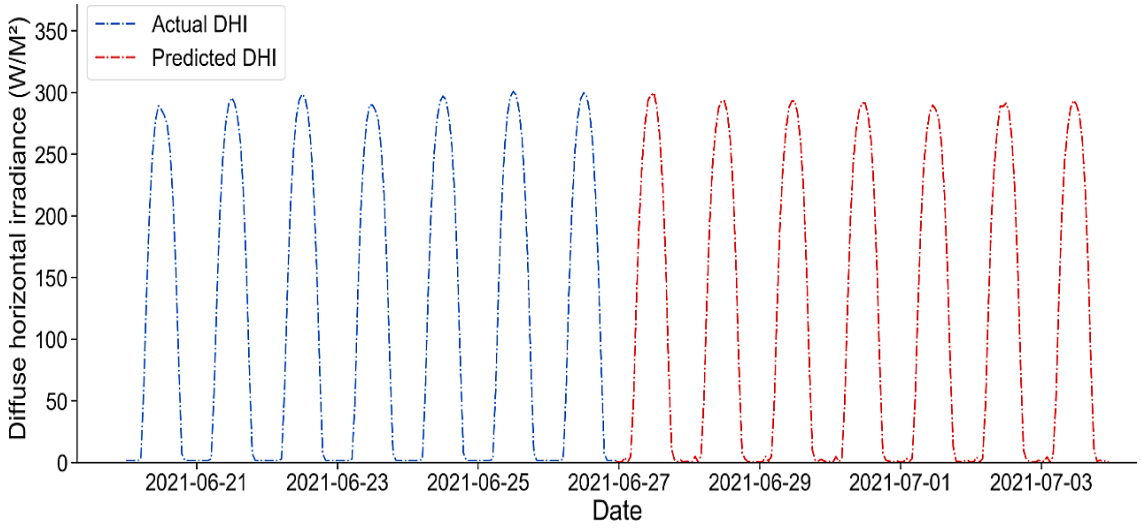

Figure A.3-24. The DHI's predicted future values for the next 169 hours for Qatar.

Table A.3-4. Forecasting accuracy indicators for Qatar prediction using the BI-LSTM model.

No.	Metric	GHI (W/M²)	DNI (W/M²)	DHI (W/M²)
1	RMSE	8.08	8.92	2.59
2	MAE	4.93	7.50	1.99
3	MSE	65.63	79.53	6.71
4	MAPE (%)	4.45	44.42	36.70
5	*p*-value (%)	2.88×10^{-27}	2.60×10^{-29}	9.49×10^{-27}
6	R^2 (%)	99	99	99

A.3.5 Solar Irradiance Prediction for Bahrain Using BI-LSTM Model

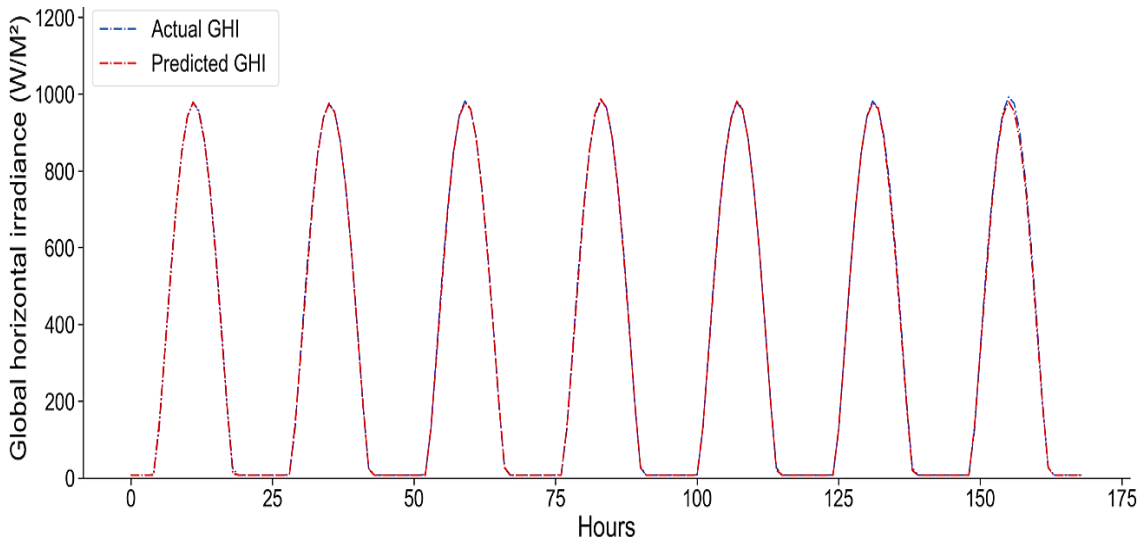

Figure A.3-25. Bahrain real and predicted values of GHI, which show the fit and performance of BI-LSTM model.

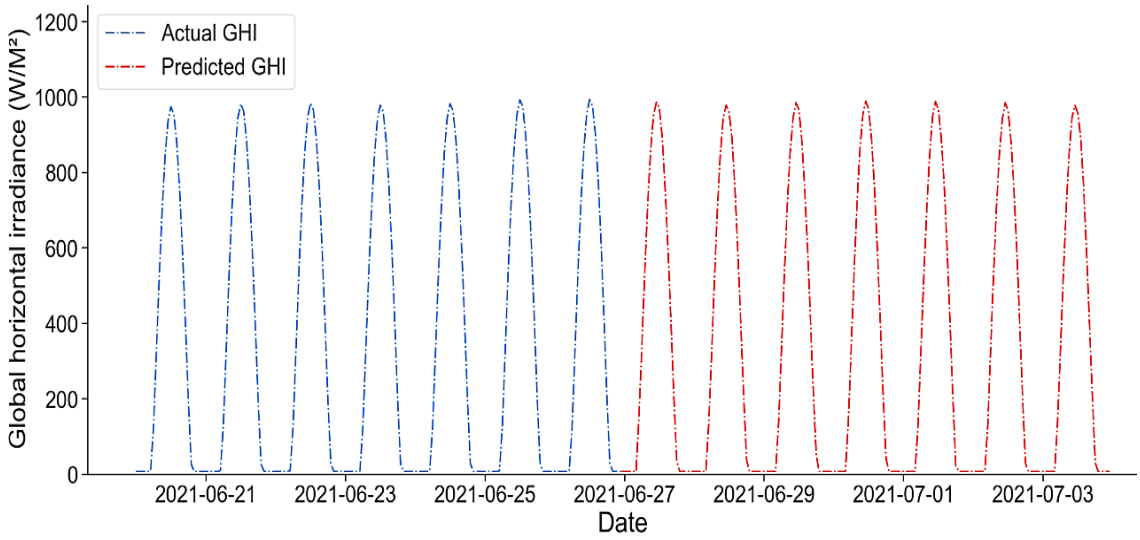

Figure A.3-26. The GHI's predicted future values for the next 169 hours for Bahrain.

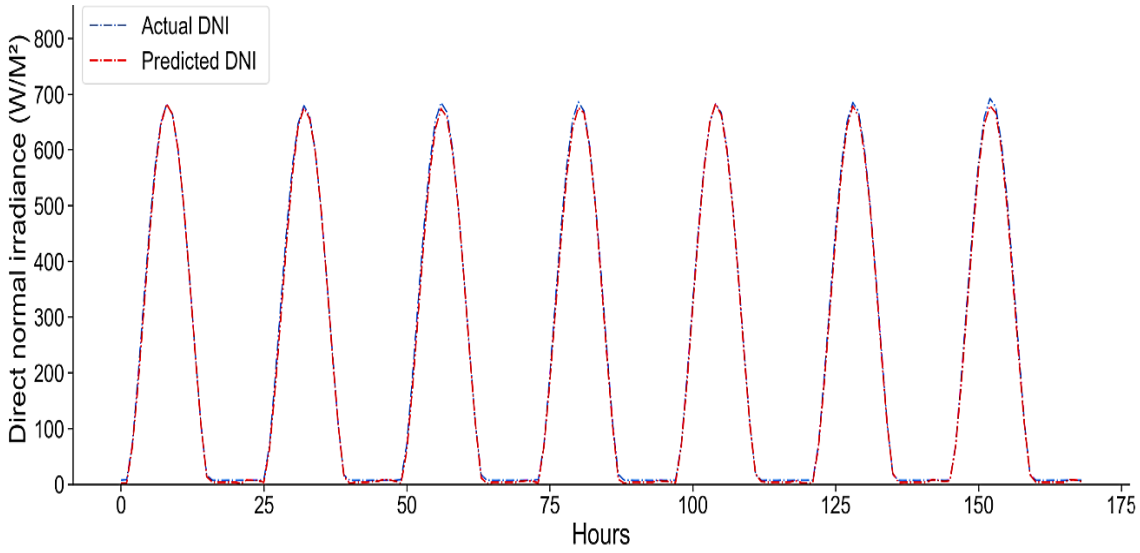

Figure A.3-27. Bahrain real and predicted values of DNI, which show the fit and performance of BI-LSTM model.

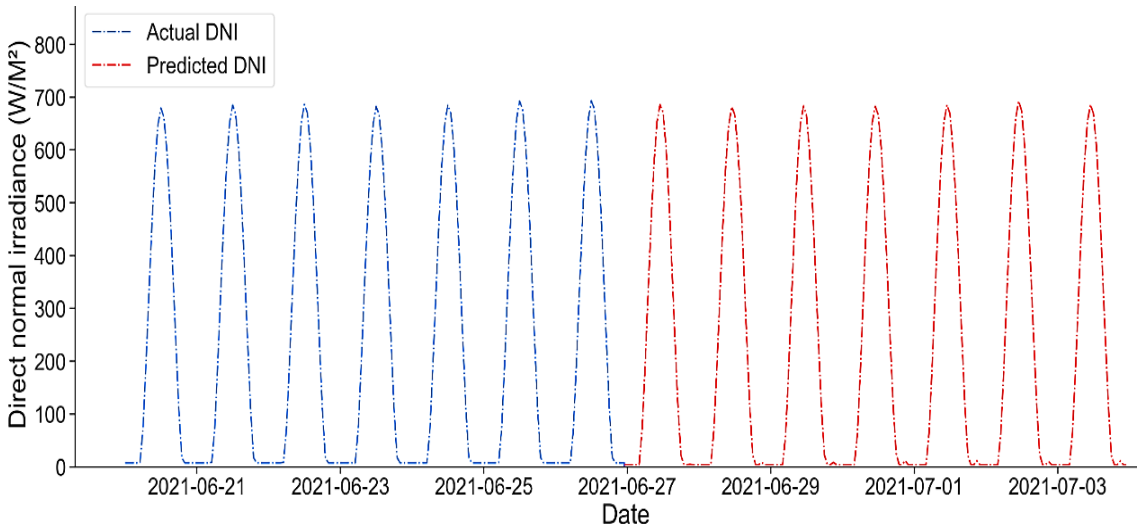

Figure A.3-28. The DHI's predicted future values for the next 169 hours for Bahrain.

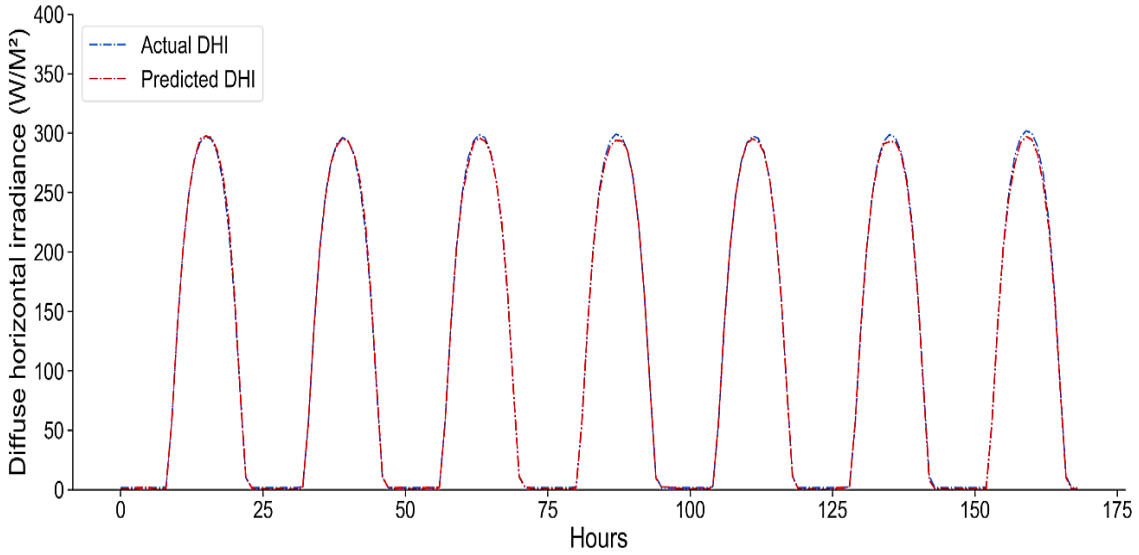

Figure A.3-29. Bahrain real and predicted values of DHI, which show the fit and performance of BI-LSTM model.

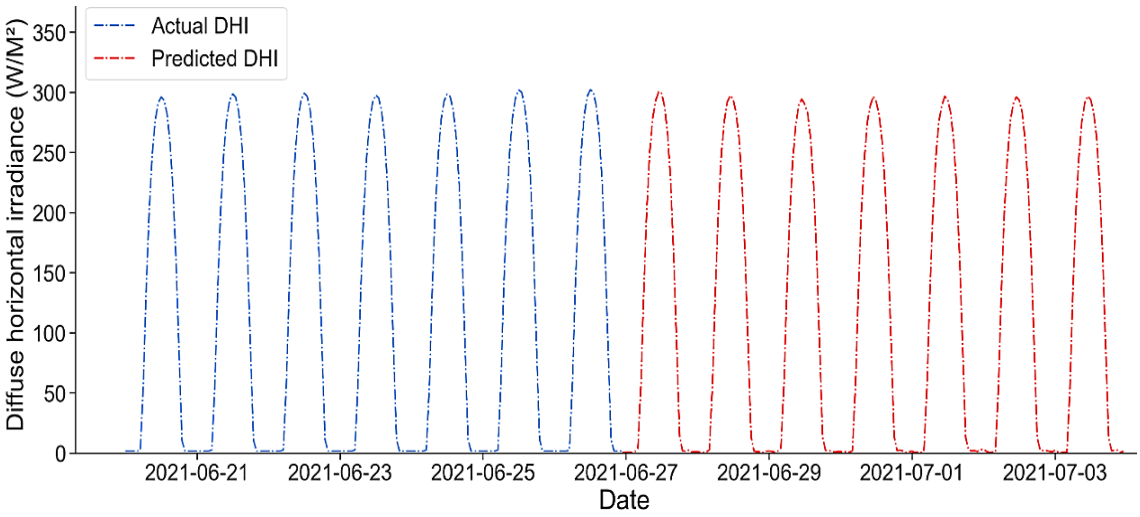

Figure A.3-30. The DHI's predicted future values for the next 169 hours for Bahrain.

Table A.3-5. Forecasting accuracy indicators for Bahrain prediction using the BI-LSTM model.

No.	Metric	GHI (W/M²)	DNI (W/M²)	DHI (W/M²)
1	RMSE	7.21	9.73	2.58
2	MAE	4.27	7.82	1.90
3	MSE	52.07	94.82	6.66
4	MAPE (%)	2.41	40.95	24.87
5	*p*-value (%)	2.97×10^{-28}	8.56×10^{-30}	8.15×10^{-28}
6	R^2 (%)	99	99	99

A.4 Appendix 4 – GCC Countries Future Scenario Using GRU Prediction Model

A.4.1 Wind Speed and Temperature Prediction for Oman Using GRU Model

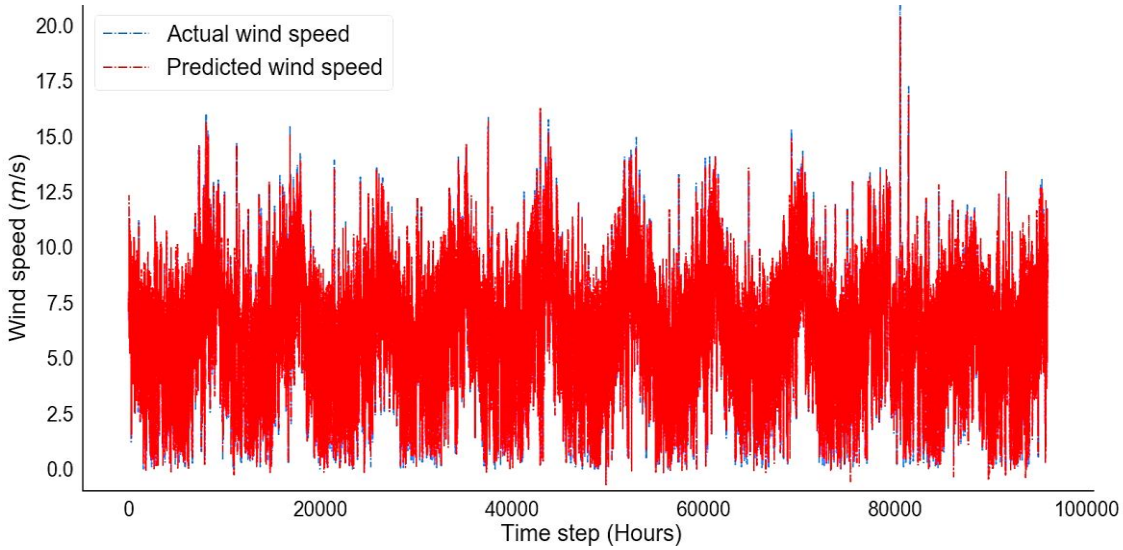

Figure A.4-1. The actual and predicted wind speed performance for Oman.

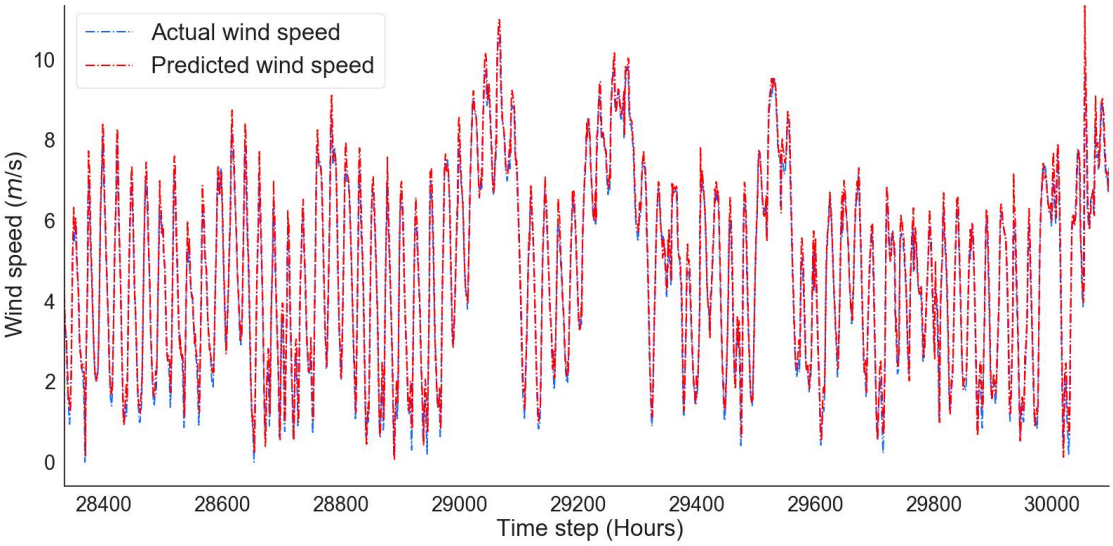

Figure A.4-2. Real and predicted values of wind speed for Oman, which show the fit and performance of the GRU model.

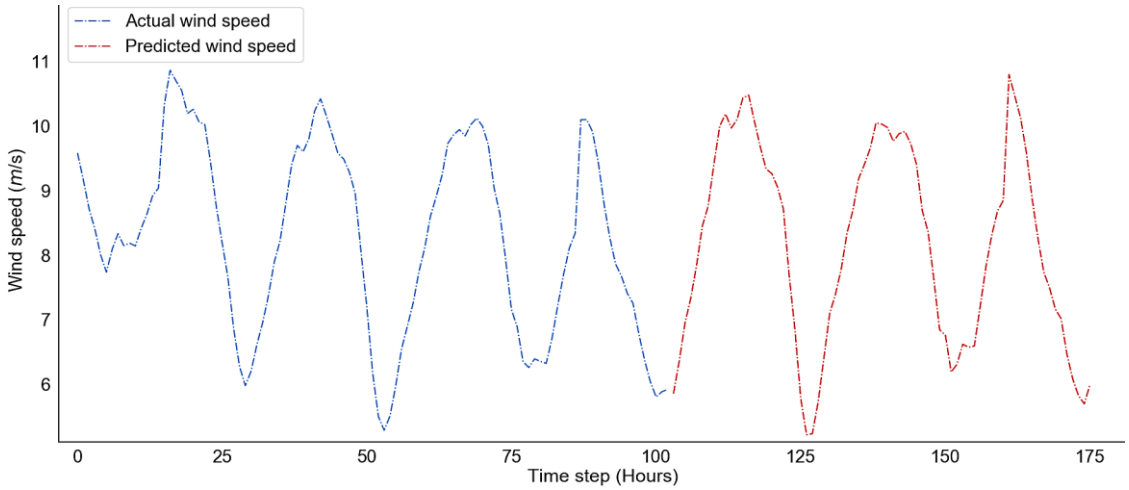

Figure A.4-3. The wind speed's predicted future values for the next 169 hours in Oman.

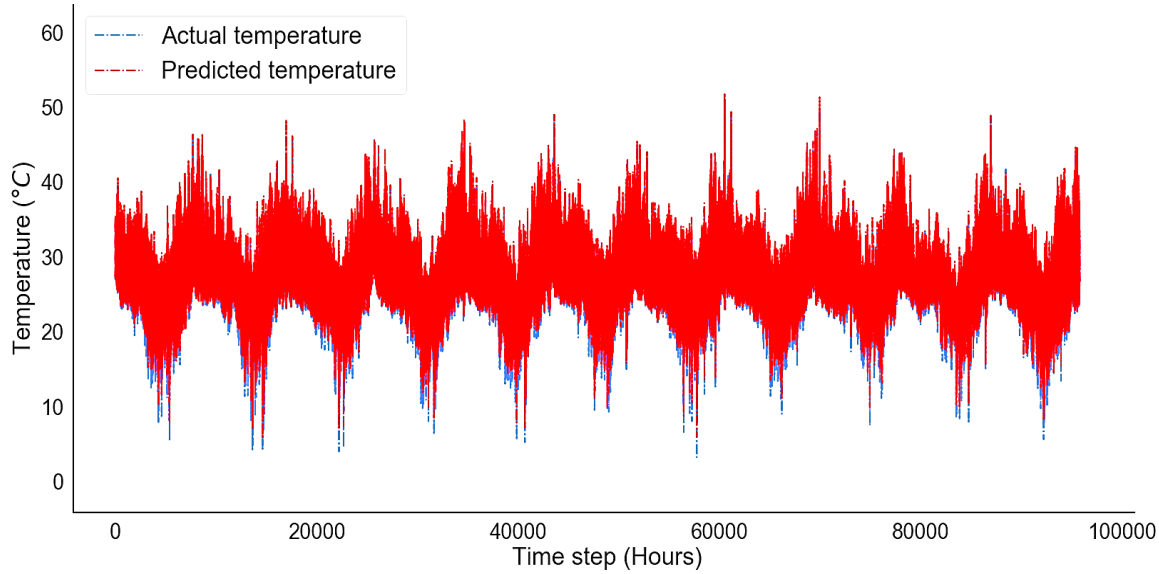

Figure A.4-4. The actual and predicted temperature performance for Oman.

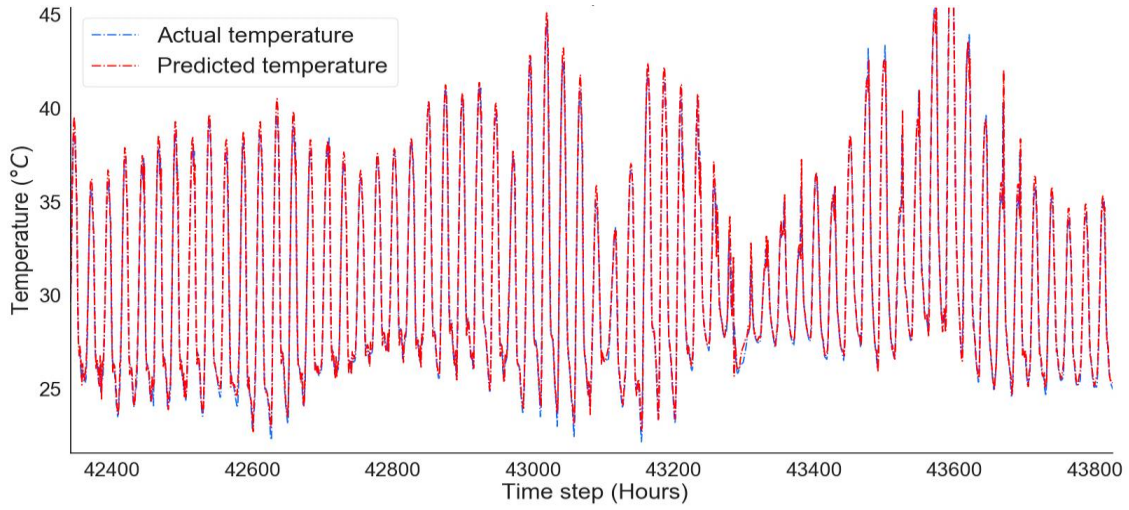

Figure A.4-5. The actual and predicted temperature performance for Oman show the model fitting.

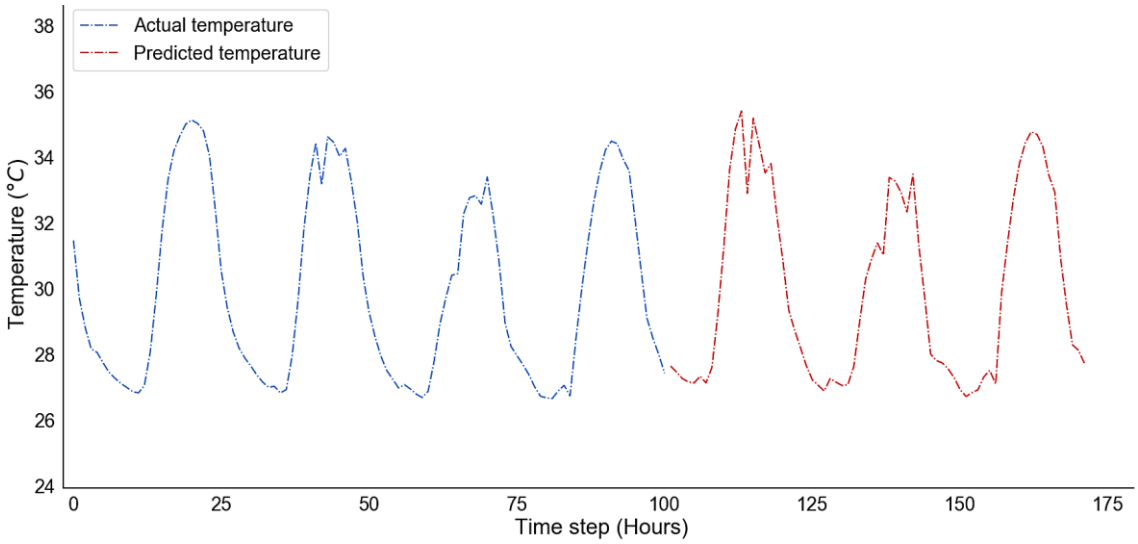

Figure A.4-6. The future predicted values of the temperature for 169 hours ahead in Oman.

Table A.4-1. Forecasting accuracy indicators for Oman prediction using the GRU model.

No.	Metric	Wind speed (m s^{-1})	Temperature (°C)
1	RMSE	0.41	0.91
2	MAE	0.29	0.68
3	MSE	0.17	0.83
4	MAPE (%)	5.04	2.52
5	*p*-value (%)	0.00	5.43×10^{-23}
6	R^2 (%)	95	97

A.4.2 Wind Speed and Temperature Prediction for UAE Using GRU Model

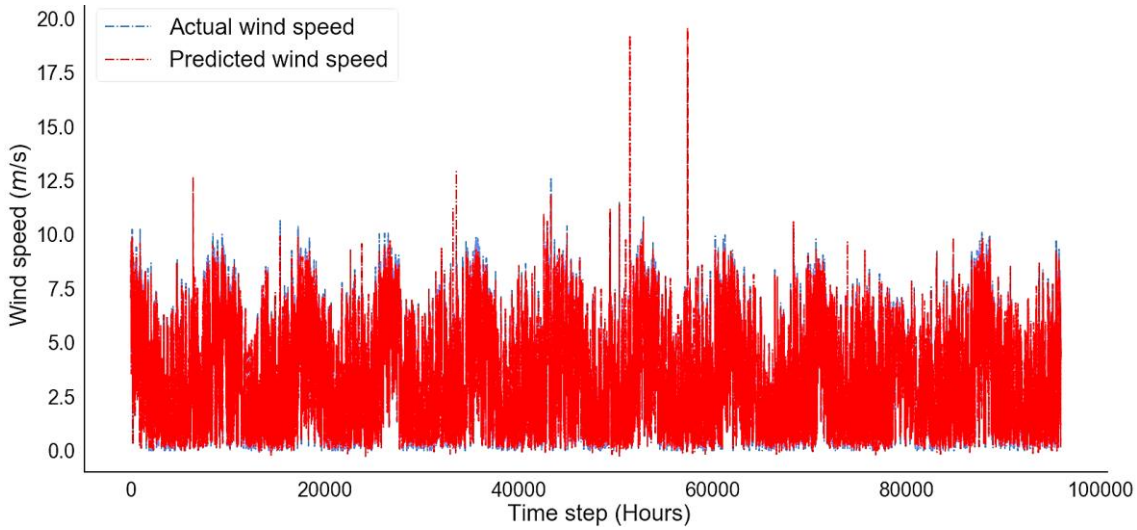

Figure A.4-6. The actual and predicted wind speed performance for UAE.

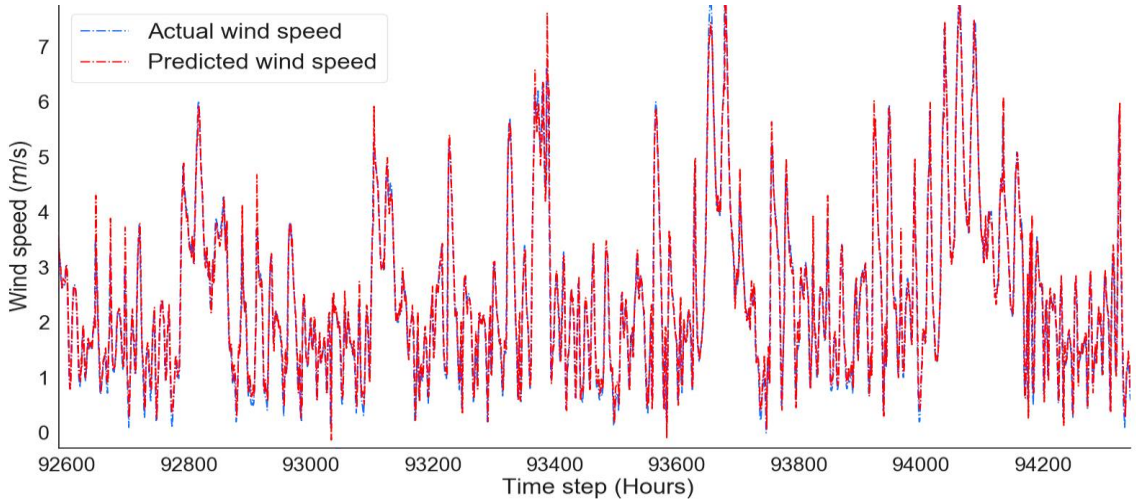

Figure A.4-7. Real and predicted values of wind speed for UAE, which show the fit and performance of the GRU model.

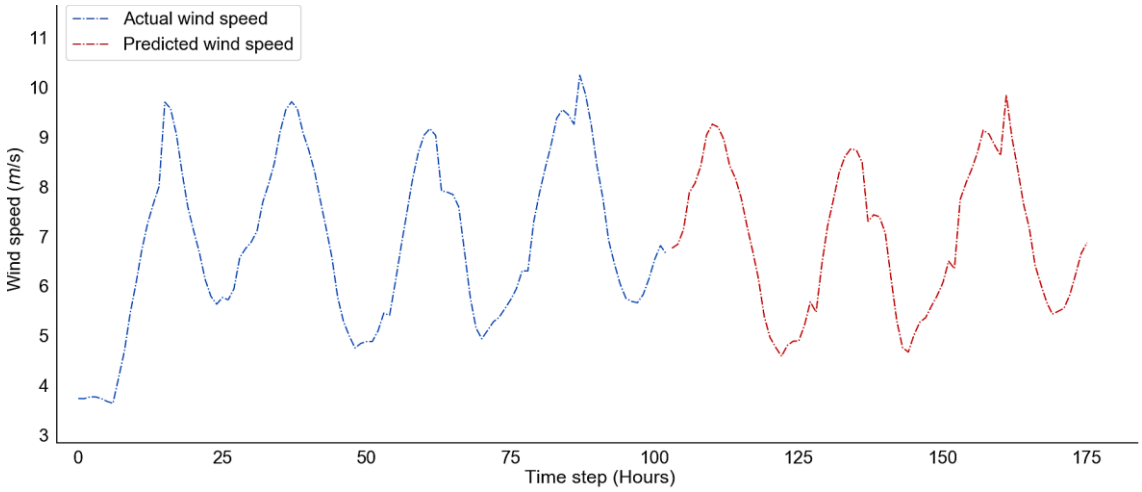

Figure A.4-8. The wind speed's predicted future values for the next 169 hours in UAE.

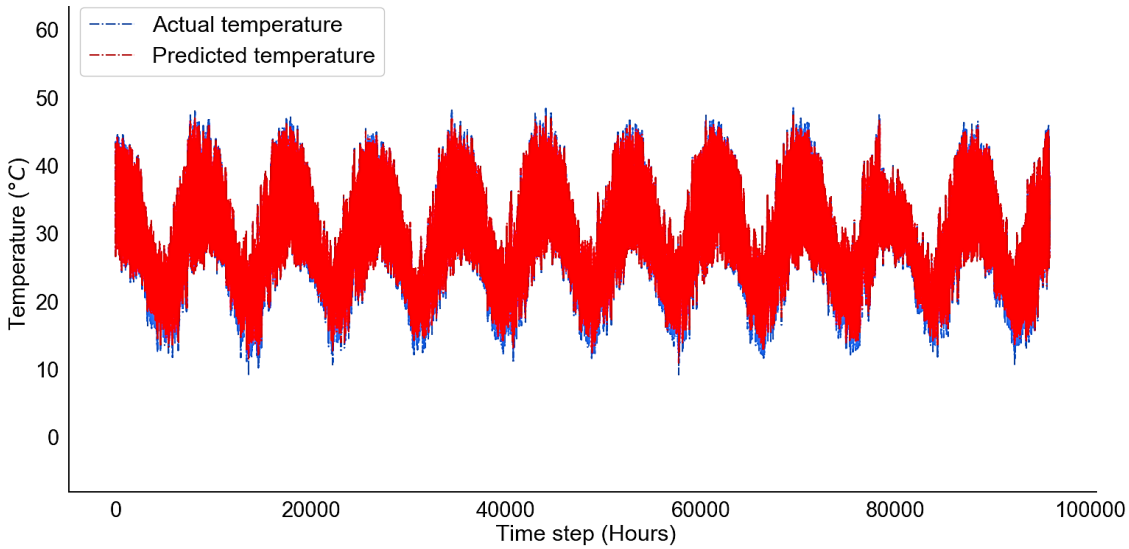

Figure A.4-9. The actual and predicted temperature performance for UAE.

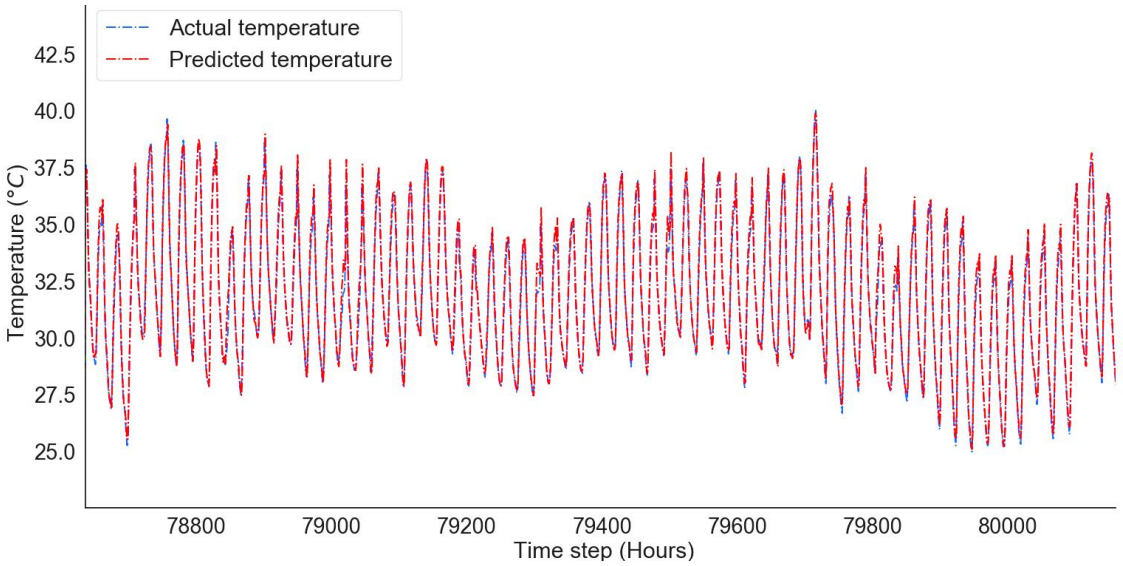

Figure A.4-10. The actual and predicted temperature performance for UAE show the model fitting.

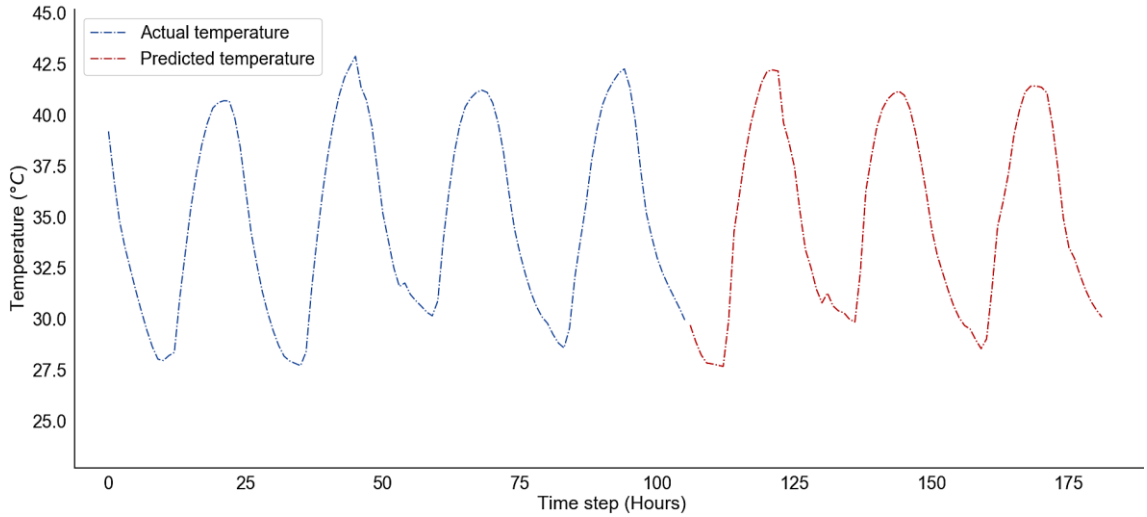

Figure A.4-11. The future predicted values of the temperature for 169 hours ahead in UAE.

Table A.4-2. Forecasting accuracy indicators for UAE prediction using the GRU model.

No.	Metric	Wind speed (m s^{-1})	Temperature (°C)
1	RMSE	0.36	0.78
2	MAE	0.22	0.53
3	MSE	0.13	0.60
4	MAPE (%)	4.39	1.77
5	*p*-value (%)	0.01	5.58×10^{-15}
6	R^2 (%)	97	98

A.4.3 Wind Speed and Temperature Prediction for Kuwait Using GRU Model

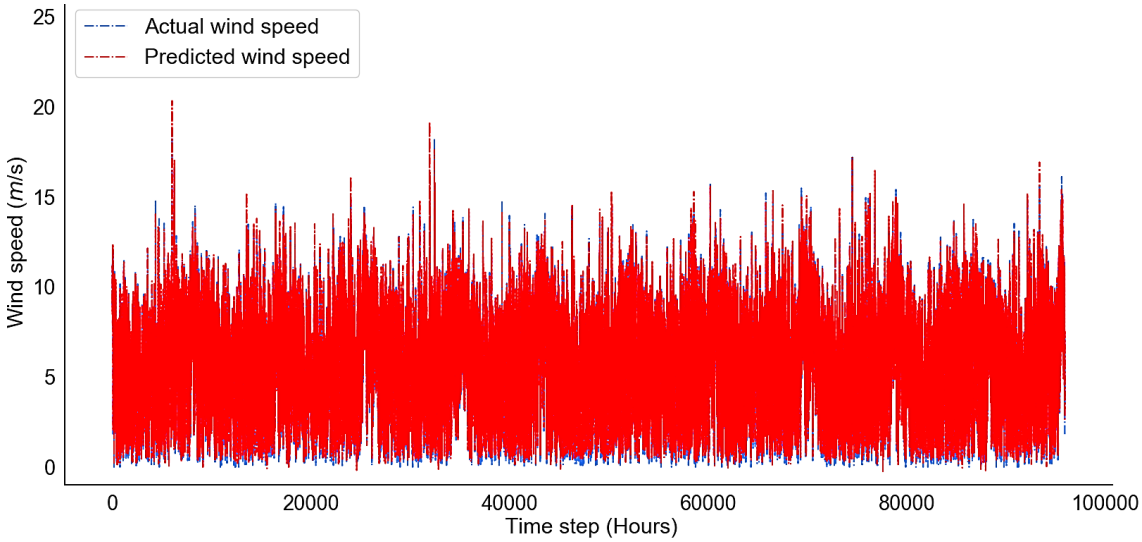

Figure A.4-12. The actual and predicted wind speed performance for Kuwait.

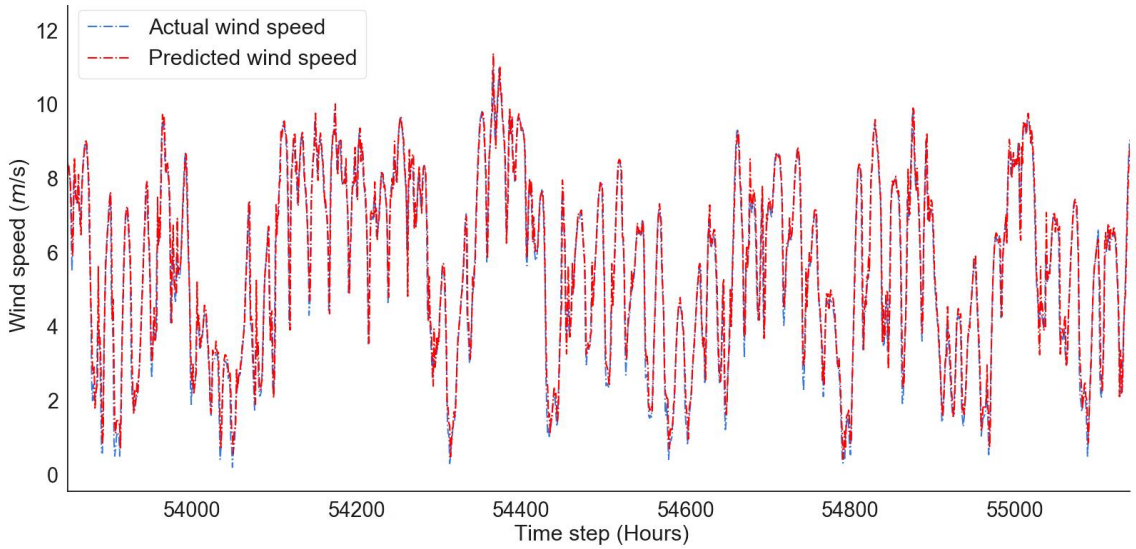

Figure A.4-13. Real and predicted values of wind speed for Kuwait, which show the fit and performance of the GRU model.

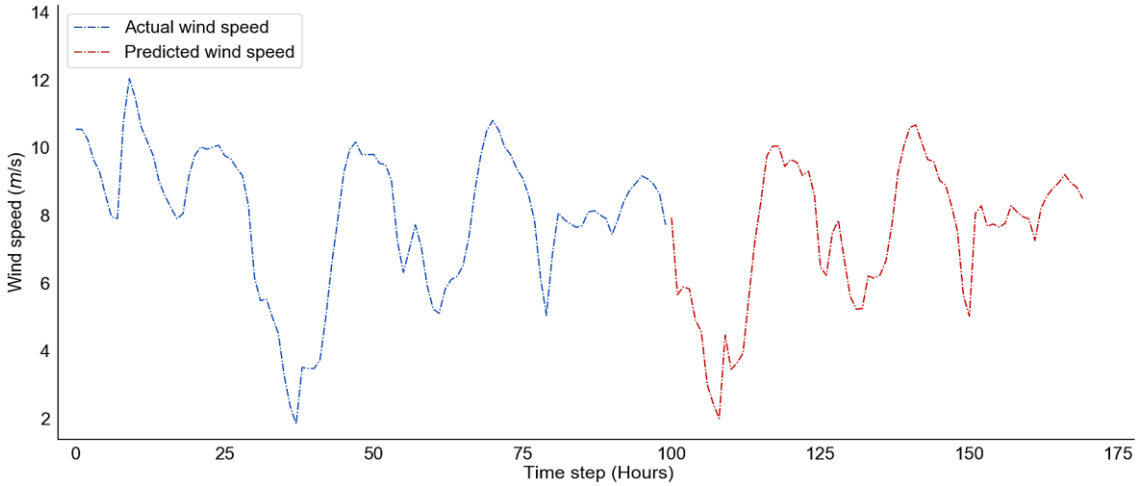

Figure A.4-14. The wind speed's predicted future values for the next 169 hours in Kuwait.

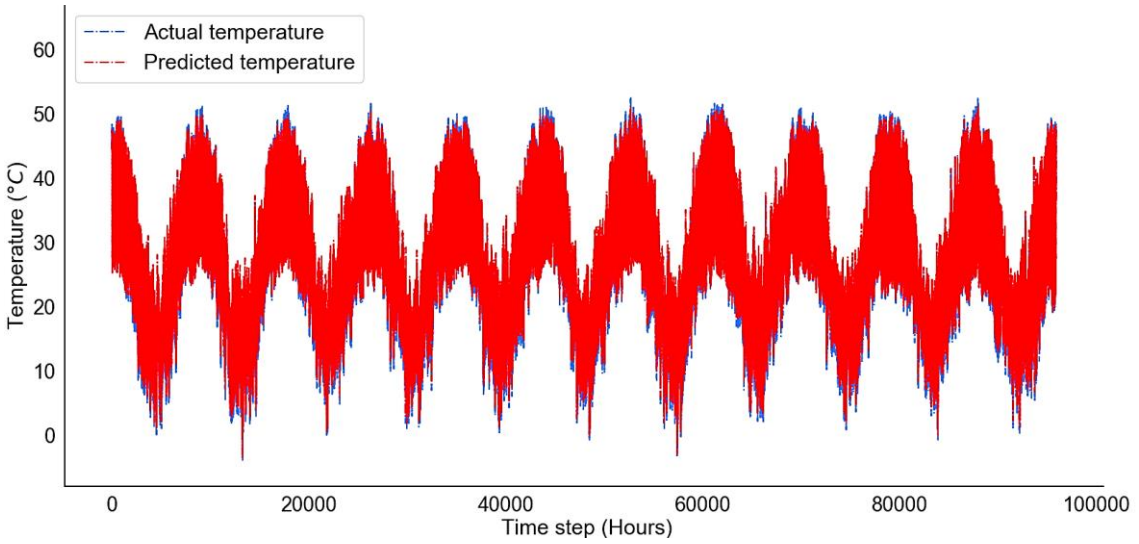

Figure A.4-15. The actual and predicted temperature performance for Kuwait.

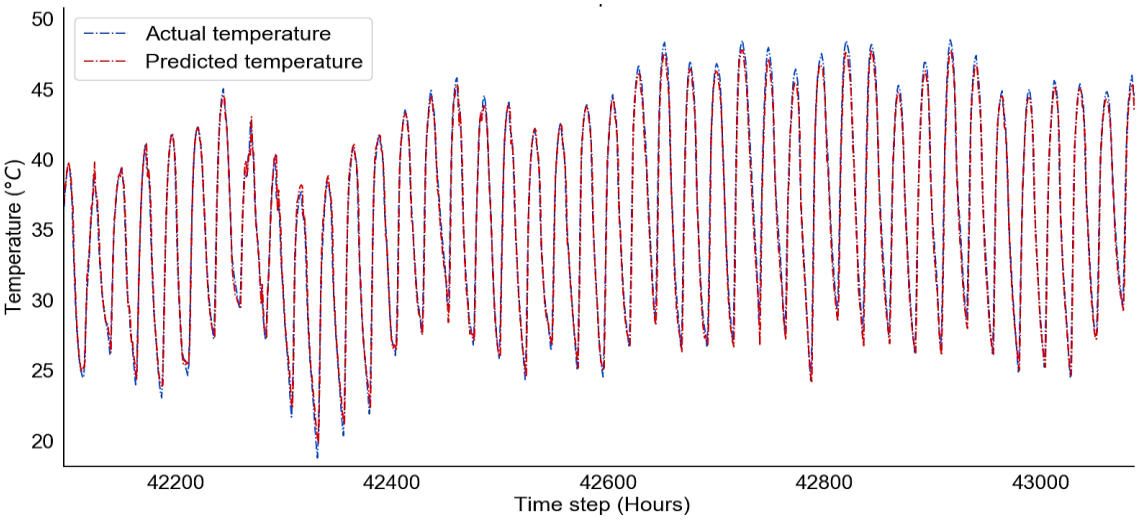

Figure A.4-16. The actual and predicted temperature performance for Kuwait show the model fitting.

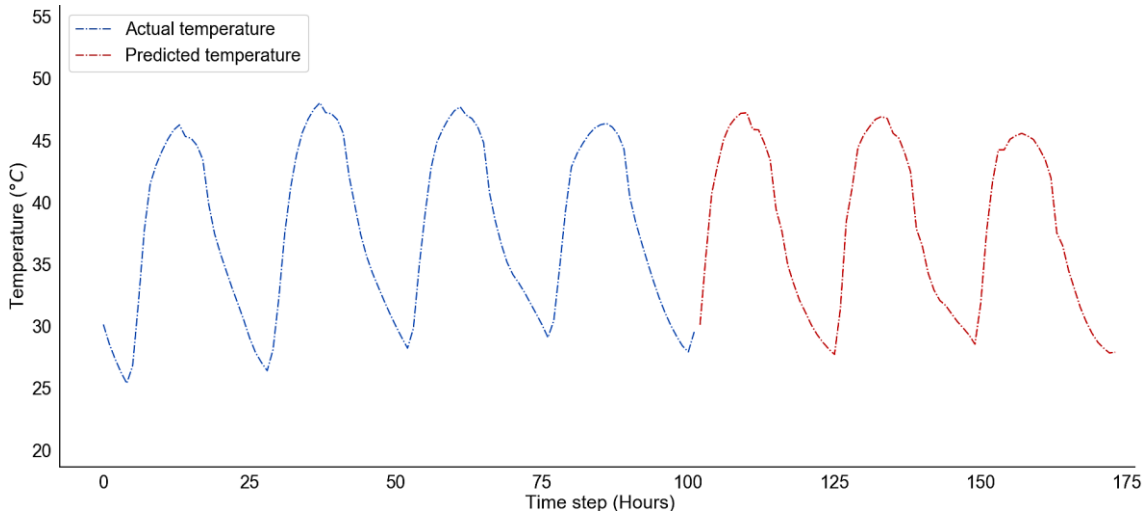

Figure A.4-17. The future predicted values of the temperature for 169 hours ahead in Kuwait.

Table A.4-3. Forecasting accuracy indicators for Kuwait prediction using the GRU model.

No.	Metric	Wind speed (m s^{-1})	Temperature (°C)
1	RMSE	0.66	1.27
2	MAE	0.44	1.04
3	MSE	0.43	1.61
4	MAPE (%)	5.40	2.69
5	*p*-value (%)	0.00	1.39×10^{-12}
6	R^2 (%)	94	98

A.4.4 Wind Speed and Temperature Prediction for Qatar Using GRU Model

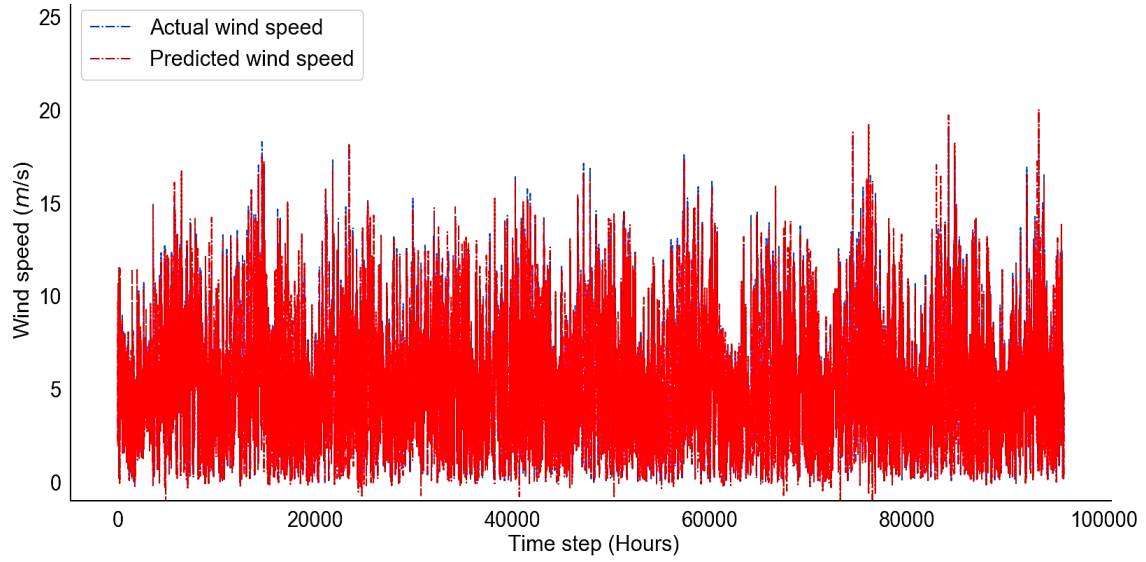

Figure A.4-18. The actual and predicted wind speed performance for Qatar.

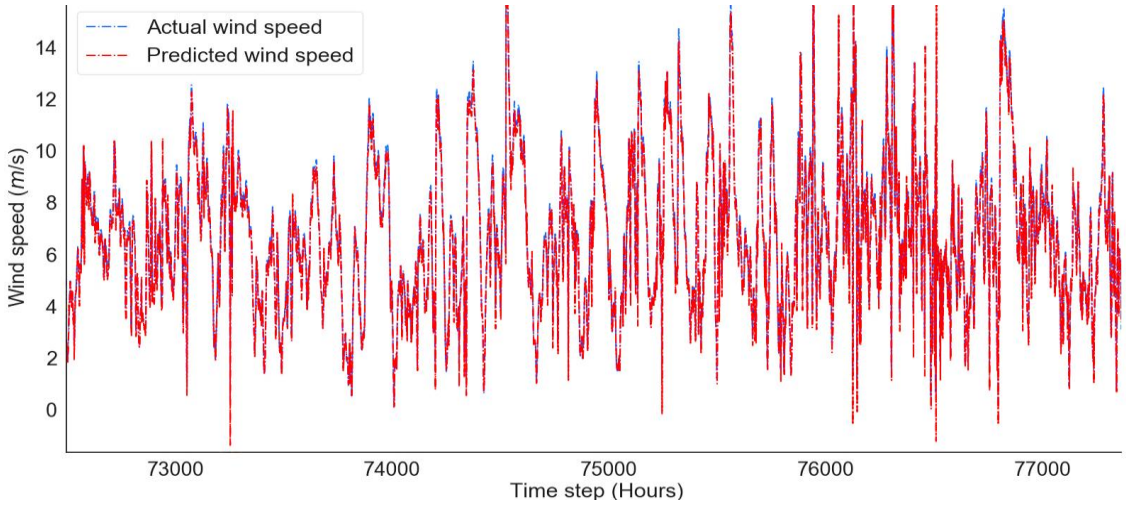

Figure A.4-19. Real and predicted values of wind speed for Qatar, which show the fit and performance of the GRU model.

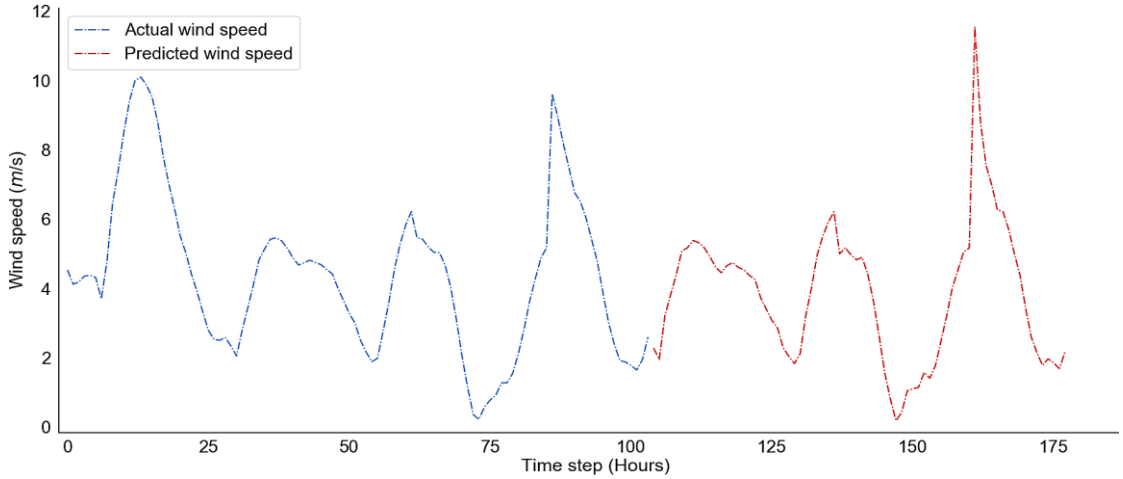

Figure A.4-20. The wind speed's predicted future values for the next 169 hours in Qatar.

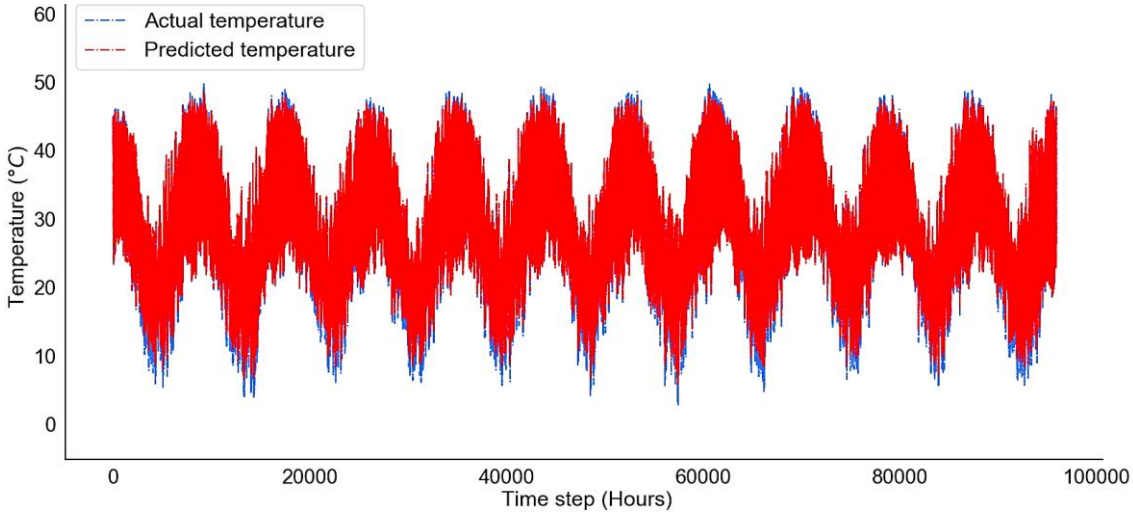

Figure A.4-21. The actual and predicted temperature performance for Qatar.

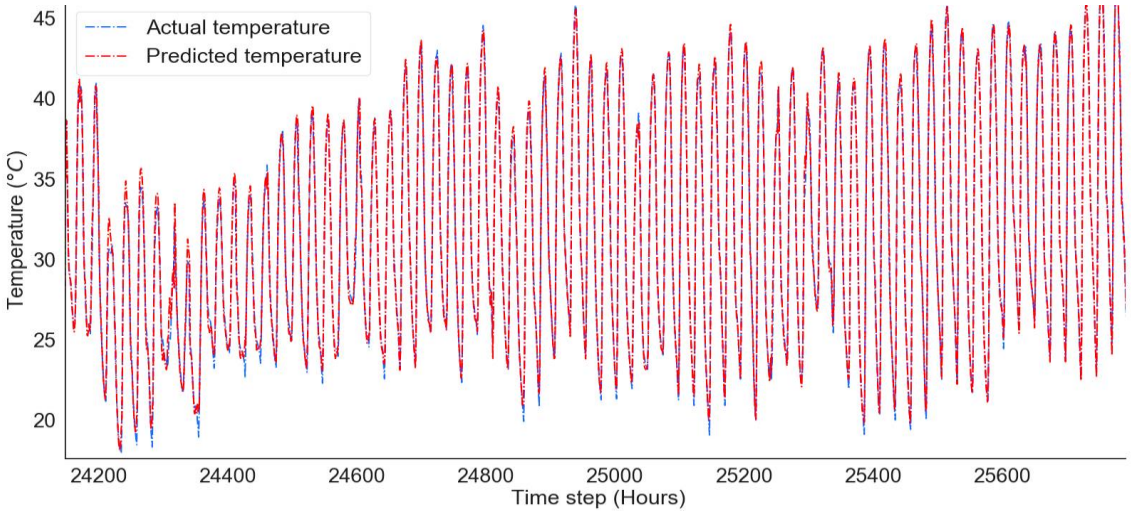

Figure A.4-22. The actual and predicted temperature performance for Qatar show the model fitting.

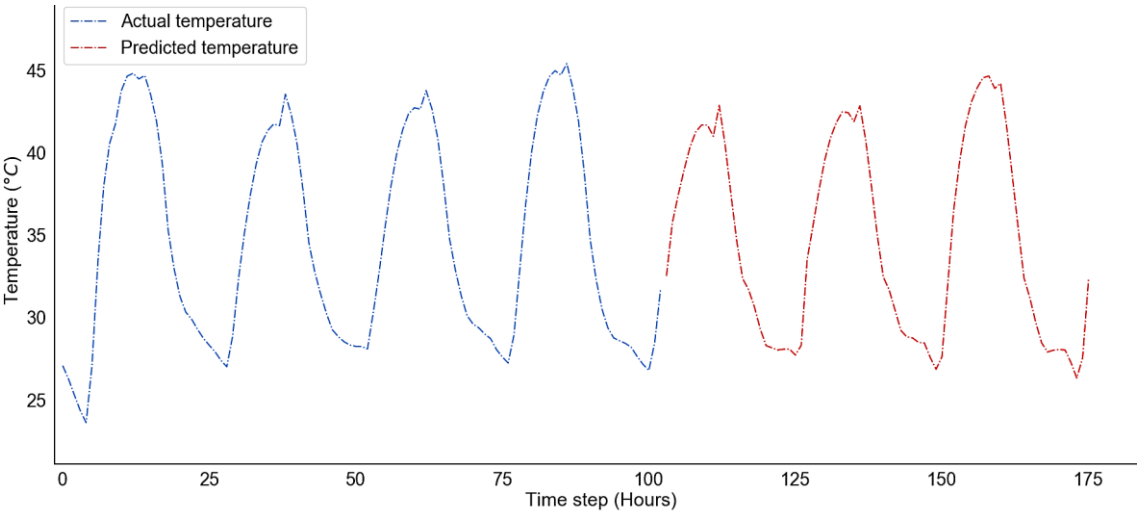

Figure A.4-23. The temperature predicted future values for the next 169 hours in Qatar.

Table A.4-4. Forecasting accuracy indicators for Qatar prediction using the GRU model.

No.	Metric	Wind speed (m s^{-1})	Temperature (°C)
1	RMSE	0.52	0.91
2	MAE	0.32	0.63
3	MSE	0.27	0.83
4	MAPE (%)	9.77	1.84
5	*p*-value (%)	0.00	1.87×10^{-15}
6	R^2 (%)	96	98

A.4.5 Wind Speed and Temperature Prediction for Bahrain Using GRU Model

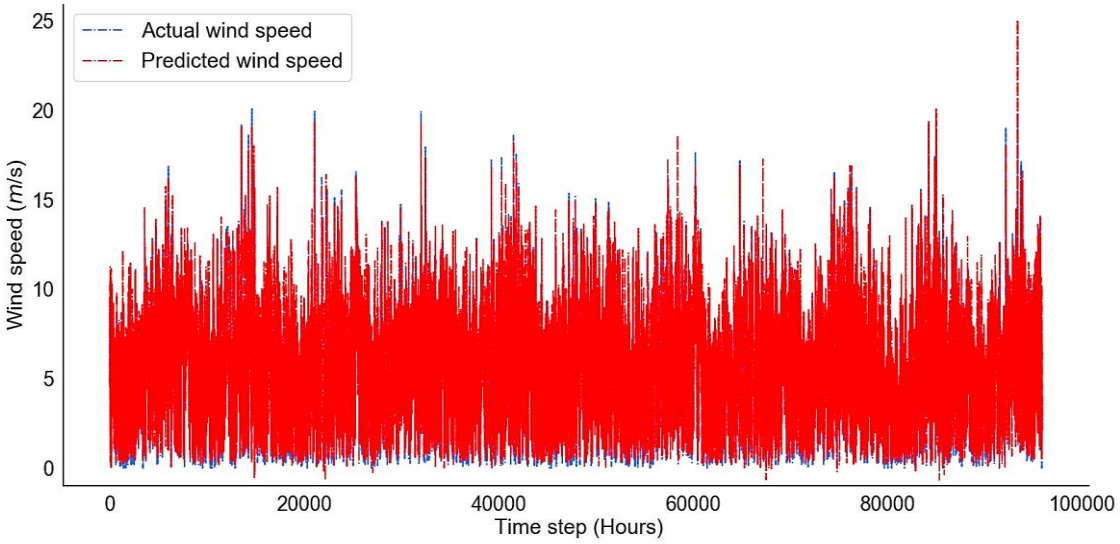

Figure A.4-24. The actual and predicted wind speed performance for Bahrain.

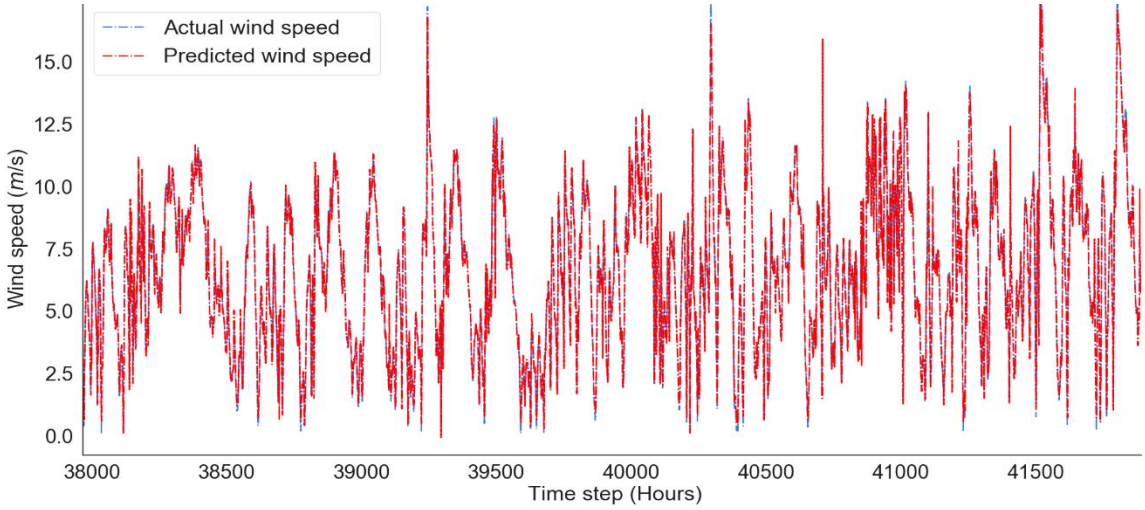

Figure A.4-25. Real and predicted values of wind speed for Bahrain, which show the fit and performance of the GRU model.

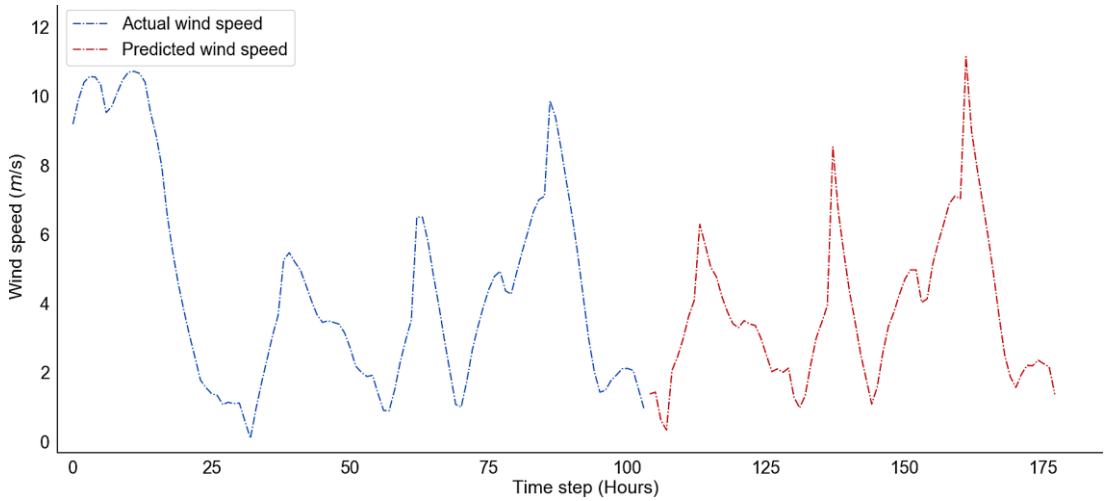

Figure A.4-26. The wind speed's predicted future values for the next 169 hours in Bahrain.

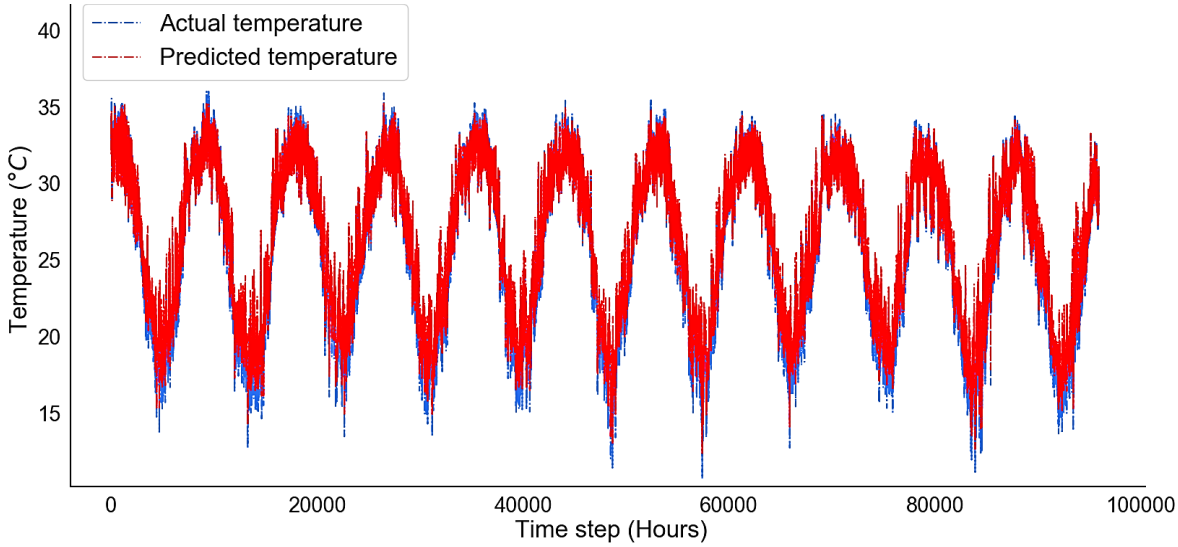

Figure A.4-27. The actual and predicted temperature performance for Bahrain.

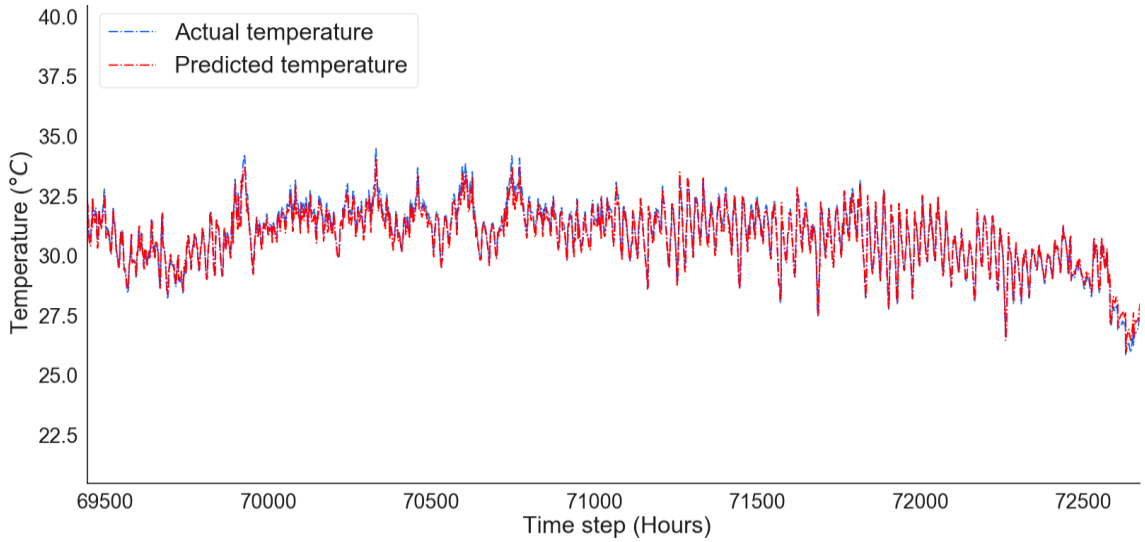

Figure A.4-28. The actual and predicted temperature performance for Bahrain show the model fitting.

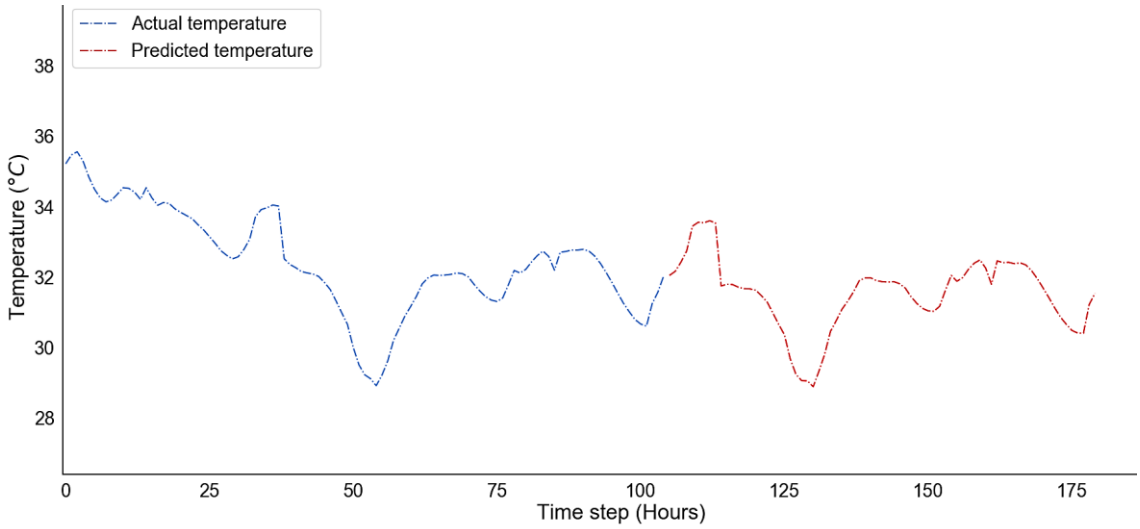

Figure A.4-29. The temperature predicted future values for the next 169 hours in Bahrain.

Table A.4-5. Forecasting accuracy indicators for Bahrain prediction using the GRU model.

No.	Metric	Wind speed (m s^{-1})	Temperature (°C)
1	RMSE	0.54	0.81
2	MAE	0.33	0.66
3	MSE	0.29	0.67
4	MAPE (%)	15.13	2.04
5	*p*-value (%)	0.01	1.86×10^{-12}
6	R^2 (%)	96	97

A.5 Appendix 5 – GCC Countries Historical Data

A.5.1 Oman Historical Solar Irradiance, Wind Speed and Temperature Data

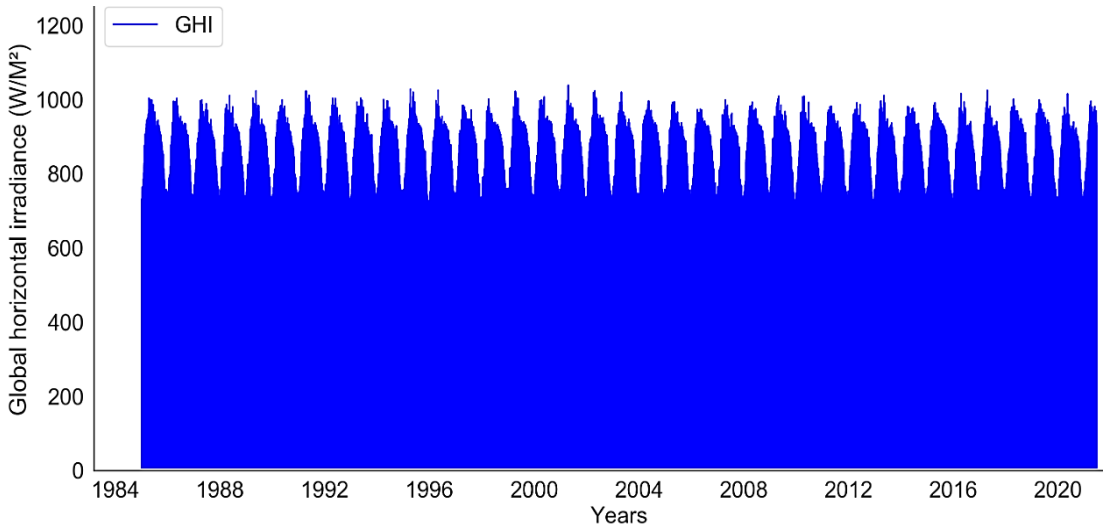

Figure A.5-1. Oman hourly intervals historical performance of the GHI over 36 years.

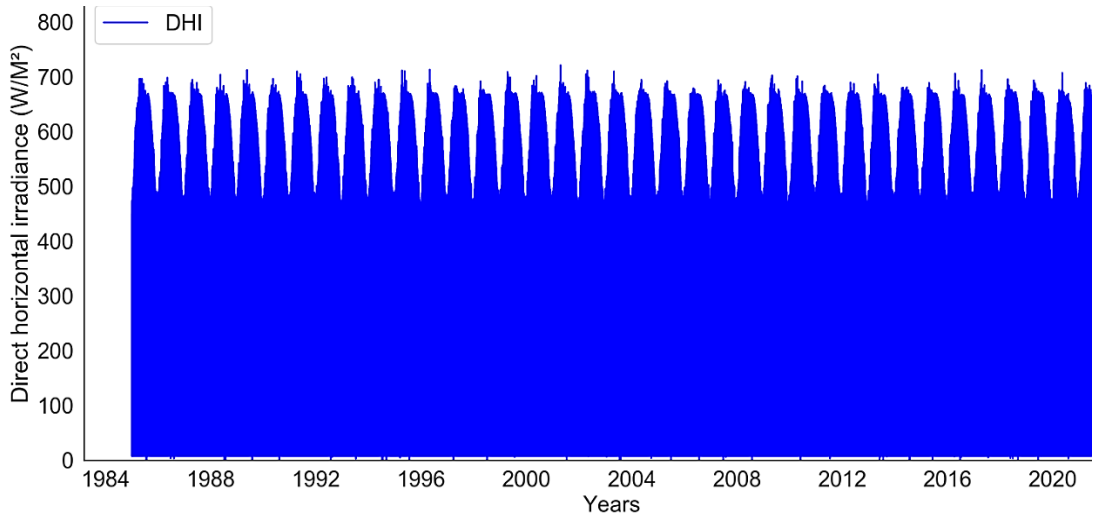

Figure A.5-2. Oman hourly intervals historical performance of the DNI over 36 years.

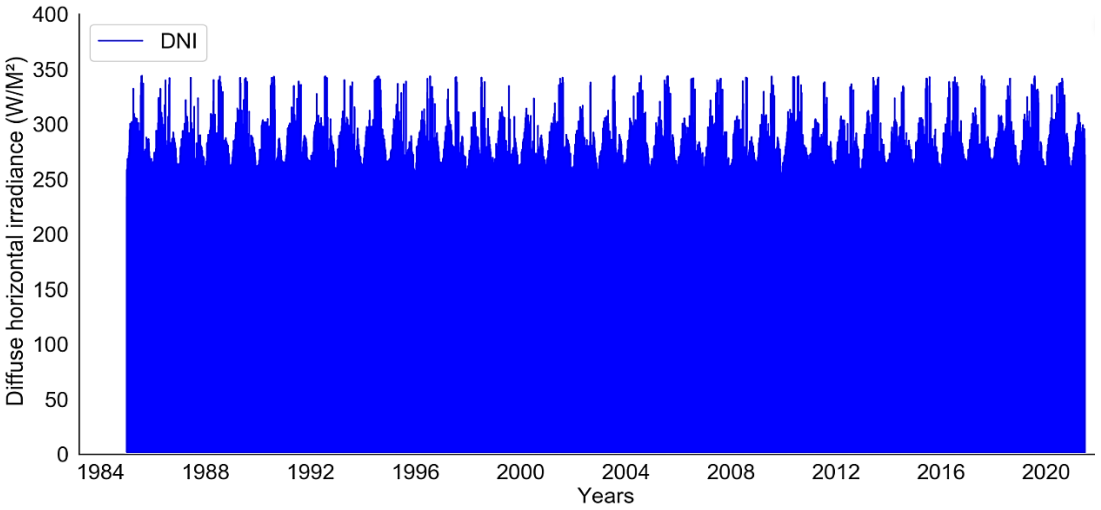

Figure A.5-3. Oman hourly intervals historical performance of the DHI over 36 years.

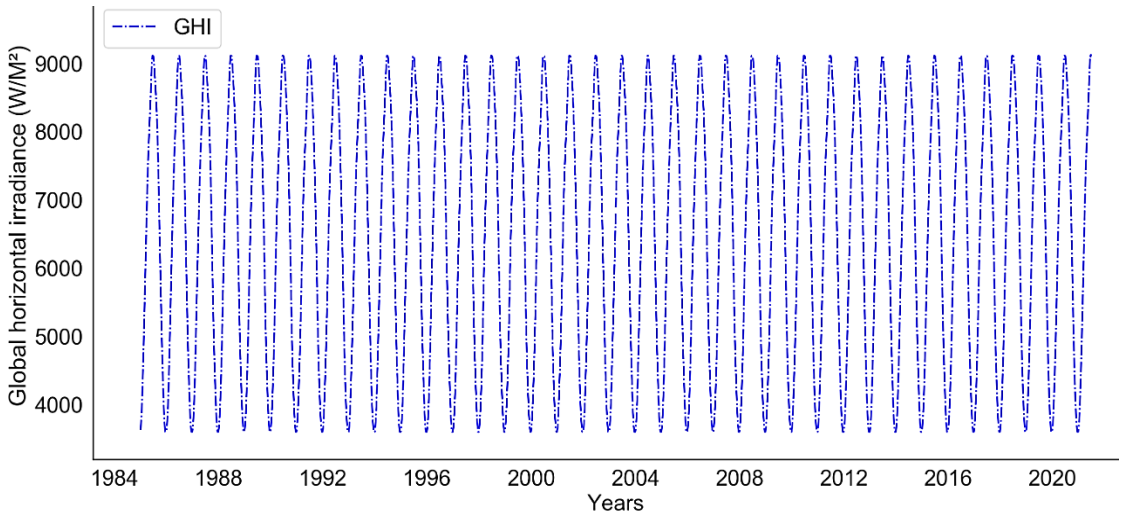

FigureA.5-4. Oman daily intervals historical performance of the GHI over 36 years.

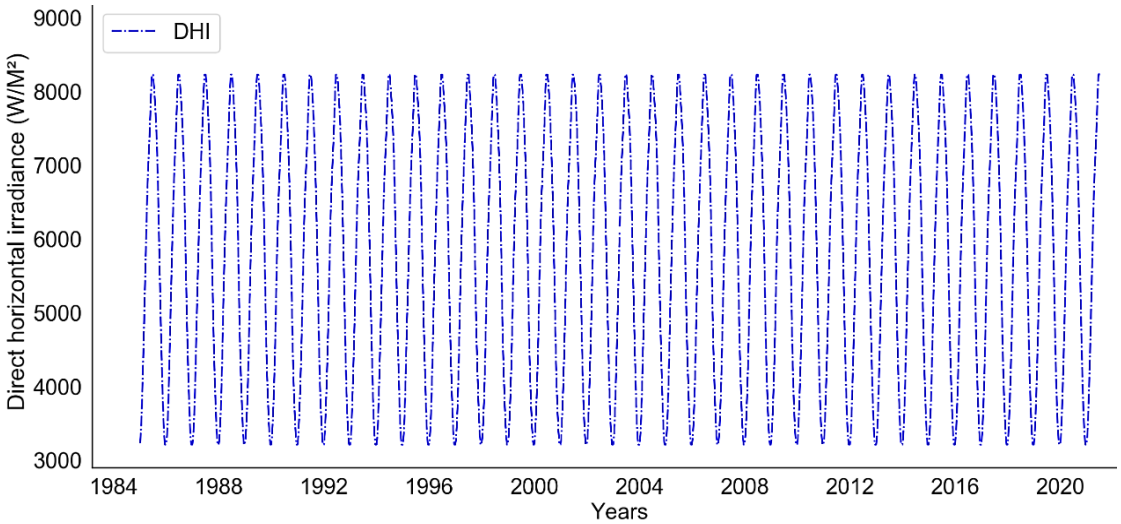

Figure A.5-5. Oman daily intervals historical performance of the DHI over 36 years.

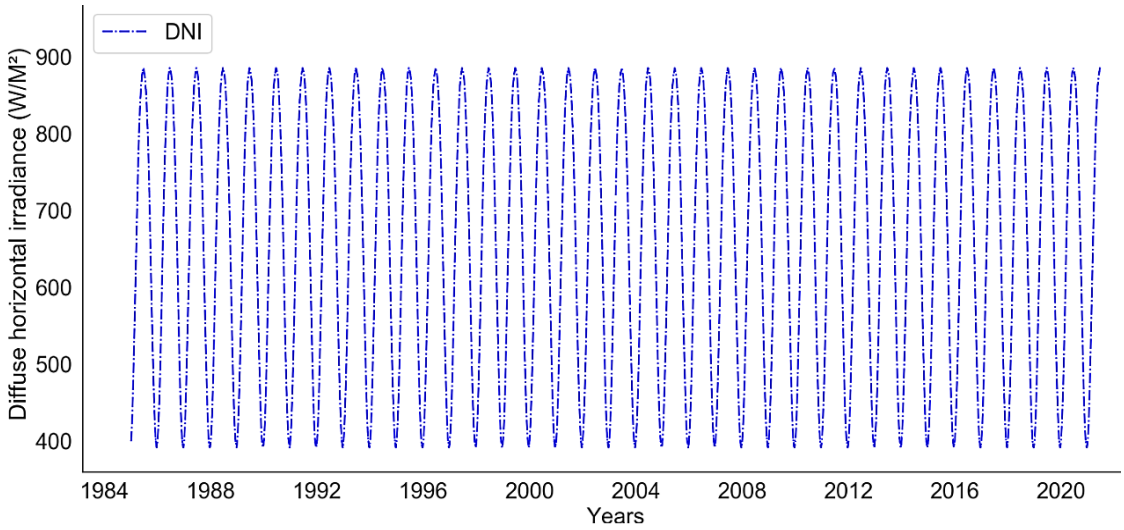

Figure A.5-6. Oman daily intervals historical performance of the DNI over 36 years.

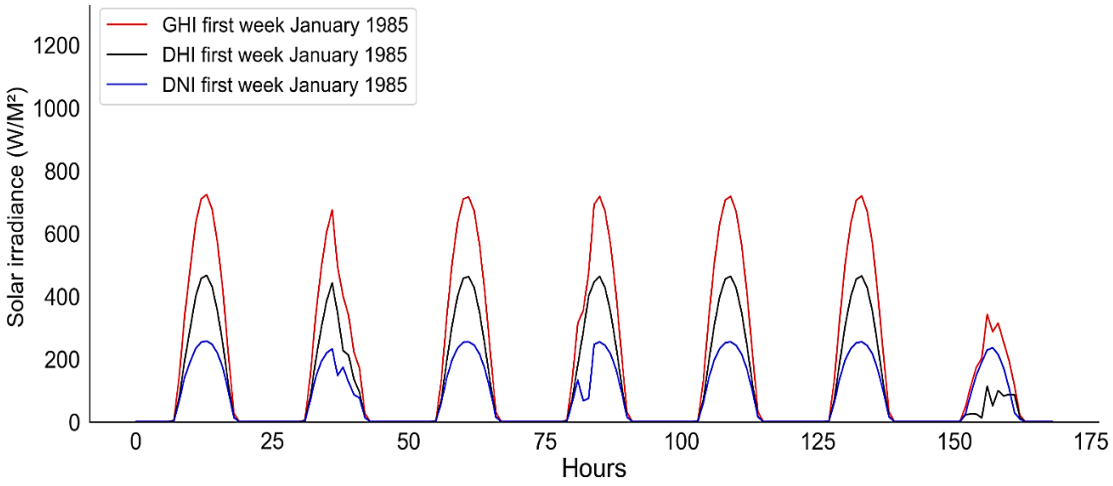

Figure A.5-7. Oman hourly intervals historical performances of the GHI, DHI, and DNI during January 1985.

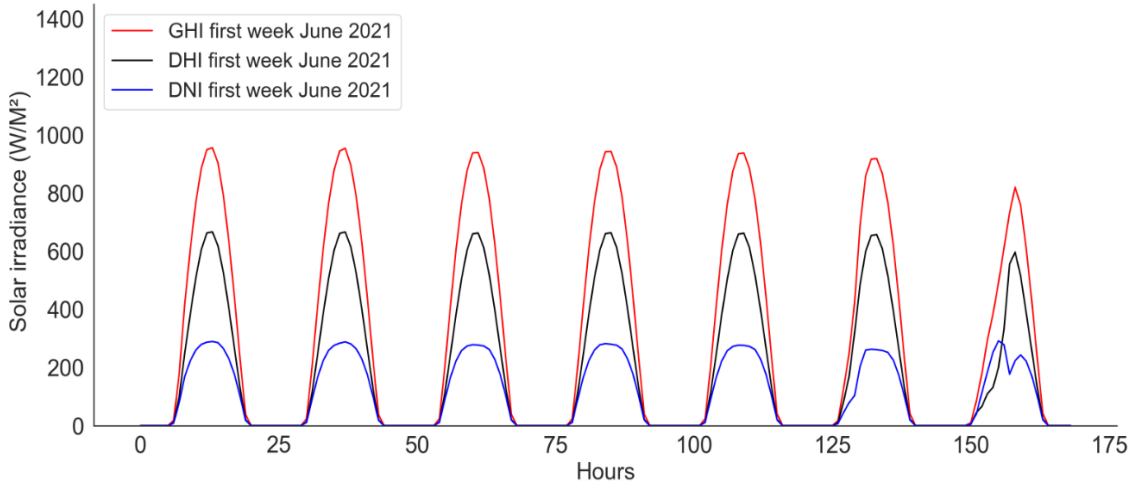

Figure A.5-8. Oman hourly intervals historical performances of the GHI, DHI, and DNI during January 2021.

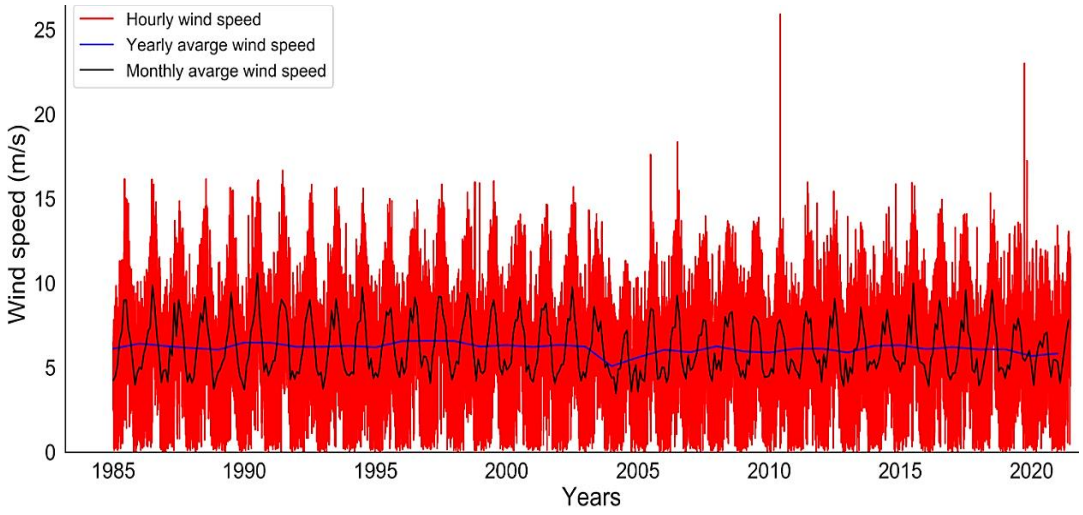

Figure A.5-9. Oman hourly monthly and yearly intervals historical wind speed performance over 36 years.

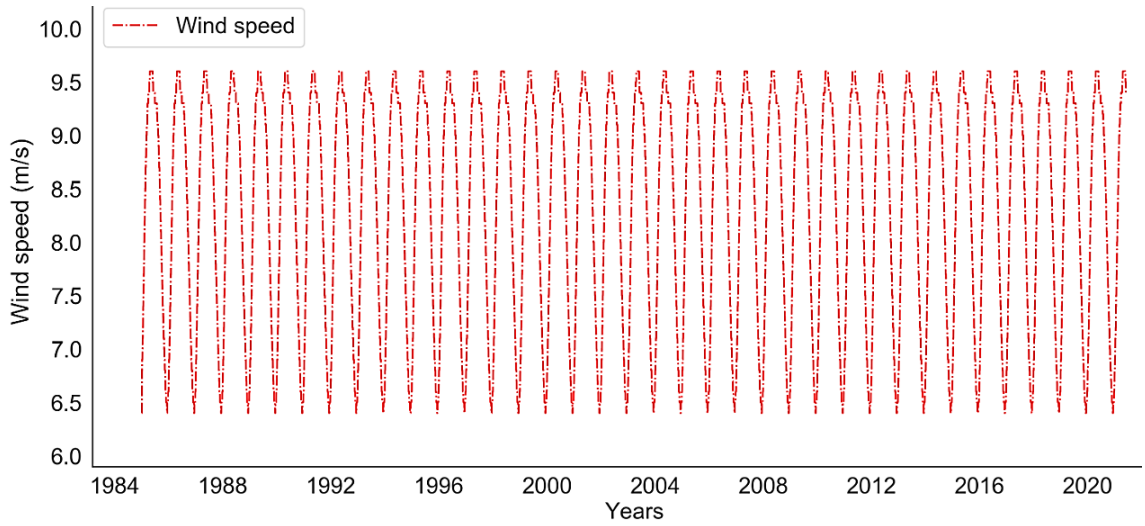

Figure A.5-10. Oman daily intervals historical wind speed performance over 36 years.

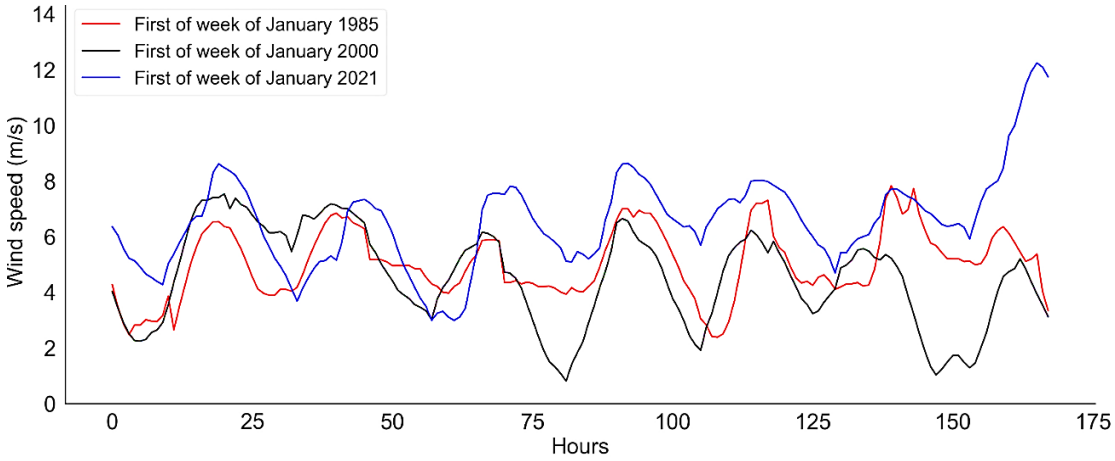

Figure A.5-11. The first three historical weeks of wind speed performance for Oman during January at hourly intervals.

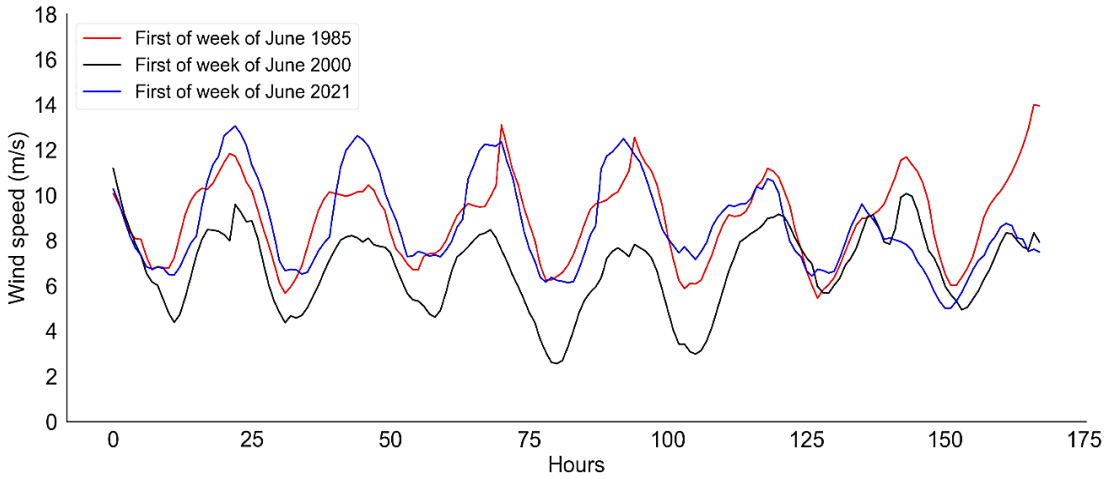

Figure A.5-12. The first three historical weeks of wind speed performance for Oman during June at hourly intervals.

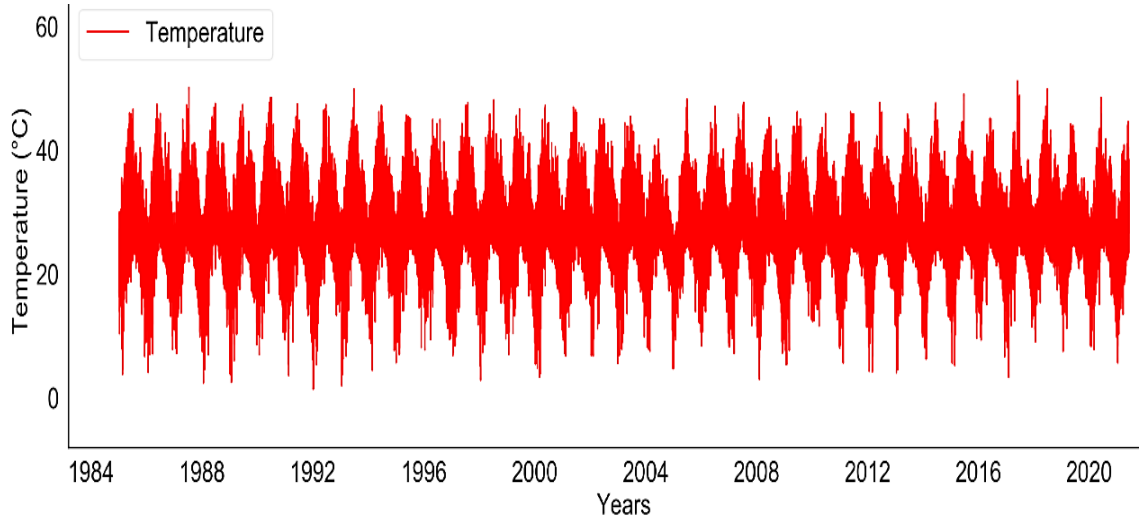

Figure A.5-13. The historical temperature performance over 36 years at hourly intervals for Oman.

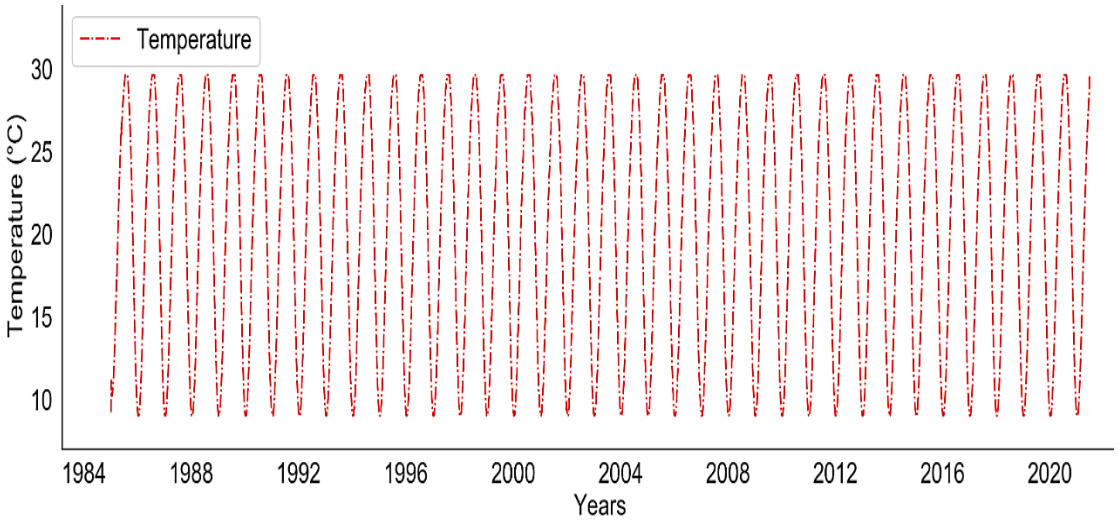

Figure A.5-14. The historical temperature performance over 36 years at daily intervals for Oman.

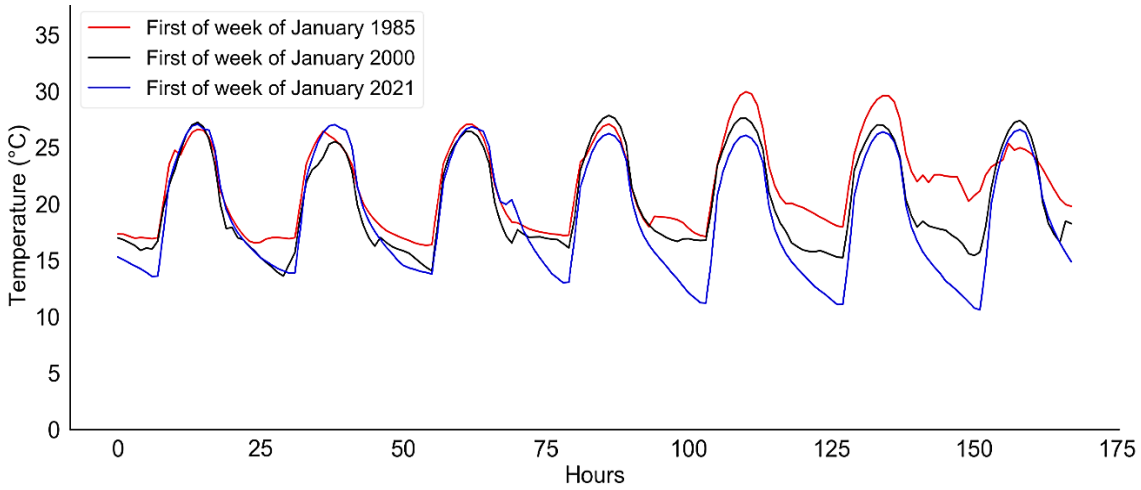

Figure A.5-15. The first three historical weeks of temperature performance for Oman during January at hourly intervals.

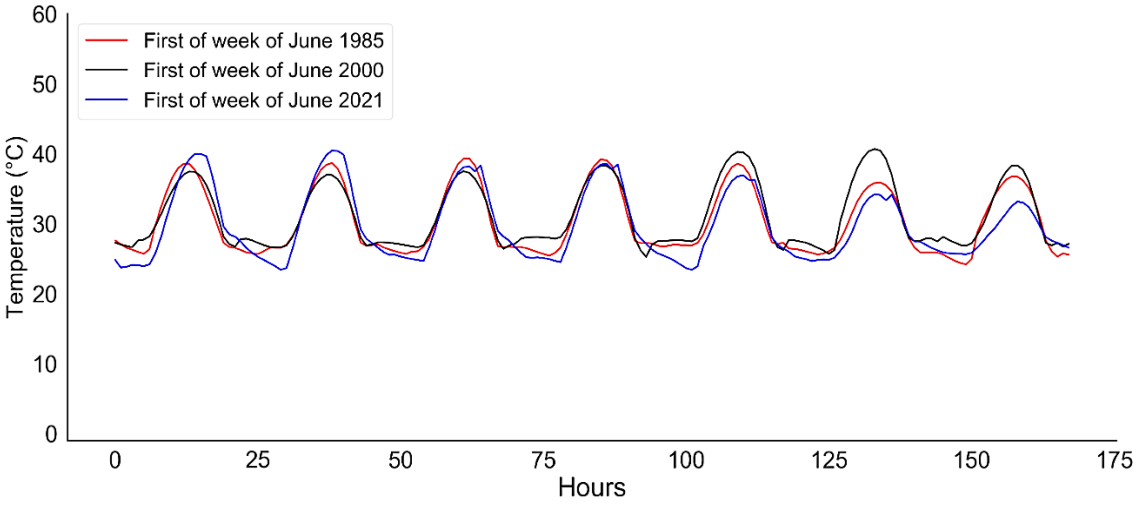

Figure A.5-16. The first three historical weeks of temperature performance for Oman during June at hourly intervals.

A.5.2 UAE Historical Wind Speed and Temperature Data

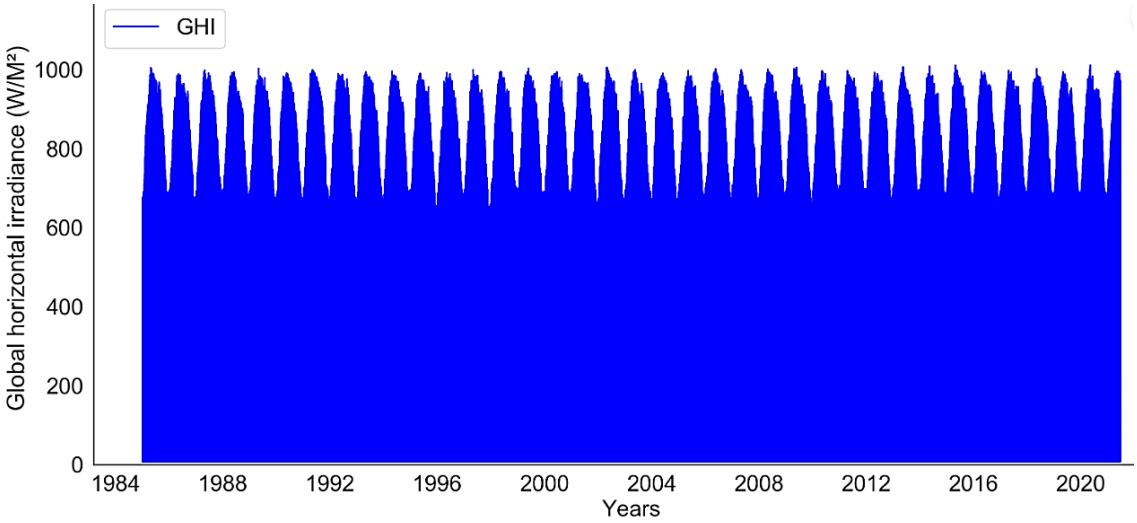

Figure A.5-17. UAE hourly intervals historical performance of the GHI over 36 years.

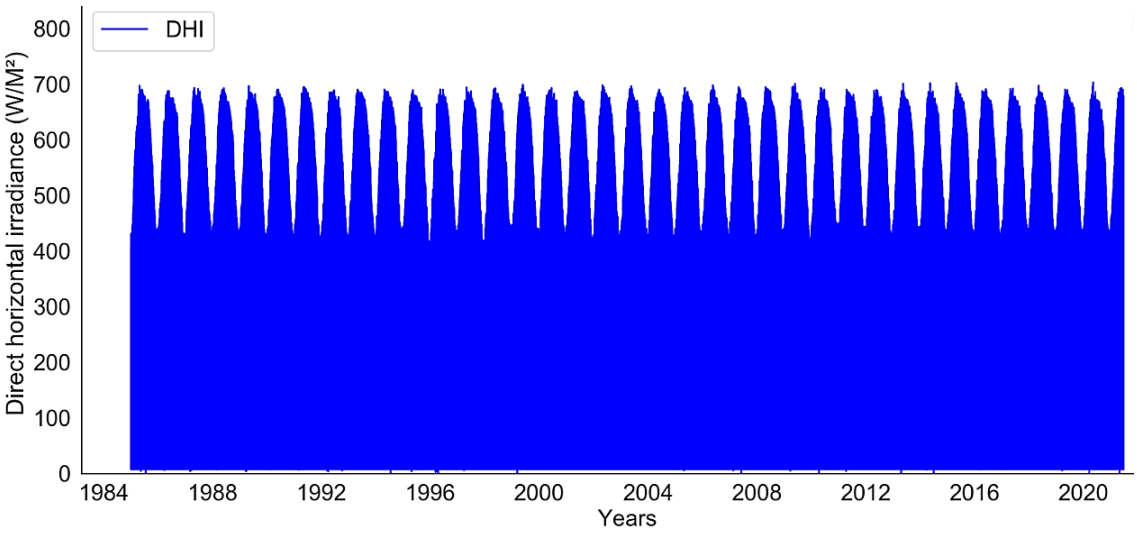

Figure A.5-18. UAE hourly intervals historical performance of the DNI over 36 years.

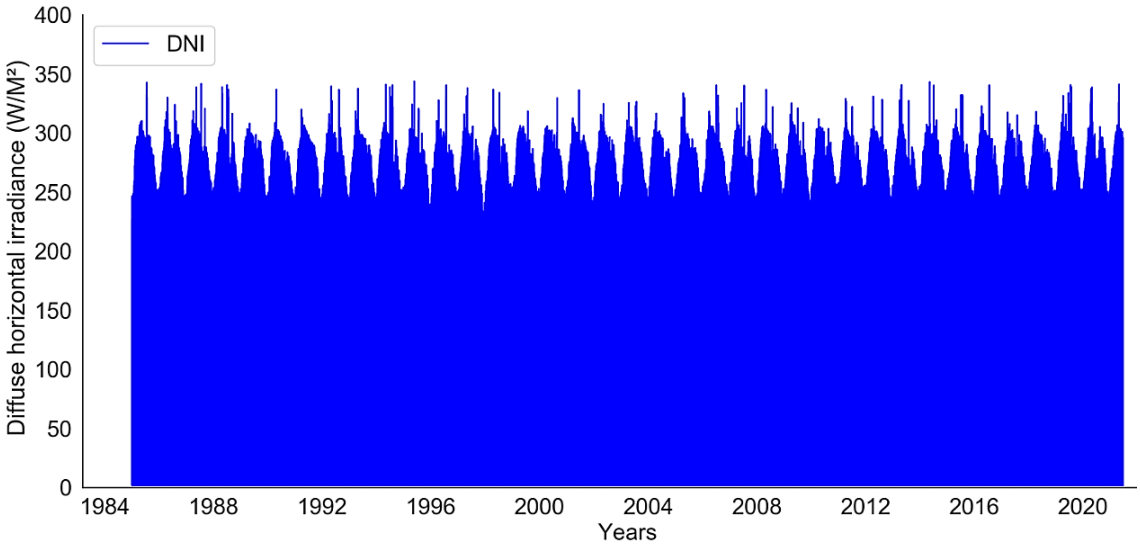

Figure A.5-19. UAE hourly intervals historical performance of the DHI over 36 years.

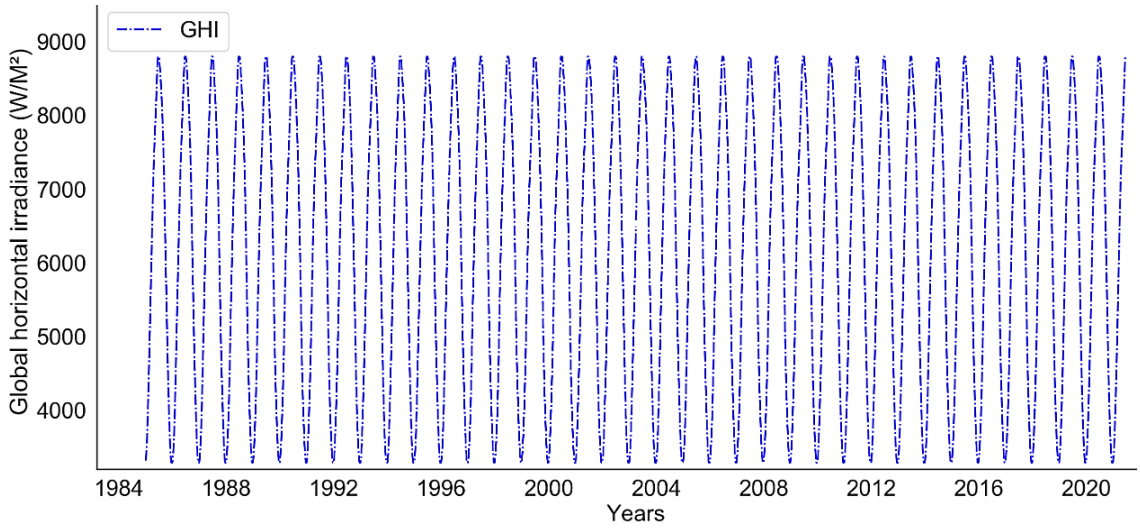

Figure A.5-20. UAE daily intervals historical performance of the GHI over 36 years.

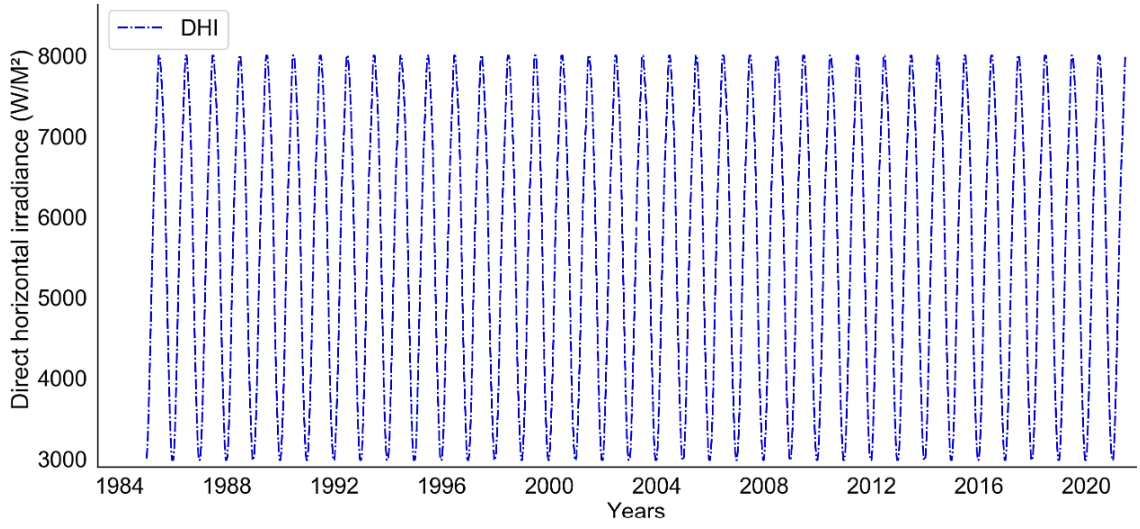

Figure A.5-21. UAE daily intervals historical performance of the DNI over 36 years.

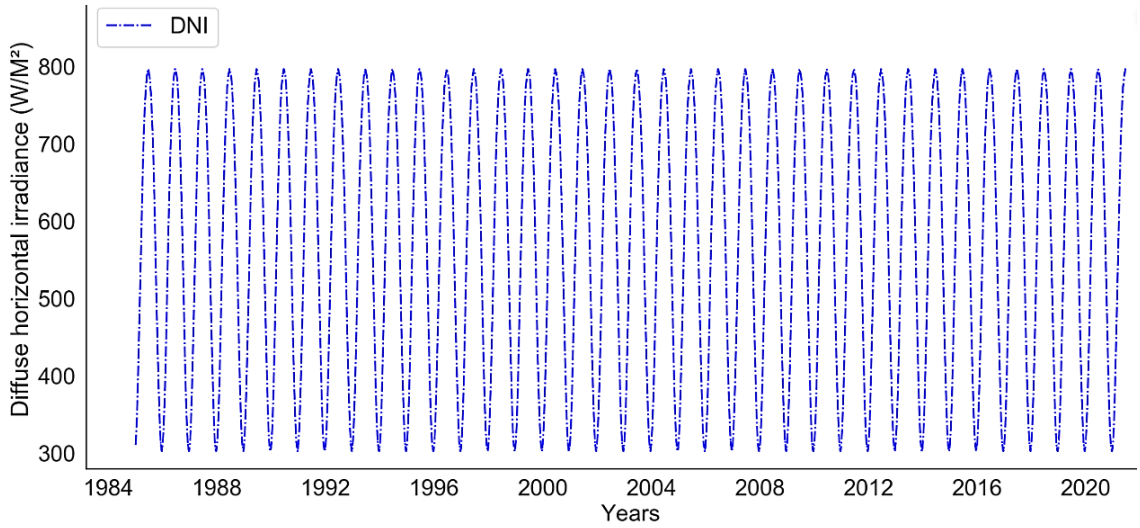

Figure A.5-22. UAE daily intervals historical performance of the DHI over 36 years.

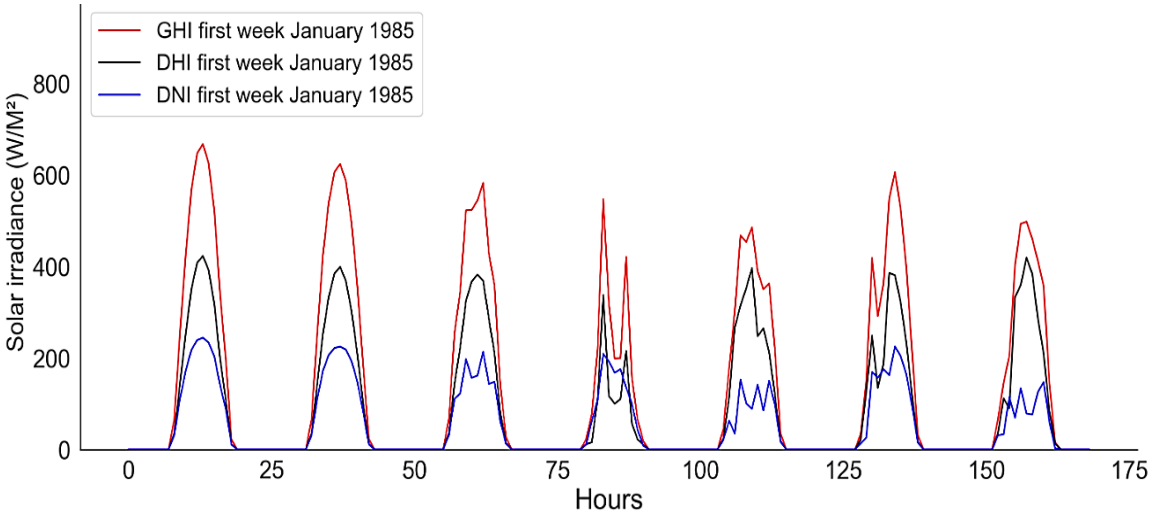

Figure A.5-23. UAE hourly intervals historical performances of the GHI, DHI, and DNI during January 1985.

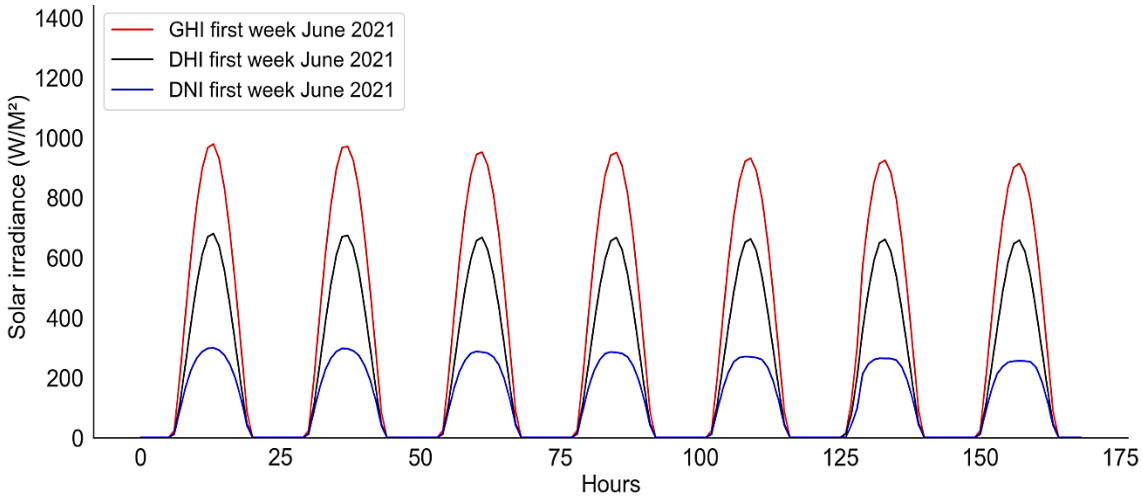

Figure A.5-24. UAE hourly intervals historical performances of the GHI, DHI, and DNI during January 2021.

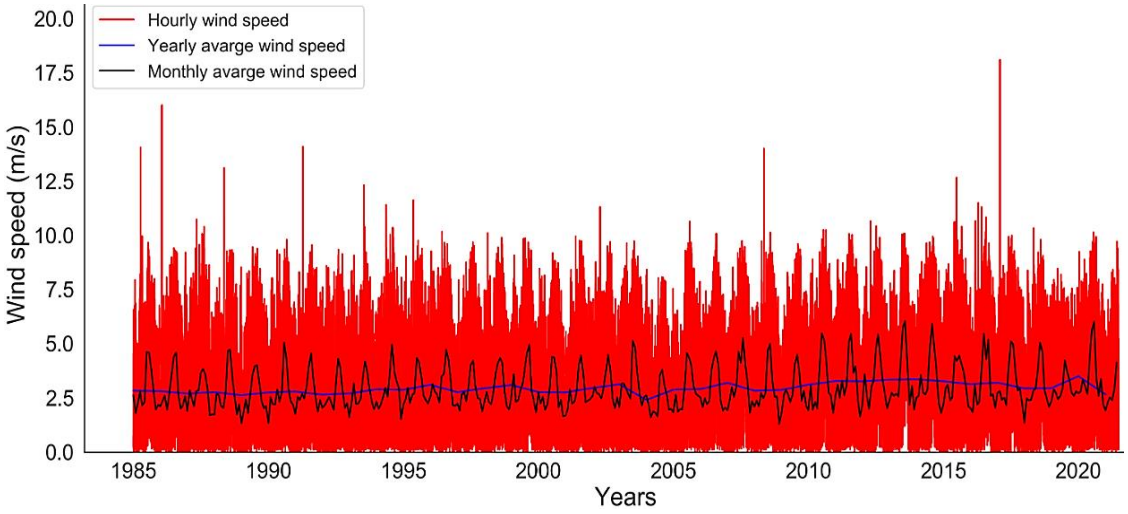

Figure A.5-25. UAE hourly intervals historical wind speed performance over 36 years.

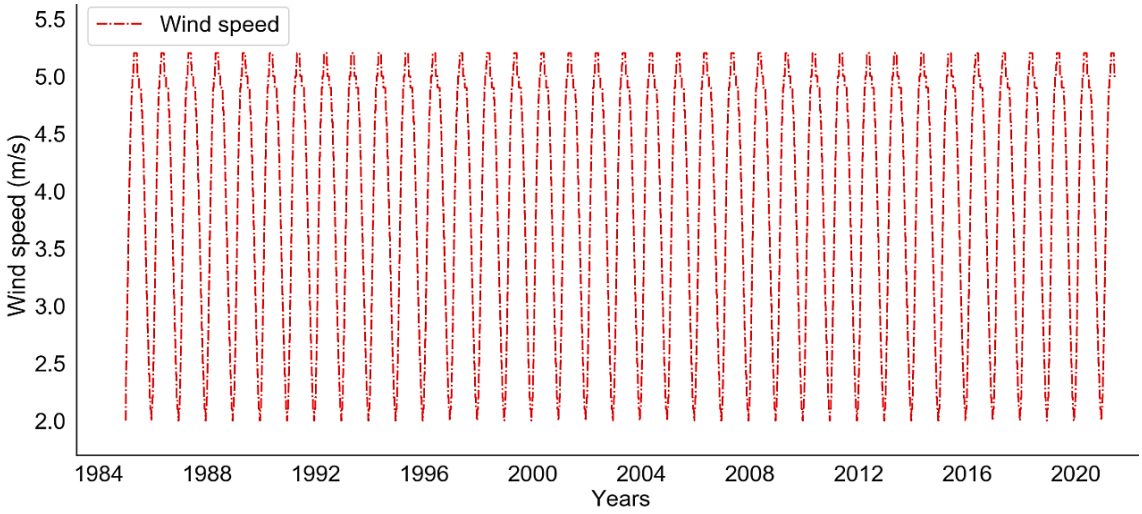

Figure A.5-26. UAE daily intervals historical wind speed performance over 36 years.

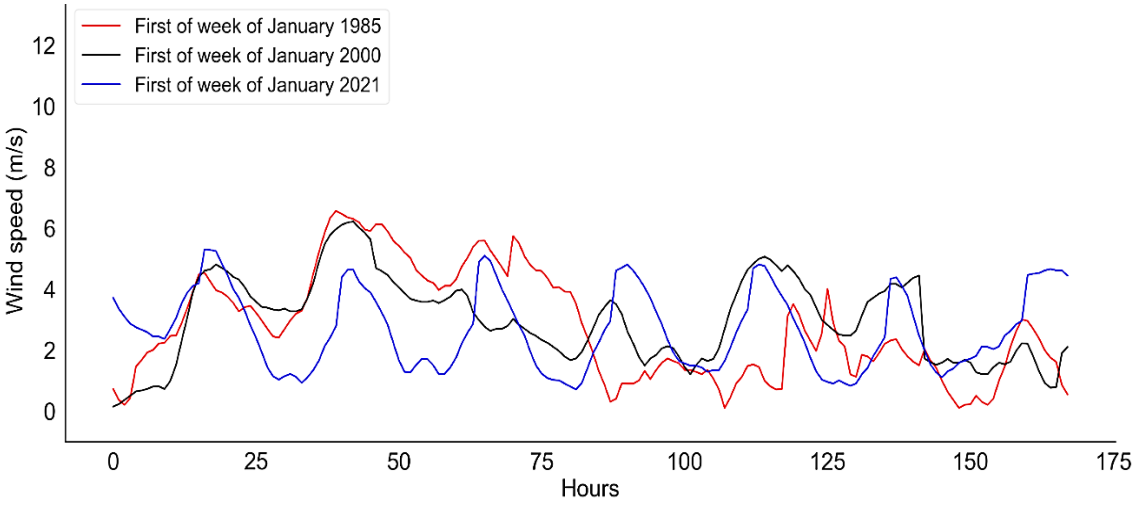

Figure A.5-27. The first three historical weeks of wind speed performance for UAE during January at hourly intervals.

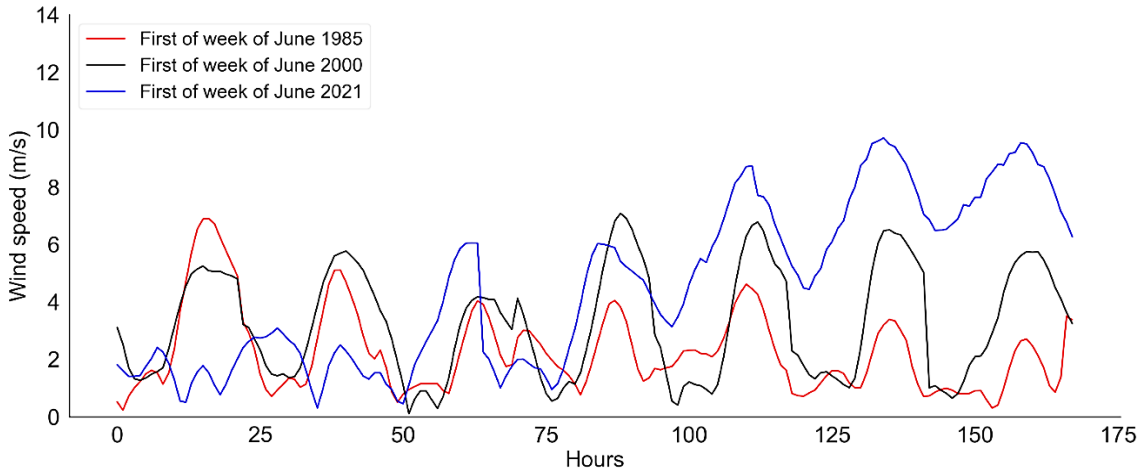

Figure A.5-28. The first three historical weeks of wind speed performance for UAE during June at hourly intervals.

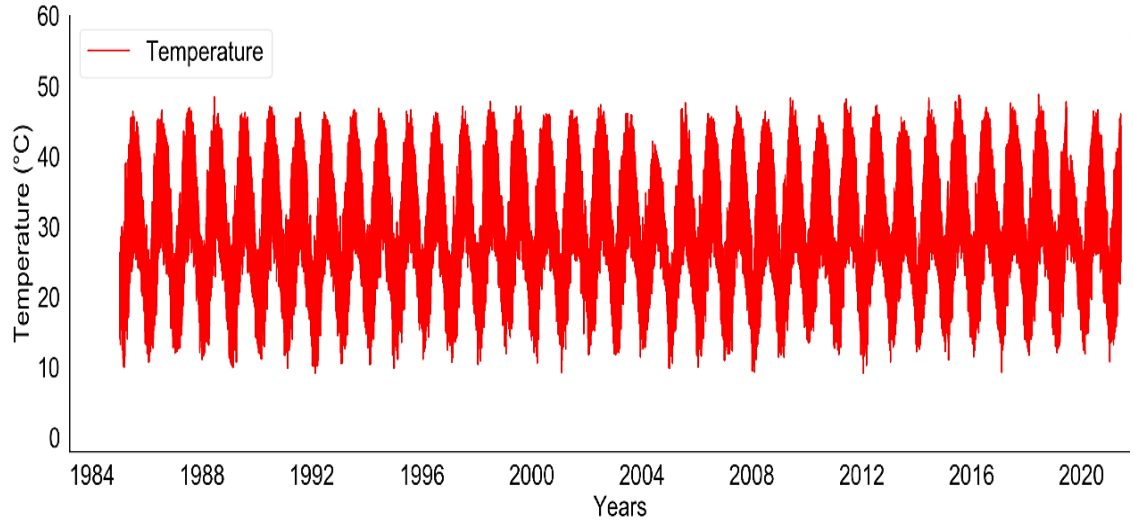

Figure A.5-29. The historical temperature performance over 36 years at hourly intervals for UAE.

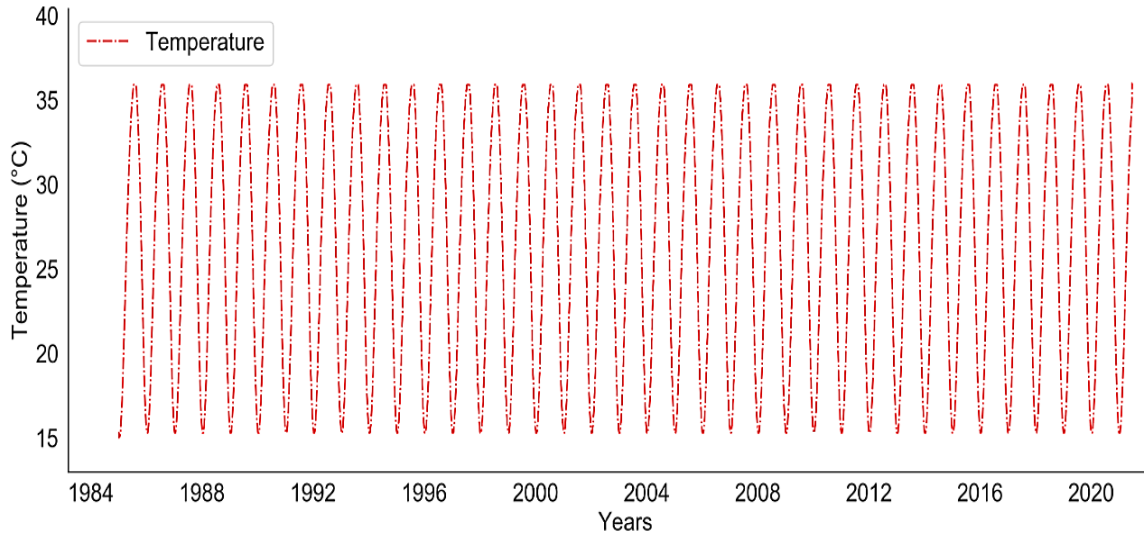

Figure A.5-30. The historical temperature performance over 36 years at daily intervals for UAE.

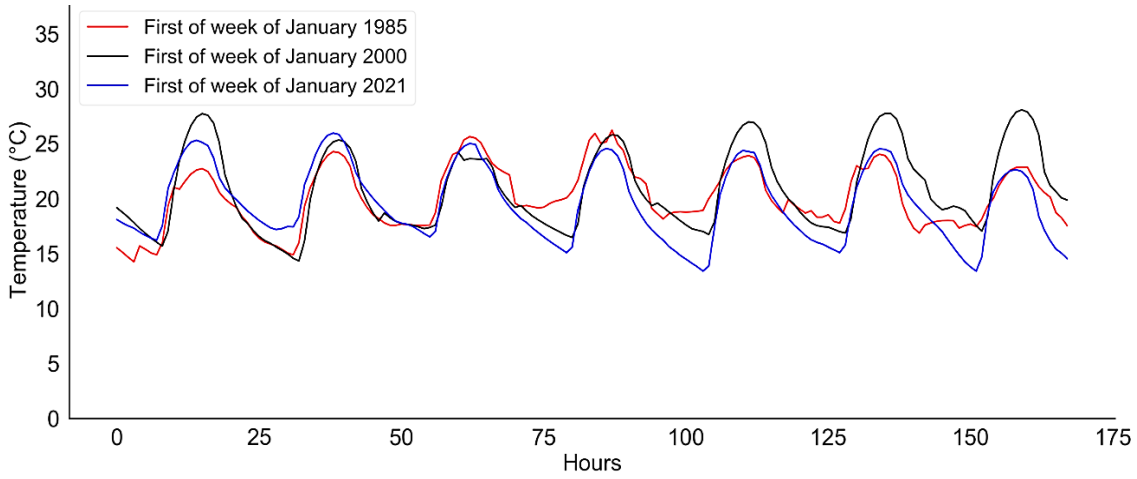

Figure A.5-31. The first three historical weeks of temperature performance for UAE during January at hourly intervals.

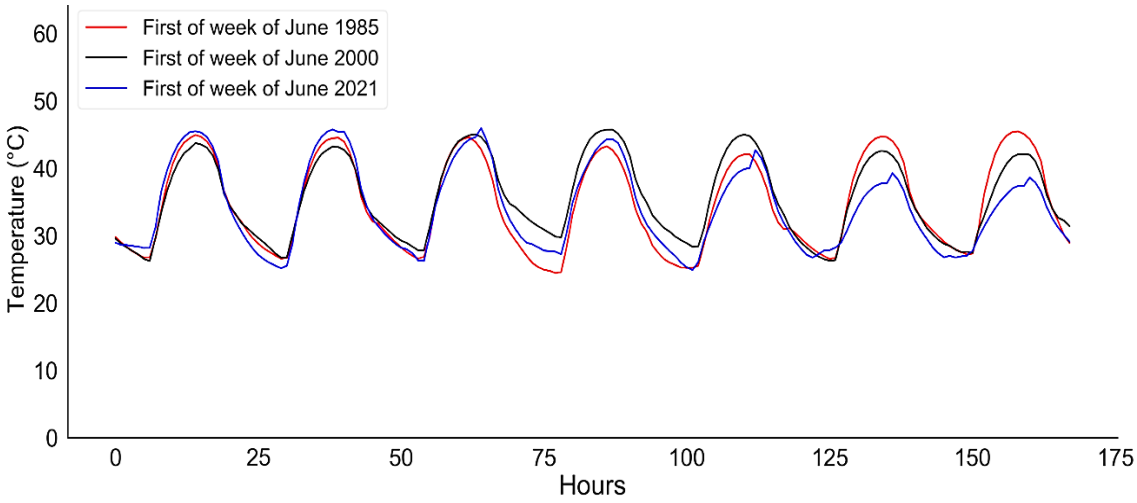

Figure A.5-32. The first three historical weeks of temperature performance for UAE during June at hourly intervals.

A.5.3 Kuwait Historical Wind Speed and Temperature Data

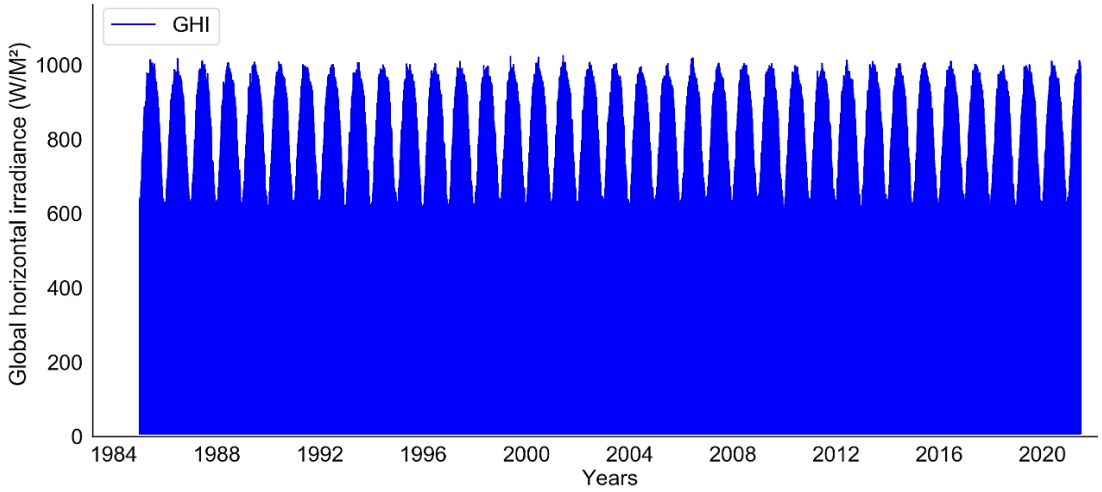

Figure A.5-33. Kuwait hourly intervals historical performance of the GHI over 36 years.

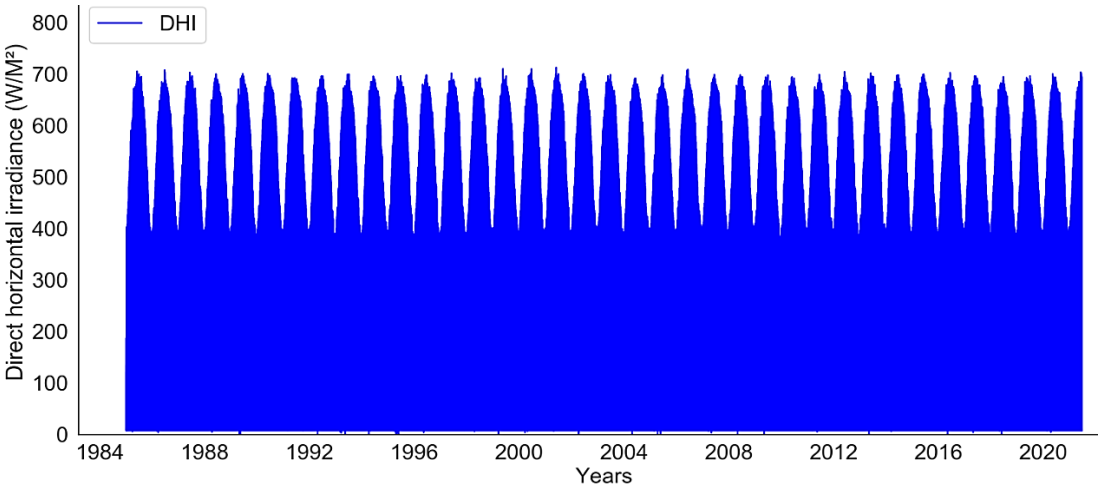

Figure A.5-34. Kuwait hourly intervals historical performance of the DHI over 36 years.

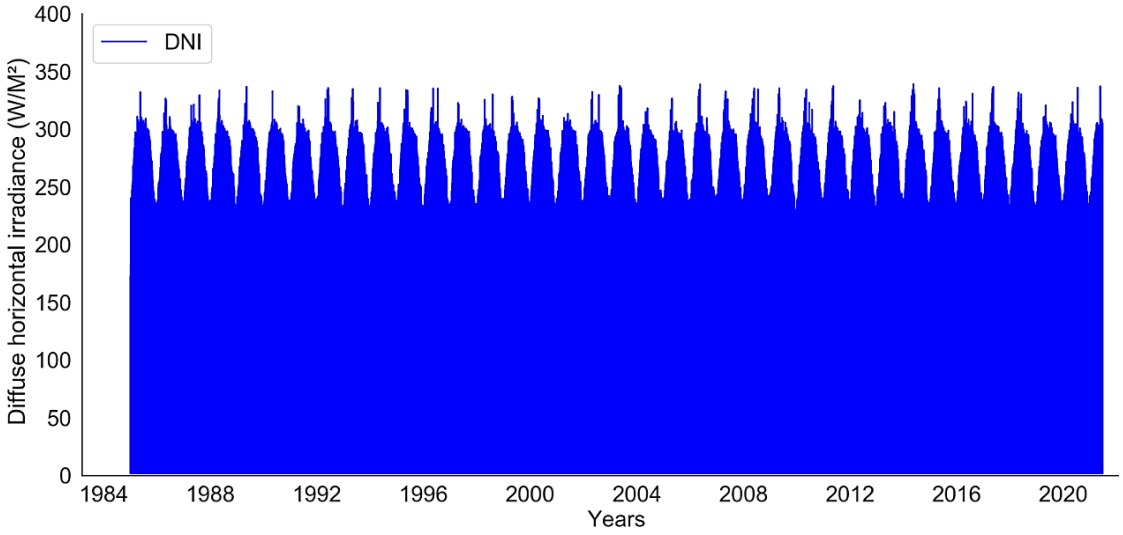

Figure A.5-35. Kuwait hourly intervals historical performance of the DNI over 36 years.

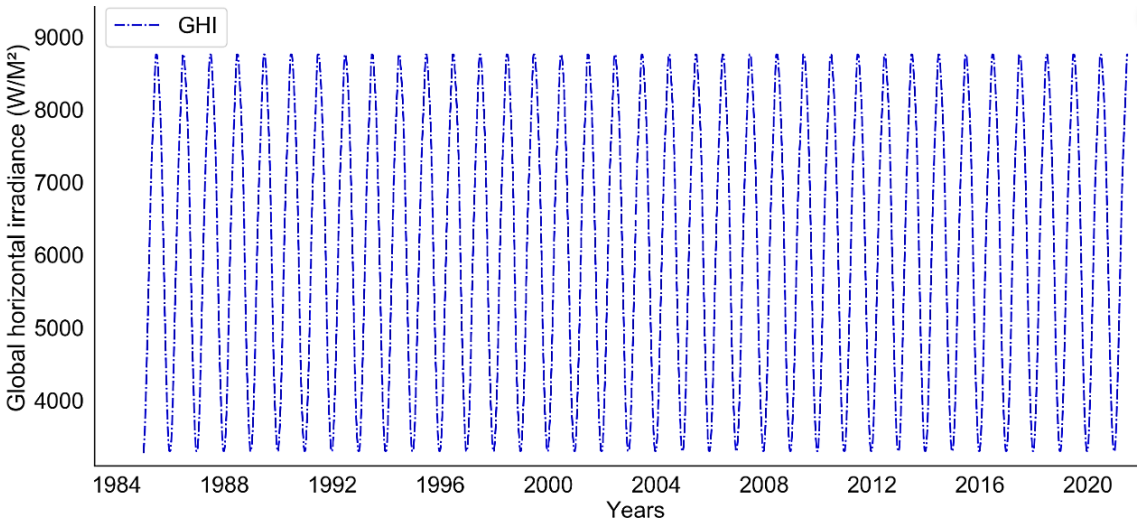

Figure A.5-36. Kuwait daily intervals historical performance of the GHI over 36 years.

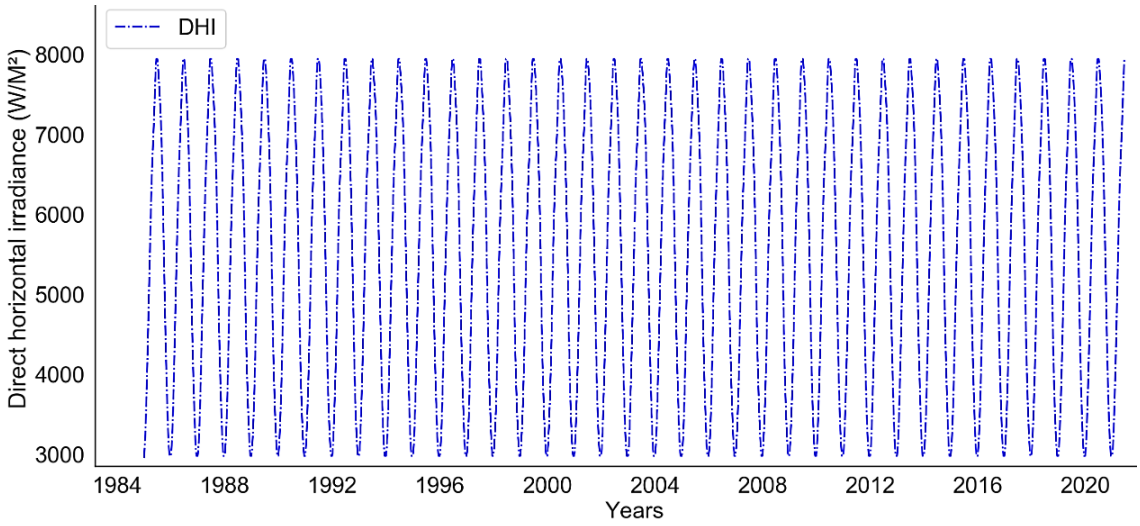

Figure A.5-37. Kuwait daily intervals historical performance of the DHI over 36 years.

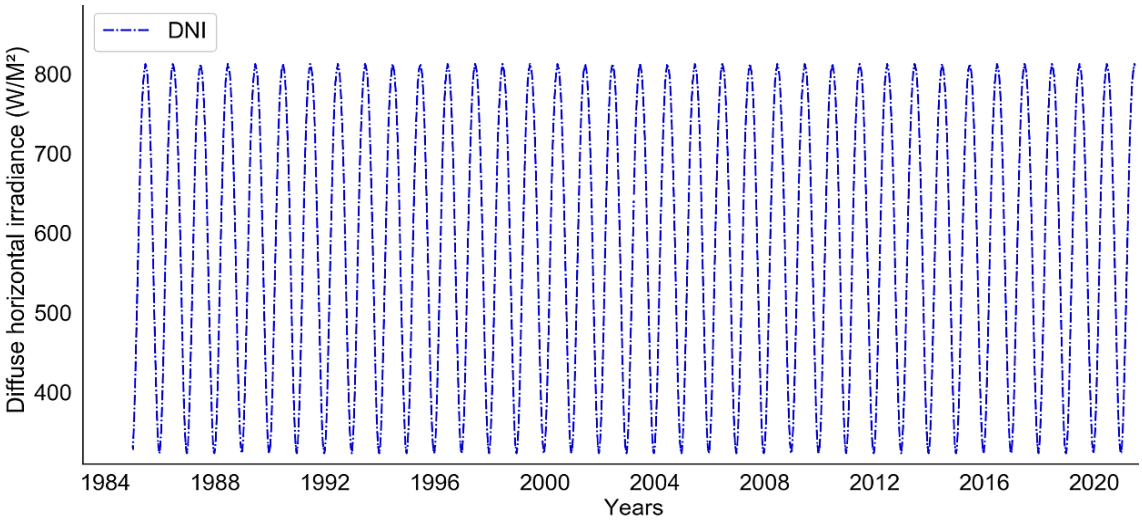

Figure A.5-38. Kuwait daily intervals historical performance of the DNI over 36 years.

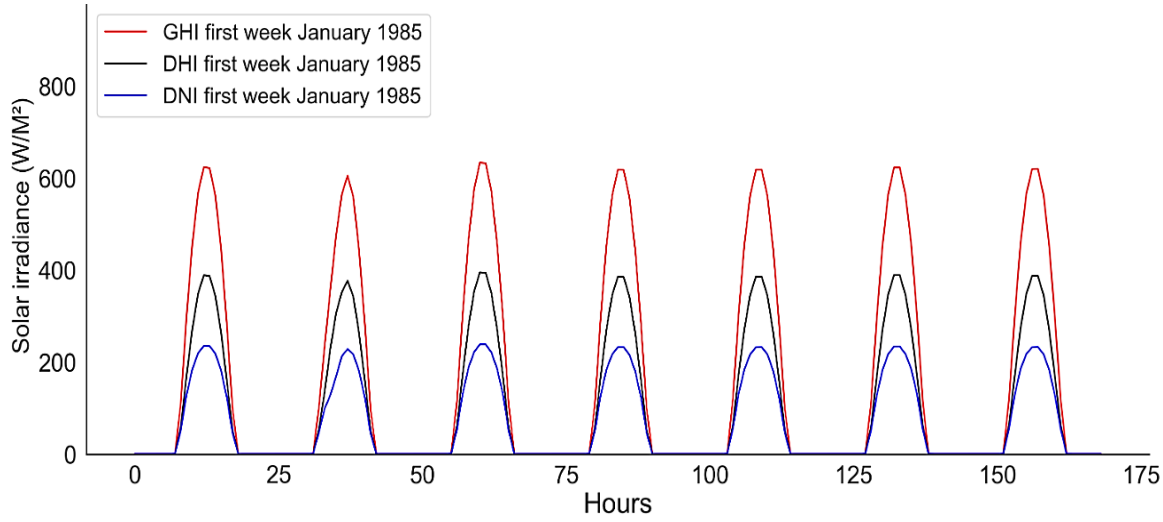

Figure A.5-39. Kuwait hourly intervals historical performances of the GHI, DHI, and DNI during January 1985.

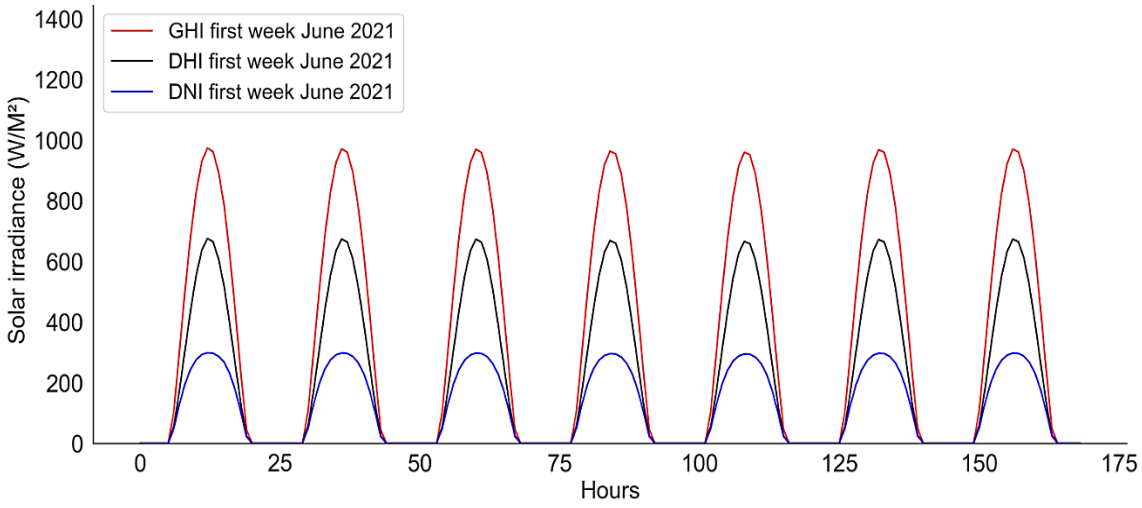

Figure A.5-40. Kuwait hourly intervals historical performances of the GHI, DHI, and DNI during June 2021.

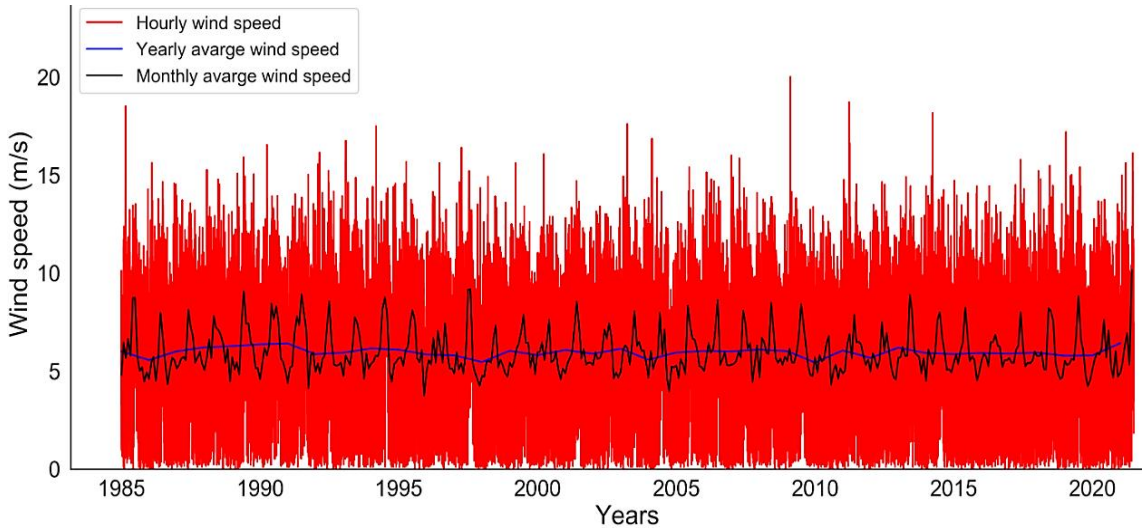

Figure A.5-41. Kuwait hourly, monthly and yearly intervals historical wind speed performance over 36 years.

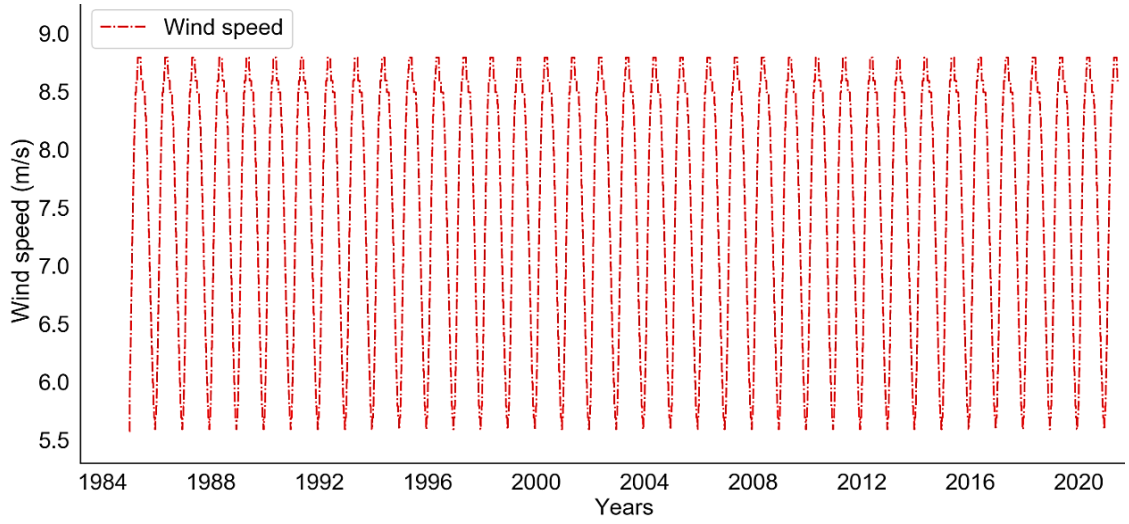

Figure A.5-42. Kuwait daily intervals historical wind speed performance over 36 years.

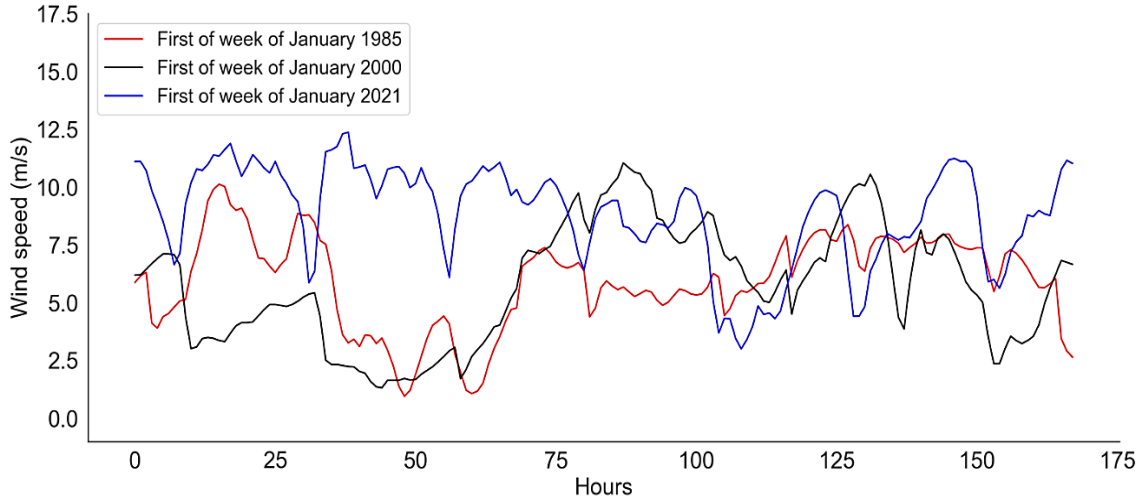

Figure A.5-43. The first three historical weeks of temperature performance for Kuwait during January at hourly intervals.

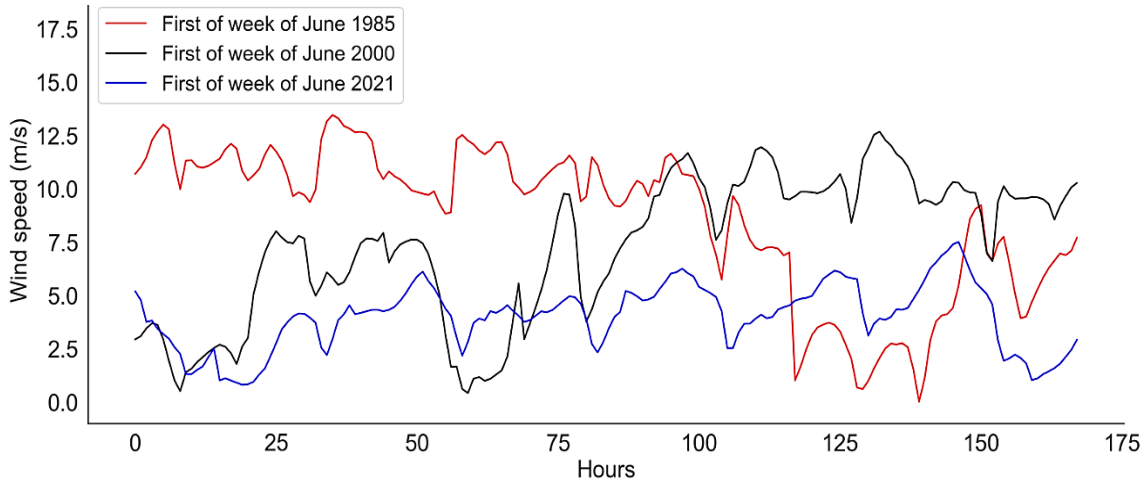

Figure A.5-44. The first three historical weeks of temperature performance for Kuwait during June at hourly intervals

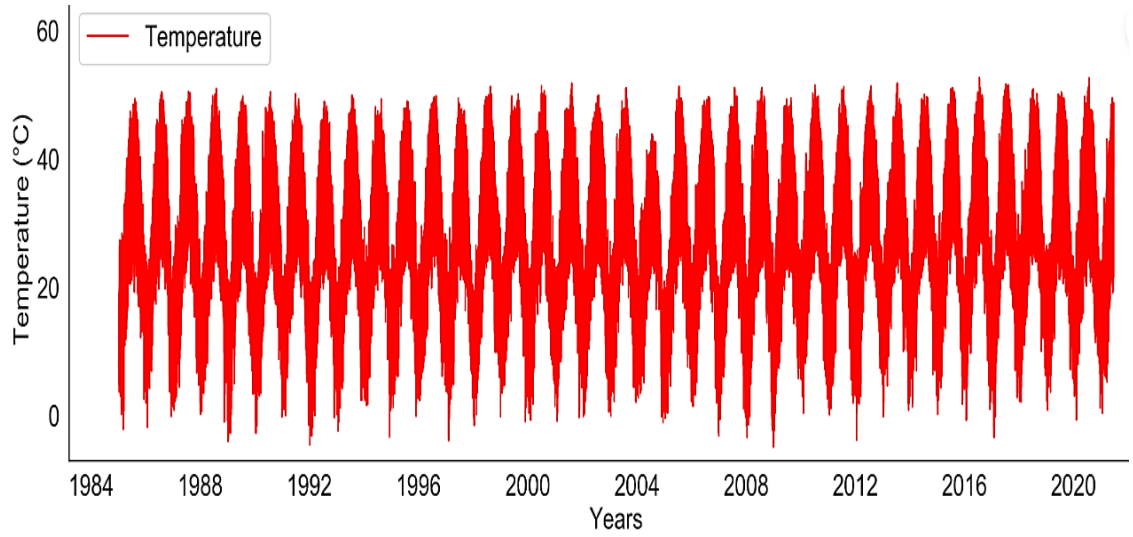

Figure A.5-45. The historical temperature performance over 36 years at hourly intervals for Kuwait.

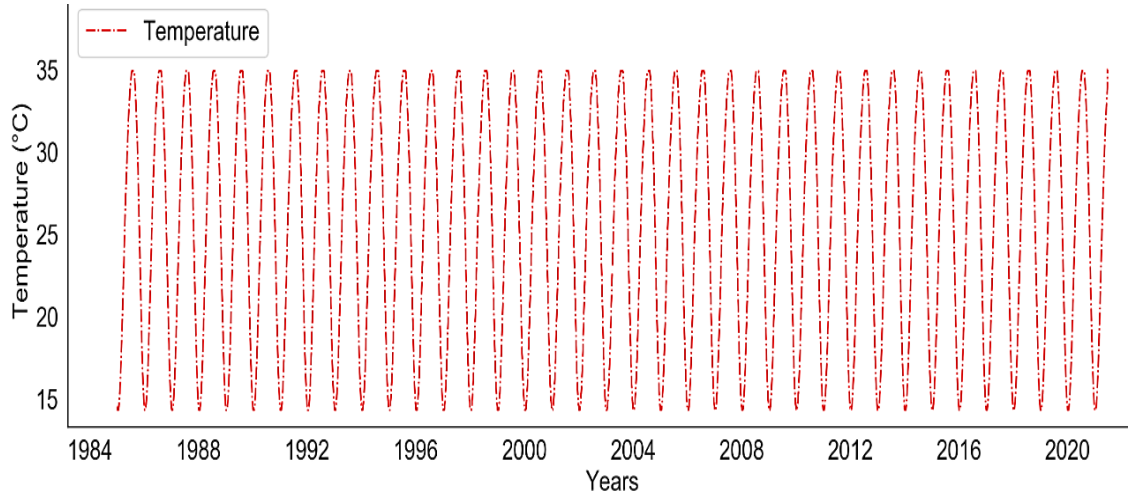

Figure A.5-46. The historical temperature performance over 36 years at daily intervals for Kuwait.

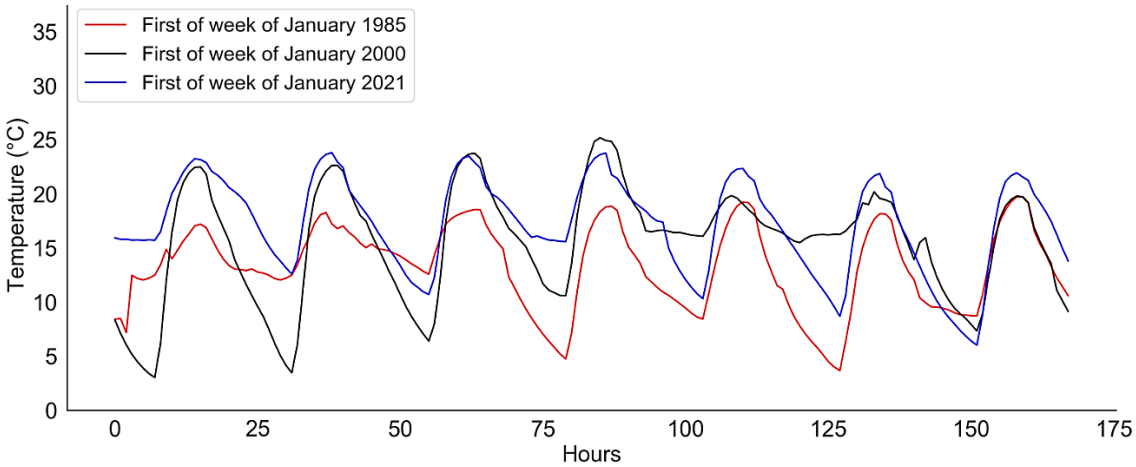

Figure A.5-47. The first three historical weeks of temperature performance for Kuwait during January at hourly intervals.

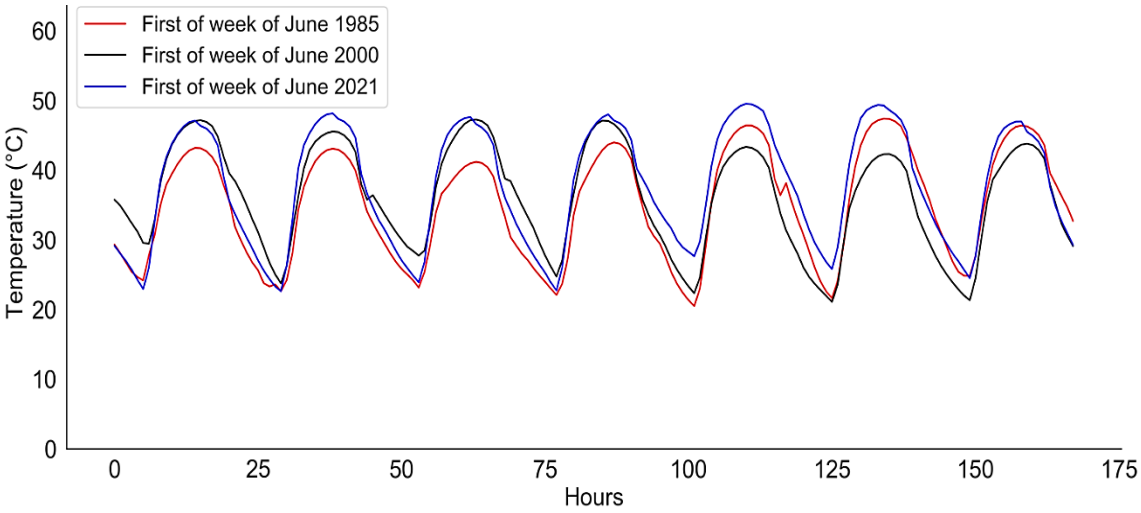

Figure A.5-48. The first three historical weeks of temperature performance for Kuwait during June at hourly intervals.

A.5.4 Qatar Historical Wind Speed and Temperature Data

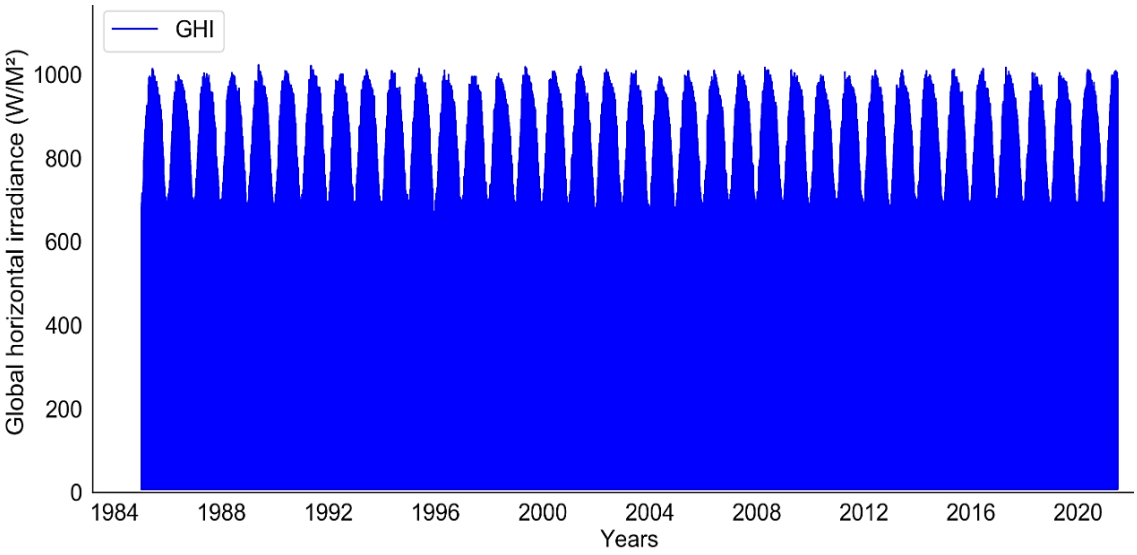

Figure A.5-49. Kuwait hourly intervals historical performance of the GHI over 36 years.

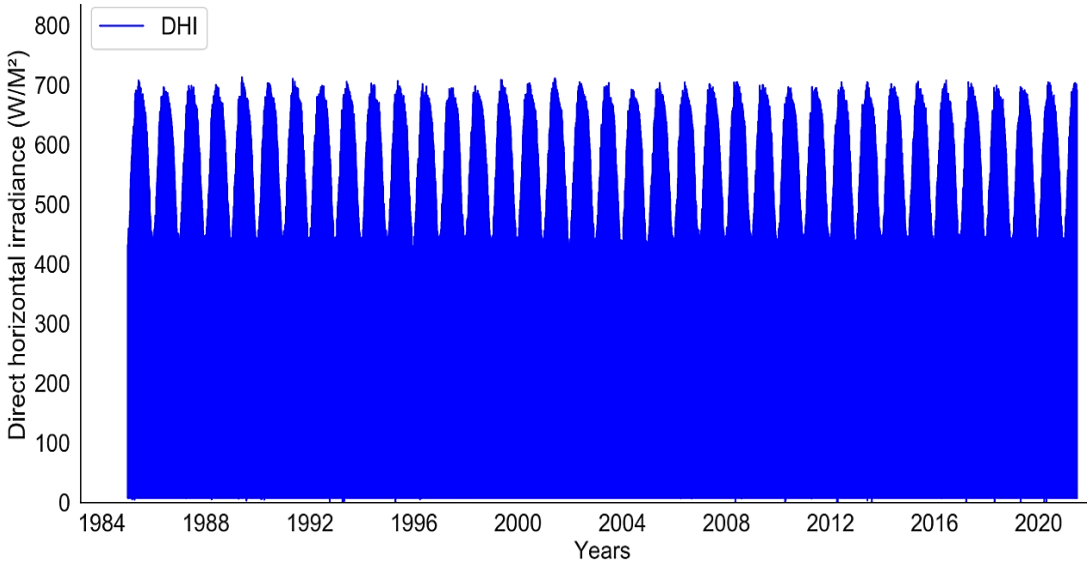

Figure A.5-50. Kuwait hourly intervals historical performance of the DHI over 36 years.

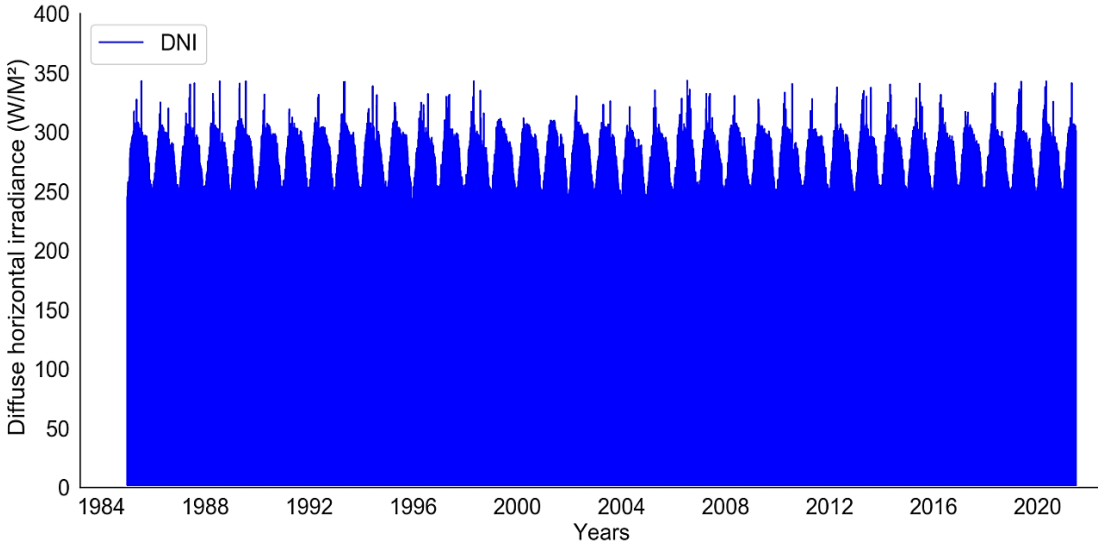

Figure A.5-51. Kuwait hourly intervals historical performance of the DNI over 36 years.

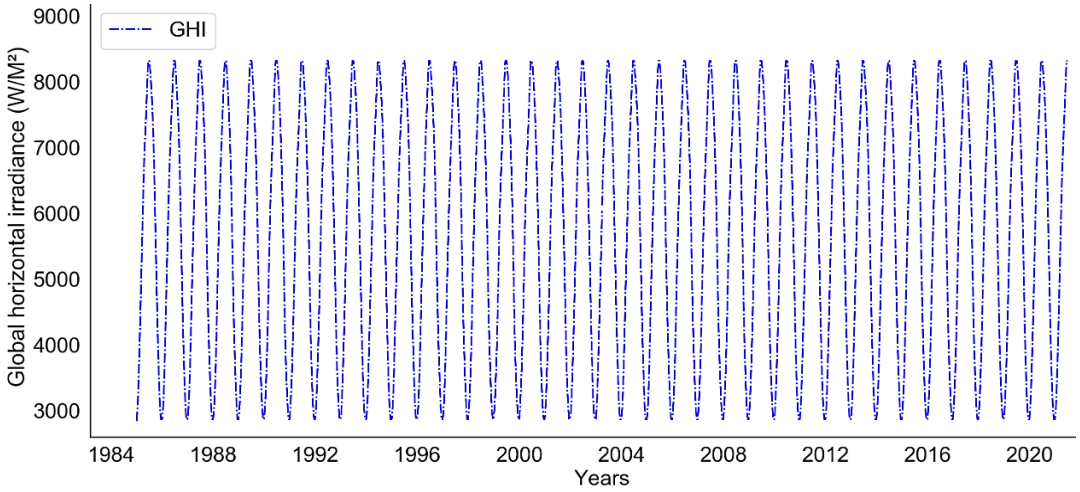

Figure A.5-52. Kuwait daily intervals historical performance of the GHI over 36 years.

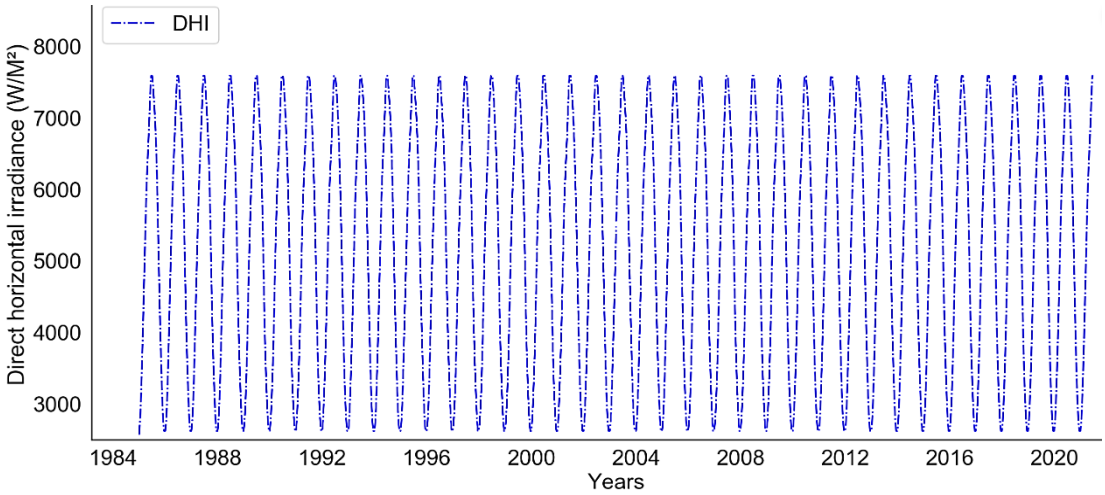

Figure A.5-53. Kuwait daily intervals historical performance of the DHI over 36 years.

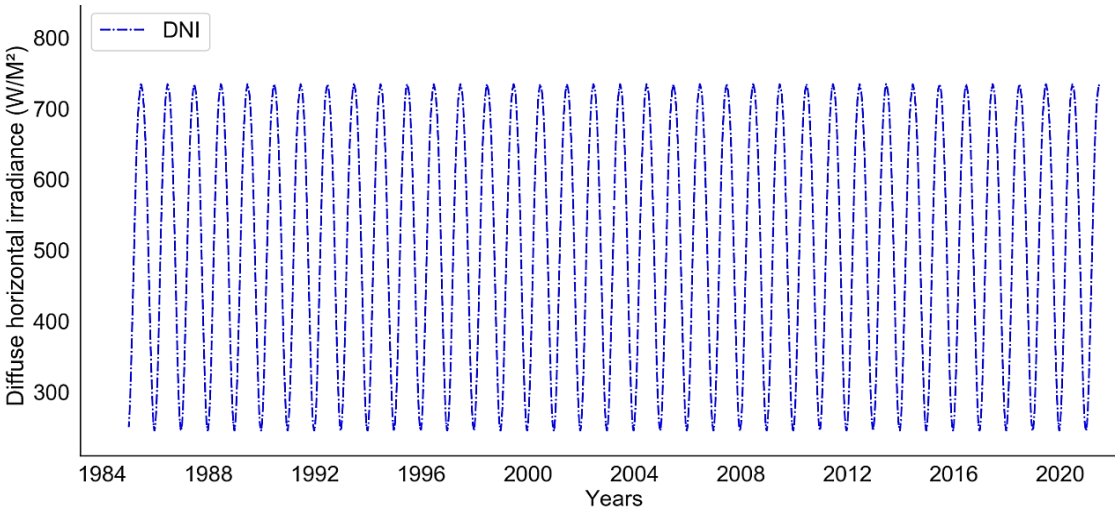

Figure A.5-54. Kuwait daily intervals historical performance of the DNI over 36 years.

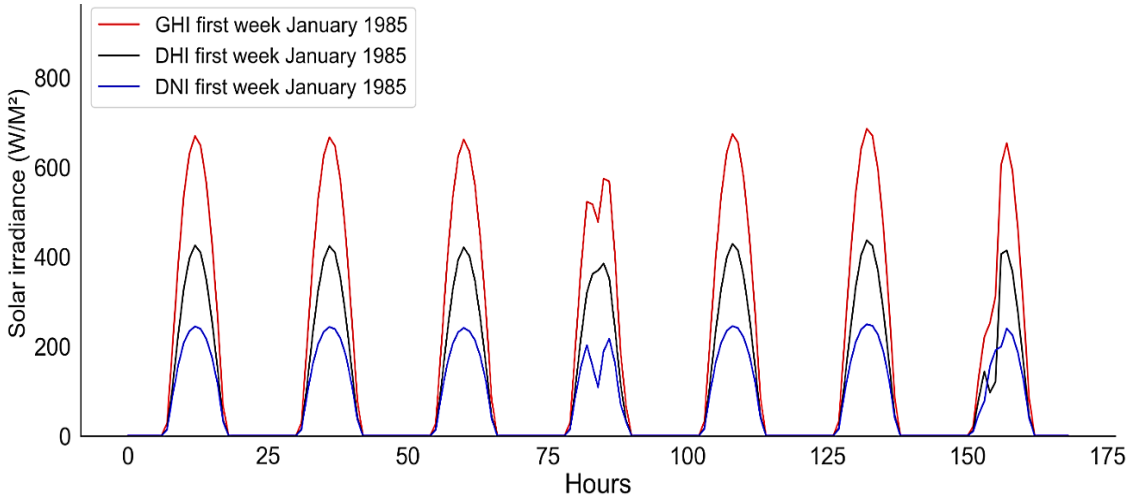

Figure A.5-55. Kuwait hourly intervals historical performances of the GHI, DHI, and DNI during January 1985.

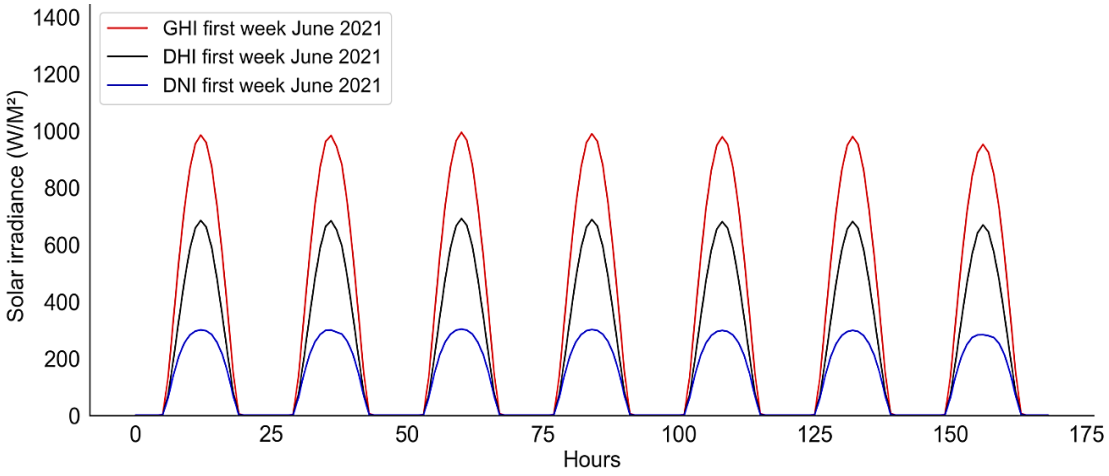

Figure A.5-56. Kuwait hourly intervals historical performances of the GHI, DHI, and DNI during June 2021.

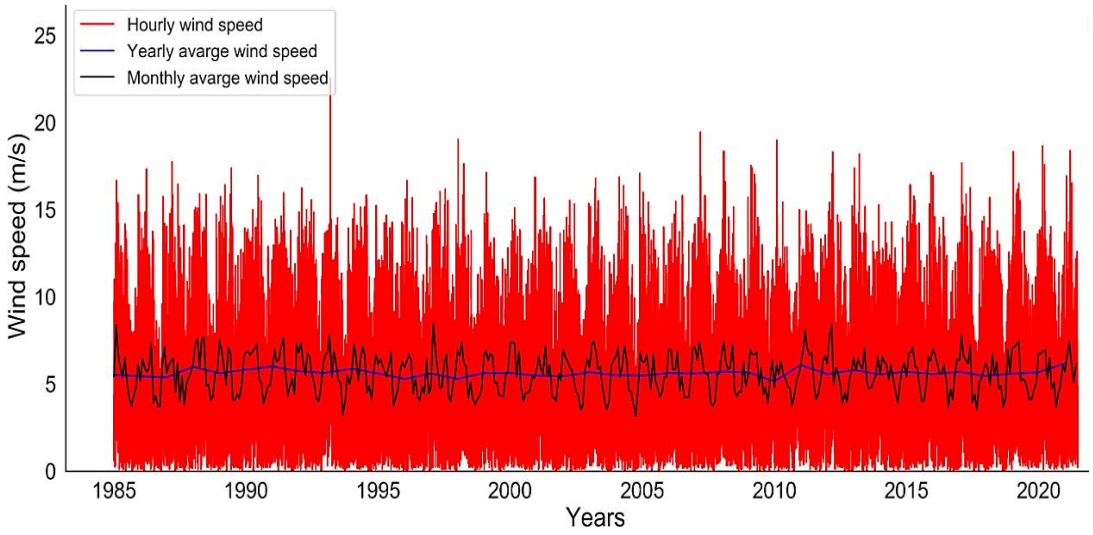

Figure A.5-57. Qatar hourly, monthly, and yearly intervals historical wind speed performance over 36 years.

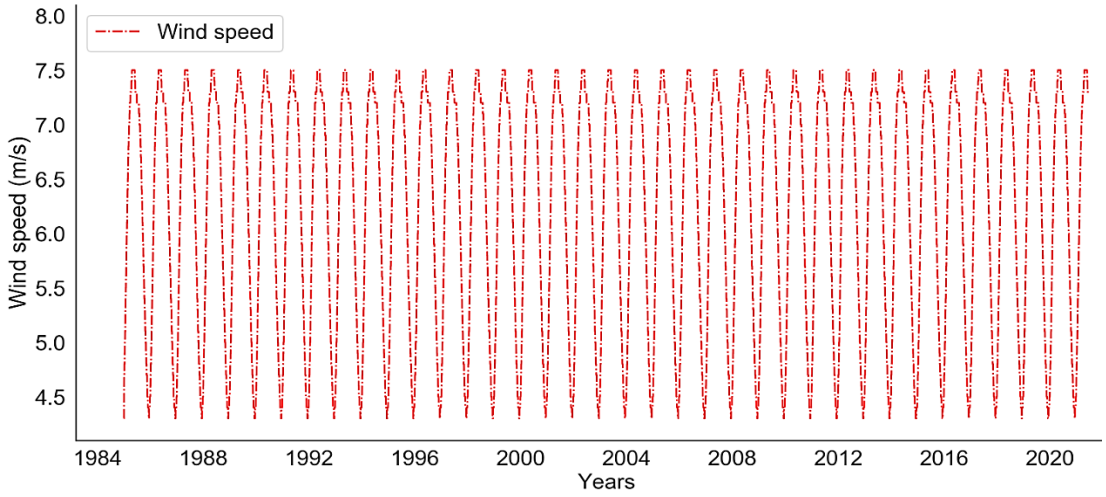

Figure A.5-58. Qatar daily intervals historical wind speed performance over 36 years.

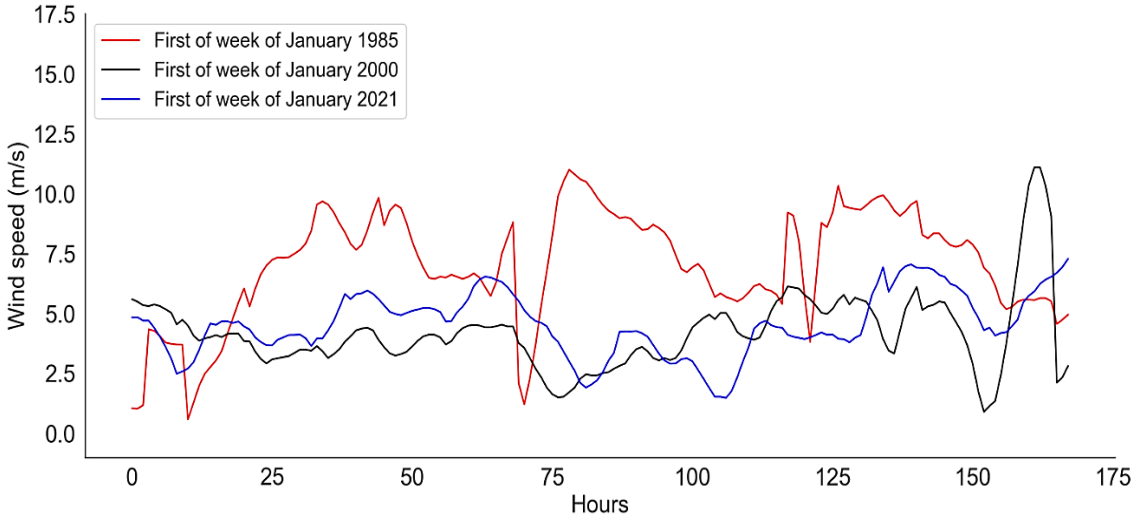

Figure A.5-59. The first three historical weeks of temperature performance for Qatar during January at hourly intervals.

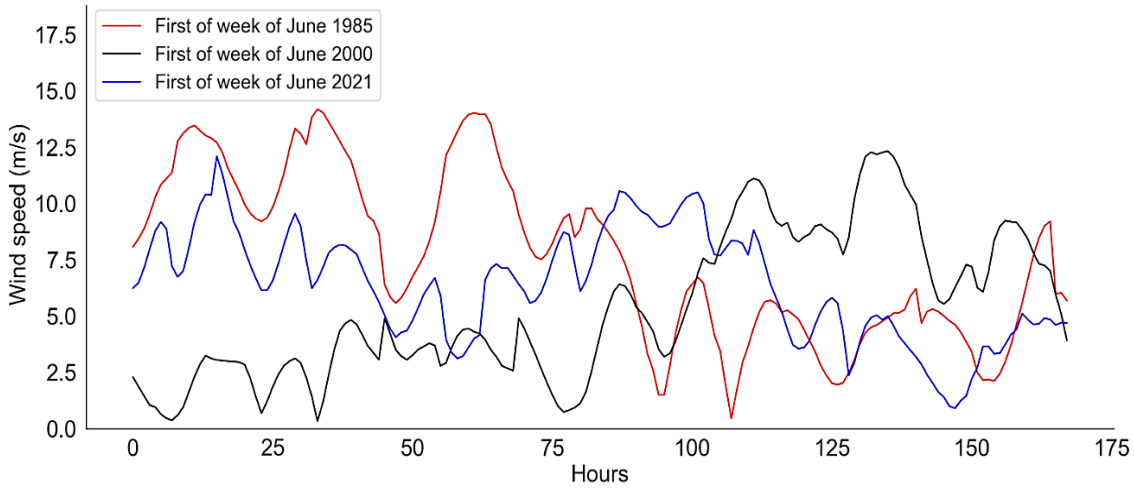

Figure A.5-60. The first three historical weeks of temperature performance for Qatar during June at hourly intervals.

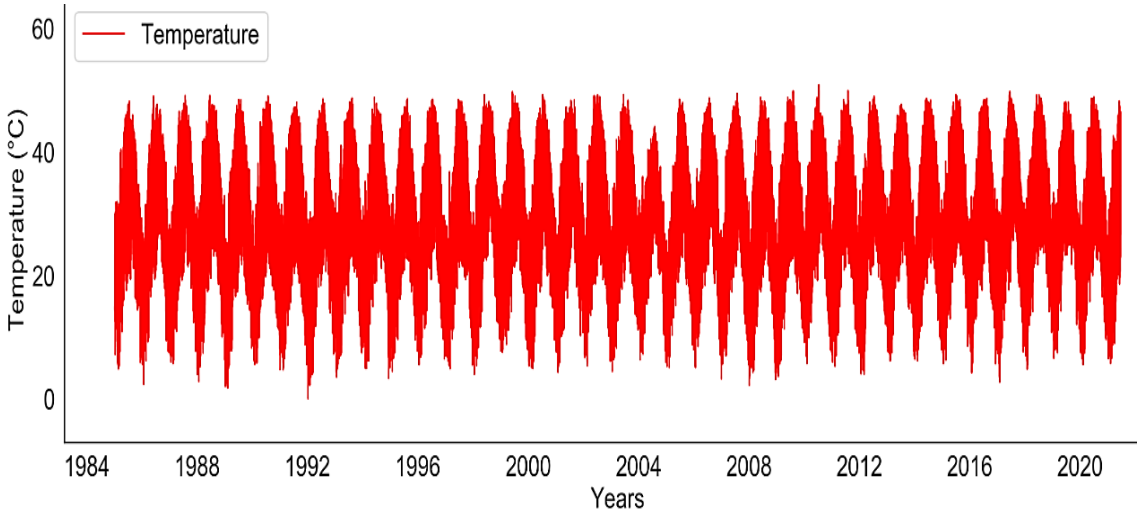

Figure A.5-61. The historical temperature performance over 36 years at hourly intervals for Qatar.

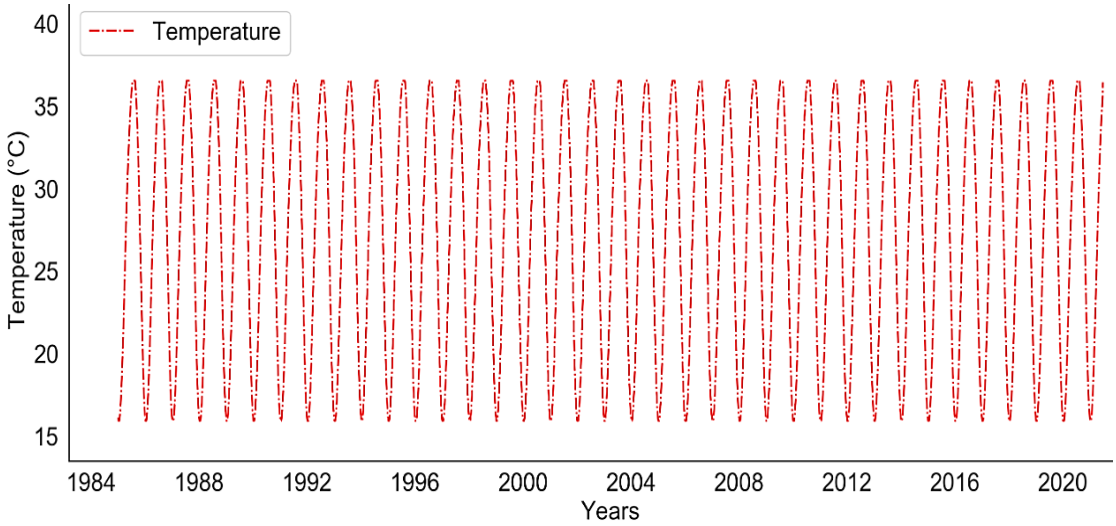

Figure A.5-62. The historical temperature performance over 36 years at daily intervals for Qatar.

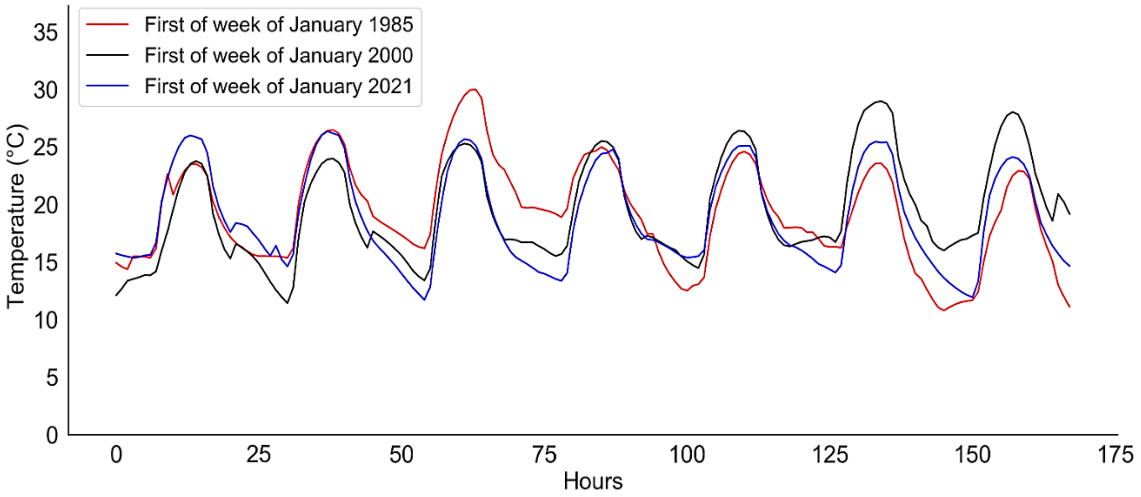

Figure A.5-63. The first three historical weeks of temperature performance for Qatar during January at hourly intervals.

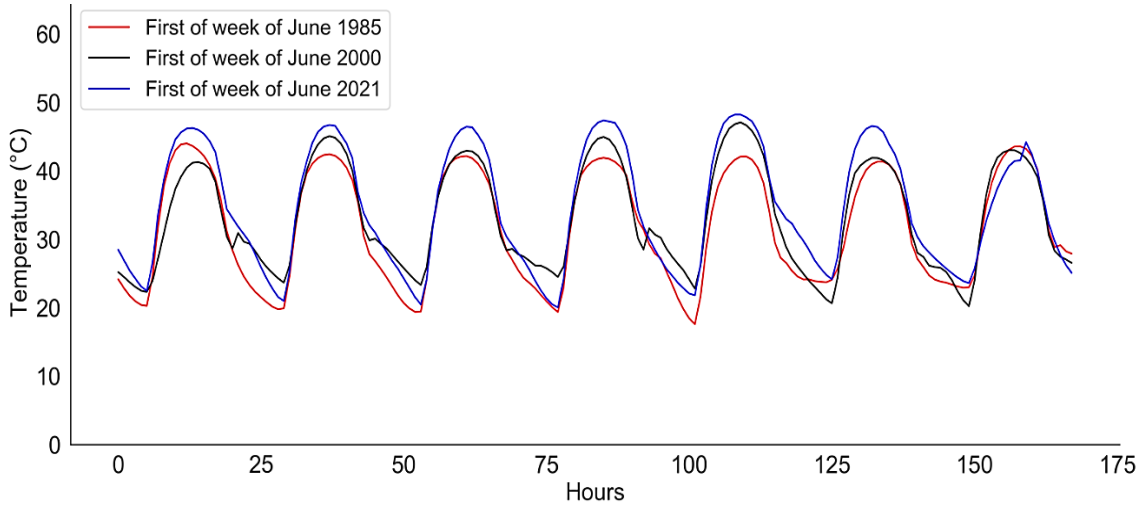

Figure A.5-64. The first three historical weeks of temperature performance for Qatar during June at hourly intervals.

A.5.5 Bahrain Historical Wind Speed and Temperature Data

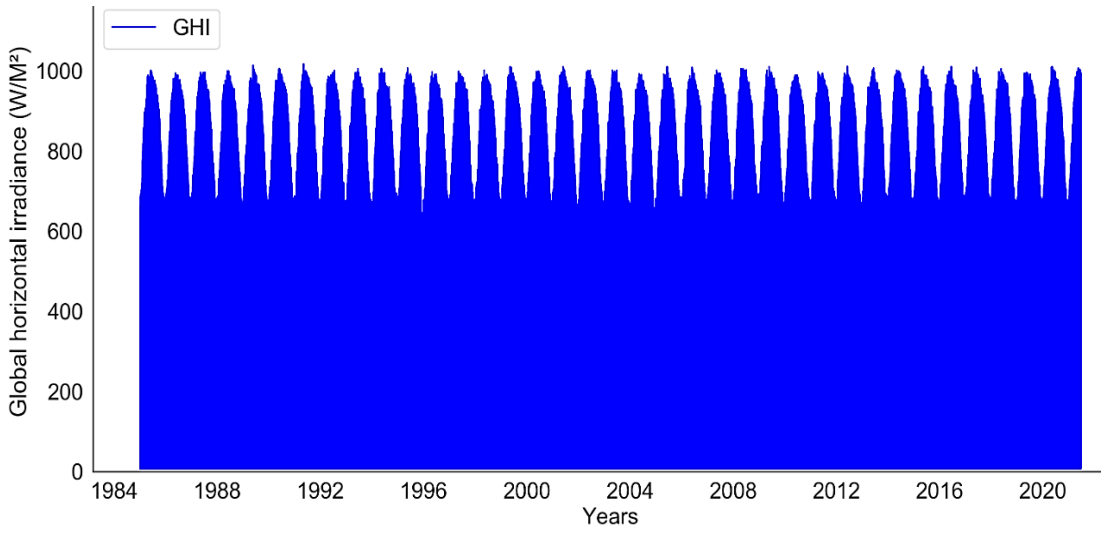

Figure A.5-65. Bahrain hourly intervals historical performance of the GHI over 36 years.

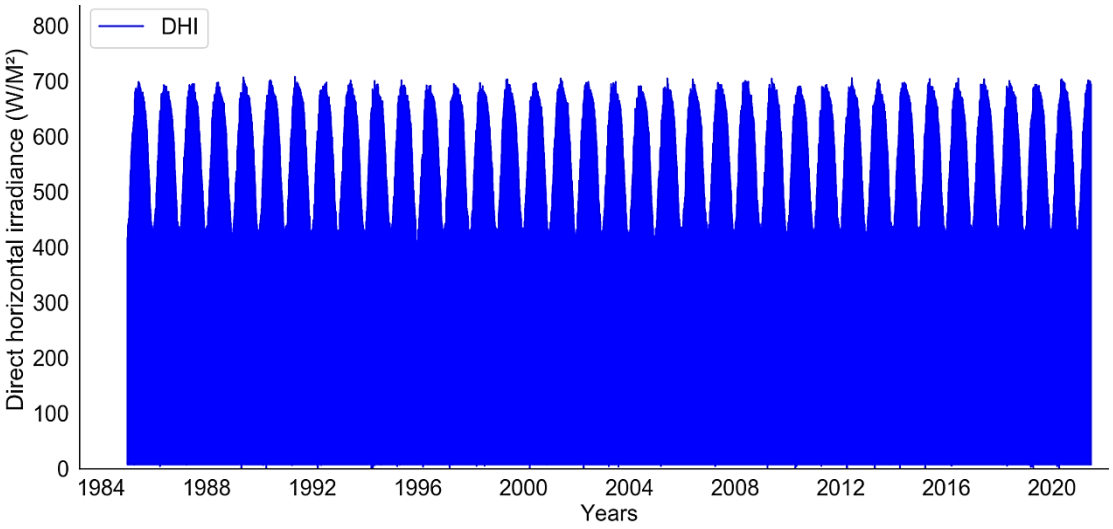

Figure A.5-66. Bahrain hourly intervals historical performance of the DHI over 36 years.

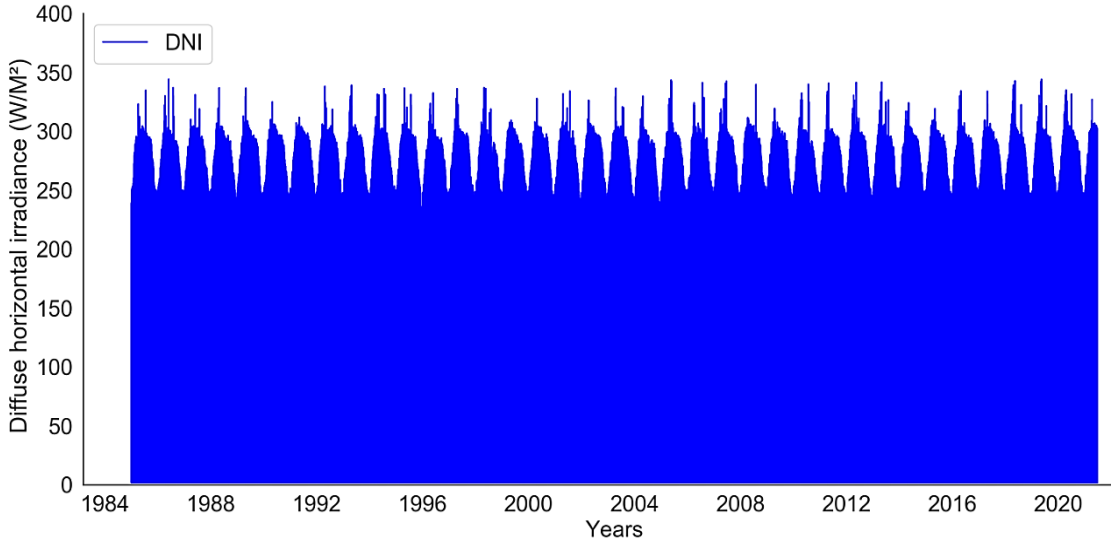

Figure A.5-67. Bahrain hourly intervals historical performance of the DNI over 36 years.

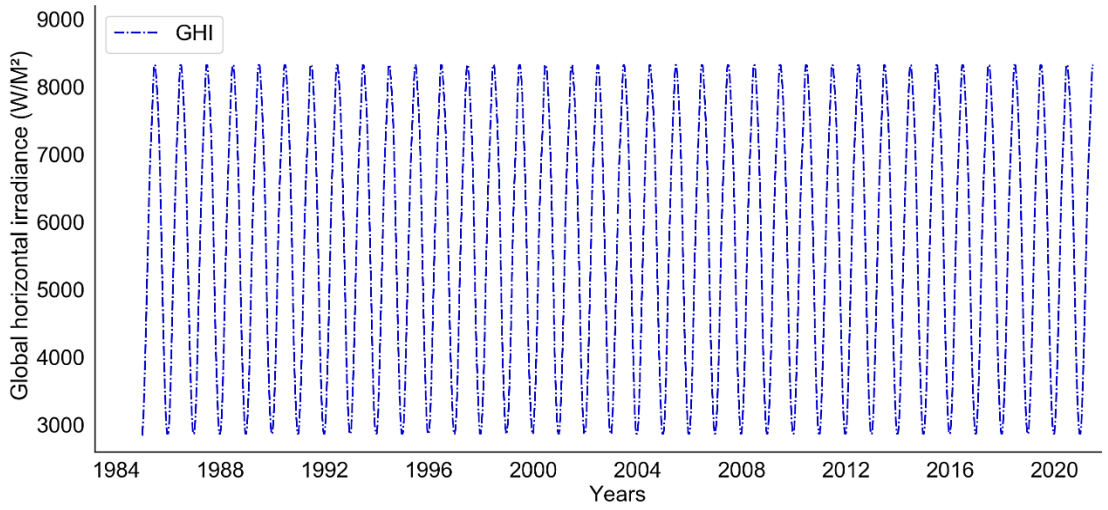

Figure A.5-68. Bahrain daily intervals historical performance of the GHI over 36 years.

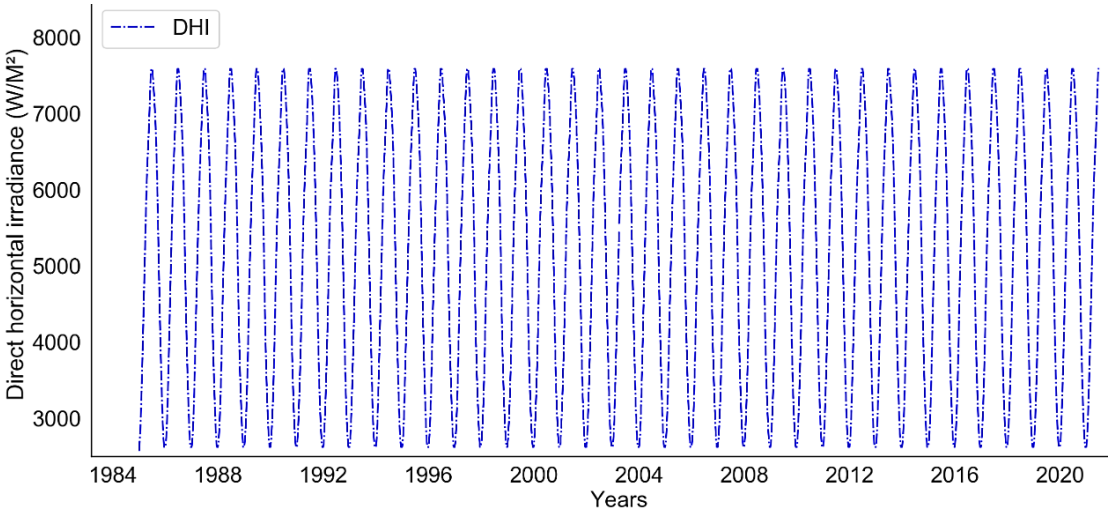

Figure A.5-69. Bahrain daily intervals historical performance of the DHI over 36 years.

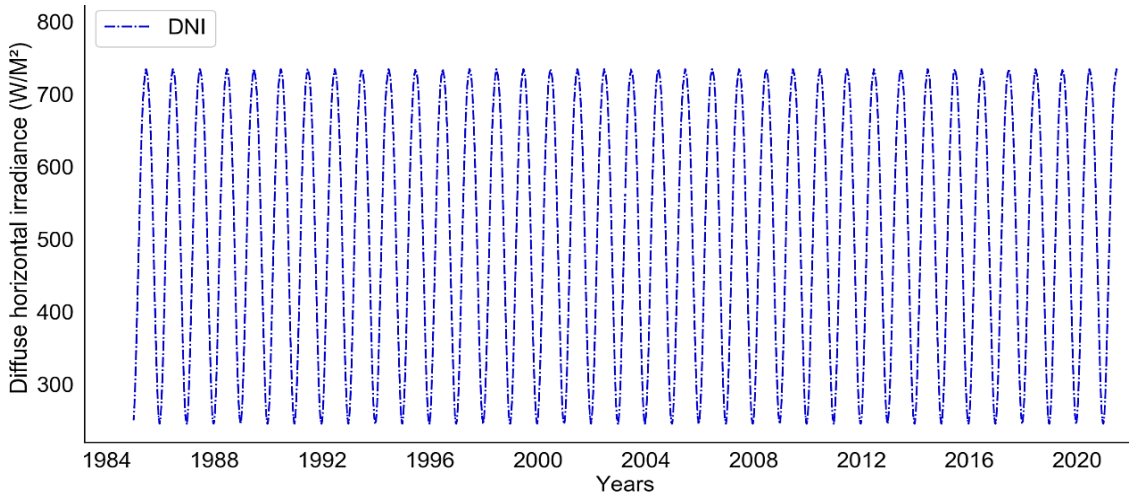

Figure A.5-70. Bahrain daily intervals historical performance of the DNI over 36 years.

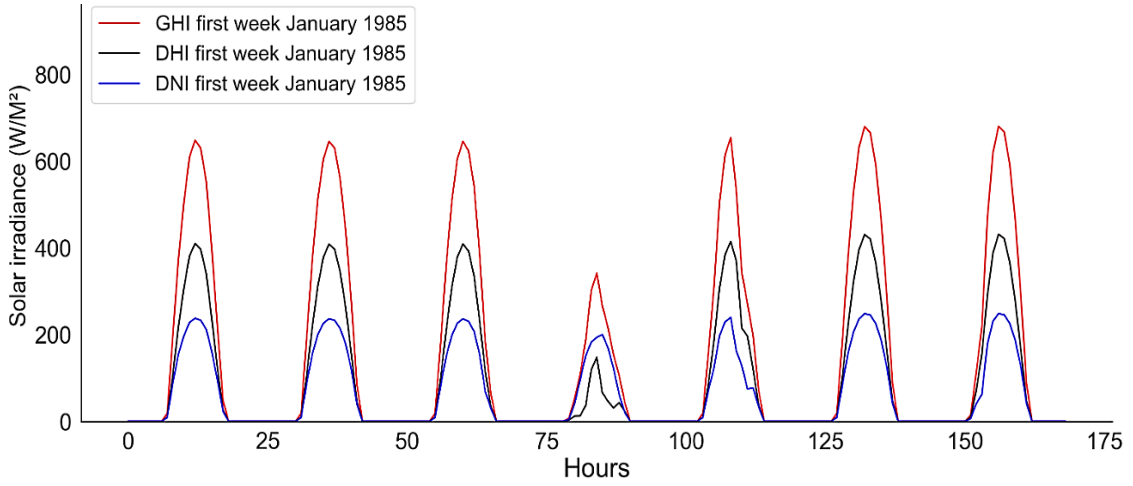

Figure A.5-71. Bahrain hourly intervals historical performances of the GHI, DHI, and DNI during January 1985.

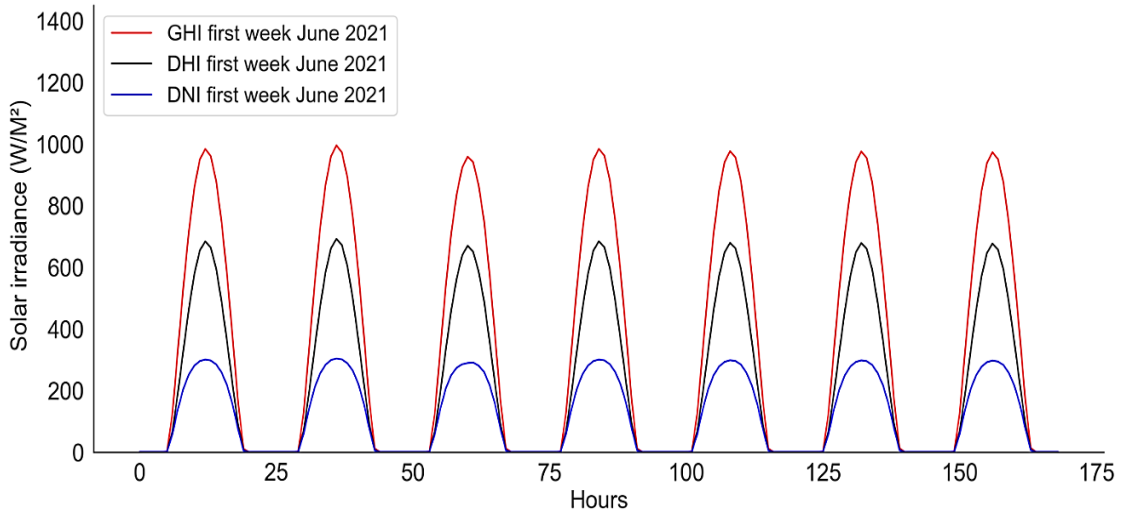

Figure A.5-72. Bahrain hourly intervals historical performances of the GHI, DHI, and DNI during June 2021.

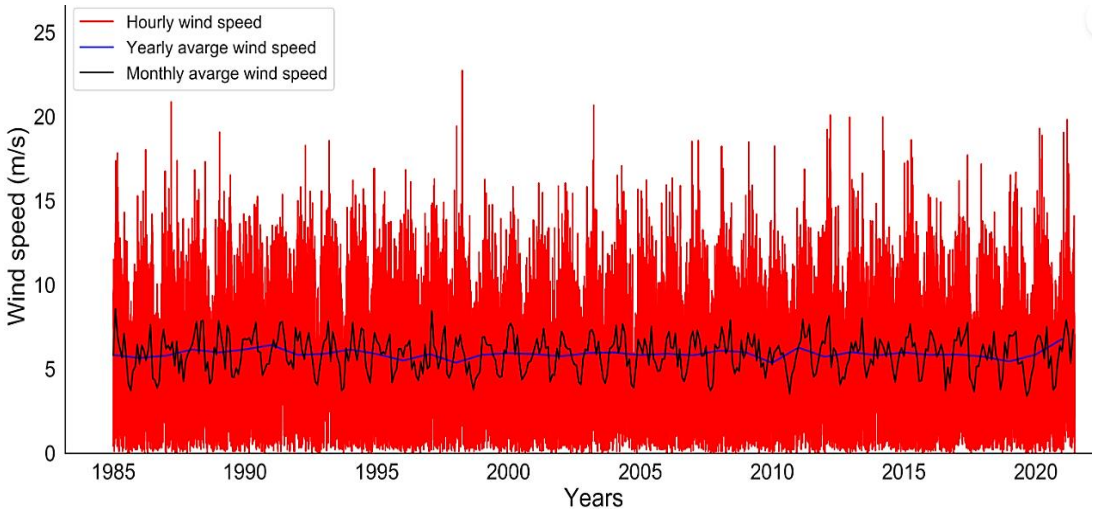

Figure A.5-73. Bahrain hourly, monthly and yearly intervals historical wind speed performance over 36 years.

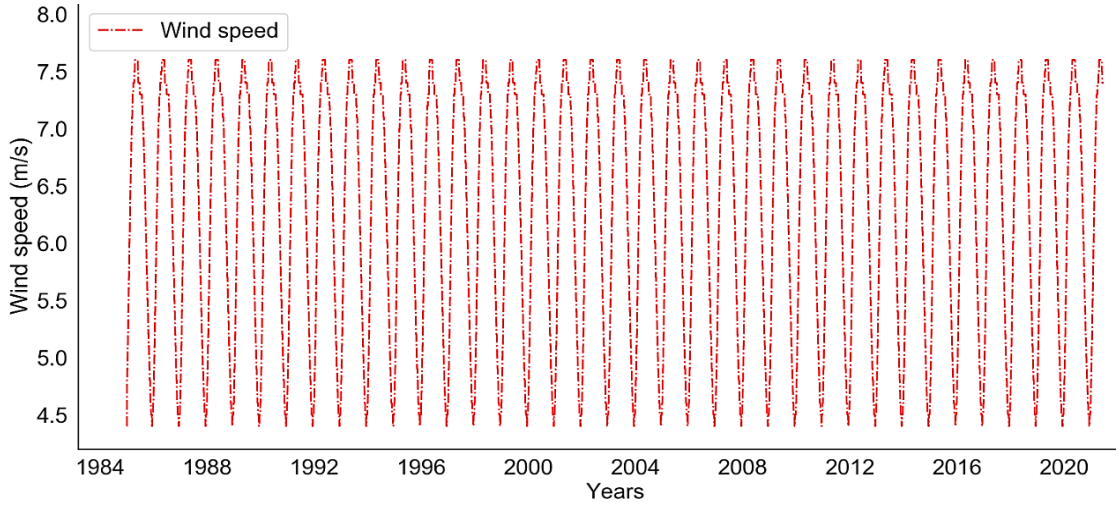

Figure A.5-74. Bahrain daily intervals historical wind speed performance over 36 years.

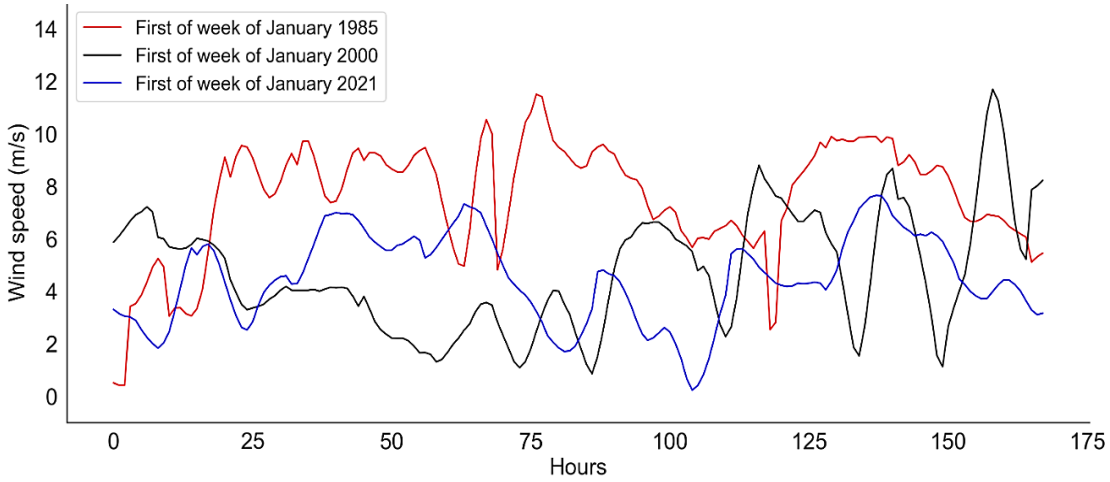

Figure A.5-75. The first three historical weeks of wind speed performance for Bahrain during January at hourly intervals.

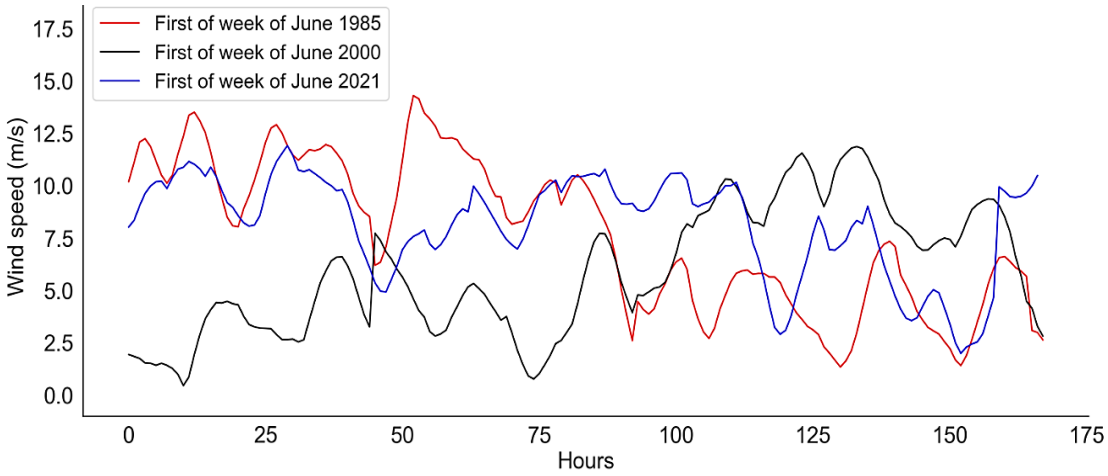

Figure A.5-76. The first three historical weeks of wind speed performance for Bahrain during June at hourly intervals.

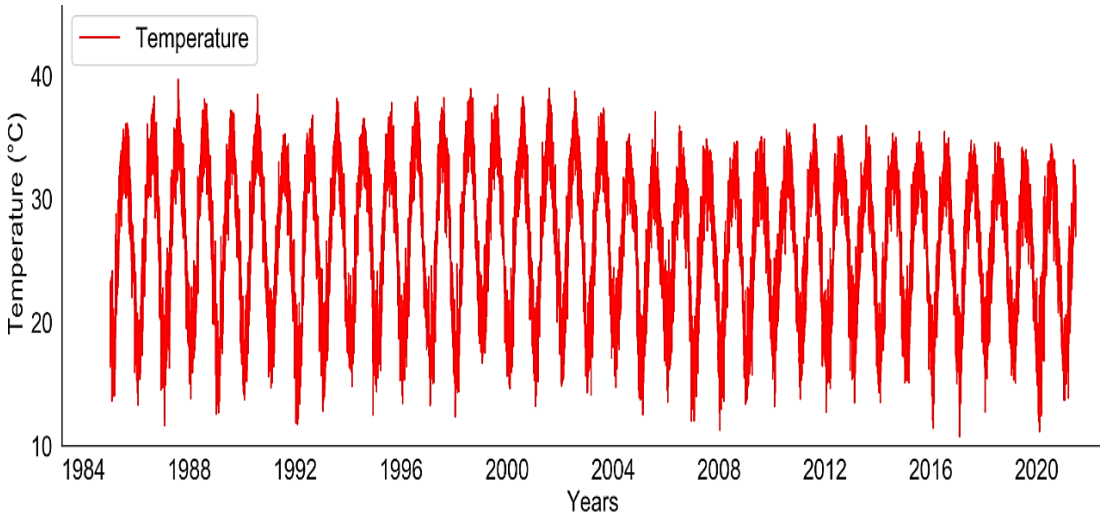

Figure A.5-77. The historical temperature performance over 36 years at hourly intervals for Bahrain.

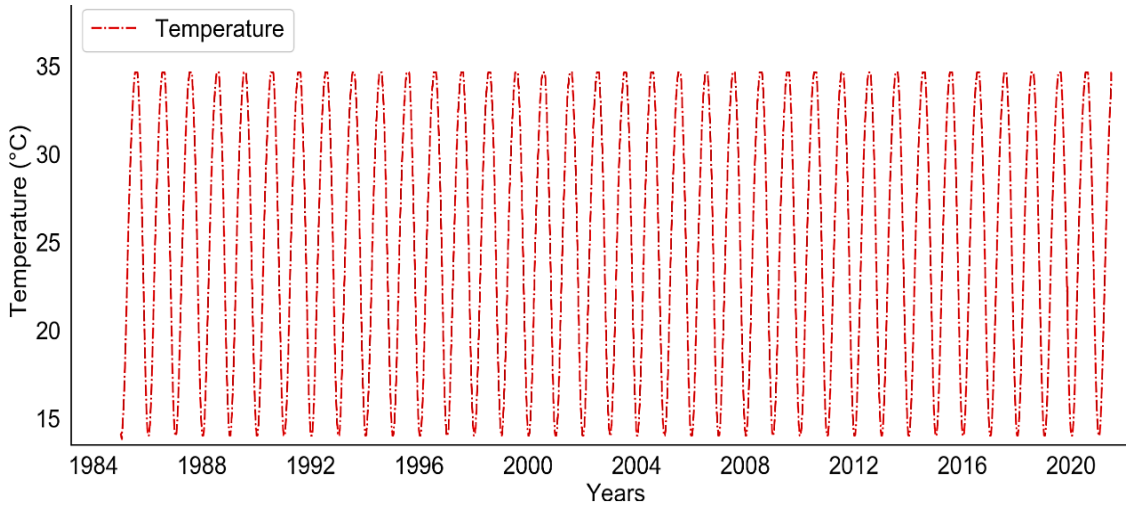

Figure A.5-78. The historical temperature performance over 36 years at daily intervals for Bahrain.

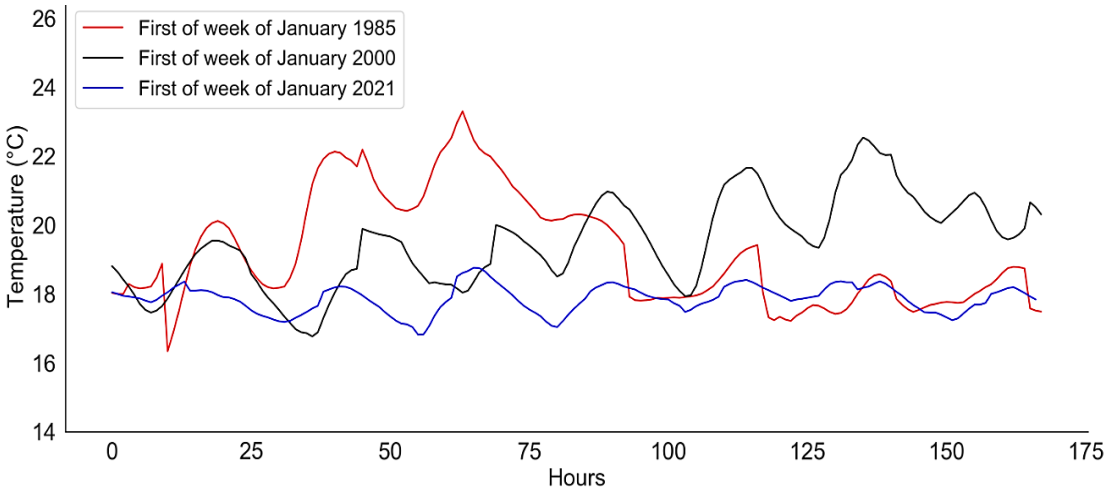

Figure A.5-79. The first three historical weeks of temperature performance for Bahrain during January at hourly intervals.

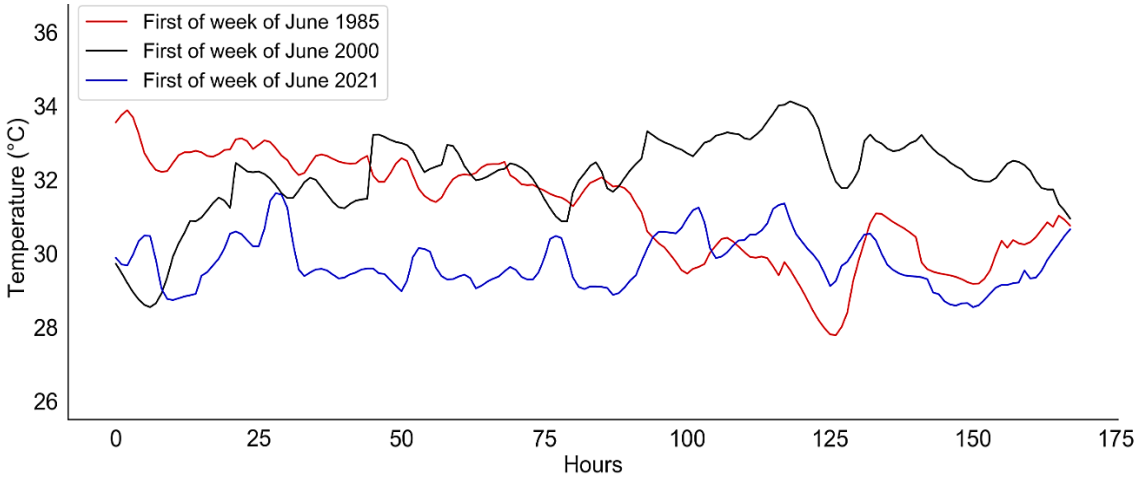

Figure A.5-80. The first three historical weeks of temperature performance for Bahrain during June at hourly intervals.